Coal-Fired High Performance

Power Generating System

DOE/PC/91155--7/2

DE-AC22-92PC91155

Final Report

August 31, 1995

Prepared for

Pittsburgh Energy Technology Center

Pittsburgh, Pennsylvania

United Technologies Research Center

411 Silver Lane, East Hartford, Connecticut 06108

DISCLAIMER

DISCLAIMER

Portions of this document may be illegible electronic image products. Images are produced from the best available original document.

Coal-Fired High Performance
Power Generating System

DE-AC22-92PC91155

Final Report

August 31, 1995

Prepared for

Pittsburgh Energy Technology Center

Pittsburgh, Pennsylvania

United Technologies Research Center

411 Silver Lane, East Hartford, Connecticut 06108

CONTENTS

TABLES

FIGURES

1.0 EXECUTIVE SUMMARY

As a result of the investigations carried out during Phase I of the Engineering Development of Coal-Fired High-Performance Power Generation Systems (Combustion 2000), the UTRC-led Combustion 2000 Team is recommending the development of an advanced high performance power generation system (HIPPS) whose high efficiency and minimal pollutant emissions will enable the US to use its abundant coal resources to satisfy current and future demand for electric power. The high efficiency of the power plant, which is the key to minimizing the environmental impact of coal, can only be achieved using a modern gas turbine system. Minimization of emissions can be achieved by combustor design, and advanced air pollution control devices.

The commercial plant design described herein is a combined cycle using either a frame—type gas turbine or an intercooled aeroderivative with clean air as the working fluid. The air is heated by a coal-fired high temperature advanced furnace (HITAF). The best performance from our cycle is achieved by using a modern aeroderivative gas turbine, such as the intercooled FT4000. A simplified schematic is shown in Figure 1.0-1. In the UTRC HIPPS, the conversion efficiency for the heavy frame gas turbine version will be 47.4 % (HHV) compared to the approximately 35% that is achieved in conventional coal-fired plants. This cycle is based on a gas turbine operating at turbine inlet temperatures approaching 2500°F. Using an aeroderivative type gas turbine, efficiencies of over 49% could be realized in advanced cycle configuration (Humid Air Turbine, or HAT). Performance of these power plants is given in Table 1.0-1.
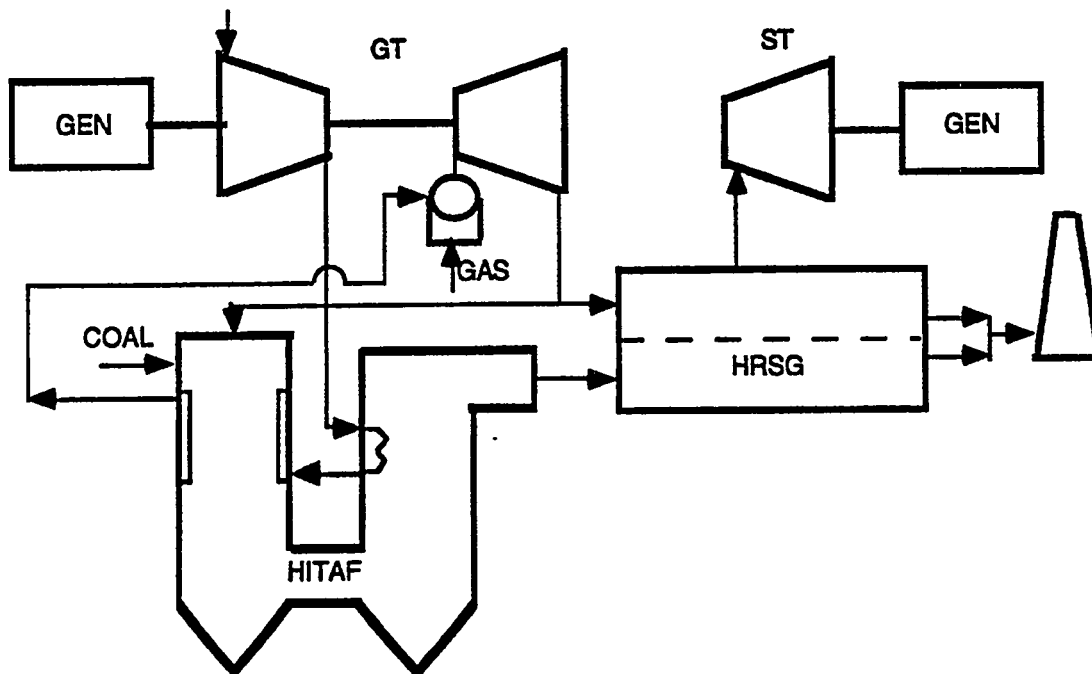
Figure 1.0-1   Simplified Schematic of HIPPS/HITAF.

1

Table 1.0-1 Performance of HITAF Power Plants

Application	GT Type/Size MW	Steam Conditions psi/°F/°F	ST Size MW	Efficiency %
Greenfield	Frame/160	2400/1000/1000	150	47.4
Greenfield	Aero/120	2400/1050/1050	101	48.5
Repowering	HAT/203	N/A	N/A	49.5
Repowering	Aero/109	2400/1050/1050	219	43.5
Repowering	Aero/109	2400/1050/1050	112	46.5
Repowering	Aero/109	1450/950/950	104	45.1
Repowering	HAT/184	2400/1050/1050	124	47.0

The use of the aeroderivative engine configurations was also investigated for repowering, i.e., using the gas turbine to supply heat, either as combustion air and/or to heat feedwater, to an existing steam turbine. Efficiencies from 43% to over 47% could be realized for a wide variety of plant sizes and steam conditions. A new furnace would be required in most cases for the designs studied. This new furnace would use only the convective air heater portion of the HITAF. The radiant air heater can also be used in repowering, depending on specific requirements. Repowering is a low-risk approach to the HITAF and could be demonstrated in commercial size early in the next century. Performance of selected repowering systems is also given in Table 1.0-1.

The emissions from these plants meet a proposed standard which is 10% of current NSPS for coal-fired steam stations; i.e., SO_x and NO_x are 0.06 lb/MMBtu, and particulates are 0.003 lb/MMBtu. Preliminary costing was done only for the frame-type power plant. The ten-year levelized cost of electricity was about 5% less than that of a conventional coal-fired plant meeting current NSPS.

1.1 Objectives

The primary objective of the UTRC HIPPS Phase I investigation was to identify the technical and economic feasibility of UTRC's advanced power concept by:

1) producing conceptual designs for key components;

2) comparing the economics of our concepts with alternative power systems, and

3) identifying the technical issues that must be addressed in order to realize a commercial demonstration before the end of the century.

1.2 Technical Issues

Because the gas turbine technology is already being developed to meet the >47% efficiency goal, the key to the success of the HIPPS program is the development of an integrated combustor/air heater that will fire a wide range of US coals with minimal use of natural gas and with the reliability of current coal-fired power plants.

- The air heater must be capable of raising the temperature of clean air to about 1700°F (2500°F for the all coal design) by extracting heat from coal combustion products that contain ash.

- The temperature of the coal combustion products in the furnace is about 3000°F. Since the air panels do not extract nearly as much heat as water walls, the wall surface temperature will be above the ash fusion temperature of most coals. Therefore our design incorporates slagging walls and wet bottom operation.

- The most efficient combined-cycle system will maximize the gas turbine compared to the steam turbine cycle. In our commercial plant designs, at least half of the heat from the coal combustion is used in the gas turbine.

- The compatibility of the slagging combustor with the high temperature radiant air heater is the critical challenge

1.3 Technical Approach – HITAF

The design of the HITAF system is complicated by the close coupling between the operating conditions of the combustor and the integrated air heater, combined with the need to control the flow and disposition of the ash. In Phase I, the approach has been to design the components with a "top down" methodology. That is, we first select an available turbine and then match the component designs with realistic operating conditions. The operating conditions imposed on the combustor/air heater were determined by a detailed cycle analysis. Once the power cycle requirements are known, thermodynamic considerations determine the conditions for the air heater and, in turn, the combustor. The arrangement of the UTRC HITAF components is presented in Figure 1.0-2.

1.3.1 The High Temperature Combustor

The HITAF combustor provides for the safe, complete combustion of a wide range of coals with minimal pollutant emissions. Most of the development risks are concentrated in the percentage and type of coal that can be burned and the ash management strategy.

Because the combustor is a new design and not just a deviation from conventional pulverized coal-fired boiler technology, there are many options for controlling the coal combustion to minimize NO_x formation. In addition, the HITAF has been designed to provide optimal conditions for the application of selective non-catalytic reduction of NO_x (SNCR).

Two HITAF combustor concepts are under consideration: (a) long axial flame, which was carried through the preliminary design stage; and (b) tangential firing, which was included during the extension to Phase I. The long flame is a relatively new approach which offers the potential for lower NO_x production and minimum ash impingement on the walls. Tangential firing, on the other hand, is a well-demonstrated commercial approach. Both concepts rely on diffusional mixing and natural reburn to control NO_x production. Preliminary results are available for the long flame. These two approaches will be evaluated for temperature profile control, ash impingement, NO_x production and development and construction costs.

3
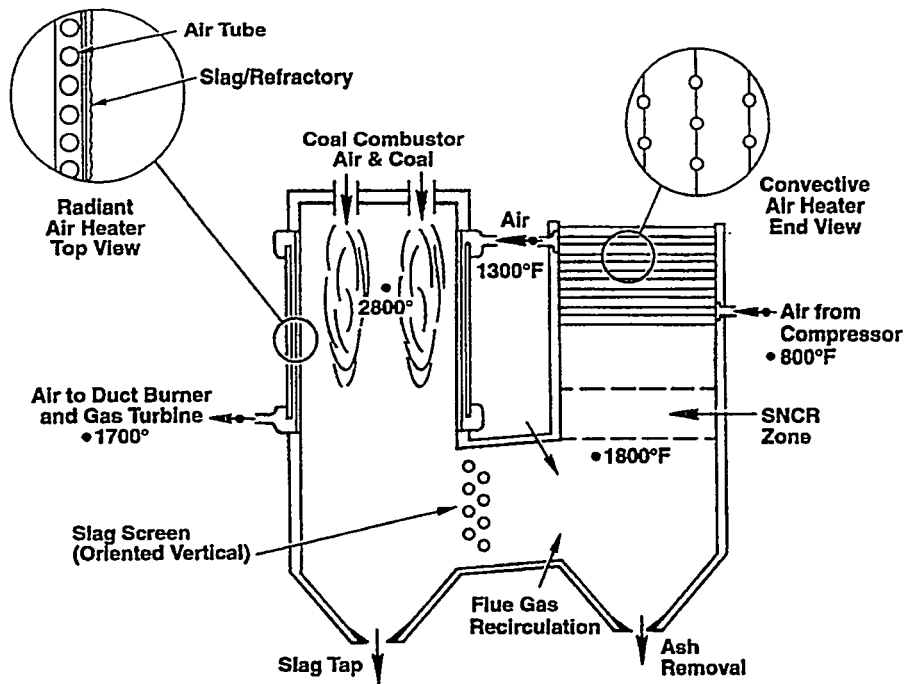
Figure 1.0-2.   UTRC Arrangement of HITAF Components.

1.3.2 The HITAF Air Heater

An air heater has been designed that is readily compatible with the gas turbine. Our designs recognize the interactions and conflicts between combustor and air heater, and the program included many trade-off studies. The failure risk of an air heater exposed to hot coal combustion products was a major concern of this study. (The alternative of allowing coal combustion products to enter a gas turbine is immeasurably worse. Even ppm levels of alkali and sulfur can have a deleterious effect on the precision components of a turbine. The design of a corrosion resistant air heater is a technological possibility, whereas a *high performance* gas turbine that can operate in a corrosive environment without loss of efficiency is not a possibility in the foreseeable future.) Our air heating is separated into (a) a high temperature radiant heater and (b) a lower temperature convective air heater. At the higher temperatures, the walls will be sufficiently hot (ca. 2600°F) that most ashes will be slagging. At the lower temperatures, the walls will be cool enough that the dry ash will only slowly densify. By this approach, we can avoid having the ash pass through its solidus temperature within our air heater. Even with a slag screen, a good deal of the ash will pass into the air heater and if it were collected there, it would eventually clog. Our radiant air heater design consists of panels cast from alloy with interior passages for the air. The corrosion protection is provided by a high temperature ceramic refractory coating, not unlike those used in blast furnaces. Laboratory scale tests of this concept have successfully demonstrated the ability to heat air from 1300°F to nearly 1800°F in an an alloy tube by radiation with flowing slag on refractory coatings. A variety of refractory coupons were tested for over 100 hr.

Our design for the convective air heater combines aspects of plate and fin with tube type heat exchangers. By adding fins along the length of the tubes to form "tube sheets" we have designed a

hybrid air heater that minimizes circumferential temperature gradients. We are convinced that the unique design can be fabricated and offers many potential advantages.

Most of the major HITAF components have been demonstrated. For example, down-fired slagging furnaces are sold commercially in Europe and the duct heater, which burns methane to raise the temperature of the air from the HITAF to desired gas turbine conditions, has been operated in a sub-scale test. The radiant air heater will be tested in a later phase of this program and, if operational lifetimes are too short for $T_{exit} = 1700°F$, the thermal load can be reduced to $T_{exit} = 1600°F$ and still achieve the goal of 47% thermal efficiency. The combined result of these features is an all-alloy design of significantly reduced risk and, therefore, a high probability of success. Our approach will allow a steady path of performance improvements as the high temperature materials technology evolves.

2.0 INTRODUCTION

The need for generating electric power with increased efficiency and decreased emissions is widely accepted. This is especially true for coal-burning power plants. In fact, according to the DOE's National Energy Strategy of 1992, the use of coal for power generation will increase steadily over the next 50 years and, even for a minimum growth scenario, would double by the year 2030. When this growing demand for coal is considered along with the fact that by the year 2000, nearly one-half of the coal-fired power plants in the U. S. will be 30 years old or more, the opportunity for both new systems and repowering designs becomes evident.

For the short term (approximately 5 years) the low price of natural gas favors the use of gas turbine combined cycle plants as a reasonable alternative for filling growing demands for electric power. In the longer term, the limitations on gas pipeline infrastructure and, perhaps, the increased cost of natural gas will necessitate a return to coal-fired designs. Several options are available in addition to the normal pulverized coal steam boilers. The use of pressurized fluidized bed combustion (PFBC) in a combined cycle and the integrated gasification combined cycle (IGCC) have received considerable attention in recent years. While these approaches appear to be attractive in some applications, they are limited by difficulties with hot gas cleanup and high capital costs.

All the proposed options for coal-fired power plants have technical risks and uncertainties in costs, both capital and operating. While direct comparisons of the various alternatives are difficult, some guidelines are possible. Any design must be capable of using a range of coals, be suitable for large installations >300 MWe and be economically viable early in the 21st century. A recent study by the International Energy Agency (IEA) indicates all of the new technology approaches have difficulties in producing electricity at lower cost than present day systems. Only when the additional requirements of increased efficiency and reduced emissions are considered, do most of these technologies have increased appeal. This is especially true for many coal-fired plants which will have to undergo expensive modifications to meet the provisions of the Clean Air Act as amended. The goal of improving the thermal efficiency of coal-burning power plants while decreasing their environmental burden can only be achieved by use of Brayton cycles (gas turbines) rather than Rankine cycles (steam turbines).

The DOE, recognizing this opportunity, began the High Performance Power Generating System (HIPPS) program which utilizes coal-fired air heaters to indirectly heat air for gas turbines. The indirect heating excludes all coal combustion products from contaminating the gas turbine working fluid, thus avoiding the expense of hot gas cleanup and/or the corrosion of turbine blades by coal ash. In the HIPPS, however, because the gas turbine working fluid (air) is heated indirectly, the highest air temperatures that can be reached by coal combustion are limited by heat exchanger materials and will fall short of the ideal turbine inlet temperatures for highest efficiency. To achieve the desired turbine inlet temperatures (approximately 2500°F for heavy frame machines and higher for aeroderivative machines) the program allows for up to 35% use of a premium fuel (e.g., natural gas or no. 2 heating

oil) in a topping cycle. The designs are still required to have a growth path to all coal as improvements in materials allow for a high temperature, corrosion-resistant heat exchanger. For the near term (<5 years) it is unlikely that there will be a structural ceramic available that can withstand molten coal ash at high pressures and temperatures of $\geq 2700°F$ for long times (10,000 hours). Therefore, the present designs must be based on materials available now or by the year 2000 and accept the temporary limitations on the air temperatures from coal combustion.

The most critical technical issues for the HIPPS program are all reducible to the HITAF air heaters requirements. The air heater is the major feature of the HITAF that distinguishes it from steam boiler designs and results in the higher wall temperatures that necessitate slagging ash and the wide range of materials problems. Most of the technical issues that arise from pursing the environmental goals of the HIPPS program (e.g., NO_x, SO_x, and particulates) are similar to those encountered by modern steam boiler designs, as highlighted by the LEBS program. Only the goal of high thermal efficiency, which requires adapting coal combustion to the Brayton cycle is unique to the HIPPS program. This is the feature that makes the high temperature air heater essential.

During Phase I of the HIPPS program, the UTRC-led Combustion 2000 Team have identified a number of ways to integrate various designs of air heaters into a HITAF system. From these options, we have been led inexorably to the following design considerations:

- The high temperatures require a slagging ash and down fired operation is preferable for wet ash.

- To avoid intolerable fouling problems, the air heater must be separated into a dry ash, lower temperature convective heater and a slagging, higher temperature radiant heater.

- Managing the high quality heat is crucial. For the 65/35 coal to premium fuel split, all the premium fuel must be burned in the topping cycle, the use of low quality heat must be optimized and the heat from coal combustion must be maximized in the Brayton cycle (our designs have about 50% utilization).

The following report presents the results of the Phase I investigations. The design of the commercial power plant and preliminary investigations of repowering systems discussed in Section 3.0 are based on the component technology described in Section 4.0. In Section 5.0, recommendations for Phase 2 effort are put forth, based on the results and conclusions drawn from our Phase I work.

7

3.0 PRELIMINARY COMMERCIAL GENERATING PLANT DESIGN

During Phase I of this three phase program, the multi-disciplined Combustion 2000 Team led by the United Technologies Research Center has developed a conceptual commercial HIPPS generating plant design of nominal 300 MW that meets, or exceeds, the HIPPS goals of high efficiency (>47% HHV), reduced emissions (originally 25% of current NSPS, but further reduced to 10% NSPS), and reduced cost of electricity (<10% reduction in COE compared to current PC plants). This design is based on current state-of-the-art technology, or technology which could be commercialized by the year 2000. Sections 3.1 through 3.10 deal with the heavy frame machine-based combined cycle. The aeroderivative-based systems are covered in later sections.

3.1 Process Overview

The HIPPS conceptual design developed by the Combustion 2000 Team is shown in a simplified schematic in Figure 3.1-1. The three major elements of the system are the High Temperature Air Furnace (HITAF), the gas turbine, and the steam turbine. The HITAF supplies 65% of the heat required by the gas turbines, bringing the compressor discharge air to 1700°F. The air then goes to a duct burner where natural gas boosts the temperature to that required by the turbine. The turbine exhaust stream, along with that from the HITAF, furnishes waste heat to a heat recovery steam generator (HRSG) and steam turbine. The overall efficiency of this system exceeds 47%, approximately 35% better than typical PC plants. Detailed descriptions of the equipment and of overall system operation are given in the following sections.

In Figure 3.1-1, it can be seen that the compressor discharge air is sent to a convective air heater in the HITAF exit stream. From there, it goes to a radiant heater located in the highest temperature portion of the HITAF, and then to the duct heater where the temperature is raised to the required combustor exit level. The exhaust from the gas turbine is split; one portion is sent to a "clean" HRSG while the remainder is used as preheated combustion air for the coal (Illinois No. 6) in the HITAF. The exhaust from the HITAF is sent to a "dirty" HRSG, baghouse, and FGD. To maintain the temperature required for a selective non-catalytic converter in the HITAF, as well as assure that the temperature for the convective section does not exceed 1800°F, a portion of the HITAF exhaust is recirculated. The steam bottoming system is atypical of currently installed combined cycles, with higher operating conditions of 2400 psi/1000°F/1000°F made possible by the HITAF exhaust temperature level.

3.2 Design Scope and Assumptions

The plant design scope is a non site-specific, greenfield power generation plant and includes all facilities required for power production. Consistent with the June, 1993 EPRI TAG™, the HIPPS plant boundaries for design and cost estimates include all the major operating systems such as the HITAF unit, heat recovery steam generators, gas turbine, environmental control equipment, auxiliary equipment and all support facilities needed to operate the plant (shops, offices, cafeteria, fuel handling and storage equipment, water intake structures, and waste treatment facilities). The plant

Figure 3.1.1   Simplified Process Flow Sheet.

includes the high voltage buss of the generator step-up transformer, but not the switchyard and transmission lines. The switchyard and lines are generally influenced by transmission system specific conditions and hence are not included with the cost or design.

In addition to the unique HITAF equipment, the commercial power plant design includes a single modern frame-type gas turbine and a Rankine cycle steam bottoming turbine. The nominal generating capacity of the HIPPS plant is 300 MWe. The plant is planned for a baseloaded duty cycle with limited load following capability.

Technical and economic criteria for the study use the EPRI TAG^{TM}, Volume 1: Rev. 7; June, 1993 as a basis. If criteria different from the TAG's are used, they are highlighted and explained, and compared to a TAG criteria.

3.2.1 Site Location and Conditions

For design calculations, the plant location and site conditions are taken from the TAG, and are as follows:

9

Site related:

Plant site	Central USA[1] (Kenosha, WI)
Site elevation (above mean sea level)	600 feet
Seismic zone	0 (UBC)[2]
Water transportation	Lake Michigan
Water makeup source	Lake Michigan
Electric power source for startup	Grid
Fuel storage capacity	60 days at 100%
Unit train coal delivery with rotary dump cars	

[1] EPRI identified region: E/W Central US

[2] Uniform Building Code

Meteorological

Average annual conditions	
Dry bulb temperature, − °F	60
Wet bulb temperature − °F	52
Atmospheric pressure − psia	14.4
Rainfall, inch/year	31
Other meteorological data	
Max. dry bulb temperature − °F	95
Max. wet bulb temperature − °F	75
Minimum temperature − °F	20 (performance)
Minimum temperature − °F	−20 (freeze protection)

3.2.2 Plant Performance Criteria

The following are the major criteria specified for the design and cost assessments.

Service conditions: The plant is to be designed for baseload operation. However, in recent years an important market aspect has surfaced in the power generation business: load profiles increasingly indicate a need for flexible plant operations, and new plant designs should account for daily output requirement swings. A minimum turndown of 50% is very desirable; operational flexibility will be examined further in Phase II.

Design life: The nominal design life is 30 years.

Target efficiency: The net efficiency of the reference commercial plant is to be 47% or higher (maximum heat rate 7260 Btu/kWh, HHV) at ISO conditions.

Design basis fuel: The plant burns Illinois No. 6 bituminous coal as the primary fuel. Coal is burned to supply 65% or more of the total heat input to the HIPPS. Properties of the design coal are listed in Table 3.2-1. Natural gas will serve as auxiliary and warmup fuel. Natural gas may provide up to 35 % of the energy requirements at the HIPPS design point. Composition and properties of natural gas are listed in Table 3.2-2.

TABLE 3.2-1 COAL PROPERTIES

(Illinois Bituminous 1993 EPRI TAG)

Proximate Analysis		
	Average	
Higher heating value (Btu/lb)	10,982	
Sulfur % wt	3.28	
SO_2/MMBtu	5.98	
Grindability index (Hardgrove)	51	
(% wt)		
Moisture	12.25	
Ash	10.97	
Fixed carbon	41.48	
Volatile matter	35.30	
	100.00	
Ultimate analysis (% wt)		
Moisture	12.25	
Carbon	61.00	
Hydrogen	4.25	
Nitrogen	1.25	
Chlorine	0.07	
Sulfur	3.28	
Ash	10.97	
Oxygen	6.93	
	100.00	
Ash analysis (% wt)		
SiO_2	50.66	
Al_2O_3	19.00	
TiO_2	0.83	
Fe_2O_3	20.30	
CaO	2.24	
MgO	0.89	
Na_2O	0.67	
K_2O	2.54	
P_2O_3	0.17	
SO_3	1.90	
Undetermined	0.58	
TOTAL	100.00	
Ash fusion temperature (°F)	**Reducing**	**Oxidizing**
Initial deformation	1950	2250
Softening (H=Q)	2030	2300
Fluid	2150	2450
(Ash fusion data from 1989 TAG)		

11

TABLE 3.2-2 GAS PROPERTIES

Ultimate analysis (%wt)	
C	73.25
H	24.26
N	1.87
O	0.62
Composition (mole %)	
CH_4	96.67
C_2H_6	1.80
C_3H_8	0.11
CO_2	0.32
H_2S	0.0004
N_2	balance
Average molecular weight	16.55
Higher heating value	
(dry gas at 60°F, 30 inches Hg)	
Btu/scf	1,013
Btu/lb	23,171

Environmental criteria: The original Phase I goal for environmental impacts of the HIPPS plant was 25% of New Sources Performance Standards (NSPS). However, at the suggestion of DoE, more restrictive limits, 10% of NSPS, were used in the commercial plant design. Atmospheric emission limits for Phase II are:

SO_2	0.06 lb/MMBtu
NO_2	0.06 lb/MMBtu
Particulates	0.003 lb/MMBtu

Liquid discharges are treated to meet NSPS requirements. Solid wastes (ash and FGD sludges) are stabilized and shipped for off site disposal.

3.2.3 Code of Accounts

Table 3.2-3 presents the code of accounts, or identification system employed with the HIPPS plant. The account numbers are used on the block flow diagram and cost estimate to ensure consistency and understanding of the plant's technical and cost estimating scope. The code is consistent with other parts of the DOE HIPPS program.

TABLE 3.2-3 CODE OF ACCOUNTS

Account No. Code of Account Items	Account No. Code of Accounts Item
Power Generation	**Balance of Plant**

1.0 Solids Feeding and Removal
    1.1 Coal Preparation and Feeding
    1.2 Limestone (FGD) Preparation and Feeding
	10.0 Solid Materials Handling
	    10.1 Coal Receiving, Storage, and Handling
	    10.2 Limestone Receiving, Storage, and
	          Handling
	    10.3 Ash Handling and Disposal

2.0 Steam Generation Island
    2.1 High Temperature Air Furnace
    2.2 Blank
    2.3 Heat Recovery Steam Generation
    2.4 Stack and Low Temperature Ducting
    2.5 Induced Draft Fan
	11.0 Water Systems
	    11.1 Cooling Water and Heat Reduction
	    11.2 Raw Water Supply and Treatment
	    11.3 Process and Plant Effluent Treatment

3.0 High Temperature Heat Exchangers
    3.1 Radiant Air Heaters
    3.2 Convective Air Heater
	12.0 Support Services
	    12.1 Service and Instrument Air
	    12.2 Natural Gas Supply
	    12.3 Electrical Distribution
	    12.4 Instrumentation and Controls
	    12.5 Interconnecting Piping
	    12.6 Fire Protection
	    12.7 General Service

4.0 High Temperature Piping and Ducting	
5.0 Process Systems 5.1 In-duct Gas Fired Heater	

6.0 Gas Turbine Generator	13.0 Civil Structure
	    13.1 Site Preparation and Facilities
	    13.2 Buildings and Structures

7.0 Steam Turbine and Boiler Feed Water	

8.0 Emission Control Systems
    8.1 Particulate Control
    8.2 Flue Gas Desulfurization Control
    8.3 Selective Non Catalystic Reduction (SNRC)
          NO_x Control	

3.2.4 Design Philosophy

The HIPPS commercial plant design is based on the EPRI TAG design philosophy, including equipment sparring: expensive spare and redundant equipment to maintain high availability are not used. A target availability of 90%, exclusive of planned maintenance, is retained by using proven commercial equipment in all balance of plant process areas and designing for simplicity, as much as possible, the processes interconnected to the advanced HITAF. Two lines of HITAF operation in the 300 MW plant will also increase availability. Major equipment where spares are installed are noted in the equipment lists. These instances reflect the philosophy of commercial power plant design and construction.

3.3 Plant Design/Description

In this section, the engineering and design work conducted in Phase I is reported. All the significant technical and cost issues are addressed for the heavy-frame combined cycle system. The performance for the aeroderivative-based systems is given in a later section.

3.3.1 Block Flow Diagram

Figure 3.3-1 is the Block Flow Diagram (BFD) developed for the preliminary HIPPS commercial power plant. The identification numbers assigned to various boxes, or sets of boxes, correspond to the code of accounts.

13

COAL →

| 10.1 |
| COAL RECEIVING STORAGE, AND HANDLING |

| 1.1 |
| COAL WARMING | ← FLUE GAS

| 5.1 |
| IN-DUCT GAS FIRED BURNER |

GAS TURBINE EXPANDER

TRANSPORT AIR →

| 1.3 |
| AIR HEATING |

| 1.2 |
| COAL PREPARATION AND FEEDING |

NATURAL GAS

HEATED COMPRESSED AIR

STEAM COND

| 2.1 |
| HIGH TEMPERATURE FURNACE |

| 3.1 |
| HITAF RADIANT AIR HEATER |

SAT HP BFW ←

| 2.3 |
| HRSG #1 HOT |

SAT HP STEAM →

SAT HP BFW ← | HRSG #2 HOT |

HP STEAM

| SLAG SCREEN |

BFW

| CARBON BURNOUT |

| 2.2 |

| GAS QUENCH | ←

FLUE GAS TO COAL WARMING

HP STEAM

| WATER WALL |

BFW

| 8.3 |
| SELECTIVE NONCATALYTIC REDUCTION |

| 3.2 |
| HITAF CONVECTIVE AIR HEATER | ←

PROCESS WASTEWATER TO TREATMENT

BOTTOM ASH →

| 10.3 |
| ASH HANDLING AND DISPOSAL |

FLYASH

SOLID WASTE BYPRODUCT/DISPOSAL

218A4p14.DGN

HIPPS Overall Block Flow Diagra

Figure 3.3-1 Bloc

AIR

GAS TURBINE
COMPRESSOR

GAS TURBINE
GENERATOR

IN-PLANT
POWER
CONSUMPTION

18 MW

161 MW

293 MW → NET POWER
TO GRID

150 MW

W. STEAM

EXHAUST
TO STACK

[2.3]
HRSG #1 COLD

[7.0]
STEAM TURBINE
GENERATOR

[8.4]
SELECTIVE
CATALYTIC
REDUCTION

HRSG #2 COLD

W. STEAM

FLUE GAS
FROM COAL
WARMING

[8.1]
PARTICULATES
REMOVAL

BFW

FEEDWATER
SYSTEM

MAKEUP
BFW

[11.2]
RAW WATER
SUPPLY AND
TREATMENT

WATER

MAKEUP COOLING
WATER

I.D FANS [2.5]

[8.2]
FLUE GAS
DESULFURIZATION
(FGD)

BOILER
BLOWDOWN

[11.]
CIRCULATING
WATER
SYSTEM

HEAT
REJECTION
SYSTEM

FLUE GAS

BLOWDOWN

FGD SOLID
BYPRODUCT/
WASTE

EXHAUST FROM
HRSG #1

PROCESS
WASTE
WATER

[11.3]
EFFLUENT
TREATMENT

TREATED
EFFLUENT

[2.4]
STACK

TO
ATMOSPHERE

[1.4]
LIMESTONE
PREPARATION
AND FEEDING

[10.2]
LIMESTONE
PREPARATION
AND FEEDING

LIMESTONE

Bechtel

San Francisco

HIPPS POWER PLANT
DOE/UTC

21884

Flow Diagram.

14

3.3.2 Plot Plan

Figure 3.3-2 shows the conceptual plot plan for the power plant. The facilities were designed and sized based on experience with similar pulverized coal-fired plants. The solid materials handling equipment and areas are designed for 60 days storage and an annual consumption of 350,000 tons. Conveyors, bins, storage piles and other items are sized for operations to efficiently receive and store materials, and to feed the HITAF units. Figures 3.3-3 and 3.3-4 show the plan and elevation views of the HITAF and associated major power island equipment.

The major components shown on the BFD and the plot plan are briefly described below. Except for the HITAF, and the way it is incorporated into the power plant, all the power generation and auxiliary equipment and processes are commercially available and used by the power industry.

The estimated land requirement is 49 acres inside the fence line. Solid waste disposal is offsite. The land requirement will vary over a wide range depending on the site and disposal method. Capital and operating costs for solids disposal are excluded from the plant estimate.

3.3.3 Power Generation Facilities Description

Solids Feeding and Removal — Code of Accounts Item 1.0

The coal preparation and feeding system is similar to those used in pulverized coal-fired power plants. Reclaimed coal from storage is pulverized and dried prior to use as fuel in the combustor. Two operating trains of equipment with 50% (35 tph) capacity each, and two installed spare trains are used. Each grinding and drying train supplies coal to one of the two combustor units.

Coal Warming/Drying Process Description — As an efficiency improvement step, coal at 60°F from the day bin is fed to a countercurrent rotary warmer/dryer where the coal is heated to 120°F and its moisture level reduced from 12.25 to 10.3 %. Warmed coal is sent to surge bins directly ahead of the coal pulverizers. Heat for the warming process is taken from the HITAF flue gas, which enters the process at 258°F and leaves at 170°F.

Coal Preparation and Feeding Process Description — Coal from the surge bins is weighed and fed to pulverizer mills where it is ground and dried. The pulverization and drying is performed by commercial gas swept mills commonly used in the pulverized coal-fired power generation industry. Each HITAF has two parallel trains with 100% pulverizing capacity per train. The ground coal is internally classified and pneumatically transported to the combustor. The transport fluid is ambient air, preheated to 457°F. The transport fluid is labeled Primary Air on the block diagram. The primary air and entrained coal leave the pulverizer at 179°F.

Transport Air Heating — The primary air is preheated to 457°F in a heat exchanger using 477°F, 550 psia steam generated in HRSG No. 2A.

Limestone Preparation and Feeding Process Description — Limestone is required for the flue gas desulfurization system. The process is commercially used at many power plants. Slurry

15

21B84P10.DWG

N

PLANT BOUNDARY

RAW WATER INTAKE FROM WATER SUPPLY

LIMESTONE SILOS

WATER TREATMENT AND STORAGE

COOLING TOWERS

LIMESTONE SLURRY PREPARATION AND GYPSUM DEWATERING

SWITCH YARD

TURBINE BUILDING

AUXILIARY BOILER

FLY ASH SILO

BOTTOM ASH SILO

LIMESTONE STORAGE

PLANT GATE

PARKING

ADMINISTRATION BUILDING

CONTROL BUILDING

GUARD HOUSE

PARKING

GAS TURBINE BUILDING

COAL & LIMESTONE PREP. BLDG.

PARKING

WAREHOUSE

MAINTENANCE SHOPS

SERVICE GATE

NATURAL GAS TO GT COMBUSTOR

ON-LINE SAMPLING AND ANALYSIS

PLANT FEED CONVEYOR

RECLAIM CONVEYOR

ACTIVE COAL SIL

IN

EMERGENCY COAL PILE

COAL DUMP HOPPER

RAI

PLANT BOUNDARY

8   7   6   5

Figure 3.3-

RUNOFF
POND

VE COAL PILE

PUR

AREA = 49 ACRES.

10' 50'
0 25'   100'   200'

GRAPHIC SCALE
1"=100'-0"

H
G
F
E
D
C
B
A

4   3   2   1

Plot Plan.

16

COAL PREPARATION AREA   ASH HANDLING AREA

SNCR

CONVEC-
TIVE AIR
HEATER

HEAT
RECOVERY
STEAM GEN'R #2
(HRSG)

SCR

COAL FEED
DAY BIN

PULVERIZER

AIR TO RADIANT HEATER

COAL
DRYER

WATER WALL
SECTION

RAW COAL
CONVEYOR

RADIANT
ZONE

COAL
DRYER

COAL FEED
DAY BIN

PULVERIZER

WEIGH
FEEDER

HEAT RECOVERY STEAM GEN'R #1
(HRSG)

GAS TURBINE
GENERATOR
BUILDING

GAS TURBINE

COAL FEED
DAY BIN

PULVERIZER

COAL
DRYER

RAW COAL
CONVEYOR

RADIANT
ZONE

WATER WALL
SECTION

COAL
DRYER

COAL FEED
DAY BIN

PULVERIZER

AIR TO RADIANT HEATER

SCR

WEIGH
FEEDER

COAL PREPARATION AREA   ASH HANDLING AREA

SNCR

CONVEC-
TIVE AIR
HEATER

HEAT
RECOVERY
STEAM GEN'R #2
(HRSG)

8   7   6   5

Figure 3.3-3 HIPPS I

STEAM TURBINE GENERATOR BUILDING

STEAM TURBINE

ELEV.

ELEV.

BAGHOUSE

LIMESTONE
PREPARATION

LIMESTONE
DAY BIN

BALL
MILLS

LIMESTONE
SLURRY
TANK

A

ABSORBER
SO2 REMOVAL

FANS &
PUMPS

ID FAN

FANS &
PUMPS

ABSORBER
SO2 REMOVAL

ID FAN

STACK

FILTER HOUSE

GYPSUM
SLURRY TANK

RETURN
WATER TANK

GYPSUM
DEWATERING

BAGHOUSE

SCALE   1" =20'-0"

20   10   0   20   40 FT

| | 7-20-94 | ISSUED FOR INFORMATION | | | | | | |

1"=20'   T.M.CARLSON   TMC/ACAD

Bechtel

San Francisco

HIPPS POWER PLANT
DOE/UTC

GENERAL ARRANGEMENT
HITAF AND TURBINE AREA WITH AIR PREHEATER
PLAN BELOW EL 75'-0"

| | 21884 | SK-P-321 | A |

4   3   2   21884P11.dwg /20-Jul-1994 /110726   1

quipment Plan View.

17

21884P13.DWG

RAW COAL
CONVEYOR

COAL
FEED
DAY
BIN

PULVERIZER

BURNER
ZONE

HITAF AIR
HEATER

CONVE:
AIR HE

WATER WALL
SECTION

SNCR

8   7   6   5

Figure 3.3-4 HIPPS Equ

SEE DWG SK-P-310

ABSORBER
SO2 REMOVAL

SEE DWG SK-P-311

VE
CR ┌─ SCR

HEAT RECOVERY
STEAM GENERATOR #2
(HRSG)

BAGHOUSE

ID FAN

10 5 0   10   20   40   80

GRAPHIC SCALE
1/16"=1'-0"

4   3   2   1

oment Elevation View.

18

preparation begins with limestone grinding in wet ball mills. The as-received 3/4 inch limestone is ground to 90% passing 200 mesh. The resulting 60% solids by weight ball mill slurry is diluted to 20% by weight and pumped to the limestone slurry tank for use in the absorbers. Grinding is performed in a single mill and the plant includes an installed spare mill.

Steam Generation Island – Code of Accounts Item 2.0

High Temperature Air Furnace – The HITAF represents the major unproven technology in the commercial plant design. Two HITAF units (Figure 3.3-5) of approximately 685 million Btu/hr each are used; the gas turbine engine located between them. The octagonal-shaped combustor units are down fired with the coal injectors located around the top. A short, refractory-lined adiabatic section allows flame stabilization prior to the radiant section. Temperatures are high enough to keep slag running down the refractory walls of the radiant exchanger to a wet bottom collector. Finely pulverized coal and reburn air are introduced in the radiant section.
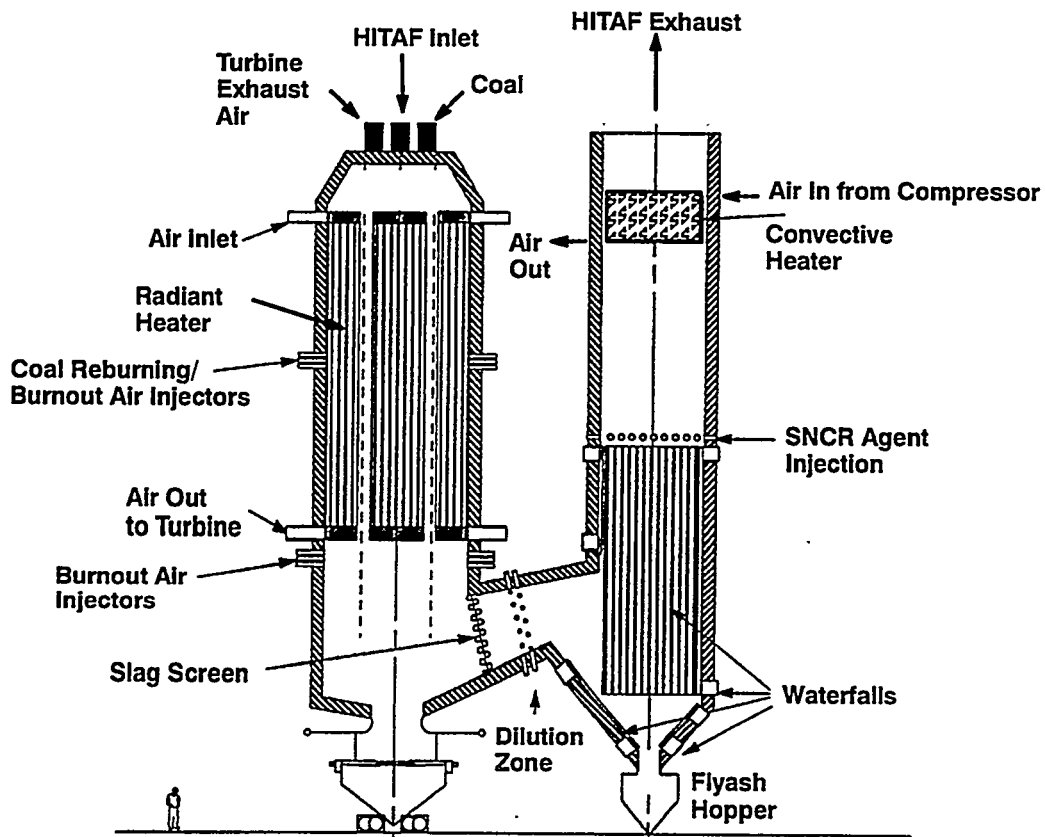
Figure 3.3-5   HITAF Cross Section.

The flow is turned 90° and passes through water-cooled slag screens and a waterwall section to freeze slag and reduce particulate carryover. A portion of the HITAF exhaust is recirculated to further reduce temperature and again turned 90° upwards before entering the SNCR and the convective heat exchanger. The exhaust exits the HITAF into a "dirty" heat recovery steam generator.

19

Considerable effort has been directed at identifying the refractory and heat exchanger materials. Currently, a castable alumina refractory is favored while a castable nickle-based alloy possibly lined with a newly developed FeCrAl alloy is proposed for the radiant exchanger. While use of an alloy limits the outlet temperature of the air heater to about 1900°F, the fabricability and joining capability of the alloy lowers the risk of HITAF development. The addition of ABB/Combustion Engineering to the Combustion 2000 Team has allowed considerable insight into fabrication and construction of the HITAF and will, by the end of Phase I, result in the lowest risk design.

Heat Recovery Steam Generators Process Description – Two HRSG's are used in the system to generate steam for electricity production. The "clean" HRSG (No. 1) operates with the gas turbine exhaust flow, and the two "dirty" HRSG's (Nos. 2A and 2B) use the HITAF flue gas as the source of thermal energy. Steam conditions are 1000°F and 2400 psia, with reheat to 1000°F and 480 psia. The HRSG's supply a single steam turbine and share a common feedwater and condensate system. Further details are provided in the equipment list. Also included in item 2.0 are the flue gas release stacks, induced draft fans and low temperature ducting.

High Temperature Heat Exchangers – Code of Accounts Item 3.0

At the preliminary commercial plant level of conceptual design, these heat exchangers are included with the total HITAF cost estimate. Heat transfer from the hot coal combustion products to the gas turbine air will be done in two successive components consisting of a convective air heater and a radiant air heater. The respective names of the two heaters denotes the principal mode of heat transfer from the coal combustion products to each heater. Forced convection is the primary mode of heat transfer to the gas turbine air from both heaters. To maximize the driving force for heat transfer between the air and the coal combustion streams, the overall arrangement of the two gas streams will be counterflow. Separate radiant and convective air heaters have been chosen to deal effectively with the predominant types of coal products present in the different temperature regimes of coal combustion.

While the radiant air heater will operate at a sufficiently high temperature level to ensure gravity-driven flow of slag from heater surfaces, the convective air heater will operate at a lower temperature regime which will ensure that dry ash deposits on heater surfaces can be removed by conventional soot blowing. A slag screen will be located between the radiant and convective air heaters to accurately establish the interface between wet slag and dry ash and to remove most of the ash from the hot gas stream before it can enter the convective air heater. To prevent excessive sintering of ash deposits on convective air heater surfaces and to provide a suitable temperature zone for selective non-catalytic reduction of NO_x, the coal combustion gas will be tempered by introducing flue gas recirculation upstream of the convective air heater. The arrangement of the air heaters and the slag screen and design configurations for the two air heaters are shown schematically in Figures 4.2-1 to 4.2-3 along with expected operating temperature levels. The rationale for this arrangement, the

unique features of the air heaters, and their operating conditions are discussed in detail in Section 4.2 HITAF Air Heaters.

The radiant air heater consists basically of many long hollow structural panels which almost completely line the inside walls of the coal combustion furnace. The gas turbine air is distributed to many small passages within these panels by an arrangement of headers, manifolds, and ducts which will be staged to avoid excessive thermal stresses. A ceramic refractory coating or tiles is applied to the fire side of the hollow panels to prevent slag-induced corrosion of the panels. Support for the entire radiant air heater is provided by a massive structural shelf at the bottom of the furnace, probably consisting of furnace brick masonry. For air outlet temperatures of 1700°F or less, when supplemental heating of the gas turbine air is available by direct combustion of natural gas or fuel oil, nickel-based metal alloys developed for the gas turbine industry will be suitable for construction of the radiant air heater panels. Additional protection from slag-induced corrosion and oxidation will be provided to these nickel-based metal alloys by depositing a thin layer of alumina/chromia on both inner and exterior surfaces. However, if higher air outlet temperatures are required to reduce the use of supplemental heating, structural ceramic materials will be needed for construction of the radiant air heater

The heat exchanger configuration chosen for the convective air heater is a modification of the shell and tube type where the air flows through banks of tubes and the hot combustion gas flows over and perpendicular to the tubes. This modification of the shell and tube configuration, called the finned-tube-sheet configuration, consists of a sheet or fin extension between adjacent tubes in rows along the direction of the hot gas flow. The finned-tube-sheet configuration was created to enhance the hot gas side conductance relative to the high pressure air side, provide additional structural rigidity, reduce circumferential thermal stresses in the tubes, and provide an aerodynamic shape which will reduce ash deposition on heater surfaces. A two-pass, cross-counter flow arrangement, with two air passes and one hot gas pass, provides the desired effectiveness without excessive pressure drops and with reasonable heat exchanger dimensions.

Since maximum wall material temperatures for the convective air heater are not expected to exceed 1600°F, nickel-based alloys with suitable alumina/chromia coatings for preventing corrosion and oxidation have been selected for construction of this heat exchanger.

High Temperature Piping and Ducting – Code of Accounts Item 4.0

This item includes the piping, valves, ducting and insulation for systems connecting the HITAF to the gas turbine and other equipment. Costs were estimated by an allowance after inspecting the conceptual plant plot plan and equipment arrangements. Material quantity take-offs will be performed after further engineering.

Item 5 includes the in-duct burner used to supplement the coal-fired HITAF thermal input to the gas turbine. Fuel for the burner constitutes about 35% of the total energy input for the plant. The preheated air is heated from 1700°F to 2450°F prior to entering the gas turbine.

Gas Turbine Generator — Code of Accounts Item 6.0

The frame-type gas turbine selected for the combined cycle system is based on a commercially available design. A cut out projection of this engine is shown in Fig. 3.3-6; an out board combustor configuration has been retained for this application to ease integration with the HITAF. Selected performance parameters are given in Table 3.3.1.
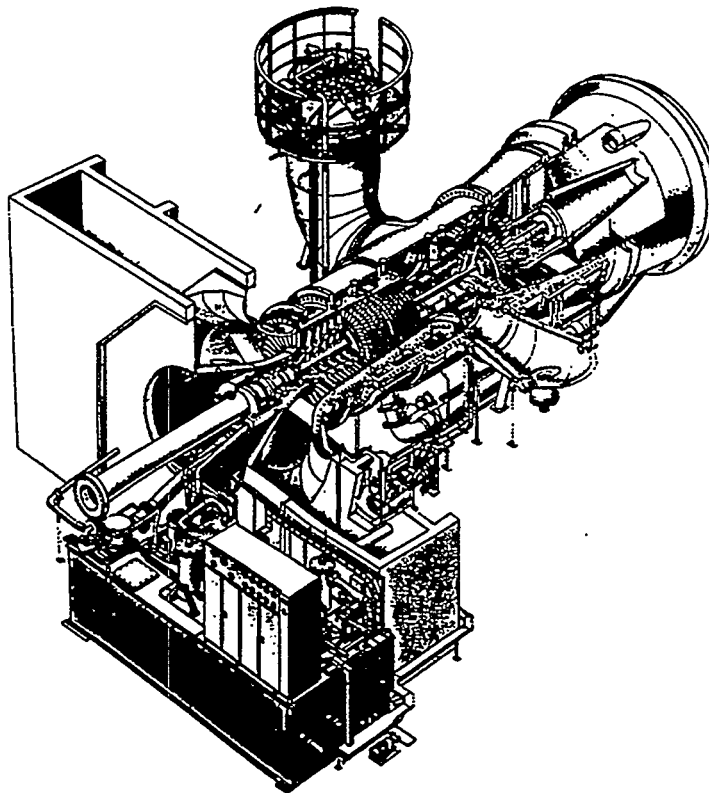
Figure 3.3-6   Heavy Frame Gas Turbine.

Table 3.3-1 Selected Gas Turbine Characteristics

Inlet Flow — lb/sec	918
Rotor Speed — rpm	3600
Pressure Ratio	16
Rotor Inlet Temperature — °F	>2350
Exhaust Temperature — °F	1005
Power — MW (nominal)	150

22

The duct burners which bring the hot turbine supply air to the desired turbine inlet temperature are located at the piping/engine interface and are arranged around the engine much like current can-annular combustor practice. The specially designed rapid mixing in these burners minimizes NO_x formation from gas combustion as well as providing minimum size for ease of installation.

Steam Turbine and Boiler Feed Water — Code of Accounts Item 7.0

Steam and Condensate — Process Description — Two heat recovery steam generator sections are thermally integrated to generate 2400 psia/1000°F superheat and 480 psia/1000°F reheat steam. The steam is used in a multiple pressure turbine to generate electric power. Steam from the low pressure turbine exhausts at 1.8 inches Hg absolute and is condensed by a shell and tube deaerating surface condenser. The cooling water flow is 97,860 gpm. The condenser thermal duty is 739 million Btu/hr. Boiler feedwater makeup (15,800 lb/hr) is added to the condenser. From the condensate pump discharge the feedwater flows through HRSG No. 1 low pressure heaters, and then is pumped to boiler pressure and fed to the economizer. Most of the high pressure evaporation occurs in the HITAF slag screen and water wall sections. A small additional amount of steam is generated in HRSG No. 1. Most of the steam superheating occurs in HRSG's Nos. 2A and 2B. Figure 3.3-7 shows the temperature versus cumulative heat transfer profiles for the three HRSG's used in the process.

LEGEND:
EC-ECONOMIZER, EV-EVAPORATOR, SH-SUPERHEATER,
RH-REHEATER, Q-CUMULATIVE HEAT TRANSFERRED
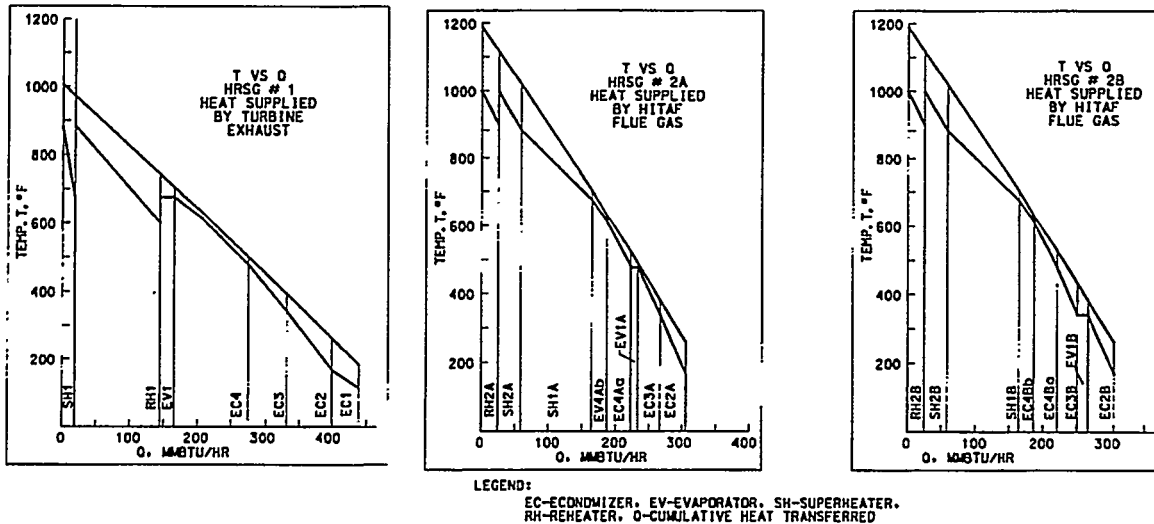
Figure 3.3-7 Temperature Profiles for HRSG's.

Boiler Feedwater Treatment: The raw water analysis data indicates that a boiler feedwater pretreatment system will be required to meet the following impurity limits:

Total Hardness as $CaCO_3$	<10 ppbw
Iron as Fe	<10 ppbw
Silica as SiO_2	<20 ppbw
Total Dissolved Solids	<100 ppbw

The boiler feedwater treatment system will be required to provide about 7700 lb/hr of demineralized makeup water for the high pressure steam cycle. The wastewater generated from the demineralizer system consists of backwashes and rinses and caustic wastes. These streams must be neutralized prior to reuse or discharge.

Emission Control Systems — Code of Accounts Item 8.0

The systems selected for the commercial plant design, and alternative technologies which were examined during Phase I, are briefly discussed below. Additionally, the team is aware of parallel DOE and industry programs, such as the low emissions boiler system (LEBS). These programs' progress and data will be reviewed in Phase II to determine if equipment or processes can be used with the HIPPS commercial design or the demonstration plant.

· **Particulate Control Process Description** — The HITAF design uses a baghouse located between the HRSG and the FGD systems for particulates control. This scheme provides adequate particulate emissions control, and is probably best available control technology (BACT). However, there are alternatives to the baghouse which might be more attractive in meeting the more restrictive emission goals. The technical capabilities of these alternatives will be more fully examined in Phase II with other systems that arise from LEBS or other development programs.

In summary, the commercial HIPPS design uses a baghouse and likely qualifies as a BACT. For Phase II engineering, the potential for cost reductions will be examined for particulates control integrated with SO_2 control. This alternative uses a moderate efficiency ESP followed by a CT-121 FGD system. Hot gas cleanup has both a higher cost and risk and does not seem justified at this time. However, if warranted, a catalytic hot baghouse for particulates and NO_x control may be considered in Phase II.

Flue Gas Desulfurization Process Description — The limestone forced oxidation process with a limestone-water slurry and throw-away product system is used for the conceptual design. The process selection is based on engineering experience and the estimated process economics, auxiliary power requirements (pressure drop) and potential for sulfur reduction. The throw-away product assumes there is not a market for gypsum, and if that assumption were to change, the process design selection may be reviewed.

The FGD design has two absorber towers to serve the two combustion trains. Each tower is sized at the maximum load, 105% of design gas flow. For the design coal higher heating value, SO_2 removal of 99 % would be needed to match an emissions requirement of 0.06 lb/MMBtu of coal fired. However, combining the coal and natural gas fuels, an SO_2 removal of 98.5% is sufficient to meet the 0.06 lb/MMBtu emission limit. The scrubbed flue gas from the two absorbers is sent to a 350 foot tall stack and released to the atmosphere. Exhaust gas from the gas turbine heat recovery steam generator is sent to the same stack where it mixes with the flue gas and provides some reheat energy. The estimated temperature of the mixed stack gas is 157°F at the stack exit. In summary, for near term application,

24

the wet limestone FGD is the most cost effective and reliable system for SO_2 control. Although a generic system is used in the present design, other proprietary systems, including CT-121, Saarberg Holter and Pure Air, will be examined in during our Phase 2 effort. As emission control performance of the processes is about the same, a selection will depend on the competitive bidding and guarantee conditions.

NO_x Control Process Description — The HITAF design includes low NO_x burners in the coal combustor and both selective noncatalytic reduction (SNCR) downstream of the radiant heating section where the temperatures range from 1600 to 1900°F, and selective catalytic reduction (SCR) in a lower temperature zone of the HRSG. By using the SCNR as the primary NO_x control, the SCR can be relatively small and more cost effective. These controls are designed to reduce the NO_x to 0.06 lb/MMBTU of total energy input to the plant (coal and natural gas).

The SCR process injects ammonia into the flue gas and passes the gas mixture through a catalytic bed with temperatures from 650 to 850°F. The ammonia reduces the NO_x to N_2 and H_2O. As reported in the literature, commercial SCR technology in combination with low NO_x burners and overfire air systems can achieve 0.1 lb of NO_x/MM Btu. The HITAF combination of SCNR and SCR is estimated to limit NO_x to the 0.06 lb/MMBtu desired for post-2000 regulations.

The NOXSO process will be examined as a possible combined SO_2 and NO_x system in Phase II, as will other processes from the LEBS and other research programs.

3.3.4 Balance of Plant Facilities Description Solid Materials Handling — Code of Accounts Item 10.0

Coal Receiving, Storage and Handling Process Description — The major items in the design of this system include the following:

- Railcar receiving and unloading
- Active coal storage in concrete silos (25,000 tons — 16 day supply)
- Inactive (dead coal) and emergency storage in open, ground storage piles (60 day supply)
- Conveyors and other material handling equipment required to transport coal safely and with minimum environmental impacts

The major equipment list in the appendix at the end of Section 3 provides specifics about the equipment at a level of detail sufficient for conceptual cost estimating.

Limestone Receiving, Storage and Handling Process Description — Three-quarter inch limestone is received by truck or rail, and delivered by movable conveyors and mobile equipment to two 5000 ton silos. The combined capacity is equivalent to 60 days of limestone reserves. Limestone is reclaimed from the silos and sent to a 200 ton day-bin prior to slurry preparation.

Water Systems — Code of Accounts Item 11.0

Heat Rejection — Process Description — Cooling water for the steam condenser is cooled from 80°F to 63°F with a forced draft wet cooling tower. A wet bulb temperature of 52°F is used to design

25

the cooling tower. The cooling water makeup rate is about 1520 gpm. The makeup accounts for evaporation losses of 1215 gpm, blowdown of 206 gpm (after 5 cycles) and a drift loss of 98 gpm.

Raw Water Supply and Treatment – **Process Description** – The plant's raw water will require treatments for sedimentation, clarification, filtration, carbon adsorption, chlorination and softening to provide potable and process quality water.

Process and Plant Effluent Treatment Process Description – Environmental issues, including waste water treatment, will significantly impact plant cost and schedule. A state mandated National Pollutant Discharge Elimination System (NPDES) permit for air and water is required before a construction license can be issued.

The major sources of wastewater streams for power plants can be identified as:

- Coal and limestone preparation systems
- Pretreatment and demineralizer washes
- Cooling tower and HRSG blowdowns
- Rainfall runoff from coal piles and FGD/ash disposal areas
- Equipment washes
- Sanitary waste treatment effluent
- FGD wastewater stream

The conventional discharge parameters are based on EPA guidelines for power plants, and include pH, oil and grease, suspended solids, residual chlorine, iron and copper. Other parameters restricted by state NPDES permits (depending on the receiving stream classification) may include dissolved oxygen, phosphorous, temperature, other trace metals (such as zinc, nickel, etc.), and dissolved solids.

Conventional waste treatment often involves combining wastewater streams according to treatment categories and treating those streams prior to discharge. As a minimum, the following are considered conceptual design requirements for treating the waste streams prior to discharge:

- Oil/water separator for removing traces of oil and grease from the floor drains and runoff streams
- Neutralization of the waste streams to adjust the pH, generally between 6.5 and 8.5
- Settling and clarification to remove solids

The single largest category of wastewater from the plant is blowdown from the wet cooling tower. This stream must be treated to meet phosphorous and TDS limits, temperature, residual chlorine, copper, iron, other metals and pH requirements.

FGD Wastewater – During combustion, chloride in coal is converted to hydrogen chloride which, being highly soluble, is captured by the FGD scrubber. The reactivity of limestone is reduced by

26

high chloride concentrations, and blowdowns of the system are necessary to remove and dilute the scrubber chloride concentration, and to limit the chlorides to a predetermined concentration. A bleed stream is withdrawn from the oxidation tank and dewatered to yield a filter cake (usually about 20% by weight residual moisture) and chloride-rich water. To limit the chloride concentration in the scrubber loop (10 to 15 g/l is tolerated), some of the separated water is purged and the rest is returned to the scrubber or as limestone slurry makeup water. The purged water stream is treated to meet NPDES limits.

Sanitary Wastewater – This effluent is collected at a central wetwell and routed to the treatment plant. Sanitary wastewater is treated by an extended aeration process. The effluent from the second stage flows into a clarifier zone where biological solids settle out and are recycled. Clarified effluent may be used as a cooling tower makeup water, or can be mixed with other waste streams for further treatment to meet NPDES limits before discharge.

Rainfall runoff and drains from plant equipment washes are combined and treated for the removal of oil, grease, and suspended solids prior to discharge. The rainfall runoff from the temporary FGD/ash storage and disposal areas must be monitored for pollutants.

Support Systems – Code of Accounts Item 12.0

The systems required for supporting power generation operations include the following.

- Service and Instrument Air
- Natural Gas Supply
- Electrical Distribution
- Instrumentation and Controls
- Interconnecting Piping
- Fire Protection
- General Services

They are defined for inclusion in the cost estimate. Each support system is available commercially, only requiring engineering specification prior to procurement. Costs are estimated from experience with similar PC power plants.

Civil Structural – Code of Accounts Item 13.0

This item includes the site preparation and facilities, buildings and structures. For cost estimating, the plant's civil materials (concrete, steel, architectural and others) and their installation are accounted for in this item. Costs are estimated based on experience.

3.3.5 Process Flow Diagram, Material and Energy Balance

Figure 3.3-8 shows the process flow diagram (PFD) with numbered state points on the process flow lines. The material and energy balance is also shown. The stream numbers at the top of the table are the PFD state points. Table 3.3-2 is the estimate of auxiliary power requirements.

27

Figure 3.3-8 Detailed P1

RECOVERY STEAM GENERATOR #1

BOILER &
SUPERHEATER

ECONOMIZER

⟨30⟩ ⟨31⟩

⟨29⟩

⟨28⟩

⟨27⟩

⟨26⟩

GENERATOR
150 MW

⟨36⟩ TO
ECONOMIZERS

CONDENSER

⟨33⟩

FLUE GAS
DESULFURIZATION

⟨25⟩

⟨21⟩

⟨24⟩

SUPERHEATER

ECONOMIZER

⟨15⟩

BAGHOUSE
PARTICULATES
REMOVAL

⟨16⟩

⟨22⟩ ⟨23⟩

RATOR #2

Bechtel

San Francisco

HIPPS POWER PLANT
DOE/UTC

21884

cess Flow Sheet.

28

GAS STREAMS

Stream Number	1	2	3	4	5	6	7	
Description	Air to GT Compressor	Cooling Air	Air to Preheat	Air to Rad Heater	Air to GT Combustor	Natural Gas	Air to Expander	Exh
Temperature, F	60	731	731	1300	1700	611	2495	10
Pressure, psia	14.4	235	235	232	229	275	225	1!
Lb/s CH4	0.00	0.00	0.00	0.00	0.00	8.32	0.00	0.
C2H6	0.00	0.00	0.00	0.00	0.00	0.29	0.00	0.
C3H8	0.00	0.00	0.00	0.00	0.00	0.03	0.00	0.
O2	211.08	44.05	167.02	167.02	167.02	0.00	132.66	17(
N2	686.95	143.38	543.57	543.57	543.57	0.17	543.74	68!
Ar	11.93	2.49	9.44	9.44	9.44	0.00	9.44	11
CO2	0.41	0.09	0.33	0.33	0.33	0.08	24.15	24
H2O	7.64	1.59	6.04	6.04	6.04	0.00	25.29	2f
SO2	0.000	0.000	0.000	0.000	0.000	0.000	0.000	0.!
NO2	0.000	0.000	0.000	0.000	0.000	0.000	0.000	0.
Total lb/s	918.00	191.60	726.40	726.40	726.40	8.88	735.28	92
Heat*, Btu/s								
Sensible	-3,765	31,188	118,242	227,718	308,430	3,028	496,540	221
Latent	8,026	1,675	6,351	6,351	6,351	0	26,580	28
HHV	0	0	0	0	0	205,655	0	
Total Btu/s	4,261	32,863	124,593	234,068	314,781	208,684	523,120	24!

GAS STREAMS

Stream Number	25	27	29	30	31
Description	Oxidation Air	Oxidation Tank Vent	Cleaned Gas	HRSG #1 Exhaust	Flue Gas to Stack
Temperature, F	206	130	129.8	180	157.4
Pressure, psia	29.4	14.4	14.5	14.6	14.4
Lb/s CH4	0.00	0.00	0.00	0.00	0.00
C2H6	0.00	0.00	0.00	0.00	0.00
C3H8	0.00	0.00	0.00	0.00	0.00
O2	1.36	0.86	12.81	109.50	122.31
N2	4.43	4.43	300.95	425.74	726.69
Ar	0.08	0.08	5.22	7.39	12.61
CO2	0.00	0.00	87.66	15.02	102.68
H2O	0.05	0.05	44.13	16.66	60.79
SO2	0.000	0.000	0.034	0.000	0.034
NO2	0.000	0.000	0.035	0.000	0.035
Total lb/s	5.92	5.42	450.84	574.30	1,025.14
Heat*, Btu/s					
Sensible	185	70	6,121	14,589	20,715
Latent	52	52	46,384	17,507	63,891
HHV	0	0	11	0	11
Total Btu/s	237	122	52,516	32,096	84,617

SOLIDS AND WATER STREA

Stream Number	
Description	(
Temperature, F	!
Pressure, psia	i
Lb/s C	2
H	1
N	(
S	1
O	!
Ash	!
H2O	∢
CaCO3	(
Gypsum	(
Total lb/s	3
Heat*, Btu/s	
Sensible	∢
Latent	
HHV	3!
Total Btu/s	3!

*All stream enthalpies reference fiduciary state of 77°F, H2O(L)

Figure 3.3-8 (Cont'd.) I

	9	10	11	12	14	15	16	17	20	21	22
	GT Exhaust to HRSG	GT Exhaust To Reburn	GT Exhaust To HITAF	Primary Air	Exh from Convect Htr	HRSG #2 Exit Gas	Dust-Free Flue Gas	Flue Gas Recycle	Flue Gas to Warmer	Flue Gas frm Warmer	Flue Gas to FGD
	1005	1005	1005	138	1189	256.8	249	258	258	170	249
	15.6	15.6	15.6	22	15.0	14.8	14.5	15.2	15.2	14.8	14.8
	0.00	0.00	0.00	0.00	0.00	0.00	0.00	0.00	0.00	0.00	0.00
	0.00	0.00	0.00	0.00	0.00	0.00	0.00	0.00	0.00	0.00	0.00
	0.00	0.00	0.00	0.00	0.00	0.00	0.00	0.00	0.00	0.00	0.00
	109.50	12.55	54.68	12.03	19.80	19.80	21.74	6.94	1.94	1.94	12.87
	425.74	48.78	212.59	39.14	462.52	462.56	507.66	161.61	45.10	45.10	300.95
	7.39	0.85	3.69	0.68	8.02	8.02	8.80	2.80	0.78	0.78	5.22
	15.02	1.72	7.50	0.02	132.37	·132.37	145.27	46.24	12.91	12.91	86.12
	16.66	1.91	8.32	0.44	42.47	42.51	47.39	15.07	4.21	4.87	28.11
	0.000	0.000	0.000	0.000	3.490	3.490	3.831	1.220	0.340	0.340	2.271
	0.000	0.000	0.000	0.000	0.105	0.053	0.058	0.019	0.005	0.005	0.035
	574.30	65.80	286.78	52.30	668.78	668.81	734.75	233.90	65.28	65.94	435.57
	137,240	15,724	68,531	772	200,527	30,295	31,847	10,675	2,979	1,548	18,880
	17,507	2,006	8,742	457	44,642	44,642	49,806	15,842	4,421	5,121	29,543
	0	0	0	0	33	0	18	6	2	2	11
	154,747	17,730	77,273	1,229	245,202	74,937	81,671	26,523	7,402	6,671	48,434

	18	19	23	24	26	28	32	33	34	35	36
	Secondary Coal	Solid Waste	Sorbent	Makeup Water	FGD Waste	Thickener Evaporation	HP Turbine Inlet Steam	LP Turbine Inlet Steam	Boiler Feed Water	Sat. Steam from HITAF	Condensate to HRSGs
	(With Stream 13)	1400	60	58	130.7	80	1000	1000	674	674	114
		15.1	14.4	14.4	14.4	14.4	2400	480	2700	2600	40
	0.00	0.14	0.00	0.00	0.00	0.00	0.00	0.00	0.00	0.00	0.00
	0.00	0.00	0.00	0.00	0.00	0.00	0.00	0.00	0.00	0.00	0.00
	0.00	0.00	0.00	0.00	0.00	0.00	0.00	0.00	0.00	0.00	0.00
	0.00	0.00	0.00	0.00	0.00	0.00	0.00	0.00	0.00	0.00	0.00
	0.00	0.00	0.00	0.00	0.00	0.00	0.00	0.00	0.00	0.00	0.00
	0.00	0.70	0.15	0.00	0.15	0.00	0.00	0.00	0.00	0.00	0.00
	0.00	0.00	0.08	17.75	0.32	0.23	218.38	215.45	228.48	200.74	228.48
	0.00	0.00	3.67	0.00	0.17	0.00	0.00	0.00	0.00	0.00	0.00
	0.00	0.00	0.00	0.00	6.01	0.00	0.00	0.00	0.00	0.00	0.00
	0.00	0.84	3.90	17.75	6.66	0.23	·218.38	215.45	228.48	200.74	228.48
	0	3,359	-15	-340	106	0					
	0	0	0	0	0	239					
	54	2,248	-2,813	0	-7,558	0					
	53	5,607	-2,827	-340	-7,452	240	309,211	317,981	159,825	208,168	8,454

...tailed Process Flow Sheet.

29

Table 3.3-2 Estimated Auxiliary Power Requirements

Item	Operating kWe
Coal handling and preparation	3,350
Limestone preparation and FGD	3,250
Large fans, blowers, plant and instrument air	2,300
Steam and condensate	2,450
Heat rejection (cooling tower) and water systems	4,450
Plant lighting, miscellaneous and transformer losses	1,000
SUBTOTAL	16,800
Gas turbine utilities	800
TOTAL	17,600

3.3.6 One Line Electrical Drawing

Figure 3.3.-9 presents the conceptual one line electrical drawing for the commercial HIPPS power plant.

3.4 Projected Performance

Table 3.4-1 shows the design point performance projections for the HIPPS power generation plant. For reference, similar projections are shown for a commercial pulverized coal-fired power plant with FGD and SCR. The PC plant is more fully discussed in Section 1.10, where the HIPPS is compared to a combination of stand-alone PC and gas turbine combined cycle power plants.

Table 3.4-1 HIPPS Generation and Emissions Performance

	300 MW	300 MW
Energy Inputs (MMBtu/hr)	HIPPS	PC Plant
Natural Gas	740.4	None
Coal	1,370.0	2,960
Total	2,110.4	2,960
Generation Performance (MWe)		
Gas Turbine	161.0	None
Steam Turbine	150.0	324
Total Gross Power	311.0	324
In–house Power Consumption	17.6	24
Net Power Production	293.4	300
Plant Efficiency, HHV Input/Output %	47.4	34.6%
Heat Rate (HHV) Btu/kWh	7,195	9,870
Environmental Emissions (lb/MWh)		
SO_2	0.42	2.95
NO_x	0.43	1.18
CO_2	1,260	2,040
Particulates	0.02	1.00
Solid Wastes	130	261
Liquid Effluents (Boiler blowdown)	25	60

2LB64P16.DWG

TO 230KV GRID

ISOLATED PHASE BUS, 3ø, 1200A

146 MVA, 3ø
DA/FA, 65°C
230-13.8 KV

ISOLATED PHASE BUS, 3ø, 7500A

8000A SF6

2400V
1000A,2.4Ω

UNIT AUX. XMFR
12/16/20 MVA,
DA/FA/FA 3ø
13.8-4.16 KV

100 KVA, 1ø
9000A · SF6
120/240V

0.720
GRD 80 KV.
RES 300V

GAS TURBINE GENERATOR

3000A N.C.

160 MW, 0.9 PF,3ø
13.8 KV (TYP.)

4.30 KV, 3000A, 350 MVA (S/C)

1200A   1200A   1200A   1200A   1200A

1-3/C-350MCM   1-3/C-350MCM   3-1/C-500 MCM

SPARE   1200A

1-3/C-350 MCM   LC A1

4.16 KV, 1200A, 350 MVA (S/C)   4.16 KV, 1200A,350 MVA (S/C)   4.16 KV, 1200A, 350 MVA (S/C)

600A 600A   600A 600A   600A (TYP.)   600A (TYP.)

1200A   1200A   1200A   400A (TYP.)

1100 HP 1100 HP   450 HP 450 HP   2000 HP 1250 HP   600 HP 450 HP 900 HP 500 HP 900 HP 350 HP 500 HP

600A   CTYP. FOR ALL 4KV MOTORS)   600A   150E   ID FAN

65E

2 CIRCULATING WATER PUMPS   2-SO2 SCRUBBER   2-SO2 SCRUBBER   FEEDWATER PUMP   2 UNITS FEEDWATER PUMP   2-SO2 SCRUBBER   ID FAN COAL PULVERIZER

INSTR/PLANT AIR COMP.   PRIMARY AIR BLOWER

FLUE GAS RECYCLE FAN

1-3/C-250MCM   1500 KVA DA, 65°C 4.16 KV-480V

500 KVA DA, 65°C 4.16 KV-480V

300 KVA DA, 65°C 4.16 KV -480V

750 KVA DA, 65°C 4.16 KV -480V

1000/ AA/F 4.16 K

600A N.C.

1600A

490V, 2000A, 42 KA(S/C)   480V 800A   22 KA(S/C)   480V, 600A, 14 KA(S/C)   480V, 1600A, 42 KA(S/C)   480V, 2000A, 42 KA (S/C) LC B1   2000A

LC   LC   MCC   MCC   LC   LC

800A 800A 400A 800A 800A   600A 400A   600A 800A 800A N.O. 1600A N.D.   800A 800A N.D.

3-1/C -#1/0   3-1/C -500MCM   MCC   3-1/C -500MCM   3-1/C -500MCM   MCC   3-1/C 500MCM   3-1/C -350MCM   2 MCC'S

200 HP 250 HP 125 HP 200 HP   100 HP   350 HP   200 HP   650 KV, 0.85 PF,3ø 480V

400A N.O.

9 UNITS COOLING TWR. FANS   3 UNITS AUX. COOLING WATER PUMPS   CONDENSATE PUMP   OXIDATION AIR COMPRESSOR   FIRE PUMP   MCC GAS TURBINE AUX'S

BUS DUCT 1000 AMP EMG DIESEL GENERATOR

4 UNITS AUX. COOL. RECIRC. WATER PUMPS   AUX. WATER PUMP   STEAM TURBINE AUX.   RAW WATER SYSTEM   BALANCE OF PLANT (BOP)

COOLING WATER SYSTEM

8   7   6   5

Figure 3.3-9   On

NOTES

1. THE ◯ DENOTES AN ELECTRICAL CONNECTION BETWEEN HEXAGONS OF THE SAME NUMBER.

2. GENERATOR CIRCUIT BREAKER WILL BE PROVIDED WITH SYNCHRONIZING GENERATOR CONTROL AND PROTECTION DEVICES.

3. UNIT AUXILIARY TRANSFORMER WILL BE SIZED TO CARRY TOTAL PLANT LOAD.

LEGEND

CIRCUIT BREAKER WITH DISCONNECT SWITCHES, 230 KV

MOTOR OPERATED DISCONNECT SWITCH

TRANSFORMER

CIRCUIT BREAKER, POWER, 4.16KV, 480V, DRAWOUT

CIRCUIT BREAKER, MOLDED CASE, 480V

FUSES

ELECTRICALLY INTERLOCKED

CONTROLLER

LOAD BREAK SWITCH

230 KV   13.8 KV   4.16KV & 7.2KV   480 V

TO 230KV GRID   1200A

1200A

1200A

230KV MAIN SWITCHYARD

200 MVA, 3φ
65°C
230-13.8 KV

ISOLATED PHASE BUS, 3φ, 1200A

ISOLATED PHASE BUS, 3φ,10000A

100 KVA, 1φ
8000A : SF6 120/240V

GRD RES   0.720
80 KW,
300V

STEAM TURBINE GENERATOR
150 MW, 0.9 PF,3φ
13.8 KV

UNIT AUX. XMFR
12/16/20 MVA,
DA/FA/FA 3φ
13.8-4.16 KV

2400V
1000A,2.40

3000A N.C.

4.16 KV, 3000A, 350 MVA (S/C)

1200A N.O.

1200A   1200A   1200A   1200A   1200A

SPARE

SPARE

3-1/C 500MCM

4.16KV, 1200A, 350MVA (S/C)

4.16 KV, 1200A,
350 MVA (S/C)   LC A2

1-3/C-350 MCH

600A (TYP)
400A (TYP)

600A

600A

65E

1200A

3-1/C-350MCM

3-1/C-350MCM

1200A

600 HP   600 HP   900 HP   350 HP   450 HP   450 HP

INSTR/PLANT AIR COMP.

COAL PULVERIZER PRIMARY AIR BLOWER

2-SO2 SCRUBBER   2-SO2 SCRUBBER

500 HP

2 UNITS COAL SILO FEED CONVEYOR

FLUE GAS CYCLE FAN

150E

1000/1333 KVA
AA/FA, 150°C
4.16 KV-480V

750 KVA
DA, 65°C
4.16 KV
-480V

300 KVA
DA, 65°C
4.16 KV
-480V

1000/1150 KVA
DA/FA, 65°C
4.16 KV
-480V

1000/1150 KVA
DA/FA, 65°C
4.16 KV-480V

83 KVA
150°C
-480V

480V, 2000A,
42 KA (S/C)   LC B2

600A
1600A
N.C.

600A
N.C.

480V, 2000A, 42 KA (S/C)

480V, 2000A,
42 KA (S/C)

LC B

3-1/C
-350MCH

800A N.D.

480V,
800A,42 KA (S/C)   LC

480V,
600A, 14 KA (S/C)   MCC

LC
480V,
2000A, 14 KA (S/C)

LC
3-1/C-
500MCH

1200A
800A

800A

400A

800A   800A   800A

3-1/C
-350MCH

800A

1/C-500MCM

2 MCC'S
2(3-1/C-500MCM)

3-1/C
-350MCM

3-1/C
-500MCM

3-1/C
-#1/0   3-1/C
-#1/0   3-1/C
-500MCM   MCC

3-1/C
-350MCM

3-1/C
-250MCM

MCC
GAS TURBINE AUX'S

1   FIRE PUMP

200 HP

2   GYPSUM FILTER

150 HP

125 HP   125 HP   3 MCC'S

TRANSFER CONVEYOR   2 UNITS ROTARY KILN DRYER

3 MCC'S

EMERGENCY STORAGE

200 HP   125 HP

LIMESTONE PULVERIZER

BALANCE OF PLANT   RAW WATER SYSTEM   SOLID HANDLING SYSTEM

Bechtel   San Francisco

HIPPS POWER PLANT
DOE/UTC

PLANT SINGLE LINE DIAGRAM

21884

21884P16.dwg /18-JUL-1994 /15:23:59

4   3   2   1

-Line Electrical.

3.4.1 Part Load Performance

The part load performance is given in Table 3.4-2.

Table 3.4-2 Part Load Performance (Nominal 50% Point)

Gas Turbine Output, MW	64.1
Steam Turbine Output, MW	95.5
Total	159.6
Aux. Load, MW	10.6
Net	149.0
Coal Flow, Btu/sec	282,944
Methane flow, Btu/sec	54,617
Efficiency at 50% Load	41.8%

3.5 Emissions

The emissions for the commercial plat are listed in Table 3.4-1 and conform to the program goals as shown in Table 3.5-1.

Table 3.5-1 DOE Emissions Goals

	Phase I	Phase II	NSPS
Pollutant Emissions			
NO$_x$ (lbs NO$_2$/MBTU fuel)	0.15	0.06	0.6
SO$_x$ (lbs SO$_2$/MBTU fuel)	0.15	0.06	0.6
Particulates (lbs/MBTU fuel)	0.0075	0.003	0.03

Liquid effluents and solid wastes are treated as needed prior to release or disposal so they meet current environmental requirements.

3.6 Operating and Maintenance Characteristics

3.6.1 Startup and Shutdown

The HIPPS is a combination of a gas turbine with low thermal inertia (fast response) and a HITAF with a high thermal inertia (slow response). While the close integration of these components will be a challenge to the control system, the system also provides the customer with the capability to operate at part power (gas turbine) while the remainder of the system comes on-line.

Startup and shutdown capabilities for the turbine are shown in Fig. 3.6-1. While the times shown are for emergency situations, it is clear that the turbine can respond in seconds and minutes. The HITAF, with its large inventory of refractory, must come up to temperature slowly, on the order of 50°F per hour, so startup from cold will be measured in hours and days.
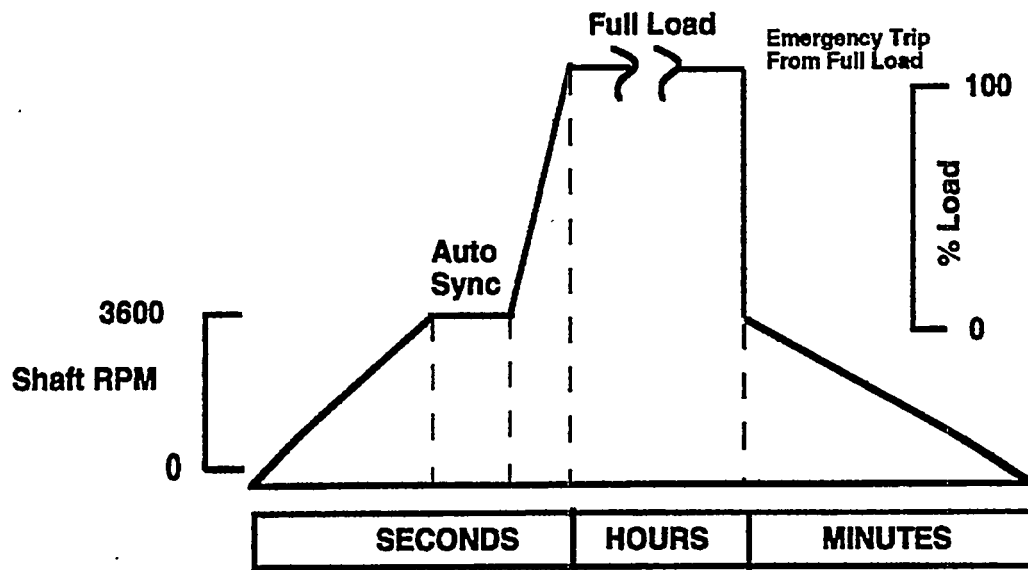
Figure 3.6-1   Startup/Shutdown for Gas Turbine.

At this point in the design study, the following general procedure is anticipated for startup. Gas is supplied to the turbine duct burners and the turbine is brought up to full power, providing the customer with 160 MW within minutes. Simultaneously, gas is fired in the HITAF (using partially vitiated gas turbine exhaust) at an increasing rate to heat the refractory. As the refractory comes up to temperature, compressor discharge air is sent to the HITAF, removing excess heat and maintaining alloy temperature in the radiant and convective heaters. At the point that the refractory temperature can maintain running slag, coal is introduced into the HITAF and the system balanced between gas and coal until all coal is attained. Water is circulated in the HRSG's and they are .brought up to temperature along with the HITAF. (Current HRSG's are capable of keeping up with gas turbine ramp rates.) The heat from the HRSG's is sent directly to the condenser until steam conditions allow the steam turbine to be brought on line.

Shutdown is essentially the reverse; coal flow is reduced and gas used in the HITAF to assure liquid slag. The gas is maintained when coal flow goes to zero to bring the HITAF down slowly to protect the refractory. Compressor discharge air (or air from another source TBD in Phase II) continues until the temperatures are within the capability of the heater alloys.

Attaining full power operation is much slower for the HIPPS than for a typical PC steam plant. However, responding to load changes down to approximately 50% would be much quicker through the use of the gas fuel fraction. Because of the higher efficiency of the HIPPS, it would be dispatched at base load for maximum time with minimum startup/shutdown cycles.

The most severe operating condition occurs at loss of electrical load (drop load). In the normal combined cycle, fuel is immediately cut to the 30% level in the turbine, equivalent to the synchronous

33

idle, no load condition. (Turbine temperature is around 1250°F, resulting in low temperature exhaust supplying heat to the HRSG.) The engine responds in nearly instantaneous fashion. Steam flow is momentarily cut off, then, as steam conditions reduce, flow is adjusted to allow the turbine to reach idle conditions.

In the HIPPS, gas fuel cut off would result in 1700°F heat to the turbine, well above idle. A fraction of the compressor discharge air will be bypassed to the duct burner (now unfired) to temper the air from the HITAF. Simultaneously, coal flow will be reduced to meet the reduced flow (around 50%) to the heaters. The steam turbine will come down as in the normal combined cycle, except steam will be bypassed to the condenser for a longer period because the HITAF exhaust temperature will not be reduced as quickly as the gas turbine exhaust temperature. Dynamic modeling of the operation of the HIPPS will be necessary to establish transient times and identify the key control parameters.

3.6.2 Part Load Operation

Typically, part load for gas turbines in combined-cycle operation is obtained by reducing inlet flow through the use of variable inlet guide vanes (IGV). Exhaust temperature is maintained nearly constant down to about 50% load (gas turbine). Part load characteristics for the turbine are shown in Figure 3.6-2 for IGV use. For the HIPPS application, the actual method of load following will be a customer input. For example, if fast response is desired, reducing gas turbine firing temperature by reducing fuel gas flow will more quickly follow load, but at a reduced efficiency versus using the IGV approach.
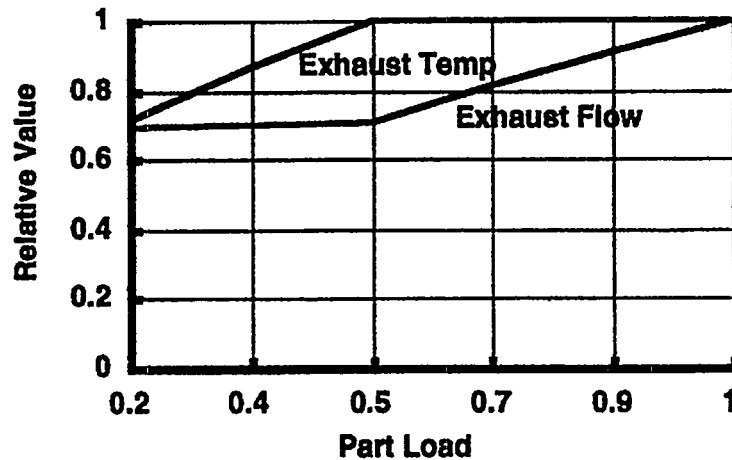
Figure 3.6–2   Part Load Characteristics for Gas Turbine.

The conventional approach has been used to estimate the HIPPS part load performance. In this mode, the HITAF exhaust temperature stays nearly constant and the steam performance does not suffer significantly. The steam system is run in a sliding pressure mode with the temperatures at the superheater and reheater exit held constant; the pressure is a direct function of flow rate. Temperature conditions are maintained at design levels, minimizing transient effects. Since the temperature of the

high pressure air leaving the HITAF remains constant, any reduction in turbine temperature means a reduction in methane flow.

At the 50% load point, 64 MW are from the gas turbine and 95 MW from the steam turbine. The efficiency is estimated to be nearly 42% compared to 32% at the same part load for a PC plant. Coal supplies almost 84% of the cycle heat at the 50% power level. Projected part load performance of the HIPPS and of conventional combined cycles are shown in Figure 3.6-3.
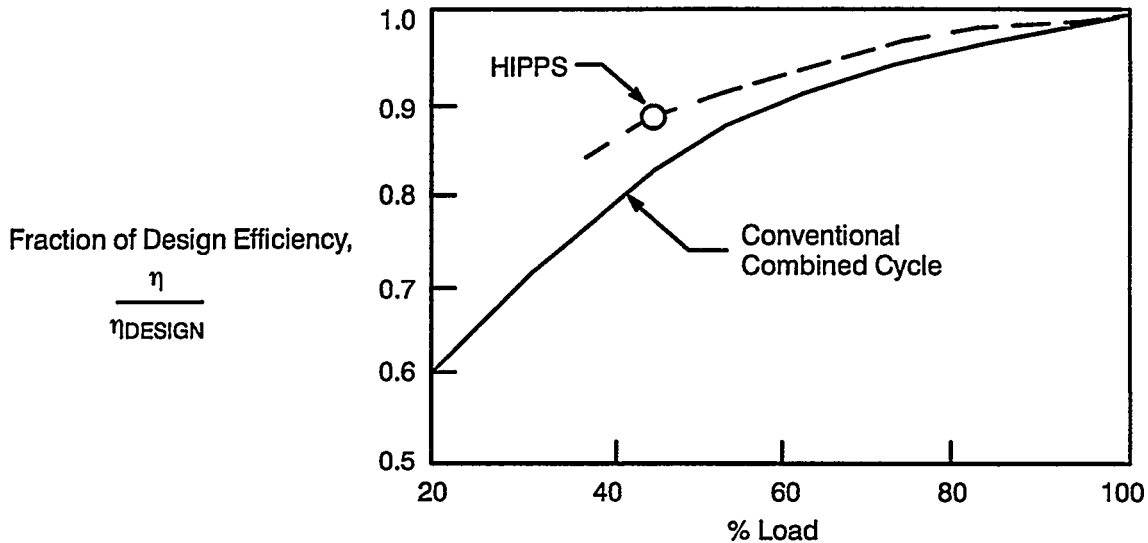
Figure 3.6−3   Part Load Comparison of HIPPS and GTCC.

3.6.3 Maintenance Considerations

The reliability and availability of combined cycles is quite good. For example, a recent study for EPRI indicated that a combined cycle would have an availability of 92.5% and a reliability of 97.2% compared to 84% and 94% for a PC plant. These values are based on hot end inspection intervals of 10,000 fired hours with blade recoating (or replacement) at 25,000 fired hours. In the HIPPS application, where firing in the engine is less severe and the circumferential temperature variations relatively low, these intervals could easily be extended.

Maintenance schedules for the HITAF are more difficult to predict. Refractory lifetime is the major concern and will be a function of coal type, local temperature differentials and ramp rates, and bonding/support mechanisms. Using the limited experience of coal gasifiers, it is anticipated that refractory inspection and replacement could be coincident with gas turbine hot end inspection and coating replacement.

3.6.4 Operational Uncertainties

The majority of the equipment in the HIPPS is currently, or will soon be, in wide-spread use in the power industry. The exception is the HITAF. Even in that component, much of the operation is well

35

understood: coal feeding, down firing, wet bottom operation, soot blowing (convective air heater), FGD, etc. The major uncertainties are those associated with the refractory and the radiant heater. These uncertainties are relatable to materials-based problems (e.g., slag/refractory interaction; long term creep of the alloy) and will succumb to technology as experience is gained in operation and specific problem areas are identified.

One key area that is currently undefined is that of system control. HIPPS presents a very dynamically complex system with many unknown factors and non-linearities. The novel HITAF furnace will be combined with conventional power plant subsystems (steam turbine, HRSG, gas turbine, emission control equipment, etc.). The HITAF must meet targets for performance and emissions. The ease and cost of meeting these targets will be influenced by the control system. The HITAF is a new furnace design, one that has never been built. While the task of designing such a system may seem daunting, the fact that HITAF is being designed "from scratch" provides an unprecedented opportunity to instrument the furnace and to create a control system, which takes maximum advantage of advances in sensors and diagnostics. Control system definition will be a key task in Phase II, where an overall system integration approach will be taken to conceptualize the power equipment/combustion/emissions control system.

From a performance standpoint, the operational limits are both technical (mostly materials related) and programmatic (the desire to have at least 65% coal). The two are related. Current heavy-frame gas turbines require combustor exit temperatures of around 2500°F; the new generation of aero-derivative turbines will operate at 2700-2800°F. Both of these are well above the capability of identifiable materials that can be fabricated and joined in complex headers and collectors. Thus, in our low-risk approach, the HITAF radiant heaters are of alloy construction, limited to 170°F outlet temperature. Using the allowed 35% gas fuel fraction, combustor outlet temperatures of 2450°F can be attained. If it is desired to raise this temperature to use the capabilities of newer turbines, either new materials must be identified that would allow higher radiant heater outlet temperatures, or additional coal must be burned to balance the increased gas. The latter would usually result in decreased system efficiency as a larger fraction of the total heat added is not used at the highest temperature point in the cycle.

These limits can be extended either by development of new materials or by taking advantage of new power cycle developments such as the Humid Air Turbine (HAT) cycle. The HAT cycle uses normally discarded waste heat to humidify compressor discharge air. This means that low-temperature heat is used to vaporize water in the compressor discharge stream resulting in significant increases in power and efficiency. For example, the FT4000, an aero-derivative industrial gas turbine being developed by P&W, has a nominal output of 115 MW and a simple cycle efficiency of about 42% (gas HHV). In HAT configuration firing gas, the output is over 200 MW at an efficiency of nearly 56% HHV.

3.7 Projected Costs

3.7.1 Commercial Plant Capital Cost Estimate

The HIPPS plant boundaries for design and cost estimates are those defined in Section 3.2 and consistent with the June, 1993 EPRI TAG^{TM}. The expected accuracy for the estimate is in the range of 30% based on the level of conceptual engineering performed. It should be understood, that the 30% value is solely dependent on the conceptual level of engineering and the engineering data contained in the drawings, tables, calculations and discussions presented in the report. If, for example, major revisions to the HITAF or other equipment were found to be required by more detailed engineering at some later date, the estimate's 30% accuracy level is not intended to account for such changes to the defined scope.

3.7.2 Cost Basis

The estimate of total conceptual plant investment and capital requirement is shown in Table 3.7-1. These costs reflect the plant scope noted above and the power generation process as defined by the flow sheets and other engineering documents.

Table 3.7-1 Costs by Code of Accounts

Account No.	Code of Account Item	300 MW HIPPS Power Plant (Millions $)	
	POWER GENERATION		
1.0	SOLID FEEDING AND REMOVAL		7.80
	1.1 Coal Warming/Drying	0.80	
	1.2 Coal Preparation and Feeding	4.90	
	1.3 Transport Air Heating	0.20	
	1.4 Limestone (FGD) Preparation and Feeding	1.90	
2.0	STEAM GENERATION ISLAND/HITAF		47.70
	2.1 High Temperature Furnace	45.00	
	2.2 Slag, Burnout, Quench and Water Wall Systems	with HITAF	
	2.3 Heat Recovery Steam Generator Systems	with HITAF	
	2.4 Stack and Low Temperature Ducting	2.79	
	2.5 Inducted Draft Fan	with baghouse	
3.0	HIGH TEMPERATURE HEAT EXCHANGERS	with HITAF	
	3.1 Radiant Air Heater		
	3.2 Convective Air Heater		
4.0	HIGH TEMPERATURE PIPING AND DUCTING		8.00
5.0	PROCESS SYSTEMS		0.60
	5.1 In-duct Gas Fired Burner	0.60	
6.0	GAS TURBINE-GENERATOR		42.90
7.0	STEAM TURBINE AND BOILER FEEDWATER		30.10
8.0	EMISSION CONTROL SYSTEMS		36.90
	8.1 Particulate Control	7.80	
	8.2 Flue Gas Desulfurization Control	21.70	
	8.3 Selective Non-Catalytic Reduction (SNCR) NO_x Control	4.40	
	8.4 Selective Catalytic Reduction (SCR) NO_x Control	3.00	
9.0	BLANK		

	BALANCE OF PLANT		
10.0	SOLID MATERIALS HANDLING		11.60
	10.1 Coal Receiving, Storage And Handling	6.80	
	10.2 Limestone Receiving, Storage and Handling	1.50	
	10.3 Ash Handling and Disposal	3.30	
11.0	WATER SYSTEMS		7.80
	11.1 Cooling Water and Heat Rejection System	3.70	
	11.2 Raw Water Supply and Treatment	1.70	
	11.3 Process and Plant Effluent Treatment	2.240	
12.0	SUPPORT SYSTEMS		58.30
	12.1 Service and Instrument Air	0.80	
	12.2 Natural Gas Supply	0.50	
	12.3 Electrical Distribution (switchyard excluded)	26.00	
	12.4 Instrumentation and Controls	5.70	
	12.5 Interconnecting Piping	23.00	
	12.6 Fire Protection	1.30	
	12.7 Other Mechanical & General Studies	1.00	
13.0	CIVIL STRUCTURAL		53.80
	13.1 Site Preparation And Concrete	31.30	
	13.2 Building and Structures	22.50	
	TOTAL DIRECT FIELD COST		305.50
	Indirect Costs (12%)		36.70
	PROCESS FACILITIES CAPITAL COST		342.20
	General Facilities and Engineering Fee (10%)		34.20
	SUBTOTAL		376.40
	Project Contingency (15%)		56.50
	Process Contingency (30% of HITAF)		13.50
	TOTAL PLANT COST		446.40
	TOTAL CASH EXPENDED (Mixed Year Dollars)		428.80
	Allowance for Funds During Construction (AFDC)		48.00
	TOTAL PLANT INVESTMENT		476.80
	Owner Costs*		21.00
	TOTAL CAPITAL REQUIREMENT		497.80

*   Owner Costs:
  − Prepaid Royalties   − Initial Cost for Catalyst and Chemicals
  − Preproduction (or Startup) Costs   − Land
  − Inventory Capital (Fuel Storage, Consumables, etc.)

Costs for the commercially available power generation and balance of plant items (Account No. items 1, and 4 through 13) were estimated from informal budget quotes by potential suppliers and experience from similar power generation projects.

Items No. 2 and 3, the HITAF furnace system, were estimated as a unit by comparison with commercial steam generation systems and air heat exchangers, adjusted for the unique HITAF requirements. The adjustments reflect HITAF material, temperatures and pressures shown on the engineering documents. Because of the advanced nature of the HITAF, engineering judgments are also used to estimate the costs. Thus, the HITAF has a greater degree of cost uncertainty than other items, and has a special contingency applied as explained below. However, the HITAF is roughly 1/6 of

the total direct field cost, and even by adding, for example, 50% more to the HITAF, the total direct field cost is only increased by approximately 7%. The factors used to estimate costs are given below. The direct field level are consistent with the EPRI 1993 TAG.

- Indirect costs are for construction items that can not be allocated to a single Account No., but are known from experience to be required for plant construction. These represent 12% of the total direct field cost.

- General Facilities and Engineering Fee is estimated as 10% of the process facilities capital cost. This value is lower than the range of 12 to 35% recommended by EPRI. For the HIPPS estimate, all the known general facilities are included with the items 1 through 13.

- Project contingency is 15% applied to the subtotal cost line. This percentage is justified because the great majority of the plant is commercially available, mature technology. The EPRI TAG, for examples use 10% for pulverized coal-fired power plants.

- A process contingency of 30% is applied to the installed cost of the HITAF. This contingency is to account for the uncertainty of design at this stage of development. If the scope of the design were to change, i.e. an all coal HITAF, the costs must be reexamined.

- The allowance for funds during construction and owners' costs are taken in the same proportions as the EPRI TAG pulverized coal plant.

3.7.3 Operating Cost Estimate

The O&M cost estimate is shown on Table 3.7-2. Costs were estimated from experience with pulverized coal and gas turbine combined cycle power plants, the literature and EPRI TAG information. Engineering judgment was used to adjust the commercial technology cost to HITAF conditions. The fuel costs are discussed below during the levelized revenue requirement (cost of electricity) calculations.

Table 3.7-2 O&M Costs

Operating and Maintenance Cost Estimate

Fixed Cost $/kW-Yr	38.9
Incremental Cost Mills/kWH	
• Variable Costs	1.4
• Consumables	1.4
• Byproducts	0.0
TOTAL INCREMENTAL COST	2.8

3.7.4 Economics

All costs are expressed in mid-1994 dollars, and the 1993 EPRI TAG is used to calculate a levelized revenue requirement using the current dollar methodology.

The HIPPS requires both coal and natural gas fuels. The 1993 EPRI TAG projections for the fuels have been examined and the following decisions reached for fuel prices.

39

- The EPRI coal closest to the Illinois No. 6 fuel used in the process design is the Perry County, Illinois Basin coal delivered to the East Central U.S. The 1990 cost is given as $1.44, and the year 2000 forecast delivered price is $1.36 per million Btu.

- For the Illinois Basin coal, little or no real escalation is forecast over the 10 and 20 year investment time frames examined. Thus, 0 real escalation is assumed and the price of coal in 1994 dollars is taken as $1.40 per million Btu.

- The TAG has similar fuel forecasts for natural gas. The price of $2.84 per million Btu (in 1994 dollars) delivered to the North Central U.S. on a long term contract is estimated from the TAG. The forecast real escalation rate in the TAG for this fuel is about 3%. Both 3 and 5% escalation of the fuel price were examined, and the difference between those cases was small. The 3% escalation case is presented here.

- The TAG levelizing factors for current dollar calculations use an inflation rate of 4.1% and an after tax discount rate of 9.2%.

- EPRI's current dollar carrying charge factors are based on a 20 year tax recovery period and book life of 30 years for coal based power generation.

Table 3.7-3 shows the results from calculating the levelized revenue requirements for 10 and 20 year investment time frames. The HIPPS results are compared to a 300 MW pulverized coal-fired power plant (Exhibit 2 in the TAG — a 300 MW subcritical PC plant with flue gas desulfurization). The costs for that plant were taken from the 1993 EPRI TAG. Escalation of 7% was added to bring the TAG costs to a mid-1994 level, and a selective catalytic reactor was added for NO_x control and consistency with the DOE emissions requirements. While the HIPPS plant is nominally 310 MW, the actual net production, some 293 MWe are, of course, used to compute economics.

The HIPPS revenue requirement is some 5% less than for the conventional PC plant.

Table 3.7-3 Summary of Levelized Revenue Requirements

300 MW HIPPS and Subcritical PC Power Plants
(Mills per kWh — 10 Year Investment Time Frame)

	HIPPS – 300 MW	PC Plant – 300 MW
Investment and Expenses	64.4	69.7
Fuel Costs	18.2	16.9
Total Levelized Revenue Requirement	82.6	86.6

300 MW HIPPS and Subcritical PC Power Plants
(Mills per kWh — —20 Year Investment Time Frame)

	HIPPS – 300 MW	PC Plant – 300 MW
Investment and Expenses	61.3	66.4
Fuel Costs	22.4	19.3
Total Levelized Revenue Requirement	83.7	85.7

3.8 Backup Strategies and Performance Shortfalls

In the current commercial plant design, approximately 160 MW are provided by the gas turbine and approximately 150 MW from the steam turbine. The duct burners in the gas turbine have the capability to furnish full temperature rise; thus, our approach offers the customer the capability to generate at least 160 MW using gas. If the customer desired, it would be possible to bypass the HITAF section and divert the gas turbine exhaust to the dirty HRSG's where auxiliary gas firing could be used to raise the required steam for the steam turbines. In that way, 100% power could be attained even if one or both HITAF units were down for scheduled or unscheduled reasons.

The major concern for performance shortfall is the possibility that radiant heater outlet temperature, 1700°F in the current commercial plant design, could not be attained. This could be due either to material limitations or because of less than expected heat transfer. Analysis has been made at lower outlet temperatures showing that 47% cycle efficiency is possible at values as low as 1550°F. In this case, additional coal is burned to match the increase in gas consumption (100°F higher rise in the duct heater) resulting in higher HITAF outlet temperature. This allowed higher steam temperatures (1050°F vs. 1000°F in the baseline) and a higher steam cycle efficiency (and cost). The increase in steam cycle efficiency did not completely offset the decrease in overall powerplant efficiency; i.e., a lower fraction of the heat from coal is used at combined cycle efficiency. At air heater outlet temperatures below 1550°F, performance would be below the 47% goal.

As indicated above, the system performance is very dependent on the air heater outlet temperature, since this dictates the amount of gas required to complete the needed rise to turbine inlet temperature. Ultimately, the goal is to reduce the gas fraction to zero for normal operation (the all coal case). The all coal case represents the most serious technical challenge, as all the cycle heat must be transferred through heat exchanger walls requiring materials that can operate in the neighborhood of 2600°F in an oxidizing atmosphere and in the presence of coal slag. If materials cannot be identified to meet this requirement, lower turbine inlet conditions will result and cycle efficiency will be reduced. Again, steam conditions can be increased, but even a very high performance steam cycle (e.g., 4500 psi/1100°F/1100°F/1100°F) is limited to around 44-45% (HHV) with lower overall plant efficiencies.

Alternative power cycles could be used. If, for example, the air heater outlet were to be limited to 1800°F-2000°F, the turbine exhaust (which would be non-vitiated) could be used as preheated combustion air at temperatures around 800°F-900°F. This is the so-called "hot-firebox" approach sometimes used in repowering of older steam stations. When combined with the high performance steam system, overall powerplant performance could be improved to around the 45% level, but detailed economic studies would be required to establish any benefit from this system design versus a super performance steam system.

3.9 Commercial Acceptability and Deployment

The power generation industry will have the need for highly efficient, environmentally clean coal-fired systems in the relatively near future — say the next 10 years. After 15 or more years of

reduced new capacity planning, the industry finally appears ready to plan and build new baseload power plants.

A recent survey shows 188 units totaling 69 gigawatts in various stages (most still in early stages) of planning. Coal is planned for almost half (30 GW) of the new capacity. The average coal plant size is 370 MW, which is smaller than in previous surveys, but compares well to the HIPPS commercial plant design. Seventy-nine coal units are planned. There is also a significant market potential for repowering with the HIPPS technology. In a brief review of only three coal producing states, Pennsylvania, Ohio and Illinois, the number of plants with initial operations starting prior to 1964 represent a significant installed capacity (Figure 3.9-1). If only part of the aging units are replaced with larger coal-fired technologies, the market for HIPPS repowering is still on the order of 1000's of megawatts.
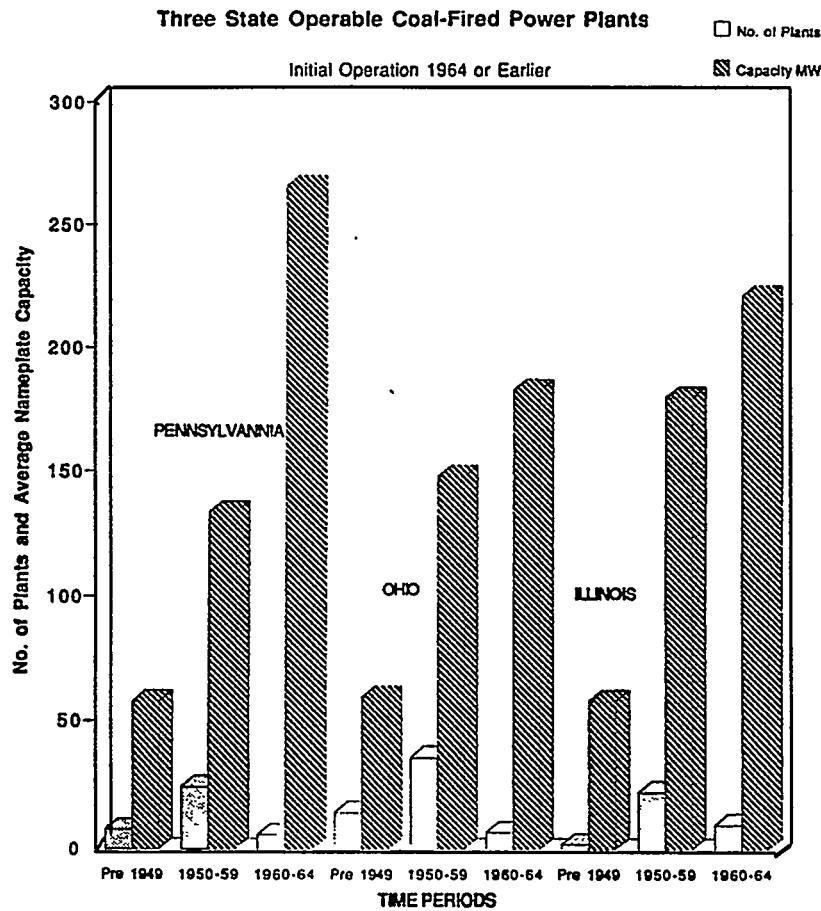
Figure 3.9-1   Installed Capacity.

What remains uncertain is the development path and continued success to prove the generation and environmental performance of the HIPPS. There is little doubt that when an all coal HIPPS is demonstrated that utilities and others in the industry will apply the technology.

- Cost of electricity: the Phase I cost of electricity is estimated to be almost 20% lower than for a comparable pulverized coal-fired power plant.

- Reliability: plant reliability should be comparable to PC plants, operations starting prior to 1964 represent a significant installed capacity (Figure 3.9-1). If only part of the aging units are replaced with larger coal-fired technologies, the market for HIPPS repowering is still on the order of 1000's of megawatts.

- Availability and maintainability: these should compare favorably with commercial PC plants. At 300 MW, two lines of HITAF equipment will help operators to plan maintenance, reduce unplanned maintenance and increase availability.

- Risk: the technical and financial risks related to a HIPPS plant after the technology has been demonstrated will be basically the same as for a PC power plant.

- Load Following and off-design performance: the use of natural gas to supply 35% of the energy allows rapid load following comparable to a normal gas turbine down to about 60% load. The decrement in efficiency is much less than a PC plant.

- Startup/shutdown requirements: startup and shutdown requirements are significantly different from normal powerplant routine. Because of the large inventory of refractory, startup from cold can take several days. Shutdown will require about the same time. Hot startup, in which the refractory has been kept at or near required temperature, would be comparable to PC plants.

- Fuel flexibility: the gas turbine will be capable of generating full load (160 MW) on natural gas and on a backup liquid fuel. Other sources of gaseous or liquid fuels, such as coal-derived fuels, have been used commercially in the heavy frame engine and can be accommodated in this application. As material technologies are developed and the coal fraction can be increased, it will eventually be possible to attain full load on all coal.

3.10 Comparison of HIPPS with PC Plant and PC/GTCC Combination

The preliminary HIPPS commercial plant was compared to separate pulverized coal-fired and gas turbine combined cycle power plants with a combined nominal capacity equal to the 300 MW HIPPS plant.

The criteria used to prepare the HIPPS design, and estimates of generation and emissions performance are provided earlier in the preliminary commercial plant design. This part of the proposal compares the HIPPS commercial plant to a pulverized coal-fired plant of the same size and baseload operations, as well as to power generation by a PC plant and a gas turbine combined cycle (GTCC) plant. The PC and GTCC plants are not necessarily related in any way except they provide power to the same utility, and the investment and operating philosophies are consistent. The combined PC and GTCC plant capacity is nominally 300 MW, and the natural gas to coal fuel ratio is the same as used by the HIPPS preliminary commercial design case (i.e., 65/35%).

43

3.10.1 HIPPS Cost Estimates

The capital, operating and maintenance conceptual cost estimates have been fully documented in Section 3.7 and are presented in Tables 3.7-1, -2 and -3. Those values are used here in comparing the three generating scenarios.

3.10.2 Description of Comparative PC and PC/GTCC Plants

A proprietary software program and data were used by Bechtel to conceptually define the performance of a 300 MW PC plant as well as both the 150 MW PC and 160 MW GTCC plants used in the comparison. Figure 3.10-1 presents a simplified block diagram accompanied by a material and energy balance for the 300 MW PC plant. It is coal fired with startup on light oil. The plant uses a 2400 psi/1000°F single reheat steam cycle and is designed for baseload with limited cycling capability. Coal used is the same as in the HIPPS baseline plan.

Emissions are controlled using an electrostatic precipitator for particulate removal, a wet limestone FGD system to remove 95% of the SO_2, and selective catalytic reduction (SCR) to reduce 80% of the NO_x present in the exhaust. Ammonia slip is limited to 5 ppm and SO_3 conversion to a maximum of 1%.

The 175 MW plant associated with the GTCC has the same characteristics as the 300 MW plant with all of the related flows reduced in proportion to the net output.

The block diagram with mass and energy balance for the GTCC plant is given in Figure 3-10-2. The plant produces 125 MW. When operated in concert with the 175 MW PC plant, the two produce 300 MW with a 65/35% coal/gas fuel split. Because the gas combustion produces no SO_x, only a SCR is included for NO_x reduction.

While it is unlikely that either a PC or GTCC plant will be available in these exact sizes, the primary intent is to examine the performance and cost that can be achieved when using current technology to produce power using a 65/35% split between coal and natural gas. Thus, performance and costing are based on practical sizes in the general range of interest.

3.10.3 Performance and Emission Comparison

Table 3.10-1 shows the predicted performance for the HIPPS plant along with the conventional comparison plants described in the previous section. The first two columns of that table give the data for the two separate plants making up the PC/GTCC combined plant. It is this PC/GTCC combined plant that is to be compared with the HIPPS plant since it uses the same 65/35% coal/natural gas split in producing the same net total power as the HIPPS but at a lower efficiency. The fourth column gives data for the pulverized coal plant while the last column repeats the data developed and presented in Section 3.4 for the HIPPS plant. Of significance in the table are the differences in plant efficiencies and emission levels. The HIPPS plant offers an efficiency about the same as that of a GTCC plant while burning a 65/35% mixture of coal/natural gas fuel. The differences in heat rate between the combined

44
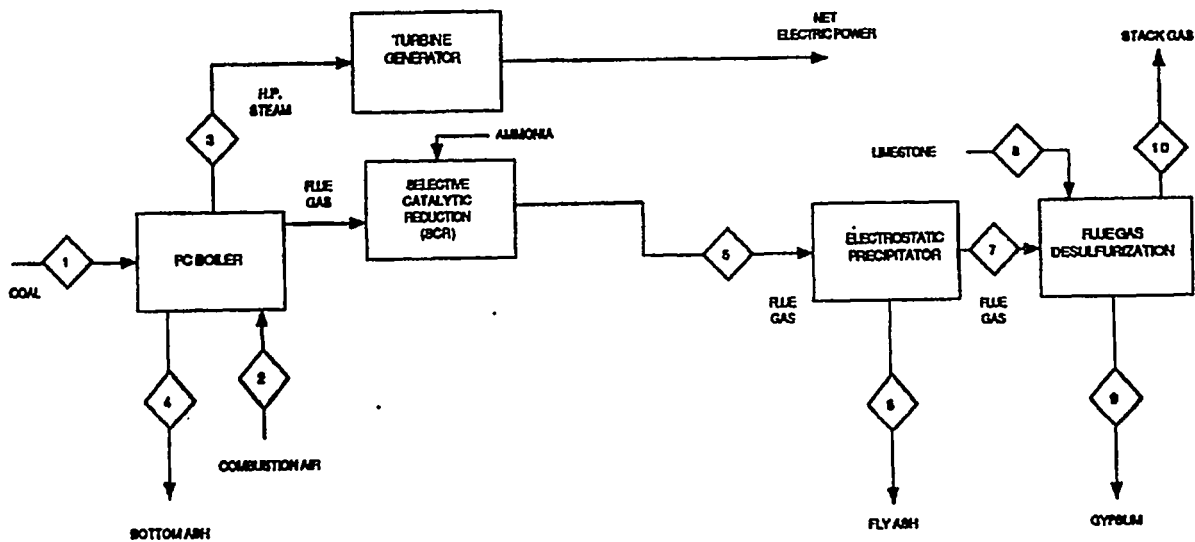
		Major Stream Flows for Subcritical Combustion with FGD and SCR					User		Coal		
Stream No.		1	2	3	4	5	6	7	8	9	10
Stream		Coal Fired	Comb Air	HP Stm to T/G	Bottom Ash	Flue Gas to ESP	Fly Ash fm ESP	Flue Gas to FGD	Limestone to FGD	Gypsum fm FGD	Flue Gas to Stack
	Units	0	0	0	0	0	0	0	0	0	0
Coal, def	lb/h	207,063	0	0	0	0	0	0	0	0	0
Sorbent	lb/h	0	0	0	0	0	0	0	29,232	0	0
Ash/Slag	lb/h	29,584	0	0	6,104	24,418	24,122	296	0	0	296
$CaSO_4 2H_2O$	lb/h	0	0	0	0	0	0	0	0	48,138	0
Water	lb/h	33,036	0	2,144,040	0	0	0	0	0	5,349	0
Subtotal	lb/h	269,684	0	2,144,040	6,104	24,418	24,122	296	29,232	53,487	296
O_2	lb/h	0	636,212	0	0	116,431	0	116,431	0	0	116,431
N_2	lb/h	0	2,096,575	0	0	2,099,934	0	2,099,934	0	0	2,099,934
CO_2	lb/h	0	0	0	0	600,237	0	600,237	0	0	600,237
H_2O	lb/h	0	8,231	0	0	149,229	0	149,229	0	0	149,229
SO_2	lb/h	0	0	0	0	17,687	0	17,687	0	0	884
NO_2	lb/h									355	
Subtotal	lb/h	0	2,741,018	0	0	2,983,518	0	2,983,518	0	0	3,109,863
TOTAL	lb/h	269,684	2,741,018	2,144,040	6,104	3,007,936	24,122	2,983,814	29,232	53,487	3,110,159
Pressure	psia	0	0	11	0	0	0	0	0	0	0
Temperature	deg F	32	32	1,000	2,496	292	291	306	32	86	128
Total Energy	mmBtu/h	2,962	9	3,130	8	354	12	365	0	1	377

Figure 3.10–1 Block Diagram with Material and Energy Balance for the PC Plant.
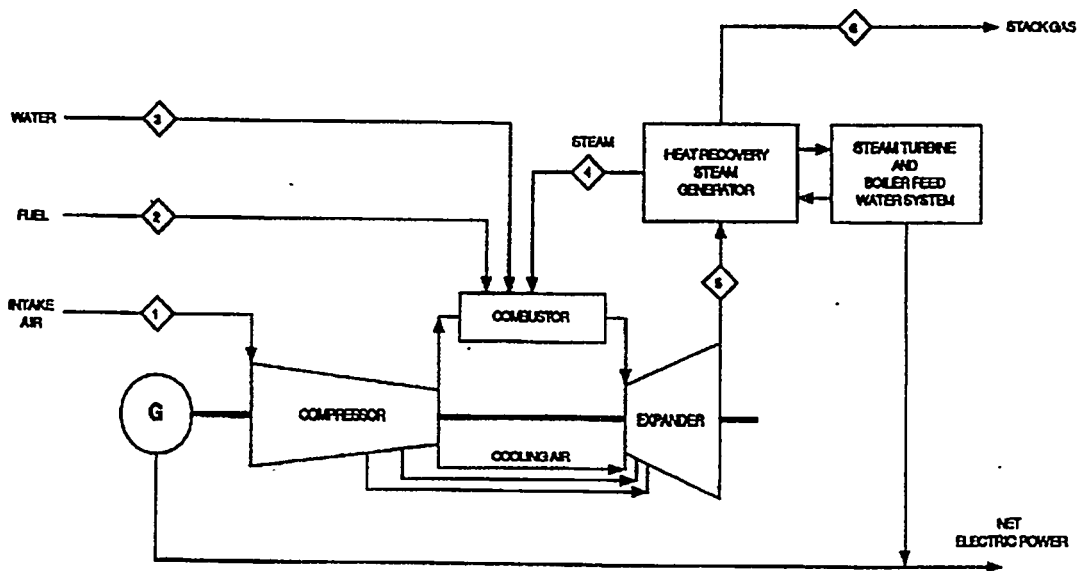
45

| ![logo] Major Stream Flows for GT Based Power Production | | Combined Cycle fuel: User | | | | NOₓ Control SCR | | |

Major Stream Flows for GT Based Power Production **Combined Cycle fuel: User** NOx Control SCR

© BECHTEL GROUP INC. 1992, ALL RIGHTS RESERVED

Stream No:		1	2	3	4	5	6	7	8
Stream	Units	Air to Turbine	Fuel to Turbine	Water to Combustor	Stream to Combustor	Turbine Exhaust	Stack Gas		
Water/Oil	lb/h	0	0	0	0	0	0	0	0
Subtotal	lb/h	0	0	0	0	0	0		
O2	lb/h	372,171	0	0	0	222,703	222,703	0	0
N2	lb/h	1,225,696	719	0	0	1,226,415	1,226,415	0	0
CO2	lb/h	0	329	0	0	103,630	103,630	0	0
H2O	lb/h	0	0	0	54,049	142,614	142,614	0	0
H2	lb/h	4,841	0	0	0	0	0	0	0
CO	lb/h	0	0	0	0	0	0	0	0
CH4	lb/h	0	36,186	0	0	0	0	0	0
C2H6	lb/h	0	1,263	0	0	0	0	0	0
C3H8	lb/h	0	108	0	0	0	0	0	0
H2S	lb/h	0	0	0	0	0	0	0	0
COS	lb/h	0	0	0	0	0	0	0	0
NH3	lb/h	0	0	0	0	0	0	0	0
SO2	lb/h	0	0	0	0	0	0	0	0
NO2	lb/h	0					29	0	
Subtotal	lb/h	1,602,708	38,605	0	54,049	1,695,365	1,695,394	0	0
TOTAL	lb/h	1,602,708	38,605	0	54,049	1,695,365	1,695,394	0	0
Pressure	psia	0	1		2	0	0	0	0
Temperature	deg F	32	59		572	1,083	248	32	32
Total Energy	mmBtu/h	5	895		69	638	248	0	0

Figure 3.10−2 Block Diagram with Material and Energy Balance for the GTCC Plant.

46

PC/GTCC and the HIPPS plant results in a 22% increase in the amount of natural gas and coal that is consumed by combustion as opposed to the HIPPS plant. As can be seen, the differential between the HIPPS and PC plant is even more dramatic.

Table 3.10-1 Performance and Emission Summary

	175MW PC Plant	125 MW GTCC Plant	PC/GTCC Combined	300 MW PC Plant	300 MW HIPPS
Generation Performance					
Net Thermal Efficiency – % HHV	34.6	47.7	39	34.6	47.4
Heat Rate – HHV – Btu/kWh	9872	7157	8743	9872	7195
Net Power Output – MW	175	125	300	300	293.4
Coal Input – MM Btu/hr	1728		1728	2962	1370
Natural Gas Input – MM Btu/hr		895	895		740
Emissions					
SO_2 – lb/MWh	2.95	0	1.72	2.95	0.42
NO_x – lb/MWh	1.18	0.23	0.78	1.18	0.43
CO_2 – lb/MWh	2039	829	1535	2039	1260
Particulates – lb/MWh	0.99	0.06	0.6	0.99	0.02
Solid Wastes – lb/MWh	261	0	152	261	130
Liquid Effluents – lb/MWh	59	22	44	59	25

The increased efficiency of the HIPPs also contributes to a reduction in emissions because of the reduced fuel use. However, in examining the estimated emission (present and in lb/MWh), it is clear that the combustion and controls technology are also greatly improved and produce an order of magnitude reduction in sulfur and particulate emissions and reduce nitrogen oxides by 64% over the PC plant. The importance of the reduced emissions cannot be over emphasized since, unlike the efficiency, its effects are not reflected in the cost of electricity. For example, to bring the pulverized coal plant sulfur emissions to the same level as the HIPPS plant would require the addition of equipment capable of removing an additional 85% of the sulfur dioxide in the stack gas.

3.10.4 Cost Comparison

Using the same methodology as described in Section 3.7, cost for the HIPPS design are compared to the combination PC/GTCC plant and to a straight PC plant having net outputs of 300 MWE. Table 3.10-2 presents the results of that comparison.

Table 3.10-2 Cost Comparison

Capital Cost Summary – 1994 $/kW

	175 MW PC Plant	125 MW GTCC Plant	PC/GTCC Combined	300 MW PC Plant	300 MW HIPPS
Const, Facilities, Engrg Costs Total	1490	650	1140	1490	1255
Project Contingency[1] Process Contingency[2]	150	66	115	150	188 45
Total Plant Cost	1640	716	1255	1640	1488
Total Plant Investment	1640	739	1265	1640	1589
Total Capital Requirement	1710	761	1315	1710	1659

[1] HIPPS contingency is 15% as opposed to 10% for the other plants.
[2] HITAF contingency is 30% of HITAF cost.

Summary of O&M Costs – 1994 Dollars

	175 MW PC Plant	125 MW GTCC Plant	PC/GTCC Combined	300 MW PC Plant	300 MW HIPPS
Fixed Costs – $/kW–yr	58	30.6	46.6	47.2	38.9

Incremental Costs – Mills/kWH
    Variable
    Consumables
    Byproducts
	
	2
	2
	0
		
		0.8
		0.8
		0
			
			1.5
			1.5
			0
				
				2
				2
				0
					
					1.4
					1.4
					0

Total Incremental Costs	4	1.6	3	4	2.8

Summary of Levelized Revenue Requirements
Mills/kWh – 10 Year Time Frame

	175 MW PC Plant	125 MW GTCC Plant	PC/GTCC Combined	300 MW PC Plant	300 MW HIPPS
Investment and Expenses	81.1	32.7	60.9	69.7	64.4
Fuel Cost	16.9	29.0	21.9	16.9	18.2
Total Levelized Revenue Requirement	97.9	61.6	82.8	86.6	82.6

Referring to the capital cost summary, the top line in that tabulation titled "Construction, Facilities and Engineering Cost Total" is the same as the line labeled "Subtotal" in the detailed estimate given in Table 3.7-1. That value represents the Total Plant Cost less contingencies. It is presented here since it represents the current best estimate of construction costs for each of the listed plants. In the case of the HIPPS plant, a 15% project contingency is added in addition to a process contingency amounting to 30% of the HITAF. The other plants have a single 10% project contingency. When compared at the total cost without contingency level, the HIPPS plant is 16% less costly than the PC plant and 10% more costly than the PC/GTCC combination. After including contingency, the HIPPS cost is still less than the PC plant but the margin is much less (only 9%).

It is also worth noting that the change in HIPPS cost from Total Plant Cost to Total Plant Investment ($100/kW or 7%) is primarily due to the contingency which would be spent toward the end

of the construction schedule and results in a large portion of the plant cost being subjected to escalation over the full construction. O&M costs given in Table 3.10-2 for the PC and GTCC plants have been estimated by adjusting EPRI TAG costs for these types of plants.

Levelized revenue requirements have been estimated using the EPRI TAG procedures. They are given in Table 3.10-2 for a 10-year investment time frame. The comparison does not change significantly with lengthened time period other than due to escalation/of fuel costs. As discussed earlier (Section 3.7) no real escalation of coal is assumed and natural gas is projected to escalate at a 3% rate.

3.10.5 Comparisons

While the HIPPS plant is clearly less expensive than a PC plant, when the alternative is a PC plant and GTCC plant, the levelized revenue requirements are essentially the same. However, the advantage would still go the HIPPS by virtue of the lower emissions and higher efficiency. Moreover, since emissions from the HIPPS plant are significantly less than for both the PC and the combined PC/GTCC plants, the HIPPS offers a clear advantage in all areas, including cost, if the other plants were upgraded to meet the same emissions.

Also, and most importantly, the preliminary HIPPS commercial design is the first step in a process to develop a HITAF system operating entirely (or nearly so) on coal. If this process is successful, the comparison is strictly between the HIPPS and PC power plants or other coal-fired technologies. The HIPPS and PC comparison reported earlier clearly shows the HIPPS to be more efficient, environmentally cleaner, and economically more attractive than PC units.

3.11 Aero-Derivative Gas Turbine/HITAF Systems

A commercial plant design has been described in the previous sections. This design was based on the use of a heavy frame-type gas turbine similar to a Siemens V84, but using advanced technology. In addition to heavy frame machines, UTRC has investigated the use of aeroderivative gas turbines in conjunction with the HITAF.

An aero-derivative gas turbine is one that is based on components originally developed for aircraft application. These components are generally lighter in weight and higher in performance than heavy frame machines. Over the years, aero-derivative gas turbines such as UTC's FT3, FT4, and FT8 and GE's LM2500 and LM6000 have been successfully applied to peaking (<500 hr/yr) and intermediate duty (1000 − 5000 hr/yr) in both simple and combined-cycle configurations. They have also been used as industrial cogenerators running as baseload (>6500 hr/yr) machines. These engines have displayed reliability's equivalent to heavy frame machines and, usually, greater availability because of the shorter down times required to replace critical components.

Their applications, however, have been limited to some degree by their small outputs, e.g., 25-35 MW per unit. Many applications gang the engines so that multiple engines exhaust into a single HRSG

for combined-cycle plants of 100-200 MW. The advent of the very high thrust (>60,000 lb) aircraft turbines gave promise to larger aero-derivative gas turbines of 40-50 MW. For example, Pratt & Whitney has developed a 60-80,000 lb thrust engine, the PW4000, Figure 3.11-1. This engine has been in commercial service for several years on such aircraft as the Boeing 747, 767, and the new 777 as well as the MD-11 and Airbus. Industrial versions of this engine have been proposed such as that shown in Figure 3.11-2.

3.11.1 Technology Advantages

The engine shown in Figure 3.11-2 has multiple spools, i.e., it has separate high pressure and low pressure sections that operate at speeds close to their optimum. The multiple spool approach has several technology advantages.

Large electric generators turn at 3600 rpm (3000 rpm in 50 cycle applications). This means that the power shaft of the gas turbine must turn at 3600 rpm, unless a costly gear box is used. A single shaft machine then is limited to 3000/3600 rpm, meaning that it must be physically large to pass the air flows necessary for high power, greater than 100 MW, output. Large parts such as turbine blades are more difficult to cool than smaller blades in the higher pressure ratio aero-derivatives resulting in higher cooling penalties. The machines also have a larger footprint.

Pressure ratios for single shaft machines are generally limited to less than 20 because compressor length gets bigger requiring longer shafts and eventually leading to bearing limitations. Also, start up and part load operation of high pressure ratio single shaft machines requires many stages of movable inlet guide vanes (IGV) and of air bypass.

The application of aircraft turbine technology to large-scale utility use can be accomplished in two ways: 1) the introduction of the advanced aerodynamics and turbine cooling techniques to large, heavy frame machines; and 2) the development of advanced power cycles taking direct advantage of the high pressure ratios and high turbine temperatures. The first method is being practiced by most aircraft turbine manufacturers, including UTC, who is supplying State-of-the-Art technology to Siemens for use in their V-series of heavy frame machines. This technology transfer can be relatively slow and may not take full advantage of the advanced technology.

Under normal development conditions, the manufacturers of gas turbines will make only small, incremental advances in turbine technology over the next several years. While these turbines can be used in power systems having efficiencies around 55% (LHV), further advances can be made only by significant cycle and turbine modification. This is because machines appearing in the mid-1990 decade will have essentially reached the plateau of current turbine cooling technology based on extraction air. The attainment of higher efficiencies combined with lower emissions and comparable cost of electricity will require cycle and machinery changes including, among others, intercooling, improved turbine cooling, flow augmentation by steam or water vapor, and combustor and turbine material improvements. These advances are more readily realized in the smaller component sizes and multiple spool arrangements typical of aero-derivative engines.
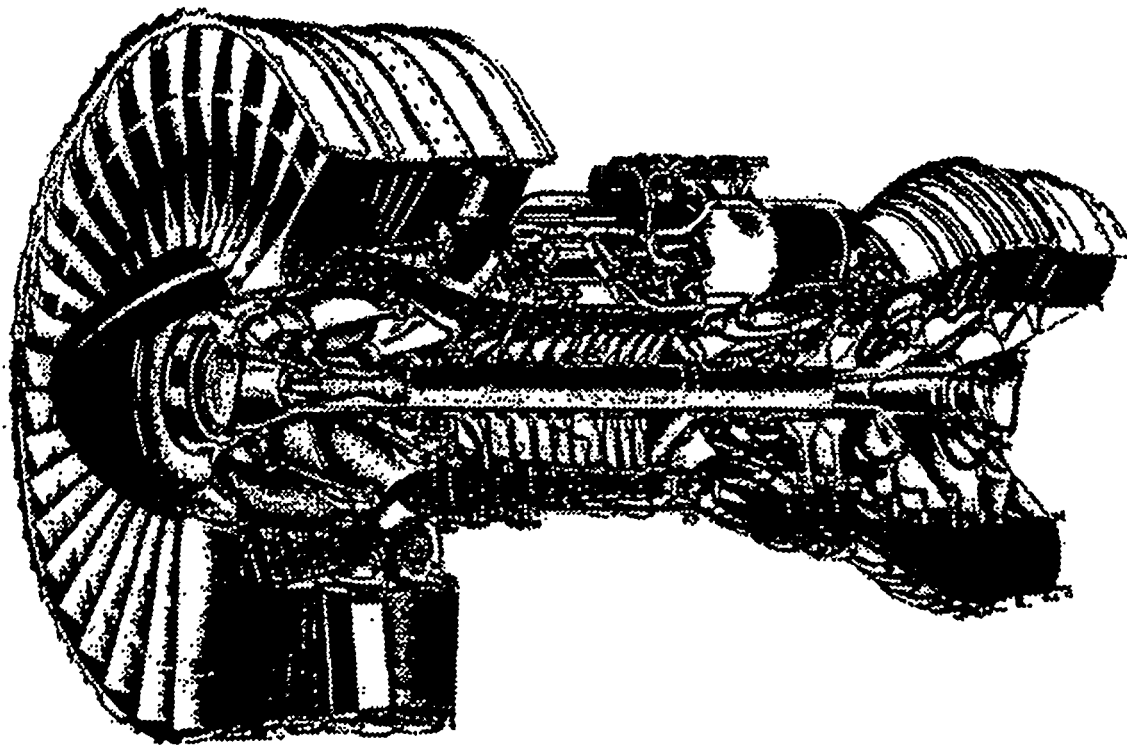
Figure 3.11-1   Cutaway of PW4000.
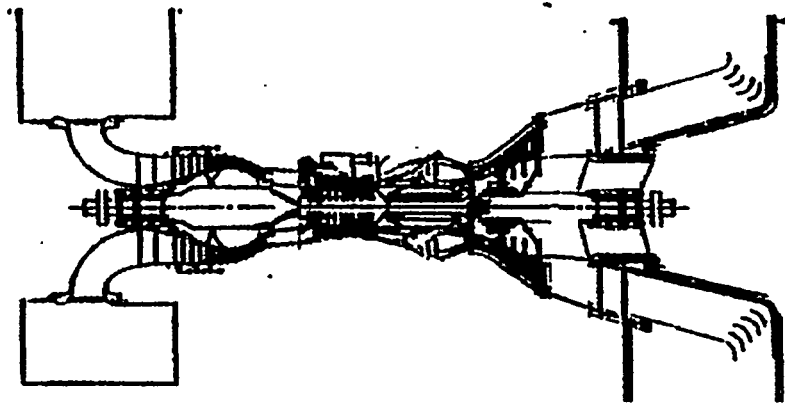
Figure 3.11-2   FT4000 Cross Section.

3.12 Baseline Aero Derivative Commercial Power Plant

A preliminary aero-derivative gas turbine baseline power plant configuration has been identified. This plant is based on the FT4000 IC, an intercooled version of the FT4000 shown in Figure 3.11-2.

3.12.1 FT4000 IC

The simple-cycle FT4000 shown in Figure 3.11-2 has been modified to an intercooled configuration to obtain more power. The high-pressure (HP) spool, which represents the largest development cost of an engine, remains the same. Intercooling allows more power output in two way: first, intercooling reduces compressor work (a cooler gas requires less work to compress it); and, secondly, for a fixed HP spool, the low pressure (LP) spool can pass more air. (The "swallowing" capacity of the HP spool is constant, thus, more lower temperature air can be passed through.)

Engine Performance

The nominal performance of the natural gas-fired version FT4000 IC is given in Table 3.12-1.

Table 3.12-1 FT4000 IC Estimated Performance

(4 in./4 in. Losses, 98% Generator Efficiency)

Generator Output — MW	100+
Efficiency — %	44.9
Combustor Exit Temp. — °F	2500+
Inlet Flow Rate — lb/sec	509
Pressure Ratio	45+
Exhaust Temp. — °F	749

System Definition

The FT4000 IC HIPPS conceptual design (see Figure 3.12-1 for a simplified schematic), developed by the Combustion 2000 Team, is based on advanced gas turbine technology, which could be commercialized by the year 2000. The three major elements of the system are the HITAF, the gas turbine, and the steam turbine. The HITAF supplies 65% of the heat to a duct burner where natural gas boosts the temperature to that required by the turbine. The turbine exhaust stream, along with that from the HITAF, furnishes waste heat to a heat recovery steam generator (HRSG) and steam turbine. The overall efficiency of this system exceeds 48%, approximately 35% better than typical PC plants.

In Figure 3.12-1, it can be seen that the compressor discharge air is sent to a convective air heater in the HITAF. From there, it goes to a radiant heater located in the highest temperature portion of the HITAF, and then to the duct heater where the temperature is raised to the required combustor exit level. The exhaust from the gas turbine is split; one portion is sent to a "clean" HRSG, while the

52

Figure 3.12-1 Combined Cycle HITAF with FT4000.

remainder is used as preheated combustion air for the coal in the HITAF. (Note: The coal used in the conceptual analyses of the heavy frame and the aero-derivative gas turbine HIPPS is a clean and dry Illinois No. 6. It differs somewhat from the EPRI TAG Illinois No. 6 subsequently identified by Bechtel for use in the preliminary commercial plant design. An ultimate analysis is given in Table 3.12-2). The exhaust from the HITAF is sent to a "dirty" HRSG, baghouse, and FGD. To maintain the temperature required for a selective non-catalytic converter in the HITAF, as well as assure that the temperature for the convective section does not exceed 1800°F, a portion of the HITAF exhaust is recirculated.

Table 3.12-2 Ultimate Analysis of Illinois No. 6 Coal Used in Conceptual Studies

Constituent (wt %)	As Received	Cleaned	Cleaned/Dried
Carbon	57.5	61.5	70.5
Hydrogen	3.7	4.2	4.8
Nitrogen	0.9	1.2	1.4
Sulfur	4.0	2.7	3.1
Oxygen	5.8	7.4	9.1
Ash	16.0	9.7	11.0
Water	12.0	12.8	–
HHV (Btu/lb)	10267	11011	12627

The steam bottoming system is atypical of currently installed combined cycles, with higher operating conditions of 2400 psi/1050°F/1050°F.

System Performance

A heat and mass balance for the Figure 3.12-1 configuration is given in Table 3.12-3. Here it is seen that the net power plant output is approximately 212 MW and the estimated overall efficiency is 48.5%.

3.12.2 FT4000 HAT

The advent of the high pressure ratio, FT4000 IC engine allows consideration of an advanced power cycle using a saturator to supply humidified air to the turbine. The Humid Air Turbine (HAT) cycle has been patented by Fluor Daniel, Inc. and has been the subject of a number of joint UTC/Fluor programs in the past several years. These include a TPM/Fluor/Texaco/EPRI study in 1991/92 on integrated coal gasification/HAT and the Cooperative Advanced Gas Turbine study for EPRI and an utility consortium in 1994.

A simplified schematic of a natural-gas fired HAT cycle is shown in Figure 3.12-2. The cycle features a very effective regeneration scheme in which low grade heat from the intercooler, an aftercooler that takes heat from the high compressor discharge, and a turbine exhaust gas exchanger that acts as a regenerator and an economizer. Low-grade heat (<400°F) is used to humidify the compressor discharge resulting in an increase in mass flow through the turbine.

Table 3.12-3 Heat and Mass Balance for Baseline FT4000 Combined Cycle

Point No.	Fluid	Temp - F	Pressure - PSIA	Flow - lb/sec	Comments
1	Air	57	14.7	509.2	
2	Air	710	701	106.2	
3	Air	710	701	403	
4	Air	1300	691	403	
5	Air	1700	680	403	
6	Methane	70	750	6.1	After Heater
7	Air	2700	657	409.1	
8	GT Exhaust	751	15.5	515.2	
9	GT Exhaust	751	15.5	264.5	
10	Coal	138	22	21.4	
11	Air	138	22	37.1	
12	HITAF Ex.	1800	14.2	465.6	
13	Flue Gas	1360	13.9	465.6	
14	Solid Waste			2.1	Sum of Both Streams
15	HITAF Ex.	240	13	465.6	
16	GT Exhaust	751	15.5	250.7	
17	GT Exhaust	180	14	574.3	TO Induced Draft Fan
18	RecycleGas	258	14.7	145.1	Recycle for Quench
19	Coal Fines				Reburn - Inc in 10 (8%)
20	GT Exhaust	751	15.5	49.4	Excess Air (20%)
21	Condensate	91	0.75	157.7	
22	Feedwater	682	3100	143	
23	Sat. Steam	682	2750	141.6	From HITAF Waterwall
24	Steam	1050	2400	141.6	
25	Steam	1050	540	141.6	

Gas Turbine Output - MW	120
Steam Turbine Output - MW	101
System Efficiency - per cent	48.5

Engine Performance

The estimated performance of the natural gas-fired version FT4000 HAT is given in Table 3.12-4.

Table 3.12-4 FT4000 HAT Estimated Performance

(4 in. Inlet Loss, 98% Generator Efficiency)

Generator Output — MW	204
Efficiency — %	58.1
Combustor Exit Temp. — °F	2700
Inlet Flow Rate — lb/sec	509
Pressure Ratio	48.4
Exhaust Temp. — °F	238

55
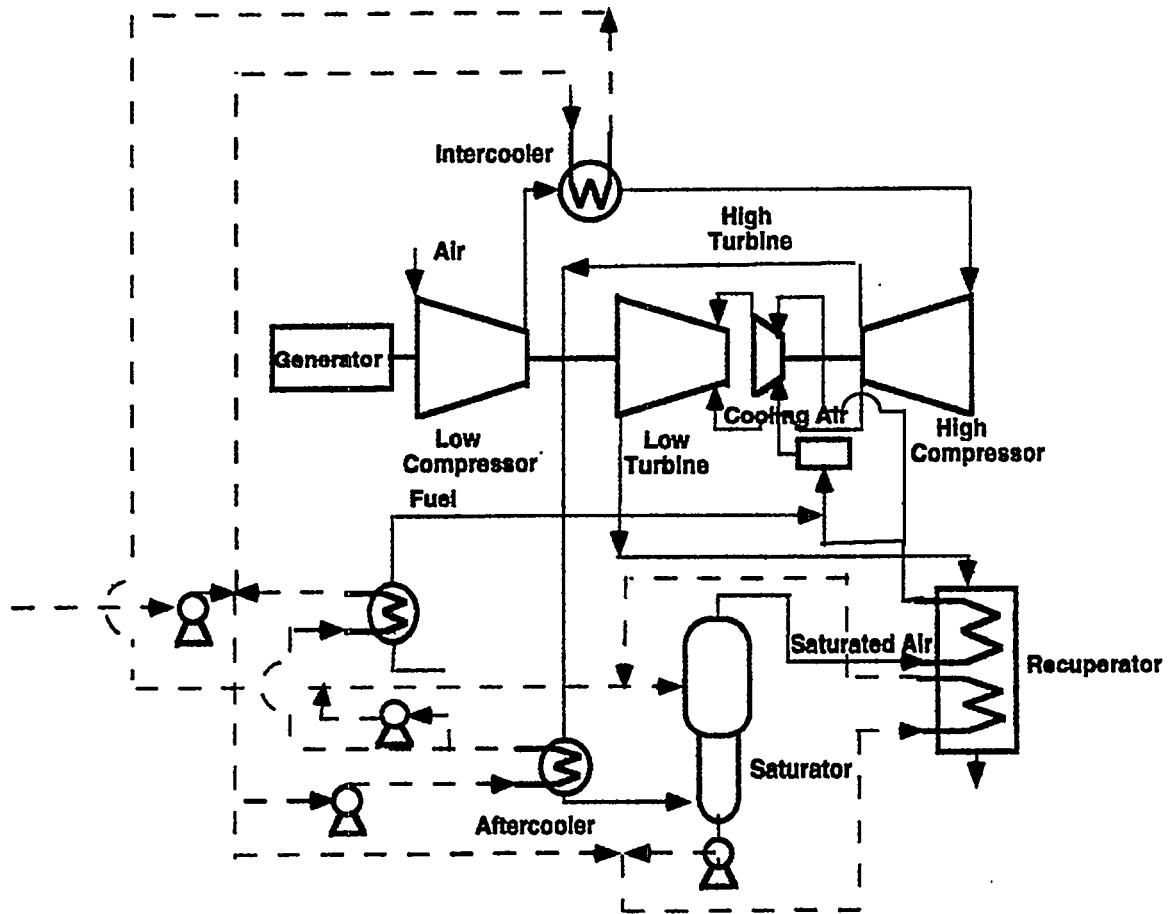
Figure 3.12-2   Natural Gas-Fired HAT Cycle.

System Definition

The adaptation of the HAT cycle to HIPPS required some changes to the engine described in Table 3.12-4. Because of the additional moisture in the gases going to the combustor, more natural gas is required to raise the temperature to the desired combustor exit temperature (2700°F). The DoE ground rule of 65%/35% coal to gas would mean that considerable excess coal would burned; excess in that the high temperature heat from the coal could not be effectively used in the HAT. This excess heat could be recovered as steam for use in a bottoming cycle, but that is counter to the philosophy of the HAT which attains high efficiencies without using steam bottoming. (A HAT /combined-cycle system was also investigated.) Also, to reduce the amount of gas required, the radiator temperature was allowed to reach 1940°F, some 200°F higher than the baseline heavy frame and baseline FT4000 IC cases. The reasoning being that the HAT cycle system would be appearing in the 2005 time frame, allowing the development of heat exchanger material that would permit the 1940°F temperature.

To make up for the power loss resulting from the lower combustor outlet temperature, the flow through the engine was increased. This was done by removing the last several stages of the high compressor and adding new front stages to the low compressor. A schematic of this system is shown in

56

Figure 3.12-3. Note that the compressor discharge air also passes through the HITAF "waterwall" section. The water-cooled walls were replaced by air-cooling to reduce the amount of steam generated in the cycle.

Figure 3.12-3   Coal-Fired HITAF Cycle.

System Performance

A heat and mass balance for the Figure 3.12-3 configuration is given in Table 3.12-5. Here it is seen that the net power plant output is approximately 203 MW and the estimated overall efficiency is 49.5%.

Table 3.12-5 Heat and Mass Balance for Baseline FT-4000 HAT

Point Number	Fluid	Temp. - F	Pressure - PSIA	Flow - lb/sec	Comment
1	Air	59	14.7	826.9	ISO Conditions
2	Air	452	106.8	826.9	
3	Air	85	98.2	625.4	
4	Air	454	590	507	Less Cooling Air
5	Air	263	573	507	
6	Humid Air	352	582	615.5	Saturator Out
7	Humid Air	787	544	615.5	
8	Humid Air	787	544	55	Vane Cooling
9	Humid Air	913	544	560.5	
10	Humid Air	1390	533	560.5	
11	Humid Air	1975	523	560.5	To Combustor
12	Methane	60	375	5.7	
13	Methane	113	523	5.7	
14	Comb. Prod.	2450	500	566.3	Combustor Exit
15	GT Exhaust	806	15.6	739.5	Turbine Exit
16	GT Exhaust	244	14.9	739.5	
17	GT Exhaust	206	14.9	739.5	
18	GT Exhaust	121	14.9	630.3	After Water Recovery
19	Air	59	14.7	201.8	HITAF Comb. Air
20	Air	220	14.7	201.8	
21	Air	958	14.6	201.8	
22	Air	59	22	24.9	Transport Air
	Coal			19.9	Includes Reburn
23	HITAF Exh'st	1033	9.7	392	
24	HITAF Exh'st	1062	16	148	Recirculation
25	HITAF Exh'st	1033	9.7	244.1	
26	HITAF Exh'st	460	9.8	244.1	
27	HITAF Exh'st	225	9.8	244.1	To Fan/FGD

Gas Turbine Output - MW   202.7
System Efficiency - per cent   49.5

57

3.13 Repowering

Repowering is the upgrading of performance, and usually emissions, of older steam plants through the replacement of obsolescent equipment with newer, higher performance equipment. Repowering generally involves the use of a gas turbine used in a variety configurations to supply heat to new or revised fired-steam boilers/heat recovery steam generators. As mentioned previously, the U.S. utility industry has a number of older, generally small (<300 MW) steam plants that are candidates for repowering. Between 80 and 90 Gigawatts of power are candidates for repowering, including more than 50 GW of coal-fired systems. Table 3.13-1 Indicates the potential base for repowering.

Table 3.13-1 Potential Repowering Sites

Size - MW	1-99	100-199	200-299
Units	380	430	175
Av. Age — yr	40	35	30

3.13.1 General Repowering Background

As previously mentioned, there are a variety of repowering options which can be covered by five general categories:

- Substitute HRSG Repowering
- Supplemental HRSG Repowering
- Hot Windbox Repowering
- Feedwater Heating Repowering
- Station Repowering

Each of these will be described briefly, as each has features that could be used in a HIPPS approach to repowering. The following summary descriptions are abstracted from EPRI Report GS-6156, Major Options and Considerations for Repowering With Gas Turbines, Jan. 1989, prepared by Bechtel Group, Inc.

Substitute HRSG Repowering

A new HRSG replaces the existing boiler and supplies steam to the existing steam turbine generator (Figure 3.13-1). A gas turbine exhausts directly into the HRSG and cooled exhaust gases are discharged to the atmosphere. Major new generation equipment includes the gas turbine generator and HRSG. This repowering system has the potential to increase plant output by 160 to 200 percent and plant efficiency by 5 to 30 percent. Environmental emissions are reduced on a per kW basis. Capital costs are typically lower than those for a grass-roots combined-cycle plant. The overall project schedule requires about 34 to 39 months. This is the option that is used most often.

Supplemental HRSG Repowering

A gas turbine exhausts into a new HRSG which produces superheated steam (Figure 3.13-2). This steam is delivered to the existing boiler at existing steam conditions. Cooled exhaust gases are

Figure 3.13-1   HRSG Substitution.

discharged into the windbox of the existing boiler. Major new generation equipment include the gas turbine generator, HRSG, steam air preheater, and stack gas cooler. This option has the potential to increase plant output by 35 to 70 percent and plant efficiency by 5 to 15 percent. Emissions on a per kW basis are lowered. Capital costs on a per kW basis are estimated to be lower than those for substitute HRSG repowering. The overall project schedule requires about 34 to 39 months. Typically, this option presents a high level of technical uncertainty because of the major modifications to the existing boiler.

Hot Windbox Repowering

The gas turbine exhausts go directly into the windbox of the existing boiler (Figure 3.13-3). This option is similar to supplemental HRSG repowering except that there is no HRSG to cool the exhaust gases. Major new generation equipment include the gas turbine generator, stack gas cooler, and steam air heater. It has the potential to increase plant output by 30 to 50 percent and plant efficiency by 5 to 10 percent. Emissions on a per kW basis are lowered. The capital costs and project schedule are the same as those for supplemental HRSG repowering.

Feedwater Heating Repowering

The gas turbine exhausts go directly into a recuperative feedwater heater where all or some of the feedwater for the existing boiler is heated (Figure 3.13-4). Cooled exhaust gases are vented to the atmosphere. The steam plant remains essentially the same except for the relocation of some
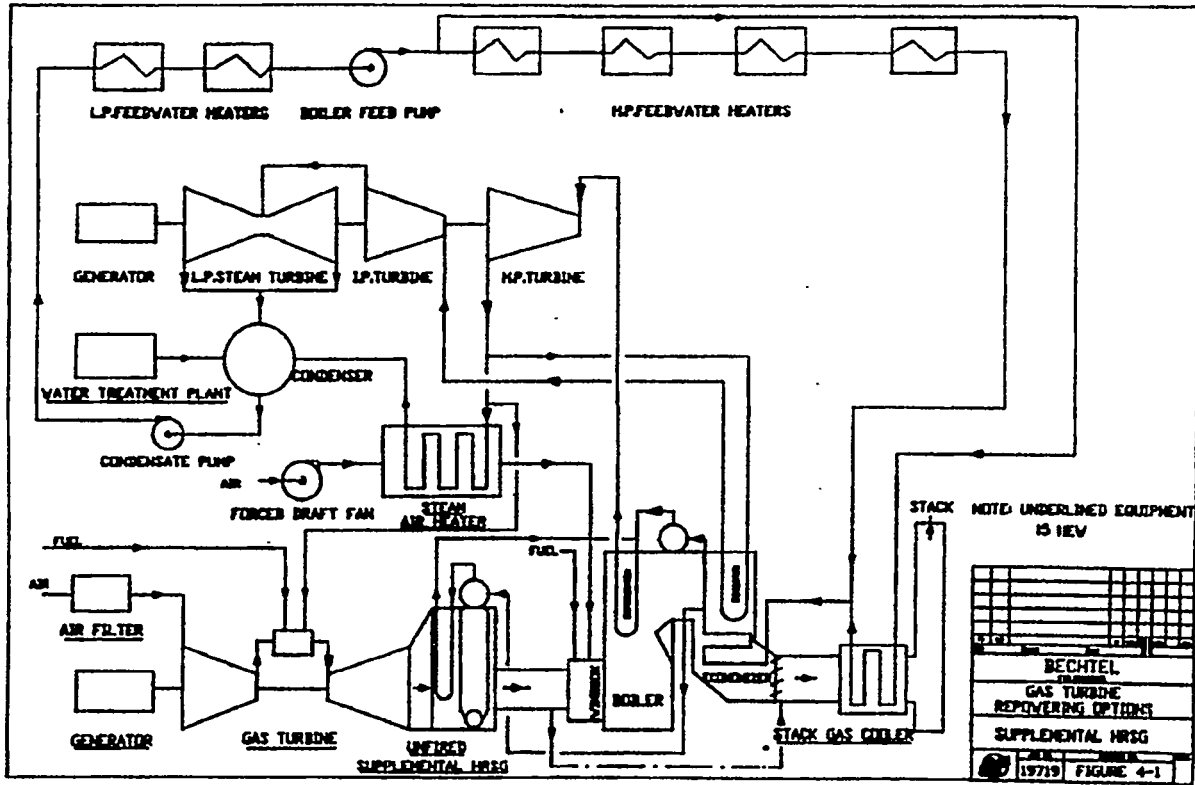
59

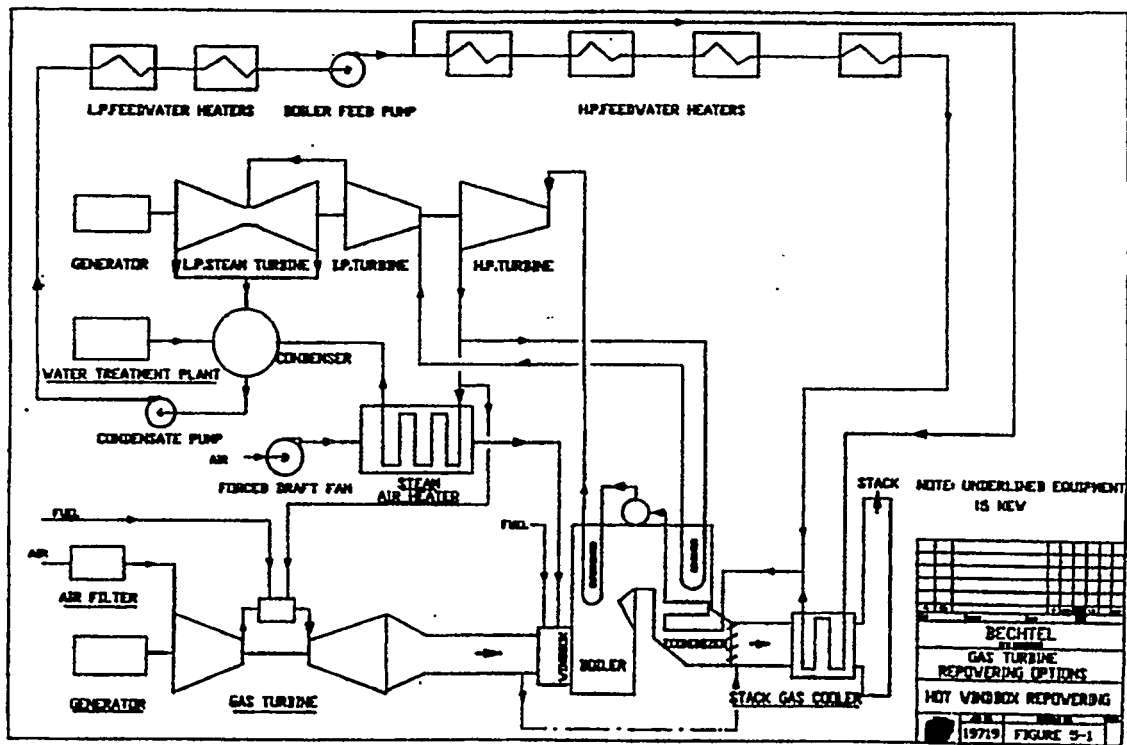Figure 3.13-2   Supplemental HRSG.

Figure 3.13-3   Hot Windbox.

60

feedwater heaters on the discharge side of the boiler feed pumps. Major new generation equipment includes the gas turbine generator and recuperative feedwater heater. This option has the potential to increase plant output by 20 to 30 percent and plant efficiency by 2 to 5 percent. This option may increase total plant emissions. Capital costs are typically low compared to all other repowering options. The typical overall project schedule requires about 30 to 33 months. This option is rarely used because of its low efficiency gain.

Station Repowering

Installation of a gas turbine or a combined-cycle plant at an existing plant site without using any existing power generation equipment is called station repowering (Figure 3.13-5). Its performance is similar to that of substitute HRSG repowering. The station output is limited only by regulatory requirements and utility needs. Since some of the existing plant infrastructure can be retained, the capital cost is typically lower than that for a grass-roots combined-cycle plant. The plant schedule is similar to that for substitute HRSG repowering.

Repowering uses proven generation technology. Its major technical risks are associated with the use of old existing equipment. Therefore, repowering requires a thorough evaluation of existing equipment conditions and performances and an assessment of required repair and refurbishment for this equipment to minimize these risks.

3.13.2 FT4000 IC/Repowering

Repowering of existing steam cycle equipment with aero-derivative engines offers a potential first step toward achieving the HIPPS program goal of replacing natural gas with coal in high-performance power generating systems while using currently available technology. Since there was no site-specific data on repowering, the approach used to make a preliminary assessment of this application was to identify the range of sizes and steam conditions that could be handled by one FT4000 IC (or one FT4000 IC-based HAT engine). This was done by defining the largest size, or "base," repowering system, the one that used all the GT exhaust as combustion air. The exhaust was then bypassed around the boiler to HRSG's that actually were used to heat feedwater. In this manner, smaller boilers were identified; the range of sizes that one engine could handle varied from less than 90 MW to over 220 MW.

The FT4000 IC is a high pressure ratio, intercooled gas turbine having a high simple cycle efficiency (>41% HHV) and is well suited to provide preheated air to a coal fired boiler as shown schematically in Figure 3.13-6. The key part of the system, shown in Figure 3.13-6 is the gas turbine combustion air (HPC discharge air) convective preheater which makes it possible to utilize a portion of the coal heat in the gas turbine cycle. This preheater, in effect, takes the place of a regenerative heat exchanger that would be used with a conventional regenerative gas turbine cycle. In the case of the FT4000 IC, the high pressure ratio design does not produce an exhaust temperature high enough to make the use of a regenerator attractive (except for the Humid Air Turbine (HAT) cycle). The exhaust
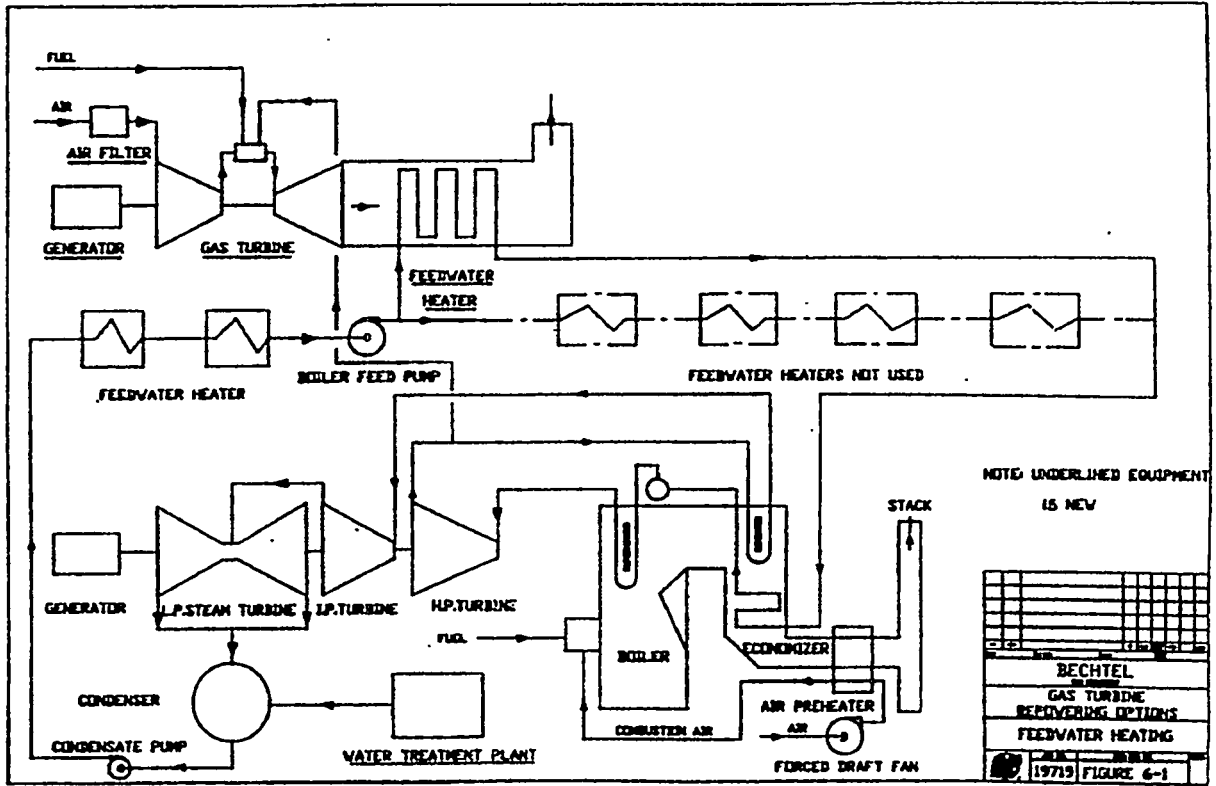
61

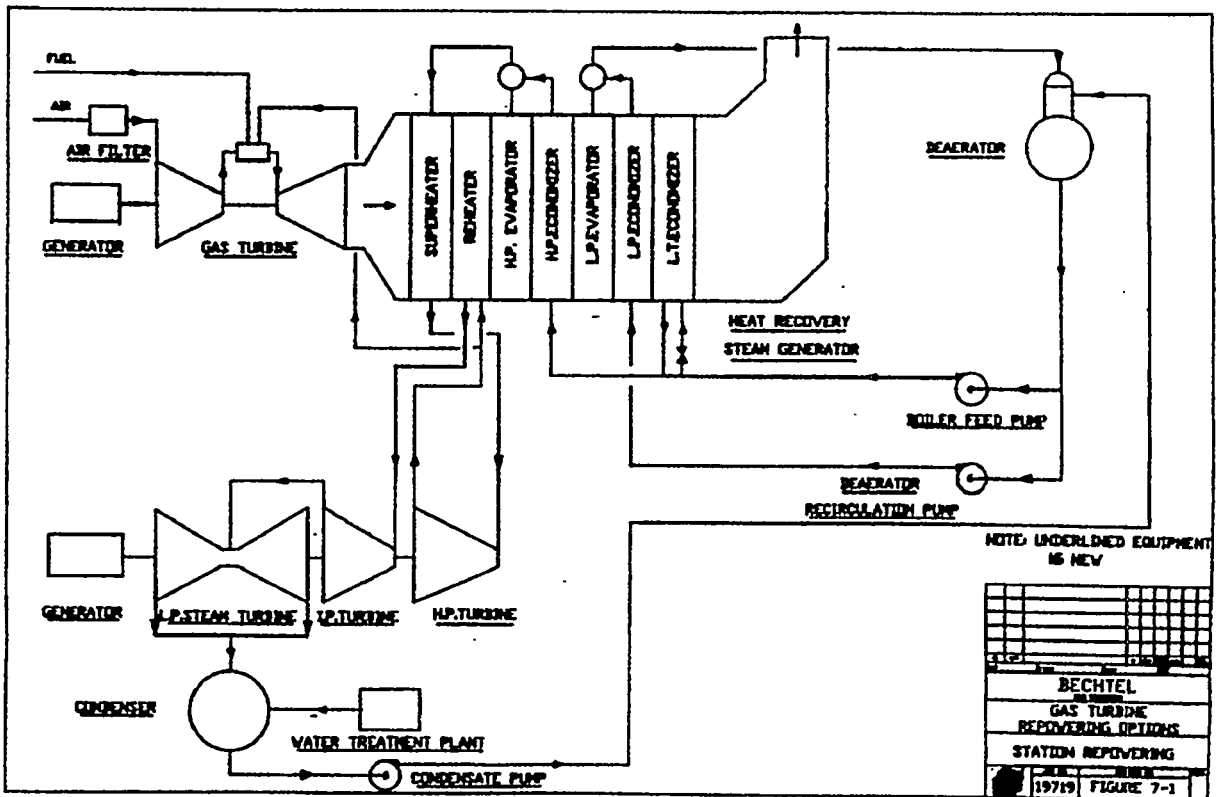Figure 3.13-4   Feedwater Heating.

Figure 3.13-5   Station Repowering.

temperature of approximately 740°F, however, makes it ideal as the combustion air for a coal fired boiler.

In Figure 3.13-6, it can be seen that the boiler is assumed to be of conventional design in regard to steam generation, superheat and reheat provisions. The absence of a regenerative air preheater allows the exhaust to be used for feedwater heating and eliminates the need for extraction heaters. The gas turbine combustion air heater (referred to as the convective heat exchanger in the HITAF system) has a design HITAF exhaust stream inlet temperature of 1800°F. This temperature was selected for the HITAF system since it is ideal for non-catalytic NO_x reduction and would permit reasonable operating times between removal of deposits to avoid densification. This convective heat exchanger would be a prototype for the HITAF system.

To make this concept applicable to existing steam equipment a flow diverter is included, allowing a portion of the gas turbine exhaust to bypass the furnace. That bypass gas is sent to a HRSG, where its heat content is used to heat feedwater for the steam cycle. Figure 3.13-7 shows the range of steam cycles that can be accommodated by varying the amount of exhaust gas sent to the HRSG. The values considered are intended to cover the range of probable steam conditions that would be encountered in a repowering operation. They range from a relatively high-performance 2400 psi/1050°F/1050°F reheat cycle to a 1250 psi non-reheat cycle. The corresponding efficiencies for each cycle are given in Figure 3.13-8 as a function of the fraction of exhaust gas sent to the HRSG. The output for each system includes the gas turbine contribution, which is constant at 108.9 MW for the cases presented. Note that the gas turbine output is slightly less than that reported elsewhere for simple cycle operation due to the lower amount of gas required in the burner and, thus, reduced turbine mass flow rate. At the baseline convective air preheat outlet temperature of 1300°F, the heat required to achieve the 2700°F firing temperature is reduced by approximately 25%. This forms the basis for the desirability of the cycle which is the reduction of natural gas consumption and its replacement by coal utilization.

As the fraction of exhaust gas sent to the HRSG is increased, the system would be expected to approach a normal combined cycle in appearance. This occurs because the fraction of turbine exhaust for boiler combustion air decreases resulting in a decrease of steam cycle output approaching levels that would be expected in combined cycle. However, the low (about 750°F) gas turbine exhaust temperatures will not support the steam temperature levels used here. Thus, there is a practical limit to the bypass fraction both from a thermodynamic as well as steam turbine size standpoint.

In the above analysis, excess air in the coal fired boiler was fixed at 20%. Also fixed was the ratio of 2:1 between transport air (ambient air) and coal. Therefore, the portion of the total heat input provided by methane or natural gas is a direct function of the split in the exhaust between the furnace and the HRSG. This relation is shown in Figure 3.13-9 for three different combustion air preheat temperatures. The effect of the increased air preheat is discussed later.

The noticeable change in slope of the curves at 20% exhaust flow to the HRSG results from an excess of low temperature heat as that flow is increased further. The slope change is more noticeable in

Condensate Feedwater → ▶ To Feedheaters

I/C

System Performance:
Total Net Power   315 MW
System Efficiency   43.5 % (HHV)

Gas Turbine

HPC   HPT   LPT   LPC

AIR

COAL Q = 501,350 Btu/sec

——— Air/Exhaust
– – – Water/Steam

Burner

TRANSPORT AIR

NAT. GAS
Q = 184,700 Btu/sec

Combustor

HP Evap

Steam Turbine

Superheater

Reheater

Convective Heater

To Condenser

From Intercooler Heater

Reheater

Feedheater

HITAF Stack

Figure 3.13-6   Repowering Configuration FT4000 IC.

⊖ 2400 PSI / 1050F / 1050F   ◇ 1800 PSI / 1000F / 1000F
△ 1450 PSI / 950F / 950F   ⊟ 1250 PSI / 950F

GT OUTPUT = 108.9 MW (CONSTANT)
G.T. AIR HEATER EXIT TEMP = 1300 F

STEAM POWER - MW

% GT EXHAUST TO HRSG
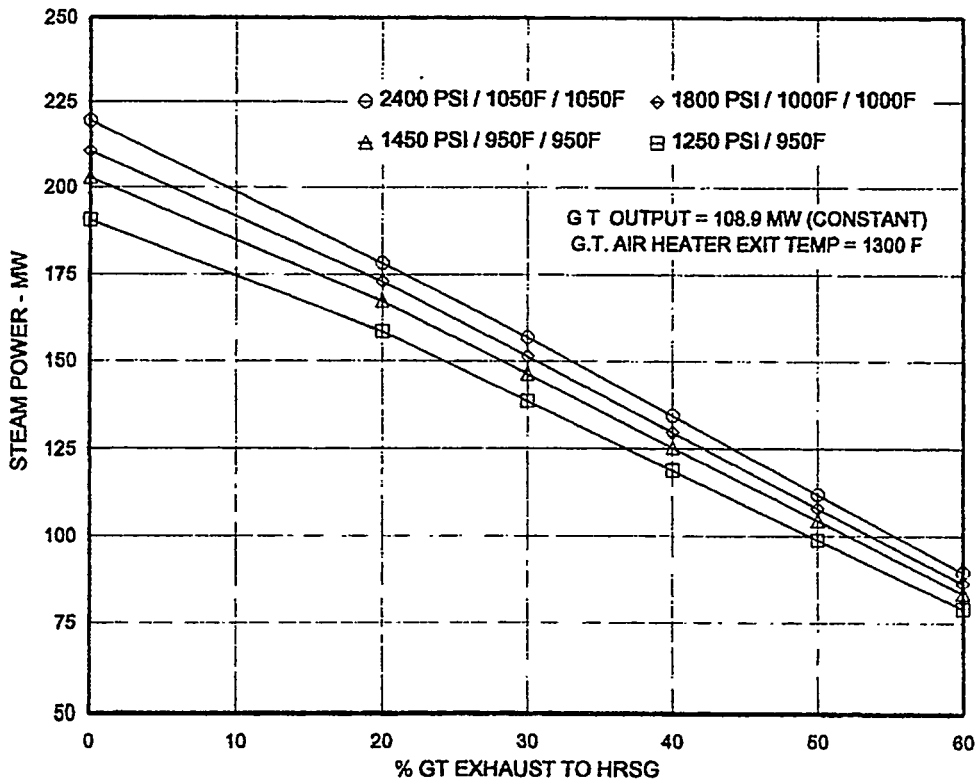
Figure 3.13-7   Steam Cycle Output.

64
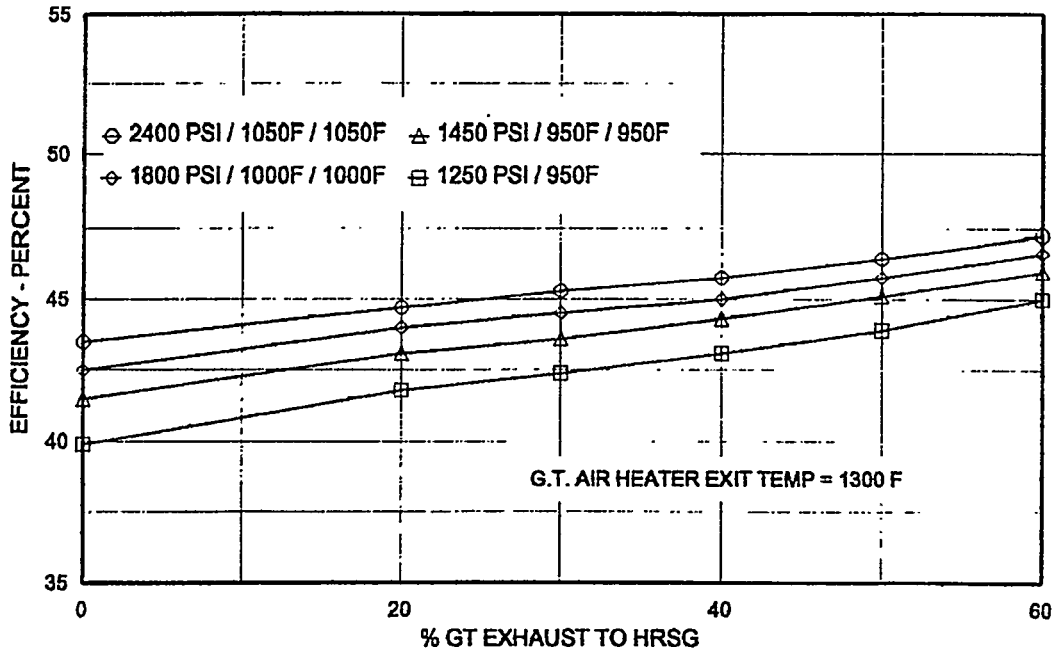
Figure 3.13-8   Overall Cycle Efficiency.
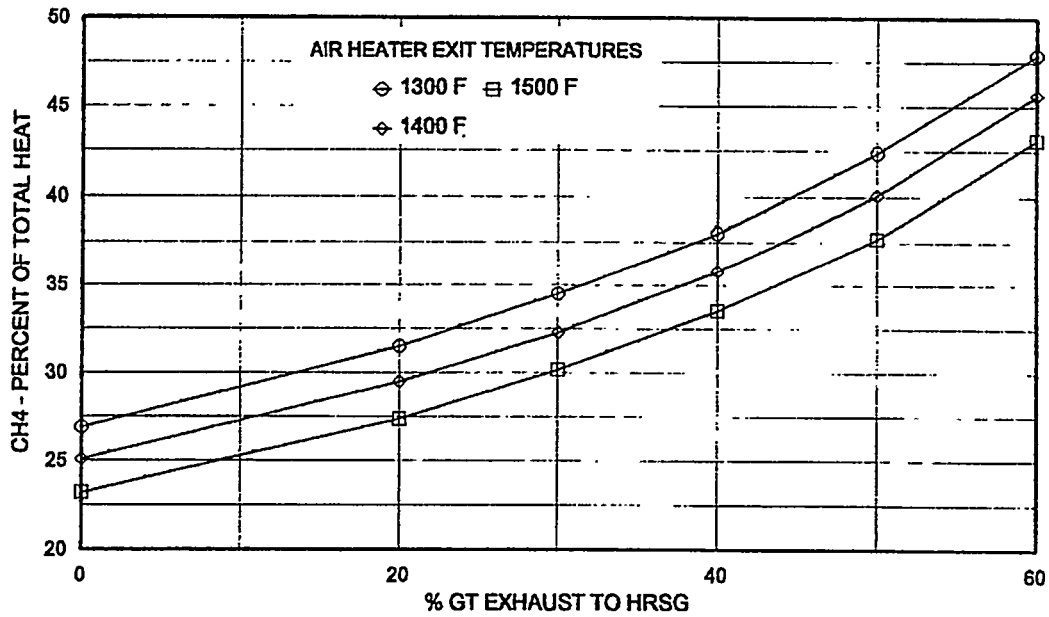
Figure 3.13-9   Methane Requirements.

65

Figure 3.13-10, discussed below, and is caused by limiting the amount of heat recovered from the gas turbine intercooler to the amount needed to heat the steam feedwater to 225°F. The remainder of the heat in that stream is sent to the cooling tower. This allows a stack temperature of 240°F to be achieved in both exhaust streams. This analytic approach is typical and indicative of the level of detail that has been used in this study.
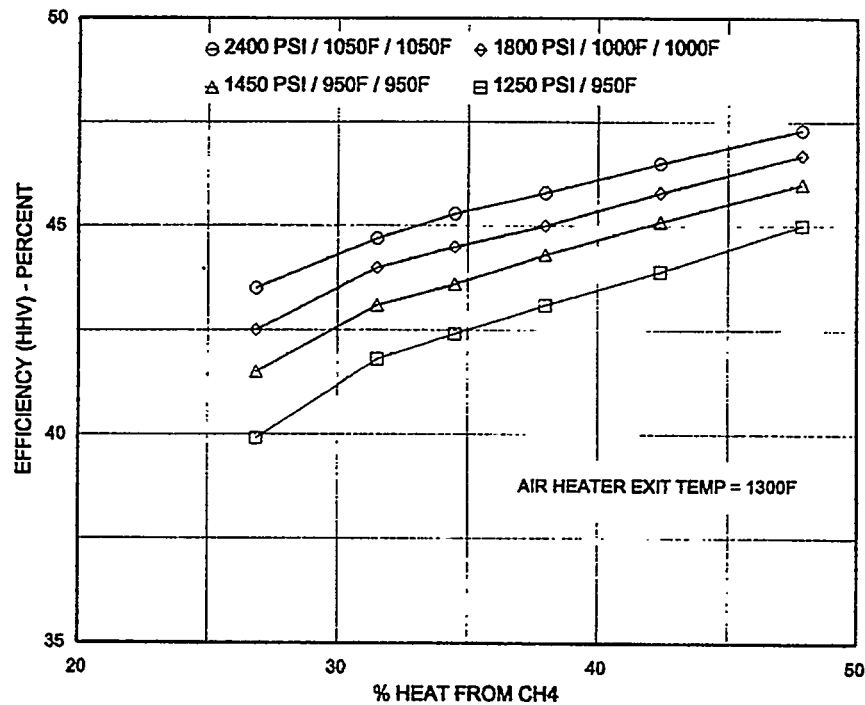
Figure 3.13-10 Efficiency as a Function of Methane Fraction.

The primary results indicate that as the fraction of gas turbine exhaust bypassing the boiler is increased, steam power decreases, efficiency increases and so does the fraction of heat from methane. Since the goals of the HIPPS program are stated in terms of efficiency and percent methane, a plot of efficiency as a function of percent methane for the various steam cycles is shown in Figure 3.13-10. That figure shows the obvious advantages to repowering with a high performance steam cycle. It also shows that with such a steam cycle an efficiency in excess of 45% (HHV) is possible and that 47% efficiency can be achieved with 40% of the heat coming from methane. The obvious break in the curves of Figure 3.13-10 is due to the need to change the arrangement of the heat recovery system as steam and, thus, feedwater flow is decreased. At relatively high steam flow rates (less than 20% flow to the HRSG) heat from the gas turbine intercooler can be used to preheat the feedwater prior to entering the economizer while achieving a 240°F stack temperature. At lower steam rates, all of that heat cannot be utilized and performance suffers. It is anticipated that in a specific case some use would be found or the excess heat would be sent overboard.

66

In the baseline HITAF cycle, air from the convective heat exchanger is heated further in the radiant section of the furnace. This additional air preheat allows us to reach the performance goal while burning only 35% methane. For the repowering configuration, increasing the duty of the convective heat exchanger was investigated. For the 2400 psi/1050°F/1050°F steam cycle the effect of increased air heater exit temperature on steam cycle output is shown in Figure 3.13-11. At full flow to the boiler (no flow to the HRSG), there is virtually no change in steam cycle output as air preheat temperature is increased. This is the result of an increase in oxygen content of the gas turbine exhaust which allows more coal to be burned making up for the increased duty of the convective exchanger. As gas turbine exhaust flow to the HRSG is increased, the heat required by the convective exchanger becomes a more significant part of the total and steam power drops off somewhat with increased air preheat temperature. It should be noted that there is a slight reduction in gas turbine output as the combustion air preheat temperature is increased. For the 1300°F, 1400°F and 1500°F conditions, the corresponding gas turbine output levels are 108.9 MW, 108.2 MW and 107.4 MW, respectively.

Overall efficiency for the system with the 2400 psi/1050°F/1050°F steam cycle is virtually unchanged with increased combustion air preheat. However, as was shown in Figure 3.13-9, preheat temperature has a marked effect on the fraction of methane used in the system. The resultant effect on efficiency as a function of the fraction of heat from methane is shown in Figure 3.13-12. There it shows that with an air preheat temperature of 1500°F, an efficiency of 47% can be achieved at a methane use rate of 35%.

3.14 FT4000 HAT

In principle, repowering with the Humid Air Turbine (HAT) cycle is much the same as with the basic simple cycle FT4000. The system is shown schematically in Figure 3.14-1. Performance at the base point (no GT exhaust bypass) with a 2400 psi/1050°F/1050°F steam cycle is significantly better than for the simple cycle version; 45.9% as compared to 43.5% for the simple cycle. The improvement comes at the expense of a higher methane use fraction. The ratio of methane heat to total heat at the base point is 0.369.

The effect of bypassing a portion of the gas turbine around the coal boiler for use as feedwater heating follows the same trend as the simple cycle with the curves being essentially parallel. This is shown in Figure 3.14-2.

As with the simple cycle repowering, gas turbine exhaust air is used as preheated combustion air in a coal fired boiler. Because the exhaust gas contains a significant amount of water vapor, boiler combustion temperature is reduced both by the effect of less oxygen as a result of combustion in the gas turbine and the added water vapor. Since the resultant combustion process differs from that of conventional boilers, it will be necessary to examine the system to determine what problems will be encountered in achieving a stable flame.

The primary variables that affect flame temperature are degree of saturation as measured by saturator exit temperature, preheat of gas turbine burner inlet air, excess air in the coal furnace and
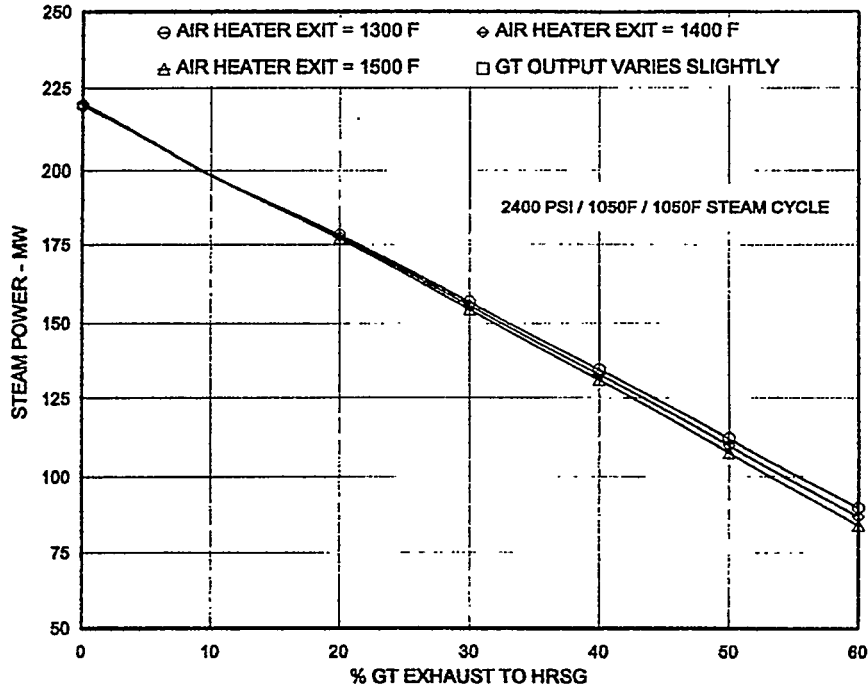
Figure 3.13-11 Effect of Air Heater Temperature.
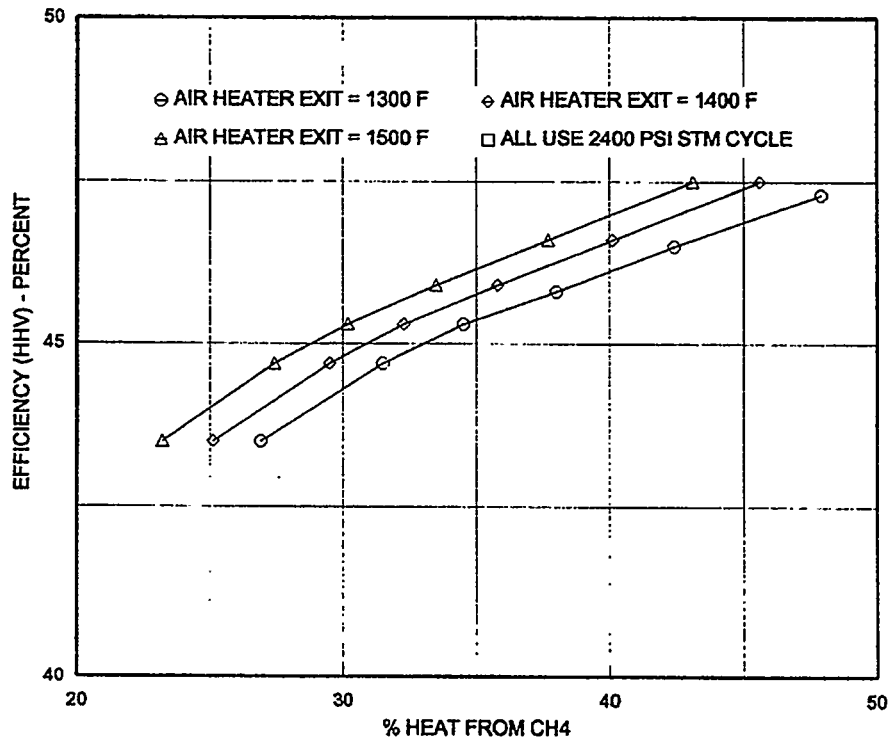
Figure 3.13-12 Efficiency as a Function of Methane Fraction.

amount of coal transport air. For this study, an excess air level of 20% was assumed and a transport air to coal ratio of 2:1 was used. Adiabatic flame temperatures in the range of 2500 to 2700°F were calculated using dry Illinois No. 6 coal. The effect of these levels on the combustion process has yet to

68
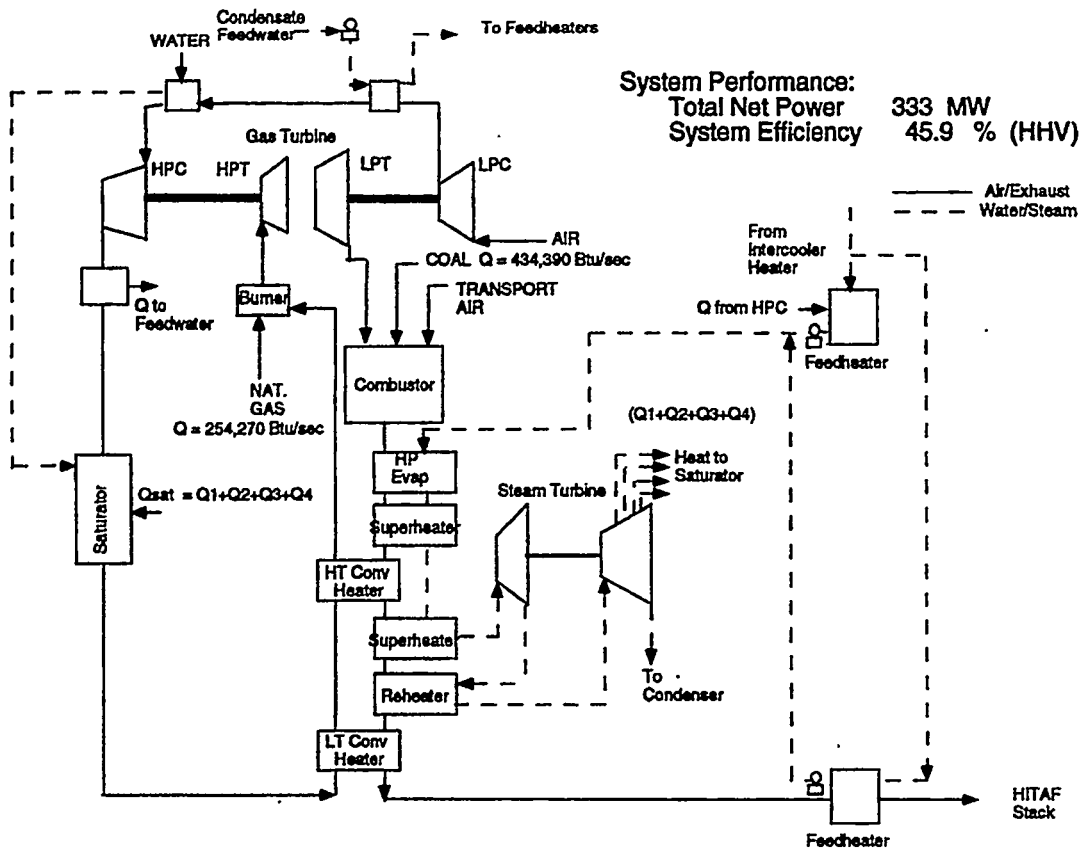
Figure 3.14-1   Schematic of HAT Repowering.
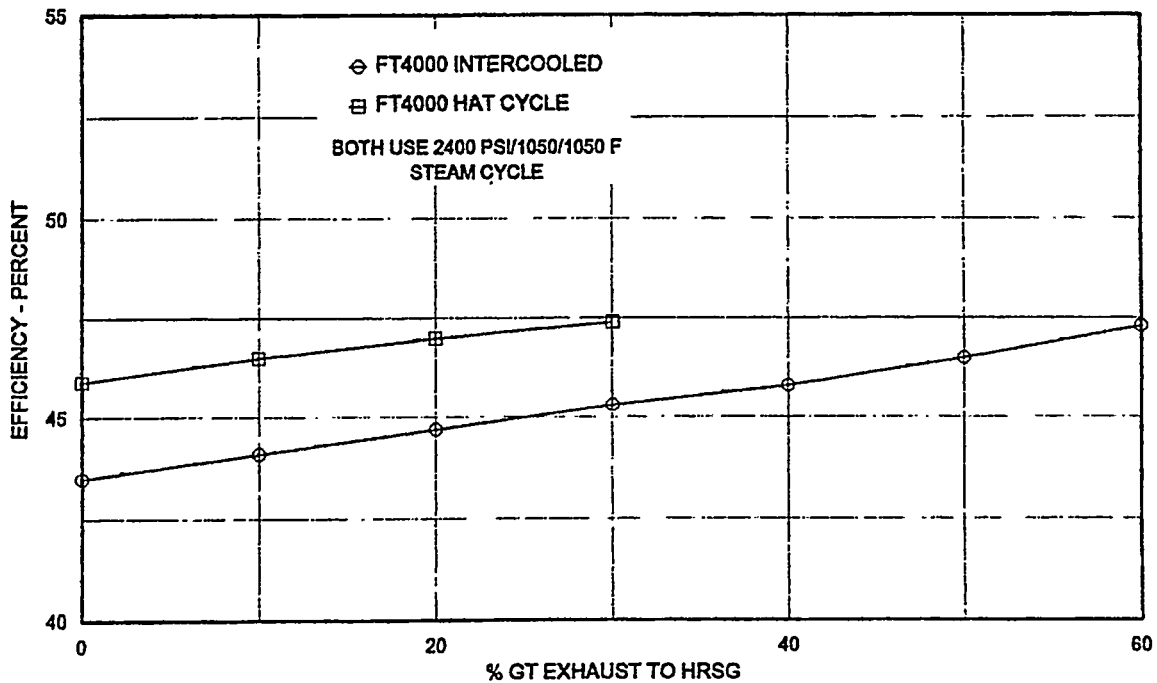
Figure 3.14-2   Effect of Air Bypass for Feed Water Heating.

69

be investigated, but various means of raising flame temperature and hopefully improving performance have been considered and are discussed later.

The other major difference in using the HAT configuration is the need to cool down the high pressure compressor exhaust and to subsequently add water vapor in the saturator. This cooling is necessary since the HP air would be cooled in passing through the saturator and the sensible heat in that stream would be utilized at a greatly reduced temperature. As shown, that heat is used in the steam cycle economizer. The reduced HP air temperature and increased mass flow rate result in a significant increase in the duty of the HP air convective heat exchanger. In order to maximize temperature differences in the various heat exchangers (and reduce cost) it will likely be necessary to make the convective exchanger in two sections as shown in the schematic.

Heat for the saturation process is provided by bleeds from the steam turbine. This is in marked difference to the conventional combined cycle, where there is an overabundance of low temperature heat. Other arrangements of the bleeds may be found desirable for a particular application, but this provided the simplest schematic arrangement for this study. It should be noted that the integration of the HAT, HITAF and steam bottoming cycles has the additional benefit of eliminating the need for the air-to-air regenerative heat exchanger, which is usually quite large to maintain efficiency. Here the reheating of the HP air stream can be done with relatively large temperature differentials. The low temperature exhaust heat can be recovered by the steam cycle feedwater, which results in a much smaller heat exchanger.

A number of other things concerning the system are worth noting. The large amount of heat required to reheat the compressor discharge after being saturated reduces the high temperature heat available for the steam cycle. Also, the water vapor in the air requires more methane to be burned to achieve the desired turbine inlet temperature, further depleting oxygen. As a result, less coal can be burned at the base condition when all of the exhaust is sent to the boiler. At the zero bypass condition, the fraction of total heat provided by methane is approximately 37% as compared to 27% for the FT4000 IC/HITAF cycle. The HAT cycle shows a less marked advantage when compared to the intercooled cycle in terms of efficiency versus methane fraction as is shown in Figure 3.14-3. The HAT cycle system experiences an excess of low temperature heat as the amount of gas turbine exhaust bypassed around the boiler exceeds approximately 26%.

The results of parametric variations and alternative schematic arrangements are worth noting. Raising the temperature of the high pressure air out of the convective heat exchanger has little effect on performance, but does reduce the methane ratio. That ratio becomes 0.35 at 1350°F and 0.338 at 1400°F out of the heat exchanger. Also noted was that some of the uses of low temperature heat, such as for pre-heating the methane, do not appear to be beneficial in this cycle.

A number of methods of raising the coal flame temperature have been considered, but have not as yet been fully investigated. There are three primary factors that affect flame temperature. The first, temperature of the combustion air has a direct effect and could be improved to a limited extent by
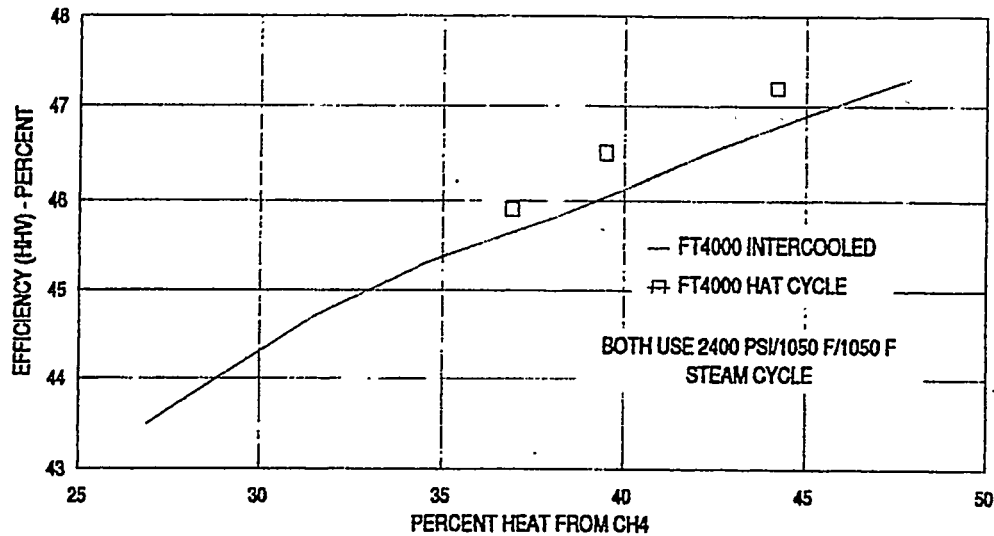
Figure 3.14-3   Comparison of HAT and FT4000 IC Cycles.

further pre-heating. The others, oxygen partial pressure and water vapor content, are closely related and are affected by other parameters such as high-pressure air preheat, saturator exit temperature, and gas turbine firing temperature. The latter is fixed for the purposes of this study, but the others have been investigated.

An increase in air pre-heat temperature of 100°F produces an increase of approximately 50°F in flame temperature due to reduced methane combustion. This is desirable since it also decreases the methane ratio while performance remains unchanged. Reduction of the saturator exit temperature has a similar effect, resulting in less methane being burned. A 10°F reduction in saturation temperature produces an 80°F increase in combustion temperature while reducing efficiency by 0.15 percentage points.

Other approaches also have been considered. In particular, cooling of the exhaust against a non-vitiated combustion air stream could provide a greater degree of flexibility to accommodate a larger range of steam cycles while improving system performance. As a rough estimate, the gas turbine exhaust contains 10% oxygen by volume. Using one half of that stream to pre-heat combustion air would permit the same amount of coal to be burned and should result in a reduced stack loss, higher availability due to increased firing temperature, and permit the other half of the stream to provide low-temperature heat.

To fully evaluate the HAT cycle, several additional things need to be done: simulation of a water loop; and revisiting the simulation of the mass transfer saturator. It appears that there are some aspects of that system that are sufficiently different from the typical combined cycle to leave room for further improvement. In both the simple and HAT cycles it appears that the use of bleed steam for feed heating could improve performance at the base case. These things are at the next level of detail that will be included in Phase II analyses.

71

3.15 Preliminary Economics for Repowering

A high-level preliminary analysis was carries out to identify the relative economics of HITAF repowering. The FT4000 IC/HITAF and the HAT/HITAF were compared to the two most likely alternative repowering schemes; aero-derivative (nominal 110 MW) and heavy frame (nominal 185 MW) machines used in the HRSG substitution mode (Figure 3.15-1). Performance and costs for the equipment were obtained from several yet unreleased reports by Fluor Daniel and from Bechtel reports. The costs were escalated to same year costs (1994). It was assumed that the plant infrastructure and steam turbine/generator and water systems were unchanged in all cases. The plant to be repowered was a 1800 psi/950°F/950°F, 200 MW system, a size that could be repowered by a FT4000 IC using turbine exhaust as the coal-fired boiler combustion air.
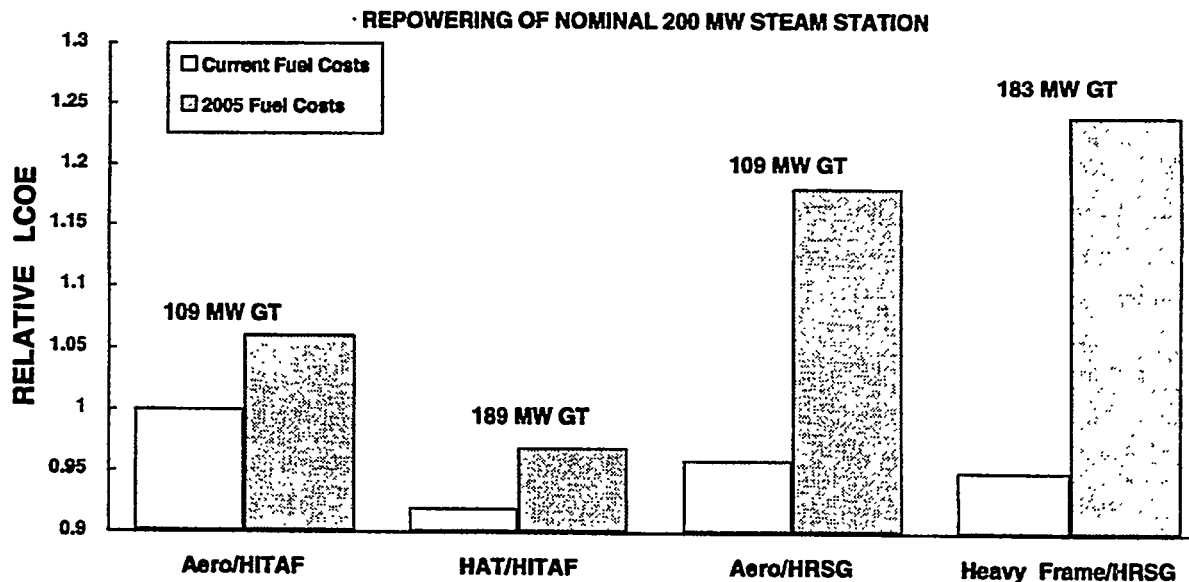
Figure 3.15-1   Comparison of LCOE.

Both the aero-derivative and the heavy frame machine required supplemental firing (gas) to generate enough steam for a 200 MW plant. Costs for gas were assumed to be roughly those used in the 1993 EPRI TAG®, i.e., current cost for gas was twice that for coal and the 10-year future cost was four times.

The cost of electricity was determined using the 10-year levelizing factors in the EPRI TAG®. The levelized cost of electricity (LCOE) for the FT4000 IC was used to normalize all the costs. (The LCOE for the aero/HITAF using current fuel prices was unity.) The results are shown in Fig. 3.15-1. At current and projected fuel prices, the HAT/HITAF has the lowest LCOE. This is because of it's projected lower capital and operating costs. As would be anticipated at current fuel prices, both the aero/HRSG and the heavy frame/HRSG are projected to have lower LCOE's. This is mostly due to their lower capital costs. Their higher efficiencies are obtained on a more costly gas fuel, and as the

gas/coal cost ratio increases in future years, their higher operating costs make them less attractive versus the HITAF configurations.

Because of the higher efficiencies possible with the FT4000 IC with bypass flow to HRSG's (feedwater heating), LCOE's for this configuration were developed and are shown in Figure 3.15-2. The savings due to higher efficiencies were offset to some extent by the increased cost ($/kW) of the smaller boiler and the cost of the HRSG/FW heater. Nonetheless, a 5% lower LCOE could be realized in the maximum bypass case.
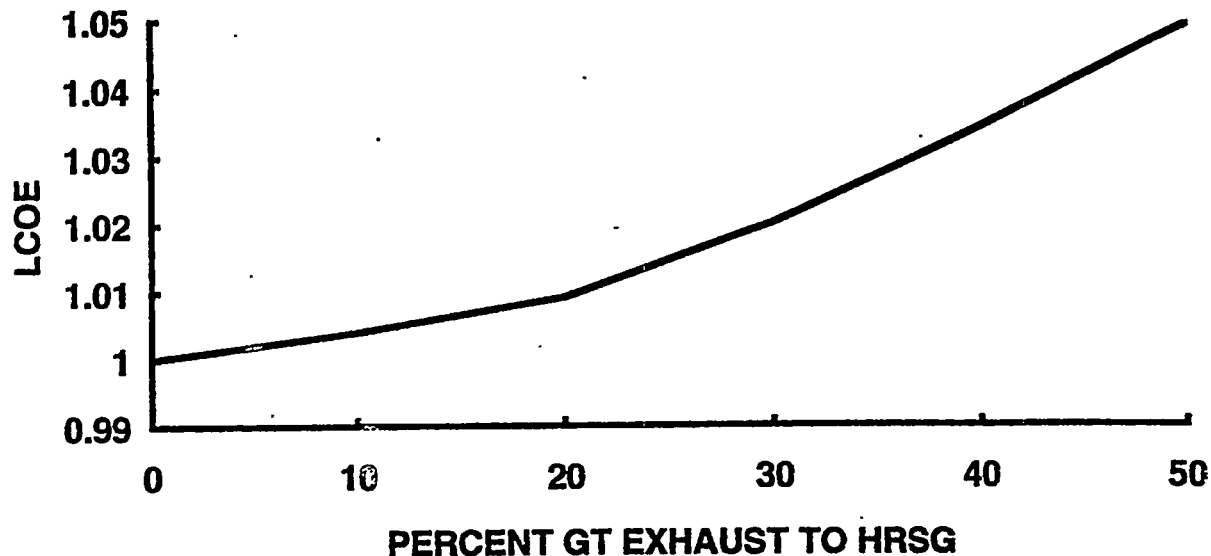
Figure 3.15-2   LCOE for FT4000 with Feed Water Heating.

3.16 Concluding Remarks on Power Systems

The use of the aero-derivative engine with the HITAF offers higher efficiencies and potentially lower capital costs, in HAT configuration, than realizable with heavy frame machines. The technology advancements in materials and cooling techniques developed for aircraft engines shows up more quickly, giving the aero-derivative engine even more of a potential advantage in the future.

When used in repowering, these engines could add as much as 10 or 12 points (around 30-35%) to the efficiencies of older steam stations. The repowering configurations do not have to use the radiative heat exchangers, somewhat simplifying the HITAF, and should result in systems having lower overall cost of electricity than current repowering alternatives. These advantages are realizable with coal providing 60-70% of the cycle input heat requirement.

4.0 COMPONENT TECHNOLOGY

While the UTRC Combustion 2000 Team's overall design is innovative compared to existing PC boiler plants, this innovative design does not equate with high risks. Many of the distinctive features of the scheme have been demonstrated in practical systems or are straightforward extensions of proven systems. For example:

- The HITAF operates at higher wall temperatures than a normal steam boiler furnace but downfired slagging wall furnaces are in commercial operation.

- One of the prime candidates for the HITAF refractory coating is fused cast alumina similar to the practice in glass melting furnaces.

- The fuel-flexible duct heater is a variant of the Pratt & Whitney Vorbix combustor, which has undergone extensive testing under two major NASA programs.

- The major high temperature structural material will be a superalloy that is manufacturable and weldable with a long projected lifetime at the conditions of our initial design.

These engineering choices have been made with a goal of achieving 47% thermal efficiency with materials that will be available and tested by the year 2000. This approach precludes the use of structural ceramics at the high temperatures of our radiant air heater because there are no reliable sealing and joining techniques that can accommodate the thermal expansion without excessive leakage. The design, however, does accommodate a growth to all coal at a time when advances in materials technology allow for a manufacturable and sealable ceramic heat exchanger that can operate at 2500°F and high pressure. The air heater must also be able to heat air from the compressor discharge temperature to the turbine inlet temperature without clogging up with ash. In other words, the system must manage the wet/dry interface to control ash buildup.

In this lower risk approach, the air heater is separated into a low temperature convective unit (750-1300°F) and a high temperature radiant unit (1300-1700°F) for our baseline case. For the all-coal case, the convective air heater would range from 750°F to 1500°F and the radiant air heater from 1500°F to 2500°F. The refractory wall temperature of the radiant section is always kept above the T_{250} value for the coal ash and is therefore completely slagging. Between the two sections of the divided air heater are the slag screen and flue gas recirculation (FGR) sections where the HITAF exhaust gas temperature is lowered from around 2800°F to about 1800°F. Thus, the ash particles entering the convective air heater are all at temperatures designated as "dry." A single air heater designed to operate from wet ash to dry ash, with the ash solidus temperature somewhere in the middle, is a recipe for disaster.

4.1 HITAF Combustor

The major components to be considered in the design of the HITAF combustor are: 1) the firing system; 2) the radiant furnace; 3) the slag screen; 4) the dilution zone, and 5) the SNCR zone. Since neither the material nor the method of construction are proven for the radiant air heater panels, an exact configuration for the HITAF is not possible at present. The initial design studies were carried out assuming that the radiant heater would be constructed of ceramic panels coated with refractory. It was later determined that the performance goals could be achieved using alloy panels, thus reducing the complexity of construction. Figure 4.1-1 shows the general characteristics of the current HITAF configuration, a "U" design with a down fired chamber followed by a horizontal dilution section. The SNCR zone and the convective air heater are in the upward length. Several alternative configurations were evaluated, but this configuration was selected because:

- Heat exchanger considerations require that the radiant heater be operated under flowing slag conditions. Not only is the thermal resistance of dry ash high, but it is not possible to design an all coal HIPPS without a slagging radiant chamber. If the system is slagging, then down fired is a reasonable compromise. Gravity helps slag flow but the pulverized coal must be transported to a relatively high elevation;

- The "U" design allows the exit from the convective air heater and the entrance to the radiant air heater to be positioned at the same elevation, and in close proximity. In addition and very importantly, the hot gas ductwork from the exit of the air heater to the gas turbine can be minimized;

- The design of the slag screen can be optimized for particle collection and as a reflector to maintain the temperatures at the slag tap;

- The dilution zone can be optimized to provide ideal conditions for SNCR and optimize the performance of the convective air heater; and

- With the exception of the radiant panels, all the components can be considered as commercial. The down-fired combustion chamber is similar to conventional wet bottom boiler technologies and entrained flow gasifiers. Slag screens are used routinely; only the dilution zone presents a design challenge because a homogeneous mixture is required at the entry to the SNCR zone.

4.1.1 Firing System Design

European experience with wet bottom boilers stresses the importance of firing system design and operation in order to increase refractory lifetime in the firing chamber. Precise control of burner stoichiometry is emphasized to avoid the formation of localized reducing atmospheres. The HITAF imposes other potential requirements on the firing system: minimization of overall radiant furnace size by maximizing heat transfer to the radiant panels and optimization of NO formed in the HITAF. Both of these requirements affect cost. Furnace size has an obvious impact on capital cost; the higher the NO_x emissions at the exit of the HITAF, the more stringent will be the requirement for any
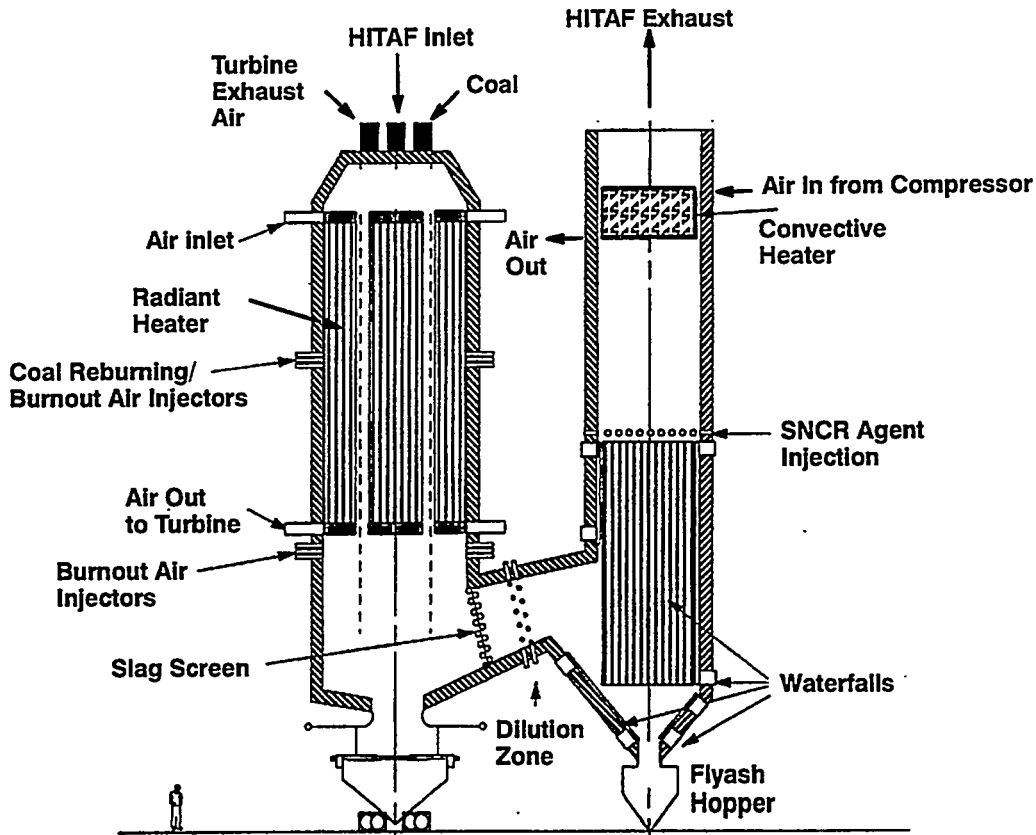
Figure 4.1-1   HITAF Cross Section.

downstream clean-up system. The cost of the power plant would obviously be minimized by preventing the formation of NO rather than removing it by costly downstream clean-up. But there is a compromise, minimization of NO_x cannot have a major impact on heat exchanger cost.

Limiting radiant panel size was established by assuming a firing system that instantaneously generates adiabatic combustion products. A radiant air heater length of 60 ft would be required to reach the target air temperature of 1700°F. This is contrasted with an air heater length of 80 ft if a fully developed axial flame is used. There are two alternative burner designs that are being considered:

1. An array of gas stabilized, axial coal injectors in a low velocity axial air flow. The delayed mixing between the fuel and air produce a naturally staged flame. Ignition stability close to the injector is important for low NO_x, and gas stabilization is preferred because it minimizes fuel air mixing in the early stages of the flame. Preliminary testing indicates that the required flame stability can be achieved with a gas flow equivalent to 2 percent of the burner heat input. This approach minimizes particle deposition on the heater walls. However, it has the disadvantage that it takes some distance to release significant energy, thus requiring a larger ignition muffle. The size of this adiabatic section can be minimized through the use of multiple fuel injectors, and although multiple injectors are

76

required for start-up, shut-down and turndown, there is a cost penalty associated with multiple fuel injectors.

2. In a tangential-fired boiler, pulverized coal is admitted at each corner of the combustion chamber through vertically arranged compartments. Air is supplied and controlled by distribution dampers along the height of the windbox, and coal/air mixing can be varied by the distribution of the air to the various elevations. The flame envelope location can be varied by raising or lowering the tilt of the coal and air nozzles, thus effectively controlling the heat absorbed by the furnace walls, and subsequently the heat transfer in the convective section. Flame is stabilized by the impingement of the laterally adjacent hot streams and resultant eddies. Except for the global vortex in the furnace, coal and air are mixed by gradual entrainment and the resulting fireball can be considered as a series of impinging long diffusion flames. Corner-fired boilers are inherently lower NO_x emission devices, and emissions can be reduced further by operating with overfire air ports. NO_x emissions below 200 ppm at 0% O_2 are reported with 100% of the theoretical air in the firing zone.

Experience with slag tap boiler refractories has demonstrated the importance of precise control of the air/fuel ratio at each burner, it is important that the cross-sectional area of the burner openings remain constant during operation and are not damaged by heat or distortion. Also, the air flow to each burner must be controlled separately (i.e., a common windbox is not recommended).

4.1.2 Evaluation of HITAF NO_x Strategies

The program goals for the HIPPS program require that NO_x emissions from the HIPPS facility be controlled to a level of 0.06 lbs/MMBtu. One approach to achieve the potentially large reduction in NO_x on a wet-bottom system is through the addition of back-end SCR. Although the target level is extremely low (approximately 10% of the current NSPS), it is likely that an optimized SCR system (perhaps in conjunction with a carbon prefilter) could meet the emission target; however, achieving the simultaneous 10% reduction in the cost of electrical power may be more challenging. Extensive experience with SCR on coal-fired systems in Germany has shown that the capital costs of SNCR are less than one third of the costs of SCR, including all design and engineering costs. In addition, operating costs for SCR are approximately 40% higher than SNCR (assuming no unusual catalyst failure) and it is much easier to do load following with SNCR. Also, due to its location in the system, NH_3 slip − if any − is much easier to deal with in SNCR systems as there is typically a scrubber downstream. For SCR, however, the system is the last element encountered by the flue gas. SCR also typically requires reheat prior to release of combustion products to the atmosphere.

Thus, during Phase I of the HIPPS program, experimental studies have been carried out focusing on ways to achieve ultra-low NO_x emissions by utilizing a combination of:

- stabilized, axial jet flames with staged air addition;
- reburning in conjunction with dilution air addition, and

77

- optimized SNCR.

The integration of these techniques can produce emissions below the DOE emission target level and the amount of reduction produced in each zone can be varied to fit differences in local site conditions and fuel availability.

Results of Optimization Experiments

A large number of tests have been performed using the 100,000 Btu/hr, refractory-lined combustion research facility (located at the University of Utah) to quantify the impact of the combustion and design parameters on emissions performance. The facility, described in a previous quarterly report (for the period January 1 – March 31, 1992), has a main firing chamber 16 cm in diameter by 7.3 m long and is constructed of composite refractory walls to minimize heat losses. The facility is divided into three zones: primary combustion, convective (for reburning) and SNCR.

The U furnace is equipped with a specially designed coal burner which feeds pulverized coal and primary air through the center of the burner surrounded by an annular gas stream and a weakly-swirling secondary air flow. The burner is designed to produce a naturally staged, axial jet flame with a fuel-rich center core. The annular natural gas is provided to ensure that the ignition front is stable on the fuel injector. Second stage combustion air can be added at multiple locations down the length of the vertical section. Reburning fuel and burnout air are added, as appropriate in the horizontal section and NH_3 or other selective reduction agents can be added at the appropriate temperature in the final vertical section.

Prior to the detailed NO_x control experiments, a series of tests were conducted to characterize the emissions under conventional combustion conditions. Figure 4.1-2 illustrates typical excess air (c.a. 5% O_2) data with the Utah bituminous coal and medium swirl for the hot wall configuration (no wall heat removal other than normal conduction). The data are reported as a function of fuel injector position which had little effect on these high temperature flames. As expected, the NO_x emissions were in excess of 900 ppm (dry, 3% O_2) which corresponds to about 1.25 lbs/MMBtu. These data are in good agreement with the full scale data on wet wall systems and confirm that NO_x emissions from wet wall systems are higher than conventional water-wall boilers unless aggressive measures are taken to achieve control. The following sections summarize results obtained for the various NO_x control strategies applied separately and as optimized combinations.

Staged, Gas Stabilized, Axial Flames

This section examines the influence of the primary zone combustion parameters on exhaust NO emissions based on the idea that it is important to prevent the initial formation of NO_x to the maximum extent possible. In these experiments the fuel injector was a single hole axial coal injector designed to produce a coal jet velocity of approximately 20 m/s. A stabilization gas was added via an annulus with discrete axial jets (issuing parallel to the primary coal jet) unless otherwise noted. Figure 4.1-3 illustrates the effect of the primary coal jet velocity on the NO_x emissions as a function of the amount
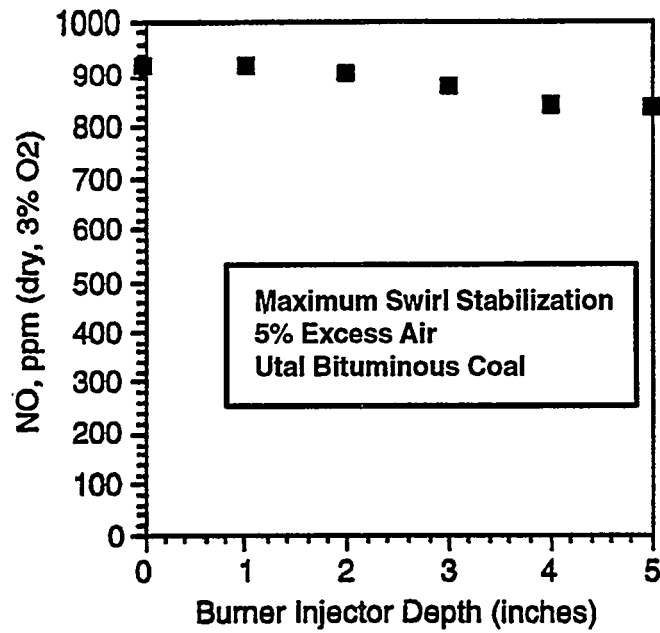
Figure 4.1-2   NO$_x$ Emissions under Conventional Conditions.

of stabilization gas used. In these experiments, the coal jet velocity was changed by changing the diameter of the fuel injector; the primary air flow was held constant in both cases. Initially both flames produced relatively high NO$_x$ emissions when the stabilization gas was completely off; however, as the gas rate was increased to 5%, the flame was more securely anchored on the fuel injector and the emissions dropped. These results on the effect of stabilization gas rate are consistent with many obtained throughout the study. Clearly, it is important to use sufficient gas to fully stabilize the axial jet flame although the amount of gas required depends somewhat on the design of the fuel injector as will be discussed later. Figure 4.1-3 also shows that the primary jet velocity has a significant effect on the exhaust emissions; decreasing the velocity to 10 m/s decreased the emissions at all stabilization gas flow rates almost certainly because of decreased secondary entrainment in the base of the flame.

Figure 4.1-4 shows the results of a similar test series focusing on the design of the stabilization gas injection system. Here the discrete axial holes are compared to a simple annulus (which completely surrounded the coal jet). In terms of overall minimum emissions, the results were approximately the same; however, the annular design produced a more inherently stable axial jet flame (even without any stabilization gas) and it required only about 3% stabilization gas to reach the low initial emission level. This design was, therefore, used in most of the subsequent ultra low NO$_x$ tests with reburning and SNCR.

In the HIPPS cycle, the clean air from the turbine outlet is subsequently used as the oxidant for the primary combustion zone. Since the cycle also contains a duct heater which is directly fired into the clean air prior to the turbine inlet, the entire stream contains significant moisture and the oxygen level is reduced to approximately 17 to 18%. To evaluate the impact of this vitiation on the NO$_x$ emissions in the primary zone of the coal combustor, tests were conducted with both normal air at conventional

79
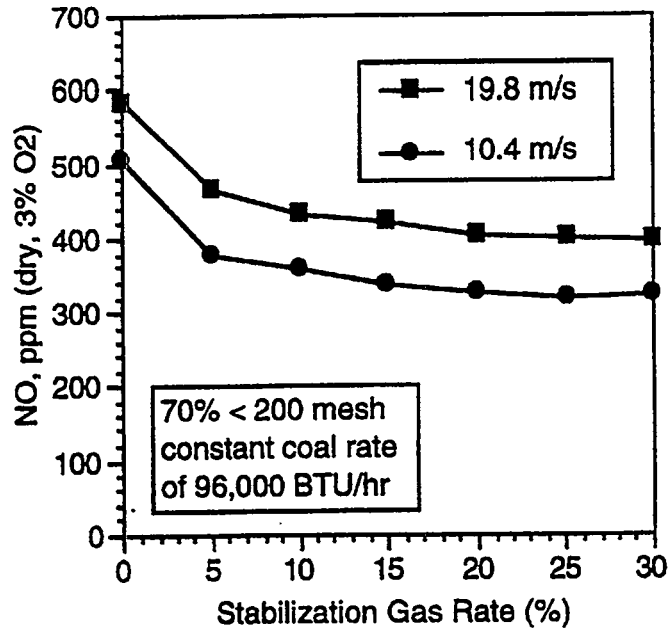
Figure 4.1-3   Effect of Primary Coaljet Velocity on NOx Emissions.
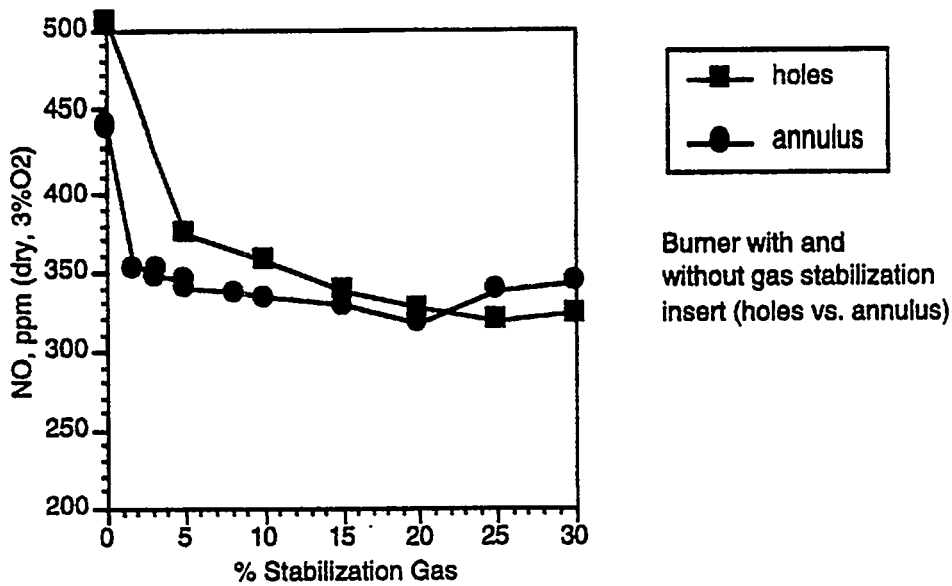
Figure 4.1-4   Gas Stabilization Effects on NO$_x$ Emissions.

preheat temperatures (650°F) and a 17.5% oxygen vitiated air stream at 1050°F. The preheat on the vitiated air was chosen to approximately match that expected from the turbine outlet and, for scientific reasons, to match the overall adiabatic flame temperature of the non-vitiated case. The results of these tests are summarized in Figure 4.1-5, where the NO$_x$ emissions are plotted as a function of gas stabilization rate. In general, the vitiation appears to have had little effect on the NO$_x$ formation. This result was typical of several other cases under different combustion conditions where vitiated air combustion was compared with normal air combustion. As long as the flame temperature was

maintained the same between the two cases (by increasing the air preheat to compensate for the reduced oxygen concentration), there was no distinguishable difference in the NO_x emissions between burning the Utah coal in normal air and in the vitiated oxidant. The investigators did, however, notice qualitatively that the vitiated air flames were more difficult to work with and seemed inherently somewhat less stable, although this was not directly reflected in the measured NO_x emissions.
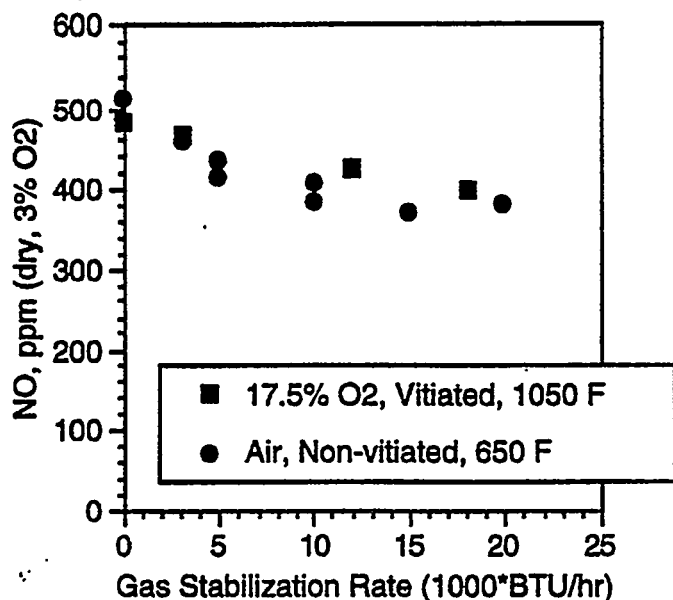
Figure 4.1-5   Vitiation Effects on NO_x Formation.

The previous data have suggested that it is possible to achieve approximately 350 ppm NO_x even in a hot wall system with properly designed gas stabilized axial flames, but the NO_x prevention can be further enhanced by operating the primary flame in a staged combustion mode. Figure 4.1-6 shows typical results on the effect of primary stoichiometry for two different first stage residence times with the staged axial flames. As expected, increasing the rich zone residence time significantly decreases the NO_x formation (because the burnout air addition is delayed and more of the fuel nitrogen will be converted N_2 prior to the point at which excess oxygen is available). By operating with a primary zone stoichiometry of approximately 0.9 and a first stage residence time of 580 ms, it is possible to limit the initial NO formation to approximately 150 ppm which represent a total fuel nitrogen conversion of less than 10%. Even lower emission levels can be achieved by further increases in primary zone residence time, although for most systems this would not be practical.

From a fundamental perspective, it is interesting that the optimum first stage stoichiometry for the gas stabilized axial flames is approximately 0.85; this is in marked contrast to conventional swirl stabilized, well mixed pulverized coal flames where the optimum stoichiometry is normally approximately 0.7. This difference is likely due to the fact that the axial flames are inherently staged due to the limited initial mixing, so it is not necessary to run the overall combustion process under such fuel rich conditions. This is advantageous both from the perspective of wall material concerns and also
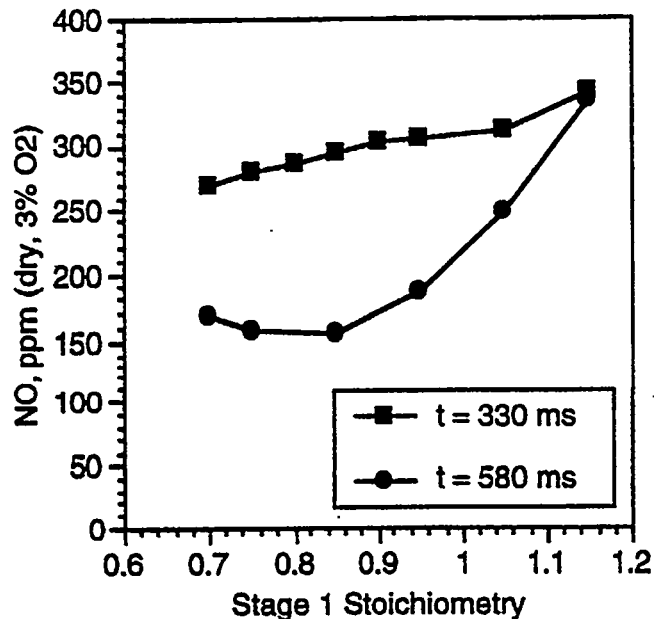
Figure 4.1-6   Effect of Primary Staging with Different Residence Times.

the need to operate the flame near stoichiometric to maximize the peak temperature and radiant heat flux.

Several experiments were also conducted to evaluate the effect of coal particle size, since the authors have previously shown that finer particles favor lower emissions under conventional staged combustion conditions. Figure 4.1-7 shows typical results with both the conventional pulverized coal and a micronized (90% less than 325 mesh) sample of the same coal. As expected, the micronized coal was considerably easier to stabilize even with no natural gas and the overall emissions were consistently lower. These data were taken with the large diameter axial fuel injector under excess air conditions (no staging). The results confirm the desirability of fine particle size from a combustion perspective, but the additional pulverization costs may not ultimately be justified because the difference in emissions can be compensated for within the SNCR zone if necessary as will be discussed later.

Reburning

Reburning is a NO_x abatement technique in which secondary fuel is injected downstream of the fuel-lean primary combustion zone of the furnace. The second stage or reburning zone is usually operated at overall fuel-rich conditions, allowing a significant fraction of the primary NO to be reduced to N_2 and other nitrogenous species. In the third zone, additional air is introduced to establish overall fuel-lean conditions and allow for the burnout of remaining fuel fragments. This form of NO_x abatement has been applied to full scale units and appears to be a viable NO_x control strategy. Therefore, reburning has been tested in the bench-scale furnace described above under conditions relevant to the HIPPs project.

82
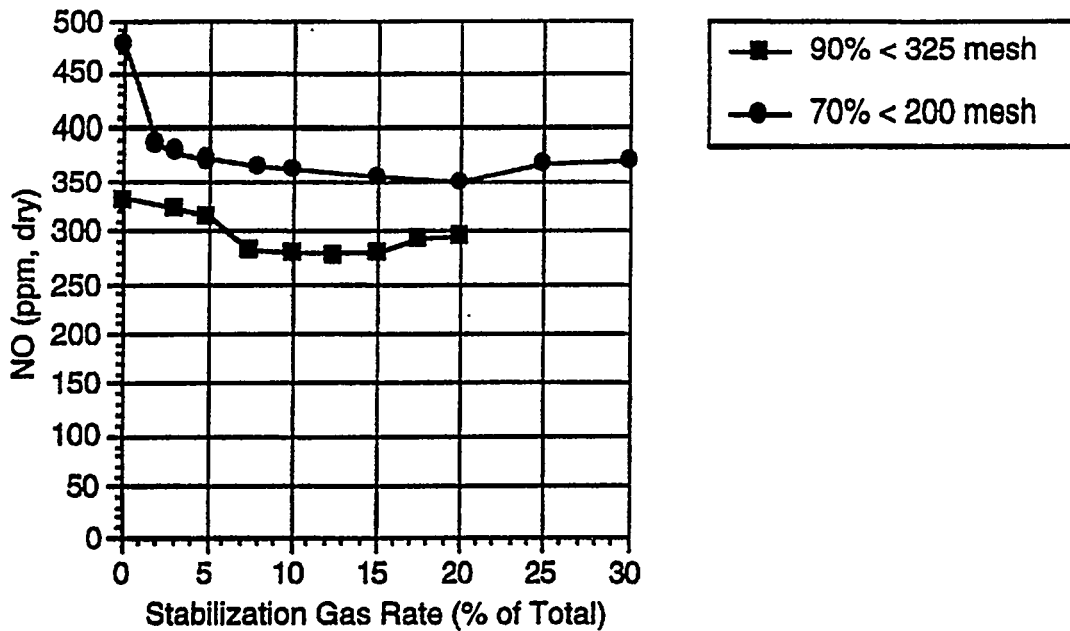
Figure 4.1-7   Micronized Coal vs. Conventional Pulverized Coal Results.

The effectiveness of reburning depends upon several key parameters, as indicated in Figure 4.1-8, for coal reburning. The parameter of greatest significance is the reburn stoichiometry which gives optimal NO reduction at a stoichiometric ratio (SR) of about 0.85. A stoichiometric ratio of 0.85 corresponds to a reburn firing rate that is approximately 20% of the total firing rate. The temperature at which reburning occurs is also significant. As shown in Figure 4.1-8, higher temperatures shift the optimum reburning stoichiometry toward more fuel rich conditions (lower SR) for coal reburning with better NO reduction occurring at lower temperatures for the higher reburn stoichiometries. However, CO emissions can increase quite dramatically at lower reburn temperatures which can make coal reburning at low temperatures impractical.

Another important parameter in reburning is the residence time that is provided in the fuel-rich reburning zone. As indicated in Figure 4.1-9, a residence time of at least 0.4 seconds is necessary for effective reburning with both natural gas and coal. Figure 4.1-9 also indicates that natural gas is slightly more effective than coal as a reburning fuel and may require less residence time in the fuel-rich zone.

This introduces another important parameter for reburning — fuel type. Several fuel types have been investigated in the current program, as indicated in Figure 4.1-10. For the higher temperature reburning conditions of Figure 4.1-10, most of the fuels tested were very effective reburning fuels. Coal performs about as well as the other solid fuels and natural gas, and would be the most likely candidate for reburning fuel type in the current program. However, the possible availability of biofuels or natural gas led to the investigation of two wood types and gas, with CO and coke being investigated for comparison. Surprisingly, all of the fuels (except perhaps CO) are quite effective at reducing NO_x from an initial value of 500 ppm to about 200 ppm.

83
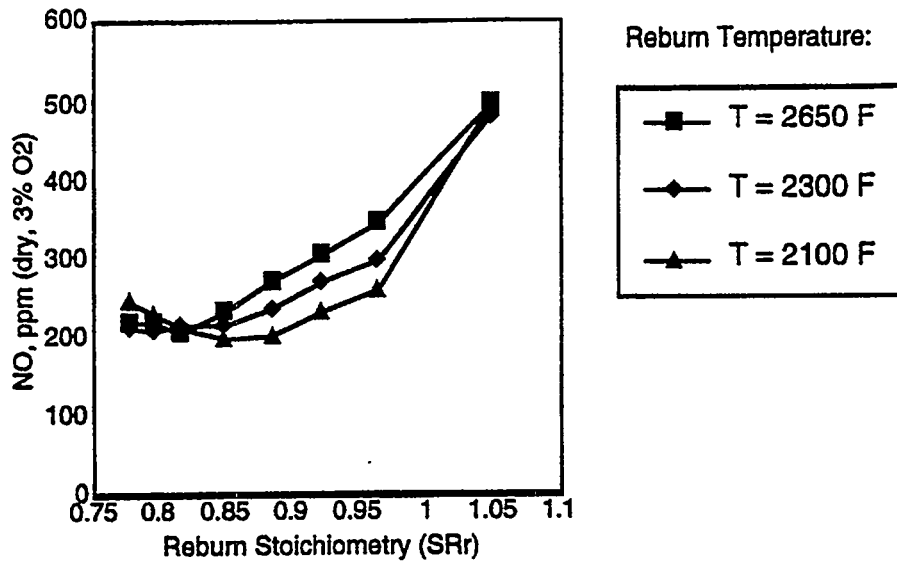
Figure 4.1-8   Reburning Effectiveness as a Function of Stoichiometry.
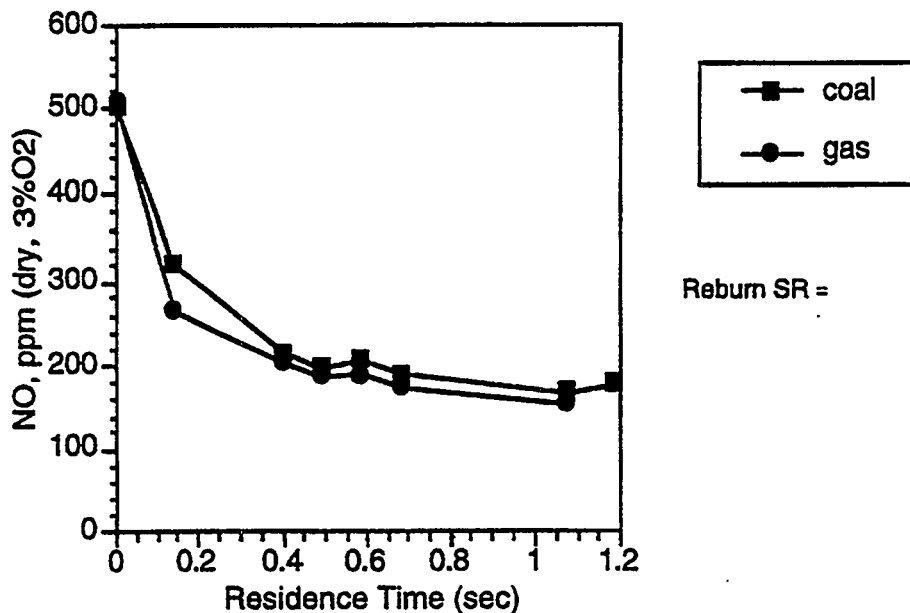
Figure 4.1-9   Effect of Residence Time on Reburning with Gas and Coal.

However, at low initial NO levels the ranking of these fuels is dramatically changed, as shown in Figure 4.1-11. At an initial NO level of 200 ppm, coal is clearly inferior to wood and natural gas for reburning. This difference is most likely due to the greater fuel nitrogen content of coal compared to wood or gas (about 2% for coal vs. 0.1% and 0% for the wood and gas, respectively). Therefore, if low NO values are expected in the reburning zone of the proposed design, reburning would be especially attractive if natural gas or wood can be used as the reburning fuel.
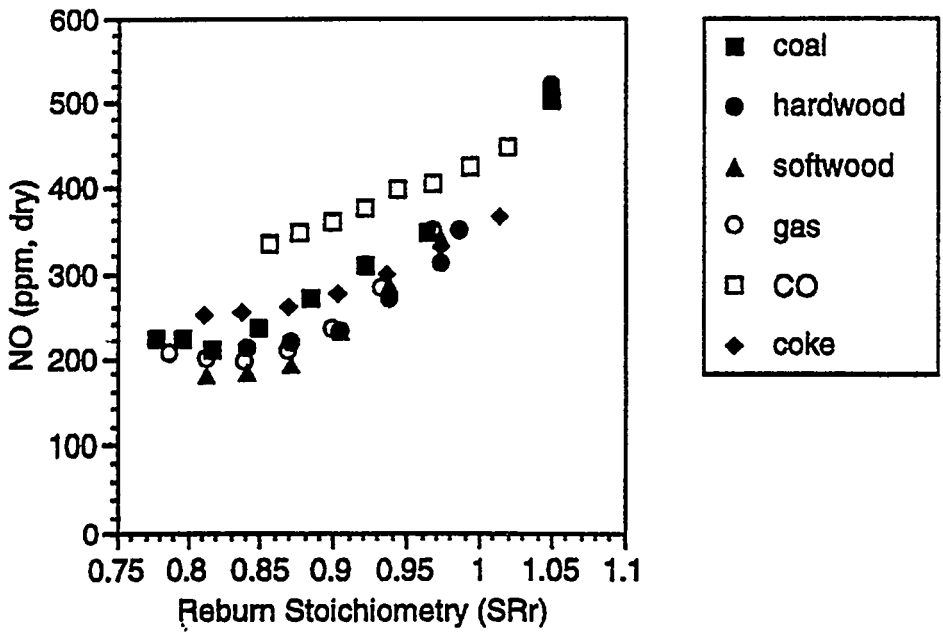
Figure 4.1-10   Effect of Fuel Type on Reburning Effectiveness.
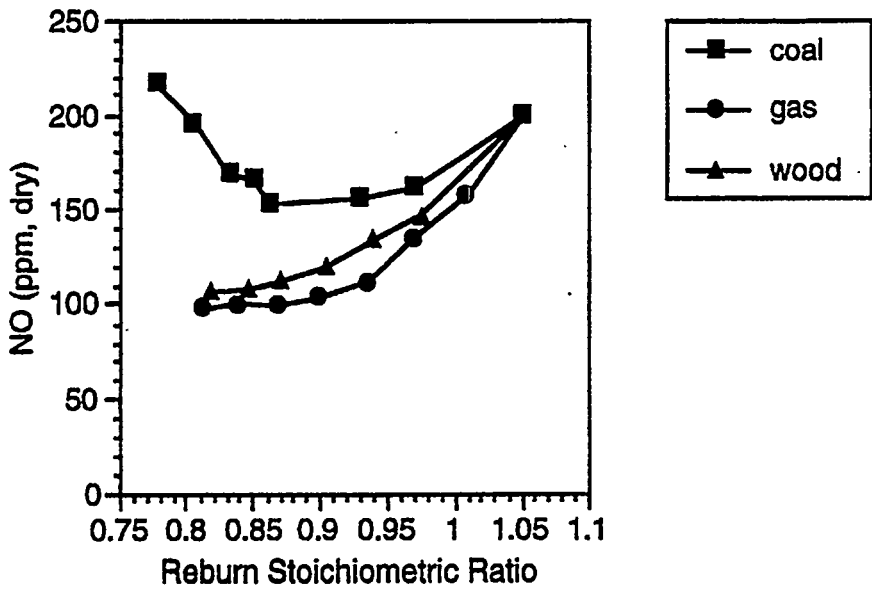
Figure 4.1-11   Effect of Fuel Type on Reburning Effectiveness – Low Initial NO.

85

Optimized SNCR

Selective Non-Catalytic Reduction (SNCR) is a NO_x reduction technique that involves the introduction of a reagent (e.g., ammonia, urea, cyanuric acid) into the exhaust stream in a specified temperature window, which allows the reduction of NO_x to N_2 by reaction with the reagent. Figure 4.1-12 shows the effectiveness of injecting ammonia into the current facility operating at 120,000 Btu/hr of coal fired in a gas-stabilized axial flame mode. NO is reduced from about 380 ppm to about 40 ppm by the injection of NH_3 at a ratio of 3:1 to the initial NO. High NH_3/NO_i ratios may not be desirable, however, because of the cost of the reagent and the increased likelihood of NH_3 emissions (or ammonia slip). In the current facility, ammonia slip was generally low (less than 20 ppm) even at NH_3/NO_i ratios of 3.0. Most practical systems would operate with NH_3/NO_i of about 1.5 to 2.0, in which case reduction of NO to about 50 ppm was achieved for the configuration of Figure 4.1-12.
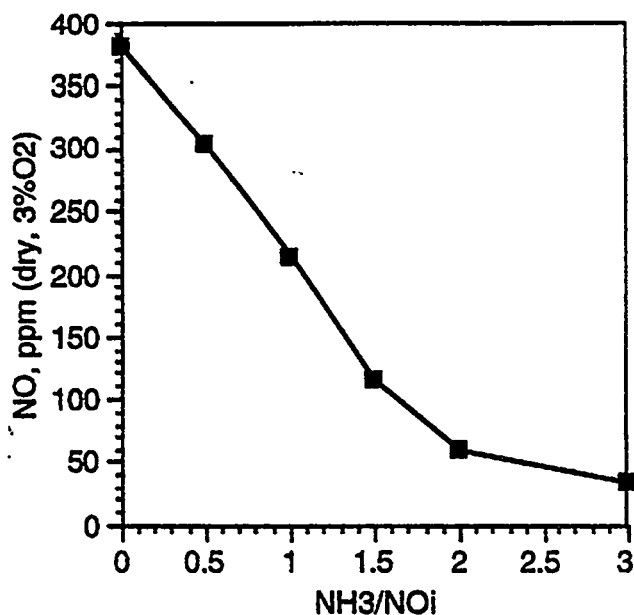
Figure 4.1-12   Effectiveness of Ammonia Injection with Current Facility.

The effectiveness of SNCR also depends upon the initial NO levels entering the SNCR zone, especially at lower reagent injection levels as indicated in Figure 4.1-13. It is interesting that at NH_3/NO_i greater than 1.5, the final NO levels achievable with SNCR appears to be independent of inlet NO, and may even decrease with increasing inlet NO. This trend is also observable in detailed chemical kinetic calculations indicating that under these conditions higher reagent and NO levels may enhance SNCR effectiveness through changes in the radical pool.

When used in conjunction with other NO_x reduction techniques, such as those described above, one must beware of interactions that might adversely affect SNCR. Figure 4.1-14 shows data obtained for conditions in which an axial, gas-stabilized coal flame was staged, with reburning applied to the products of this primary zone. The resulting NO values from this configuration range from about 80 to 100 ppm. However, as indicated in Figure 4.1-14, the distance between the reburning zone and the

86
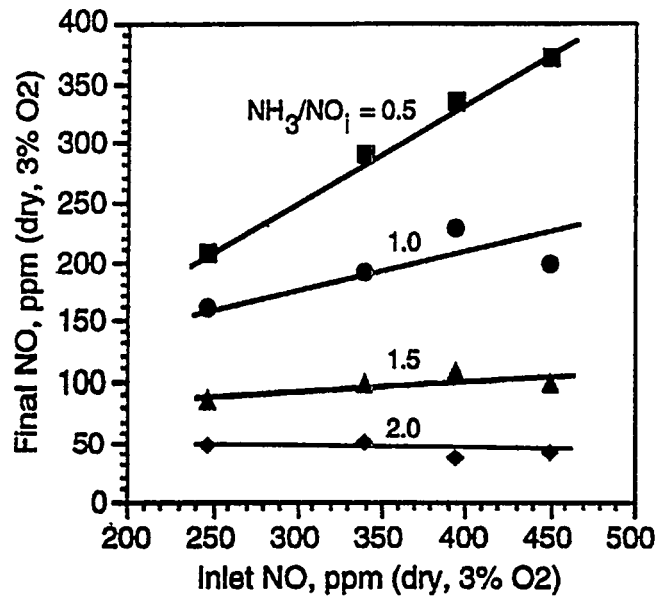
Figure 4.1-13   SNCR Effectiveness with Varying Initial NO Level.

SNCR zone dramatically affects SNCR, and actually determines whether SNCR reduces or produces NO. For the case in which the distance between the reburning zone and the SNCR zone is 0 inches (i.e., the reagent is injected with the burnout air), NO is produced in the SNCR zone due to a shifting of the temperature window to lower temperatures caused by the presence and reaction of fuel fragments from the reburning zone.
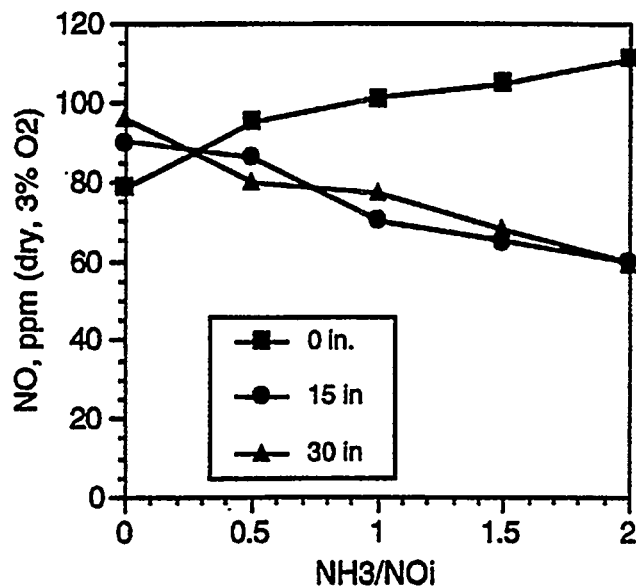
Figure 4.1-14   Combustion of Staging Returning and SNCR-Effect of Reburning Zone Location.

The optimization of SNCR can be accomplished primarily through the careful control of temperature at the point of the reagent injection and throughout the SNCR zone. Other parameters of

87

importance in SNCR include the presence of CO or other fuels or fuel fragments which tend to shift the optimal SNCR conditions to lower temperatures. Figure 4.1-15 indicates the significance of temperature and quench rate in the SNCR zone. Notice that as the injection temperature is decreased from 1303°K to 1267°K, NO_f/NO_i more than doubles in both the model and the experiment. Also, as the quench rate increases from 418 to 2420 K/s, NO_f/NO_i more than doubles. The model also captures the effect of injection momentum as accomplished by increasing the diluent nitrogen flow. As shown in Figure 4.1-15, increases of injection momentum consistently result in higher NO_f/NO_i in the absence of CO.
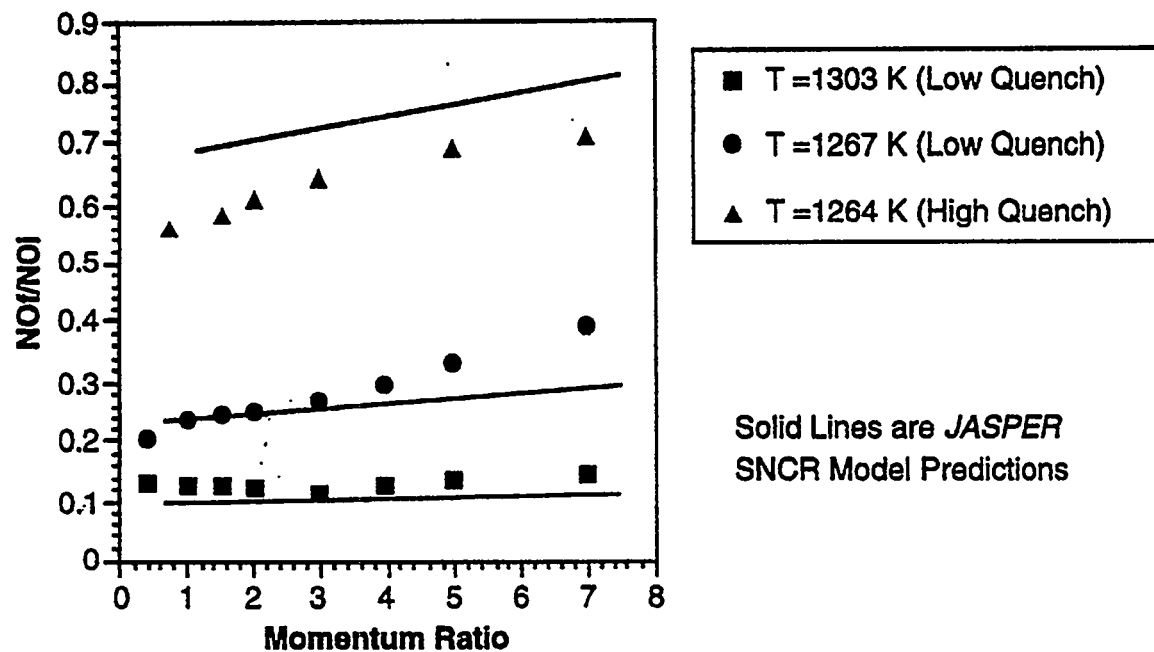
Figure 4.1-15 Significance of Temperature and Quench Rate.

It is important to note that at high temperature, low quench conditions, reduction efficiencies of about 90% have been consistently observed in the current facility (as indicted in Figure 4.1-12, Figure 4.1-13, and Figure 4.1-15), suggesting that a well designed SNCR section in the proposed design could be a very effective NOx reduction technique that is significantly cheaper than selective catalytic reduction (SCR).

Integrated Combustion Controls

The previous sections have shown that:

- NO_x formation can be largely prevented by the use of staged gas stabilized axial flames even in hot wall systems.
- Reburning, particularly with natural gas, is a powerful tool for NO_x control.
- Optimized SNCR can be almost as effective as catalytic de-NO_x schemes.

88

A wide variety of tests were conducted to evaluate various combinations of these schemes. Figure 4.1-16 summarizes the different experiments conducted with the integrated system and indicates the range of emissions which can be achieved with the various combinations of techniques. From a commercial perspective, the optimum configuration appears likely to be a staged, gas stabilized axial flame with optimized SNCR, although other alternatives may be more economically attractive in different locations depending on the local conditions.
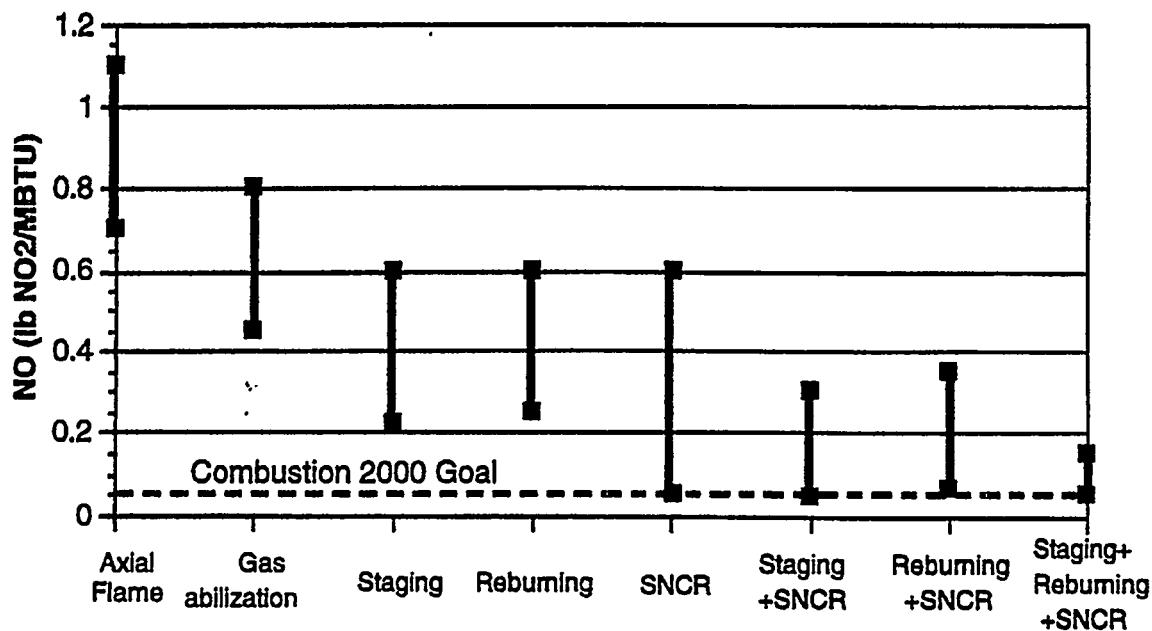
Figure 4.1-16   Summary of Integrated NO_x Control System Experiments.

4.1.3   Evaluation of Heat Transfer Efficiency in the HITAF

Evaluation of heat transfer from long axial flames to the radiant heat exchanger panels within the HITAF has been carried out by computer simulation. A series of HITAF simulations were performed which determined heat transfer sensitivity to geometric variations (length and diameter changes) and deposit thickness. This information was subsequently utilized to develop the current HITAF design.

A bench-scale experiment was also carried out to provide additional information on the heat transfer characteristics of long axial flames. Experiments were performed in the 100,000 Btu/hr test facility at the University of Utah using a Utah bituminous coal. A small heat transfer panel was designed and mounted flush with the furnace wall. The location of the probe allowed for formation of a flowing slag layer on the surface of the probe once the furnace reached a steady-state mode of operation. The probe was duel jacketed and used water as the heat transfer medium. Measured water temperatures at the inlet and outlet of the probe were used to determine levels of heat absorption by the probe.

Once the heat transfer flux panel was installed, initial experimentation began using a natural gas flame. The furnace was run for two days using natural gas and after an initial period of stabilization, several "soot blowing" experiments were performed. The steady-state heat flux measured during gas

89

flame experiments was approximately 79,000 Btu/hr/ft^2 (as shown in Figure 4.1-17). During soot blowing, the heat flux rose nearly 10,000 Btu/hr/ft^2 and quickly decayed back down to the average value.
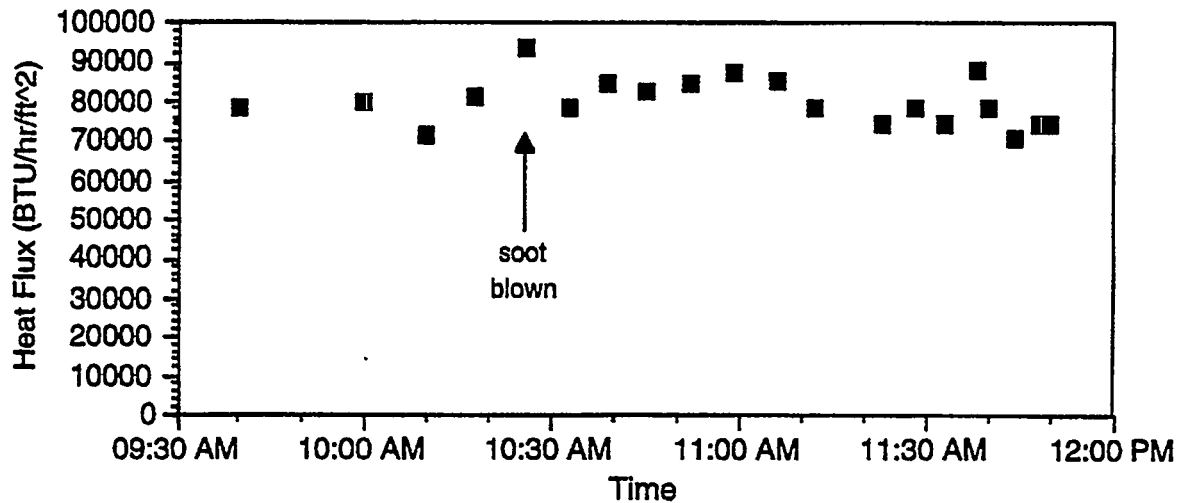
Figure 4.1-17   Steady State Heat Flux Measurements Made Using a Natural Gas Flame Firing at Nominally 100,000 Btu/hr.

The coal burner was subsequently ignited and the effect of coal firing on the heat flux to the panel was measured. As shown in Figure 4.1-18, there was an initial period of large variation in the measured heat flux as the coal flame was igniting and stabilizing. Then, a steady-state slag layer began to form and the average heat flux measured at the wall probe began to decrease. The coal flame heat flux finally steadied after 90 minutes at a level of approximately 70,000 Btu/hr/ft^2 and remained essentially constant for the next 16 hours. The levels of steady-state heat flux obtained in the University test facility (70,000 Btu/hr/ft^2 for coal and 78,000 for natural gas) fall in the middle of the 'normal range' of standard boiler wall heat flux levels of 50,000-90,000 Btu/hr/ft^2 indicating that the long flame (at this scale) provides acceptable heat flux values.

When the experiment was terminated and the probe removed, it was apparent that there had been a flowing slag layer on the surface of the probe with a thickness on the order of 1 mm or less. The presence of the slag layer appeared to decrease the overall net heat flux to the panel by approximately 8,000 Btu/hr/ft^2.

These heat flux measurements were compared with values obtained in the full-scale HITAF computer simulation. The values obtained in the 100,000 Btu/hr experimental test facility were somewhat higher than those obtained in the computer simulation (by approximately a factor of 2), although of similar magnitude. It should be noted that the values from the computer simulations were obtained with single, slow-mixing flames. The coal flame in the experimental test facility provided a greater flame volume (relative to the surface area of the furnace walls) than that of the single flame

90
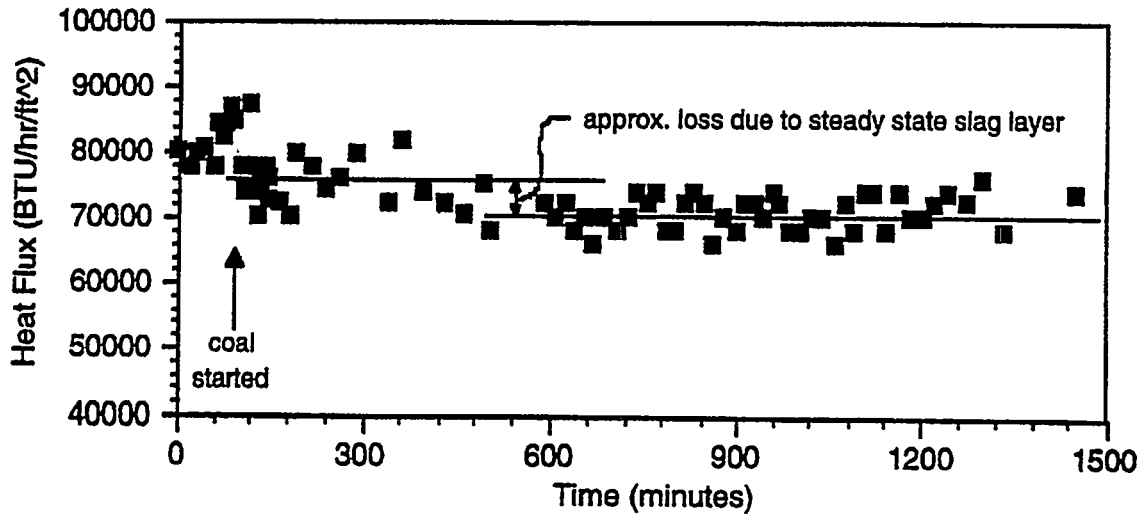
Figure 4.1-18 Heat Flux Measurements during Coal Firing Showing Onset
of Steady State Slag Layer and Subsequent Effect.

HITAF; particularly in early regions of the furnaces. The use of multiple long flames (anticipated with the HITAF) will provide for slightly enhanced mixing due to interactions between individual burners. Also, multiple flames will provide a larger, more dispersed body of radiating combustion gases earlier in the HITAF. Careful design of these burners can result in such enhanced mixing, while still providing the low NO_x emissions anticipated from a long axial flame. These detailed design issues will be addressed in Phase II computer simulations.

4.1.4 Full-Scale HITAF Simulation

In order to evaluate the performance of different HITAF design options, computer simulations were used to predict full-scale performance as a function of combustion parameters. The computer models utilized for the combustion simulations are steady-state, two- and three-dimensional computational-fluid-dynamics codes which fully couple the effects of reacting gases and particles with the impacts of turbulence and radiation. The turbulence is simulated using a two-equation model (κ-ϵ) for closure. The gas-phase equations are solved using an Eulerian framework and the coal-particle trajectories, solved in a Lagrangian framework, are coupled with the gas-phase equations through particle source terms in both mass- and energy-continuity equations. The gas-phase kinetics are assumed to be mixing-limited; therefore, the gaseous combustion is modeled using a statistical probability density function based on the mixture fraction of the inlet streams. The statistics of the mixing of the coal off-gas is similarly computed. Devolatilization of products from the coal particles, char oxidation, and particle swelling and fragmentation are included in the comprehensive simulation based on time-mean properties of the surrounding gas phase. Particle and gas-phase radiation are modeled using the discrete ordinates method.

91

Throughout the Phase I program, these computational tools have been used to analyze the feasibility of the full-scale HITAF. Different combustor concepts were evaluated based on their ability to achieve both heat transfer and emission goals. In addition, the simulations provided important deposition information which allowed analysis of slagging/freezing conditions. The majority of the Phase I simulations, however, focused on modeling the main combustion chamber of the HITAF; i.e., from the burners to the end of the radiant combustion zone. The reason for this focus was a compromise between the need to identify heat transfer capabilities of particular designs while maintaining reasonable turnaround in computation time.

After completion of the basic combustion chamber design, however, computer simulations were initiated that modeled the entire HITAF; i.e., from the burners through the transition zone up to the convective air heater. The purpose of such an extended simulation was to evaluate the impact of firing chamber operation on many of the downstream components of the HITAF. Such a simulation is vital to provide other C2000 team members with information needed for other tasks in the program. For example, information on flow profiles and particle distribution entering the slag screen will be required for the detailed calculations and simulations involved in the design and placement of the slag screen. Temperature distributions on walls in the transition zone will be necessary to provide insight into locations of different types of ash deposits and their subsequent ash management. Flow patterns and temperatures entering the SNCR zone will assist in the placement and design of injectors. Information on the flow and temperature distributions approaching the convective heater will be important in its final design and placement.

An initial simulation of the full HITAF has been completed and the geometry modeled is shown in a three-dimensional computer rendering in Figure 4.1-19. The important features of the HTIAF can be seen in these views of the outer shell. The opening for the five coal burners used in this simulation can be seen at the top left of each view. The octagonal shape of the radiant zone is also apparent. The horizontal transition section and the slag tap and dry ash hopper are visible at the bottom of each view. This simulation utilized approximately 310,000 computational nodes or grid points to define this geometry, and required considerable computer time to achieve a solution.

Results from this simulation are shown in Figure 4.1-20. The small inset on the left shows an overall view of the HITAF and the red box indicates the portion of the HITAF shown in the expanded view. The horizontal transition section was chosen for a detailed view because of the complexity of the flow of combustion products through that portion of the HITAF. The detailed view shown is made up of several planes of velocity vectors providing information about the flow of gases and particles as they turn and pass through the slag screen and subsequently turn upwards into the riser portion of the HITAF. It is apparent that the slag screen is functioning as a flow straightener and distributor. The extent of this behavior will depend on the design of the screen; particularly the pressure drop.

Also evident is the behavior of particle clouds as they pass into the slag screen. The particle cloud trajectory is indicated by the black line encircled by rings that starts in the burner closest to the

Actual geometry modeled in HITAF simulation

View of computational mesh

Radiant zone

Location of air heater

SNCR zone

Transition zone

Slag tap

Five long flame coal burners

Location of slag screen

Dry ash hopper
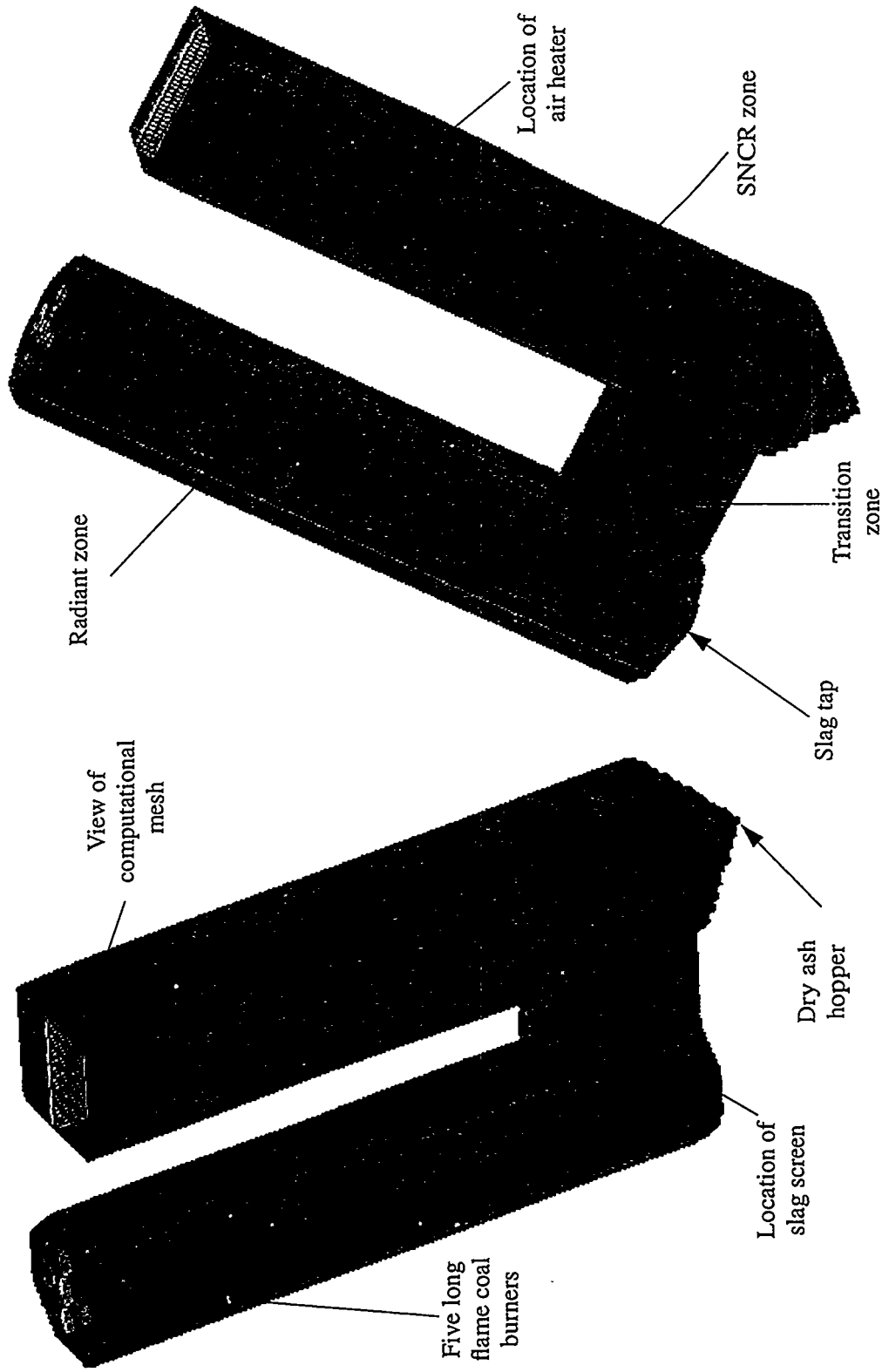
Figure 4.1-19 Computer Rendering of HITAF.

Five Burner Case - Long Axial Flames

Recirculation zones

Particle cloud trajectory being 'shaved' by and impinging on slag screen tubes

Slag screen locations

Particle trajectory with dispersion

Computational mesh

Overall HITAF

> 15 m/s

Velocity Magnitude (of expanded view)

0 m/s
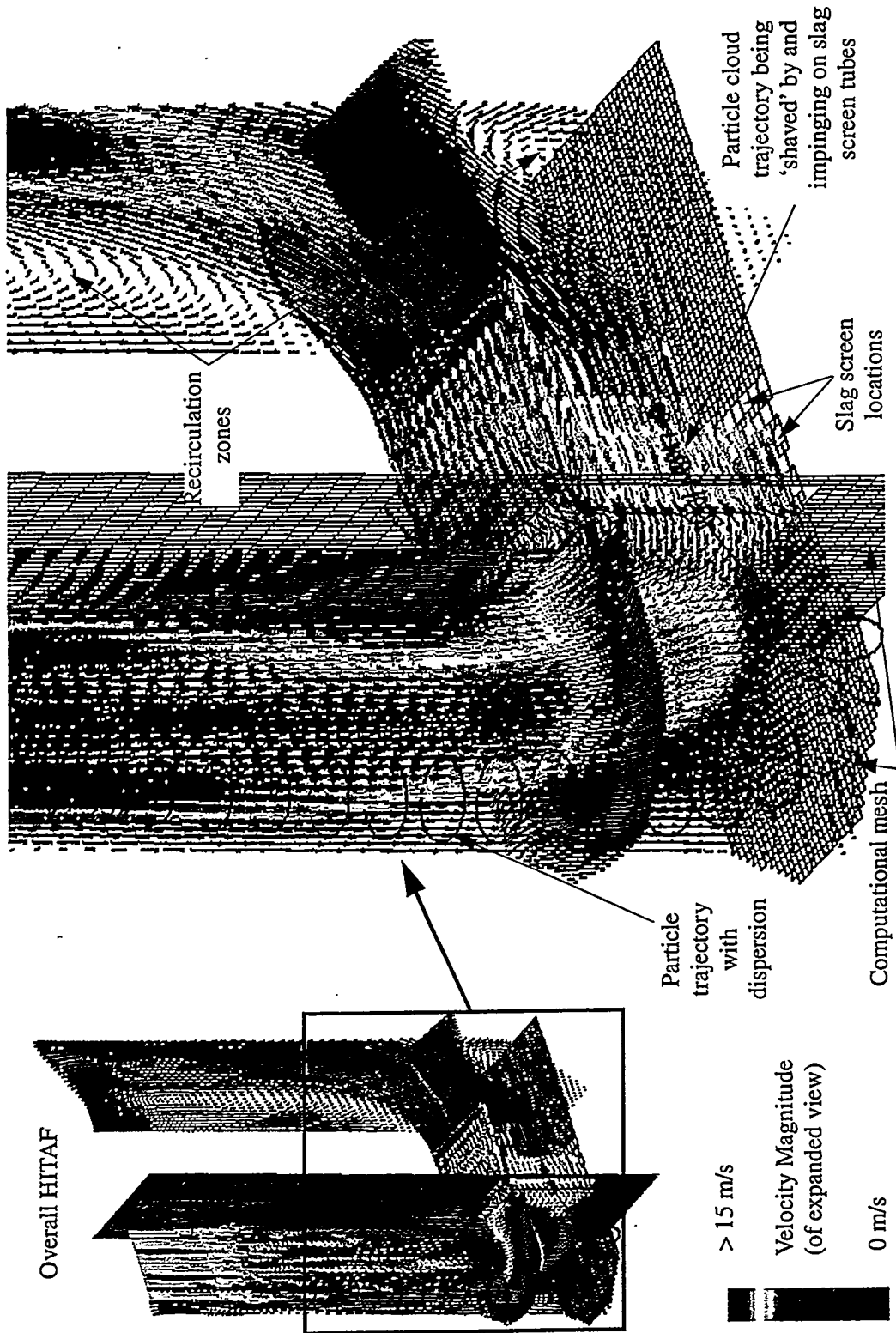
Figure 4.1-20 HITAF Velocity Distributions through Horizontal Transition Section.

left-most wall, and flows downward towards the slag tap. The rings shown indicate the dispersion of the cloud of coal/ash particles around their mean trajectory. As shown in the detailed view, prior to encountering the bottom of the furnace the mean particle path turns outward and then rises up and into the slag screen. The cloud of particles is 'clipped' by deposition on slag screen tubes and this particular trajectory ultimately collides with a screen tube after passing through more than 75% of the slag screen rows.

Also shown is the behavior of the combustion gases upon exiting the horizontal section into the ash hopper and riser portion of the HITAF. The bulk pathway of the gases is upwards towards the HITAF exit and the result of this upward motion is a flow recirculation in the ash hopper region. It is also apparent that the flow becomes detached from the inner wall of the riser portion upon exiting the horizontal section, resulting in an additional recirculation zone. The sharp 90° turn makes it difficult for the flow to remain attached and results in a flow recirculation that persists to the exit of the HITAF. This recirculation forces the bulk of the gases towards the outermost wall of the riser. The persistence of this recirculation zone will be altered by the presence of the convective heat exchanger (not included in this simulation) and its subsequent pressure drop. Also, the introduction of the carrier for the SNCR reagent will potentially affect the recirculation zone as well. It is apparent that knowledge of such flow behavior will be important in the design and placement of the SNCR injectors. For the current simulation, the distribution of SNCR reagent may need to cover only a fraction of the riser cross-section for adequate NO reduction. Inclusion of the convective air heater will be required for more accurate determination of these riser duct flow patterns, however.

The HITAF simulation will necessarily include the calculation of SNCR chemistry to provide an overall prediction of NO emissions from the HITAF. The NO emissions predicted in earlier HITAF simulations corresponded to the outlet of the radiant zone only; however, with the overall simulation there is the potential to analyze different staging, reburning and SNCR configurations to predict exhaust NO emissions at full scale. Earlier discussions (Section 4.1.2) of experimental work indicated the possibilities of low NO_x emissions from long flames using various combinations of staging, reburning or SNCR. The model will provide the means for scaling these findings to the HITAF. Previous results have shown the ability of the computer model to predict not only NO formation from coal flames (Smith et al., 1993 Joint Symposium on Stationary Combustion NO_x Control, Miami Beach, Florida) but NO reduction via SNCR chemistry as well.

4.2 HITAF Air Heater

Because the high temperature products of coal combustion provide the heat source for the HITAF concept, the air heaters must be capable of operation under unusually severe conditions. While conventional coal-fired steam power plants experience similar operating conditions, the air temperature required from the HITAF is of the order of 1700°F or more compared to only about 1000°F for steam, and air is a poor heat transport fluid compared to steam. The process of transferring heat from coal combustion products at temperatures up to 3000°F to high pressure air will require special structural design of the air heaters in order to avoid excessive mechanical and thermal stresses. Moreover, the mineral content of most coals at typical combustion temperatures produces ash particles in the combustion gas stream, resulting in potential for heat transfer performance degradation, and corrosion, and erosion of air heater surfaces. Although erosion of air heater surfaces by impinging ash particles is not expected to be a problem because gas and particle velocities will not be excessive, special provisions will be made to minimize heat transfer degradation and to prevent corrosion.

In order to produce the high air temperature required for acceptable gas turbine efficiency, the coal combustion temperature will have to be sufficiently high to produce molten slag which can potentially foul and corrode heat transfer surfaces. Since the entire air heater cannot be maintained hot enough to produce continuous slag flow from all heat transfer surfaces, the transition from wet slag to dry ash will be controlled by separation into two different types of air heaters which will be designed to deal exclusively with a specific type of deposit. Specifically, separate radiant and convective air heaters will be used to deal with the different temperature levels and properties of slag and ash, respectively. The radiant air heater (RAH) will operate at the higher temperature levels required, while the convective air heater (CAH) will function at the lower temperature regime. The air heaters will be arranged for counter flow of the gas turbine air and the coal combustion gas so as to achieve the highest possible temperature differential. A slag screen will be located between the two air heaters to establish the wet-dry interface (wet slag to dry ash) and to remove most of the ash from the hot gas stream before it can enter the convective air heater.

To prevent excessive sintering of ash deposits on heater surfaces and to provide a suitable temperature zone for selective non-catalytic reduction of NO_x, the combustion gas temperature will be tempered to about 1800°F by introducing flue gas recirculation immediately upstream of the convective air heater. This arrangement of the air heaters and the slag screen are shown schematically in Figure 4.2-1, along with expected operating temperature levels. The rationale for this arrangement of the air heaters, their respective operating conditions, and unique design features are discussed below in relationship to operating temperature levels and slag and ash environments.

4.2.1 Rationale for Air Heater Concepts

The rationale for selection of heat exchanger concepts for transferring heat from coal combustion products to high pressure air for driving the gas turbine are based primarily on the types of
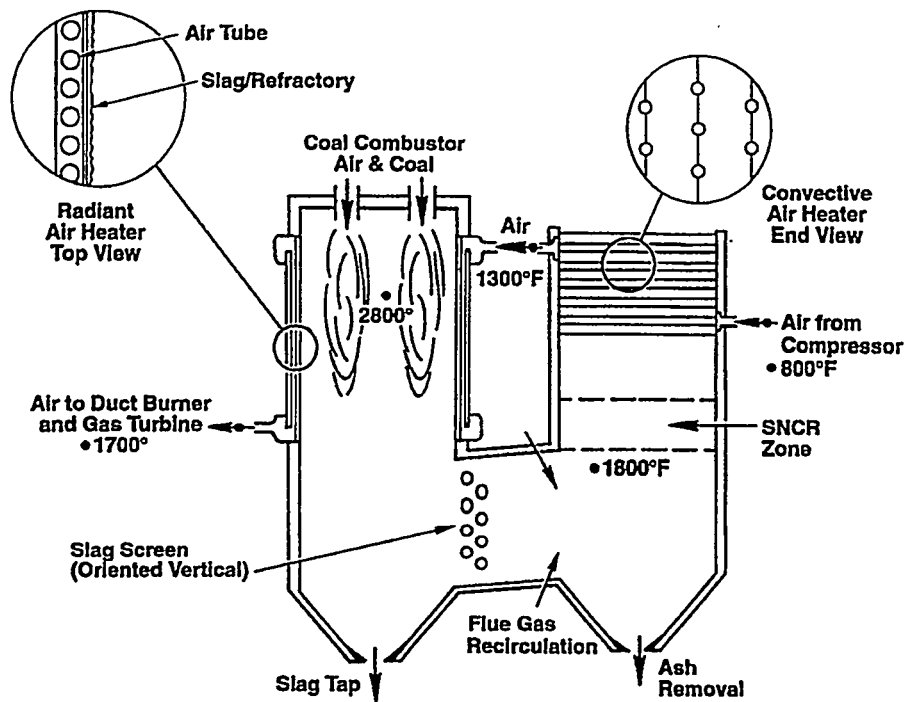
Figure 4.2-1   UTRC Arrangement of HITAF Components.

mineral deposits and the associated temperature regimes of the hot combustion gas. Depending on the temperature of coal combustion products, there are two general types of deposits, molten or liquid slag at high temperatures and dry ash at low temperatures, with varying amounts of the two types of deposits present at intermediate temperatures. For most coals, the distinction between the two types of mineral deposits can be controlled precisely by regulating the temperature of the combustion gas stream within two fairly broad temperature regimes. Specifically, liquid slag is predominant at high temperatures above about 2200 to 2600°F and dry ash prevails at lower temperatures below about 1800°F. Therefore, heat exchanger concepts and materials of construction will be chosen so as to be compatible with the types of mineral deposits present in the combustion gas stream, the corrosive nature and mechanisms of the prevailing type of deposit, the temperature regime, and the optimum modes of heat transfer available. In general, radiation heat transfer is best suited for the high temperature regime while convective heat transfer is appropriate for the lower temperature regime.

The radiant heat transfer mechanism offers several ideal features for transferring heat from coal combustion gases at the highest temperature regime to the gas turbine air. First, since radiant heat transfer is most efficient at high temperatures, the percentage of high quality heat from coal combustion which can be transferred to the Brayton cycle is unrestricted by thermal conductance. Second, since radiant heat transfer is a non-contact process which acts at a distance, slag deposition on heater surfaces can be minimized by proper design and location of the heater and the coal combustor. Third, since some small amount of slag deposition on heater surfaces is unavoidable, ceramic refractory coatings can provide long-term protection of heater surfaces from slag-induced corrosion.

97

Ceramic refractory coatings are currently used to protect radiant-heated steam boilers from slag-induced corrosion.

Although the thermal resistance of the refractory reduces the heat flux somewhat, the refractory serves the more important dual functions of preventing corrosion of the underlying structural air passages and maintaining a sufficiently high heater surface temperature to ensure slag removal by gravity-induced flow. The latter function is important because slag cannot be allowed to solidify in thick layers on heater surfaces since this will impede heat transfer adversely and solidified slag is difficult to remove. In practice, the refractory will gradually dissolve into the flowing slag and the refractory will have to be replaced periodically. By proper selection of the refractory, however, experience with steam boilers has shown that the cost and frequency of replacement of the refractory can be acceptable. A key task of this program will address the development of a ceramic refractory coating for protecting the radiant heater surfaces. Also, methods will be investigated under this program for *in situ* replacement of depleted refractory coating by periodically seeding the pulverized coal with appropriate metal oxides which will promote solidification of the slag on the radiant air heater surfaces.

The coal combustion product gas in the lower temperature regime is characterized by a gas temperature below about 1800°F, dry ash deposits, and potential for alkali-induced corrosion. Since the temperature of the gas in this second regime is too low for efficient radiant heat transfer, the air heater concept in this regime will have to be based on convective heat transfer. Since heat flux levels for convective heat transfer are typically low, compared to radiant heat transfer, deposition of ash on convective air heater surfaces will have to be controlled. Fortunately, techniques and equipment are readily available for cleaning of coal ash deposits from heater surfaces. By limiting the combustion gas temperature to a maximum of about 1800°F, ash deposits will not densify excessively beyond 75% of full density in about eight hours and the ash deposits will be removable from heater surfaces by conventional soot-blowing methods at reasonable time intervals. Although there will be a potential for alkali-induced corrosion of convective air heater surfaces, this problem has been controlled effectively in conventional coal-fired steam power plants. To ensure against alkali-induced corrosion of the convective air heater, the ash management and materials development tasks for this program will utilize this experience base to identify methods for avoiding alkali condensation and to develop metal alloys which are resistant to alkali corrosion.

4.2.2 Radiant and Convective Air Heater Design Concepts

Conceptual designs for the radiant and convective air heaters are shown in Figures 4.2-2 and 4.2-3, respectively. The radiant air heater will consist basically of many long hollow structural panels which will line the inside walls of the coal combustion furnace. The gas turbine air will be distributed to the many small passages within these panels by an arrangement of headers, manifolds, and ducts which will be staged to avoid excessive thermal stresses. A ceramic refractory coating or tiles will be applied to the fire sides of the hollow panels to prevent slag-induced corrosion of the panels. Although the radiant air heater is adaptable for either parallel or counter flow of the hot and cold gas streams,

parallel flow will enhance draining of liquid slag from the radiant heater surface by producing the highest heater surface temperature at the lowest point of the heater. Structural support for the entire radiant air heater will be provided by a massive structural shelf at the bottom of the furnace, probably consisting of furnace brick masonry.
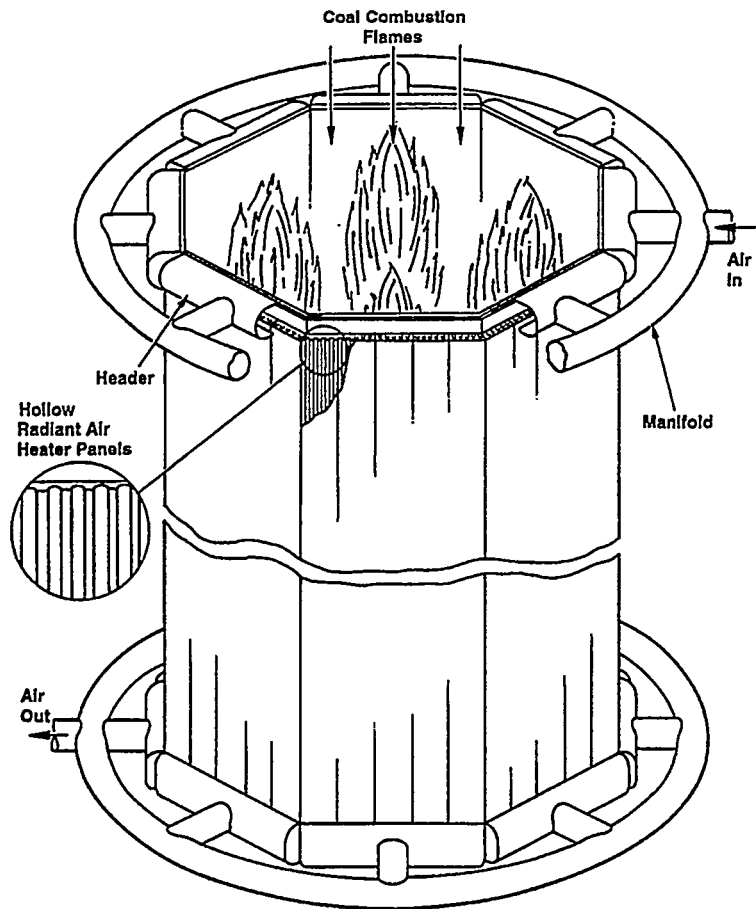
Figure 4.2-2   Radiant Air Heater Conceptual Design.
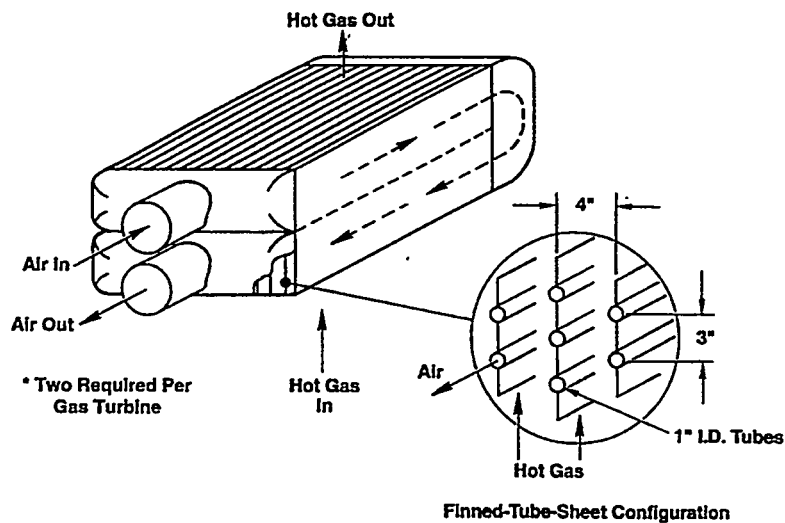
Figure 4.2-3   Convective Air Heater Conceptual Design.

99

The high temperature coal combustion products at 2800°F or higher will heat the panels by radiant transfer and, as the gas turbine air flows through the panels, the air will be heated by forced convection from about 1300°F to 1700°F or higher, depending on heater material capabilities and availability of supplemental heating by direct combustion of natural gas or oil. If the air temperature out of the radiant heater is limited to 1700°F, nickel-based metal alloys which have been developed for the aircraft gas turbine industry can be used to withstand an expected maximum heater temperature of about 1900°F. However, if higher air outlet temperatures are required, for example, to reduce the use of supplemental fuel heating, either super alloys with possibly thermal barrier coatings or ceramic materials will be required for construction of the radiant air heater.

As shown in Figure 4.2-3, the heat transfer surface configuration for the convective air heater is a modification of the shell and tube heat exchanger, where the air flows through the tubes and the hot combustion gas flows over and perpendicular to banks of tubes. This simple modification of the shell and tube heat exchanger, which is called the finned-tube-sheet configuration, consists of a sheet or fin extension between adjacent tubes in rows along the direction of the hot gas flow.

There are a number of advantages to using the finned-tube-sheet configuration for the convective air heater. First, because the heat convection coefficient for the hot gas side is only about one-fourth of the coefficient for the air side, the enhanced surface provided by the finned-tube-sheet configuration provides an overall heat conductance which is closer to the ideal balance for minimizing the convective air heater size. This enhanced surface area has been estimated to reduce the convective air heater size by about one-third as compared to a plain tube configuration. Second, the integrated structure of the finned-tube-sheet configuration is stronger and more rigid than plain tubes and less susceptible to circumferential thermal stresses. By joining adjacent tubes together by fin sheets (i.e., connecting the hottest and coldest circumferential positions together), circumferential temperature gradients in tube walls will be reduced. Third, because the smooth external surface contour of the finned-tube-sheet is aligned with the hot gas streamlines and there are no spaces between tubes for gas recirculation, ash deposition on air heater surfaces will be dramatically reduced. Finally, by limiting the hot gas temperature to 1800°F, the finned-tube-sheet configuration can be manufactured in modular units from metal alloys using conventional fabrication processes. In summary, use of the finned-tube-sheet configuration for the convective air heater will increase the hot gas side surface area, provide additional structural integrity, reduce circumferential thermal stresses in the tubes and reduce ash deposition, resulting in a smaller, stronger, less costly, more reliable, and lower operating cost heater.

For the rather modest effectiveness requirement of 53% for the convective air heater, a two-pass, cross-counter flow arrangement, with two air passes and one hot gas pass as shown in Figure 4.2-3, will produce the desired heating and temperature rise of the gas turbine air with a reasonable size heater. While additional passes of the gas turbine air could slightly reduce the size of the convective air heater, this would increasing the air side pressure drop and require additional return headers. As shown in Figure 4.2-3, large domed headers will collect and distribute the gas

100

turbine air to the convective air heater passes. Since the maximum air side temperature from the convective air heater is not expected to exceed 1500°F, the structural shell of these headers will be constructed of metal alloy, similar to the alloy to be used for the convective air heater tubes. The exterior surfaces of these headers will insulated and the interior surfaces may be lined with a ceramic to minimize heat loss to the ambient and to reduce the metal alloy temperature, respectively.

4.2.3 Air Heater Materials

Materials are the key enabling technology for successful operation and commercialization of the HIPPS system. The use of high temperature heat exchangers in a coal combustion environment, coupled with the cost constraints imposed by the desired capitalization (and related electricity) costs make proper materials selection a considerable challenge. Nonetheless, utilization of state of the art materials and joining methods, as well as advanced oxidation and corrosion resistant coatings, should yield acceptable results.

Air Heater — Materials — Radiant — The Radiant Air Heater (hereafter "RAH") must tolerate running coal slag on it's inner surface, while providing protection and reasonable heat transfer to the working fluid (air) contained near the outer walls of the coal combustor. Phase I efforts have indicated that the optimum design for the RAH is an alloy panel or tube bank protected by a cast refractory coating similar to the linings used in glass melting furnaces.

The use of an alloy based RAH, particularly under temperatures and environments afforded by the 65% coal combustion case offers several advantages:

- ease of fabrication, (i.e., conventional processes can be used to shape and weld components);
- existence of a significant supplier base; and
- superalloys offering high strength at baselline

The superalloys offer superior performance compared to the steels, currently utilized in similar applications, such as water wall slagging coal combustors. However, it is clear that for the radiant air heater section, a system of refractory ceramic linings (with or without supplemental thin coatings on the base alloy) will be required to protect the alloy from the slagging coal ash environment. A diagram of a RAH wall cross-section is shown in Figure 4.2-2.

The use of structural ceramics and/or fusion cast refractories to convey the working fluid (air) have disadvantages, such as joining and sealing technologies which are not well developed. For structural ceramics, while a supplier base exists for producing relatively large tubes, production costs remain high. Moreover, fusion cast ceramics are not normally produced as hollow shapes. Nonetheless, the allowable use temperatures of these ceramic materials make them the primary alternatives for use in the "all coal" combustion case when the working fluid is heated to 2500°F or higher.

The metal based approach to the RAH clearly offers a high probability of success for fabricating and operating a prototype HIPPS system, provided that material temperatures are moderated via partial use of natural gas as a supplemental fuel. All of the various material elements (metals, coatings, and ceramics) that make up this approach to the Radiant Air Heater wall will require careful selection and screening to determine survivability in coal combustion environments. In addition to selecting and testing of metals, coatings, and refractory ceramic liners, consideration must be given to both on-line and off-line repair of the materials during use. Techniques for bonding, joining and attaching both the dissimilar materials of construction and individual wall subsections will require development and validation.

Metals for the Radiant Air Heater — The selected alloys must possess the required properties such as ductility, high temperature strength, and resistance to creep. The materials must be able to be shaped and joined. Some typical high temperature mechanical properties of cast, wrought and sheet alloys are presented in Figure 4.2-4, and the methods to produce them are summarized in Table 4.2-1. The alloys selected must be capable of forming scales that limit the rate of wastage when exposed to hot oxidizing and corrosive gases. However, it is anticipated that the primary resistance to oxidation and corrosion of the alloy components is to be provided by special protective coatings developed to resist attack from the hostile environment.
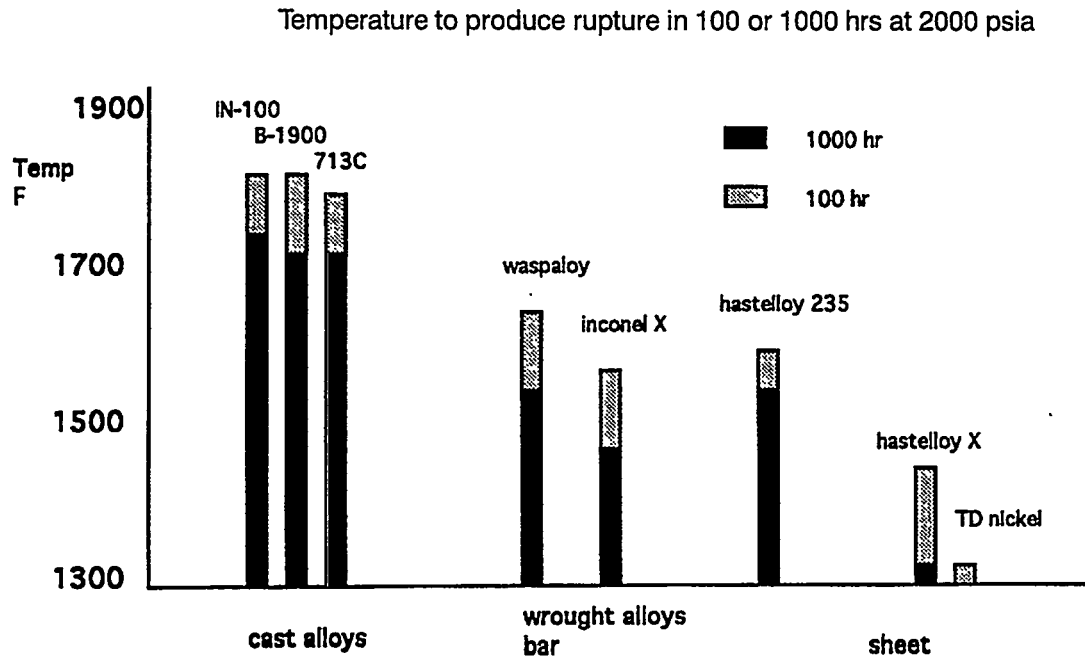
Figure 4.2-4   Temperature Capability.

TABLE 4.2-1 Production Melting Processes and Typical Alloys

Process	Alloys	Use
Vacuum Induction Melt + Vacuum Arc Remelt (VIM+VAR)	Waspaloy,A-286 IN-718, B-1900	General forgings and investment castings
Vacuum Induction	Mar-M246, 713C	Remelt for castings some sheet product cast into slab ingot
Electo-Slag Remelt + Vacuum Arc Remelt (ESR +VAR)	IN 718, H-188 H-230	Primarily for sheet products from slab molds

Two types of alloys will be·considered for use in construction of "metal based" RAHs. One uses the very strong, oxidation resistant cast nickel base superalloys, while the other takes advantage of the wrought nickel base family. In the first, the RAH will be constructed from a cast nickel base superalloy such as B-1900 The high temperature strength of these materials, as shown in Figure 4.2-4, is far greater than required for the RAH conditions. Parallel pipeds containing shaped passageways will be cast using technology developed for the gas turbine industry, and joined together by transient liquid phase bonding. This process produces bonds as strong as the parent metal, and are typically free of any line defects normally associated with welded structures. The oxidation resistance of the internal passageways will be provided by an aluminide coating applied prior to the bonding process.

The second approach utilizes the wrought alloys represented by Haynes 230 or Hastelloy X. These alloys are commercially available as pipe. Their limited oxidation and hot corrosion resistance will be enhanced by co-extrusion with the Alpha-IV alloy. Alpha-IV is a ductile iron base alloy that forms a protective alumina scale which exhibits outstanding resistance to oxidation and hot corrosion. Unfortunately the Alpha-IV alloy is too weak to serve as the prime structural material.

The cast nickel base superalloys for the RAH application are joined by transient liquid phase bonding process. In this process, a low melting point alloy first dissolves and then diffuses into the adjacent metal structure, leaving a metallurgical bond without any evidence of localized liquidation. Shielded-metal arc, gas tungsten arc, and gas metal arc processes are used to join wrought superalloys. The tests employed to evaluate all joined superalloys include, restraint cracking tests, variable strain tests, as well as hot ductility tests.

Thin Protective Coatings for Metals — The nickel base superalloys require additional protection from oxidation and corrosion by the air being heated within the exchanger. Even the relatively clean air from a stationary turbine compressor contains small quantities of salts and other accelerants that promote spallation of the protective oxide scales. The most desirable scale is alumina, an oxide that forms on the coatings used to extend the life of many types of turbomachinery components (Figure 4.2-5).

The major classes of environmental protection systems for superalloys are (1) aluminides, (2) overlays and (3) ceramics. The principle features of each are summarized in Table 4.2-2. These coatings have the ability to form a protective and adherent oxide scale to resist the service environment. The choice of a system is generally based upon protective capability, ease of application, and cost.
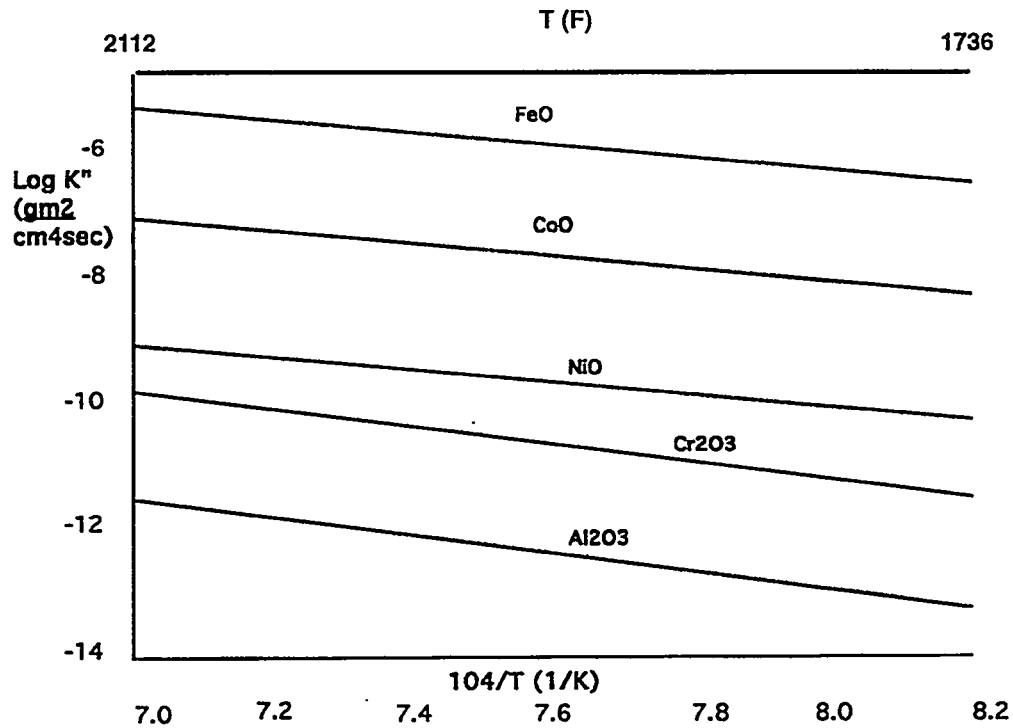
Figure 4.2-5   Oxidation Temperature Dependency.

TABLE 4.2-2 INTERNAL PROTECTIVE COATINGS FOR ALLOYS

Coating System	Method of Application	Major Elements	Primary Protective Oxide	Major Physical Characteristics
Aluminide	Pack CVD Slurry	Al,Cr,Si	Al_2O_3	Intermetallic Brittle Low temp DBTT
Overlay	PVD LPPS Thermal spray	Ni,Co,Cr,Al	Al_2O_3	Multiphase alloy similar to matrix
Ceramic	PVD CVD LPPS Thermal spray	Zr,Al,Cr,O	$ZrO_2Al_2O_3$	Thermal barrier Corrosion resist

The relative oxidation resistance of various alloys and coatings are shown in Figure 4.2-6. Aluminide coatings are the leading option for enhancing the oxidation resistance of the internal passageways of the RAH. Aluminide coatings are typically applied via Chemical Vapor Deposition

(CVD) processes, utilizing either a pack to generate the desired gases, or via direct generation of gases and subsequent reaction with the substrate to form the aluminide coating.

```
                  |
          1000X   |
                  |                        aluminide
 Relative         |                        coated
 performance      |             aluminide  B-1900    Alfa-IV
                  |             coated
          100X    |             Hastelloy X  |          |
                  |           .              |          |
                  |                          |
                  |             B-1900
          10X     |               |
                  |
                  |       hastelloy X
          base    |————————|————————————————————————
                  |
```
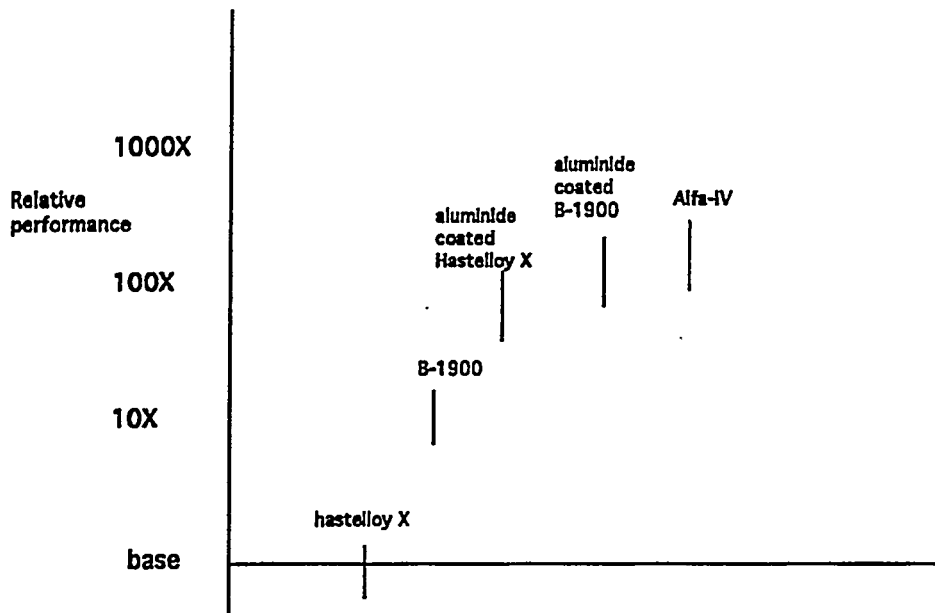
Figure 4.2-6   Relative Oxidation Resistance at 1950°F.

Thin Protective Coatings – The coatings used to extend the life of structural alloys are generally defined as a surface layer of material, metallic or ceramic or combinations thereof, that is capable of preventing damage related to the interaction between the substrate and the environment. The damage can be surface regression by oxidation or corrosion, or the loss of mechanical integrity associated with the diffusion of harmful species into the metallic substrate.

The elevated temperature oxidation and corrosion resistant coatings afford protection by the interaction of the coating with the oxidant to form protective scales rather than by acting as inert barriers. These coatings are relatively thin (less than 0.003 to 0.050 inch), and hence are referred to as thin coatings to differentiate them from the refractory ceramic liner.

The thin coatings, used to protect metallic structures, contain sufficient quantities of those elements that readily form adherent oxide scales such as aluminum, chromium or silicon. It is equally important that the coating material be chemically and mechanically compatible with the metal substrate. Diffusion of elements alters the mechanical and chemical properties of both the matrix and the coating. Thermal stresses can be of sufficient magnitude to cause separation of or cracking of the coating from the substrate.

The role of thin coatings for alloy component exterior sections in the Radiant Air Heater are: 1) to provide oxidation protection for the metallic substrate, 2) to transfer heat into the metallic structure and 3) to provide corrosion protection from gaseous and condensed coal combustion products that could seep, flow, or otherwise penetrate the refractory ceramic liner. An additional requirement

unique to the Radiant Air Heater application is that the thin coating must be simultaneously both mechanically and chemically compatible with the metallic substrate and the ceramic barrier liner.

The principle candidates, previously described in Table 4.2-2, are the overlay coatings (MCrAlYs), and the ceramic coatings. Overlay coatings currently afford oxidation and hot corrosion resistance to industrial gas turbine components. It is anticipated that the ceramic coatings would offer superior resistance to molten coal ash, in the event of failure in the thick refractory ceramic liner.

Thermal barrier coatings (TBCs) are widely employed in aircraft and industrial gas turbine engines. These materials consist of a ceramic separated from the metallic substrate by a bond coat, which is metallurgically bonded to the substrate. They are applied to the substrate using plasma spraying, flame spraying or physical vapor deposition. A typical example is yttria stabilized zirconia, bonded to the nickel base superalloy by a nickel base alloy rich in aluminum and chromium.

The TBCs developed for the industrial and aircraft gas turbine engines, as well as the family of overlays, will be evaluated for protection of the RAH. The concentration of the stabilizing phase, or the chemistry of the stabilizer, may be altered as determined from the test program. Candidate stabilizers include magnesia as well as calcia. Additionally, the same techniques employed to produce the TBCs will be used to produce an outer ceramic layer consisting of a solid solution of the oxides of alumina and chromia. The chemical composition of this layer will closely resemble that of the candidate refractory liner materials. These coatings are most resistant to the corrosive attack of fused alkali salts and provide superior resistance to oxygen transport relative to zirconia.

Refractory Ceramic Linings for the Radiant Air Heater – The key requirements for corrosion/erosion resistant refractory linings include: (1) resistance to liquid slag attack at temperatures up to 1450°C (approx. 2650°F); (2) mechanical and chemical durability and stability; (3) thermal shock and spalling resistance; (4) compatibility with metal heat exchanger components (thermal, mechanical, heat transfer, chemical); (5) ease of application, attachment, and repairability; and, (6) affordable cost.

The chemical and microstructural composition (phases, grain size, porosity, grain boundary and other impurities) of the refractories have a major impact on items 1-5 above. In addition, the methods used to process and manufacture the refractories have a strong effect on their chemical and microstructural features, as well as on items 5 and 6 above. The refractories which are most likely to meet the above requirements contain various combinations of the following constituents: Al_2O_3, MgO, mullite, ZrO_2, Cr_2O_3, $MgCr_2O_4$ (spinel), $Al_2O_3.Cr_2O_3$ (solid solution), SiO_2, plus various additives such as SiC and cements.

The choice of corrosion resistant refractories depends on many factors, including the specific slag and conditions of exposure. The results of study at ANL by Greenberg and Poeppel, where 8 different refractory materials were exposed to different liquid slags at 1600°C for 24 hours are as follows. The results indicate that the rate of recession of the refractories is strongly dependent upon

the refractory type (composition, type of bonding, and hence, processing), on the type of slag, on slag flow rate, and on impurities. The most erosion resistant refractory was processed by fusion casting, followed by the high fired, direct-bonded brick. The study concluded that refractory composition by itself is not a satisfactory guide in determining corrosion resistance, and that microstructural, manufacturing process, and other factors must be considered. In the proposed program, the testing of various types of refractories exposed to specific slags is a crucial part in arriving at the best refractories for application in the radiant heat exchanger lining.

The performance of the refractories is directly related to the choice of raw materials (minerals, oxides, purity, grain size, impurities); processing (forming the right combination of phases by heat treatment-calcining, fusing, etc.); and on the forming of the final refractory microstructures (final balance of phases, grain size distribution, porosity, etc.) and shape. Refractory candidates and their processing and shaping methods are listed in Table 4.2-3.

The chemical compositions to be studied include selected combinations of MgO, Al_2O_3, Cr_2O_3, ZrO_2, SiO_2 and additives such as SiC. The selections will consider a wide variety of refractories from various suppliers. Where possible, past experience will provide some guidelines on the most corrosion resistant refractories to coal ashes and slags.

The fusion cast refractories appear to offer the best resistance to coal slags. Indeed, these refractories are widely used to line glass tank furnaces, and operate for many thousands of hours exposed to flowing glasses. Molten coal slag shares somewhat similar composition and behavior with glasses used for various applications (container, fiberglass, etc.). Drawbacks of these types of refractories are high cost and relatively poor thermal shock resistance. However, the goal in determining the best refractory ceramic lining material will be to balance material lifetime and performance against cost.

Attachment of the refractory liner to the metallic air heater sections also requires careful consideration, due in part to the large thermal expansion mismatch between the metal substrate and refractory materials, and the required close contact between the liner and substrate (for high heat transfer). Gunnable and castable refractories have been traditionally attached to water cooled metallic walls via metal anchoring pins. The high temperatures of the HITAF preclude this approach. A system of ceramic anchors will require design and testing. Use of sintered or fused cast block refractories will also require unique attachment methods to accommodate the issues discussed above. A system of cooled metal pins, or ceramic pins, in combination with periodic support shelves is envisioned.

All Ceramic Construction for Growth to All Coal Case – The ultimate goal of the HIPPS system is to employ only coal as the fuel. The working fluid (air) within the Convective and Radiant air heaters would be heated to temperatures above 2500°F. No metallic materials possess the necessary strength and oxidation resistance to withstand operation in air at these temperatures. Replacement of the

107

TABLE 4.2-3 COMPARISON OF REFRACTORY MATERIALS FOR COATING THE RADIANT AIR HEATER

Refractory Type	Comp. Avail.*	Form	Raw Mat'l Processing	Type Bonds (grains)	Method of Application	Porosity (%)	Slag Corr. Resistance	Strength	Ther. Shock Resistance	Ease of Appl. & Repair	Cost
Shaped											
Fused cast	①-⑦, ⑧	slabs, bricks, etc.	fuse & cast	direct	lay-up shapes	0-10	excellent	moderate	poor	poor	high
Sintered	①-⑦, ⑧	slabs, bricks, etc.	press & sinter	direct	lay-up shapes	6-20	good - excellent	moderate - high	moderate	poor	moderate - high
Castable (prefabricated)	①-⑥, ⑧	slabs, shapes	cast, dry, fire	cement	lay-up shapes	10-25	fair - moderate	low	excellent	excellent	low - moderate
Unshaped											
Castable (site fabricated)	①-⑥, ⑧	powders	powder + cement mix w/H$_2$O	cement	cast to shape	10-25	fair - moderate	low	excellent	excellent	low - moderate
Ram mix	①-⑥, ⑧	powders	powder + cement or cer. bond mat'l	cement or cer. bond	ram or tamp to shape (in removable support)	10-20	fair - good	low	good	excellent	low - moderate
Gunning mix	①-⑦, ⑧	powders (wet/dry)	mix with H$_2$O in spray gun or torch	cement or cer. bond	spray (wet) spray (hot)	10-20	fair - moderate	low - moderate	good	excellent	low - moderate

*Compositions:

① Al$_2$O$_3$ - SiO$_2$, mullite
② zircon, zirconia
③ basic refractories (MgO, Cr$_2$O$_3$ - bearing)
④ high Al$_2$O$_3$

⑤ Al$_2$O$_3$ + SiC
⑥ Al$_2$O$_3$ - Cr$_2$O$_3$
⑦ Al$_2$O$_3$ + ZrO$_2$ + SiO$_2$
⑧ combinations of above

metal heat exchanger passageways with structural ceramics or fusion cast ceramics would allow the current general HITAF configuration to operate at progressively higher temperatures.

Structural ceramics such as silicon carbide or newly available silicon carbide particulate/alumina composite ceramics offer:

- high temperature strength and oxidation resistance to 2500°F,

- some resistance to acidic coal slags (generally, from bituminous coals), and

- good thermal expansion match with most protective coatings and linings.

Drawbacks include:

- low resistance to basic coal ash,

- high costs (due to low production volumes),

- manufacturing limitations for large, complex shapes, and

- failure effects concerns for brittle materials (e.g. tube fragments could enter the turbine hot section).

Mechanical properties of various structural ceramics candidates are listed in Table 4.2-4.

TABLE 4.2-4 POTENTIAL CERAMIC MATERIALS FOR GROWTH TO ALL COAL CASE

Material	Supplier	Ave. Flexural Strength at 1400°C	SCG Param. "n"* at 1400°C	Notes on*** Preliminary Slag Exposure
Sintered Beta SiC	Coors Ceramics	54.5	250 **	Sintered Alpha SiC — no st. loss at 1090°C
DIMOX SiCp/ Alumina	Dupont/ Lanxide	30.0	N/A excessive creep	No strength loss at 1090 and 1260°C expos.
NT230 SiSiC	Sain Gobain/ Norton	26.0	15.5	Significant strength loss at 1090°C expos

*	SCG — slow crack growth parameter measured by dynamic fatigue technique at ORNL
**	No SCG observed
***	Coal ash exposures in Wyodak and Illinois #6 static test, 300 hours, followed by room temperature flexural testing. Phase I DOE HITAF Program

Another unique approach to exchanger passages having higher temperature capability would be to employ fusion cast ceramics. As discussed above, these materials are used to line glass tank furnaces, an environment similar to molten coal slag. Manufacturers have limited experience in fabricating hollow shapes from these materials; currently they are limited to relatively large wall thickness shapes (0.5 to 1.0 inch), limiting heat transfer area for a given radiant wall section to a low level. The unique feature of this approach is the combination of air passageways and slag resistance in

a single material. If fusion cast refractory ceramics show promise under Phase II development, tube fabrication may be considered for Phase III efforts.

Ultimately the greatest limitation to the use of structural ceramics for the RAH is the present inability to seal and join these complex structures while accounting for their differential thermal expansion. Several seal designs were reviewed in Phase I but none seemed close to providing reliable operation at the conditions of this program.

Air Heater Materials – Convective – All surfaces of the Convective Air Heater (hereafter CAH) design for the 65% coal burning Prototype HIPPS system will operate at elevated temperatures in a highly oxidizing and corrosive environment. The inner surfaces will be exposed to the same oxidants and corrodants currently encountered in land based industrial gas turbine engines. Oxidation and corrosion of the external surfaces will be further exacerbated by the presence of "dry" coal ash and condensed alkali salts. Thus many of the same materials issues discussed above for the RAH must also be addressed for the CAH. These include base alloy selection, selection and screening of thin protective coatings, development and testing of joining techniques, and evaluation of repair technologies.

Metals and Coatings for the Convective Air Heater – The CAH will be fabricated from a wrought superalloy. The relatively weak iron base superalloy Alpha IV, exhibits outstanding resistance to oxidation and hot corrosion. This alloy is often considered as a candidate coating for the protection of stronger wrought and cast alloys. One approach for the CAH components is to strengthen this alloy without adversely affecting oxidation and corrosion resistance. In the event that additional high temperature strength is required, the primary candidate materials will be the stronger, less oxidation and corrosion resistant wrought nickel base superalloys. These alloys will require thin coatings for protection from coal ash deposits and alkali sulfate condensates. The various coating materials and techniques are described in the previous section.

The CAH panels will require joining and sealing to headers and support structures. The use of finned tubes would require manufacturing development efforts to establish low cost fabrication technology. Techniques for welding wrought alloys are discussed above. Welding will also be considered as a repair technique for this component.

Partial Ceramic Construction for Growth to All Coal Case – Issues surrounding the use of structural ceramics were described in Section entitled **All Ceramic Construction for Growth to All Coal Case** above. The CAH may or may not need protective coatings or linings if constructed from structural ceramics such as sintered silicon carbides, even at the higher operating temperatures dictated by the all coal combustion case. Techniques for joining and sealing would require development, again as described above. As part of any Phase II effort, technological progress in the area of fabricating large complex shapes from silicon carbide structural ceramics will be monitored, and if significant progress is made, these materials will be given renewed consideration for HITAF CAH construction.

Another option for growth to the all coal combustion CAH would be to transfer materials and design technology from the RAH. The RAH materials will be proven (in 65% coal design) for operation at the higher temperatures expected in the all coal CAH.

Refractory-Superalloy Compatibility Tests — Gaseous Reaction Products — Gases are released whenever coal slags or ashes are reheated. The weight change associated with the thermal decomposition of Illinois No. 6 slag and ash as well as Rochelle ash were experimentally determined. The Rochelle and Illinois ashes are stable up to 900°C (1650°F), after which they exhibit a continual weight loss until liquidation occurs at approximately 1300°C (2370°F). The Illinois slag differs in that it exhibits a continual weight loss until about 900°C (1650°F), after which the material gained weight consistent with an oxidation process. The chemical composition of the ashes and the experimental data are shown in Table 4.2-5 and Figure 4.2-7, respectively.

Experiments were performed to evaluate the degree of interaction between the metal and the candidate ceramics in contact with the products of decomposition of ashes and slags. The experimental apparatus to assess the potential for corrosion is sketched in Figure 4.2-8. The position of the metal and slags or ashes are shown and the reaction cavity in the lid allows the gases generated to simultaneously contact the ceramic and the metal.

The appearance of the superalloy, after exposure for 336 hrs at 2000°F, and the ceramics (fusion cast AXS and bonded fused grain chromia alumina) with Illinois No. 6 slag or ash or Rochelle ash are shown in Figure 4.2-9.

The interactions between the ceramic and the gases generated from the slags and ashes was assessed based on metallographical examination. For comparative purpose, specimens of the superalloy were exposed in the same furnace, and the microstructure of the "blank" after test, is shown in Figure 4.2-10. The high strength oxidation resistant alloy formed a thin oxide scale, separated from the unaffected matrix by the normal depleted zone, which is approximately 1.2 mils thick. The metallography associated with the superalloy in the AZS refractory exposed to the decomposition products of the Illinois ash, Illinois slag and Rochelle ash, and the superalloy in the bonded fused grain chromia-alumina refractory exposed to the same conditions, is shown in Figures 4.2-11 and 4.2-12, respectively. In summary, the microstructure for all of the specimens is comparable. It appears that the decomposition products of the candidate ashes and slags are relatively innocuous with respect to the metallic substrate.
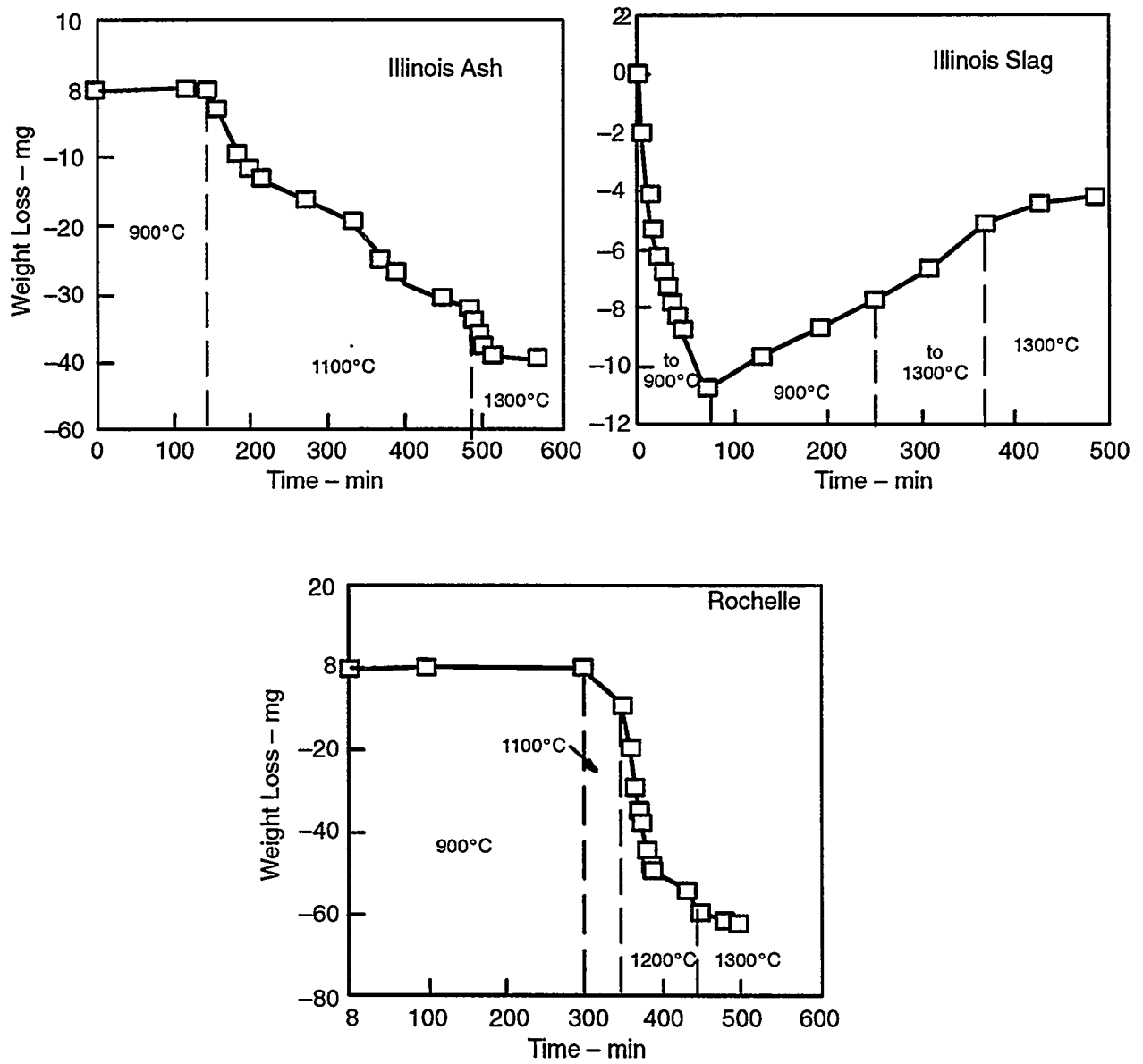
Figure 4.2-7   Thermal Decomposition of Selected Ashes and Slags.

Candidate
ceramic

lid

reaction cavity

base

nickel Superalloy
B-1900

Candidate slag or
ash
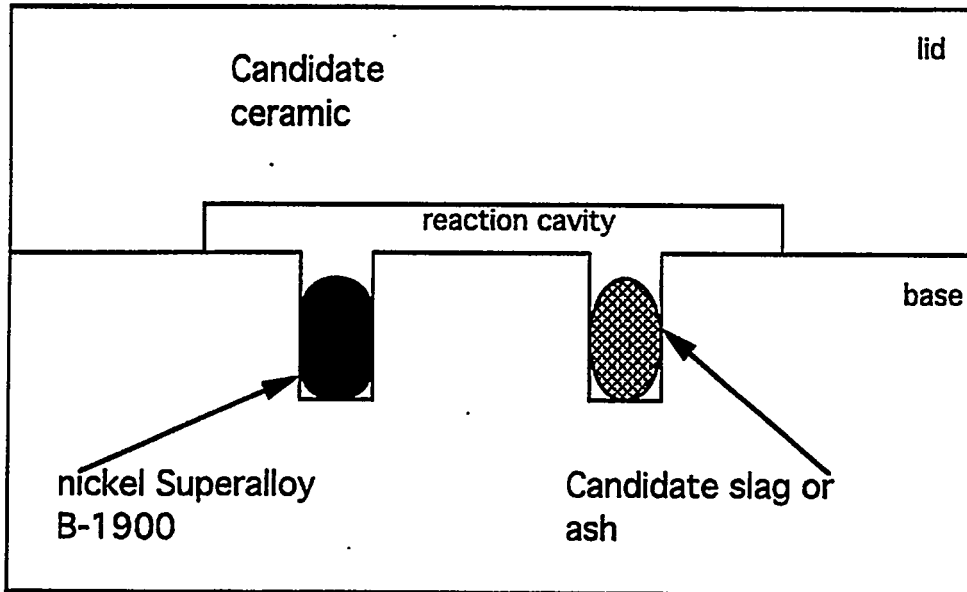
Figure 4.2-8   Gaseous Compatibility Studies.

113
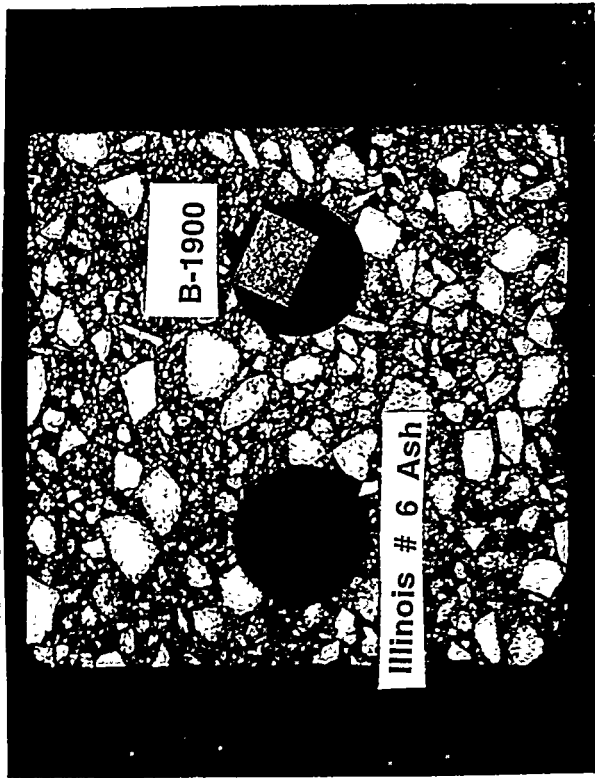
3X

Illinois No. 6 Slag

3X

Illinois No. 6 Ash

3 x

Rochelle Ash

Figure 4.2-9a Gaseous Compatibility Studies – Bonded Fused Grain (336 hrs – 2000°F).

114

3X

Illinois #6 Slag

Illinois No. 6 Slag

3X

B-1900

Illinois #6 Ash

Illinois No. 6 Ash

3X
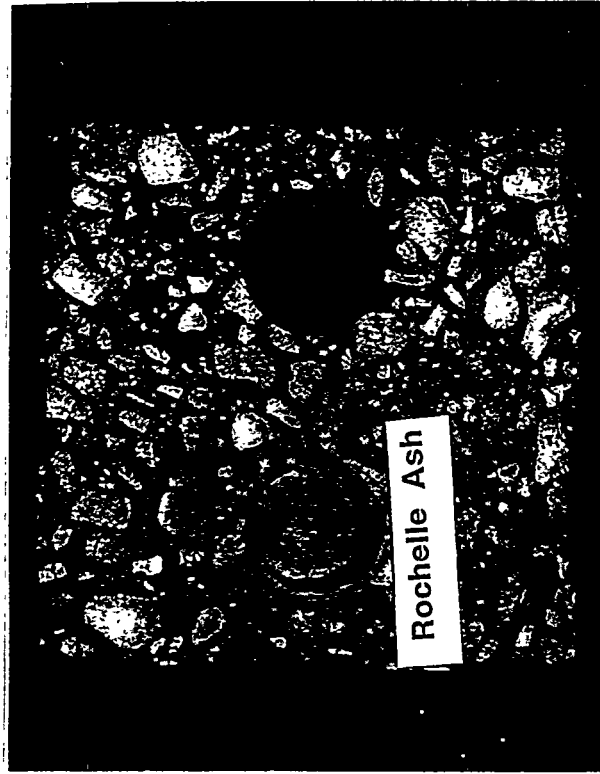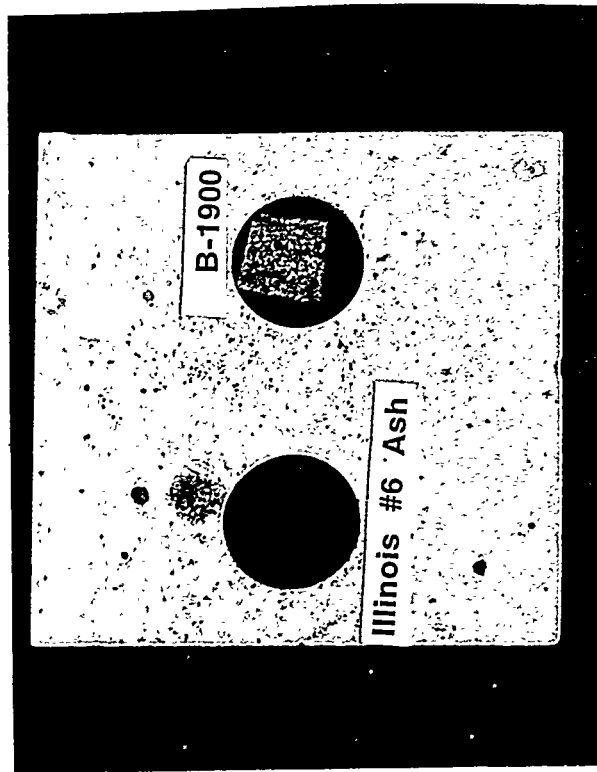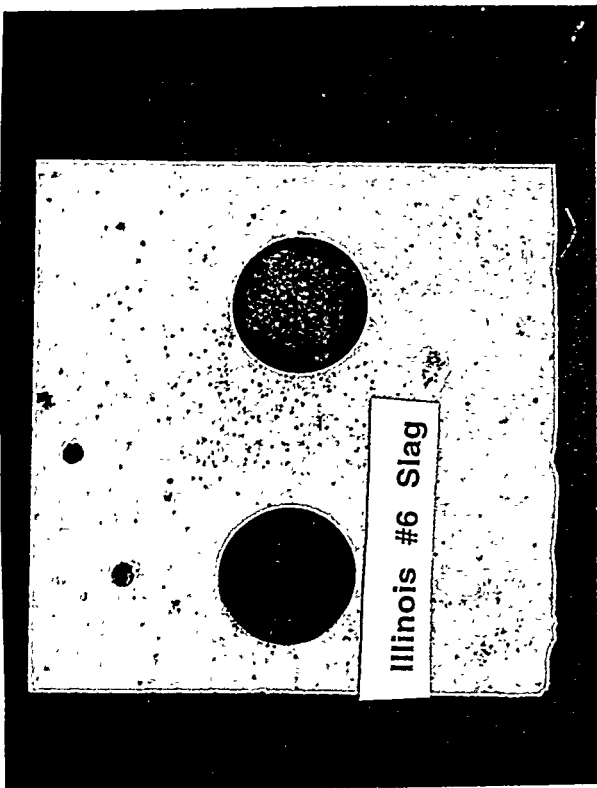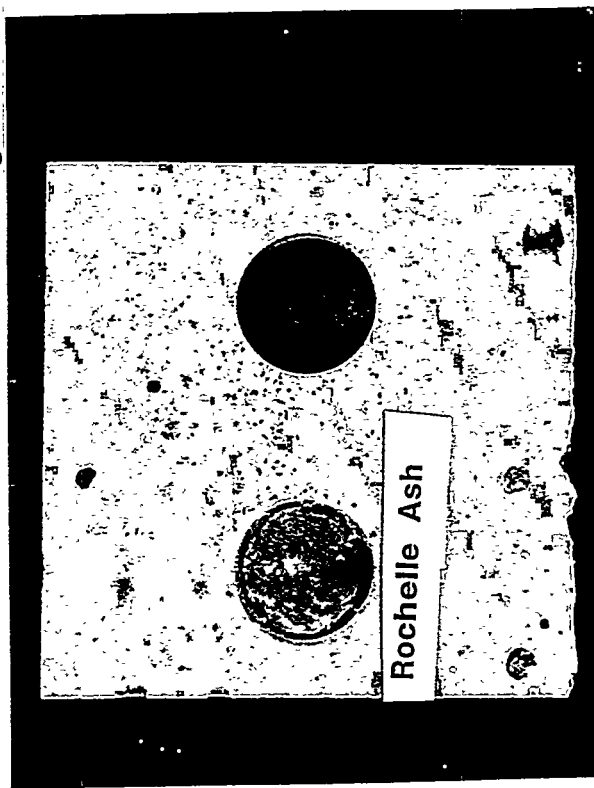
Rochelle Ash

Rochelle Ash

3X

Figure 4.2-9b Gaseous Compatibility Studies – Fusion Cast AZS (336 hrs – 2000°F).

115

100X

Oxide Scale

Denuded Zone
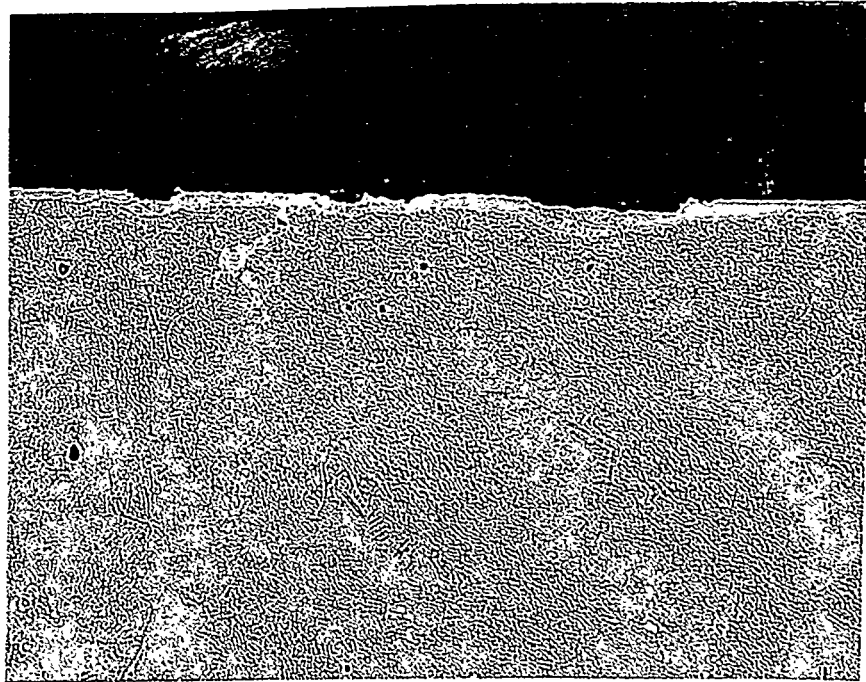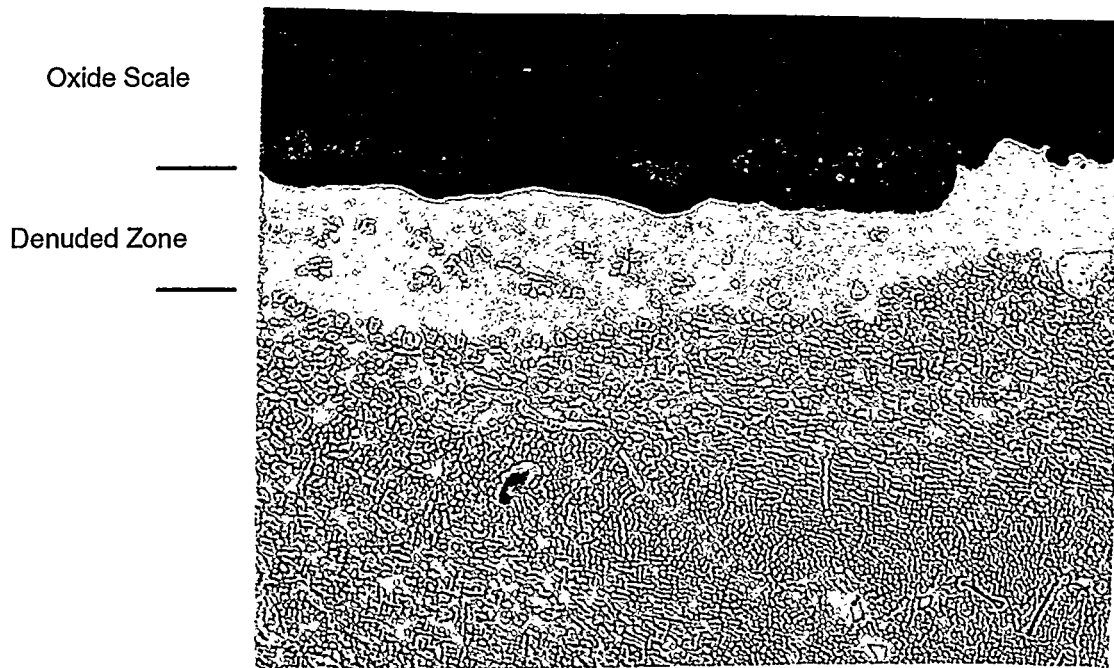
500X

Figure 4.2-10   Microstructure of B-1900 Exposed for 336 hrs at 2000°F.

116

500X

Illinois No. 6 Ash

500X

Illinois No. 6 Slag

500X

Rochelle Ash

Figure 4.2-11 Microstructure of B-1900 in AZS, Exposed 336 hrs at 2000°F to Decomposition Products of Coal Ashes and Slags.

117

Illinois No. 6 Ash   500X   Illinois No. 6 Slag   500X
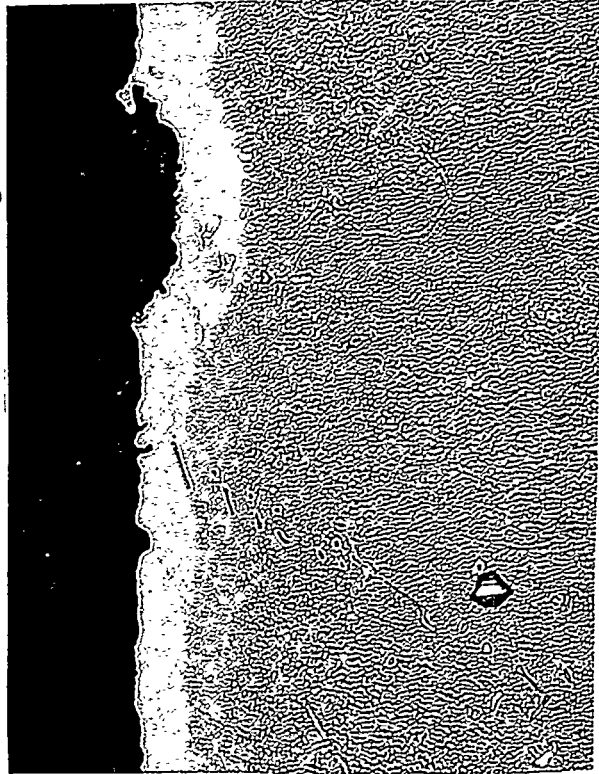
Rochelle Ash   500X

Figure 4.2-12 Microstructure of B-1900 in Bonded Fused Grain Chromia-Alumina Exposed 336 hrs at 2000°F to Decomposition Products of Coal Ashes and Slags

118

TABLE 4.2-5 CHEMICAL COMPOSITION OF CANDIDATE ASHES AND SLAGS[1]
(WEIGHT PERCENT)

Oxide	Illinois No. 6 Ash	Illinois No. 6 Slag	Rochelle Ash
SiO_2	48.12	52.89	38.73
Al_2O_3	18.63	16.57	17.13
Fe_2O_3	16.93	12.92	6.26
TiO_2	0.85	0.72	1.35
P_2O_3	0.18	0.17	0.89
CaO	5.18	12.95	22.17
MgO	1.42	1.27	5.58
Na_2O	0.57	0.84	1.38
K_2O	1.82	1.57	0.14
SO_3	6.31	0.1	10.40
[1] EERC Data			

Ceramic-B-1900 Compatibility — At elevated temperatures, the oxides that form on the surface of the nickel base superalloy will interact with the ceramic and elements present in each matrix will interdiffuse. The driving force is established by the relative activities of the elements in each matrix. In order to evaluate the compatibility of the alloy with the ceramics, the alloy must be in intimate contact with the ceramic. Advantage is taken of the differences in coefficients of thermal expansion of the materials. Intimate contact is achieved, as shown in Fig. 4.2-13. The chemical composition of the test ceramics is shown in Table 4.2-6

TABLE 4.2-6 REFRACTORY CANDIDATE

Ceramic	Cr_2O_3	Al_2O_3	MgO	SiO_2	Fe_2O_3	Na_2O	ZrO_2	Other
Fused Cast Cr_2O_3-Al_2O_3	27.1	58.6	6.1	1.6	5.9	0.3	–	0.4
Bonded Fused Grain Chromia Alumina	29.9	63.1	0.22	1.9	0.06	0.12	2.8	Bal
Fusion Cast AZS	–	45.5	–	12.2	–	1.0	41.0	Bal
Bonded Fused Grain AZS	–	49.5	–	18.5	–	1.0	30.0	1.0
Fusion Cast Beta Alumina	–	98.0	–	–	–	–	2.0	2.0

The metallic substrates, tightly wedged at temperature, contracts from the ceramic when the specimens are removed from the furnace. Visual examination, confirmed by metallographic analyses, indicate that for the two chromia rich ceramics, the bond fails at the metal-oxide interface. For the

metal

ceramic

0.250

0.625

0.750

1.50

0.25

0.50

1.00

2.00

front view

side view

a

B-1900 Alloy

0.650

0.125

0.25

b
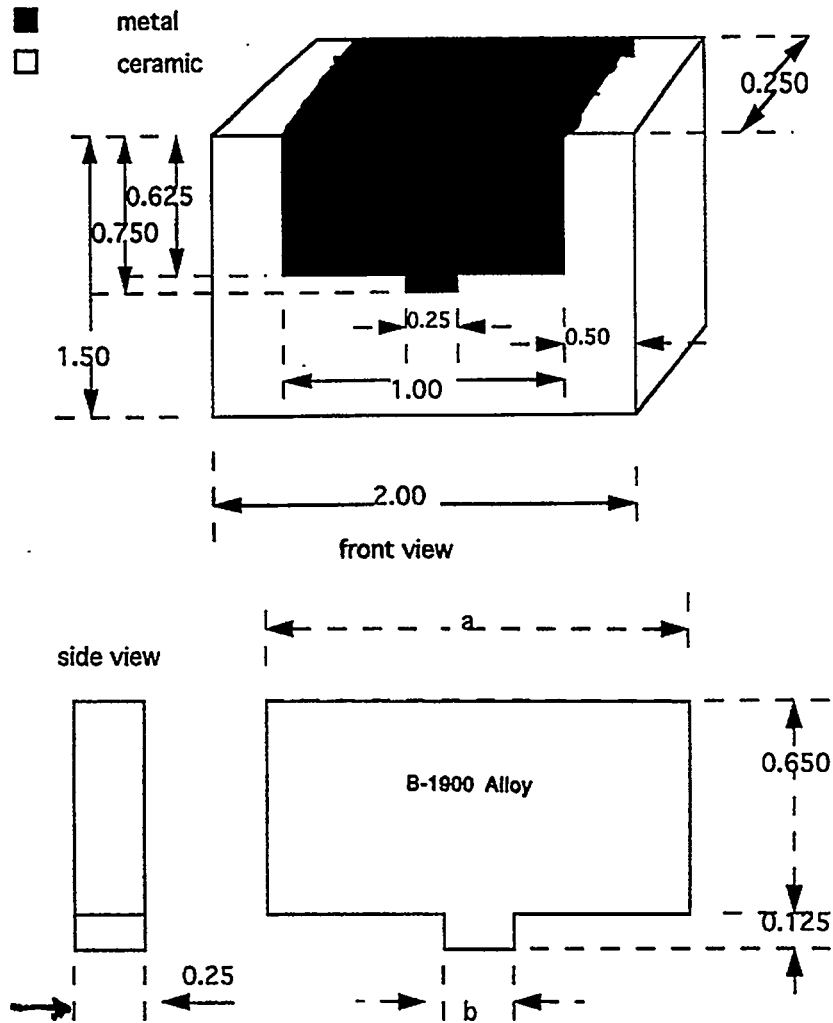
a inches	b inches	ceramic	Temp F
0.993	0.248	ER-300	1600
0.994	0.248	1711/Jm	1600
0.995	0.249	k3	1600
0.99	0.248	ER-300	1800
0.992	0.248	1711/Jm	1800
0.993	0.248	k3	1800
0.996	0.247	ER-300	2000
0.99	0.247	1711/Jm	2000
0.992	0.248	k3	2000
0.98	0.245	ER-300	2200
0.985	0.246	1711/Jm	2200
0.989	0.247	K3	2200

Figure 4.2-13   Compatibility Assessment.

120

others, debonding occurs primarily at the ceramic-oxide interface. This visual appearance of the specimens exposed at 2200°F is shown in Figure 4.2-14

In the depth of interaction of the superalloy and the ceramic is determined from the thickness of the "depletion" zone that separates the outer oxide from the unaffected substrate. The depletion zone is the result of diffusion of element(s) from the superalloy and the ceramic. Based upon the metallographic data, outward diffusion predominates for the couples between B-1900 and the ceramic candidates: (1) bonded fused grain chromia-alumina, (2) fusion cast chromia-alumina, and (3) fused cast beta-alumina. This conclusion is based on the visual identification of the row of Kirkendall voids within the depleted zone. The zirconia rich ceramics do not display any evidence of Kirkendall void formation. The depth of the depletion zones and the primary mode of separation of the B-1900 and ceramic candidates are summarized in Table 4.2-7.

TABLE 4.2-7 SUMMARY OF COMPATIBILITY DATA
(B-1900/Ceramic 2200°F)

Ceramic	Depth of Depletion Zone (mils)	Debonded at
Fused Cast Chromia-Alumina	7.0	B-1900 Oxide Interface
Bonded Fused Grain Chromia-Alumina	2.8	B-1900 Oxide Interface
Fusion Cast Beta Alumina	1.0	B-1900 Oxide Interface
Bonded Fused Grain AZS	1.0	Ceramic/Oxide Interface
Fusion Cast AZS	0.6	Ceramic/Oxide Interface

In summary, the important findings of the compatibility tests are as follows:

Accelerated oxidation (corrosion) related to the gaseous products of decomposition of coal slags and ashes is not anticipated.

A protective coating is needed if the preferred ceramic is represented by fused cast chromia-alumina or bonded fused grain chromia-alumina.

B-1900 is very compatible with fusion cast AZS, bonded fused grain AZS and fusion cast beta alumina.

An aluminide intermetallic compound will be used to extend the durability of B-1900 and perform as a compliant zone. The experimental data indicates that debonding of the alumina scale formed on the intermetallic compound will occur at the ceramic/oxide interface for the zirconia rich ceramic candidates. Although the development of Kirkendall porosity is of concern, the potential for premature disbonding can be largely attenuated through modification of substrate chemistry.

4.2.4 Air Heater Structural Modeling

Stresses in pressurized heat exchanger components occur due to three factors: 1) thermal gradients, 2) thermal mismatch, and 3) pressure. A representation of these effects are shown in Figure

Alloy Depleted
Zone

500X

Figure 4.2-14a Compatability Studies — B-1900/Fused Cast Beta Alumina

122

Alloy Depleted
Zone

500X

Figure 4.2-14b Compatability Studies – B-1900/Bonded Fused Grain Chromia-Alumina

123

Alloy Depleted
Zone

500X

Figure 4.2-14c Compatability Studies — B-1900/Fusion Cast Chromia-Alumina.

124

Alloy Depleted
Zone

500X

Figure 4.2-14d Compatability Stuies – B1900/Bonded Fused Grain AZS.

Oxide Scale
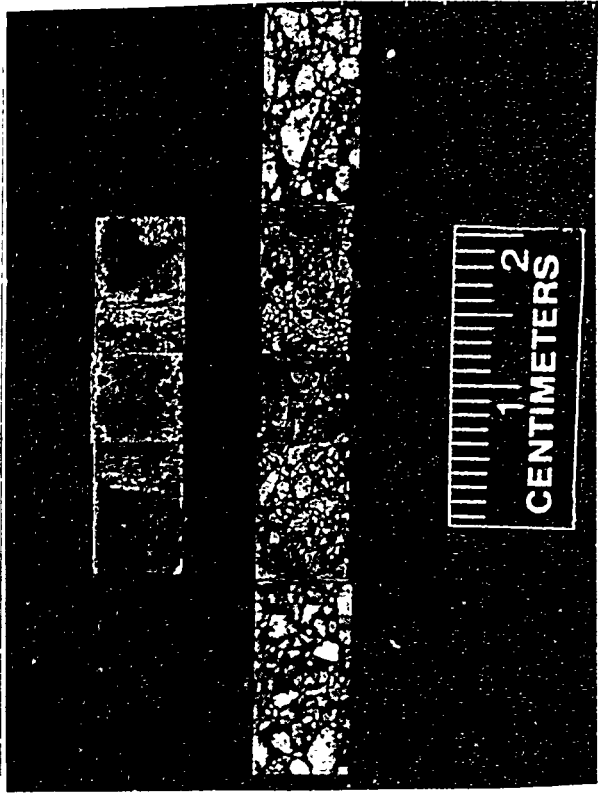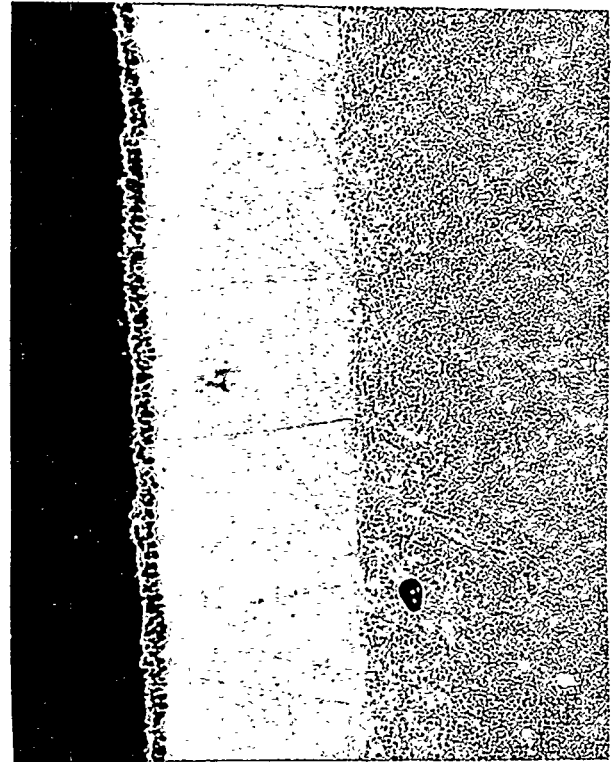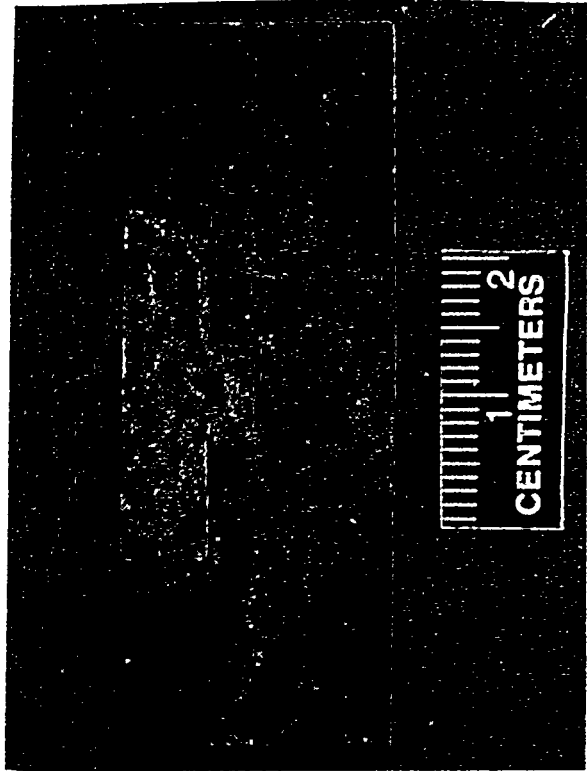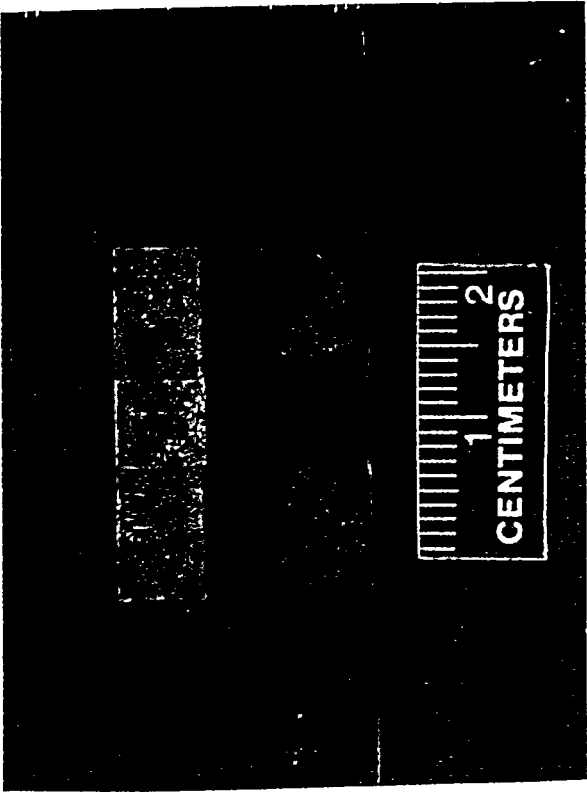
Alloy Depleted
Zone
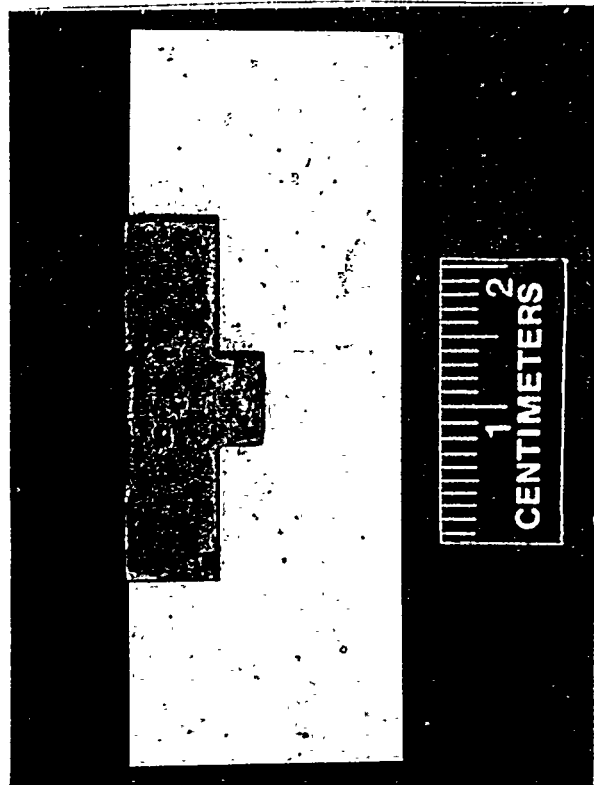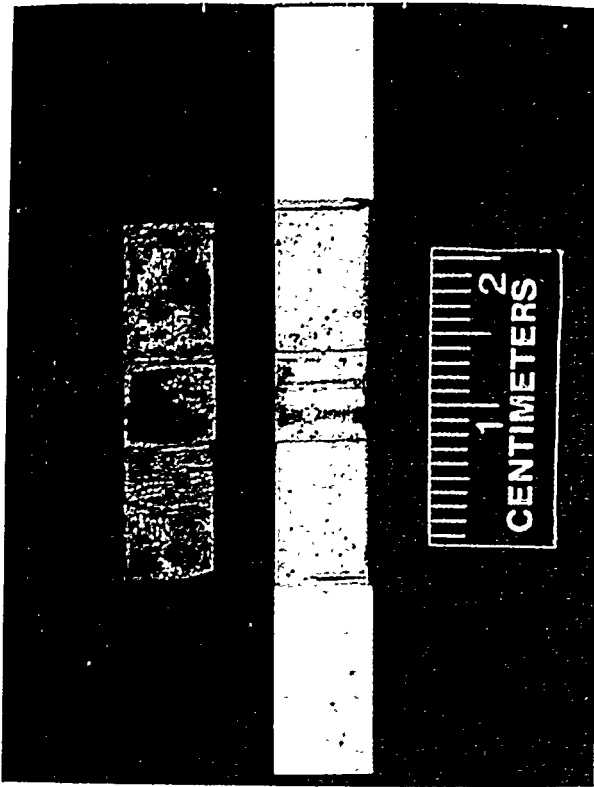
Figure 4.2-14e Compatability Studies B-1900/Fusion Cast AZS.^{500X}

4.2-15. Thermal gradient stresses occur when significant temperature changes occur across small distances, such as a tube wall. Thermal mismatch occurs when two different materials attached at an interface experience a temperature change. Since the materials want to expand differently, a thermal fight ensues causing stress. Thermal mismatch is typically found in layered or coated structures, such as a tube or panel with a refractory coating. Pressure and other applied loads cause stress either locally at a support point, or globally as in a pressurized tube.
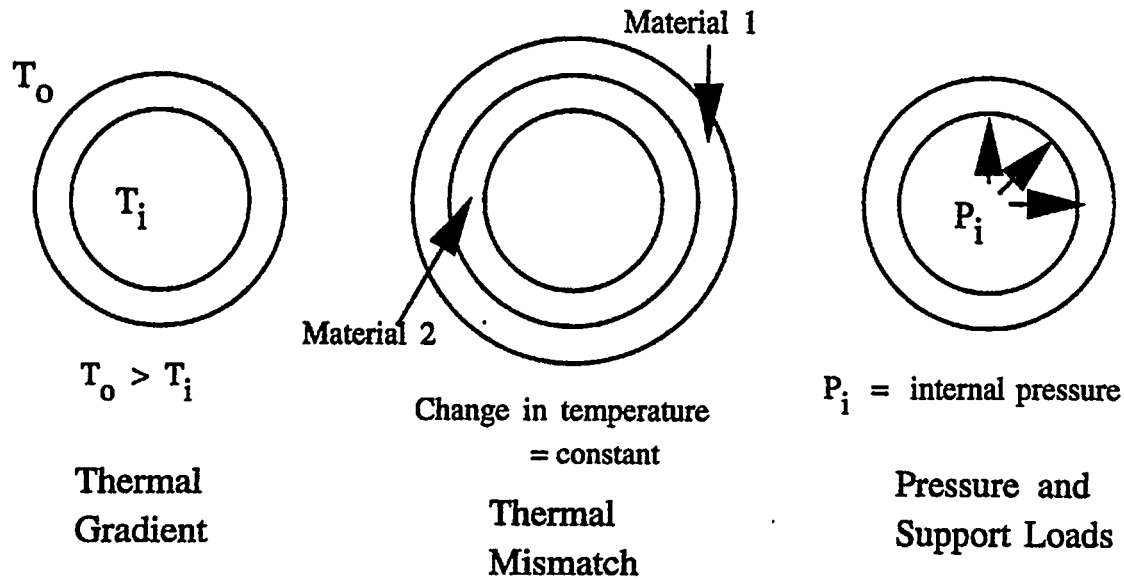
Figure 4.2-15   Three Sources of Stress in Air Heater Components.

Modeling of air heater components, consists of three main steps. The first step is the prediction of the temperature distribution throughout the component using heat transfer finite element analysis. The geometry, thermal material properties, and thermal environment must be accurately defined to obtain physically-realistic results. In the second step, a thermal stress analysis is performed using the temperature distribution from step one as the thermal loading. In addition, all support constraints and any additional mechanical loading, such as pressures, must be defined. Temperature-dependent material properties must be used, due to the severe thermal environment. Nonlinear creep effects will be included in the analysis. Results from the thermal stress analysis consist of displacements, strains and stresses throughout the component.

Step three is the prediction of the service life of the component using the current design. Ceramic materials exhibit brittle failure, and therefore life prediction is typically described using probabilistic failure analysis. In probabilistic failure analysis, a large number of ceramic specimens are loaded to failure, and the failure stresses are used to define a Weibull failure curve. Based on the stress results, the probability of survival of the current component design is determined.

Metal materials exhibit ductile failure, and a deterministic failure method can be employed. The stress level in the current design can be compared to the yield stress to determine if plastic deformation and yielding have occurred. If stresses are below yield, the life can still be limited due to creep effects. Creep is the progressive deformation of a material at constant stress, encountered in temperature ranges that are typically 0.35 to 0.70 times the melting point. Permanent strain from creep will occur over time, and can lead to eventual failure by rupture. Even if rupture does not occur, the stress will relax, thus changing the reference temperature of the material. This change will cause residual stresses to be present after cycling to room temperature, and these stresses will also be calculated to determine their effect on life.

Joint and seal design provides an additional technical challenge. Due to the severe thermal environment and size of the components, a large amount of movement must be permitted at joints, yet structural integrity must be achieved and leakage must be kept to a minimum. Structural analysis can predict the material behavior at a joint, but leakage rates can only be estimated, and testing will be required to obtain a final design. In the following sections, the technical issues concerning the convective and radiative air heater designs are presented. Preliminary design concepts with sample stress and life calculations are shown and compared to more traditional or existing designs. Discussions of preliminary joint and seal design is presented, and experimental testing is described.

Convective Air Heater – The preliminary convective air heater design consists of a series of shell and tube heat exchangers is depicted in Figure 4.2-16. Hot gas combustion enters the convective air heater at 1800°F and exits toward the steam cycle at 1250°F. The air from the compressor is fed into the tubes of the convective air heater at 732°F, and exits toward the radiant air heater at 1300°F. The heat exchanger preliminary design has approximate dimensions of 2 feet wide by 26 feet long panels with tube wall thicknesses and fin thicknesses to be selected as part of the design process. Internal pressure in the tubes is assumed to range from 200 psi to 450 psi. The actual design pressure depends on the total system requirements.

The heat exchanger design must be able to withstand the high temperature levels, the thermal gradients through the wall thicknesses, and the internal pressure loading. Traditional shell and tube heat exchangers consist of round tubes connected by flat fins. This design has several disadvantages for this application, including high thermal stresses due to changes in temperature between hotter fins and cooler tubes, and the particulate build-up of ash in the irregularly-shaped external profile where the tube meets the fin. A proposed enhanced heat exchanger design consists of a shell and tube configuration in which the tubes are elongated to an elliptical shape with the same cross-sectional area as a round tube. The advantages of this design are an enhanced surface area on the hot gas side, reduced thermal stresses due to more efficient cooling, reduced ash particulate build-up, and better access to remove particulates. However, the elongated inner tube shape may incur large localized stresses due to the internal pressure. The proposed design effort will seek the optimized geometry, which could be a hybrid of the round and elliptical designs. Possible cross-sectional tube and fin shapes are shown in Figure 4.2-17.
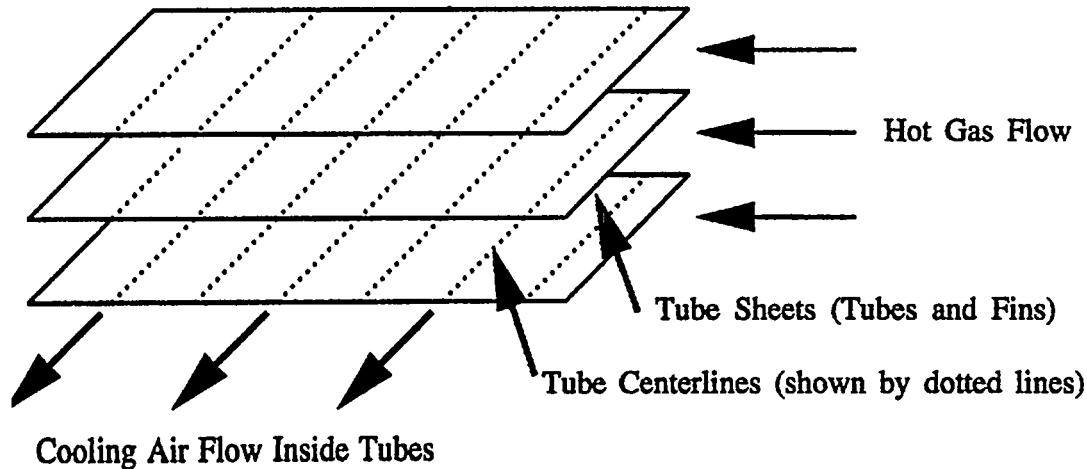
Figure 4.2-16   Convective Air Heater Design.

Circular Tube and Fin   Elliptical Tube and Fin   Hybrid Tube (Elliptical on
                                                            Outside and Circular on Inside)
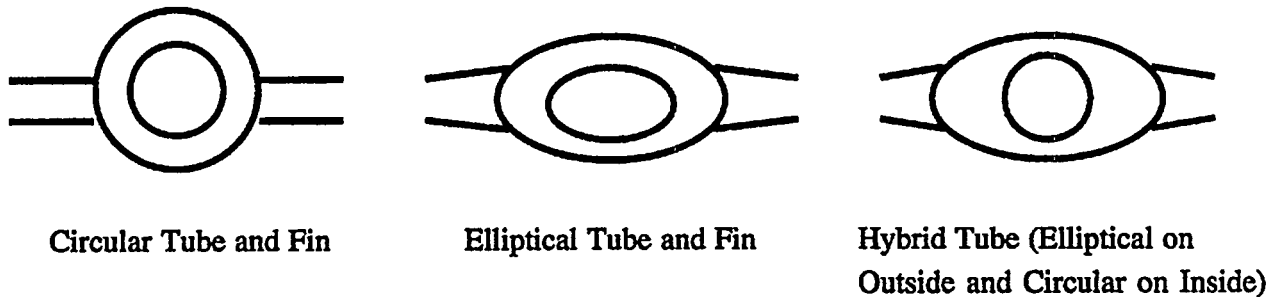
Fig. 4.2-17   Convective Air Heater Tube and Fin Designs.

Structural Analysis of Convection Air Heater – Preliminary finite element analyses have been performed to predict the stresses and subsequent life of shell and tube heat exchangers based on the thermal environment and pressure loadings assumed in the convective air heater. Assumptions used in this study are listed below.

1. Symmetry of geometry and loading is assumed, so only one-quarter of a shell and tube section is modeled.

2. A two-dimensional generalized plane strain representation is used to model the geometry. This formulation accounts for out-of-plane thermal expansion.

3. Worse-case hot-side steady-state conditions are used to define the temperature distributions

4. The tube internal pressure is 400 psi.

129

5. Silicon carbide is used in the ceramic design, and ALFA-IV ferritic stainless steel alloy is used for the metal design.

The steady-state thermal boundary conditions are entered into the analysis as convection conditions on the inner and outer surfaces of the air heater. These conditions consist of a heat transfer coefficient and a sink temperature. For the preliminary study, the following values are defined:

$$h_{in} = 1.91 \times 10^{-4} \; Btu/(sec-in.^2-{}^{\circ}F)$$

$$T_{in} = 1300{}^{\circ}F$$

$$h_{out} = 6.37 \times 10^{-5} \; Btu/(sec-in.^2-{}^{\circ}F)$$

$$T_{out} = 1800{}^{\circ}F$$

a. All-Ceramic Design Stresses

Figure 4.2-18 contains the finite element grid for the elliptical tube and fin geometry, with the temperature distribution from the hot region of the ceramic air heater superimposed. Both the temperature magnitude and range have been reduced compared to the circular tube and fin model. The maximum temperature is 1475°F, and the minimum temperature is 1448°F. The maximum stress component due to the thermal and pressure loading has shifted to the y direction at the inner radius of the tube and has a magnitude of 6.81 ksi. This stress is much higher than the round tube design and is caused by the pressure loading which has created a stress concentration region. Figures 4.2-19 through 4.2-21 contain the stress contours for the normal stresses in the x, y and z directions, respectively.

Although the elliptical design contains less severe temperature gradients than the circular design, the circular design is more suited to evenly distributing the stresses due to the internal pressure. An optimum design will most likely have a circular inner geometry and an elliptical external profile.

The finite element formulation used in this study is two-dimensional generalized plane strain, which assumes that the out-of-plane normal strain is constant over the cross-section. Thus a prediction of the total thermal expansion in the out-of-plane axial direction can be obtained based on the assumed length of the tube sheet. For example, assuming a 26 ft length of tube sheet, both configurations (round and elliptical) will expand 1.0 inch over a 26-ft section based on the hot side thermal conditions in the ceramic convective air heater. This information is useful for the design of joints and headers.

b. Life Prediction of Ceramic Convective Air Heater

The thermal and mechanical environment are used to predict the displacement, strains and stresses in the ceramic components. The life in terms of probability of survival can be estimated based on this information and ceramic failure data using the CARES/LIFE computer program. CARES (Ceramic Analysis and Reliability Evaluation of Structures) is used to calculate the fast-fracture reliability or failure probability of macroscopically isotropic ceramic components subjected to
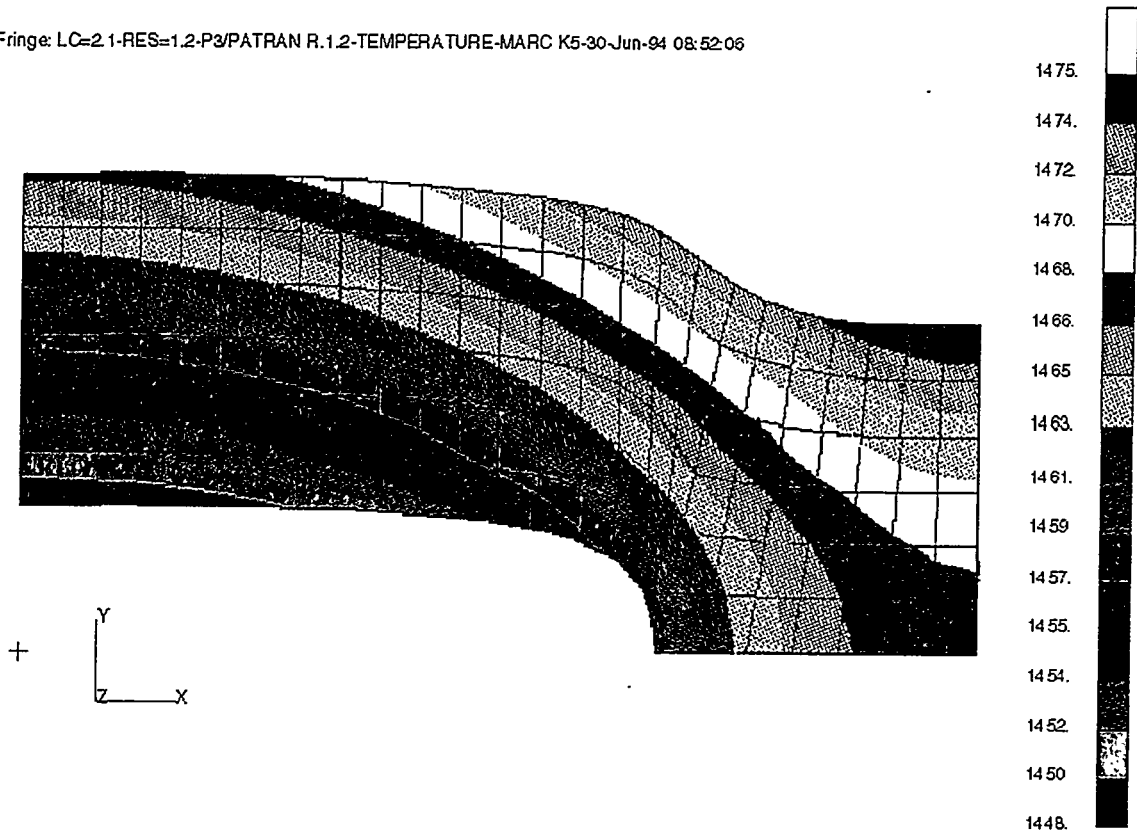
Figure 4.2-18   Temperature Distribution in Elliptical Tube and Fin Air Heater.

Figure 4.2-19   Normal Stress in X-Direction in Elliptical Tube and Fin.

131

| 6807. |
| 6141. |
| 5476 |
| 4810 |
| 4145 |
| 3479 |
| 2814. |
| 2148. |
| 1483. |
| 817.3 |
| 151.8 |
| -513.6 |
| -1179. |
| -1845. |
| -2510. |
| -3176. |

Figure 4.2-20   Normal Stress in Y-Direction in Elliptical Tube and Fin.

Fringe: LC=3.2-RES=3.1-P3/PATRAN R.1-(Tensor-ZZ)-MARC K5-30-Jun-94 08:54:22

| 1950 |
| 1701. |
| 1453. |
| 1204. |
| 955.1 |
| 706.4 |
| 457.7 |
| 209.0 |
| -39.65 |
| -288.3 |
| -537.0 |
| -785.7 |
| -1034. |
| -1283 |
| -1532 |
| -1781 |
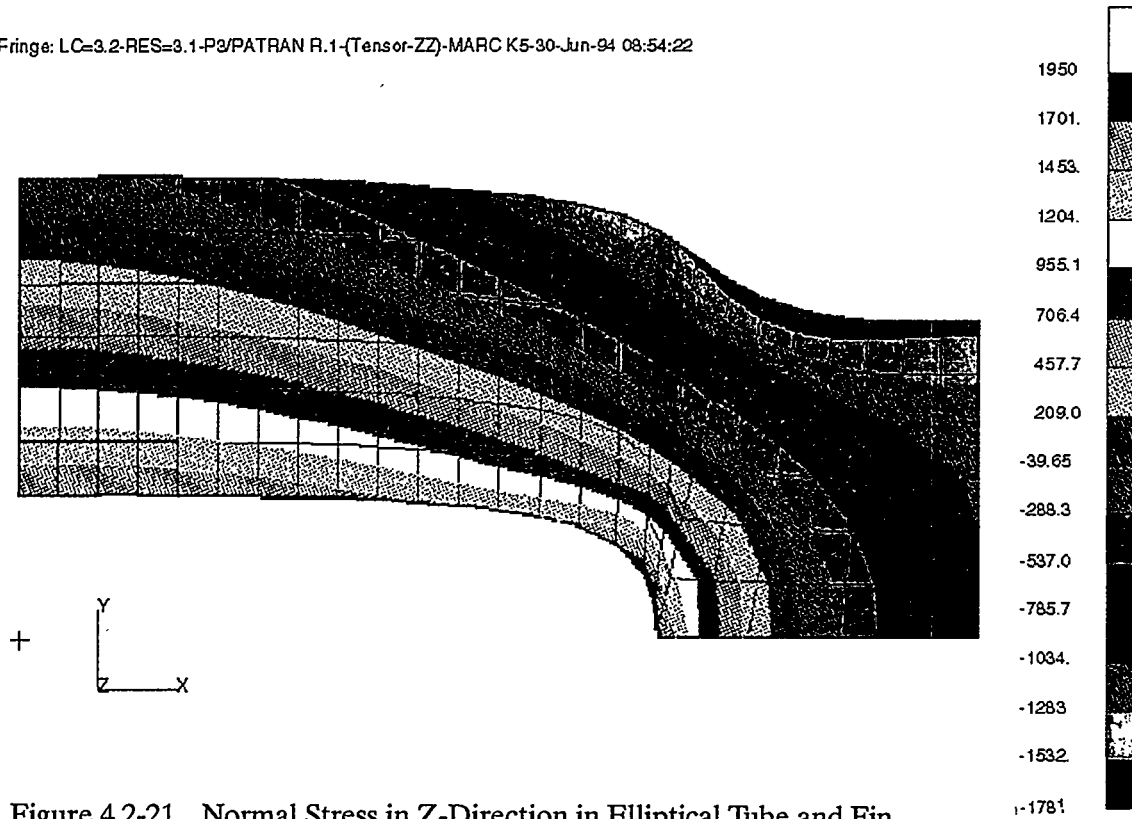
Figure 4.2-21   Normal Stress in Z-Direction in Elliptical Tube and Fin.

132

complex thermomechanical loadings. CARES utilizes the Batdorf model and the two-parameter Weibull cumulative distribution function to describe the effects of multiaxial stress states on material strength. CARES LIFE is an extension of the CARES code which calculates the time-dependent reliability of ceramics by utilizing the power or Paris law relations.

As an example of the use of CARES, an analysis was performed to determine the probability of failure of the circular tube and fin design. A MARC user-subroutine has been developed which automatically generates the input for CARES during a finite element analysis. Sample failure data for silicon carbide has been obtained and used to define the failure distribution. The failure data consists of 93 failure stresses ranging from 21.0 ksi to 31.75 ksi. Based on the finite element results, which contain a maximum stress of 2.06 ksi, the probability of failure predicted by CARES is one failure in 4.5×10^{15} for the quarter-section model. Since the actual tube sheet is assumed to be 2 feet wide and 26 feet long, the one-quarter section represents 119984 of an entire sheet. Therefore, the probability of failure of a tube sheet is one failure in 4.5×10^{11}.

Based on this study and its assumptions, the ceramic convective air heater tube sheets would be deemed acceptable. More detailed analysis, including support loads and headering conditions, must be performed to determine the final design and probability of failure.

c. All-Alloy Design Stresses

The same elliptical tube and fin design, boundary conditions and loads were used in an analysis of the convective air heater made of ALFA-IV, a ferritic stainless steel alloy. ALFA-IV is exceptionally resistant to oxidation at high temperature under both continuous and cyclic thermal conditions. The physical properties as a function of temperature are known and have been used in the analyses, including coefficient of thermal expansion, thermal conductivity, yield strength and modulus of elasticity. The analysis procedure used in this preliminary study assumes linear, elastic material behavior including temperature-dependent material properties. Therefore, the results will only predict if the elastic stresses exceed the yield stress, indicating plastic deformation of the air heater. The actual inelastic behavior is not modeled. However, the proposed design study will include non-linear analysis which will include yielding due to plastic deformation as well as other inelastic effects such as creep and rupture.

Results from the all-alloy analysis indicate that the main difference between the metal air heater and the ceramic air heater is that the metal air heater has a significantly higher temperature gradient than the ceramic air heater. For a round tube and fin design with 0.5 inch walls, the temperature varies from 1580°F to 1479°F, a range of 101°F. The temperature range in the ceramic air heater is 40°F.

The alloy and ceramic materials also behave much differently at high temperature. Ceramic materials typically do not exhibit a degradation of material properties at high temperatures, whereas the elastic modulus and yield stress of the alloy greatly decrease at temperatures in the range found in the air heater environment. For the round tube and fin alloy design with 0.5 inch thick tube walls and

133

assuming hot-side conditions and 400 psi internal pressure, the maximum predicted stress is 4.50 ksi, which corresponds to 78% or yield at that temperature range.

As in the ceramic analysis, generalized plane strain formulation was used, permitting the calculation of the thermal extension of the metal tube sheet along the tube length. For the hot-side conditions, a 26 foot section would expand 3.5 inches.

d. Life Prediction of Alloy Convective Air Heater

A deterministic approach is used for predicting life in metal structures, since failure in metals can be predicted with reasonable accuracy based on a maximum allowable stress level. As stated previously, the round alloy tube and fin design has a maximum stress that is 78% of yield and therefore remains in the elastic range under the assumed load condition. At elevated temperatures and pressures, additional effects can limit the life of metals even when loaded under the yield point. Creep occurs under these conditions, causing permanent deformation of the metal over time and possibly leading to rupture. Limited creep data exists for the alloy under consideration in this study. The data that is available is in the form of time to rupture as a function of applied stress and temperature. For example, at a temperature of 1562°F and an applied stress of 1.0 ksi, the ALFA-W alloy will rupture in approximately 400 hours, based on the data. This data indicates that for the worst case conditions modeled in this preliminary study, rupture will occur within 400 hours.

More detailed analysis and possibly experimental creep testing is required before determining the actual life prediction of the alloy tube sheet design. However, adequate life in an alloy design can be achieved by reducing the stress levels, reducing the temperatures, and selecting an alternate alloy that has improved high temperature strength and creep properties. The proposed analytical and experimental work will provide these improvements.

Radiative Air Heater — The radiant air heater consists of a large cylindrical or octagonal furnace that contains hot gas with air-cooled panels on the outer circumference. The inside region of the furnace contains pulverized coal and air heated at temperatures of approximately 3000°F to form a hot combustion gas. The circumference consists of a series of flat panels that will be approximately 2 feet wide and 60 feet long. The panels will be designed considering an all-ceramic and all-alloy construction. The panels contain passages to allow the flow of cooling air to facilitate the heat transfer. The surface of the panels facing inward toward the hot gas will have a refractory coating layer applied. In addition, refractory surface temperatures in excess of 2600°F will permit slag ash to flow over on the surface. A description of the radiant air heater design and a conceptual drawing are presented earlier in this Section.

The preliminary design of the system heat transfer assumes that the cooling air will enter the radiant air heater at 1300°F and exit at 1800°F. Although these temperatures may change as the design progresses, the air heater panel material will experience much higher temperatures than in the convective air heater. It can therefore be expected that the thermal gradients through the heater walls

will be significant, the refractory coating layer will provide a possible thermal mismatch with the air heater material, and the selected material must be able to withstand the cooling air pressure at elevated temperatures.

Structural Analysis of Radiant Air Heater – Due to the high temperatures, the design of the radiant air heater must be made in concert with the system heat transfer models and the material selection effort. A small change in the system heat transfer model will change cooling temperatures, which will change the radiant panel temperatures. Even small changes in material temperature at these elevated temperature levels may provide for much greater strength and life of a material, and even allow alternate materials to be used. Initial structural analysis has been performed to provide guidance in reaching a final design. Sample calculations, using analytical expressions and finite element solutions, will be described.

The first step in modeling the radiant panels is to predict the temperature distributions through all layers for various conditions in the radiant air heater using heat transfer calculations. Based on system heat transfer results, the gas temperature as a function of the air heater length and type of gas flow, parallel or counterflow, is predicted. This information, along with the flow conditions, is used to estimate heat transfer coefficients at the hot surface and in the cooling air channels. These data are then entered into a one-dimensional heat transfer analysis to determine the temperature distribution through the walls of the layers.

One example considered is a case of constant flue gas temperature of 2800°F, assuming parallel gas flow. The radiant air heater panels are assumed to have properties of ceramic material with a refractory coating. The two conditions which have been modeled will be considered here: axial locations x = 0 and x = 60 feet. Axial location x = 0 is where the cooling air first enters the radiant heater, and the air temperature is 1300°F. At the other end of the radiant heater at x = 60 feet, the cooling air temperature has increased to 1800°F. For this flow condition, no ash layers are present. Based on a one-dimensional finite element heat transfer steady-state solution with 1.0 inch refractory coating thickness and 0.25 inch thick ceramic panel walls, the following temperatures are predicted:

	x = 0 ft	x = 60 ft
Gas Temperature	2800°F	2800°F
Refractory Surface Temperature	2340°F	2510°F
Outer Surface of Air Heater Wall	1770°F	2120°F
Inner Surface of Air Heater Wall	1740°F	2100°F
Air Temperature	1300°F	1800°F

Based on additional heat transfer analyses, both ceramic and alloy walls range in temperature from 1700°F to 1800°F for the lowest temperature (1300°F) and from 2000°F to 2100°F for the highest air temperatures (1800°F). Increasing the wall thickness increases the wall temperature. Both

ceramic and alloy materials can be found to withstand temperatures between 1700°F and 2100°F. However, the air heater walls are subjected to stress caused by 1) thermal mismatch with refractory layer, 2) thermal gradients through wall thickness, and 3) internal pressure from cooling air.

The thermal mismatch is based on the amount each layer wants to expand from some initial stress-free state and the strength of the layers. The stress-free state can be estimated as the temperature at which the refractory is applied to the wall, since at that temperature the layers are bonded and are assumed to contain no stress. An estimate of this temperature is 1300°F. Thus, at operating conditions, the temperature rise that is used to produce stress can be as high as 700°F or more. In the case of the ceramic air heater panels with a refractory coating, the thermal coefficient of expansion is similar, although high stresses that will lead to cracking of the refractory coating are possible. For an alloy panel, the difference in thermal coefficient of expansion is much greater, and it is likely that the stress in the coating will lead to cracking.

One variation on the radiative air heater design that will be examined is to provide for a small gap between the panel and the refractory coating. The details of this configuration have not yet been identified, but the implications of separating the refractory from the panel wall are that thermal mismatch stresses will be eliminated. This is because both materials will be able to expand without being impeded by the adjacent layer. By separating the refractory coating from the air heater walls, the remaining sources of stress in the air heater walls are the thermal gradient through the wall and the internal cooling air pressure. As an initial analytical prediction of the stresses from these sources, a model was developed that combines these stress components. The model assumes circular passages, and the stresses due to a thermal gradient and internal pressure on a thick-walled cylinder are derived. The input to the model consists of the inner and outer radii of the cylinder, the internal pressure, the inner and outer wall temperature, and the material properties of the cylinder material defined at the temperature range of the problem. Using this simple model, effects on the stress and life of the component can be determined based on wall thickness, temperature gradient, internal pressure and material properties including temperature effects.

Parametric studies were performed to determine the effect of the different factors on the stress and life of the radiant air heater. Some results are obvious; for example, increasing the pressure and increasing the thermal gradient through the wall increase the stress. Also, increasing temperature range in an alloy design will decrease the elastic modulus, yield stress, and rupture stress. Increasing the thickness, however, increases the thermal stresses but decreases the pressure stresses. In addition, increasing the thickness will also increase the temperature gradient as well.

To illustrate the effect of wall thickness on stress in a cylindrical air passage, consider a cylinder constructed of a high-temperature alloy, in this case Haynes Alloy 230, subjected to an internal pressure of 230 psi. The cylinder has an inner radius of 0.5 inch, and the outer radius is varied between 0.6 and 1.5 inch. The inner and outer temperature for each case was calculated separately based on a heat transfer calculation of the radiative air heater system. The table below (Table 4.2-8) lists the inner

136

and outer wall temperatures, the total stress, and the components from thermal and pressure effects as a function of the outer radius.

The stress listed in the table is the maximum tangential stress in the cylinder, which occurs at the inner radius. The radial stress component is much lower than the tangential for this application.

Table 4.2-8 Stress in Radiant Air Heater Tubes

	Temperature (°F)		Stress Components (ksi)		
Outer Radius	Inner Wall	Outer Wall	Total	Thermal	Pressure
0.6	1739	1766	2.50	1.22	1.28
0.7	1731	1771	2.57	1.86	0.71
0.8	1723	1803	4.32	3.79	0.52
0.9	1715	1820	5.50	5.06	0.44
1.0	1708	1837	6.69	6.31	0.38

The results from the table indicate that the thermal stress increases as the thickness is increased, due to the larger gradients that occur. Note that the change in temperature across the wall is 27°F for a 0.1 inch wall, and 129°F for a 0.5 inch wall. The stress from the pressure loading decreases as the thickness is increased. Thus, for a 0.1 inch thick wall, the pressure stress is 1.28 ksi, which is over five times greater than the applied pressure of 0.23 ksi. It is indicated from the table that the thermal stress tends to dominate the behavior, and that a thin wall of 0.1 to 0.2 inch will provide the lowest total stress value of 2.5 ksi.

In the range of 1700-1800°F, the yield stress for Haynes Alloy 230 is approximately 20.0 ksi. All the stresses in the table are well below the yield stress of the material. Rupture stresses are also available as a function of temperature. For the current temperature range, the stress to cause rupture in 1000 hours is 6.0 ksi, and the stress to cause rupture in 10,000 hours is 3.5 ksi. The smaller outer radii meet this criteria and will not rupture in 10,000 hours, based on the assumptions in this study. The alloy used in this study contains rupture data which indicates that at 1900°F, the material will rupture at very low stress levels. Therefore, cooling air temperatures may have to be decreased to prevent temperatures in the panel walls from reaching 1900°F. Further structural and heat transfer analysis is proposed in the development of the radiative air heater. Simple calculations like those described herein will be used in the early design process to determine the feasibility of different conditions and different materials and configurations. As the design matures, more advanced two- and three-dimensional finite element analyses will be necessary. Probabilistic failure analysis for the all-ceramic design, and nonlinear creep analysis for the all-alloy design will be used to predict life.

Joints and Seals — In both convective and radiative air heaters, components will be manufactured in sections that must attach to other sections or to headers. At these connections, expansion of the material due to high temperatures must be permitted without creating additional stresses that would limit the life of the component. In addition, leakage of pressurized cooling air must

be kept to a minimum for maximum efficiency of the heat exchanger. Any materials used for sealing or joining purposes must perform in the high temperature environment in the air heaters.

Joints and seals will be designed much differently based on the selection of alloy or ceramic air heater components. Joining of alloy components can be achieved using welding of the alloy. Expansion at headers can be handled using more traditional methods, such as bellows or expansion pipe joints. Ceramic joints create a technical challenge, since welding cannot be used and many types of joints can create large local stresses which could crack a brittle material like a ceramic.

Finite element analysis techniques can be used to predict the behavior of joints. The finite element method can predict displacements, strains and stresses due to large movement and interaction of sections at a joint. Leakage rates can be estimated based on either deformed geometric configurations or on the final densities of seals. More accurate leakage predictions could be made using experiment.

Joints For Alloy Air Heaters – Alloy air heater components will deform and expand a large amount based on the temperature ranges designed for this application. To account for expansion on the order of inches, yet prevent air leakage from air heater tubes, welding of alloy sections is is a possible solution. The effect of expansion of air heater components can be minimized at joints by permitting large motion of the components without a large increase in joint stresses. A bellows geometry allows for large expansion without large stresses. A bellows geometry or an expansion loop in tube allows for large expansion without large stresses. This procedure is used in steam boiler applications and uses the same principle of allowing larger geometric displacement without large stress. Finite element methods can be used to determine stresses and life estimates of welded joints based on large amounts of expansion of the alloy components.

Joints For Ceramic Air Heaters – A preliminary investigation on the design of high-temperature, high-pressure seals for use in ceramic joints has indicated that this application is currently an unresolved problem. However, several potential designs for tube-to-tube and tube-to-header joints show promise.

For tube-to-tube joints assuming ceramic tubes, three designs have been identified as having a good chance of success, and are listed below:
- Glass-filled relaxing seal
- Silicon brazed permanent seal
- Spherical compression seal

The glass-filled relaxing seal consists of a concentric tubes with a glass fill in the interface. The glass exhibits viscous properties which allow the tubes to slide relative to each other longitudinally while maintaining a gas-tight seal. A silicon brazed seal is similar to the glass-filled seal, but silicon is used as the bonding agent instead of glass. This seal has great strength, but does not compensate for

138

thermal expansion. The spherical compression seal consists of a spherical seat on which rests an appropriately-shaped tube end.

For tube-to-header joints in ceramics, four proposed designs are listed:

- spherical compression seal
- fiber tube seal
- cemented tube seal
- fiber layer seal

The spherical compression seal works the same way as in the tube-to-tube application. The fiber tube seal consists of ceramic fibers wound around the section of the tube that extends through a header plate, which allow for expansion of the joint. The cemented tube seal has the same geometry as the fiber tube seal, but a phosphate-bonded alumina cement is used instead of the fiber wrap. This design does not allow for large expansion. The fiber layer seal is shown in Figure 4.2-22. In this configuration, a ceramic fiber layer is used to seal the joint in addition to providing a compliant joint. The ceramic fiber layer is on the inside of the header plate, and the pressure inside the header is used to press down on a plate with in turn compresses the ceramic fiber layer and sealing the joint.
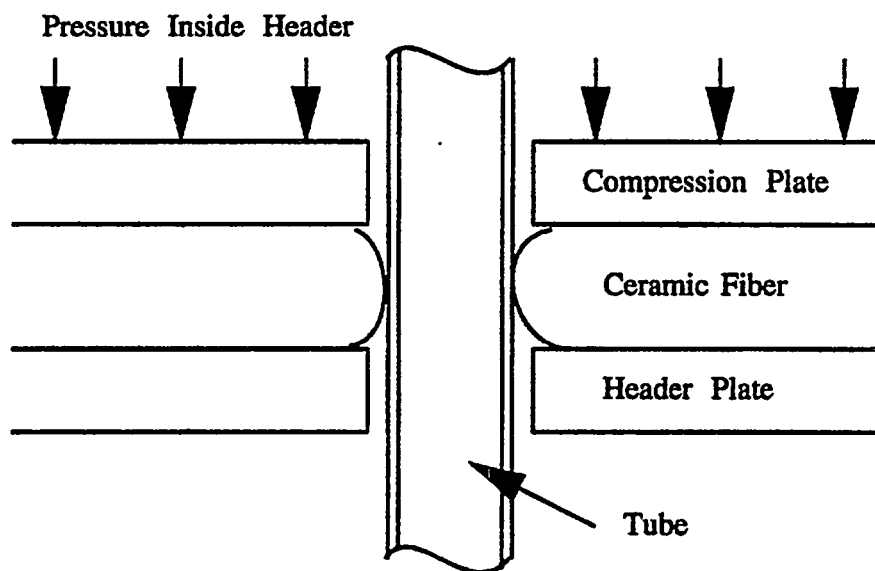
Figure 4.2-22 Fiber Layer Seal.

139

4.3 Ash Management and Solid Wastes

In order to explore the effect of coal type on the HITAF operation, four coals were chosen for study under Phase I. These coals were selected such that they were significant for the end user in that they will have large reserves. Only bituminous and subbituminous coals were selected as the unique combustion behavior of lignites typically requires a different combustor design.

4.3.1 Coal Selection

Although the ultimate goal is utilization of most U.S. coals, it is prudent to begin with a limited range and expand this as both ash research and the HITAF design progress. The goal of burning a wide range of coals can be met by careful design of the combustor and by selective use of cleaning or additives.

In p.c. boilers, coals are currently selected on the basis of several criteria including higher heating value, Hardgrove grindability, percent moisture, percent volatiles, percent ash, percent sulfur, and ash fusion temperatures. For western coals, percent alkali may be added to the list. Unfortunately, these criteria do not begin to address the particulate nature of deposit initiation, and as such, are insufficient for the proper development of a HITAF system.

Percent ash is useful only in assessing the quantity of ash that will need collection and disposal; it does not address the issues of deposition propensity or corrosion. Percent sulfur is a rough indicator of the pyrite level of coals, but provides no information as to whether pyrite is included and hence prone to form corrosive iron aluminosilicates, or excluded with the potential for deposition of iron oxysulfides within the combustor. Ash fusion temperatures help define the temperature at which a slag layer will flow, but provide no information as to whether that layer will be comprised of all the ash constituents contained within a coal. Each individual ash particle formed during the combustion process will have a viscosity-temperature relationship that differs, sometimes by hundreds of degrees, from the bulk viscosity-temperature relationship as expressed by the ash fusion temperature.

Based upon preliminary HITAF designs, conditions in the furnace and air heater have been defined. The ash management issues that affect coal selection can be summarized in terms of potential problems as follows:

1. Corrosion of alloys and refractories by liquid slag at the high temperatures characteristic of the radiant zone surfaces;

2. Corrosion of alloys or ceramics by alkali, particularly sodium at temperatures characteristic of the convective air heater;

3. Formation of liquid slag throughout the radiant air surface in the primary HITAF combustion chamber; and

4. Formation of ash deposits that can easily be removed *on-line* which reduce heat transfer in the convective air heater.

The slagging tendency of a coal in conventional p.c. boilers is evaluated using the ash fusion temperature and one or more empirical indices. One common index is the base-to-acid ratio which is the ratio of basic oxides to acidic oxides in the ash (based on bulk ash composition).

$$R_{b/a} = \frac{Fe_2O_3 + CaO + MgO + K_2O + Na_2O}{SiO_2 + Al_2O_3 + TiO_2}$$

The oxides are expressed as weight percent of the ash. The value of $R_{b/a}$ for most bituminous coals falls between 0.2 and 0.4. To prevent slagging in p.c. boilers, a maximum value of 0.5 is sometimes specified. For cyclone-fired boilers, on the other hand, flowing slag is essential and the value of $R_{b/a}$ should exceed 0.27. An alternate measure of the ability of slag to flow is the ash fusion temperature or the temperature at which the ash attains a viscosity of 250 poise (T_{250}). The latter index should be less than 2600°F for cyclone-fired boilers.

Ash fusion temperature and T_{250} help define the temperature at which a slag layer will flow, but provide no information as to whether that layer will be comprised of all the ash constituents contained within a coal. They also imply that ash particles or molten slag are homogeneous materials which can be described by a single composition. Each individual ash particle formed during the combustion process will have a viscosity-temperature relationship that differs, sometimes by hundreds of degrees, from the bulk viscosity-temperature relationship as expressed by the ash fusion temperature.

High values of $R_{b/a}$ have been associated with high corrosion rates for certain ceramics, although it is not clear if this effect is due to low ash viscosities associated with high base to acid ratios or the chemical interactions with the deposit. The base to acid ratio based on the bulk ash composition will give an indication of the corrosivity of the ash. A maximum value of $R_{b/a}$ may be specified to avoid corrosion.

Corrosion of metals and silicon carbide by alkali vapors has been well documented in the literature. Experiments have been conducted under more severe conditions than expected in a coal combustion system, however. At this point, it is not possible to define a clear specification for sodium in coal. The ratio of sodium to silica in the coal ash was used as a preliminary specification.

Clearly, coals which avoid the above problems will be easier to work with in the initial stages of the program, enabling HITAF design and materials development to proceed as required. In the later stages, coal preparation and HITAF aerodynamic modifications will be employed to expand this range. Some knowledge of ash particle size and composition is therefore essential to the coal selection task.

The coals chosen should be significant from the end user's point of view in that such coals will have large reserves. At this stage, lignites will not be considered. The combustion behavior of lignites is substantially different from bituminous coals and this usually implies a different combustor design.

141

Restricting the search to bituminous and subbituminous coals includes almost all the important U.S. reserves.

Fourteen coals were chosen (Table 4.3-1), representing ten different seams; in some cases data are presented for seams which have different names but which are considered to be geologically equivalent. Much of the data were obtained from CQIS, including several recent entries from the DOE/EPRI Coal Quality Expert project. Other coal data sources included DOE Report DOE/PETC/ TR-90/7 and the 1992 Keystone Coal Industry Manual, as well as data provided by PSIT and EERC for certain coals. Each data set contains four types of information:

- Standard analyses for raw and cleaned (if available) coals, including proximate analysis, ultimate analysis, ash composition, ash fusion temperatures, and grindability;

- Trace element analysis (for seven of the ten seams);

- Initial cleanability potential for all ten seams, based on float/sink washability analysis and amount of "near-gravity" material at selected specific gravities; and

- Some indication of the seam's reserve base and recent production trends.

TABLE 4.3-1 PRELIMINARY COAL SELECTION: PROPERTIES

Seam	Type	State	Raw % S	Raw % Ash	Clean % Ash	B/A	Na/Si
Upper Freeport	Bit.	PA	1.93	31.7	10.4	0.20	0.014
Pittsburgh 8	Bit.	PA	2.39	27.5	8.2	0.32	0.006
Pocahontas No. 3	Bit.	WV	0.70		10.9	0.12	0.01
Pocahontas No. 3	Bit.	VA	0.86	26.5	5.0	0.20	0.009
Cedar Grove/Alma	Bit.	WV	0.87	8.4	6.9	0.18	0.009
Pratt	Bit.	AL	2.13	25.9	11.0	0.25	0.011
Illinois No. 5	Bit.	IL	2.92	24.5	9.4	0.32	0.017
Kentucky No. 9	Bit.	KY	3.93	16.1	8.1	0.49	0.010
Illinois No. 6	Bit.	IL	4.61	18.5	9.0	0.44	0.009
Kentucky No. 11	Bit.	KY	3.78	35.4	10.1	0.33	0.017
Blind Canyon	Bit.	UT	0.49	10.3	4.6	0.26	0.079
Wyodak	Subbit.	WY	0.30	6.2	5.9	0.68	0.037
Wyodak/Anderson	Subbit.	WY	0.38	7.3	5.6	0.84	0.063
Rosebud/McKay	Subbit.	MT	0.78	10.7	9.0	0.43	0.032

Of the ten seams selected as candidate coals for this project, five are bituminous from the Appalachian Region, two are bituminous from the Interior Region, one is bituminous from the Western Region, and two are sub-bituminous from the Western Powder River Basin.

We chose up to four coals a) for materials testing and b) for a detailed coal cleaning study by CQ Inc. Note that the latter study will only involve conventional physical cleaning. We selected representative coals from major mines and from different regions in the country. Very high ash coals were avoided because at this point we do not know how difficult ash removal from the furnace or air heater will be. When a coal had very high ash, the ease of cleaning or data on cleaned coals provided by CQ Inc. was used to decide if the cleaned version is acceptable. High sulfur coals were deemed acceptable since we will scrub the SO_2 from the flue gas.

The Upper Freeport and Pratt coals were eliminated because of their high ash content. The Pittsburgh coal is marginal in terms of ash and we may want to consider it. The Pocahontas coals are cleanable, but based on PSIT experience they are difficult to ignite and burn out, so they were eliminated. Of the Appalachian coals, Cedar Grove/Alma is not known to cause any problems in operation and should be "safe" for operation of a non-slagging combustor. The Illinois basin coals all have high ash, but the ash is removed effectively by cleaning; the cleaned coals have less than 10% ash with reasonable energy recovery. The coals selected for testing or analysis were:

- Wyodak, subbituminous coal from the Powder River Basin;
- Blind Canyon, bituminous coal from Utah;
- Illinois No.6, bituminous coal from Illinois;
- Cedar Grove/Alma, bituminous coal from West Virginia.

Three coals were selected for a coal cleaning evaluation study in which the cost of cleaning by conventional means was calculated. The Wyodak and Blind Canyon coals would not benefit from conventional cleaning. The Illinois 6 and one other eastern coal (Pittsburgh 8) will be evaluated as discussed in the next section. The Cedar Grove coal will be evaluated in a similar fashion after data have been obtained from the coal company.

4.3.2 Coal Cleaning Evaluation

The important parameters for conventional coal cleaning are heating value, ash fusion temperature, ash reduction, and SO_2 emissions. In addition, the cost of cleaning coal must be weighed against the improved combustion or emission characteristics. Since the HITAF is not a conventional pulverized coal combustor, the desired cleaned product may differ from the conventional product. As the combustor design and ash management strategies become more clearly defined, the coal cleaning requirements will become more specific.

In this coal cleaning study, the following processes were considered. Heavy-media and water-only cyclones separate coal (with a specific gravity of about 1.25) from mineral fragments (with specific gravity of greater than 2). Froth flotation is then used to recover energy from the coal fines. The variables that affect the cost and energy recovery are crushed and topsize, cyclone geometry, heavy media specific gravity, and additives used in the flotation process.

One of five coal-cleaning process flow sheets were evaluated by CQ Inc. for each coal. The choice of flow sheet depended on the coal size.

1. Coarse jig plant in which fines and scalped off

2. Jig plus water-only cyclone

3. Heavy media vessel plus heavy media cyclones

4. Jig followed by water-only cyclone and froth flotation circuit

5. Heavy medial vessel, heavy media cyclones, plus froth flotation circuit.

PSIT and CQ Inc. selected conventional coal cleaning processes for consideration based on the cleanability definition in terms of a) total ash reduction, b) energy recovery, and c) decrease in detrimental ash constituents. CQ Inc. assessed the cleanability and costs of cleaning the specified coals and provided the following information:

• Washability comparison

• Trace element composition of cleaned coal and coal cleaning waste streams

• Select conceptual flowsheet designs

• Order-of-magnitude cost estimates.

To determine the capital cost and operating and maintenance (O&M) cost, the EPRI Coal Cleaning Cost Model (CCCM) was used. The CCCM is a workbook for engineers with limited cost-estimating experience to estimate the economics of coal cleaning processes to within an accuracy of ±20%. The CCCM requires that a flowsheet, plant feed rate, and the yield of each circuit within the flowsheet be determined first. For this study, a coal preparation plant flowsheet with coarse coal jig, water-only cyclone, and froth flotation circuits was selected. This is a very common circuit that can be successfully used to produce the required clean coal quality from easily cleaned coals such as the Pittsburgh Seam and Illinois No.6 Seam coals.

For this coal cleaning cost determination, the clean coal quality was required to have an ash content of less than 10%, energy recovery of at least 90%, and an annual output of 500,000 tons per year (tpy) at a heating value of at least 13,610 Btu/lb. The last requirement is to guarantee sufficient coal for the 270 MWe design plant. If a clean coal heating value of 13,610 Btu/lb could not be achieved, the annual output would be adjusted accordingly to achieve the required energy output. Using float/sink washability data of the two raw coals-Pittsburgh Seam and Illinois No.6-a plant simulation was performed to determine the clean coal quality and the yield. The results of the simulation are summarized in Table 4.3-2.

The simulator used for prediction of clean coal quality and quantity is the Coal Cleaning Simulator (CCS) being developed by Aspen Technology, Inc. of Cambridge, Massachusetts, under DOE Contract No. DE-AC22-89PC89908. The CCS contains models for conventional coal cleaning equipment: jigs, heavy media vessels, heavy media cyclones, water-only cyclones, spirals, concentrat-

ing tables, and froth flotation. Screens, classifying cyclones, and dewatering equipment are also part of the program. This program is currently the best-available, state-of-the-art coal cleaning simulator.

TABLE 4.3-2 RAW AND CLEAN COAL QUALITY OF SELECTED COALS

	Illinois No. 6	Pittsburgh
Raw Coal (dry basis except moisture)		
Total Moisture (Wt%)	9.5	11.7
Ash (Wt%)	15.4	27.2
Total Sulfur (Wt%)	4.4	2.2
Heating Value (Btu/lb)	11,771	10,741
SO_2 Emission Potential (lb/MBtu)	7.5	4.1
Clean Coal (dry basis except moisture)		
Total Moisture (Wt%)	5.3	7.2
Ash (Wt%)	10.1	9.4
Total Sulfur (Wt%)	3.2	1.8
Heating Value (Btu/lb)	12,661	13,765
SO_2 Emission Potential (lb/MBtu)	5.1	2.6
Performance		
Yield (Wt%)	89	70
Energy Recovery (Wt%)	96	90
Ash Reduction (%)	34	65
SO_2 Reduction (%)	32	37

CQ Inc. engineers configured the conventional coal cleaning flowsheet specific to this program. The flowsheet unit operations and the size fractions of coal that they process are:

- Coarse coal jig: top size x 3/8 in.

- Two-stage water-only cyclone: 3/8 in. x 0

- Froth flotation: 100 mesh x 0

Both cleaned coals were able to meet the ash and energy specifications. However, the cleaned Illinois No.6 Seam coal, with a heating value of 12,661 Btu/lb, did not meet the heating value specification equivalent to 500,000 tpy capacity. Therefore, the cleaning plant output was adjusted to 540,000 tpy (by increasing the operating time of the preparation plant) to achieve the design energy throughput.

Today, 500 tph cleaning plants are usually the smallest plants built due to the high costs associated with labor, O&M, and capital investment relative to the amount of coal processed; for these two cases, a plant feed rate of 500 tph was used for the simulation. With clean coal properties and yields as shown in Table 4.3-2, it would require a 500 tph plant cleaning Pittsburgh Seam coal to operate 1,681 hours per year, and a plant cleaning Illinois No.6 Seam coal to operate 1,428 hours per year, with both plants operating at 85% availability. Plant availability means the percentage of a day that the plant would produce clean coal, allowing for daily plant start up and equipment breakdown.

The CCCM estimates the capital cost of a preparation plant based on actual major equipment costs. From the selected flowsheet and a prediction of the circuit yields, a major equipment list was generated. Sizing and costing of the major equipment were determined from the CCCM. Equipment costs obtained from the CCCM are actual costs solicited from various equipment vendors. Installed in-plant equipment costs were determined by applying established construction factors to major equipment costs. Installed costs for out-of-plant equipment (coal receiving, storage, loadout facilities, etc.) were also determined by the CCCM. The CCCM does not attempt to address indirect costs such as financing, depreciation, taxes and insurance.

The CCCM estimated that the capital costs of a 500 tph cleaning plant would be $12.3M for the Pittsburgh Seam coal and $11.6 million for the Illinois No.6 Seam coal. Since the location of the plant is not specified, the capital costs of out-of-plant equipment may be different from those used in these calculations.

The O&M costs are shown in Table 4.3-3 in terms of the cost per ton of raw coal and the cost per ton of clean coal. The costs were determined by taking the annual O&M cost and dividing by the annual raw or clean coal tonnage, respectively. The total cost of the cleaned coal (dollars per ton) is determined by adding the cost of the raw coal to the cleaning cost shown in Table 4.3-3. For example, if raw Illinois No.6 Seam coal were purchased at $20 per ton, the total cost of the cleaned coal would be $22.20 per ton; costs to transport the cleaned coal to its final destination would be additional. Thus for these eastern bituminous coals, the cost of cleaning is reasonable, on the order of 10% of the coal cost, to produce a product with less than 10% ash and greater than 90% energy recovery.

TABLE 4.3-3 OPERATING AND MAINTENANCE COST SUMMARY FOR COAL CLEANING

	Illinois No. 6	Pittsburgh
Annual O&M Cost	$1,234,558	$2,252,857
Annual Raw coal Processed (Tons)	606,742	714,286
Cost Per Ton Raw Coal	$2.03	$3.15
Annual Clean Coal Produced (Tons)	540,000	500,000
Cost per Ton Clean Coal	$2.29	$4.51

4.3.3 Ash Deposition And Removal In HITAF

The High Temperature Advanced Furnace (HITAF) required to heat turbine inlet air to high temperatures has many features in common with conventional pulverized coal combustors. Yet there are certain key differences that necessitate a careful investigation of the management of ash in the combustor. In this section, the HITAF design is presented together with an overview of the processes affecting ash production, deposition, and removal. In subsequent sections, the deposition and removal mechanisms at critical points in the HITAF are investigated, followed by an overall ash mass balance in HITAF. The UTRC HITAF design has been discussed in Sections 4.1 and 4.2

146

At the heart of the HITAF design there will be a radiant air heater, composed of panels of alloy material. The panels will be covered with refractory, probably alumina or silicon-carbide castable refractory. Temperatures will be high enough in the radiant heat transfer section to allow slag to flow down the walls to a wet bottom collector. Flow of slag in the radiant section is discussed in more detail in a later section.

Injectors for burnout air and reburning fuel will be located in the radiant zone. Vitiated air or turbine exhaust will be used to convey the reburn fuel (finely pulverized coal) into the combustion chamber. A wet ash hopper will be located directly underneath the combustion zone. The wet hopper should be designed as short and fat as possible with a 30° slope into the seal box. The hopper will also be equipped with clinker grinders, pumps, water control, and transport conveyor.

At the bottom of the combustion zone, below the radiant panels, the combustion gases turn 90° to enter the dilution/quench zone. At this point, the cross section of the furnace changes from octagonal to rectangular. There will be a convergent section before the slag screen to increase the inlet gas velocity to approximately 200 ft/s. The combustion gases enter the slag screen at approximately 1800 K (2800°F). The slag screen is made of a staggered array of water-cooled metal tubes. Retractable sootblowers will be installed in the walls to clean the slag screen. Details of the slag screen design are presented later.

Following the slag screen, dilution is accomplished through injectors designed to deliver FGR and/or turbine exhaust into the duct at a velocity of 150 ft/s. Since the gas temperature at the inlet to the dilution zone will still be high (1700 to 1750 K or 2600 to 2700°F), the injectors must be protected from build-up of wet slag. The injectors will be designed for removal to clean slag as required. The temperature of the gas exiting the dilution zone will be 1370 K (2012°F).

Following the dilution zone, the gas turns and flows upward through a waterwall section with a cross section of 12.5 ft by 30 ft. The waterwall section is designed to reduce the gas temperature to 1256 K (1800°F). Wall blowers will be installed to remove the dry ash that accumulates on the walls. A dry ash hopper is located directly below the waterwall section. The hopper will remove ash which is blown from the water walls or the convective air heater. The sloped sides of the ash hopper are lined with waterwall surface. Above the waterwall section is the SNCR area in which urea is injected into the gas stream at a location allowing enough residence time for reduction of NO_x prior to the entrance to the convective air heater.

Flue gas flows upward through the convective air heater at an inlet temperature of 1256 K (1800°F) and leaves at 941 K (1234°F). Air is heated from 662 K (732°F) to 978 K (1300°F) in a two-pass, cross-counter flow heat exchanger consisting of parallel finned-tube sheets in the direction of hot gas flow. The tube sheets are made of alloy; each sheet contains 1 in. diam. tubes spaced 3 in. apart (center to center). Tube sheets are spaced 4 in. apart. Deposition and sintering of deposits in the convective air heater is described in detail in Section 3.4 Dry ash accumulation on the convective air

heater surface will be controlled by the use of retractable sootblowers. Ash will be directed into the dry ash hopper below.

Slag Flow in Radiant Air Heater

In the Combustion 2000 program, we need to model the flow of a slag layer on a hot, vertical wall in order to model heat transfer through the slag. The primary source for this is the Ph.D. work of Rodgers (1979) on flow of MHD slags. First, it is useful to discuss the critical viscosity of glasses which is necessary to understand the behavior of slag deposits.

Coal slags exhibit Newtonian flow at high temperatures. There is a sharp increase in viscosity below a certain temperature (Figure 4.3-1). This viscosity is called the critical viscosity and the temperature is denoted by T_{cv}. The rapid increase in viscosity as the slag cools is due to formation of crystals in the liquid. The critical viscosity for coal slag is in the range of 102 to 104 poise (Raask, 1985). As Figure 4.3-1 shows, the viscosity often shows some hysteresis from heating to cooling since formation and dissolution of crystals does not necessarily occur at the same temperature.
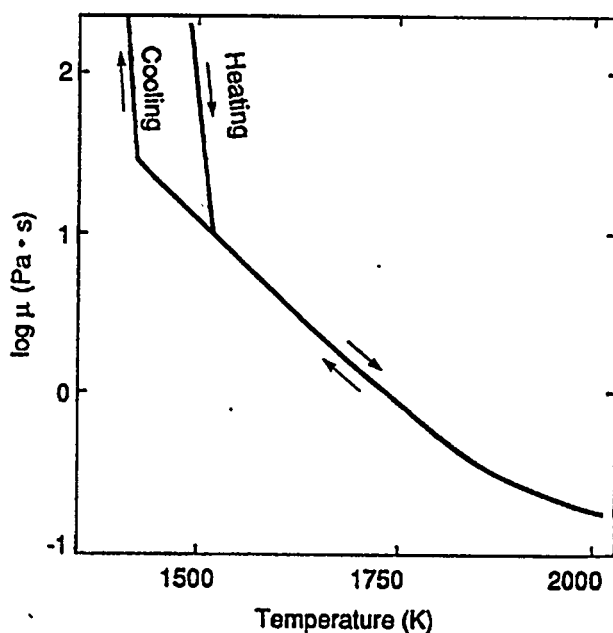
Figure 4.3-1   Viscosity of Coal Slags, after Raask (1985).

A glass can exhibit Newtonian behavior at temperatures below T_{cv} if it is cooled so as to prevent crystal formation. PSIT's viscosity database contains hundreds of viscosity measurements at these lower temperatures. These were made in the laboratory; slag deposits are a different matter.

The temperature of critical viscosity is a function of composoition. Hay et al. (1965) developed a

correlation for T_{cv}:

$$T_{cv}[K] = 3263 - 1470\alpha + 360\alpha^2 - 1478\beta + 0.15\beta^2 \qquad (1)$$

where $\alpha = SiO_2/Al_2O_3$, $\beta = Fe_2O_3 + CaO + MgO$, and $SiO_2 + Al_2O_3 + Fe_2O_3 + CaO + MgO = 100$ [wt%]

Figure 4.3-2 reproduces the viscosity-temperature curves for two slags taken from Reid and Cohen (1944). Below T_{cv}, the slags are Newtonian fluids. Between T_{cv} and T_f, the solidus temperature or freezing temperature, the slags show plastic behavior. Reid and Cohen also provided data on shear stress as a function of temperature. Table 4.3-4 provides T_{cv} and T_{250} for the program coals.
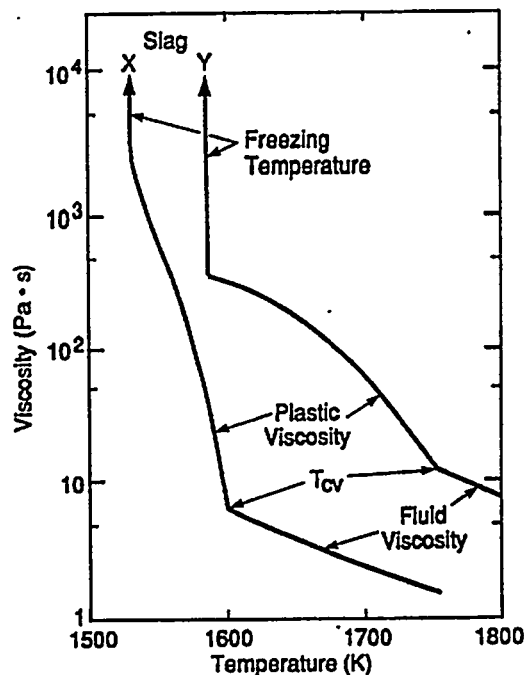
Figure 4.3-2   Slag Viscosity for Two Coal Slags from Reid and Cohen (1944).

Rodgers used these data to test some simplifying assumptions in his model of slag flow. The results of these calculations show us that as an approximation, the temperature of critical viscosity can be taken as an effective freezing temperature.

TABLE 4.3-4 CALCULATED VALUES OF T_{CV} AND T_{250} (OXIDIZING CONDITIONS)

Coal	T_{250} - K (°F)	T_{cv}, K (°F)
Wyodak	1475 (2195)	1414 (2085
Illinois No. 6	1790 (2762)	1498 (2237)
Blind Canyon	1760 (2708)	1637 (2487)
Cedar Grove	1820 (2816)	1617 (2451

149

Using the data of Reid and Cohen, Rodgers calculated the surface temperature and layer thickness for one of the flowing slags. This was called Case 1, the baseline, and should have been fairly accurate since it used actual viscosity and yield stress data. He then calculated several other cases.

Case 2. Slag "freezes" at T_{cv}: Newtonian flow at $T > T_{cv}$ and infinite viscosity at lower temperatures.

Case 3. Slag "freezes" at T_f: Reported plastic viscosity assumed for $T_f < T < T_{cv}$, but zero yield stress.

Case 4. No freezing: Newtonian viscosity and zero yield stress assumed for $T > 1200$ K.

The calculated slag layer thicknesses for the four cases are shown in Figure 4.3-3. The numbers in parentheses indicate the surface temperature. Cases 2 and 3 show similar layer thicknesses as Case 1 and have an error in the surface temperature of approximately 10 K. Case 4, on the other hand, shows much larger errors in surface temperature and layer thickness. Thus, assuming that the slag "freezes" at T_{cv} is a good approximation. The next level of complexity is to use a more sophisticated model of heat and mass transfer as did Rodgers.
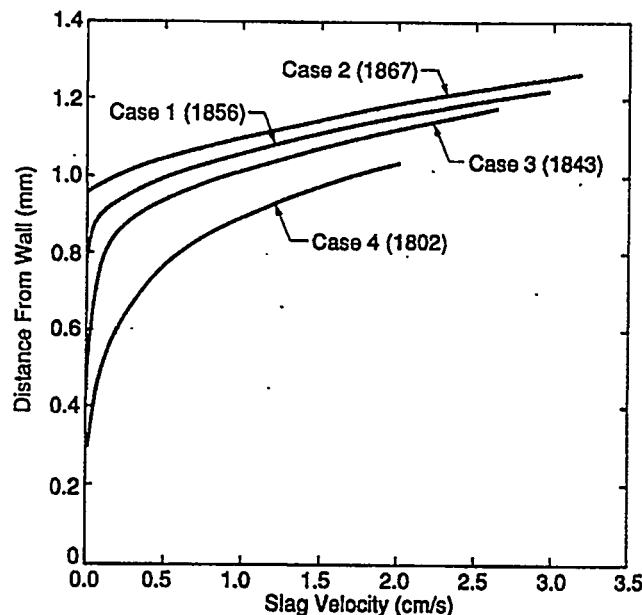
Figure 4.3-3   Slag Layer Thickness with Slag Surface Temperature in Parentheses (Source: Phillips and Muan, 1959).

The flowing slag model treats the flow of slag on a vertical surface (Figure 4.3-4). The equations used will be conservation equations for momentum, energy, and mass. The x-component for the momentum equation (steady, two-dimensional flow) is

$$\varrho u \frac{\partial u}{\partial x} + \varrho v \frac{\partial u}{\partial y} = \frac{dp}{dx} + F_x + \frac{\partial \tau_{xy}}{\partial y} \qquad (2)$$

150

where ϱ is the fluid density, u and v are the velocity components in the x- and y-directions. τ_{xy} is the shear stress component acting in the x-direction on a surface normal to the y-direction, and F_x is the body force in the x-direction. The Reynolds number in the slag layer will be small because viscosity will be high for slag flow, thus the inertia terms can be neglected. For a falling film with a free surface, the pressure term (dp/dx) can be neglected. The term F_x is equal to the gravitational force ϱg.
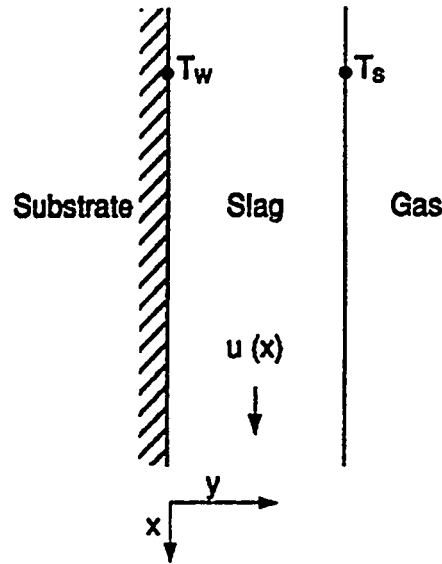
Figure 4.3-4   Flowing Slag Layer Model.

Thus the momentum equation is

$$\frac{\partial \tau_{xy}}{\partial y} = \varrho g \; .$$ (3)

We will assume Newtonian flow in the slag for temperatures above the critical viscosity temperature and thus

$$\tau_{xy} = \mu \, \frac{\partial u}{\partial y} \; .$$ (4)

The energy equation takes the form of the steady boundary layer equation for an incompressible liquid

$$\varrho u C_p \, \frac{\partial T}{\partial x} + \varrho v C_p \, \frac{\partial T}{\partial y} - \frac{\partial}{\partial y} \left(k \frac{\partial T}{\partial y} \right) - \mu \left(\frac{\partial u}{\partial y} \right)^2 = Q$$ (5)

where C_p is the slag specific heat, T is the temperature, k is the thermal conductivity, and Q is an energy source term. For low Reynolds numbers, the convective and viscous terms are neglected.

151

In this system, there is no energy source giving

$$\frac{\partial}{\partial y}\left(k\frac{\partial T}{\partial y}\right) = 0 \tag{6}$$

The conservation of mass can be expressed as the integral of the velocity profile

$$\dot{M}_s = \int_0^s (\rho u)dy \tag{7}$$

where M_s is the mass flow rate per unit width of slag layer and $y=s$ is the location of the slag surface. The mass flux is also equal to the integral of the ash deposition flux from the gas:

$$\dot{M}_s = \int_0^x \dot{m}_s(x)dx \tag{8}$$

where $\dot{m}_s(x)$ is the local ash deposition flux. The other boundary conditions can be stated as

$$u(x,0) = 0 \tag{9}$$

$$T(x,0) = T_w(x) \tag{10}$$

$$\tau(x,s) = \tau_s(x,T_s) \tag{11}$$

$$q(x,s) = q_s(x,T_s) \tag{12}$$

where T_s is the surface temperature. Equation (10) assumes an axial wall temperature profile. Eq. (11) represents a surface shear force and Eq. (12) is a surface heat flux.

To aid in solving these equations, the independent variables are transformed from (x,y) to (x,T) which gives

$$\frac{\partial y}{\partial T} = \frac{k}{q(x,T)} , \tag{13}$$

$$\frac{\partial u}{\partial T} = \frac{k}{q(x,T)\mu}\tau , \tag{14}$$

$$\frac{\partial q}{\partial T} = 0 \tag{15}$$

Solving Eq. (15) gives

$$q(x, T)) = q_s(x, T) \tag{16}$$

or the heat flux through the slag layer is equal to the surface flux. To solve Eqs. (13) and (14) assume that ρ and k are constant, that τ_s is equal to zero and that the viscosity is given by

$$\text{for } T > T_{cv} \tag{17}$$

Equation (13) can be integrated as

$$y(x, T) = \frac{k(T - T_w)}{q_s(x, T_s)} \tag{18}$$

noting that the slag layer thickness is found by setting $T = T_s$ in Eq. (18). Equation (14) can be integrated to give

$$u(x, T) = \frac{k}{q_s(x, T_s)} \int_{T_w}^{T_s} \frac{\tau(x, \theta)}{\mu(\theta)} \, d\theta . \tag{19}$$

Once the velocity is known, the mass flux can be calculated from

$$\dot{M}_s(x) = \frac{\rho k}{q_s(x, T_s)} \int_{T_w}^{T} u(x, \theta) d\theta . \tag{20}$$

At any axial position, Eq. (20) can be solved iteratively as a function of T_s. That is, the root of the equation

$$\int_0^x \dot{m}_s(x)dx - \dot{M}_s(x, T_s) = 0 \tag{21}$$

can be found.

A parametric study was completed using the new version of the radiant heat transfer model, incorporating the variable viscosity slag model. The following parameters/conditions were varied:

- Air flow (parallel versus countercurrent)
- Gas temperature
- Refractory wall thickness
- Ash deposition rate

Parallel flow produces a dry ash layer of constant thickness with a slowly increasing liquid slag layer. Countercurrent flow, in contrast, produces a rapid increase in the dry ash layer thickness at the

153

bottom of the reactor where the air is cold. Parallel flow seems preferable because a nearly constant heat flux is maintained down the length of the air heater. Furthermore, at a gas temperature of 2900°F with parallel flow, the refractory surface temperature is in the range of 2200 to 2400°F. For countercurrent flow, the refractory surface temperature reaches 2500°F at the top of the combustor. To reduce the risk of refractory corrosion, the refractory surface temperature should be kept low. This may provide another reason for preferring parallel flow.

Decreasing the thickness of the refractory layer causes the dry ash layer thickness to increase. There is almost no effect on the length of the radiant air heater, although the overall resistivity increases as the refractory is made thinner because the ash layer has a lower thermal conductivity than the refractory. This seems to indicate that if the refractory reacts with the ash and is gradually "replaced" by dry ash, there shouldn't be a major change in heat transfer.

Deposition in Radiant Air Heater

Ash transport to heat transfer surfaces can occur by several mechanisms: Brownian diffusion, turbulent or eddy diffusion, thermophoresis, vapor condensation and inertial impaction. The dominant transport mechanism for flow parallel to the walls under the conditions of the HITAF is by turbulent diffusion. Assuming the flow to be turbulent and all particles to follow the turbulent fluctuations (i.e., no size dependency of a particle's ability to follow turbulent eddies), the mass flux of ash to the wall is

$$\dot{m}_A = \varrho' \, u' \, f_A \qquad (22)$$

where ϱ' and u' are turbulent fluctuation intensities in gas density and velocity, respectively, and f_A is the mass fraction of ash in the gas flow. Estimates for the turbulent fluctuations as a fraction of the mean flows vary from 0.01 to a maximum value of 0.15. Denoting this fraction as ε_0, we rewrite $\dot{m}_A$ as

$$\dot{m}_A = \varepsilon_0^2 \, (\varrho \, u \, f_A) \; . \qquad (23)$$

The above equation states that the turbulent flux of ash particles to the wall is ε_0^2 times the axial flux of ash in the main flow. For the case where the turbulent fluctuation is 4% of the mean value, the ash flux to the wall will be 0.16% of the total mass flux of ash in the bulk gas flow. For a typical velocity of 20 m/s at 2700°F (1750 K) and an ash loading of 0.01 kg ash/kg air in the radiant section (i.e., a coal containing approximately 10% ash), the ash flux is calculated as 6.4×10^{-5} kg/(m$^2 \cdot$s). Note that because of the high temperatures in the radiant section, the sticking coefficient of unity is assumed for all particles that arrive at the wall.

The above estimate represents an upper limit because ash transport was based on turbulent parameters in the bulk flow. Lower effective turbulent diffusivities in the wall boundary layer are expected to lead to even lower ash deposition rates than estimated. A better evaluation of ash buildup due to turbulent diffusion is presently underway based on work in the literature. For example,

154

particulate deposition from turbulent streams onto solid wall surfaces was analyzed by Im and Chung (1983). Their model describes the flow near a wall as consisting of three regions: a laminar sublayer next to the wall, a buffer or transition layer in which turbulence is lower compared to the main flow, and a fully developed turbulent region. The fluid turbulence causes particles to diffuse to the vicinity of the laminar sublayer and penetrate it to the wall. Their analysis shows that the deposition rate increases with particle size up to a limiting particle size, because drag in the viscous sublayer is more likely to slow down smaller particles. Beyond a certain particle size, however, the momentum imparted to the particles decreases as the particles cannot effectively follow the turbulent fluctuations, and the deposition rate decreases. Two points are worth noting in their treatment vis-a-vis Eq. (2): turbulent diffusion through the boundary layer is slower than in the bulk flow and the diffusion coefficients are a function of particle size. The above calculation (Eq. (2)) therefore represents a very conservative upper estimate of the ash mass deposition rate.

4.3.4 Slag Screen

Slag Screen and Capture Efficiency

In order to determine what size ash particles will be captured most efficiently by the slag screen, an analysis was performed to determine the collection efficiency of a single tube. The capture efficiency of this type of collector in a high velocity flow field is mainly determined by an inertia parameter characterizing the particle motion, termed the Stokes number. The Stokes number can be viewed as the ratio of the characteristic stopping time of the particle to the characteristic flow time around the collector. For low Reynolds number flow, the particle stopping time may be computed by applying the Stokes drag law. The drag experienced by the particle in high Reynolds number flow is non-Stokesian. Israel and Rosner (1983) developed engineering correlations for the inertial parameter for particle capture by a cylinder as:

$$Stk_{eff} = \psi(Re_p) \cdot Stk \tag{24}$$

where $Stk = \varrho_p d_p^2 U / (18\mu)$, $Re_p = d_p \varrho_g U_\infty / \mu_g$, and $\psi(Re_p)$ is the correction factor for non-Stokes behavior given by

$$\psi(Re_p) \simeq \frac{3}{0.0628\,Re_p}\left[\left(0.0628\,Re_p\right)^{1/3} - \tan^{-1}\left(0.0628\,Re_p\right)^{1/3}\right]. \tag{25}$$

For a circular cylinder collection geometry and $Stk_{eff} > 0.14$, the following correlation for the capture fraction (if each impacting particle "sticks") was presented:

$$\eta_{cap} \simeq \left[1 + 1.25\left(Stk_{eff} - \tfrac{1}{8}\right)^{-1} - 1.4 \times 10^{-2} \cdot \left(Stk_{eff} - \tfrac{1}{8}\right)^{-2} + 0.058 \times 10^{-4}\left(Stk_{eff} - \tfrac{1}{8}\right)^{-3}\right]^{-1}. \tag{26}$$

For the near critical range (Rosner and Tassopoulos):

$$0.125 < Stk_{eff} < 0.14$$

(27)

$$\eta_{cap} = 0.043\left(Stk_{eff} - \frac{1}{8}\right)^{0.11} .$$

These correlations were used to calculate the impaction efficiency of ash particles for three cases to provide an estimate of the particle size likely to be removed by the slag screen under HITAF conditions. The three conditions considered were a) d_{tube} = 2 in., v_{gas} = 200 ft/s; b) d_{tube} = 2.875 in., v_{gas} = 200 ft/s, c) d_{tube} = 2.87 in., v_{gas} = 160 ft/s. Figure 4.3-5 shows the impaction efficiency as a function of particle size. As a reference, the 10 μm particles were collected with an efficiency of 28% for case a) and an efficiency of 15% for case c). The corresponding values for the 20 μm ash particles were 63% and 48%, respectively.
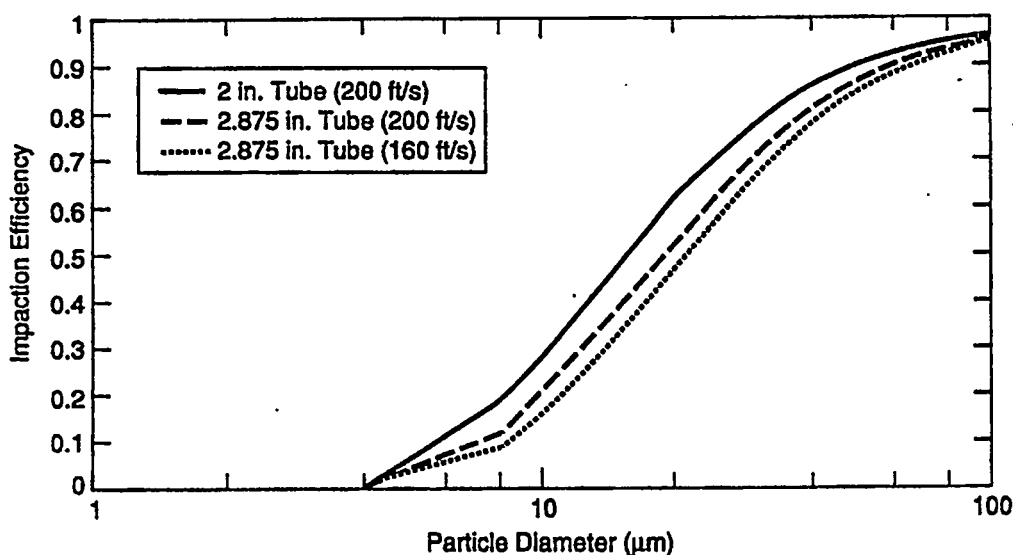
Figure 4.3-5   Impaction Efficiency as a Function of Particle Size.

The next step in the preliminary design process was to estimate the overall particle collection efficiency of multiple rows of several cylindrical tubes. The collection of particles from gas streams by impaction on multiple spherical targets has been examined by Jacober and Matteson (1985) in a experimental study of impaction 10 μm droplets of dioctylphthalate (DOP) and isopropanol onto 6 mm targets. A numerical study of particle laden gas flow past tubes was conducted by Schuh et al. (1989). Experimental particle tracking and visualization work has also been performed by Shaffer et al. (1989). A review of tubular separation performance was provided by Calvert et al. (1975). From all of these studies, it becomes clear that the collection efficiency for single collectors cannot be directly applied to a collector array since the wakes of the leading spheres strongly influence both the particle concentration and velocity before the trailing spheres on the array.

In particular, the work by Jacober and Matteson (1985) demonstrated that the target collection efficiencies may be enhanced or reduced depending on inter-collector spacing and alignment. With an in-line arrangement of target tubes, a marked shielding effect created by the lead target reduced the efficiencies of subsequent targets. The multiple tube collection efficiency did not equal the isolated, single tube value until 20 target diameters downstream at low gas velocities. At higher gas velocities, the collection efficiencies of downstream targets were always lower than that of the lead target.

A staggered tube arrangement, on the other hand, exhibited a higher collection efficiency for downstream tubes compared to the leading tube for certain arrangements. Analysis of the experimental data indicated the formation of a wake behind the leading target containing relatively high concentrations of ash particles. These data suggest that the capture efficiency of the slag screen can be maximized by placing successive tubes within the wake boundary from the preceding tube. However, these experimental results were based on single cylinders, not banks of tubes. When additional tubes are included in each row, as in the slag screen, the wakes from individual tubes may interfere with the wakes from neighboring tubes, redistributing the particles across the flow field and negating the effect of placing tubes in the predicted wake location.

For a bank of staggered tubes placed within the particle laden flow, the overall removal efficiency may be examined in two limits. The lower limit is one in which ash particles are redispersed uniformly throughout the flow between any two rows of tubes. If η is the impaction efficiency for one tube, collection efficiency for a row is given by

$$\eta_{row} = \eta \frac{A_r}{A_f} \ . \tag{28}$$

where A_r is the projected tube area per row and A_f is the tube flow area. Efficiency of the tube bank is then given by:

$$\eta_{tot} = 1 - (1 - \eta_{row})^n \tag{29}$$

where n is the number of rows. This limit is approached as the rows are spaced apart significantly - so that the ash particles have sufficient time to redisperse across the flow field before approaching the next tube row.

The upper limit occurs when the tubes are spaced fairly closely together. In this configuration particles are concentrated in the "jet" formed by the preceding row and impact the tube. The maximum collection efficiency is given as:

$$\eta_{tot} = \eta \frac{A_{tube}}{A_f} \ ; \ \eta_{tot} \le 1 \ . \tag{30}$$

Based on the estimated collection efficiency of the various configurations, the slag screen will consist of 2-1/2 in. Schedule 160 tubes with an O.D. = 2.875 in. and an I.D. = 2.125 in. The spacing

within a row will be between 6 and 9 in. on centerline and between rows will be 6 to 18 in. on centerline. The staggering between two rows will be such that the tube is centered between the two preceding tubes. A six-row tube bank is recommended for efficient removal of large particles. Table 4.3-5 provides the minimum and maximum efficiency of the slag screen for three particle sizes.

TABLE 4.3-5 OVERALL COLLECTION EFFICIENCY OF SIX-ROW SLAG SCREEN

(200 ft/s, 2875 diameter tubes)

Particle Size	8 μm	10 μm	20 μm
η_{min}	0.20	0.325	0.68
η_{max} ($\approx \eta_{actual}$)	0.23	0.4	1.0

Pressure Drop and Heat Loss Calculations

The slag screen collection efficiency calculations described in the previous sub-section indicate that a staggered arrangement of tube rows will maximize the ability of the slag screen to remove large (>20 μm) particles. Another important design consideration is the effect of tube placement on the slag screen operation. For example, the slag screen must not appreciably add to the total pressure drop of the HITAF. High temperature drops in the slag screen must also be avoided to maximize the efficiency of the convective air heater and minimize the potential for fouling of the slag screen by frozen ash.

In order to explore the effect of tube placement on the slag screen pressure and temperature drop, a set of general correlations, presented by Kzukauskus (1972), were used. These correlations were developed for cross-flow heat exchangers, and are applicable here. The pressure drop correlation (Fig. 4.3-6) plots a dimensionless pressure drop, , as a function of Re for various configurations. The parameters are as follows:

$$a = S_n/d_{tube}$$

$$b = S_p/d_{tube}$$

The pressure drop for various configurations were then calculated using the parameters from Figure 4.3-6 and Eq. (8), assuming the following conditions:

U	=	60 m/s (200 ft/s)
ϱ	=	0.2 kg/m^3
μ	=	5.85 x 10^{-5} Pa-s
T_g	=	1755 K
d_{tube}	=	0.073 m (2.875 in.)
T_f	=	1034 K
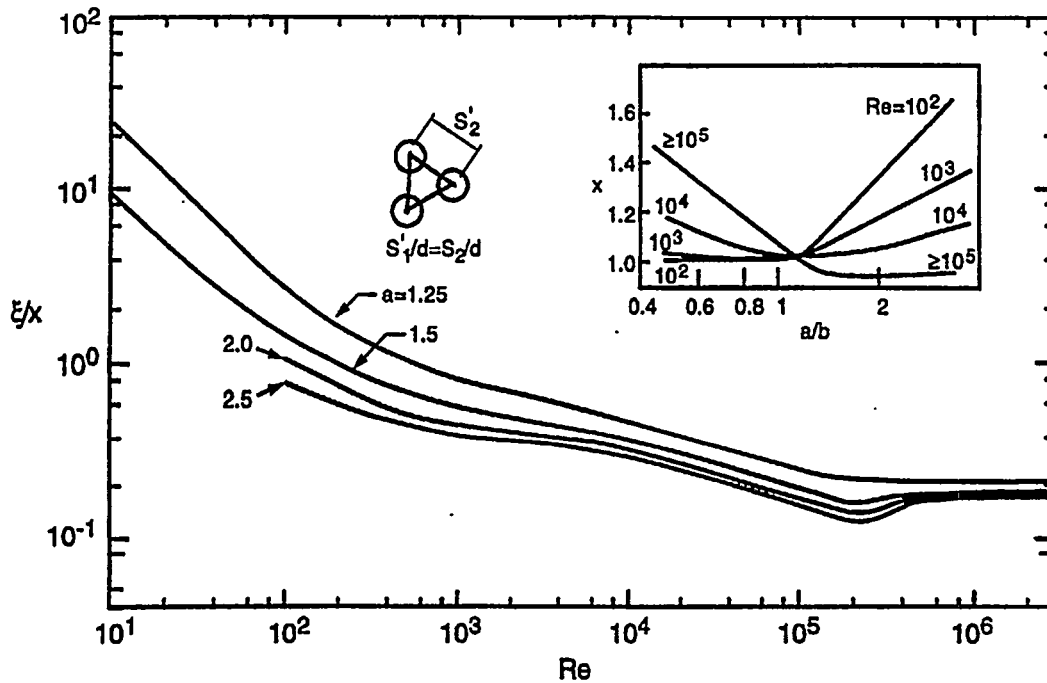
Figure 4.3-6   Pressure Drop Coefficients of Staggered Banks as Referred to the Relative Transverse Pitch a (Kzukauskus, 1972).

T_w = 313 K

ϱ_f = 0.34 kg/m^3

μ_f = 4.3 x 10^{-5} Pa-s

k_f = 0.069 W/m s

C_p = 1.15 x 10^3 J/kg °C

M_{air} = 73 kg/s

From the values in Table 4.3-6 it is obvious that the dimensionless tube spacing a is the most important parameter for pressure drop in a tube bank. The data also suggest that a $\geq$ 2 yields reasonable design pressure drops. Therefore, the centerline tube spacing should be at least 6 in. to avoid high pressure drops in the slag screen.

$$\Delta p = (\xi/x) \; x \; \frac{U_0^2 \; \varrho}{g_c} \tag{31}$$

TABLE 4.3-6 EFFECT OF TUBE CONFIGURATION ON SLAG SCREEN TEMPERATURE AND PRESSURE DROP

a/b	a	x	ξ/x	Δp (in. H₂O)	ΔT (°C)
3	2.5	1.15	0.30	6.0	162
	2.0	1.15	0.32	6.4	180
	1.5	1.15	0.38	7.6	225
	1.25	1.15	0.50	10.0	298
2	2.5	1.03	0.30	5.4	162
	2.0	1.03	0.32	2.7	180
	1.5	1.03	0.38	6.8	225
	1.25	1.03	0.50	8.9	298
1	2.5	1.03	0.30	5.4	162
	2.0	1.03	0.32	5.7	180
	1.5	1.03	0.38	6.8	225
	1.25	1.03	0.50	8.9	298
0.6	2.5	1.10	0.30	5.9	162
	2.0	1.10	0.32	6.1	180
	1.5	1.10	0.38	7.3	225
	1.25	1.10	0.50	9.5	298

The Nusselt number of the *clean* slag screen, defined in Eq. (32), was estimated from Eq. (33) (Kzukauskus, 1972) using the parameters outlined above. The maximum heat loss in the slag screen was then estimated assuming a total of 11, 2.4m long, tubes in each row. The surface temperature was defined as 313 K. The values in Table4.3-6 suggest that decreasing a, i.e., placing the tubes in each row closer together, results in much higher heat losses. Note that these calculated heat losses represent the maximum heat losses for the slag screen. When an insulating slag layer forms on the tubes, the heat transfer to the tubes drops dramatically, lowering the overall drop in the gas temperature drop as it passes through the slag screen.

$$Nu = \frac{h \, d_t}{k_f} \tag{32}$$

$$Nu = 0.40 \left[U_{max} \, \varrho_f \, \frac{d_{tube}}{\mu_f} \right]^{0.60} Pr^{0.36} \tag{32}$$

Effect of Deposit Buildup on Slag Screen Operation

The temperature and pressure drop calculations presented in the previous sub-section were based on clean cylindrical tubes. However, under normal operation there will be some ash on the tubes which will effect the temperature drop, and possibly the pressure drop in the slag screen. Although the slag screen is designed to operate "wet," where molten ash flows down the tube surfaces, there will be some frozen ash layer on the tubes. This frozen ash layer is beneficial in the slag screen for the exact reason deposits are detrimental in conventional pc fired plants − the frozen layer acts as a

160

thermal insulator and inhibits heat transfer from the hot combustion gases to the water cooled tubes. Therefore, the surface of the deposit is closer to the combustion gas temperature and is, normally, hot enough for ash to flow. In order to better define the temperature drops in the slag screen and estimate the effect of deposit buildup on the pressure drop in the slag screen, a number of more detailed calculations were performed.

Another design consideration that must be addressed for a dirty slag screen is cleanability of the tubes. This issue may become critical in the event of the gas temperatures drop below the critical flow temperatures of the slag causing the slag screen to operate "dry." The tubes must also be cleanable to prevent bridging of the slag screen for high ash deposition fluxes. Tube cleanability was explored by determining the effect of placing water lance channels in the slag screen on heat transfer and ash collection efficiency.

Effect of deposit buildup on slag screen pressure drop

The change in pressure drop, caused by the presence of a frozen ash layer, may be due to changes in tube roughness, shape, and size. As there has not been a great deal of quantitative work in this area, we used a simple analysis to make an estimate of the effects of these properties on the slag screen pressure drop.

If we neglect the effects of corrosion, the scale of roughness on the tube can be thought of as the size of the items sticking into the flow stream divided by the tube diameter. As a "worst case" estimate, we will assume no sintering occurs. In this case, the individual particles located on top of the deposit represent the "items sticking into the flow." However, these particles are very small as compared to the tube diameter, so we can expect the relative-roughness of the tube to change very little as deposit builds up.

Even in the case of significant surface roughness, studies presented elsewhere (Goldstein, 1965) suggest that the increase in surface roughness actually causes a decrease in the drag coefficient of a cylinder in the flow regime we are considering.

Figure 4.3-7 illustrates some of the "typical" forms of deposits in boilers. As can be seen from this figure, the deposit tends to make the tubes more aerodynamic in shape (i.e., the drag coefficient is reduced). Therefore, there shouldn't be any significant increase in pressure drop due to the shape change caused by deposit buildup. However, care must be taken to design the slag screen to prevent the extended deposits from bridging with the preceding tubes – significantly restricting the flow.

Previously, we determined that the tube spacing in each row is the controlling parameter for pressure drop in the tube bank. If we perform a "thought experiment" for the effect of deposit buildup on the tube spacing in each row, we see that there should be no significant change in the total pressure drop because, at least initially, deposits do not reduce the effective spacing between tubes. At the side edges of each tube (the tube edge at the gap between tubes) we would expect the particle deposition to be limited to non-inertial effects (e.g., diffusion and thermophoretic effects). However, these are

161
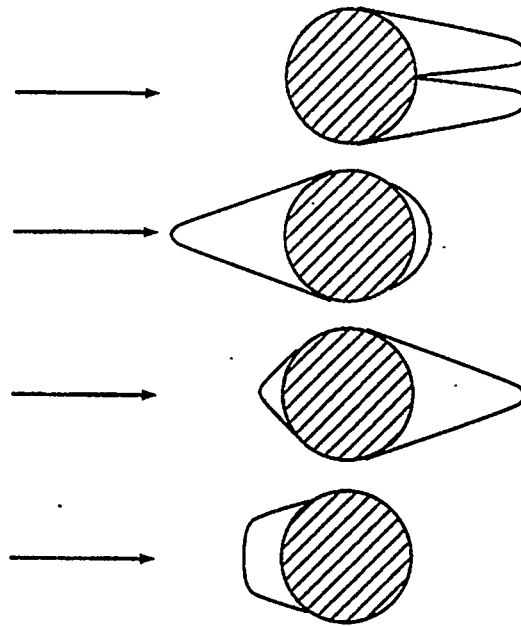
Figure 4.3-7   Typical Forms of Deposits Observed in Boilers.

likely to cause much slower deposition rates than from inertial impaction on the leading edge of the tube. This suggests that the deposit on the leading edge grows much faster than the deposits between the tubes (this is supported by the typical deposit forms found in industry). Therefore, in the event of an excessively large frozen ash layer, or if the slag screen must be operated "dry," the tubes will probably need to be cleaned to prevent bridging between rows before the deposit growth in the gap becomes significant.

Thickness of frozen ash layer on slag screen

In order to ensure that the slag flows off the slag screen, the surface temperature must be high enough to prevent slag freezing and the slag viscosity must be low enough to allow the slag to flow. The thickness of the frozen ash layer plays a major role in controlling the surface temperature. By calculating the surface temperature as the ash layer grows, we can estimate the minimum thickness required to maintain the slag flow.

The surface temperature was calculated assuming that the water in the pipes, and the *inside* wall of the pipe, is maintained at 313K.   Note that the temperature drop calculations discussed earlier assumed that the *outside* wall of the pipe was maintained at 313K. From Eq. (34), it was possible to calculate the overall heat transfer coefficient for an individual tube. For this equation r_0, r_1, r_2 were the inside tube radius, the outside tube radius, and the overall tube radius, respectively. The film properties were those presented earlier, and the film heat transfer coefficient was calculated using Eq. (33). Previous work has suggested that the thermal conductivity of an ash deposit is strongly

162

dependent on the form (e.g., porosity) of the deposit. The equation used here, Eq. (35), is based on data presented by Anderson et al. (1987) and Wain et al. (1991).

$$U_0 = r_0^{-1} \left(\frac{\ln(r_1/r_0)}{k_{tube}} + \frac{\ln(r_2/r_1)}{k_e} + \frac{1}{r, h} \right) \tag{34}$$

$$k_e = (0.861 + 2.45 \times 10^{-3} \, T_m) \, (1 - 1.254\phi + 3.9 \times 10^{-4} \, T_m - 2.73 \times 10^{-4} \, T_m) \tag{35}$$

The heat flux is given by Eq. (36), and the surface temperature is given by Eq. (37). The temperature drop in the slag screen is given by Eq. (38).

$$q_0 = U_0 \, (T_1 - T_g) \tag{36}$$

$$T_s = T_g + \frac{q_0 \, r_0}{h \, r_2} \tag{37}$$

$$\Delta T = \frac{q_0 \, SA}{m \, C_n} \tag{38}$$

In Eq. (38), SA is the total tube surface based on the *inside* diameter of the tube, m is the mass flowrate of flue gas (73 kg/s), and C_p is the gas heat capacity (1150 J/kg°C).

These equations were used to generate the plots shown in Figures 4.3-8 and 4.3-9 assuming:

u	=	200 ft/s [61 m/s]
No. Tubes	=	66
r_0	=	1.0625 in. [2.70 cm]
r_1	=	1.4375 in. [3.65 cm] (2 ½ in. Schedule 160 piping)
Tube Length	=	7.9 ft [2.408 m]
k_{tube}	=	9.4 Btu/hr ft² °F [53.4 W/m² °C] deposit
porosity	=	0.65, 0.30, 0.00 (fully sintered)

The velocity, mass flow rate, tube length, and number of tubes were chosen to correspond to a likely slag screen design.

As can be seen from these figures, the frozen ash layer has a very large effect on the surface temperature. For this configuration, an approximately 1 mm thick ash deposit is sufficient to maintain a surface temperature which is significantly higher than the slag critical viscosity. This frozen ash layer thickness might be slightly higher in the cooler, exit, region of the slag screen.

In addition, the temperature drops are significantly lower than those calculated earlier. This is likely due to the assumption used in the previous calculation that the *outside* wall temperature was

163
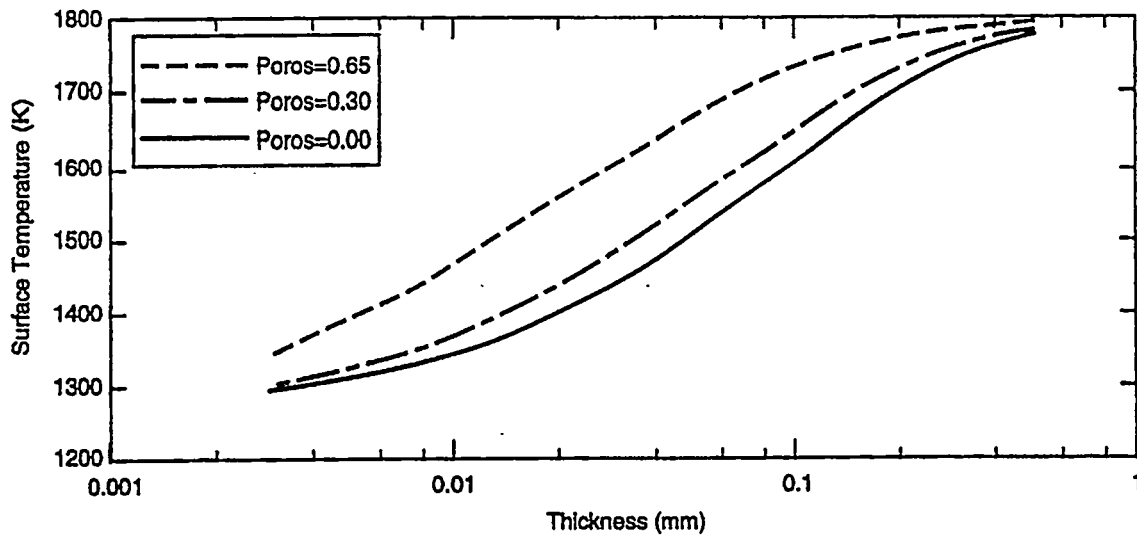
Figure 4.3-8   Slag Surface Temperature on Slag Screen Tubes.
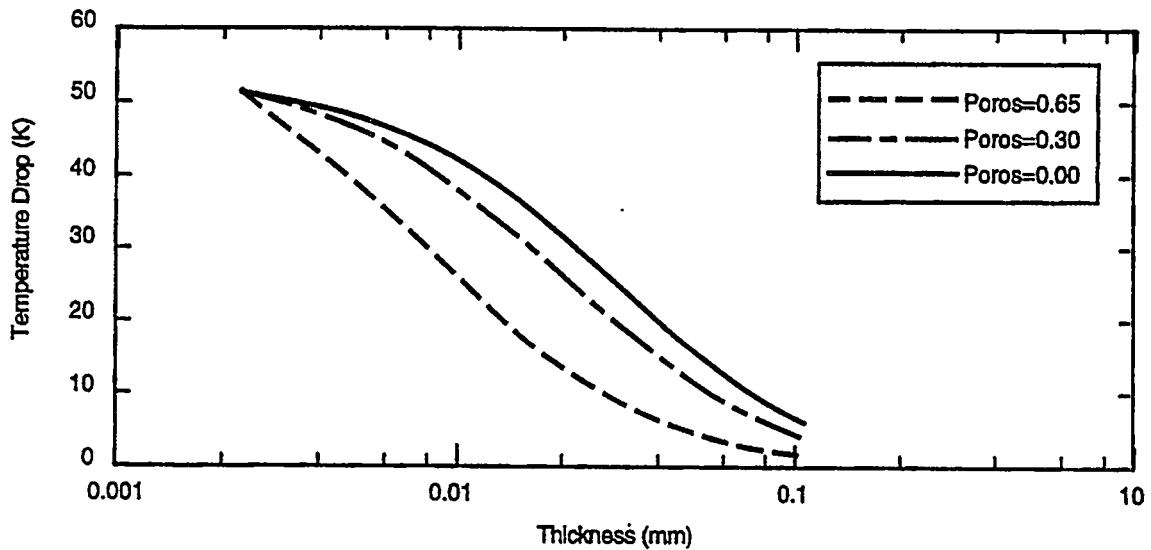
Figure 4.3-9   Slag Screen Temperature Drop.

313 K. In fact, the outside wall temperature was calculated to be approximately 1200 K in the absence of any ash deposit. The combination of these two results suggests that it should be possible to run the entire slag screen "wet," thus maximizing particle removal.

Another important issue is that of the thickness of the flowing slag layer on the slag screen tubes. To address this issue, the flowing slag model for the radiant air heater, see Section 3.2, was slightly modified. The working fluid was changed to water at a fairly high flowrate (5.6×10^9 lb/hr). The water

side heat transfer coefficient was also set such that the inside wall of the pipe was approximately the bulk water temperature. The refractory thickness was also set to zero, so that the slag screen tubes consisted of metal tubes with no coatings. As the slag screen serves as both a particle removal device and a radiation shield for the furnace, the code was modified so that the heat transfer was due to either radiation or convection. The radiation case would be more indicative of the first few rows of tubes as they "see" the furnace. The interior tubes are better modeled by the convective heat transfer case. Interestingly, the calculated surface temperatures (see Figure 4.3-10) were very similar for the two cases. Therefore it is not surprising that the calculated surface thicknesses were also similar (Figure 4.3-11). Note that this analysis used the same gas temperature for both heat transfer mechanisms. In the operating slag screen the gas temperature at the inner tube locations will be lower than the first two rows - increasing the thickness of the frozen ash layer and possibly the total slag layer. This effect was explored in more detail at the end of this subsection.
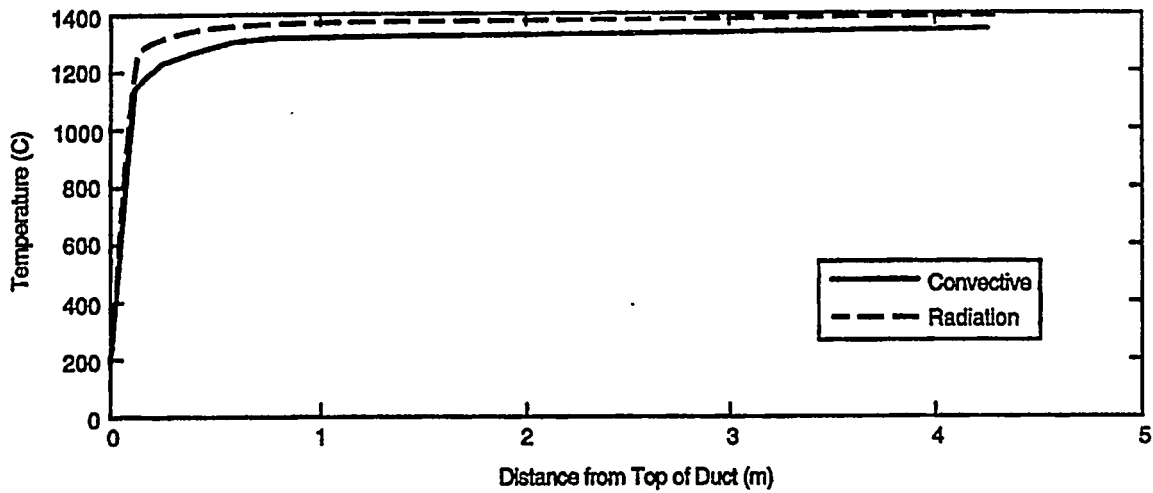
Figure 4.3-10   Calculated Slag Surface Temperatures (Includes Frozen Ash Layer).
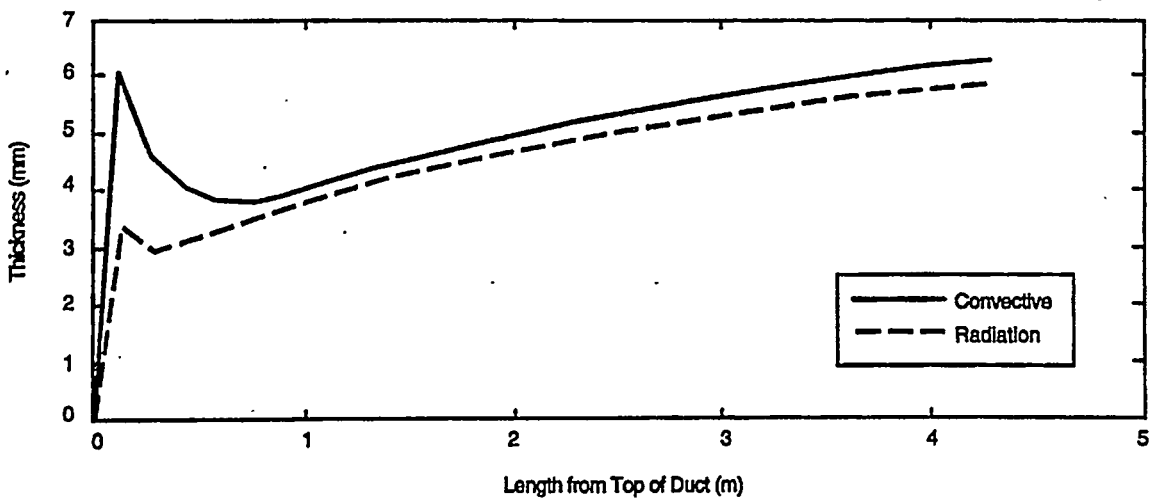
Figure 4.3-11   Calculated Slag Layer Thickness (Includes Frozen Ash Layer).

For the results plotted in Figures 4.3-10 and 4.3-11, the deposition flux in the slag screen was assumed to be approximately 4 lb/ft^2 h as calculated in the furnace ash balance calculations discussed elsewhere in this report. As can be seen from Figure 4.3-11, the slag layer (flowing and frozen) should be approximately 0.25 in. (6 mm) at the bottom of the tubes (assuming vertical tubes). This is consistent with the 1 to 2 mm thicknesses calculated for the radiant air heater, and the 2 mm frozen ash layer calculated for the slag screen. Therefore, as long as the proposed tube spacing is much larger than the flowing layer, there shouldn't be a significant pressure drop associated with restricting the flow.

Slag re-entrainment from slag screen

In order to ensure that the ash captured by the slag screen was removed at the slag tap, and not re-entrained by the gas flow, an estimate was made of the gas velocity required to shear slag droplets from the slag layer. The empirical equation derived by Ullock and presented by Calvert (1975) was used to estimate the required gas velocity to shear droplets from the flowing slag layer. The gas velocity (U_g) required is given by:

$$U_g = 35.6 \frac{\sigma^{0.127} \varrho_l^{1.27}}{\varrho_g^{0.5}}$$

where U_g is cm/sec and:

σ	=	liquid surface tension [dyne/cm]
ϱ_l	=	liquid density [g/cm^3]
ϱ_g	=	gas density [g/cm^3]

Slag surface tension range from approximately 200 to 300 dyne/cm. If we assume a value of 250 dyne/cm, the resulting gas velocity is 157 m/s. From this estimate significant reentrainment will probably not occur in the current system.

Slag screen heat transfer calculations

The next step in the slag screen design was to perform more detailed design calculations for specific slag screen designs proposed based on the preliminary calculations discussed thus far. This phase was a team effort between PSIT and UTRC personnel. Heat transfer calculations were performed by PSIT. Collection efficiency and pressure drop calculations were performed by UTRC using CFD codes. The general results from both the heat transfer calculations and the CFD calculations were used to define a specific design to be studied further under Phase II.

The preliminary CFD results obtained by UTRC suggested that the ash collection efficiency could be maximized with acceptable pressure drops for a = 1.66 (tube center to center approximately 4.8 in.) and b ranging from 1 to 2 (row center to center distances between 2.9 and 5.8 in.). The results of the heat transfer calculations for these configurations are shown in Figs. 4.3-12 through 4.3-15. The calculations were set up as follows:

166

1. The first two rows were allowed to "see" radiation from the furnace — resulting in higher surface temperatures;

2. Heat transfer was by radiation from the gas, radiation from the walls (rows 1 and 2), and convection;

3. The Nusselt number was previously defined to be a function of the tube spacing.
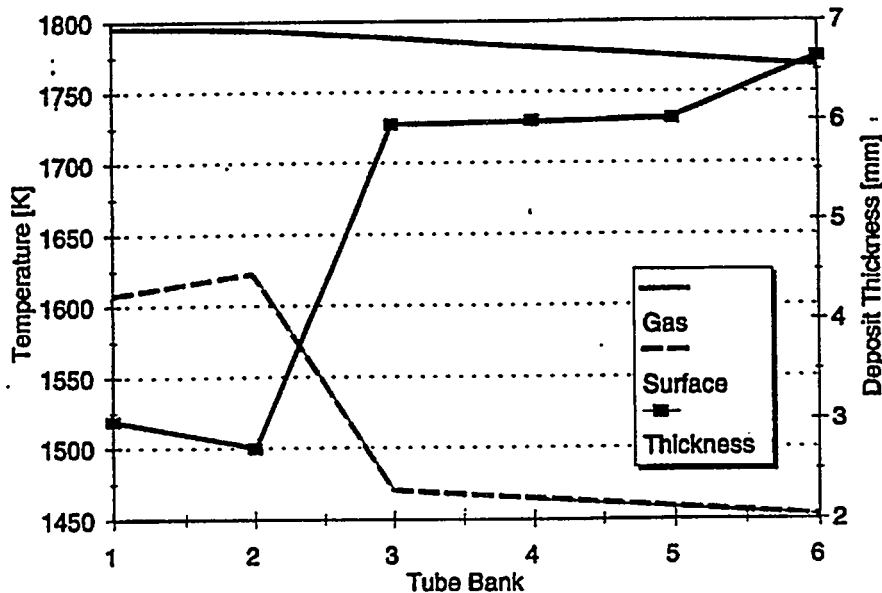
Figure 4.3-12 Heat Transfer Results - a - 1.66, b = 1.

For each tube bank, the surface and gas temperatures were estimated by assuming an average 3 mm (0.1 in.) partially sintered ash layer on each tube. Using the estimated gas temperature, the critical ash layer thickness required for the slag to flow was calculated. As can be seen from the plots, the temperature drop through the slag screen is fairly low — approximately 30 K. However, the critical frozen ash layer thickness ranged from 3 mm (0.1 in.) to 7 mm (0.27 in.). These values represent the minimum slag layer thicknesses (the flowing layer is not included). This analysis suggests that there will be serious flow restrictions in the last few rows of the slag screen for the tightly packed (b = 1) case. For this case we estimate that 70% of the flow is restricted in the last row. If we double the distance between rows (b = 2) only 35% of the flow is choked. Therefore, to avoid major operational problems, we suggest that the larger row spacing is used, in spite of its slightly lower collection efficiency.

Another issue that was addressed to define the design for Phase II was placement of the rows to facilitate cleaning. Clearly, cleaning a bank of 6 rows, even with the expanded row spacing of b = 2, can't be done with conventional cleaning apparatus. Therefore, additional calculations were performed for a design with a path at least 18 in. wide placed between the second and third rows of

167
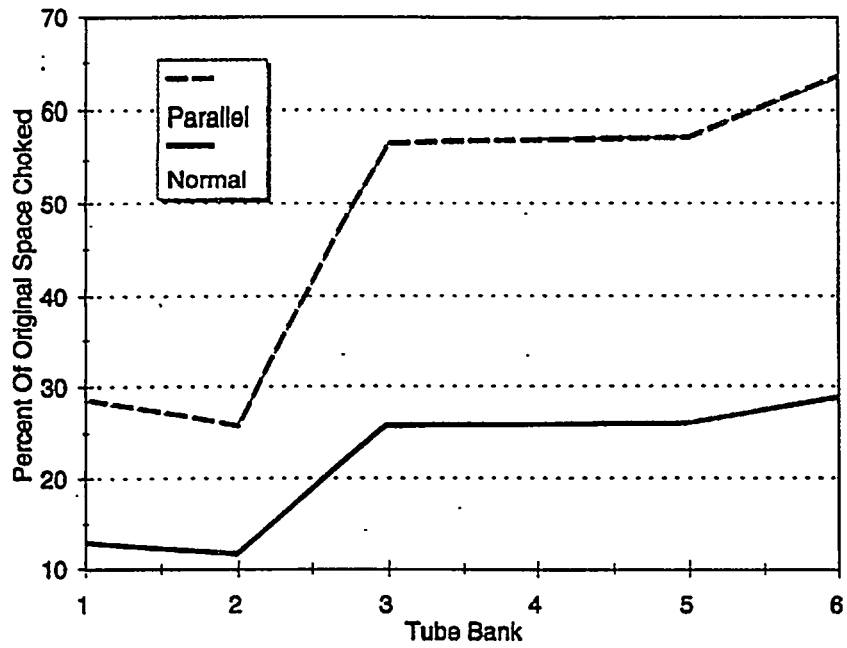
Figure 4.3-13   Percent Reduction of Flow Area by Slag Layer - a = 1.66, b = 1.
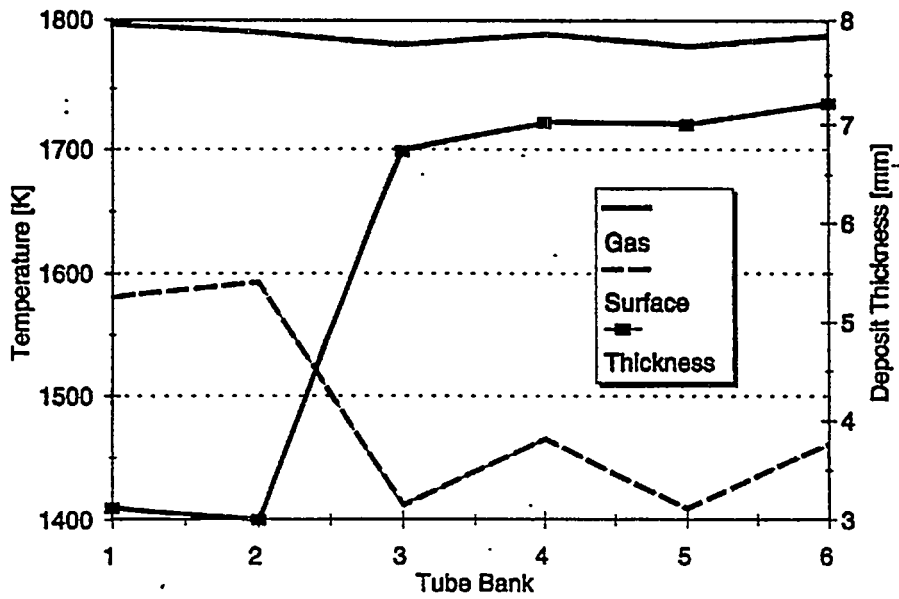
Figure 4.3-14   Heat Transfer Results - a = 1.66, b = 2.
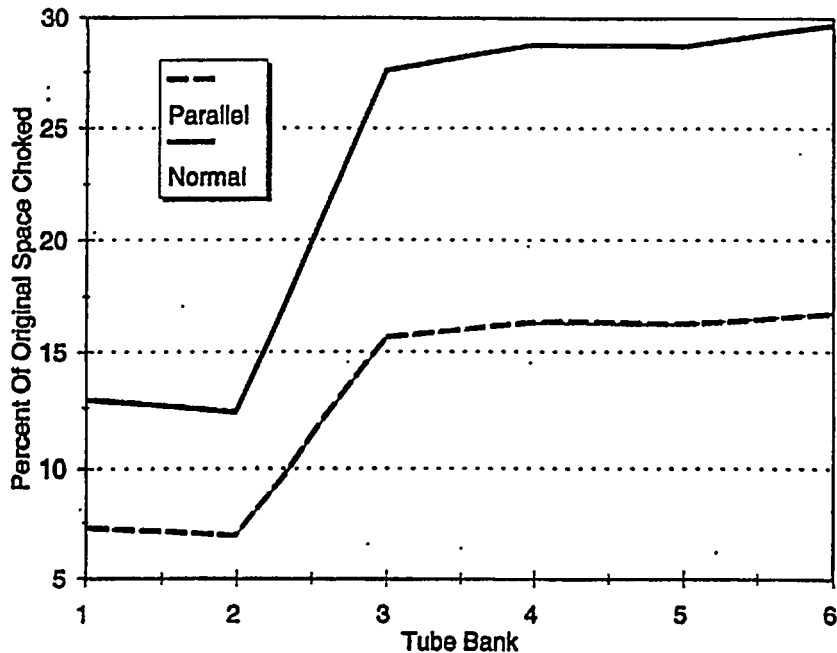
Figure 4.3-15   Heat Transfer Results - a - 1.66, b = 1.

tubes. A second cleaning path was inserted between rows 4 and 5. The rows would consist of 2.875 in. (O.D.) tubes, with a = 1.66 and b = 2. The results from the CFD calculations (performed for 4 tube rows) indicate that greater than 70% of the ash will be removed. Addition of the two rows not considered in these calculations will increase this value.

Proposed slag screen design for Phase II

Based on the analysis in this section, the following design will be explored further in Phase II, including flow visualization and feasibility testing:

Tubes:	2-1/2 in. Schedule 160
No. tubes:	11 tubes per row
No. rows:	6 rows
Tube spacing:	a = 1.66 (approximately 4.8 in. center to center)
Tow spacing:	b = 2 (approximately 5.8 in. center to center) with 18 in. clean out paths between rows 2 and 3 and rows 4 and 5

CFD analysis of slag screen performance

Computational Fluid Dynamics (CFD) was used to estimate the effectiveness of various slag screen designs in removing ash particles with a size and number density distribution representative of the anticipated ash loading from the furnace. The objective of these calculations was to identify one or more designs, in terms of tube spacing and arrangement, that remove the maximum percentage of

169

particles with minimum pressure loss. Specifically, an ash removal rate of 70 to 90 percent with an overall pressure drop of 0.1 psi was used as criteria to screen configurations; for the larger particles, a removal rate of 90+ percent was specified. In addition, it is necessary to maintain tube-to-tube spacings in excess of some minimum to allow for buildup of ash on tubes located farther downstream in the screen and therefore in a colder region of the flow; in warmer regions, the slag will remain in a molten state and will drain from the tubes. Finally, provisions for cleaning of the slag screen requires that large gaps be maintained periodically between banks of tubes.

Description of CFD cases

All of the results described herein were obtained using the commercially available computer code, *FLUENT.* This code solves the Reynolds-averaged form of the Navier-Stokes equations using a finite-volume method in general curvilinear coordinates for both two and three-dimensional flows. For turbulent flows, both eddy viscosity and differential Reynolds stress models are available. For the present results, two-dimensional flow calculations were made using the two-equation k-ε turbulence model. The gas flow and surface boundary conditions used in these computations are listed in Table 4.3-7. Note that for two cases described later, the inlet value of turbulent intensity differed from 10 percent.

TABLE 4.3-7 BOUNDARY CONDITIONS FOR CFD CALCULATIONS

Inlet velocity, fps	54.4
Inlet temperature, °F	1800
Inlet turbulent intensity, %	10
Wall temperature, °F	1445

Flow field results were first obtained in the absence of any effects due to particles. It should be noted that the particle concentrations are low enough that the effects of the particles on the gas phase are negligible, in any case. With the gas flow established, particles were introduced with the size distribution listed in Table 4.3-8. In *FLUENT,* particle laden flows may be modeled in either of two ways. In the first, only the mean particle tracks are determined; that is, the effects of turbulence on particle motion are neglected. This model is strictly applicable only for the case of relatively large, dense particles. For smaller particles, and especially for the first three or four size classes used here, turbulent dispersion of the particles may be important. In this case, the code provides a stochastic spray model in which the local gas velocity used in the determination of particle drag includes a turbulent fluctuating component based on the local value of turbulent kinetic energy (k of the k-ε turbulence model). Generally, due to inertial effects, large particles will deviate from the local flow direction as the flow turns. Small particles tend to follow the flow streamlines.

TABLE 4.3-8 INLET ASH PARTICLE DISTRIBUTION

Diameter, μ	Loading, kg/m^3
1.25	7.71E-06
3.75	8.96E-05
7.5	2.40E-04
15	3.69E-04
30	3.08E-04
60	1.38E-04
Total	1.15E-03

However, due to the random perturbations associated with the turbulence field, small particles can effectively migrate across streamlines. In terms of the design of the slag screen, a fraction of the smallest particles can be collected due to the net effect of large numbers of random perturbations that eventually cause the particles to encounter a tube. Therefore, to provide a more realistic simulation of slag screen performance, the stochastic model was used. The collection efficiencies tabulated below are based on the results of several hundred computational particles subjected to large numbers of random turbulent fluctuations over each particle trajectory.

In this study, both inline and staggered-tube bank arrays were considered. Typical examples of inline and staggered arrays are shown in Figures 4.3-16 and 4.3-17, respectively, where the flow is from left to right between the tube rows. Six inline configurations were analyzed in which the spacing between tube banks and the spacing within a tube bank varied. Seventeen staggered-tube arrangements were also modeled. The larger number of staggered-tube arrangements was due to the fact that staggered arrays rapidly emerged as better performers in terms of overall capture efficiency. In an inline array (e.g., Figure 4.3-16), large particles in the middle of the flow field will pass through the screen. In a staggered-tube array (e.g., Figure 4.3-17), the flow is turned and the inertia of the larger particles will cause some fraction to deviate sufficiently from the streamlines and impact on the upstream side of a tube. Also, some of the smaller particles will diffuse into the recirculation zones behind each tube and be effectively trapped there.

The results of these calculations are summarized in Table 4.3-9. Cases A through F represent inline (I) arrays, each with six tubes arranged in two rows of three tubes each. Cases G through W represent staggered (S) arrangements. In some staggered-tube configuration cases, the upper row contained the same number of tubes as the lower row (see Figure 4.3-17);since the computation domain usually ended in such cases at the midpoint of the last tube of the upper row, the number of tubes (#Tbs) is listed as 5.5 for these cases. To determine the effect of the last fractional tube, the results for cases N and O can be compared.

In every case except Cases Q and R, the tube diameter (D) was assumed to be 3 inches. For Case Q, the tube diameter was 4 inches. For Case R, the tube spacings (see below) were the same as in Case
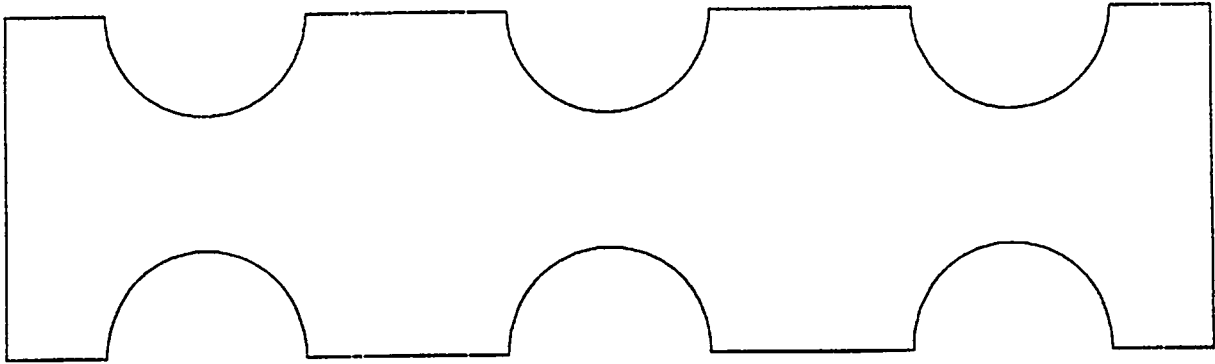
Figure 4.3-16   Inline Tube Arrangement
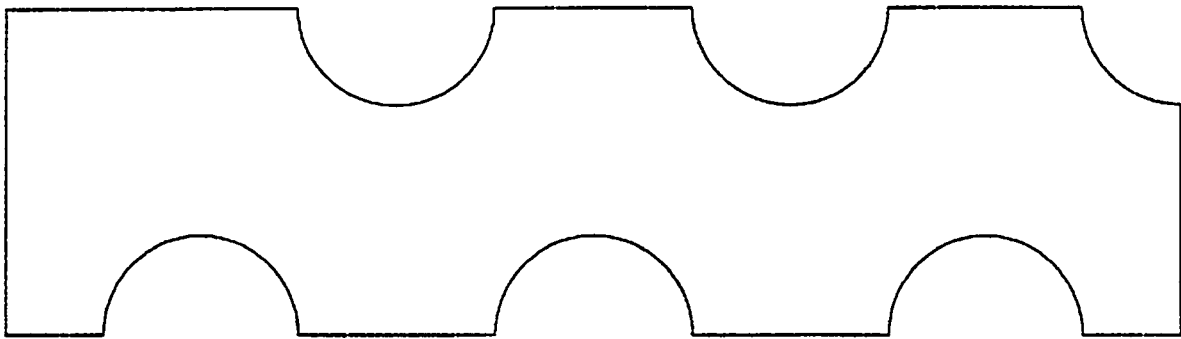
Figure 4.3-17   Staggered Tube Arrangement

M but the tube diameter was increased to 3.5 inches to represent the additional blockage due to slag buildup.

The geometric parameters listed in Table 4.3-9 are defined as follows. Reference may be made to Figure 4.3-18. The spacing between tubes in the same row is denoted as A and the center-to-center spacing in the spanwise direction between rows is designated as B; therefore, for staggered-tube arrays, the spacing between tube centers *in the same bank* is equal to 2B. The parameter A/B is essentially a tube pitch measure indicating, for example, how "close" the tubes are in each bank relative to the spacing between tubes in the same row. G1 and G2 indicate the spacing between tubes in the same row and between two banks, respectively. These are essentially measures of the open area between tubes and can be used to judge whether the tubes are spaced far enough apart to allow sufficient flow to pass through the screen as slag accumulates. Note that G2 is not the actual flow area between tubes. Instead, it is equal to the distance along the line connecting tube centers exclusive of

172

TABLE 4.3-9 PERFORMANCE OF SLAG SCREEN CONFIGURATIONS

Case	#Tbs	D,in	Arr	A	B	A/B	Percent Captured							ΔP,psi	G1,in	G2,in
							1.25μ	3.75μ	7.5μ	15μ	30μ	60μ	Total			
A	6	3	I	2	2.50	.80	13	12	9	7	20	31	14	.0088	3.000	4.500
B	6	3	I	2	2.00	1.00	17	20	22	25	32	39	27	.0146	3.000	3.000
C	6	3	I	2	1.67	1.20	28	27	28	31	40	47	34	.0253	3.000	2.000
D	6	3	I	3	3.75	.80	10	8	9	9	10	9	9	.0043	6.000	8.250
E	6	3	I	3	3.00	1.00	11	14	14	16	20	25	18	.0061	6.000	6.000
F	6	3	I	3	2.50	1.20	15	16	17	19	24	30	21	.0083	6.000	4.500
G	5.5	3	S	2	2.50	.80	13	16	17	19	25	31	21	.0074	1.500	5.080
H	5.5	3	S	2	2.00	1.00	17	20	22	24	32	39	27	.0114	1.500	3.710
I	5.5	3	S	2	1.67	1.20	27	27	28	32	41	49	35	.0181	1.500	2.830
J	5.5	3	S	3	3.75	.80	9	10	11	13	16	20	14	.0045	3.000	9.120
K	5.5	3	S	3	3.00	1.00	12	13	14	16	20	25	17	.0062	3.000	7.060
L	5.5	3	S	3	2.50	1.20	14	16	17	19	25	32	22	.0091	3.000	5.750
M	5.5	3	S	2	1.00	2.00	73	67	54	81	100	100	82	.0414	1.500	1.243
N	5.5	3	S	2	.83	2.40	90	87	83	99	100	100	95	.0648	1.500	.905
O	5	3	S	2	.83	2.40	86	81	75	99	100	100	93	.0775	1.500	.905
P	5	3	S	2	.66	3.00	95	92	93	100	100	100	98	.2046	1.500	.605
Q	5	4	S	2	1.11	1.80	56	54	43	42	85	94	61	.0323	1.000	1.979
R	5.5	3.5	S	1.71	.857	2.00	93	92	87	100	100	100	96	.0924	1.250	.743
S	5	3	S	4	.83	4.80	83	75	66	85	100	100	86	.0518	4.500	3.500
S'	5	3	S	4	.83	4.80	65	68	65	85	100	100	85	--	4.500	3.500
T	5	3	S	4	.83	4.80	73	62	54	79	100	100	80	.0510	4.500	3.500
U	5	3	S	4	.83	4.80	89	82	75	86	100	100	89	.0505	4.500	3.500
V	6	3	S	4	.83	4.80	94	90	81	89	100	100	92	.0741	4.500	3.500
W	4	3	S	4	.83	4.80	77	77	73	59	70	97	71	.0521	4.500	3.500

173
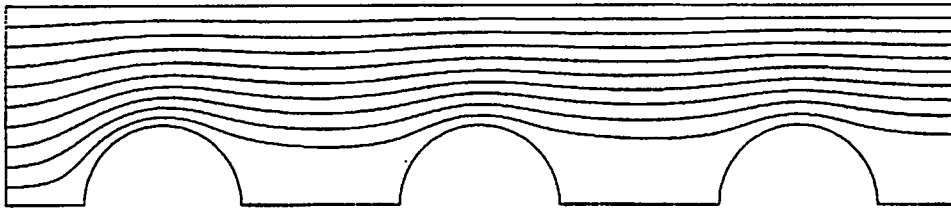
Case A - Inline A = 2 A/B = 0.8
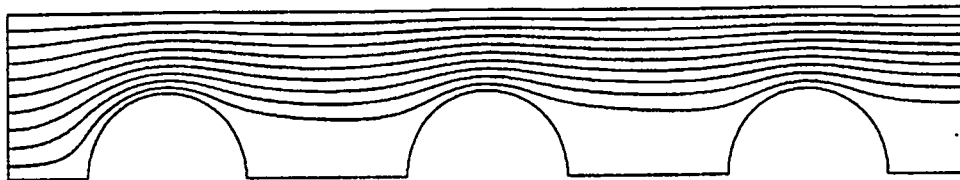
Case B - Inline A = 2 A/B = 1
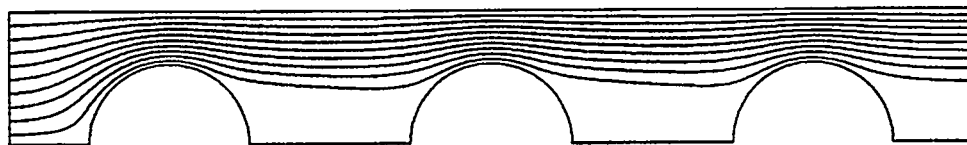
Case C - Inline A = 2 A/B = 1.2
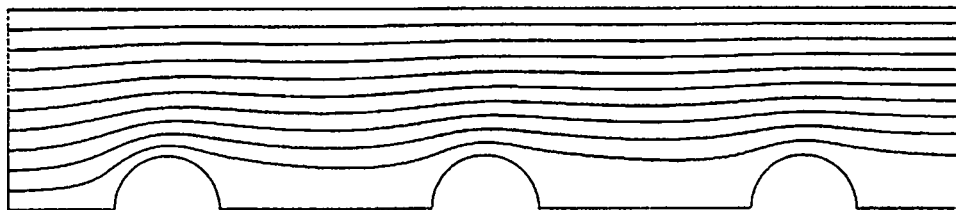
Case D - Inline A = 3 A/B = 0.8
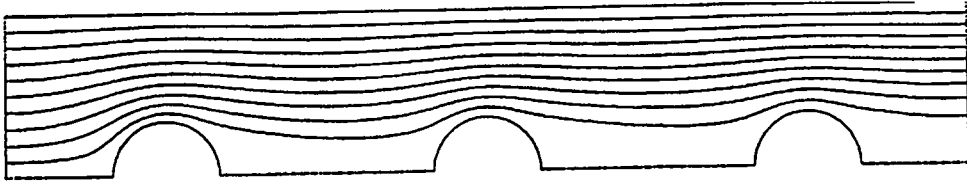
Case E - Inline A = 3 A/B = 1.0
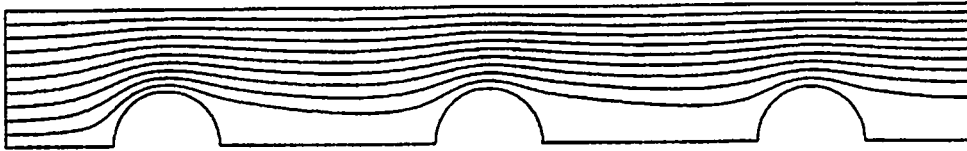
Case F - Inline A = 3 A/B = 1.2
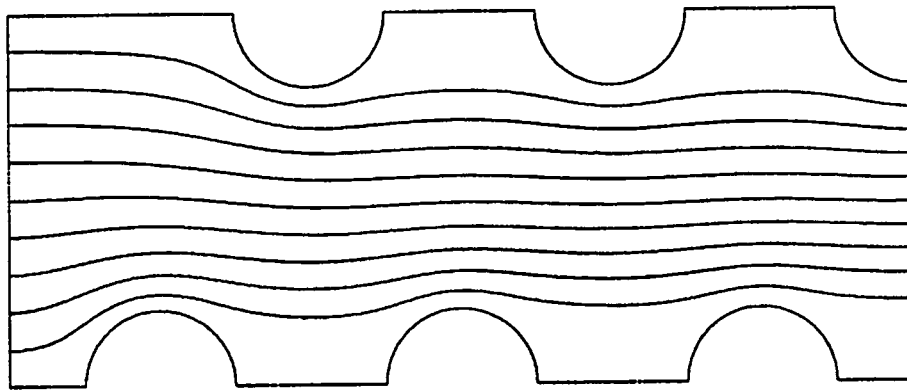
Case G - Staggered A = 2 A/B 0.8
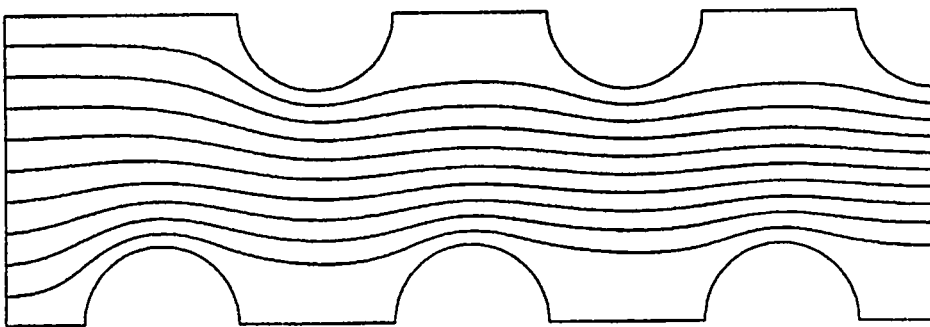
Case H - Staggered A = 2 A/B 1

175
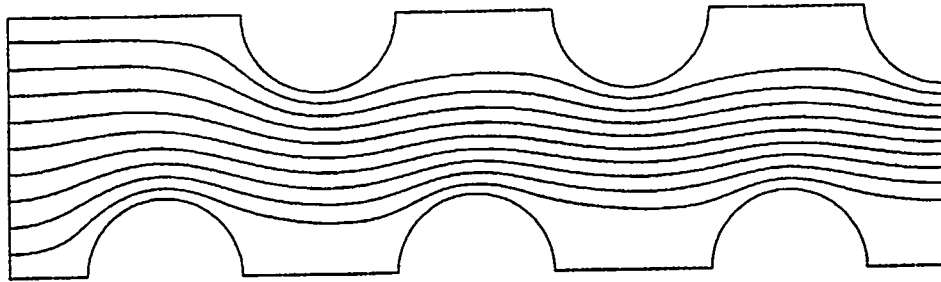
Case I - Staggered A = 2 A/B 1.2
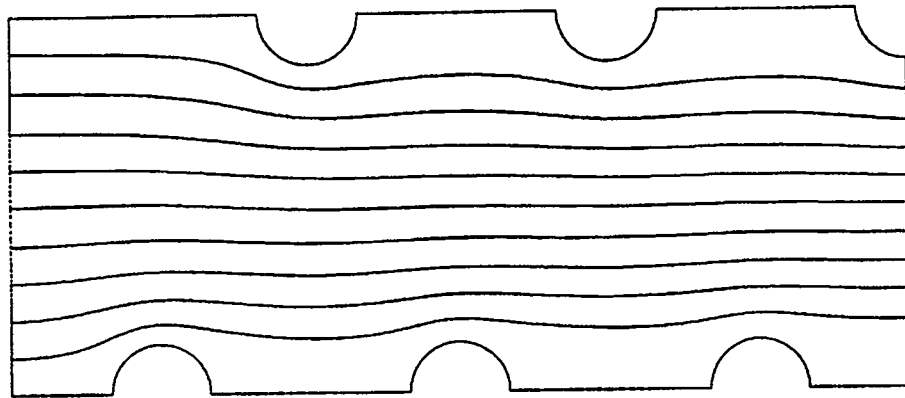
Case J - Staggered A = 3 A/B 0.8
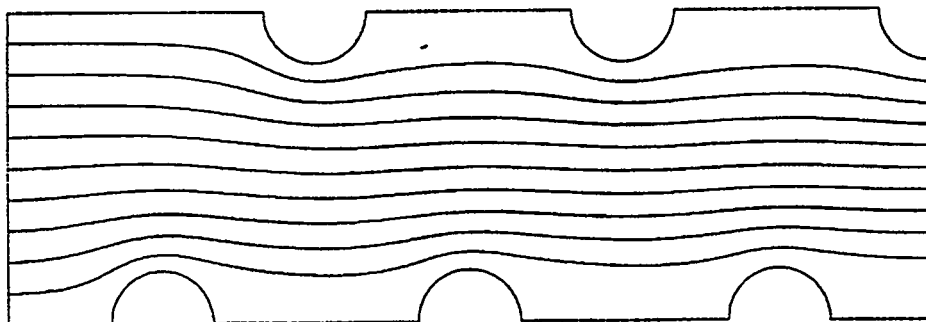
Case K - Staggered A = 3 A/B 1/0
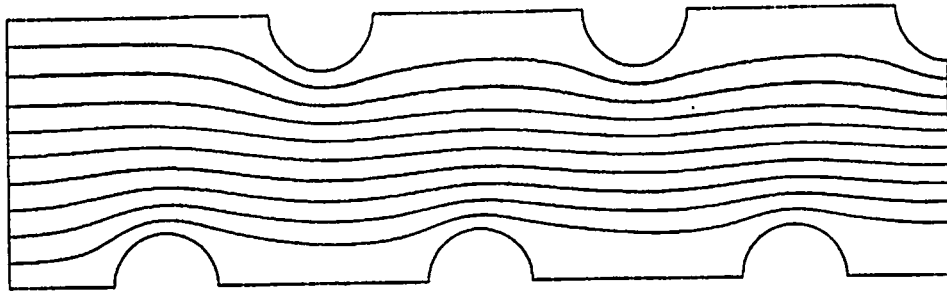
Case L - Staggered A = 3 A/B 1.2
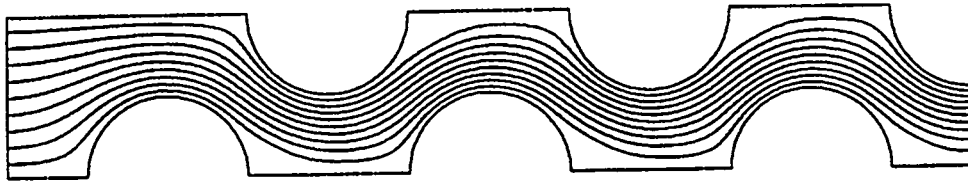
Case M - Staggered A = 2 A/B 2
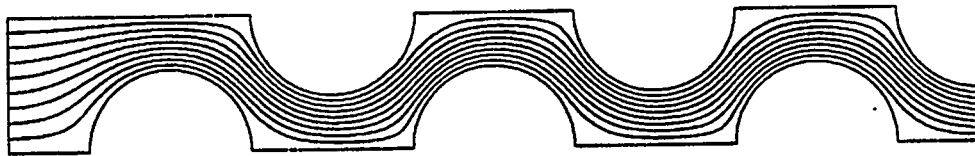
Screen Case N - A = 2 B = 2.4
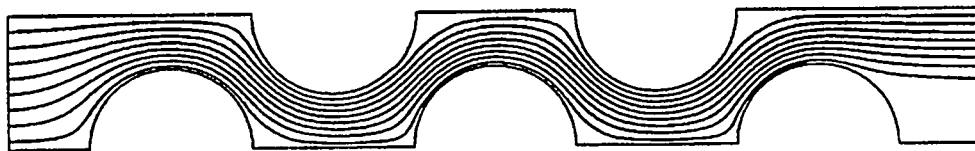
Case O - A = 2 A/B = 2.4 No Quarter Tube
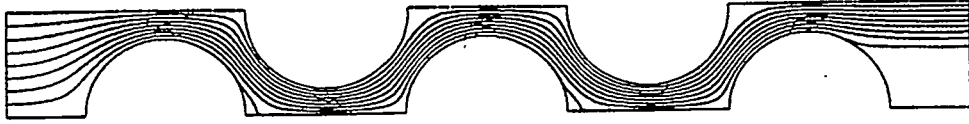
Screen Case P - A = 2 A/B = 3 No 1/4 Tube
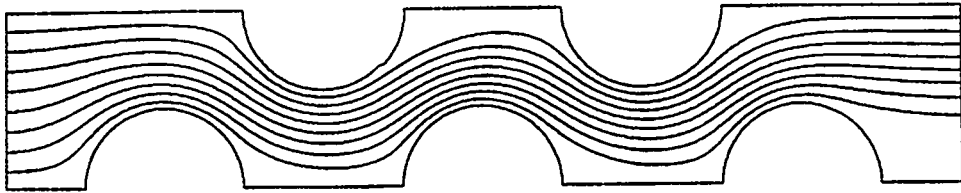
Screen Case Q - A = 2 A/B = 1.8 No Quarter Tube
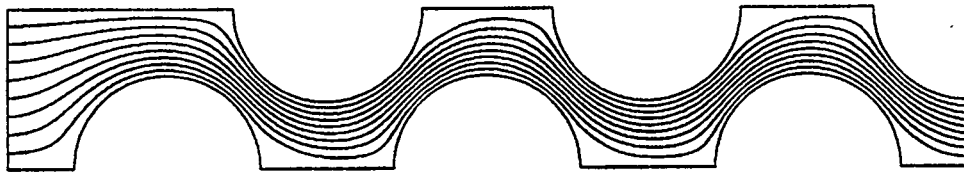
Case R - Case M With D = 3.5 In

Case S - A = 4 B = 0.83 5 Tubes
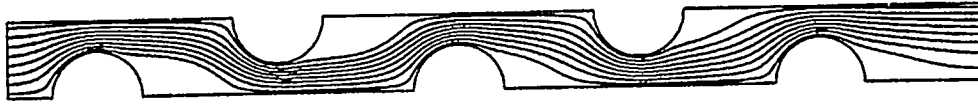
Case T - A = 4 B = 0.83 5 Tubes I = 1 Percent

Case U - A = 4 B = 0.83 5 Tubes I = 20 Percent
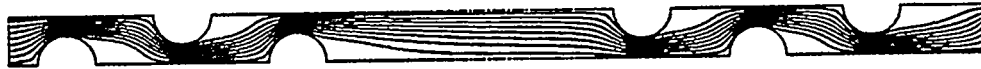
Case V - Staggered With 18 In Spacing
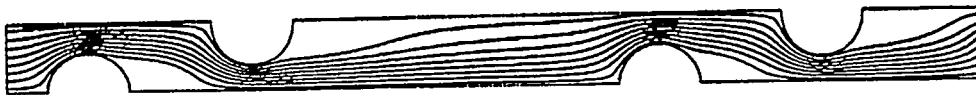
Case W - 18-In Gap Between Banks 2 and 3

the distance covered by the tubes. Its usefulness is that of an approximate measure of the open area. Cases V and W differ from the other cases in that a large (18-in) gap is left between either banks 3 and 4 or banks 2 and 3, respectively, to allow cleaning equipment to pass across the screen in the bankwise direction.
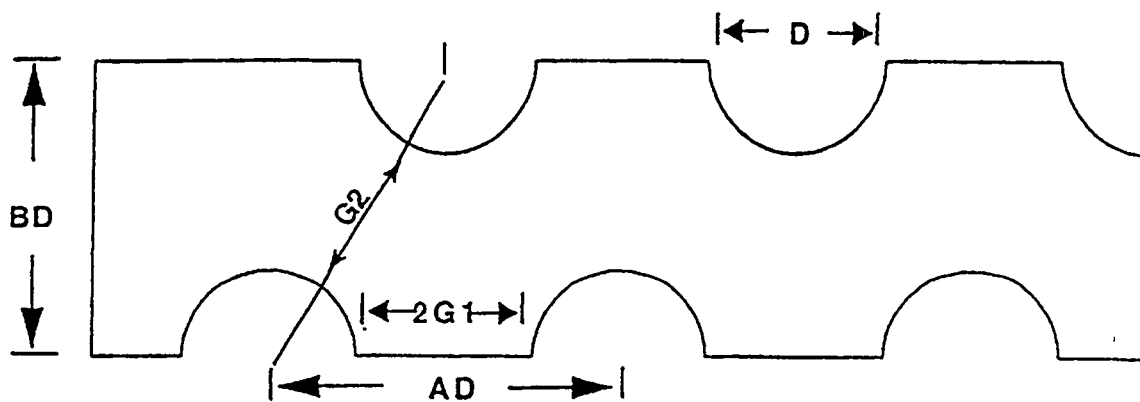
Figure 4.3-18   Definition of Geometric Parameters

In the table, the collection efficiencies for each particle class and for all of the particles are listed as well as the overall pressure drop across the screen. The total percent of particles captured is the weighted sum of the individual collection efficiencies using relative weights derived from Table 4.3-8.

Discussion of CFD results

In Appendix A, plots of streamlines for all of the cases are presented so as to provide a basis for explaining the performance of the slag screen configurations in terms of particle capture efficiency and pressure drop.

Inline-Tube Cases A through F: For the initial evaluation of the slag screen, six inline-tube arrangements were analyzed in which the tube-to-tube spacings in the streamwise and bankwise directions were varied. As can be seen from Table 4.3-9, particle capture efficiency increased with decreasing tube spacing in the bankwise direction (i.e., decreasing B). For Cases A and F, the spacing within a row (A) was increased by one tube diameter and resulted in a small increase in capture efficiency. Generally, the trajectories of larger particles that are located essentially in a direct line-of-sight with a tube are not affected by the flow field and impact on the tube. The larger spacing for Case F allows the effects of the turbulent fluctuations to cause sufficient numbers of smaller particles to diffuse into regions that permit particle capturing; the 60-micron diameter particles are unaffected by the larger spacing in Case F. Overall, the capture efficiency of the inline arrangements is well below the target range and these designs are not viable for the slag screen.

Staggered-Tube Cases G through W: In staggered-tube designs, the flow is forced to turn rapidly. It is expected that the larger particles have sufficient inertia that they are unable to follow the flow

180

streamlines as the flow turns around the tube in an adjacent row. Also, these configurations permit smaller values of B than inline configurations do; B for inline arrays is limited to one tube diameter, in which case the tubes in a bank form a solid wall to the oncoming flow. Turbulence is generated in the wakes of all of the tubes (whether in an inline or staggered arrangement) and this increase in turbulence affects the smaller particles. For the staggered-tube arrays, the combination of rapid turning and increased turbulence is expected to increase the collection efficiencies for smaller particles as well.

For Cases G through L, the ranges of both A and B were similar to those used for the inline-tube designs and the resulting performance was also similar - that is, the collection efficiency was too low. In Case M, B was reduced to unity and the collection efficiency improved dramatically for all particle classes. In Case M, the tube-to-tube gaps were small relative to those used in the previous cases (see Table 4.3-9). For Case N, B was further reduced and the collection efficiency increased further. In all cases, the pressure drop was less than 0.1 psi.

As can be seen from the figures presented in Appendix A, most of the staggered-tube cases included a section of tube located across the exit of the computational domain. Obviously, in practice the slag screen has an integral number of tubes. In Case O, this last fractional tube was eliminated. Comparing the results for cases N and O, the collection efficiency decreased slightly in the absence of the fractional tube.

Using only 5 tubes each, Cases O through Q show the effects of further decreasing B or increasing the tube diameter. For case P, the pressure drop is over 0.2 psi and represents an unacceptable design; this large increase is due to the very small tube gaps that result from the value of B used. By using a large tube diameter (Case Q), larger gaps result and the pressure drop and tube spacing are acceptable, but the particle collection efficiency is unacceptable.

During the operation of the slag screen, slag will accumulate on some of the downstream tubes. In Case R, the tube-to-tube spacings were maintained the same as those used in Case M, but the diameter of the tubes was increased to 3.5 inches to simulate the effects of accumulating a one-quarter inch layer of slag; for these calculations, the slag surface was assumed to be hydrodynamically smooth. The gap spacings decreased for this case due to the simulated slag layer. Compared to Case M, Case R shows that both the collection efficiency and pressure drop increased.

Due to concerns about maintaining large enough tube gaps to allow for slag or ash removal, Case S was run with a larger value of tube spacing within each row (A) while maintaining the same bankwise spacing as in Case O. The results for case S show that both the collection efficiency and pressure drop decreased relative to the values for Case O; however, the performance is acceptable.

Table 4.3-9 also includes case S', which is the same as Case S geometrically. The information for S' provides a measure of the uncertainty in the collection efficiency for the smaller particles. Recall that a stochastic model was used for all of the calculations described here For each particle injected

181

into the flow, the trajectory is determined by integrating the equation of motion for the particle over a large number of time steps (typically, for 50000 to 100000 time steps in these cases). Particles that are trapped in recirculation zones can remain there indefinitely. Therefore, *FLUENT* will terminate the integration of such trajectories after a preset number of time steps has accumulated. One may interpret such trapped particles as having been removed from the flow and to assume that they are effectively captured by the slag screen. This was the assumption made for all cases except Case S'. Alternatively, one can assume that random fluctuations will eventually eject the smaller particles from the recirculation zone and that it will escape from the slag screen. This was the assumption made for Case S'. As can be seen from Table 4.3-9, the capture efficiency for the larger particles is unaffected by the assumption used (these tend to collect on the upstream side of a tube by inertial separation) while that for the smaller particles is affected (these tend to collect on the downstream side of a tube). Overall, the collection efficiency is acceptable with use of either assumption.

Cases T and U were designed to address concerns about the assumed level of turbulence intensity at the inlet. For Case T, the inlet turbulence intensity was one percent. This value is obviously unrealistically low for practical combustion equipment. For Case U, the inlet value was increased to 20 percent. Comparing the results for Cases S, T and U, it is seen that the inlet value of turbulent intensity has only a small effect on capture efficiency and pressure drop. As noted above, the rapid turning of the flow and the recirculation zones behind the tubes are the dominant sources of turbulence.

Cleaning of the tubes is anticipated to occur from time to time. To allow cleaning equipment to traverse the slag screen, large gaps must be maintained between some tube banks. In Case V, an 18-in. gap is maintained between the centers of the third and fourth tubes in the lower row (refer to the corresponding streamline plot in Appendix A); in Case W, an 18-in. gap is maintained between banks 2 and 3. Case W is considered to be the more practical design since less maneuvering of the cleaning head is required to reach all of the surface of a tube. From Table 4.3-9, performance of either design is acceptable. The results for Case W were obtained using only four tube banks (versus six banks for Case V) and provides a conservative design. Case V assumes that there is sufficient volume to accommodate 6 tube banks and two 18-in gaps.

Case W represents a viable design for a slag screen. It is instructive to examine the collection efficiency by particle class at each tube bank. These results are presented in Figure 4.3-19 and show that the largest portion of the total particle mass is captured on the second bank of tubes. Based upon a limited examination of the tube-by-tube performance of some of the other designs, the relative efficiency of the first row is typical. Since large particles can deviate appreciably from the flow streamlines as the flow turns, a substantial fraction of these particles impact the front surface of the upstream tubes and are captured.

As is evident from the preceding discussion and from the results shown in Table 4.3-9, capture efficiency is directly related to pressure drop across the slag screen. This relationship is depicted in
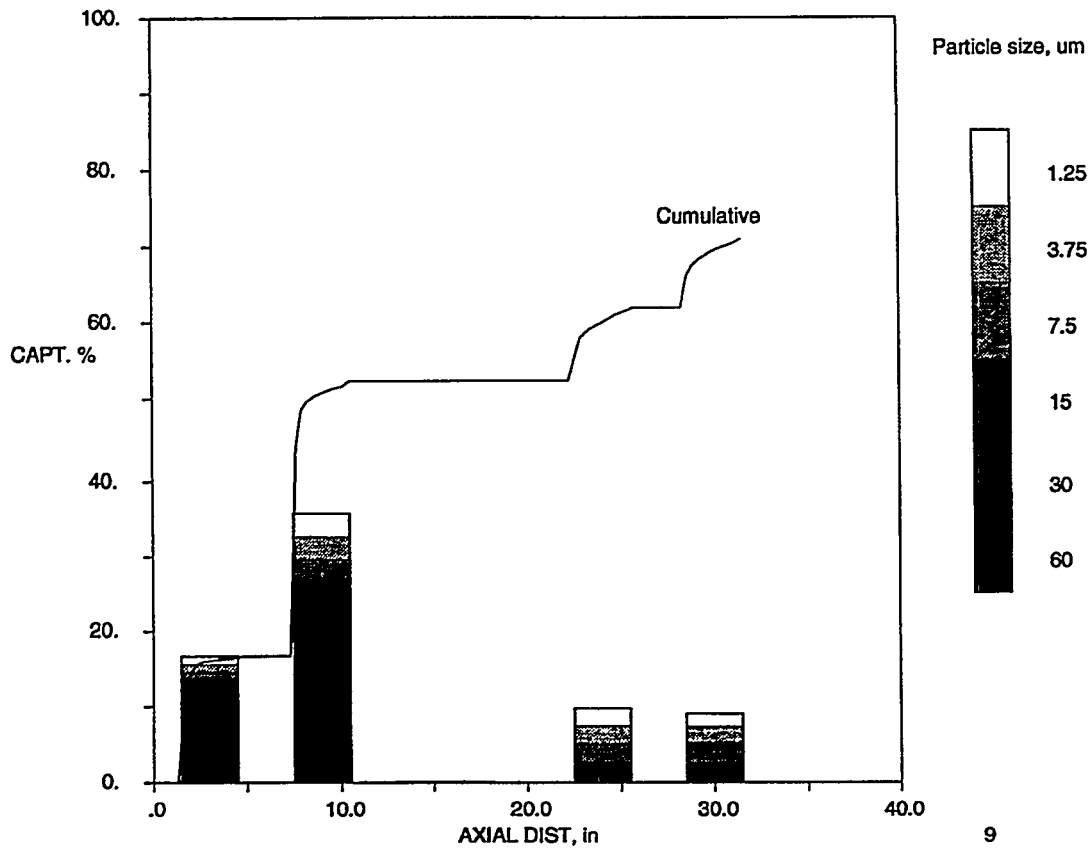
Figure 4.3-19 Capture Percentage by Particle Class and Tub Location - Case W.
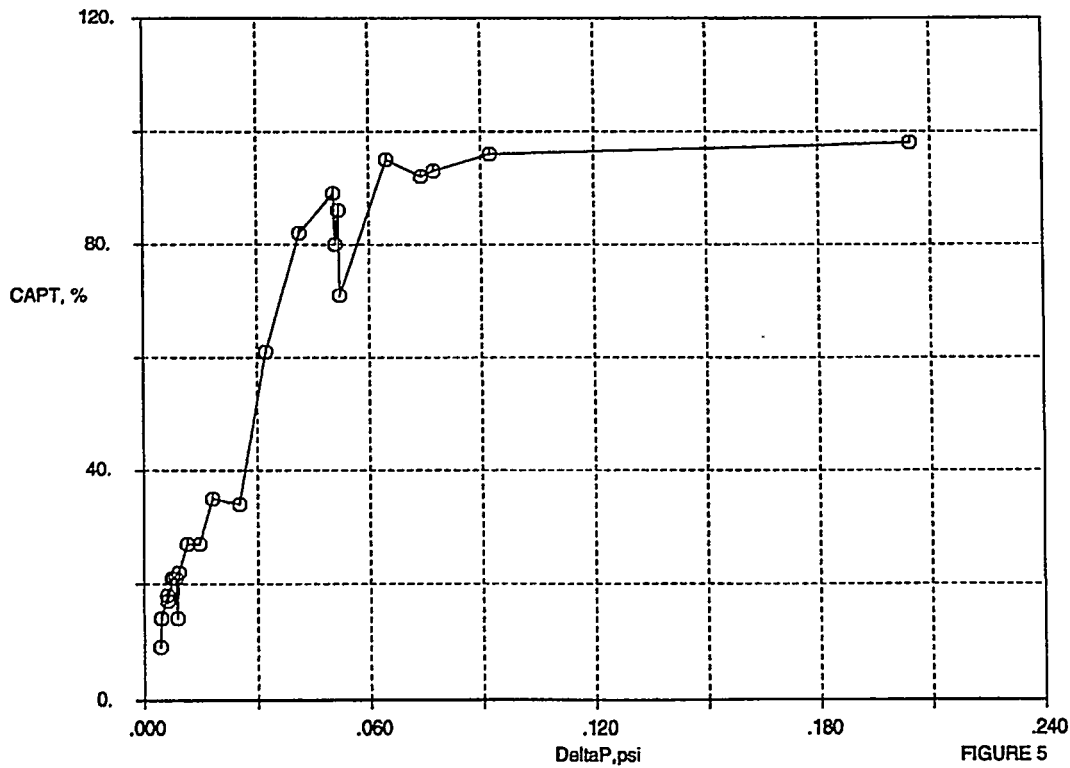
Figure 4.3-20 Capture Efficiency Increases with Pressure Loss.

183

Figure 4.3-20 for the cases studied here. Deviations from an otherwise smooth curve are associated with differences in the characteristics of each case and appear to be of second order.

As the design of the slag screen is finalized, it is recommended that CFD be used to estimate its performance. More refined tube boundary conditions can be used, including the effects of surface roughness. Some three-dimensional flow simulations should also be conducted to determine the effects of the flow in the vicinity of the endwalls on screen performance.

4.3.5 Convective Air Heater Ash Management

Maximum Inlet Temperature for Deposit Removability

We have picked four coals for detailed analysis in Combustion 2000. These coals represent a wide range of American coals:

1. Cedar Grove: Appalachian bituminous coal with very high ash fusion temperature.

2. Blind Canyon: Utah bituminous coal with high ash fusion temperature.

3. Illinois No. 6: Illinois basin coal with high iron content, giving high ash fusion temperature under oxidizing conditions, but low ash fusion temperature under reducing conditions. The analysis of uncleaned coal provided in the EPRI Technical Assessment Guide will be used.

4. Wyodak: Powder River Basin sub-bituminous coal with high calcium and low ash fusion temperature.

Using PSIT's algorithms for calculating ash viscosity, we can examine the tendency of deposits to densify and/or flow on the radiant air heater surface. Using the ASTM ash composition (Table 4.3-10), the viscosity was calculated as a function of temperature from 1000 to 1900 K. The results of these calculations were used to estimate the flowing slag layer thickness and deposit densification rates discussed below.

184

TABLE 4.3-10 ASTM ASH ANALYSIS

	Illinois 6 (EPRI TAG)	Wyodak (Rochelle)	Blind Canyon (Deer Creek)	Cedar Grove (Mingo Logan)
SiO_2	45.0	32.1	51.7	53.7
Al_2O_3	18.0	17.8	21.2	29.6
TiO_2	1.0	1.0	1.5	1.3
Fe_2O_3	20.0	5.2	4.8	9.1
CaO	7.0	24.8	8.3	1.7
MgO	1.0	10.0	1.7	0.9
Na_2O	0.6	1.0	4.1	0.5
K_2O	1.9	0.3	0.2	3.1
P_2O_5	0.2	1.2	0.2	0
SO_3	3.5	7.3	6.4	0
TOTAL	98.2	100.7	100.1	99.9

Figures 4.3-21 and 4.3-22 display the viscosity-temperature curves for oxidizing (all iron as Fe^{+3}) and reducing (all iron as Fe^{+2}) conditions. Cedar Grove coal has so little iron that the viscosity changes little with gas environment. Illinois 6 and Blind Canyon, however, have enough iron to ensure that under reducing conditions, the viscosity is much lower than under oxidizing conditions. Wyodak coal has a distinctly different viscosity-temperature relationship. Note the rapid viscosity change with temperature (1000 to 1100 K) that is characteristic of PRB coal ashes.

Raask (1985) describes the behavior of deposits on surfaces as a function of viscosity. These observations have been adapted to the program coals in Tables 4.3-11 and 4.3-12. Under oxidizing conditions, the onset of sintering is approximately 1000 K (1350°F) for the PRB coal and 1200 K (1700°F) for the bituminous coals. Formation of "flowing" slag begins at about 1400 K (2060°F) for the PRB coal and about 1650 K (2500°F) for the bituminous coals.

Under reducing conditions, the onset of sintering is still approximately 1000 K (1350°F) for the PRB coal and 1200 K (1700°F) for the Cedar Grove bituminous coal. The other two bituminous coals have enough iron, particularly Illinois 6, that the onset of sintering is approximately 1000 K (1350°F). This probably represents a maximum temperature for deposit removal by sootblowing.

What are the deposit characteristics that relate to successful deposit removal? This question was addressed by Wain et al. (1992). They measured thermal and mechanical properties of ten slags and tried to relate the measurements to sootblowing experience. The temperature change needed to reach
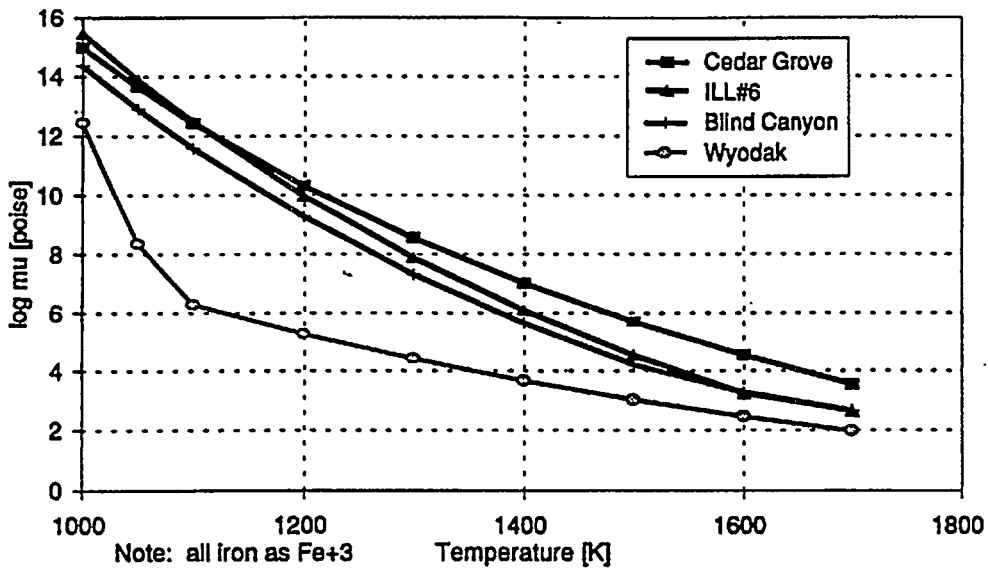
Figure 4.3-21   Viscosity-temperature Curves for Oxidizing Conditions.
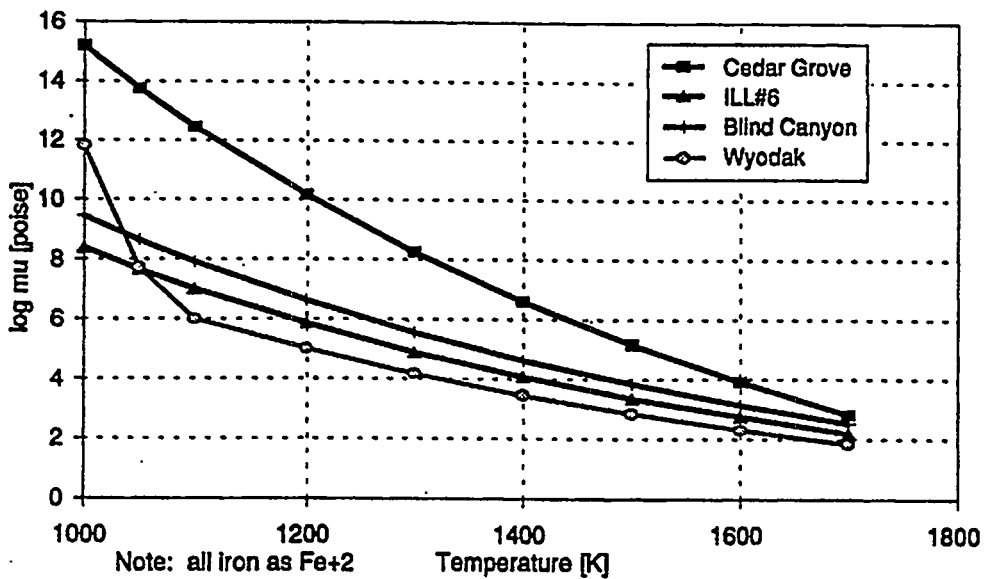
Figure 4.3-22   Viscosity-temperature Curves for Reducing Conditions.

the fracture stress level in the deposit was used to quantify sootblowing.

$$R = \Delta T = \frac{\sigma (1 - \nu)}{\alpha E} \tag{40}$$

where σ is the fracture stress, α is the thermal expansion coefficient, ν is Poisson's ratio, and E is the elastic modulus. The thermal shock parameter R depends on the composition of the deposit, the degree of crystallinity, and the porosity of the deposit.

TABLE 4.3-11 COMBUSTION 2000: EXPECTED ASH SINTERING BEHAVIOR

(Based on Raask, Table 9.1) Under Oxidizing Conditions

	log μ (Poise)	Temperature (K)			
		Wyodak	Blind Canyon	Illinois No. 6	Cedar Grove
On surfaces					
Onset of Sintering	10 to 12	1000 to 1030	1120 to 1200	1120 to 1215	1129 to 1220
Medium-Rate Sintering	8 to 10	1030 to 1060	1200 to 1300	1215 to 1320	1220 to 1330
Rapid Sintering	6 to 8	1060 to 1140	1300 to 1400	1320 to 1450	1330 to 1480
Formation of Non-Flowing Slag	4 to 5	1220 to 1460	1460 to 1550	1510 to 1600	1550 to 1650
Slow Movement by Gravity	3 to 4	1360 to 1460	1550 to 1660	1600 to 1630	1650 to 1690
Flowing Slag in Cyclone-Fired Boilers	2.4	1475	1755	1790	1820

TABLE 4.3-12 COMBUSTION 2000: EXPECTED ASH SINTERING BEHAVIOR

(Based on Raask, Table 9.1) Under Oxidizing Conditions

	log μ (Poise)	Temperature (K)			
		Wyodak	Blind Canyon	Illinois No. 6	Cedar Grove
On surfaces					
Onset of Sintering	10 to 12	1000 to 1025	to 955	to 930	1120 to 1200
Medium-Rate Sintering	8 to 10	1025 to 1050	955 to 1100	930 to 1030	1200 to 1320
Rapid Sintering	6 to 8	1050 to 1100	1100 to 1260	1030 to 1190	1320 to 1450
Formation of Non-Flowing Slag	4 to 5	1200 to 1330	1350 to 1500	1290 to 1400	1500 to 1600
Slow Movement by Gravity	3 to 4	1330 to 1400	1500 to 1575	1400 to 1550	1600 to 1660
Flowing Slag in Cyclone-Fired Boilers	2.4	1430	1714	1581	1792

The thermal expansion coefficient and Poisson's ratio are independent of the porosity of the deposit. The thermal expansion coefficient depends on the composition and the micro-structure (i.e., glassy versus crystalline). Both the fracture stress and the elastic modulus depend on the porosity of the deposit, , as follows

$$\sigma = \sigma_0 \ e^{n\varepsilon} \tag{41}$$

and

$$E = E_0 \ (1 - a\varepsilon + b\varepsilon^2) \tag{42}$$

where n, a, and b are parameters which depend on the composition of the deposit.

The compressive strength was measured as a function of porosity for ten slags. As porosity decreased, the compressive strength increased. The change in compressive strength was most dramatic as the porosity dropped below 25%. Above 25%, all the slags had similar compressive strengths. The elastic modulus showed similar trend with porosity. The authors state that, "This value of the porosity may be considered *a critical porosity* level, since above 25 vol% the mechanical properties can be predicted with a fair degree of accuracy, regardless of the composition or microstructural details." The thermal shock resistance parameter R is also fairly constant at porosities greater than 0.25 (Figure 4.3-23).
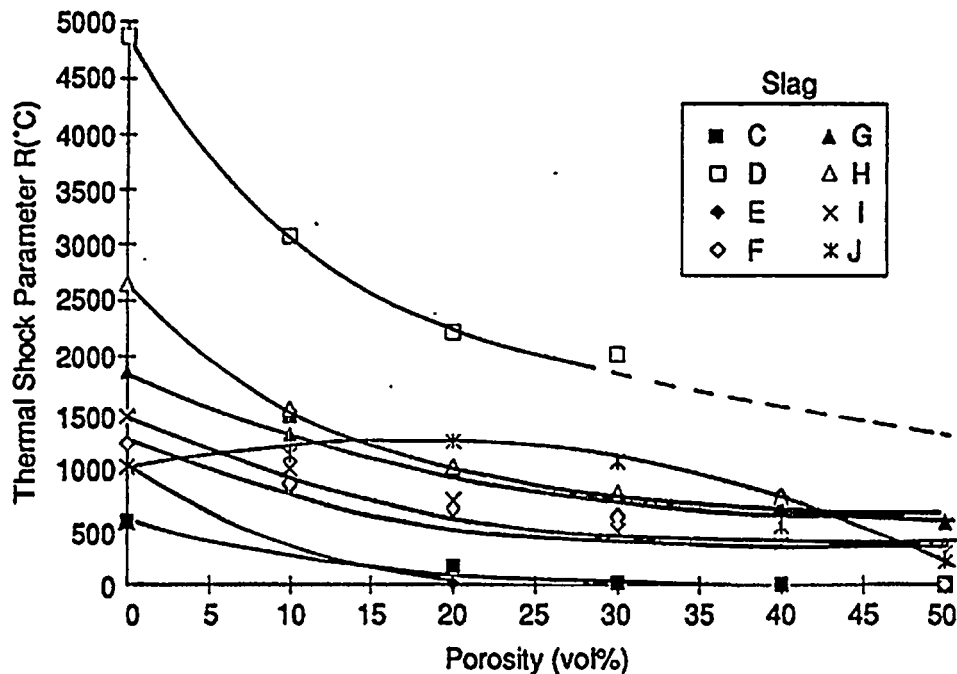
Figure 4.3-23   Variation in Thermal Chock Parameter R, Calculated for Each Slag at Porosity Values from 0- to 50 vol% (Source: Wain et al., 1992)

It is well known that reduction in porosity, i.e., sintering of the deposit, makes the deposit harder to remove by sootblowing. Since the thermal shock parameter is fairly constant for porosity greater than 0.25 (vol% = 25), we can conclude that this is a <u>critical porosity for deposit</u> removal by sootblowing.

The values of the thermal shock parameter as calculated by Wain et al. are high, 500 to 5000°C at zero porosity. The authors conclude that the absolute value of the parameter should not be used. Instead, this should be used to make comparisons between coals. They have used compressive strength instead of tensile strength to calculate R. Tensile strength (which is lower than compressive strength) is probably what should be used to calculate R, but it's easier to measure compressive strength.

The most important criterion for determination of the maximum allowable gas temperature entering the convective air heater is that the deposit must be removable by sootblowing. Since an ash deposit has a finite thickness, we can specify that the "outer" surface of the deposit must not be so sintered as to prevent easy removal by sootblowing. The criterion for easy removal will be that a porosity of 0.25 or more will be obtained in greater than 8 hours. Eight hours was picked as a convenient time for sootblowing.

Densification calculations were performed using the method of MacKenzie and Shuttleworth (1949). The bulk ash composition was used to calculate the viscosity. The initial deposit porosity was assumed to be 50% and the mean pore radius of 10 μm was assumed. Figure 4.3-24 shows a densification plot for Illinois No. 6 coal. The point at which $t = 3 \times 10^4$ s and a relative density equals 0.75 corresponds to a temperature of approximately 1180 K as shown on the figure. The maximum deposit surface temperatures are given in Table 4.3-13.
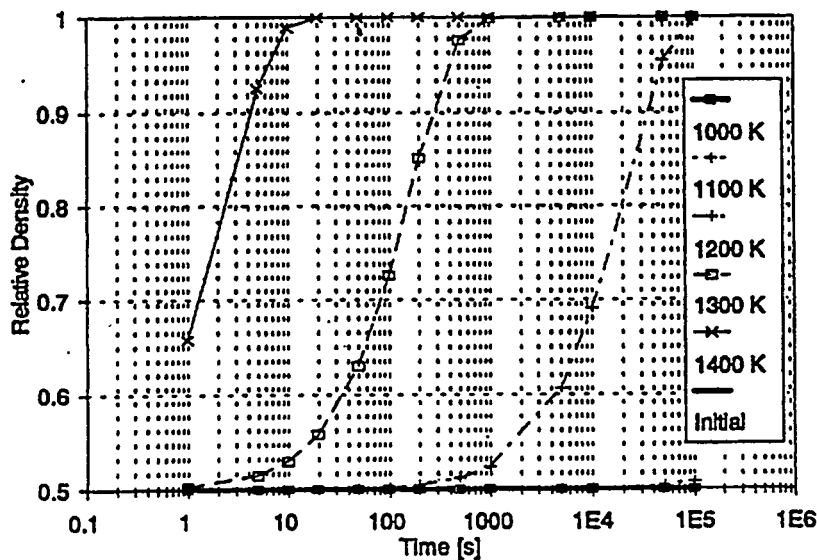
Figure 4.3-24   Densification of Illinois No. 6 (EPRI TAG) Deposit.

Calculating the gas temperature from the deposit surface temperature requires the deposit thickness. Since ash is a good insulator (particularly if it is not sintered), the temperature drop across the ash must be accounted for. The gas temperature can be calculated by solving the steady state heat transfer problem given the air and deposit surface temperatures. This involves solving three equations for three unknowns.

TABLE 4.3-13 MAXIMUM DEPOSIT SURFACE TEMPERATURE BASED ON DENSIFICATION CRITERIA

Coal	Temperature (K)
Blind Canyon	1160
Illinois No. 6	1180
Cedar Grove	1240
Wyodak	1025

As a check on the calculational approach, the maximum allowable flue gas inlet temperature was estimated for a conventional steam convective air heater. Since the first bank of tubes in a power plant (the secondary superheater) sees a lot of radiation, the second bank (the reheater) was modeled. The gas temperature entering the reheater is typically 1900°F. Ash deposits of 0.5 in. in 8 hours are typical and can be removed easily.

Table 4.3-14 gives the parameters used for the steady state heat transfer calculation applied to a conventional steam reheater. Illinois No. 6 coal was used to determine the fireside deposit surface temperature. Figure 4.3-25 shows that the maximum allowable temperature for a 0.5 in. deposit is slightly less than 2000°F. This agrees with the experience in coal-fired power plants. Thus, the estimation method for the HITAF convective air heater is reasonable.

TABLE 4.3-14 VALUES USED TO CALCULATE STEADY STATE HEAT TRANSFER IN A STEAM REHEATER

Parameter	SI Units	English Units
Steam Temperature	817 K	1010°F
304SS Thermal Conductivity	17.3 W/m-K	10 Btu/ft-hr-°F
Ash Thermal Conductivity	1 W/m-K	0.6 Btu/ft-hr-°F
304SS Thickness	$3.175 \times v10^{-3}$ m	0.125 in.
Gas Heat Transfer Coefficient	170.4 W/m^2-K	30.0 Btu/ft^2-hr-°F
Steam Heat Transfer Coefficient	1700 W/m^2-K	300 Btu/ft^2-hr-°F

Table 4.3-15 gives the values used to solve the heat transfer problem in the HITAF convective air heater. For this calculation, the heat exchanger wall was assumed to be made of 0.25 in. silicon
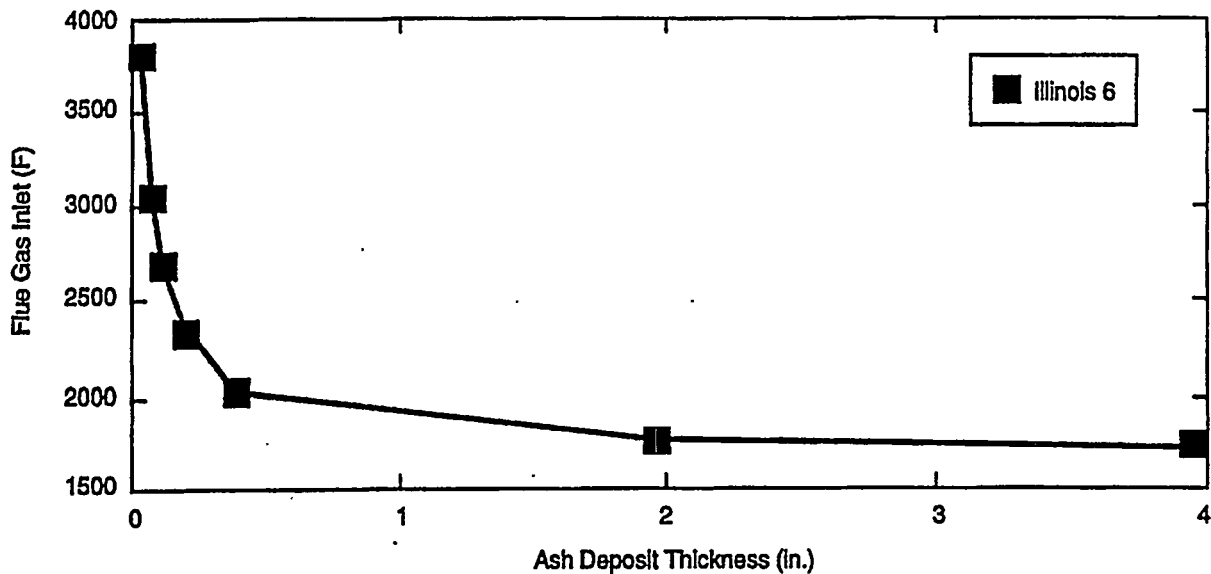
Figure 4.3-25   Maximum Allowable Flue Gas Inlet Temperature for a Steam Reheater (Illinois No. 6 Coal).

carbide. The results (as shown in Figure 4.3-26) are virtually identical for an alloy heat exchanger (0.125 in. thickness of Inconel).

TABLE 4.3-15 VALUES USED TO CALCULATE STEADY STATE HEAT TRANSFER IN CONVECTIVE AIR HEATER

Parameter	SI Units	English Units
Air Temperature	978 K	1300°F
SiC Thermal Conductivity	52 W/m-K	30.1 Btu/ft-hr-°F
Ash Thermal Conductivity	1 W/m-K	0.6 Btu/ft-hr-°F
SiC Thickness	$6.35 \times v10^{-3}$ m	0.25 in.
Gas Heat Transfer Coefficient	170.4 W/m^2-K	30.0 Btu/ft^2-hr-°F
Air Heat Transfer Coefficient	544.6 W/m^2-K	95.9 Btu/ft^2-hr-°F

The results are shown in Figure 4.3-26 for four coals. For ash layer thickness less than 6.4×10^{-3}m (0.25 in.), the allowable flue gas inlet temperature is very sensitive to deposit thickness. If the convective air heater surface is "clean," the inlet gas temperature can be high, 1500 to 1750 K (2200 to 2700°F), for the bituminous coals.

This analysis also serves to remind that the ash layer thickness is part of the convective air heater design. We must decide what amount of ash we can tolerate in the convective air heater in order to maintain adequate heat transfer. These calculations are rather simplistic since they just look at steady state heat transfer at one point in the convective air heater (i.e., the hottest point). However, when coupled with a design for the convective air heater that includes limits on the ash layer thickness, they can be used to set the maximum inlet gas temperature.
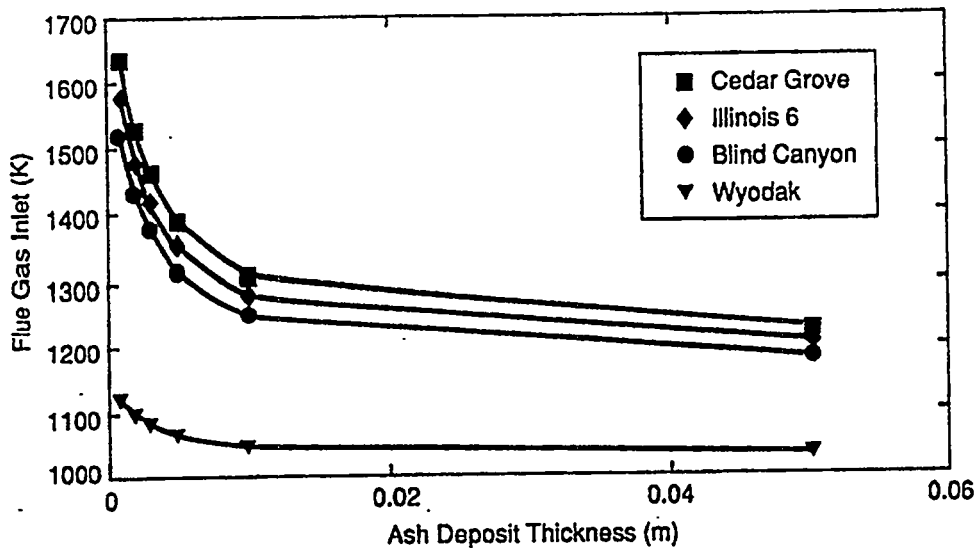
Figure 4.3-26   Maximum Allowable Flue Gas Inlet Temperature for HITAF Convective Air Heater.

Overall Collection Efficiency in Convective Air Heater

CFD calculations performed by UTRC on various convective air heater configurations (see the July through September, 1993 Technical Quarterly Report) were used to select a convective air heater configuration with favorable heat transfer and low ash deposition. The preferred arrangement features a finned tube sheet with elliptical tubes. The tube sheets are spaced 4 in. apart and consist of ellipsoidal tubes with a 5:1 aspect ratio spaced 3 in. on center. The heat exchanger has a depth of 10 ft in the flow direction (or 40 tubes).

CFD calculations were performed for the first three tubes in the tube sheet. The calculation of the overall convective air heater ash collection efficiency was calculated from these CFD results. As previously discussed in the July through September, 1993 Technical Quarterly Report, inertial deposition of large particles is largely confined to the first tube (the leading edge). In subsequent tubes, there should be some steady state deposition, a combination of inertial deposition and turbulent diffusion. Using this assumption, the calculated collection efficiency for the third tube was extrapolated to rest of the convective air heater. The CFD calculation yielded the collection efficiency for the first three tubes, 3, and the collection efficiency for the ith tube, i, was derived from this. The overall collection efficiency in the convective air heater (consisting of the first three tubes and another 37 tubes) is then given by

$$\eta_{CAH} = 1 - (1 - \eta_3)(1 - \eta_i)^{37}$$

Since the ash is no longer molten in the convective air heater, we expect ash particles to have some finite sticking probability based on their composition. This has been calculated for Illinois No. 6 ash as a function of particle size. Table 4.3-16 gives the results of these calculations. From the table, it

192

is clear that deposition of particles larger than 10 to 20 μm is very low after the leading edge of the convective air heater. The effect of a non-unity sticking probability is dramatic and reduces the amount of material collected in the convective air heater to a low level as discussed in the next section.

TABLE 4.3-16 CALCULATION OF COLLECTION EFFICIENCY IN CONVECTIVE AIR HEATER

Collection Efficiency	0 to 2.5 μm	2.5 to 5 μm	5 to 10 μm	10 to 20 μm	20 to 40 μm	40 to 80 μm
First three tubes	13.1%	12.2%	11.4%	10.9%	13.1%	13.6%
Subsequent tubes	3.3%	3.0%	3.6%	2.1%	1.1%	0.6%
Total collection (unity sticking)	74.5%	71.2%	77.0%	59.2%	42.6%	30.1%
Total collection (including sticking probability factor)	24.9%	10.5%	7.8%	4.7%	5.3%	3.2%

Ash Mass Balance in HITAF

The previous sections have provided details of ash deposition efficiencies and deposit removal at various locations in the HITAF. In this section, an overall mass balance for ash in the HITAF is created for Illinois No. 6 coal. Ash loading in the gas was calculated from the mass flow rates given in Table 4.3-17 for one HITAF combustor taken from the commercial plant design as outlined in the Phase II proposal. Figure 4.3-27 shows the points in the HITAF that correspond to the flows in Table 4.3-17.

TABLE 4.3-17 BASELINE HITAF FLOWS FOR ASH MASS BALANCE (ILLINOIS NO. 6)

No.	Stream	T (°F)	Flow, lb/s
1	Coal	138	17.3
	Gas Flows		
2	Primary Air	138	26.2
3	Secondary (Vitiated) Air	1005	143.4
4	Reburn (Vitiated) Air	1005	32.9
5	Slag Screen Inlet	2800	217.9
8	Slag Screen Outlet	2650	217.9
9	Flue Gas Recycle	256	117.0
12	Convective Air Heater Inlet	1800	334.9
13	Convective Air Heater Outlet	1190	334.9
14	Baghouse Outlet	350	334.9

PSIT's mineral transformation model (MMT) was used to generate an ash particle size distribution (psd) for Illinois No. 6 that is used as a starting point for the deposition calculations.

193
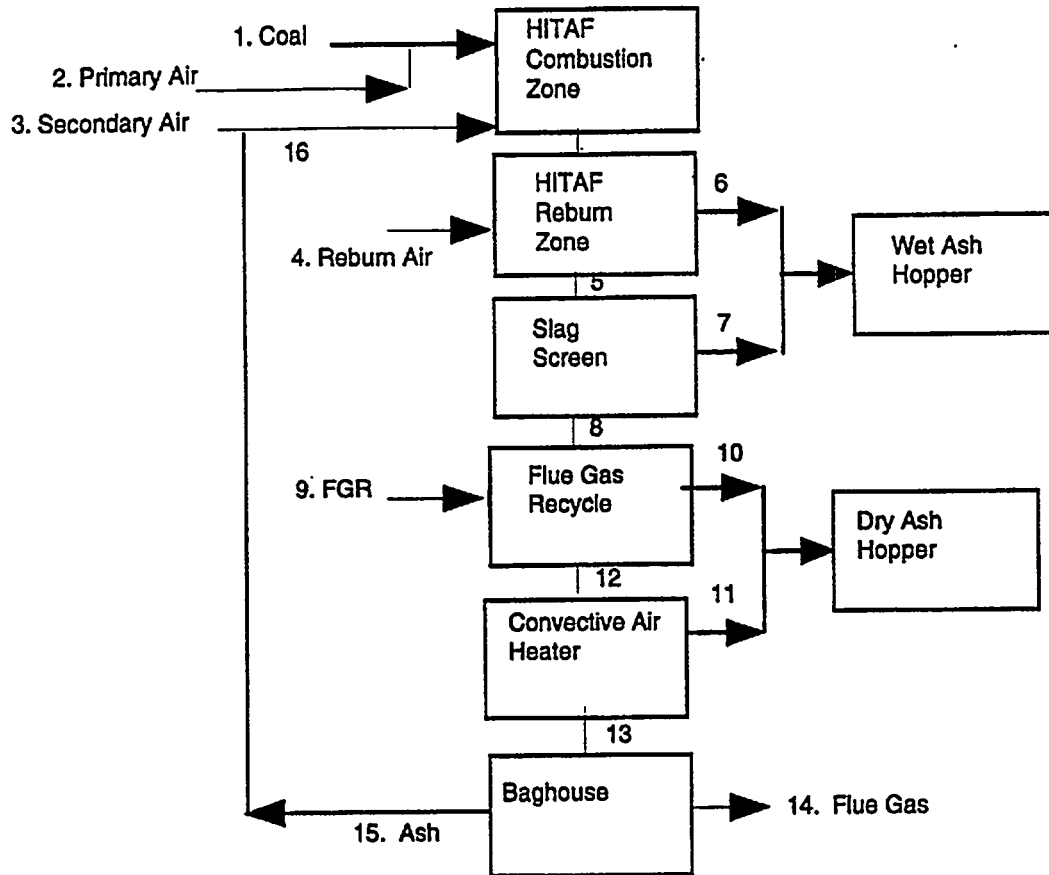
Figure 4.3-27 Ash Mass Balance in HITAF.

Deposition in the Radiant Air Heater, slag screen, and Convective Air Heater was calculated as described in the previous sections.

In brief, the PSIT mineral transformations model operates as follows: CCSEM measurement of coal mineralogy is used as the starting point of the model. CCSEM provides a statistical description of the type, size, and chemical composition of the major minerals contained in a pulverized coal sample. While CCSEM does not identify the size of coal particles and define a relationship between coal particle size and mineralogy, it is done computationally as part of the model.

The operating premise of the model is that the minerals in coal are randomly distributed according to the relative volumes of coal and mineral particles. In other words, the model assumes that there is no preferential grinding of coal along coal-mineral planes to produce preferential mineral-rich classes of coal particles. This means that the variation in mineral content from coal particle to coal particle is a random process, and can therefore be modeled using statistical techniques. The model therefore redistributes the minerals among the various size classes of coal particles using a combination of Poisson statistics and Monte Carlo techniques. Extraneous or excluded minerals are also identified. At the conclusion of this step, a "reconstituted" coal with minerals of different sizes and compositions distributed among the various size classes of coal particles is obtained.

194

Once the inorganic species are redistributed, the model begins the ash formation computation. Coalescence is allowed to proceed fully within each individual coal (char) particle, barring char fragmentation. No kinetic barriers to mineral coalescence within a burning char particle are assumed. Results calculated with this assumption incorporated into the model are in good agreement with laboratory scale combustion test data.

Modifications were made to the MMT to allow it to interface with the ash transport and deposition model. A subroutine to calculate vaporization of sodium and calcium was added to the model. Submodels for deposition in the radiant air heater, in the slag screens, and at the leading edge of the convective air heater were written and coupled to the MMT output. The combustion stoichiometry is taken from the current combustor design: 740 MBtu/hr at a stoichiometric ratio of 1.0. Secondary combustion air is assumed to be vitiated to 17.5% oxygen. Transport air, which accounts for 15% of the oxygen, is assumed to have 21% oxygen.

The collection efficiency for ash particles in the radiant air heater, slag screen, and convective air heater is summarized in Table 4.3-18. The details of calculation of these collection efficiencies were discussed above. These collection efficiencies were applied to the ash particle size distribution as calculated using PSI's MMT.

TABLE 4.3-18. ASH COLLECTION EFFICIENCY FOR HITAF COMPONENTS AS A FUNCTION OF PARTICLE SIZE

Unit	0 to 2.5 μm	2.5 to 5 μm	5 to 10 μm	10 to 20 μm	20 to 40 μm	40 to 80 μm
Radiant Air Heater	0.8%	0.3%	2.0%	2.0%	2.0%	2.0%
Slag Screen	5.0%	10.0%	50.0%	60.0%	70.0%	80.0%
Convective Air Heater	24.9%	10.5%	7.8%	4.7%	5.3%	3.2%

In order to produce a high value ash product, the fine ash collected in the baghouse can be re-injected into the furnace. All ash then leaves the HITAF through the ash hoppers, primarily through the wet ash hopper. The glassy slag produced from the wet ash hopper can then be sold for aggregate material. The ash mass balance was calculated with and without recycle of the baghouse ash. The results of these calculations are shown in Figures 4.3-28 through 4.3-31.

The amount of ash recycled was calculated for each particle size class. At steady state, the amount of ash coming in to the HITAF (in the coal) must equal the amount of ash leaving the HITAF

195
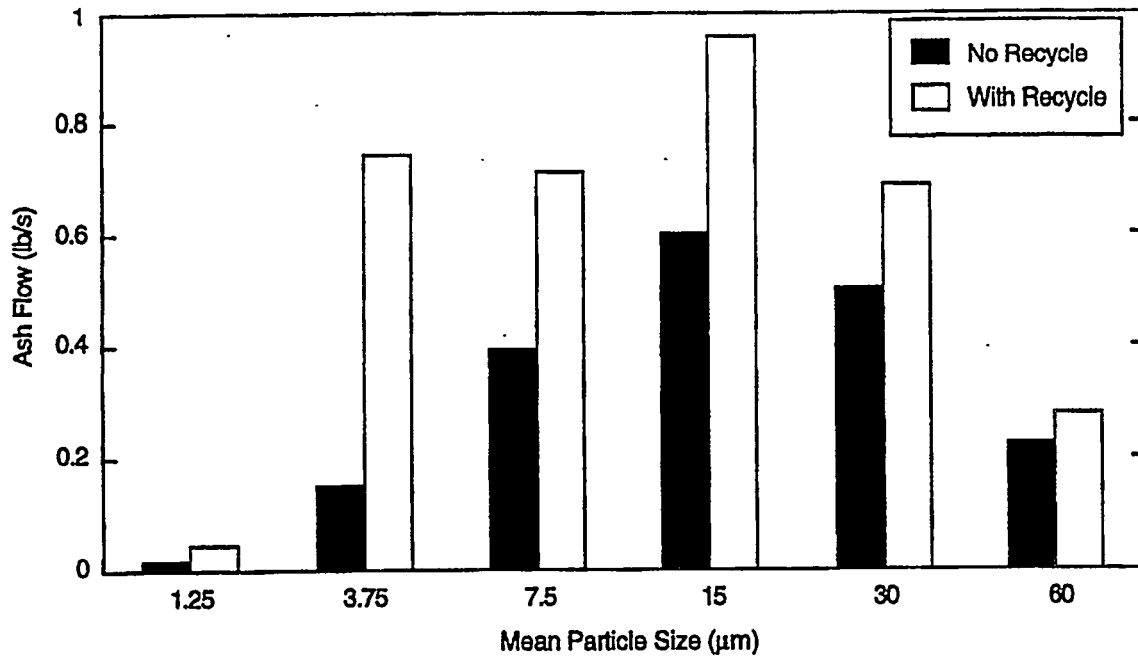
Figure 4.3-28   Ash Loading at Slag Screen Inlet as a Function of Particle Size for Illinois No. 6 Coal, With and Without Recycle of Baghouse Ash.
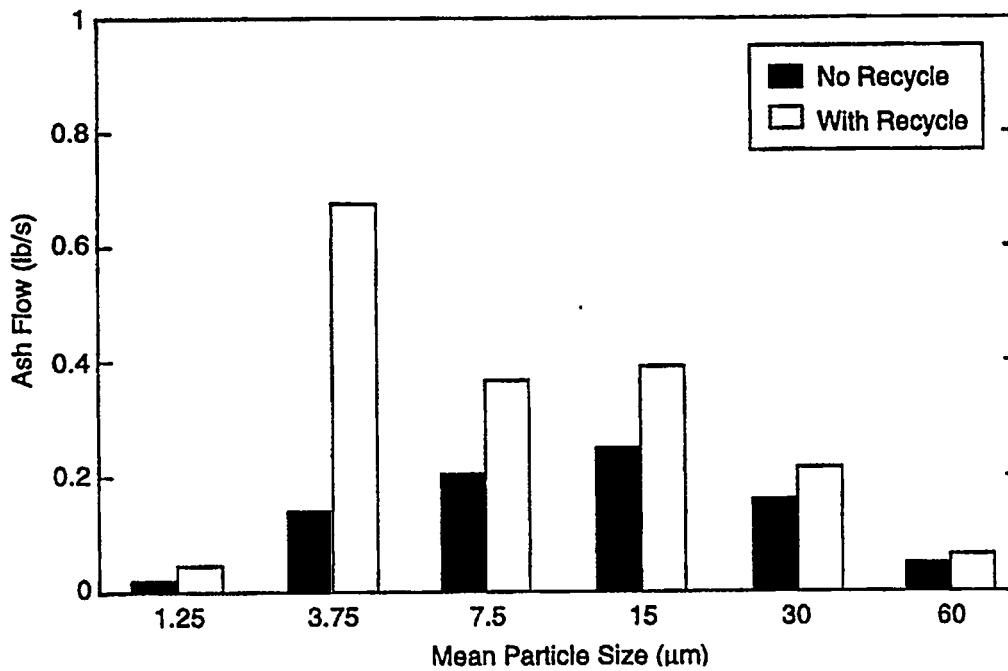
Figure 4.3-29   Ash Loading at Convective Air Heater Inlet as a Function of Particle Size for Illinois No. 6 Coal, With and Without Recycle of Baghouse Ash.
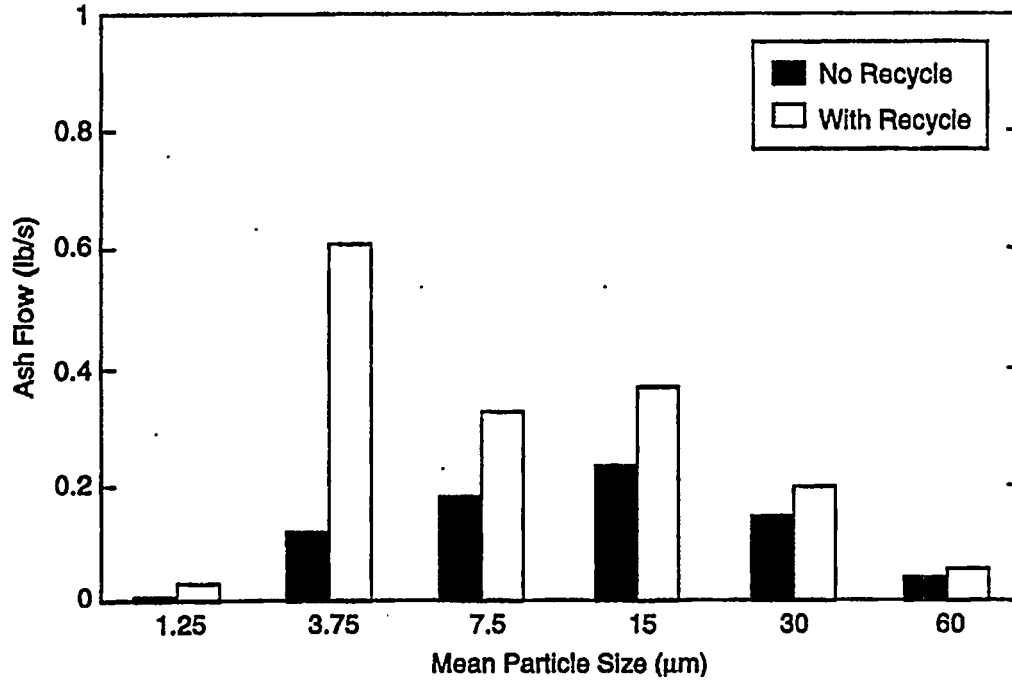
Figure 4.3-30   Ash Loading at Convective Air Heater Outlet as a Function of Particle
Size for Illinois No. 6 Coal, With and Without Recycle of Baghouse Ash.
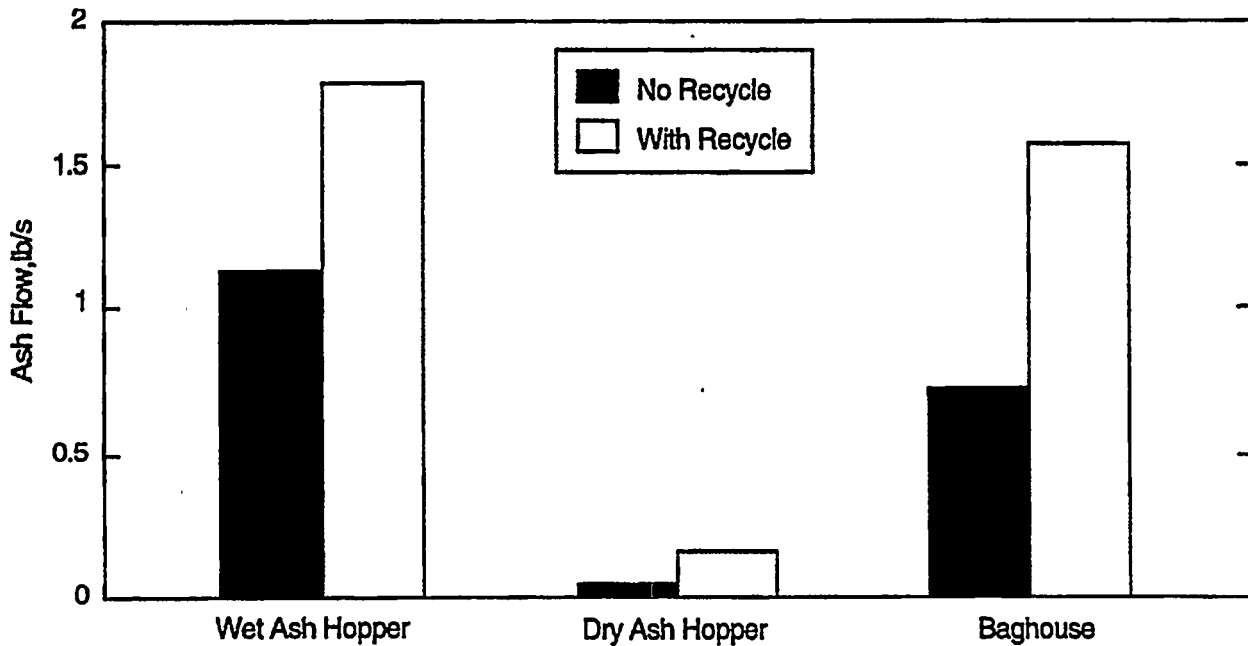
Figure 4.3-31   Ash Removal from HITAF for Illinois No. 6 Coal, With and Without
Recycle of Baghouse Ash.

through the ash hoppers if all the ash collected in the baghouse is recycled. This can be written as

$$W_{coal} = W_{RAH} + W_{SS} + W_{CAH}$$

where W_{RAH}, W_{SS}, W_{CAH} are the mass flow rates of ash removed in the radiant air heater, slag screen, and convective air heater, respectively, and W_{coal} is the mass flow rate of ash in the coal. The amount of ash in the gas entering the radiant zone of the combustor is the sum of the ash from the coal and the recycled ash, R. Thus the amount of ash deposited at the various points in the HITAF is given by the following equations.

$$W_{RAH} = (W_{coal} + R)(\eta_{RAH})$$

$$W_{SS} = (W_{coal} + R)(1 - \eta_{RAH})\eta_{SS}$$

$$W_{CAH} = (W_{coal} + R)(1 - \eta_{RAH})(1 - \eta_{SS})\eta_{CAH}$$

where the η's represent collection efficiencies in the various HITAF regions. Solving for the recycle rate at steady state gives:

$$R = W_{coal} \frac{1 - f(\eta)}{f(\eta)}$$

where

$$F(\eta) = [\eta_{RAH} + (1 - \eta_{RAH})\eta_{SS} + (1 - \eta_{RAH})(1 - \eta_{SS})\eta_{CAH}]$$

There is little change in the mass loading at the exit of the radiant heater since the turbulent diffusion flux is quite low. Thus Figure 4.3-28, the ash particle size distribution at the slag screen inlet, is nearly identical to the post-combustion size distribution for the case of no recycle. From this figure, one can see the size of particles that are recycled from the baghouse. Overall, the effect of recycle is to approximately double the ash mass flow rate from 1.7 lb/s to 3.5 lb/s. The mass loading of small particles (< 5 μm) is more than doubled as a result of recycle and there are substantial increases in the amount of larger particles. The effect of recycle will be to increase the total amount of material collected in the slag screen by about 50% which may necessitate more frequent cleaning.

Comparison of Figures 4.3-28 and 4.3-29 illustrates the effect of the slag screen on ash particle size distribution. After the slag screen, particles larger than 20 μm are significantly reduced. Recycle of baghouse ash does not significantly change the amount of large particles (>20 μm) entering the convective air heater, but substantially increases the amount of smaller particles (< 5 μm). The largest particles will be removed primarily by the leading edge of the convective air heater. The small particles will deposit throughout the convective air heater via turbulent diffusion. Unless the large

increase in fine particles causes increased sintering of deposits, recycle should not have a major impact on cleaning of the convective air heater.

Comparison of Figures 4.3-29 and 4.3-30 illustrates the effect of the convective air heater on ash particle size distribution. Because we have assumed that only a fraction of the particles actually stick in the convective air heater, the amount of ash removed in the convective air heater is small. The mass-average collection in the convective air heater is on the order of 7 to 8%.

Figures 4.3-30 and 4.3-31 illustrate the most important effect of recycling ash: the amount of ash entering the baghouse is doubled. Most of this increase is in fine particles and this should change the operation (and cost) of the baghouse somewhat. The design of the baghouse, therefore, will be dependent on whether or not ash is recycled. From Figure 4.3-31, one can see that the wet ash hopper will have to handle about 50% more slag if ash is recycled and this, too, will effect its design, although not as much as in the case of the baghouse.

4.3.6 Ash Ceramic Interactions

Introduction

The goal of this study was to a) identify mechanisms for ash-ceramic and alkali-ceramic corrosion and b) identify temperature ranges for significant corrosion reactions. We used two different silicon carbide materials (siliconized and alpha-sintered) and two different coal ashes: Western sub-bituminous and Illinois basin bituminous. Previous studies of ash corrosion of silicon carbide have characterized the silicon carbide material in detail, but the ash has not been as thoroughly characterized. Little attention has been paid to the mechanisms for corrosion by ash. Thus it is difficult to generalize about the reaction of silicon carbide to a wide range of ash compositions. In this work, we want to discover the components in the ash that contribute to corrosion of silicon carbide. This will lead to a better understanding of the impact of coal composition on corrosion and to the design of corrosion-resistant coatings for silicon carbide.

Corrosion of hot ceramic surfaces in coal combustion systems can be caused by deposition and reaction of ash or by formation of condensed alkali salts (e.g., sodium sulfate) from the vapor phase. In this study, both paths will be explored. Previous work on the corrosion of silicon carbide at high temperatures has looked at a wide range of environments. Tests of exposure to alkali salts (halides and sulfides) have been extensive (e.g., Butt et al, 1989; Fox et al., 1990; Federer, 1990). A number of tests have been conducted on the interactions between coal ash and silicon carbide (Ward et al., 1980; Ferber and Tennery, 1981; Ferber and Tennery, 1982; Easler et al., 1985).

In the burner rig and thin film studies of Fox and coworkers (Fox et al., 1990), silicon carbide material was exposed to a concentration of 2 ppm sodium sulfate at 1830°F and 4 atm total pressure. After 40 hr, a 50% strength reduction was noted for siliconized SiC and only 30% for sintered SiC. The hypothesis was that the free silicon was attacked more readily than SiC, resulting in a higher corrosion rate.

199

Butt et al. (1989) exposed siliconized SiC and α-SiC in a burner facility in which sodium silicate was injected into the burner. Volatile and particulate sodium was delivered to the samples at a velocity of 30 m/s. The temperature of the samples was 1760°F and exposure times were 243 to 373 hr. Both sintered α-SiC and siliconized SiC showed strength reductions and visual analysis showed that failures were often from large surface pits. For sintered α-SiC, the grain boundaries were attacked preferentially, while for siliconized SiC, the silicon matrix was oxidized rapidly.

Tubes of various silicon carbide materials were exposed to ash via deposition from a flowing gas in crossflow for 1000 hr (Ward et al., 1980). Ash from an Eastern bituminous coal (high silica ash) was used. Tube temperatures were in the range of 1800 to 2300°F. Siliconized silicon carbide showed no apparent oxidation layer and no preferential oxidation of the free silicon. A sintered silicon carbide tube in the same test showed a reduction of the tube wall thickness at the leading edge of the tube, indicating some reaction with ash.

Ferber and Tennery (1981, 1982) exposed various types of silicon carbide to coal ash at approximately 2200°F for 250 to 500 hr. The ash was characterized only as either acidic (high silica) and basic (low silica/high calcium). For acidic slag (Ferber and Tennery, 1981), there was no appreciable change in the microstructure of sintered SiC as a result of the exposure. Negligible change in room temperature tensile strength was observed. Siliconized SiC was also relatively stable with respect to acidic slag in a 500 hr test. Localized corrosion was observed characterized by small pits containing glass. The corrosion seemed to occur preferentially at iron-rich inclusions. A slight increase in the room temperature tensile strength was attributed to crack blunting by formation of a glassy material out of the silicon phase.

For basic ash (Ferber and Tennery, 1982), both siliconized and sintered SiC tubes showed reduced thickness after a 240 hr test. Silica content of slag increased relative to ash; formation of $FeSi_2$ was observed at slag/ceramic interface and was postulated as a mechanism for removing silicon from substrate. No significant decrease in room temperature tensile strength was noted.

Samples of sintered α-SiC were coated with two different kinds of synthetic ash classified again as acidic (high silica) and basic (low silica/high calcium), and exposed to air or gasification-type mixture at 2000 to 2300°F (Easler et al., 1985). The weight change and fracture stress of the materials were measured after exposure. Exposure times were 200 hr. At the highest temperatures, corrosion in the presence of basic slag dominated the SiC-slag interaction while at the lower temperatures, passive oxidation was more important. The reaction products from the basic slag experiments showed evidence of iron silicides which was also noted by Ferber and Tennery (1982). No significant corrosion was observed below 2300°F for acidic and basic slags, but the basic slag corroded the substrate considerably at 2300°F.

High temperature corrosion by sodium salts or by coal ash has been shown to reduce the strength of silicon carbide in some cases. The iron impurities have been linked to corrosive attack by slag. In work cited by Ward et al. (1980), the reaction of iron with silicon carbide can produce iron silicides at

200

temperatures above 1523 K. Ferber and Tennery observed the formation of iron silicides in high calcium/low silica slags at 2200°F and concluded that such alloys could effectively transport silicon away from the silicon carbide surface into the slag.

Modeling Alkali-Ceramic Interactions

Preliminary calculations were performed on sodium vaporization in order to get a better idea of the experimental conditions for the alkali corrosion experiments by calculating the amount of sodium expected in the vapor phase. Theoretical work on sodium sulfate stability (Wibberly and Wall, 1982) has shown that below the temperature range 1800 to 2060°F, condensed sodium sulfate is the preferred phase in coal combustion systems, while above this temperature range, sodium silicate or aluminosilicates, formed by interaction of vapor-phase sodium and coal ash, is preferred.

The goal of these calculations is to get a better idea of the experimental conditions for the Combustion 2000 alkali corrosion experiments by calculating the amount of sodium expected in the vapor phase. The basic assumptions used in the calculations were:

- Equilibrium calculated using SOLGASMIX with a sodium aluminosilicate liquid mixture allowed. The IMCC model was used to account for the non-ideal behavior of the liquid (Hastie and Bonnell, 1985).

- Amount of sodium vaporized was calculated from the work of Gallagher et al. (1990).

- Gas composition was calculated from the coal ultimate analysis and an equivalence ratio of 0.95. Note that the combustion "air" is actually 17% O_2.

- The calculations were run at temperatures from 1340 to 2420°F, representative of the air heater surface temperature.

- Three cases were calculated for each coal: 1) gases only, no ash; 2) excess SiO_2; and 3) excess SiO_2 and Al_2O_3 (Al/Si ratio from ASTM ash).

The results are summarized in Table 4.3-19. In general, 1 to 5% of the sodium in the coal vaporized. For these coals, the equivalent sodium concentration in the gas phase (due to vaporization) was 0.3 to 13 ppm (as Na). For Case 1 (gases only), the equilibrium values were in the range of 0.2 to 3.3 ppm Na; the two sodium species of importance were NaOH and Na_2SO_4. The dewpoint of sodium sulfate was in the range of 1700 to 2000°F (Figures 4.3-32 and 4.3-33). Below the dewpoint of Na_2SO_4, this species is the dominant gas phase sodium species, but above the dewpoint, NaOH is more important. To put it another way, below the dewpoint, most of the sodium is condensed as $Na_2SO_4(l)$ with some vapor present and above, most of the sodium is found as NaOH(g).

Addition of excess SiO_2 to the equilibrium calculation is intended to simulate a silicon carbide surface covered with a crystalline silica surface layer. At equilibrium, almost all the silicon was found as $SiO_2(cr)$. In the range of 1800 to 2200°F, a sodium silicate liquid mixture formed. Above 2200°F, the sodium was all found in NaOH(g). As a result of adding excess silica, the dewpoint of sodium sulfate changed by 0 to 75°F.
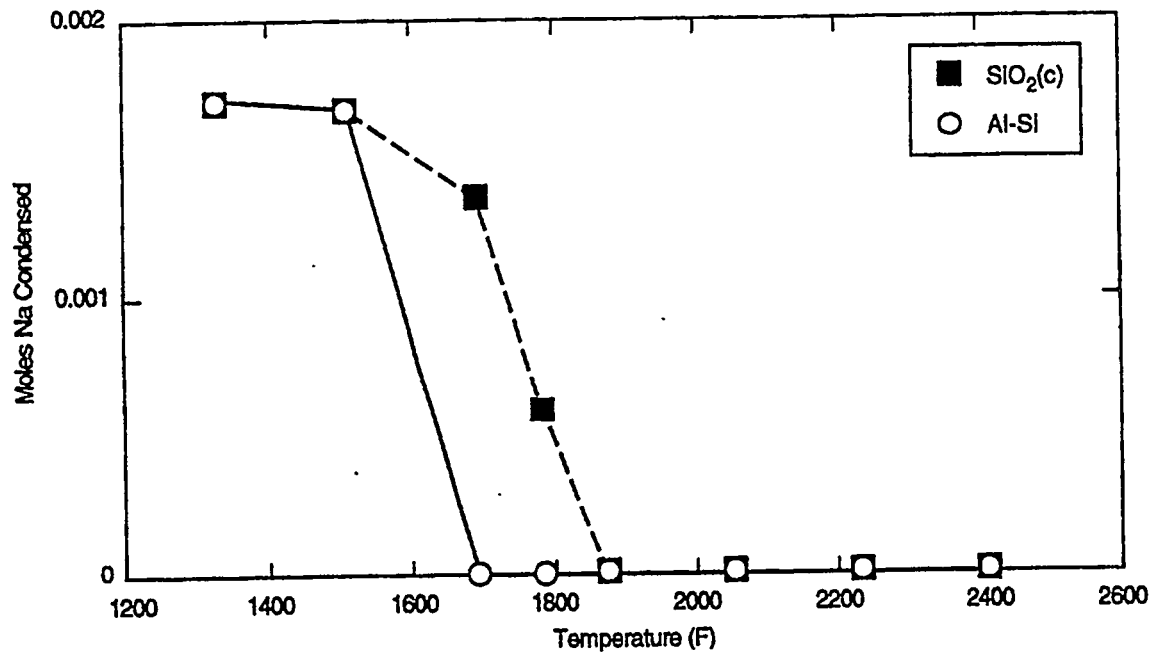
Figure 4.3-32   Condensed Phase Sodium Sulfate as a Function of Temperature for
Wyodak Ash with Excess Silica and Aluminosilicate (Condensed).
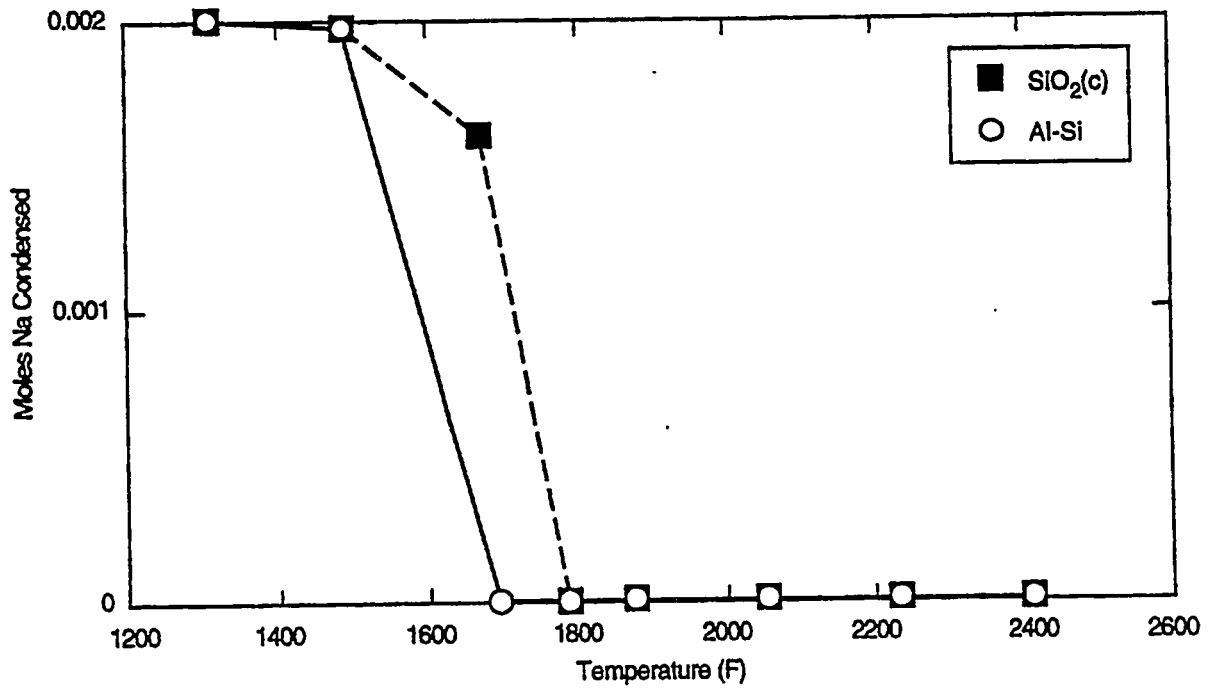
Figure 4.3-33   Condensed Phase Sodium Sulfate as a Function of Temperature for Illinois
No. 6 Ash with Excess Silica and Aluminosilicate (Condensed).

TABLE 4.3-19 SODIUM VAPORIZATION AT FLAME CONDITIONS
RESULTS OF EQUILIBRIUM CALCULATIONS FOR PROGRAM COALS

Quantity	Wyodak	Illinois No. 6	Cedar Grove	Blind Canyon
Amount of Na vaporized from coal ash	3.3%	2.2%	1.4%	5.3%
(1) Gas-phase only – no ash ppm SO_2	190	1860	480	286
ppm Na at 1800°F	1.6	1.4	0.2	3.6
Dewpoint Na_2SO_4 – °F	1760	1813	1696	1933
(2) Excess condensed SiO_2 ppm SO_2	190	1860	480	286
ppm Na at 1800°F	0.4	1.2	0.3	0.4
Dewpoint Na_2SO_4 – °F	1800	1813	1696	1786
(3) Excess condensed Al-Si ppm SO_2	190	1875		286
ppm Na at 1800°F	0.0002	0.0002		0.0002
Dewpoint Na_2SO_4 – °F	1650	1650		1650

Addition of excess Al and Si is done to approximate the presence of aluminosilicate ash on the air heater surface. This had a dramatic effect on gas phase sodium: the concentration of Na was reduced to 0.0002 ppm in all cases. The dewpoint of sodium sulfate was also reduced to 1650°F. Above the dewpoint, almost all the sodium was found in an aluminosilicate liquid mixture and very little was found in the gas phase. Although a small amount of liquid was formed, almost all the aluminum and silicon were distributed as mullite and crystalline silica. At low temperatures, however, an aluminosilicate liquid may not form based on kinetic arguments concerning the high viscosity of the liquid. While these results point to the equilibrium state, this state might not be achieved in the combustor.

The conclusions from this study are as follows:

- With no aluminosilicate ash present, the dewpoint of sodium sulfate is 1700 to 1800°F. This is just below the gas inlet temperature to the convective air heater; the air heater surface temperature will be in the range of 1400 to 1800°F. Thus we should expect condensation of sodium sulfate at the inlet of the convective air heater.

- According to the calculations for a large excess of SiO_2 in equilibrium with the gas, sodium silicate liquid only forms near the dewpoint 1650 to 1800°F, but the liquid can be stable up to 2200°F.

- The presence of aluminosilicates decreases the sodium in the gas phase by about three orders of magnitude. It implies that there should not be a problem with sodium if there is aluminosilicate ash around; this was the result even for the PRB coal (Wyodak), although a large excess of alumino-silicate was used for this calculation instead of using the sodium-to-silicon-to-aluminum ratio in the coal ash.

Generation of size-segregated ash samples

Coal ash samples were generated in the Entrained Flow Reactor Facility (ERF) at PSIT (Figure 4.3-34). The entrained flow reactor is designed to simulate heterogeneous combustion and mineral matter transformation processes under well-characterized laminar flow conditions. This furnace is capable of handling 1 to 10 lb/hr of solids feed (10,000 to 100,000 Btu/hr heat input). The flame zone is swirl-stabilized in order to simulate the high intensity, near-burner region of an industrial furnace flame, followed by a plug flow burnout region. The flame may be fueled by coal and/or natural gas. Coal particles are introduced into the vertical tube furnace via a water-cooled injector. The primary gas is typically air supplied by a regenerative blower at a nominal rate of 2 scfm. Various gases (e.g., oxygen, sulfur dioxide) can be added to the primary air as required. The particle laden gases flow through a 3-3/8 in. ID alumina tube furnace, 51 in. length, allowing residence times of up to 5s at temperatures up to 1540°C (2800°F). Three zone, electrical temperature control of the furnace is included, providing uniform or variable temperature profiles. Water-cooled sampling probes are used to isokinetically sample and rapidly quench the ash particles from the furnace. A Pollution Control Systems cascade impactor and/or cyclone are used to size-segregate the ash particles. The combustion gases are cooled and dried, and analyzed continuously for CO, CO_2, O_2, NO_x, and SO_2. A special deposition test section is used in the test facility to study ash deposit initiation and growth.
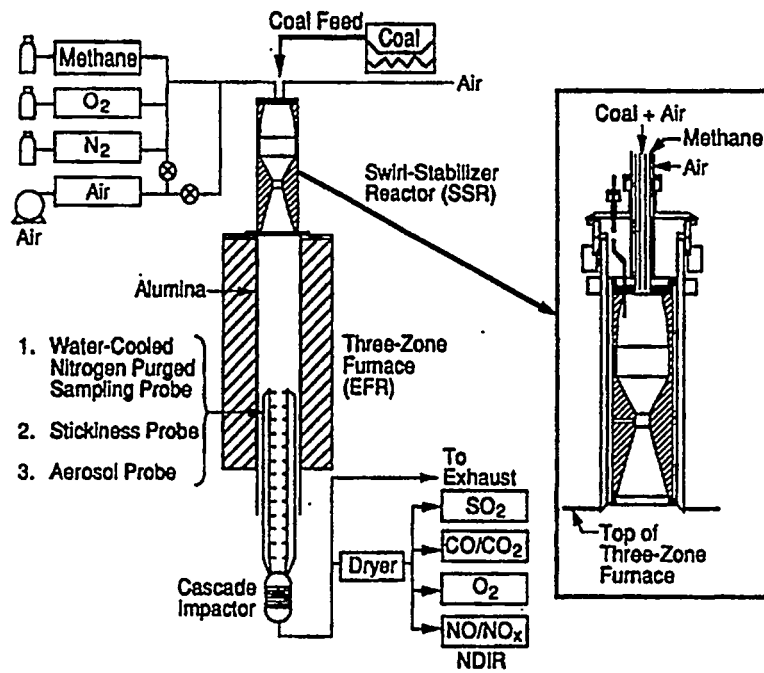
Figure 4.3-34 Entrained Flow Reactor.

Limited combustion experiments were conducted with two of the coals selected for alkali-ash corrosion experiments under convective air heater conditions. The gas temperature oxygen partial pressure, and coal particle feed rate will be adjusted to achieve coal particle temperatures equal to the flame temperature expected in the HITAF. The following samples and data were generated.

1. Collect "total filter" ash samples by extracting ash particles from the post-combustion gases in the PSIT laboratory reactor with an isokinetic sampling probe, quenching them within the probe, and depositing them on polycarbonate filters.

2. Analyze the ash particles by CCSEM (2000 to 3000 particles per sample) to obtain particle size and size-resolved chemical composition distributions.

3. Collect size-segregated ash particle samples from combustion of the standard pc grind coal sub-sample using a PSIT-owned PCSC Mark III Cascade Impactor and cyclone pre-cutter. Determine the amount of submicron fume by identifying the ash mass fraction approximately less than 5 µm in size collected with this device.

The first two coals to be used in the ceramic corrosion tests were received at UNDEERC. Three 5-gal buckets of run-of-mine crushed coal were donated by the Peabody Coal company from the Wyodak seam of the Rochelle, Wyoming, mine. This is a Powder River Basin subbituminous coal that was chosen for the sting tests to represent Western U.S. coals with basic ash. It has intermediate quantities of sodium and sulfur, and an intermediate calculated slag viscosity as compared to other Wyoming coals. Peabody states that the sample is representative of a 10,000-ton train load of coal. The second coal is Illinois No. 6 bituminous from the Burning Star mine. One barrel was provided. It was chosen to represent Eastern U.S. coals with acidic ashes.

The coals were pulverized to standard utility grind at UNDEERC. The three 5-gal buckets of Wyodak coal were pulverized in a cross beater mill. The barrel of Illinois No. 6 coal was pulverized in a hammer mill. Each of the coals were riffled into 5-gal buckets to provide more useable portions that represent the whole sample.

PSIT received the pulverized samples of the Wyodak and Illinois No. 6 coals. The Entrained Flow Reactor was set up to generate ash for the tests, including a new cyclone pre-cut device which will be used to produce size-segregated ash samples to simulate deposition in the convective air heater.

The sieve analyses of the two coals are given in Table 4.3-20. The proximate test data and ash compositions of the coals are given in Tables 4.3-21 and 4.3-22. Duplicate tests of the Wyodak coal were run to test the efficiency of the riffling procedure. The variations in the Wyodak data in both tables are within the experimental error of the analytical procedures.

TABLE 4.3-20 SIEVE ANALYSES OF PULVERIZED WYODAK AND ILLINOIS NO. 6 COALS (WT%)

Mesh	Wyodak	Illinois No. 6
100	6.67	3.49
140	3.22	6.83
200	10.07	12.12
230	3.45	6.92
270	6.29	7.65
325	1.28	.66
PAN	68.65	62.17

TABLE 4.3-21 PROXIMATE ANALYSES OF WYODAK AND ILLINOIS NO. 6 COALS (AS-RECEIVED WT%)

	Wyodak (a)	Wyodak (b)	Illinois No. 6
Moisture	21.00	21.30	8.40
Volatile Matter	34.98	34.66	34.41
Fixed Carbon	39.24	39.35	46.83
Ash	4.77	4.68	10.34

TABLE 4.3-22 ASH COMPOSITIONS OF WYODAK AND ILLINOIS NO. 6 COALS (WT%)

	Wyodak (a)	Wyodak (b)	Illinois No. 6
SiO_2	31.88	32.12	54.42
Al_2O_3	17.66	17.95	19.42
Fe_2O_3	5.16	4.86	16.21
TiO_2	1.01	0.99	1.01
P_2O_5	1.23	1.36	0.04
CaO	24.59	23.06	4.49
MgO	9.90	9.90	3.05
Na_2O	1.02	1.47	0.70
K_2O	0.27	0.28	0.56
SO_3	7.27	8.01	0.00

In addition to the standard ASTM tests, the chemical associations of the inorganic elements in the coals are being determined by chemical fractionation analyses at EERC. Chemical fractionation

consists of a series of extractions of pulverized coal with a series of aqueous reagents. The procedure uses silicon as an internal standard by assuming that none of it is extractable. The test is designed to determine what portion of the inorganic elements are present as water soluble materials, ion exchangeable cations, and acid soluble and insoluble species. The procedure is described in detail by Benson and Holm (1985). It involves extracting the coal with water to remove water-soluble elements such as Na in Na_2SO_4, or those elements that were most likely associated with the groundwater in the coal. This is followed by extraction with 1M ammonium acetate to remove elements that may be bound as salts of organic acids. The residue of the ammonium acetate extraction is then extracted with 1M HCl to remove acid-soluble species which may be in the form of hydroxides, oxides, carbonates, and organically coordinated species. The components remaining in the residue after all three extractions are assumed to be associated with the insoluble mineral species such as clays, quartz, and pyrite.

The extractions were completed on the Wyodak coal (Table 4.3-23). In addition, the size and composition distributions of the 1- to 100-μm-diam. mineral grains in the pulverized coals were determined by computer-controlled scanning electron microscopy (CCSEM).

TABLE 4.3-23 CHEMICAL FRACTIONATION OF THE WYODAK COAL
(WT% BASIS)

	Initial (ppm)	Removed by H_2O	Removed by NH_4OAc	Removed by HCl	Remaining
Silicon	8436	0	0	0	100
Aluminum	5340	0	0	32	68
Iron	1956	0	0	100	0
Titanium	427	6	0	0	94
Phosphorus	383	11	0	86	3
Calcium	9289	0	67	31	2
Magnesium	3242	0	64	33	3
Sodium	448	0	93	3	4
Potassium	137	0	49	35	16

The data indicate that an insignificant amount of the inorganic material is associated in water soluble phases such as those dissolved in the moisture present in the coal (primarily sulfates or chlorides). Large portions of the calcium, magnesium, sodium, and potassium are extracted by ammonium acetate, indicating their presence in the coal as salts of carboxylic acids. During combustion of the coals, these elements are liberated and interact strongly with existing mineral particles. Approximately 1/3 of the aluminum, all of the iron, and the remaining phosphorus, calcium, magnesium, sodium, and potassium are removed by the subsequent hydrochloric acid treatment. The extracted aluminum are usually present as either calcium aluminum phosphate or as an organic complex. The iron must have been present as a partially oxidized pyrite, or fine-grained iron

carbonate. The extracted phosphorus most often occurs as calcium aluminum phosphate. All of the titanium is insoluble; it usually occurs as one of the TiO_2 polymorphs, principally rutile. About 2/3 of the aluminum is insoluble, existing as aluminosilicate clays. The silicon was defined by the procedure to be insoluble because it most often occurs in coal as insoluble quartz or aluminosilicate clays.

CCSEM was used to determine the size, quantity, and semi-quantitative composition of mineral grains in coals (Jones et al., 1992). The semi-quantitative chemical composition data obtained were used to classify the particle into mineral or chemical categories. After the minerals are identified, the CCSEM program classifies the minerals by average diameter into six separate, user-defined size bins. In the standard analysis, three different magnifications are used to ensure a significant number of particles in each of the size bins. However, at the request of Peabody Coal Company, the Wyodak was run with two magnifications so that the data could be used with an existing computer simulation of ash deposition. The number of mineral grains and their areas are tallied in each size bin for each mineral type. As a result, the size distributions for individual mineral species can be ascertained.

Tables 4.3-24 and 4.3-25 list a summary of the size and composition distributions of the 1- to 100-μm-diam. mineral grains detected by CCSEM analyses of the Wyodak and Illinois No. 6 coals, respectively. The mineral grains in the Wyodak coal are primarily quartz and aluminosilicate clays (principally kaolinite), with some pyrite and calcium aluminum phosphate. Over 2/3 of the grains are less than 10 μm in diameter. The major minerals in the Illinois No. 6 coal are quartz, calcite, aluminosilicate clays (principally kaolinite and potassium aluminosilicate or illite), and pyrite. Like the Wyodak coal, the minerals in the Illinois No. 6 were relatively fine, with 60% of the detected particles having diameters of 10 μm or less.

TABLE 4.3-24 CCSEM ANALYSIS OF THE WYODAK COAL
(WT% OF DETECTED MINERALS)

Diameter (µm):	1.0 to 2.2	2.2 to 4.6	4.6 to 10.0	10.0 to 22.0	22.0 to 46.0	46.0 to 100.0	Totals
Quartz	5.5	10.0	9.1	10.1	6.0	3.4	44.2
Iron Oxide	0.1	0.5	0.0	0.0	0.0	0.0	0.6
Periclase	0.0	0.0	0.0	0.0	0.0	0.0	0.0
Rutile	0.3	0.6	0.0	0.0	0.0	0.0	0.9
Alumina	0.0	0.0	0.0	0.0	0.0	0.0	0.0
Calcite	0.0	0.0	0.0	0.0	0.0	0.0	0.0
Dolomite	0.0	0.0	0.0	0.0	0.0	0.0	0.0
Ankerite	0.0	0.0	0.0	0.1	0.0	0.0	0.1
Kaolinite	4.1	4.8	5.1	3.6	2.6	0.9	21.1
Montmorillonite	0.3	0.8	1.4	0.4	0.2	0.0	3.0
K Al-Silicate	0.1	0.2	0.9	0.0	0.2	0.0	1.5
Fe Al-Si	0.0	0.0	0.0	0.0	0.0	0.0	0.0
Ca Al-Si	0.1	0.1	0.0	0.0	0.0	0.0	0.2
Na Al-Si	0.1	0.0	0.0	0.0	0.0	0.0	0.1
Aluminosilicate	0.3	0.6	2.8	0.4	0.3	0.0	4.4
Mixed Al-Silicate	0.0	0.0	0.0	0.0	0.0	0.0	0.0
Fe Silicate	0.0	0.0	0.0	0.0	0.0	0.0	0.0
Ca Silicate	0.0	0.0	0.0	0.0	0.0	0.0	0.0
Ca Aluminate	0.0	0.1	0.0	0.0	0.0	0.0	0.1
Pyrite	2.1	2.6	0.0	0.5	1.2	0.0	6.4
Pyrrhotite	0.0	0.0	0.0	0.2	0.0	0.0	0.3
Oxidized Pyrrhotite	0.1	0.0	0.0	0.0	0.0	0.0	0.1
Gypsum	0.0	0.0	0.0	0.0	0.0	0.0	0.0
Barite	0.0	0.0	0.0	0.0	0.0	0.0	0.0
Apatite	0.0	0.0	0.0	0.0	0.0	0.0	0.0
Ca Al-P	2.2	5.5	2.3	0.5	0.4	0.0	11.0
Gypsum/Barite	0.0	0.0	0.0	0.0	0.0	0.0	0.0
Gypsum/Al-Silicate	0.0	0.0	0.0	0.0	0.0	0.0	0.0
Si-Rich	0.2	1.2	1.9	0.2	0.0	0.0	3.5
Ca-Rich	0.0	0.0	0.0	0.0	0.0	0.0	0.0
Ca-Si-Rich	0.0	0.0	0.0	0.0	0.0	0.0	0.0
Unknown	1.2	0.9	0.0	0.0	0.6	0.0	2.7
Totals	16.8	28.1	23.5	16.0	11.3	4.2	100.0

209

TABLE 4.3-25 CCSEM ANALYSIS OF THE ILLINOIS NO. 6 COAL
(WT% OF DETECTED MINERALS)

Diameter (μm):	1.0 to 2.2	2.2 to 4.6	4.6 to 10.0	10.0 to 22.0	22.0 to 46.0	46.0 to 100.0	Totals
Quartz	2.6	5.2	4.5	1.8	0.4	0.0	14.5
Iron Oxide	0.0	0.0	0.0	0.0	0.0	0.0	0.0
Periclase	0.0	0.0	0.0	0.0	0.0	0.0	0.0
Rutile	0.1	0.0	0.0	0.0	0.0	0.0	0.1
Alumina	0.0	0.0	0.0	0.0	0.0	0.0	0.0
Calcite	0.2	0.5	1.3	2.9	3.1	1.6	9.5
Dolomite	0.0	0.0	0.0	0.0	0.0	0.0	0.0
Ankerite	0.0	0.0	0.0	0.0	0.0	0.0	0.0
Kaolinite	2.5	5.3	3.7	2.3	0.9	0.1	14.8
Montmorillonite	1.1	1.5	0.6	0.4	0.3	0.0	3.9
K Al-Silicate	3.1	5.6	3.5	1.2	0.4	0.3	14.1
Fe Al-Si	0.1	0.1	0.1	0.0	0.0	0.0	0.3
Ca Al-Si	0.0	0.0	0.0	0.0	0.0	0.0	0.0
Na Al-Si	0.0	0.0	0.0	0.0	0.0	0.0	0.0
Aluminosilicate	0.3	0.4	0.5	0.1	0.0	0.0	1.3
Mixed Al-Silicate	0.1	0.1	0.0	0.1	0.0	0.0	0.3
Fe Silicate	0.0	0.0	0.0	0.0	0.0	0.0	0.0
Ca Silicate	0.0	0.0	0.0	0.0	0.0	0.0	0.0
Ca Aluminate	0.0	0.0	0.0	0.0	0.0	0.0	0.0
Pyrite	1.6	2.3	7.3	9.8	9.0	2.5	32.4
Pyrrhotite	0.0	0.0	0.0	0.0	0.0	0.0	0.0
Oxidized Pyrrhotite	0.0	0.3	0.0	0.0	0.0	0.0	0.3
Gypsum	0.0	0.0	0.2	0.4	0.3	0.2	1.0
Barite	0.0	0.0	0.0	0.0	0.0	0.0	0.0
Apatite	0.0	0.0	0.0	0.0	0.0	0.0	0.0
Ca Al-P	0.0	0.0	0.0	0.0	0.0	0.0	0.0
Gypsum/Barite	0.0	0.0	0.0	0.0	0.0	0.0	0.0
Gypsum/Al-Silicate	0.1	0.0	0.0	0.0	0.1	0.0	0.2
Si-Rich	0.4	0.8	0.7	0.3	0.2	0.0	2.4
Ca-Rich	0.0	0.1	0.0	0.0	0.1	0.0	0.3
Ca-Si-Rich	0.0	0.0	0.0	0.0	0.0	0.0	0.0
Unknown	1.4	1.1	0.9	0.5	0.3	0.5	4.7
Totals	13.6	23.2	23.3	19.6	15.0	5.2	100.0

210

Experimental procedure for alkali-ash interactions

Corrosion of ceramic substrates in the presence of sodium and/or ash was evaluated in a single zone, horizontal tube furnace. Coupons were placed on a shelf made of a high purity alumina "DEE" tube (Figure 4.3-35). Coupons measured approximately 0.25 in. wide, 0.5 in. long, and 0.33 in. thick. Prior to testing, each coupon was washed, rinsed with distilled water, acetone, and methanol. In some instances, a thin layer of sodium sulfate was applied to the surface using an airbrush. In order to produce a uniform coating, the coupon was heated to 390°F and an aqueous sodium sulfate solution was sprayed on the surface. A target loading of 5 mg/cm^2 was achieved by weighing the coupons before and after application. Some samples were coated with approximately 3 mg of ash. Sodium sulfate was applied to the coupon before any ash was applied to simulate the formation of an initial sodium sulfate layer.
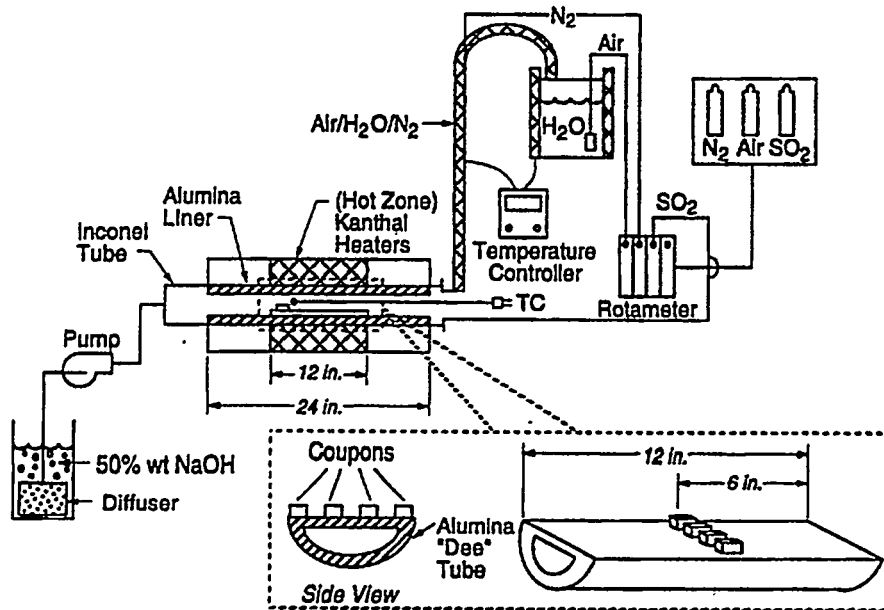
Figure 4.3-35   Alkali-ash Corrosion Experimental Apparatus.

During the experiments, simulated flue gas flowed through the reactor containing 5.0% O_2, 5.6% H_2O, 1917 ppm SO_2, and the balance N_2. The total gas flow was 125 sccm (standard cc per minute) which resulted in a complete turnover of process tube volume every 60s at 1650°F. During some of the experiments, a high purity alumina boat was placed in the furnace upstream of the samples. The boat contained 3g of Na_2SO_4 which allowed a constant atmosphere of sodium sulfate vapor to flow over the samples. At 1650°F, little of the sodium sulfate evaporated from the boat. All samples were processed at 1650 or 1790°F for 8 days (approximately 200 hr).

Coupons fashioned from two types of silicon carbide were tested. Both materials have high strength and are of very high purity, making them candidates for construction of heat exchangers. The

first material was a siliconized silicon carbide (NT-230) manufactured by Norton. This material contains silicon carbide grains with a small amount of residual silicon metal. The second silicon carbide was a sintered alpha-phase of silicon carbide (Hexoloy SA) manufactured by Carborundum. This material contains silicon carbide grains with small amounts of binder material.

Five series of experiments (Series A-E) were carried out using two different types of silicon carbide and two different types of coal ash. NT-230 is a siliconized silicon carbide manufactured by Norton. Hexoloy SA is a sintered alpha-silicon carbide manufactured by Carborundum. Coupons were analyzed at EERC. The siliconized silicon carbide (Norton NT-230) was tested at 1650 and 1790°F. The sintered silicon carbide (Carborundum Hexoloy SA) was tested at 1790°F.

Ash samples of both coals were collected from combustion in a laboratory scale combustor as described in the Section titled *Generation of size-segregated ash samples.* The high temperature experiments used total ash samples, while the lower temperature experiments used size segregated ash samples collected by excluding the larger ash fractions with a cyclone separator. Lower temperature experiments with Wyodak ash used ash with an aerodynamic diameter less than 3 μm, while the cutoff point for Illinois 6 ash was 6 μm. The composition of the size-segregated ash (as measured by XRF) is given in Table 4.3-26.

TABLE 4.3-26 COMPOSITION OF SIZE-SEGREGATED ASH SAMPLES (WT% SO₃-FREE)

Oxide	Illinois No. 6 (< 6 μm)	Wyodak (<3 μm)
SiO_2	50.14	26.55
Al_2O_3	23.69	21.75
Fe_2O_3	14.63	6.4
TiO_2	1.48	1.39
P_2O_5	0.27	2.34
CaO	5.39	29.92
MgO	1.41	10.4
Na_2O	0.79	0.99
K_2O	2.21	0.26

In each test series, the following coupons were processed:

1. As received, no Na_2SO_4 in gas phase, no ash.

2. As received, no Na_2SO_4 in gas phase, layer of Wyodak ash.

3. Coating of Na_2SO_4 on surface, with Na_2SO_4 in gas phase.

212

4. Coating of Na_2SO_4 on surface, layer of Wyodak ash, with Na_2SO_4 in gas phase.

5. As received, with Na_2SO_4 in gas phase, no ash.

Coupons from experiments 2, 3, and 4 were analyzed at EERC. The samples were set in epoxy resin and cut in half. The samples were not polished and there appeared to be some oxidation of the silicon carbide surface because of this. The cross-sections were examined via SEM and EDX analysis. Elemental composition was determined at individual points or mapped over the entire image. Experimental conditions for the coupons analyzed at EERC are summarized in Table 4.3-27.

TABLE 4.3-27 DESCRIPTION OF EXPERIMENTAL CONDITIONS

Sample	PSIT ID	EERC ID	T [K]	Material	Surface
A1	3	5182	1173	NT-230	Na_2SO_4
A2	2	5195	1173	NT-230	Wyodak
A3	4	5187	1173	NT-230	Wyodak-Na_2SO_4
B1	7	5257 5256	1248	NT-230	Na_2SO_4
B2	10	5258	1248	NT-230	Wyodak
B3	6	5265	1248	NT-230	Wyodak-Na_2SO_4
C1	14 20	5329 5365	1248	Hexoloy	Na_2SO_4
C2	11	5327?	1248	Hexoloy	Wyodak
C3	13	5328	1248	Hexoloy	Wyodak-Na_2SO_4
D2	22	5367	1248	NT-230	Illinois No. 6
D3	16	5363	1248	NT-230	Illinois No. 6-Na_2SO_4
E2	24	5368	1248	Hexoloy	Illinois No. 6
E3	19	5364	1248	Hexoloy	Illinois No. 6-Na_2SO_4

Results of Alkali-Ash Interaction Experiments

Ash-ceramic interactions

Figure 4.3-36 is a backscattered electron micrograph of the interface between the Wyodak ash and the siliconized silicon carbide after reaction at 1650°F for 200 hr. The ash is present as partially sintered agglomerates, many of which are suspended in the epoxy above the coupon. The maps of individual elements (via EDX) show that the individual ash particles in the agglomerates have a range of compositions, but are composed primarily of oxides of Mg, Al, Si, and Ca. There is essentially no reaction phase formed between the Wyodak ash and either type of silicon carbide at 1650°F.

At 1790°F, reaction phase formed composed primarily calcium, silicon, and oxygen on the surface of the NT-230 siliconized silicon carbide. This phase is generally less than 3 μm thick. No such
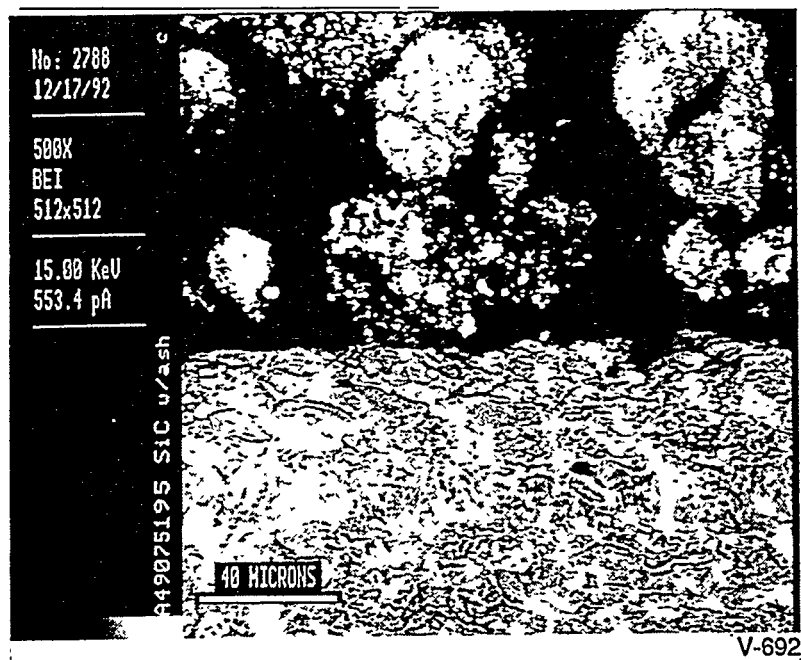
Figure 4.3-36   Backscattered Electron Micrograph of the Interface between the Wyodak
and Siliconized Silicon Carbide Coupon after Reaction at 1650°F.

reaction phase was present on the surface of the Hexoloy SA samples reacted at 1790°F. No reaction phase formed between either the NT-230 or the Hexoloy SA silicon carbide samples and the high-iron, high-silica Illinois No. 6 ash from 1650 to 1790°F.

Alkali-ceramic interactions

The first series of experiments examined sodium sulfate corrosion of silicon carbide under simulated combustion conditions. Figure 4.3-37 shows the results when a layer of sodium sulfate on an NT-230 substrate was exposed to vapor-phase sodium sulfate at 1650°F. The initial layer of sodium sulfate is calculated to be 19 μm thick based on a loading of 5 mg/cm^2. A layer of sodium sulfate approximately 20 μm thick can be seen on the surface, indicating that most of the sodium sulfate did not react with the substrate at this temperature. The most unusual feature of the sample is the silicon-rich layer, approximately 5 μm thick, which can seen in the cracks between the sodium sulfate and, in some places, actually covering the sodium sulfate. Some of the silicon in the substrate has moved into the sodium sulfate layer in discrete domains. These regions are probably silica glass, possible containing some sodium, although none was detected in the EDX maps, indicating that, if there is sodium, it is in low concentrations. Thus there is evidence for limited interaction between silicon carbide and sodium sulfate at 1650°F over 200 hr.

At 1790°F, the NT-230 sample showed increased reaction. The silicate reaction layer contains bubbles, some several hundred microns large, embedded in a sodium sulfate reaction product. As seen in Figure 4.3-38, this reaction layer is on the order of 50 μm thick. As seen in elemental maps, the reaction product is a mixture of sodium silicate and pure silica. A few areas of sodium sulfate can be

214
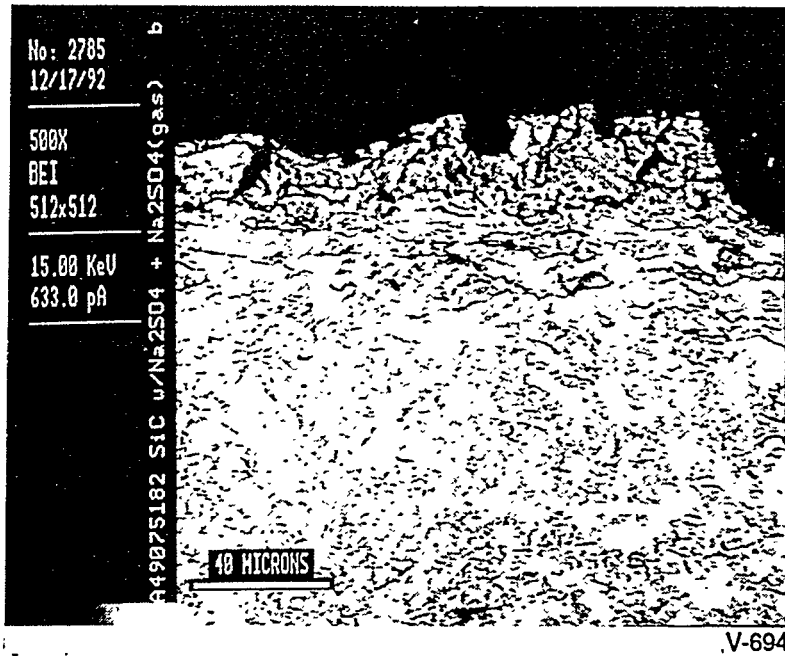
Figure 4.3-37   SEM Photograph of NT-230 Coupon After Reaction with Sodium
Sulfate at 1650°F.

seen, but very little sodium sulfate remains on the surface. Spot analyses of the reaction layer reveal that the sodium content of the sodium silicate is 16 to 18 wt%.

Comparison of the NT-230 material with Hexoloy SA at 1790°F reveals that the Hexoloy contains large bubbles, similar to the NT-230, but has a thicker reaction layer (100 to 200 µm) on top of
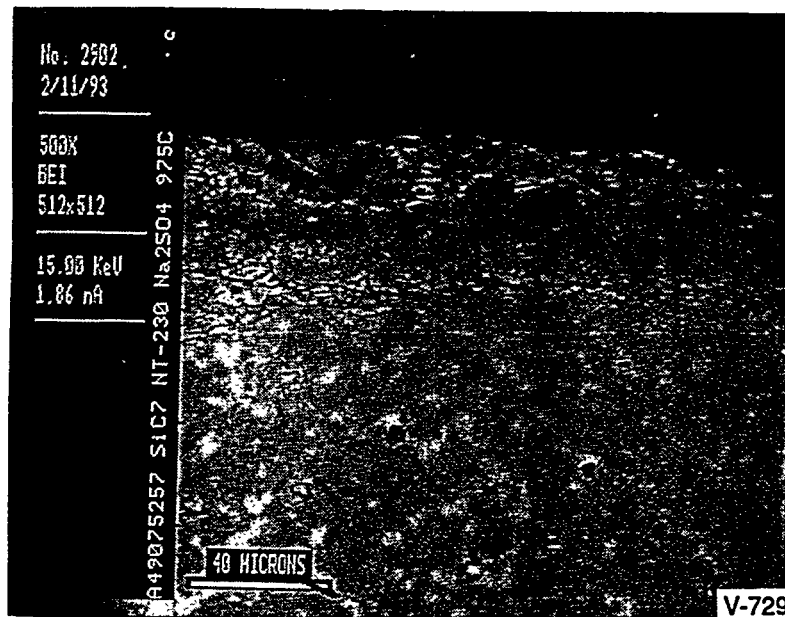
Figure 4.3-38   SEM Photograph of NT-230 Coupon After Reaction with Sodium
Sulfate at 1790°F.

the silicon carbide. As with the NT-230 sample, there are distinct composition regions of pure silica and sodium silicate. The silica layer is found at the silicon carbide interface and on top of the sodium silicate layer. A small amount of sodium sulfate was observed on top of the reaction layer. Qualitatively, the Hexoloy sample appears the same as the NT-230 sample, indicating that the mechanism for reaction with sodium sulfate is the same in both materials. Quantitatively, the Hexoloy sample shows a much thicker reaction layer than the NT-230 sample which seems to indicate that the Hexoloy reacted more extensively with sodium sulfate than did the NT-230.

Ash-ceramic interactions with excess alkali

The combination of sodium sulfate and ash was studied at 1790°F. At this temperature, sodium sulfate reacts preferentially with the ash. The ash is, however, more fluid because the excess sodium lowers its viscosity. Lowered viscosity increases the reaction between ash and silicon carbide.

The NT-230 sample reveals extensive reaction between the Wyodak ash and sodium sulfate. The ash layer consists of fused ash particles in a sodium sulfate matrix. Figure 4.3-39 shows the surface layer (with element maps). There is a reaction layer whose composition corresponds to MgO-CaO-2SiO$_2$ which is approximately 30 μm thick. Little sodium was incorporated in this reaction layer. Note that a region of trapped sodium sulfate can be seen underneath the silicate layer.
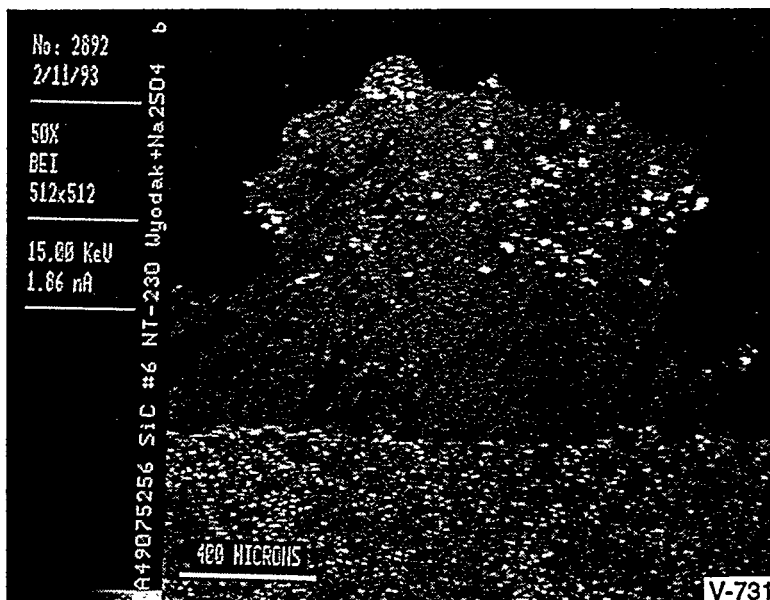
Figure 4.3-39   SEM Photograph of NT-230 Coupon After Reaction with Sodium Sulfate and Wyodak Ash at 1790°F.

The addition of sodium sulfate to Illinois 6 ash causes the formation of a glassy layer containing large (50 to 200 μm) bubbles. The composition of this glass is uniform according to element maps. Figure 4.3-40 shows pits on the surface of the NT-230 sample, indicating reaction between the ash and the silicon carbide. Such pits were also observed with the Wyodak-Na$_2$SO$_4$ sample. A few small

216

regions of sodium silicate can be seen on the surface. In contrast to the Wyodak-Na_2SO_4 sample, there is not a large, distinct reaction layer.
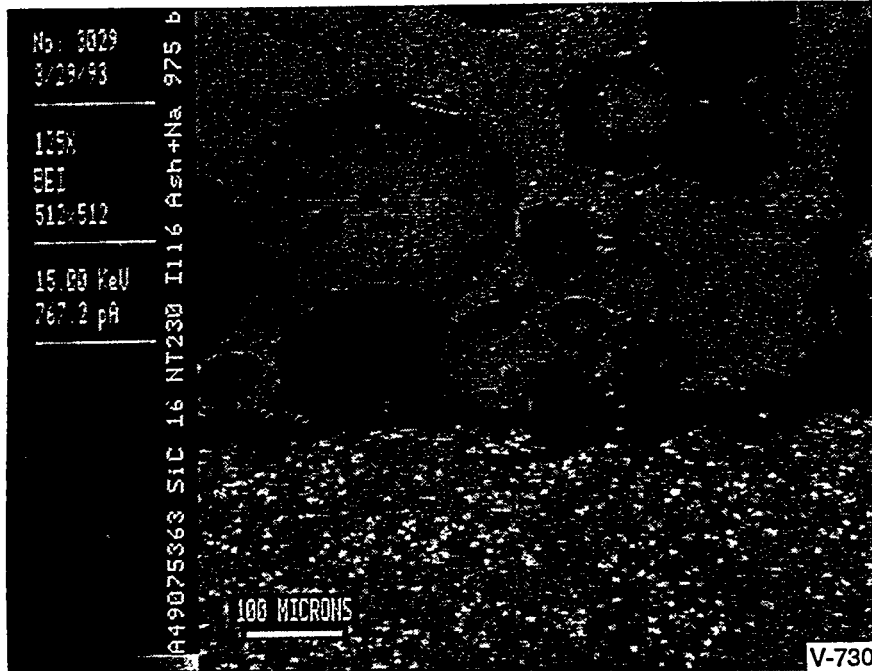
Figure 4.3-40. SEM Photograph of NT-230 Coupon After Reaction with Sodium Sulfate and Illinois No. 6 at 1790°F.

Reactions between Hexoloy SA coupons and combinations of sodium sulfate and the two ash compositions appeared similar to the NT-230 coupons. Wyodak ash produced a thick calcium-magnesium silicate reaction layer while Illinois No. 6 did not show stratification in the ash. The reaction product was probably a sodium aluminosilicate glass. Reaction was evident from the pits in the silicon carbide surface.

Conclusions

The reaction of silicon carbide with sodium sulfate proceeds by the formation of sodium silicate and silica. These are distinct phases. At 1650°F, there is limited reaction with most of the initial sodium sulfate left on the surface. At 1790°F, the reaction is extensive with almost no sodium sulfate remaining. Hexoloy had a much thicker reaction layer than NT-230, indicating that it may be more reactive. Chemical equilibrium calculations of the stability of sodium sulfate predicted the trend in reactivity as a function of temperature.

No interaction occurs between Wyodak ash by itself and silicon carbide at 1650°F. At 1790°F, limited reaction was observed to form a thin calcium silicate layer. The lowest eutectic in the $CaO-SiO_2$ system is 2600°F (Phillips and Maun, 1959), so for a relatively long test representing a metastable equilibrium, the reaction product must be a very high viscosity glass, possibly fluxed with a small amount of sodium. Diffusion of calcium ions into the reaction layer must be by solid state diffusion. The presence of mobile sodium ions in the glass should increase the diffusion rate. Illinois

217

No. 6 by itself does not react with the silicon carbide over a period of 200h in the range of 1650 to 1790°F; this is true for both types of silicon carbide.

At 1790°F, both types of coal ash combined with excess sodium sulfate react with silicon carbide. Wyodak ash reacts by forming a calcium-magnesium silicate reaction product at the surface. The mechanism appears to be the same for NT-230 and Hexoloy. The combination of Illinois No. 6 plus sodium sulfate appears to react with both types of silicon carbide at 1790°F based on the evidence of surface pits. There is not distinct reaction product layer as with the high calcium Wyodak ash.

Based on these preliminary experiments, there are implications for interactions between silicon carbide in the air heater and condensable sodium sulfate and/or ash. It should be noted that the thick layer of sodium sulfate applied to the silicon carbide samples may not be typical of what would condense in the HITAF, although these experiments provide a "worst case." Long term, dynamic testing under more realistic conditions will be needed to provide quantitative rates of corrosion. However, the results of these experiments provide insight into mechanisms for corrosion and regimes of temperature that are important.

Equilibrium calculations predict that sodium sulfate should condense at temperatures below 1900°F. At temperatures below approximately 1700°F, sodium sulfate alone (with no ash) did not react with silicon carbide. Above approximately 1900°F, sodium sulfate does not condense according to equilibrium calculations; the exact dewpoint will depend on the amount of sulfur and sodium in the coal. Thus, there is a range of temperatures (1700 to 1900°F) over which corrosion by condensed sodium sulfate may pose a problem in the convective air heater. Locations which have surface temperatures in this range should be identified. The severity of the corrosion seems to depend on the type of silicon carbide as well as the composition of the ash.

In the temperatures of the experiments (1650 to 1790°F), there was only limited interaction between ash alone and silicon carbide. The most pronounced interaction was between high calcium Wyodak ash and NT-230 silicon carbide, resulting in a thin layer of calcium silicate. Such a reaction was not observed between Wyodak and Hexoloy SA silicon carbide. Illinois No. 6 ash did not react with either type of silicon carbide.

Based on previous calculations of densification criteria, the maximum deposit surface temperature should be in the range of 1385 to 1630°F for Wyodak and Illinois No. 6. At these temperatures, neither sodium sulfate nor ash should pose a significant threat to the integrity of a silicon carbide convective air heater. However, if the air heater surface temperature exceeds 1800°F, corrosion will occur, particularly with high calcium ash.

4.3.7 Ash Utilization

Coal combustion by-products can be used successfully in a number of different applications. Some of these by-products have been established in areas of utilization for several decades. The general topic of coal combustion by-product utilization is quite complex and needs to be thoroughly

218

presented in order to fully appreciate and understand the technical and marketing aspects. Typical utilization applications fall into the broad categories of construction, industrial or manufacturing, land application, and waste stabilization.

Construction Materials

The use of by-products in cement and concrete products

Recent developments in the use of fly ash in cement and concrete products have focused on manufacturing portland cement or specialty cements, the fundamental mechanisms of fly ash reactions in concrete, the effect of fly ash addition on unwanted alkali-aggregate reactions in concrete, increased use of Class F pozzolanic fly ash, high fly ash content in structural-grade concrete, and cast concrete products.

Cement manufacture

The incorporation of fly ash in cement manufacturing can be accomplished either by substituting fly ash for the slag or rock normally used in the cement kiln or by directly blending fly ash with portland cement. The use of fly ash in cement kilns is a potentially large market in areas where suitable fly ash is produced in the immediate vicinity of the cement plant and where transportation costs are favorable. Use of fly ash in general-purpose blended cement is a more limited market in the United States because of its competition with direct replacement of cement at the ready-mix plant. However, intergrinding with the clinker or blending with ground cement and adding anhydrous $CaSO_4$ (anhydrite) can create a blended cement with characteristics closely approximating those of portland cement. In many European countries, the production of ordinary portland cement is being gradually replaced by production of portland-fly ash-blended cement (Clarke, 1993). A European blended cement that combines cement kiln technology with direct blending may offer large-tonnage use of U.S. fly ash (Manz and Mitchell, 1986). The process involves first sintering 40% fly ash with 60% limestone and fine grinding the fused material and then blending this product with additional fly ash in a 40:60 ratio.

Cement replacement - properties and mechanisms

The incorporation of fly ash as a partial replacement for portland cement in concrete has generally beneficial effects: reduced water requirements, increased ultimate strength, improved workability, extended setting time, reduced heat release, lower permeability, improved durability, and increased resistance to chemical degradation. In the sometimes problematic area of freeze-thaw durability, the practices that ensure good freeze-thaw performance for other concretes also apply for fly ash concrete (Tyson, 1991; Dunstan, 1991). Freeze-thaw performance is reported to improve with the addition of Class C fly ash up to a 50% replacement level (von Fay et al., 1993). The resistance of fly ash concrete to salt scaling due to deicing in cold climates appears overall to be similar to that of conventional concrete, and improved resistance correlates with strength and reduced permeability (Soroushian and Hsu, 1991).

219

Aggregate

Methods for the manufacture of artificial aggregates from fly ash or other coal combustion by-products can be distinguished by the conditions employed for hardening the pellets. Sintering processes (Puccio and Nuzzo, 1993) rely on the residual carbon content of the fly ash, with addition of pulverized feed as required, to heat pellets to sintering temperatures above 900°C. Hydrothermal and cold-bonding processes applied to fly ash, portland cement, and lime use steam or extended curing time at temperatures ranging from ambient to about 250°C. Sintering processes are well-established technology and have operated successfully for decades, but lower-temperature processes under development have attracted more recent attention because of their lower energy requirement and greater cost-effectiveness. Commercial production of lightweight aggregate for building block based on low-temperature processing has commenced recently in Florida using the Aardelite process (Smith, 1993; Hay and Dunstan, 1991) and in Virginia using the Agglite process (Courts, 1991).

Synthetic aggregate was experimentally produced from lime-based spray dryer FGD by-products in the early 1980s by pelletizing at pressures of 5 to 20 tons per square inch followed by extended 10- to 60-day curing under controlled moisture conditions (Donnelly et al., 1986). Strength properties were adequate for confined applications such as road base. Production costs in 1982 were estimated to be $5.20/ton in a facility sized to process by-product from a 400-MW plant burning low-sulfur western coal. Pellets produced from cool-side, limestone injection multistage burner (LIMB), and fluid-bed combustion (FBC) by-products in the Ohio Coal Development Office demonstration project have passed the American Society for Testing and Materials, (ASTM) abrasion test for use as road base aggregate (Hopkins, et al., 1993). Commercial production of lightweight aggregate suitable for use in lightweight building block commenced in Florida in 1992 using bituminous coal fly ash and FGD scrubber sludge as raw materials in the low-temperature Poz-O-Lite process (Smith, 1993).

A novel method for producing lightweight aggregate by agglomerating fly ash or sand in foamed cement has been developed in Germany (Grosline, 1986). The properties of the aggregate can be controlled to meet a range of specifications on size, strength, density, and porosity. The cellular structure imparts high strength in relation to weight and reduces the amount of cement required.

Fly ash as a cementing agent in concrete block

The technology for using fly ash as part of the cementing agent in concrete building block parallels that for concrete in general. A recent study (Wei and Golden, 1993) indicated among its key findings that the substitution of 40% Class C fly ash for cement produced blocks having a slightly higher compressive strength than a no-fly-ash reference block. Fly ash blocks, because of the slower setting characteristics of fly ash concrete, were more sensitive to curing temperature and benefited from accelerated steam curing. Fly ash blocks evidenced water absorption slightly higher than the reference block, but still within the requirement of the ASTM C55 standard. The use of bottom ash as a

replacement for natural aggregate beneficially reduced the weight of the block but also reduced strength and increased water absorption.

Autoclaved cellular concrete used in building blocks, roof slabs, and other cast products represents an important market for fly ash in Europe, but attempts to introduce the technology into the United States have not succeeded commercially (Clarke, 1993; Sauber, 1991). In this process (Pytlik and Saxena, 1991; Payne and Carroll, 1991), fly ash is combined with cement, lime, sand, and aluminum powder and mixed with hot water. The reaction of aluminum and lime generates hydrogen gas, which forms an aerated cellular structure. Curing in high-pressure steam autoclaves produces a physically and chemically stable product. Autoclave cellular concrete is currently being researched by the Electric Power Research Institute (EPRI). A small-scale mobile plant touring the United States is being hosted by several utilities.

Brick

Research on the manufacture of various types of brick from fly ash and bottom ash indicates that these products offer a good potential for achieving superior properties at reduced cost. The ash bricks are lighter and provide better sound absorption and heat insulation than clay brick. Depending upon the methods used in their production, ash bricks can offer lower shrinkage and higher resistance to freezing and thawing, but may also suffer from higher water absorption. Methods of manufacture involve either the replacement for clay in fired brick or the combination of fly ash with cement or lime binder in unfired but steam-cured bricks. Economic studies show that the use of coal ash in brick can provide substantial savings, both to the utility producing the ash and to the manufacturer of the brick (Naik et al., 1992b).

Road base

The use of fly ash alone or together with lime or cement in self-hardening road base is an evolving technology that is receiving increased attention. New information in this area includes results of laboratory testing and extended field monitoring, use of reclaimed pond ash, incorporation of flue gas desulfurization (FGD), by-products, and use of the ash-based aggregates discussed previously.

Monitoring of a 1500-ft test section using cement-fly ash base for a Michigan four-lane highway has indicated quite satisfactory performance since its construction in 1987 (Gray et al., 1991b). Some heaving and cracking occurred in winter months as a result of frost. Laboratory leachate concentrations for heavy metals using ASTM and RCRA (U.S. Environmental Protection Agency Resource Conservation and Recovery Act) procedures were near drinking water standards. Replacement of lime with Class C fly ash in the subbase for a Kansas racetrack reduced the cost by one-half; swelling potential was reduced compared to lime stabilization, but strength was reduced at soil temperatures below 40°F (Ferguson and Zey, 1991). Laboratory evaluation of fly ash stabilization of caliche, a red-brown calcareous material used for roadways in South Texas, indicated that both Class C and Class F ashes were more effective than lime for reducing plasticity and that Class C fly ash

also significantly increased strength (Keshawarz et al., 1991). Laboratory and field tests on the use of artificial aggregate produced from fly ash in asphalt paving, both as road base and in the asphalt mix, indicated that bitumen is absorbed into the pores of the aggregate, producing good bonding but a relatively dry and stiff mix; replacement of commonly used gravel with fly ash aggregate did not result in higher leaching of any of the heavy elements analyzed (Mulder and Houtepen, 1991).

Reclaimed pond ash containing fly ash and bottom ash from Canadian lignite has been used to stabilize road base for asphalt paving (Culley and Smail, 1986). The wet pond ash, when compacted in 4-inch layers using standard equipment and handling procedures, had good structural bearing, but the unconfined surface suffered rapid surface abrasion when dry. Adequate bonding between the ash subbase and asphalt paving was achieved by blade mixing the first layer of asphalt into the underlying ash. Road surface condition was adequate over time where appropriate construction techniques were used. Recent laboratory testing on strength development for a reclaimed high-calcium fly ash used along with kiln dust to stabilize road base materials indicated strengths in the range of 200 to 1000 psi (Bergeson and Overmohle, 1991).

Fly ash has been successfully used in combination with lime sludge to stabilize unstable sand in Florida road base projects (Jones, 19986). A base prepared by mixing lime and fly ash with *in situ* sand hardened sufficiently after several weeks to allow heavy truck traffic. By-products from cool-side, LIMB, and FBC sulfur control technologies are currently being evaluated for use in road base. Laboratory tests on the compaction, swelling, shear strength, permeability, and leaching properties of the cool-side FGD by-product indicate a good potential for use in road base applications, but final assessment awaits the performance of field trials and engineering analysis (Hopkins et al., 1993).

Marine Applications

Fly ash concrete, blocks, and precast products have been experimentally used in fresh and salt-water applications for break waters, reefs, substrate for marine aquaculture, and waterfront bulkheads replacing rotting timbers. Concerns in using fly ash concrete in a marine environment are the slower rate of strength gain after pouring, the possible penetration of salt water, abrasion resistance and freeze-thaw tolerance in the splash zone, aerobic degradation, and possible leaching of heavy metals. These expressed concerns have not been experienced as serious problems in documented demonstration projects, and marine applications appear to be a large potential market for coal use by-products along coastlines, inland lakes, and water ways. All of the available study reports indicated no significant heavy metal leaching or adverse effects on marine organisms (Kuo et al., 1991). The types of applications investigated are illustrated by the following case studies:

- A 500-ton reef was constructed in 1980 off Long Island, New York, using 15,000 blocks made from fly ash and FGD sludge. Laboratory studies performed to evaluate potential toxicity indicated no adverse effects on the growth of plants or the viability of shrimp or fish larvae (Parker et al., 1982).

- Long-term monitoring since 1983 on a 16,000-block reef using fly ash and FGD sludge, in the Atlantic off the Netherlands, showed several very positive results. Over this extended test period, the strength of the blocks increased about fourfold, an abundant biological growth developed, and the loss of heavy metals from the blocks was a small fraction of that indicated in laboratory leaching studies. The low leachability in the marine setting was attributed to pore blockage and reduced permeability resulting from deposition of magnesium and carbonate in the pore volumes of the block (van der Sloot, 1991).

- A 33-ton test reef in the Gulf of Mexico off Florida was demonstrated to be a very effective habitat for numerous types of plants, fish, and other marine organisms. Bioassay indicated no major accumulation of heavy metals at any level of biological organization (Livingston et al, 1991).

- Stabilized coal ash has been demonstrated to be an acceptable oyster-growing substrate replacing scarce shells in tests conducted in Delaware (Price et al., 1991) and in Texas (Baker et al., 1991). Testing showed satisfactory material strength, oyster-attraction density, growth, and absence of heavy-metal accumulation.

- High-volume use of fly ash for land reclamation from the sea, in the form of coastal extrusions or offshore islands, is technically and economically feasible according to an Israeli study (Zimmels et al., 1991). The cost of reclaiming 100 acres with an average water depth of 3 to 4 meters, estimated to be $400,000 per acre in 1985, was indicated to be favorable for development along a highly populated land-scarce coastline.

Industrial Uses

A large number of potential uses for coal combustion by-products in industrial applications have been investigated. Commercial practice is very limited in the United States, but is more common in some other countries. For example, production of gypsum from FGD facilities is common practice in Europe, and substantial amounts of fly ash brick are produced in China.

Gypsum

The production of salable by-product gypsum from FGD is an economic opportunity that presents both technical and marketing challenges for utilities. The technical requirements for producing market-grade gypsum involve process adaptations to provide sufficient aeration and reaction time in the scrubber circuit to oxidize calcium sulfite sludge to a high-quality, 92% to 95% gypsum product (Pauken and Wieskamp, 1993). Most existing lime/limestone scrubbers operating in the United States are not designed to produce gypsum, as they generally are in Europe. However, a significant number of U.S. installations could be modified to produce gypsum by adding air bubbles (spargers) and reaction tanks to facilitate the required oxidation. Alternatively, oxidation can be accomplished by reprocessing the sulfite sludge in a separate facility. Markets for gypsum are found in masonry products and wallboard manufacture. Wallboard presents the largest and most promising

223

market, wherein FGD gypsum could be substituted for part of the 26 million tons of natural gypsum consumed annually in the United States. U.S. gypsum consumption is of the same order as the total U.S. sulfur control requirement after Clean Air Act Amendments are fully implemented in the year 2000, making this market a viable target for recycling. Successful marketing of FGD gypsum requires that utilities work collaboratively with wallboard manufacturers to ensure a dependable supply of specification-grade material meeting standards for purity and low levels of moisture and soluble salts.

Land Application Uses

The role of coal use by-products in agriculture

Coal use by-products are being evaluated as soil amendments and in mine land reclamation. Soluble forms of calcium, magnesium, sulfur, and certain necessary trace metals such as boron, molybdenum, zinc, selenium, and copper that are present in coal ash and FGD by-products can be used to provide needed plant nutrients. No significant amounts of the primary nutrient elements — nitrogen, phosphorous, and potassium — are found in coal ash, but wood ash is rich in potassium and phosphorous. By-product gypsum ($CaSO_4 \cdot 2H_2O$) can be used to improve the tilth of clayey soils and mitigate the toxicity of exchangeable aluminum in acid soils. Calcium contributes to soil aggregation by displacing sodium on clay minerals and providing microscopic cementation. Concerns relating to the agricultural use of coal by-products involve the presence of soluble salts and trace concentrations of toxic metals.

Review of agricultural applications

A review of past work on the effect of coal use by-products on plant growth (Clark et al., 1993) indicates that little agricultural utilization is occurring and that information is limited. Scrubber sludge impoundments have been successfully vegetated using wheatgrass, tall fescue, sweet clover, millet, cottonwoods, and red cedars. Scrubber sludges have been successfully used as a source of boron and selenium trace nutrients. FBC bed residues are variously reported to increase maize and soybean yields and to provide a necessary source of calcium for apples. Research has been conducted by the TVA on the inclusion of lime/limestone scrubbing waste into fertilizer formulations (Santhanam et al., 1981). Research is being conducted on the agricultural use of wood-fueled power plant ash from generating units in California (Wheelabrator Shasta Energy Co., 1991; Meyer et al., 1992).

In controlled greenhouse tests on several different coal products (Clark et al., 1993), the addition of FBC residues to an acid soil of known severe aluminum toxicity served to double the yield of maize at an optimum add rate of 2% to 3% in the soil mix, but yields decreased at higher use rates. The effect of fly ash addition varied with coal type, with a bituminous Class F fly ash showing its highest growth enhancement at 3% addition, whereas lignitic Class C fly ash continued to increase yields at rates up to 25% of the soil mix. FGD by-products generally provided less growth enhancement, and optimum results were obtained at very low rates of 1% or less of the soil mix, possibly owing to detrimental effects of sulfite contained in these by-products. The use of an FGD sludge that had been processed to

convert sulfite to gypsum enhanced growth rates at add rates up to 75% of the soil mix, consistent with the known beneficial effect of gypsum application to acid soil.

A major study on land application of FGD and PFBC by-products (Beeghly et al., 1993) is in progress in Ohio, sponsored by the Ohio Coal Development Office, DOE, EPRI, Ohio Edison, American Electric Power, Dravo Lime Co., and Ohio State University. By-products from 15 sources are being investigated, representing four major clean coal technologies, including furnace injection FGD (LIMB), duct injection FGD, spray dryer FGD, and atmospheric and pressurized fluidized-bed combustion (AFBC and PFBC). These by-products are characterized by high alkalinity expressed as calcium carbonate equivalents of 25%-70%; sulfur contents of 2.4%-10.3%; fly ash contents of 10%-32%; and, with the exception of FBC bed material, a high surface area and fineness. Selected by-products, alone or in combination with sewage sludge, were mixed with acid soils and mine spoils and tested in greenhouse growth studies. Interactions of different materials gave somewhat different results. For example, growth of tall fescue was enhanced in overburden spoil, but was suppressed in acid underclay. Sulfite-bearing material did not harm seed germination. LIMB by-product was successfully composted with sewage sludge. The conclusion reached from the greenhouse tests was that the by-products tested, when used appropriately, are suitable substitutes for traditional soil-liming materials for acid soils. Field tests are under way to demonstrate the practicality of this use.

The commercial N-Viro Soil Process (Burnham, 1993) combines agricultural use with waste stabilization by composting coal ash by-products, or cement/lime kiln dust as originally used, with municipal wastewater treatment sludge. The soil conditioner produced has a low nutrient value (1% N, P, K); a high lime equivalency of 25% to 60%; good storage, handling, and spreading properties; and acceptable odor. The product is being produced from sludges produced in several municipalities and is used in agriculture and in cover for landfill. The key to the success of this process is that pathogenic microorganisms are destroyed by the alkalinity and heat associated with the addition of coal ash by-products and possibly quicklime (CaO), followed by temperature-controlled composting and air drying. Leachability tests at various pH levels have indicated that the heavy metals are below EPA toxicity limits.

Assessment of agricultural applications

The efficacy of using coal ash residues in agricultural applications cannot be generalized, since it is evident in comparing case studies that success is varied and depends on the suitability of the amendment to the soil and use conditions. For example, composting coal fly ash with field-collected waste vegetation was found to have no detrimental effect on bean germination in clayey and sandy soil, but reduced germination in a high-humus soil (Varallo, 1993). Alkaline treatment is appropriate for eastern acidic soil, but not for many midwestern soils that are already alkaline in nature. Novel applications in specialized areas may provide some of the more immediate commercial opportunities. FBC bed residues have been used at high rates of over 100 tons per acre as a mulching agent applied directly to cap the soil surface in orchards and raised-bed tomato rows (Korcak, 1993). Coal bottom ash has been demonstrated as an acceptable root medium for growing flowers in a hydroponic

nutriculture system (Bearce, 1993). Widespread acceptance of coal ash by-products in agriculture still has performance and economic barriers to overcome, but opportunities exist today where the properties of a utility's by-products meet the needs of a local market.

Some concerns still exist about the environmental safety of using coal ash by-products in agriculture, despite findings that leachable concentrations of toxic metals are very low (Beeghly et al., 1993; Burnham, 1993; Bennett et al., 1981). While results vary somewhat for different by-products and soil types, the general finding reported is that leachates are nontoxic relative to the eight RCRA toxic metals (arsenic, barium, cadmium, chromium, lead, mercury, selenium, and silver) and often approach the more stringent primary standard for drinking water. The mobility of metals depends on the mineral matrix and on pH, and solubility is generally reduced at the high pH levels associated with alkaline coal by-products. Certain beneficial trace plant nutrients present in coal fly ash, such as boron, selenium, and molybdenum, are assimilated in animal tissues (Lisk, 1981), and selenium deficiency in farm animals has been shown to be correctable by feeding the animals fly ash-grown crops. In coordinated tests on farm crops and animals (Bennett et al., 1981), there has been "little evidence" of detrimental effects on the food chain. One reason for caution is that standard tests for determining the leachability of trace metals, including the EPA EP and toxicity characteristic leaching procedure (TCLP) tests for acid solubility, do not accurately represent all utilization environments, and they may either evidence problems that do not exist or miss worst-case problems that would occur in practice. At the current stage of understanding, states will tend to regulate ash reuse on farmland as solid waste management, requiring case-by-case permitting (e.g., California [Marshack, 1992]). Well coordinated research covering a carefully selected classification of by-product materials and utilization settings will be required to provide the confidence level required for large-scale, nonrestricted use of coal ash and FGD by-products in agriculture.

Power Plant Location

The vicinity of Kenosha, Wisconsin, is the assumed site of a high-pressure power system (HIPPS) plant to be used for economic evaluation of probable power plant by-product materials. It is located approximately 60 miles south of Milwaukee on the shores of Lake Michigan. The location is significant, in that it is near major U.S. cities, such as Chicago, which utilize considerable amounts of coal combustion by-products. Another significant factor is the availability of water transportation to other major metropolitan areas.

An important aspect of assessing marketability of by-products is the use of integrative technological data manipulation software from Strategic Mapping, Inc., the Atlas® GIS (geographic information systems). GIS is a software technology that permits the input, manipulation, analysis, and display of geographically referenced data. GIS contains a set of tools to perform a variety of functions directed towards integrating both map information and associated data. This is an effective means of indicating market areas attributable to such factors as travel distances, methods of transportation, available industries utilizing coal by-products, and competing materials similar to coal by-products. In the near vicinity of the proposed HIPPS plant are several coal combustion power plants that already

market their coal by-products. The GIS mapping system is also an effective tool for identifying other potentially competing coal by-products.

The more precise a reference point available for GIS, the more beneficial its geographical application will be. For this reason, the community of Bain, Wisconsin, was chosen as the precise location of the coal combustion facility. The location of Bain is 1-2 miles southwest of Kenosha. An important reason for choosing Bain was its proximity to major railroad lines, a major method of transporting coal by-products for utilization.

Coal and Coal By-Products

Although a coal source has not officially been chosen, the leading candidate would be the Illinois No. 6 coal seam. When assessments are made on the expected chemical, mineralogical, and physical aspects of the by-products, the anticipated results will be based on this assumption. The appropriate coal and combustion characteristics used to determine the quantities of produced by-products is contained in Table 4.3-28. The combustion by-products are assumed to be approximately 80% boiler slag, 10% very fine fly ash, and the remaining 10% of by-product is assumed to become deposited throughout the system. In addition, there will also be significant amounts of FGD sludge produced. The entrained fly ash will be filtered through a baghouse. Therefore, it is anticipated negligible amounts of fly ash will enter the FGD sludge. Potential utilization of all three by-products are being assessed.

Boiler slag is a coal by-product that is extensively utilized in many parts of the United States. According to the American Coal Ash Association (ACAA, 1994), over 6,200,000 tons of boiler slag were produced in the United States in 1993, with nearly 55% utilized. The utilization of the slag by-products has been in such applications as blasting grit, roofing granules, skid-resistant material for snow and ice, cement and concrete production, grouting, and others. Nearly 80% of the utilization was in the application of blasting grit and roofing granules. For the proposed UTRC HiPPS, the quantity of slag anticipated to be produced is 30,700 tons per year.

Fly ash is the most commonly used coal by-product, generally as a partial replacement for cement in concrete. The fly ash assumed to be produced for the proposed UTRC HiPPS system is considered to be extremely fine in particle size in comparison to fly ash produced from conventional pulverized coal combustion systems. This quality is important because specific surface area is a factor in assessing the use of coal fly ash in concrete applications. The quantity of fly ash anticipated to be produced is considered to be quite minimal (7700 tons per year) when compared to conventional pulverized coal power plants. Fly ash from the proposed HiPPS plant may need to be stored in a silo until sufficient quantities are obtained to warrant their use.

TABLE 4.3-28 PROPERTIES OF DESIGN COAL, NATURAL GAS, AND SULFUR SORBENT[1]

Proximate Analysis of Coal	
Heating Value, Btu/lb	10,982
Sulfur wt%	3.28
lb of SO_2/MMBtu	5.98
Moisture Content, %	12.25
Ash Content, %	10.97
Maximum Heat Rate, Btu/kWh Composition of Natural GAs	7260
Heating Value, Btu/lb Sorbent Properties	23,171
Sorbent Ratio, Ca:S	1.05
Purity of the $CaCO_3$, %	94.1
Calculated Sulfur Rate, lb/hr	4226
[1] The net target efficiency of the commercial plant is to be 47% or higher at ISO conditions. The plant is designed for baseload operation. The baseload is assumed to be 65% coal and 35% natural gas. The annual coal consumption is estimated to be 350,000 tons per year.	

The commercial HIPPS plant conceptual design includes a wet-limestone FGD system for 98% SO_2 removal. Alternative FGD processes are designed to make by-products to be used as high-purity gypsum for wallboard manufacturing, cement production, fertilizers, and agriculture lime substitutes. As part of the desulfurization process, *in situ* oxidation can be used to produce ammonium sulfate, which can be used in fertilizer production. As a substitute for agricultural lime, the FGD by-product is used to control pH. For use as gypsum supplement, the FGD by-product is by itself of insufficient quality to be immediately utilized. By means of forced oxidation into the scrubbing slurry, a higher-purity gypsum is produced by oxidizing calcium sulfite. Additional dewatering equipment and product handling and storage facilities may be required. In 1993, over 20,340,000 tons of FGD material was produced with less than 6% (1,163,077 tons) utilized (ACAA, 1994). Quality assurance for FGD by-product gypsum is necessary to ensure gypsum consistency meets the relatively stringent commercial specifications. The quantity of FGD by-product sorbent anticipated to be produced in the HIPPS system is 76,500 tons annually at a solids content of 90%. FGD by-products is a disposal concern for many electric power utilities. Marketability of these materials is a major emphasis in research all across the United States and Canada.

Market Study

At the EERC there is a core research group, known as the Coal Ash Resources Research Consortium (CARRC, pronounced "cars"), involved in coal by-product research. CARRC is a consortium of industry and government members that performs scientific and engineering research on the properties and behavior of coal ash relating to ash utilization. The EERC and CARRC have been actively involved in promoting ash utilization for more than 20 years. To develop a thorough and up-to-date market assessment specific for the Kenosha market area, several coal ash marketing agents

and electric utility companies, were contacted for consultation. Marketers in this area are the most familiar with local logistic concerns and potential market for by-product utilization. The consultants solicited in the market feasibility study for the HIPPS power station have all been associated with CARRC activities. Overcoming technological barriers, such as laboratory testing and field demonstrations, are but an initial step in power plant by-product utilization. The greatest challenges for marketing power plant by-products include convincing potential users that power plant by-products are beneficial raw materials and not inferior waste products, and convincing regulatory agencies to develop requirements that will clarify and promote reuse options.

Coal combustion wastes are exempt from federal hazardous waste regulations (Subtitle C) under the Resource Conservation and Recovery Act (RCRA). As a result of this exemption, coal ash may be regulated under state solid waste requirements in accordance with RCRA Subtitle D. However, with no guidance on the reuse of coal ash provided by the United States Environmental Protection Agency (EPA), state regulations vary significantly. Individual state regulations can be vague and/or extremely conservative, resulting in a complicated approval process. Thus, it is important to be aware of and understand each state's regulations prior to pursuing an ash-marketing program.

In a report by the American Coal Ash Association (ACAA, 1995), a nationwide survey was performed to identify regulatory barriers to the beneficial use of power plant by-products and to identify areas where regulatory reform may be warranted. The results of the survey summarize the solid waste regulations and/or policies pertaining to power plant by-product utilization on a state-by-state basis. In Wisconsin, for example, coal ash is exempt from the hazardous waste regulation and is regulated as special waste under solid waste regulations. Provisions allow coal ash to be exempt from the state's landfill requirement if the ash is beneficially used. The ash is still considered a waste and the exemption must be requested and approved under a provision for the beneficial use of utility ash. Bottom ash (or slag) can be used as a fill material for road subbase, for foundations of a building, and under parking lots. As in Wisconsin, the state of Illinois exempts coal ash from the hazardous waste regulations. It is regulated as a special solid waste under states regulations. No specific regulations address utilization and requests are handled on a case-by case-basis.

Boiler slag

The physical characteristics of boiler slag − dark color, hard glassy texture, and course sizing − make it a very suitable material for utilization. For use as a raw material in roofing shingles, the size fractions are very specific. Generally, the boiler slag is first screened to obtain size fractions between a No. 12 (1.70-mm) and a No. 40 (425-μm) mesh sieves. Sieve fractions between these two are used to obtain the ideal level of gradation. For use as a blasting or abrasive grit, the fraction sizes are not as stringent as those required for roofing shingles. An abrasive grit may have a maximum size requirement, such as the No. 12 sieve, but the finer fractions can go down as low as No. 100 (150 μm) in size. There is also generally no requirement in the gradation for blasting grit either. Figures 4.3-41 and 4.3-42 indicate locations of potential users of abrasive-type materials such as the HIPPS boiler slag.

Included in the 100-mile radius are companies that market or utilize blasting cleaners, abrasive blasting equipment, abrasive materials, or abrasive coatings. Most of these companies are located within 50 miles of the proposed UTRC HiPPS system.
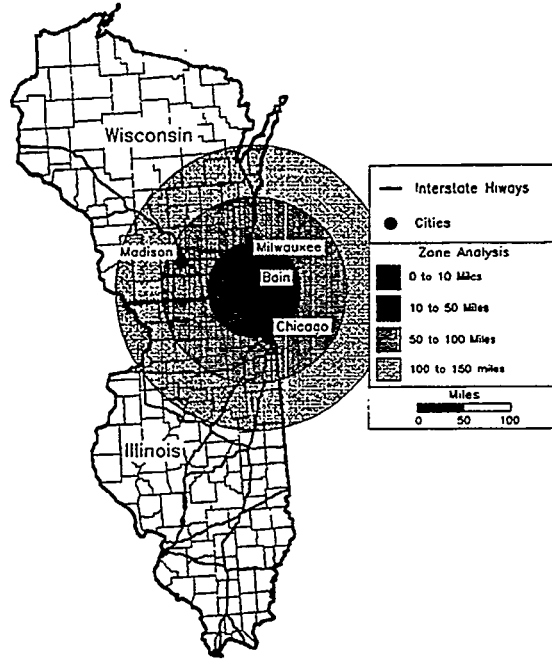
Figure 4.3-41   Potential Consumers of Boiler Slag Produced from UTRC system.
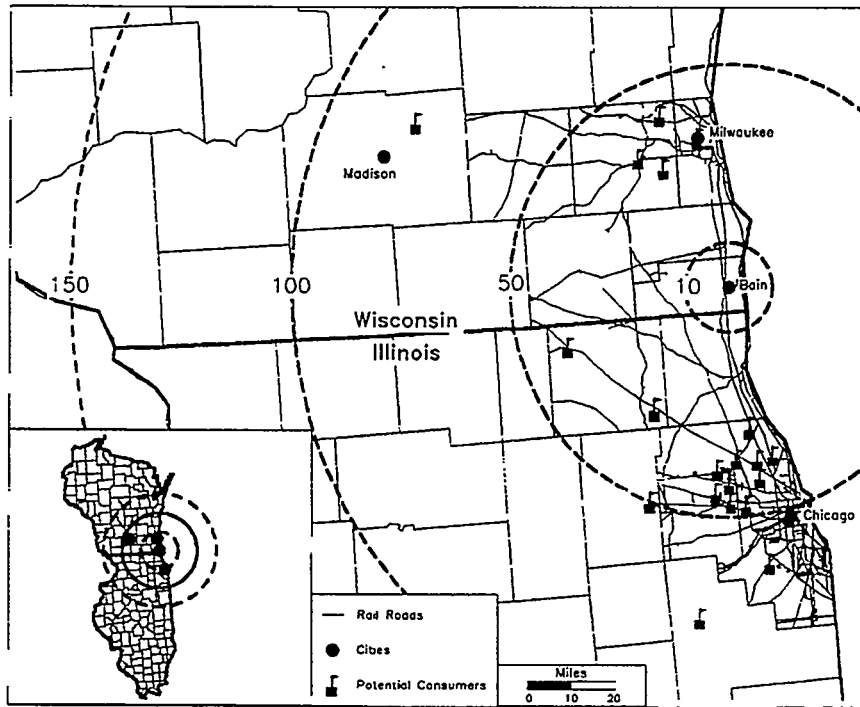
Figure 4.3-42   Potential Consumers of Boiler Slag Produced from UTRC system.

Utilities currently marketing their wet-bottom boiler slag and dry-bottom ash will grind their materials prior to transportation to customers. Figure 4.3-43 shows the locations of power generation systems that currently market portions of their boiler slag and/or bottom ash. Depending on the gradation of the boiler slag produced from the HIPPS system, pregrinding of materials may also be a prerequisite to marketability. Commercially available boiler slags can be sold for $.50 per ton. If the transportation costs are subsequently passed onto the utility, these may vary from $2 to $3 per ton, so conceivably there can still be a cost associated with marketing as opposed to disposal. Locations of other existing wet-bottom boilers is contained in Figure 4.3-43. The extended longevity of a landfill needs to be considered when determining revenue enhancement from utilization.
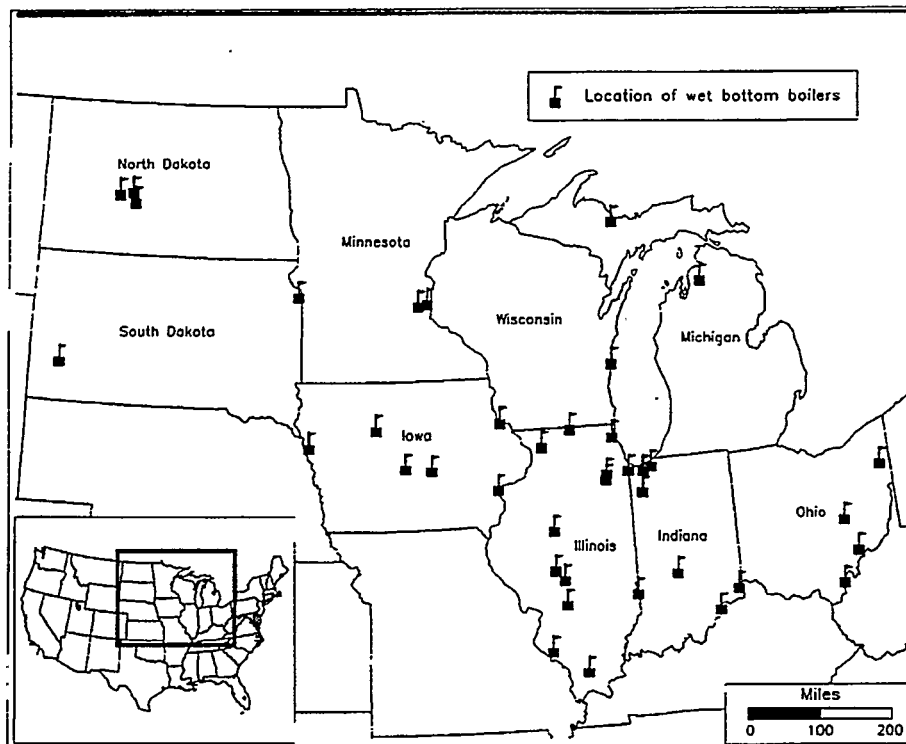
Figure 4.3-43   Locations of Existing Wet Bottom Boiler Plants that Currently
Market Boiler Slag and/or Bottom Ash.

Gypsum

The technical challenges of producing commercially usable by-product gypsum have mostly been solved and the operating changes required to use these materials in commercial applications are becoming relatively well established. The area that remains a significant challenge is structuring successful relationships between producers and consumers. Ultimately, economics is the driving force that will determine the level of utilization. However, a by-product that is less expensive than a raw material will not automatically be sought after for industrial use. The factors that govern its desirability as a product are much more diverse.

231

The commitment of the by-product gypsum supplier is critically important to encourage a partnership with consumers. Commitment is seen in numerous forms, such as supply reliability because building materials production plants operate very consistently, thus making supply interruptions difficult to manage; product quality to ensure impurities are controlled to acceptable levels; desirability of local market region; and competitive advantage over other materials. Two main areas that have received attention as process improvements are additives and forced oxidation. Additives are employed in improve SO_2 removal by increasing the liquid-phase alkalinity. Forced oxidation of sulfite to sulfate (eliminating major dewatering problems) is an important major improvement in scrubber systems. This has led to the development of the production of commercial-grade FGD gypsum.

A critical element in the economic consideration of gypsum markets, natural or synthetic, is transportation costs. Gypsum, and the two principal products made from it, cement and wallboard, are bulk items sensitive to handling and transportation costs. For this reason, location of the gypsum source and manufacturing plant, distance between the two facilities, and mode of transport are critical. Two separate sources of information have identified completely different methods of transportation as most practical. One source stated that rail was by far the most economical alternative for transporting high volumes of a coal by-product from the plant site to a industrial location. A second source stated that any transportation distance under 100 miles is commonly and most ideally performed by truck. Each method of transportation is site-specific and entirely dependent upon the type of by-product produced and the form of utilization intended for that by-product. Cement plants have traditionally been located on or adjacent to limestone or dolomite deposits, and are usually located within 100 to 150 miles of their markets. Wallboard plants located in the United States are generally within the vicinity of major urban areas. For the most part, the natural gypsum for these industries comes from those mined closest to their plants. For several gypsum operations, the economics have been such that wallboard plants are located at or adjacent to the mine.

Figures 4.3-44 and 4.3-45 show the locations of gypsum mines and wallboard plants in the United States. The economic advantage of bulk shipment by water overland has been one of the principal reasons gypsum resources from Canada have been the principal feedstock for wallboard plants located in the United States within the vicinity of major urban areas on or near the Atlantic and Gulf coasts. Most gypsum produced, which represents less than 4% of gypsum produced domestically that year, was used for wallboard and cement production. It would be reasonable to conclude that commercial-grade FGD produced at the HIPPS system would be economically competitive with natural gypsum for current markets. Over 12.5 million metric tons of FGD material was generated from 96 plants in 1993 (Barsotti and Kalyonco, 1995). For the same year, according to surveys by the U.S. Bureau of Mines, approximately 2.4 million tons of limestone and 1.6 million metric tons of lime were reported consumed in flue gas desulfurization. One can see the relative location of utilities, gypsum mines and wallboard facilities by overlaying the gypsum industry data with the utility FGD-generated data and focusing on the Upper Middle West near the proposed HIPPS system.

Buffer zones of 100 miles around wallboard facilities were generated under this arbitrary scenario (Figure 4.3-46) to provide an additional perspective in showing the closest electric power generating units to wallboard manufacturing facilities. Commercially available gypsum will generally cost approximately $9 per ton. Costs associated with the production of gypsum are for crushing and milling the raw material into a useable form by cement plants and wallboard manufacturers. Costs for transportation will need to be added onto the $9 per ton estimate.
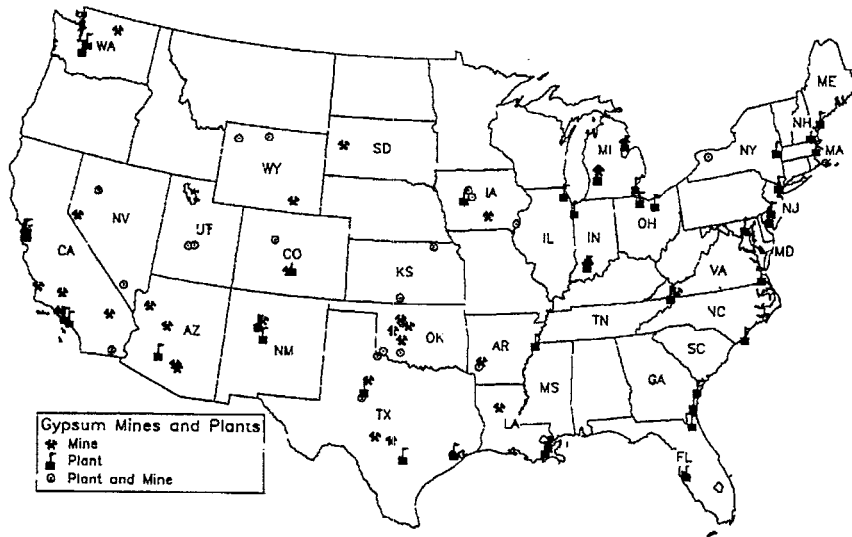
Figure 4.3-44   Location of Gypsum Mines and Plants (Source: U.S. Bureau of Mines).

Figure 4.3-45   Location of Gypsum Mines and Plants, Eastern United States (Source: U.S. Bureau of Mines).

233
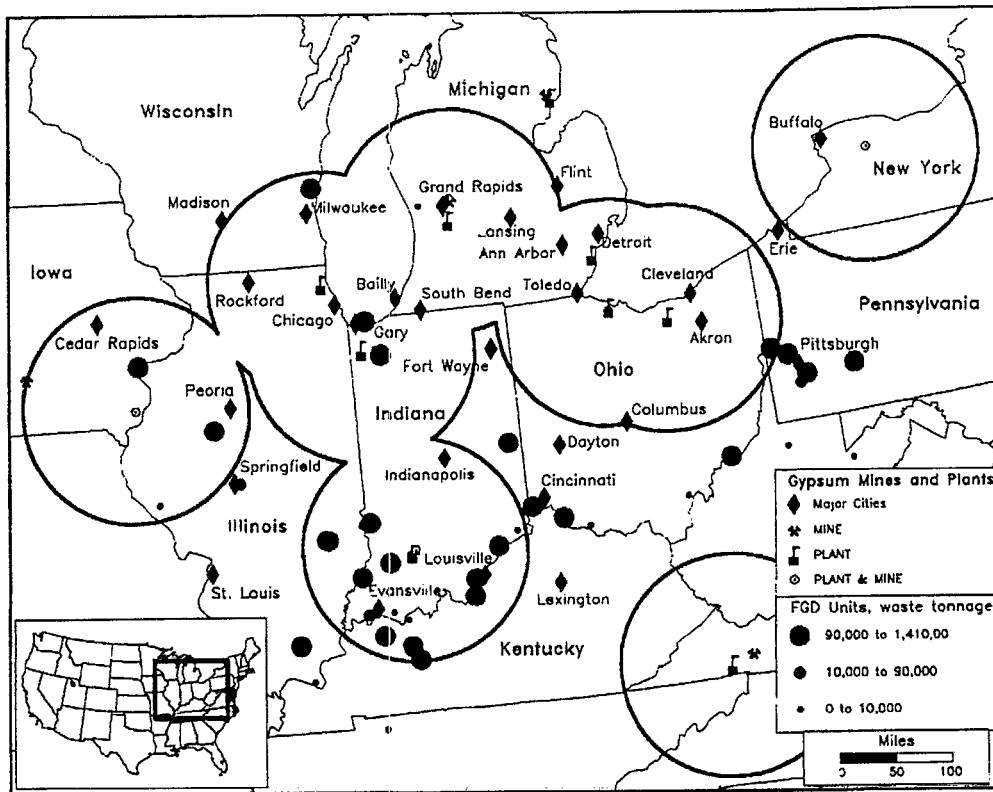
Figure 4.3-46   Location of Gypsum Mines and Plants and Coal Combustion Power Plants with
FGD Units 100 Mile Radiuses are Indicated (Source: U.S. Bureau of Mines).

Currently, FGD gypsum from the Bailey Generating Station in northern Indiana is providing gypsum to a U.S. Gypsum-owned wallboard plant within its vicinity (Henkel et al., 1993). The gypsum plant, East Chicago, has been receiving synthetic gypsum from the Bailly electric power generating station ever since the facility first added its desulfurization system in 1992. The East Chicago plant is located approximately 20 miles from the Bailly generating station. Both facilities are located near the Lake Michigan shoreline. Several key factors added together make this arrangement an ideal example of a successful coal by-product utilization program. First and foremost is the mutually beneficial business association established between United States Gypsum and the Northern Indiana Public Service Company, (NIPSCO). The success of this program has been due, in large part, to the uniform quality of the product as well as the open and frequent communications between U.S. Gypsum and NIPSCO. Additionally, the location of the two facilities has been a significant reason for the success of this FGD utilization program. The FGD product is shipped by water from the Bailey Station to East Chicago gymsum plant. The details of the business arrangements is proprietary, but the obvious financial benefit for NIPSCO has been the absence of any need to dispose of the FGD sludge since the desulfurization system and forced oxidation system were added.

234

Conclusions and Recommendations

The marketing potential of the coal combustion by-products produced with the UTRC HIPPS system should be considered a viable alternative to disposal. A key element supporting this claim is location. The HIPPS system is ideally located near major metropolitan areas that can utilize boiler slag either as a raw material or in the manufacture of another product. The market price for boiler slag can vary from $0.50 to $1.50 per ton. Transportation costs, if paid by the producer, could exceed the market value of the raw material, depending upon the method of haulage and the corresponding travel distance.

The fly ash produced and collected in the baghouse may have an application as a partial cement replacement in portland cement concrete. A typical fly ash, with an established track record of utilization, can be sold for $20-$30 per ton. This would translate into an annual product value of $150,000-$230,000 for the HIPPS fly ash. However, the quantities of fly ash to be produced are minimal in comparison to fly ash produced at pulverized combustion units already in existence in the region. The lack of substantial volumes of materials with a consistent track record in quality assurance and the existing competitive market for fly ash would limit the utilization potential for the HIPPS system fly ash. An alternative may be to recycle the entrained ash into the combustion zone, thereby melting the materials and producing additional boiler slag. If either one of the by-products is marketed separately, design conditions must be such that neither material is combined with the other during transportation and storage. The consistency of the by-product is essential to developing and maintaining a utilization program.

The FGD sludge is close to regional gypsum plants for use in the manufacture of gypsum wallboard. Currently, the FGD sludge that would be produced is unable to meet industry requirements for use as a suitable gypsum product. Process adaptation would be necessary to provide sufficient aeration and reaction time in the scrubber circuit to oxidize calcium sulfite sludge to a high-quality gypsum. Water transportation of the FGD is a significant advantage for this type of utilization. There is already in place a successful utilization program of modified FGD gypsum within the regional area of the UTRC HIPPS system. Generally the most practical form of revenue enhancement is to avoid all associated disposal costs. For one utility company in Wisconsin to develop and monitor a landfill, costs for disposal average between $10 and $20 dollars per ton. For the UTRC HiPPS system, this could translate into an annual cost savings of between $1 to $2 million dollars of avoided disposal costs for the three coal by-products produced.

To develop an effective, long-term market program, a designated representative or contact person needs to be established from the utility side. This revenue enhancement representative would work with receiving industries to ensure a quality product is produced and delivered in a fashion acceptable to both parties. This also serves to verify the commitment of the coal combustion by-product supplier to the needs and concerns of the recipient.

4.3.8 HITAF Technical Risks – Ash Management

The preliminary design work performed during Phase I suggests two major technical risks in the HITAF design. These risks are primarily caused by the criterion that the radiant section operate "wet" - that is ash depositing on the radiant heater walls be molten and flow into the slag tap. Experience has shown that molten slag can be extremely corrosive to conventional furnace refractory linings. Therefore, a better understanding of slag corrosiveness is necessary for optimum selection of the protective refractory. In addition, the slag state (solid or liquid) and thickness have a profound effect on the heat transfer characteristics of the radiant section and the slag removal in the slag screen. Therefore it is important to ensure that either the slag continues to flow easily, forming layers of minimal thickness on the walls, under all operating conditions or preventative steps have been taken to minimize the effects of ash freezing.

Refractory Lifetime in Radiant Zone - The RAH in the high-temperature advanced furnace (HITAF) will be subjected to corrosive conditions at high temperatures, which may shorten the effective lifetime of this component. To extend the ceramic lifetime and to prevent catastrophic failure of the system, a refractory coating will be applied to the ceramic. SiC refractories have thermal conductivities superior to those of conventional materials, such as alumina or chrome-based refractories, so they are useful as replaceable, corrosion-resistant coatings on surfaces through which heat flow is required.

A major hurdle to overcome in the use of SiC refractories is their rapid corrosion in the presence of coal slags. Static slag corrosion studies under Phase I of Combustion 2000 indicated that commercially available monolithic SiC-based refractories were porous and reacted quite extensively with the high-calcium and high-iron slags above 2300°F. The corrosion rates indicated that a 1-inch layer of refractory exposed to an Illinois No. 6 slag at 2300°F would be consumed in less than 6 months of operation, which was the slowest corrosion rate observed. At 2605°C, the refractory would be consumed in less than two months. The effective lifetime of the refractory in the presence of a high-calcium Power River Basin (PRB) coal at 2605°F was two weeks of operation. These lifetimes are derived from static slag corrosion tests and do not take into consideration erosional effects of flowing slag or replenishment of fresh slag in a dynamic system. In a dynamic system, corrosion rates are expected to be higher, shortening the effective lifetimes of the refractories.

Additives that would combine with the iron in slags and slow the corrosion process were also investigated. Copper promotes crystallization of spinel phases, such as hercynite ($Fe+2Al_2O_4$). The formation of hercynite would lock the iron in a stable phase and render it unable to react with the SiC and form iron silicides. The removal of the iron from the slag and the crystal formation would increase slag viscosity, which would decrease the migration of corrosive species to the ceramic surface.

A laboratory experiment was conducted to determine the effects of copper oxide additions on crystallization of a high-iron Illinois No. 6 slag. A small addition of CuO (1 wt %) was added to the ash and heated to 2550°F, then quenched. Scanning electron microscopy (SEM) revealed a high

236

concentration of blocky crystals, 5 mm in diameter, in the slag. Analyses indicated that iron and oxygen were the main elements present in the crystals, which are probably magnetite (Fe_3O_4). The formation of these crystals may influence the slag corrosion of SiC ceramics by increasing slag viscosity. The presence of crystals increases frictional forces and thus increases the viscosity of the slag. Also, magnetite formation would reduce the amount of iron in the residual slag, increasing the viscosity of the residual melt. The crystal formation also ties up the iron, a major player in SiC corrosion, in a stable phase. This may reduce the mobility and availability of iron to react with SiC.

Frozen versus Flowing Slag in the Radiant Zone - As mentioned above, experience in conventional power plants has shown that the physical state of the ash/slag dramatically effects heat transfer in the boiler. In the current HITAF design both the radiant zone and the slag screen are designed to operate under molten slag conditions. However, in the event that the gas temperatures in these sections cool below the critical point for slag to flow, provisions must be made to ensure that catastrophic loss in heat transfer efficiency does not occur. For example, during load following or furnace shut down the heat input into the furnace may drop below that required to maintain the molten slag layer. When this occurs, the slag layer on the radiant heater walls will freeze. Additional deposition on the walls will increase the ash layer thickness, and decrease the heat transfer to the working fluid with potentially catastrophic results.

The design, therefore, must include features to prevent freezing of the slag layer or operating procedures to manage the impact of a frozen slag layer. One possibility is the inclusion of small natural gas jets along the radiant heater walls and at the bottom of the furnace, in the slag tap. Under conditions where slag freezing may occur, these jets may be enabled to ensure that the slag layer remains molten. As an added preventative measure, sootblowers may be required in the slag screen for deposit removal under dry ash conditions. This area will require additional work to minimize the risk associated with operating the HITAF under dry ash conditions by identifying combinations of operating conditions and coals which cause unacceptable freezing in the radiant zone.

In the case of a coal which does cause unacceptable freezing in the radiant zone, it may be desirable to control this thickness and the temperature at which the slag freezes to assure minimum slag corrosion rates, tapping problems, and deposition in the convective pass. Increasing slag viscosity may provide a means to protect the ceramic surface. In an oxidizing atmosphere, a thin layer of SiO_2 forms on the surface of SiC and Al_2O_3 on aluminide alloys. The oxide layers can act as protective coatings to reduce corrosion rates by slowing the transport of oxygen to the underlying material unless it dissolves into the slag, leaving the material exposed directly to the slag. Since both SiC and aluminide alloys are non-oxides, they are not expected to be wetted well by the slag, and corrosion rates will depend on the rate of transport of directly corroding species. The preferred surface, oxide or non-oxide, is the one that dissolves most slowly.

The formation of the oxide layer depends on the partial pressure of oxygen at the ceramic surface, which can be influenced by the thickness of the slag layer. A viscous slag layer would not allow

rapid oxygen penetration to the ceramic surface because it would form a deeper layer through which the oxygen must diffuse, and because the diffusion rate is lower as a result of to the relatively high concentration of bridging oxygens in a more viscous melt. Also, the diffusion rates of corrosive ions such as iron to the SiC or calcium or magnesium to the aluminide surfaces are much slower in a slag with higher viscosity and levels of bridging oxygens. Therefore, increasing slag viscosity next to the HITAF surface seems to be a plausible method to reduce slag corrosiveness as long as the amount of increase is tempered with other concerns such as slag tap operation.

The viscosity of a coal slag depends on the degree of oxygen bridging, molecular clustering, and crystal formation in the melt. These factors are, in turn, determined by the temperature and composition of the melt, as well as the gas stream composition. During basalt operation of the HITAF, the gas temperature and composition are expected to be relatively fixed by burnout and efficiency requirements, although excursions for slag control will be possible. In addition, a great deal of flexibility is possible in slag composition by using blends of coals and possibly through the addition of small levels of naturally occurring nonfuel materials. Most important will be the ability to predict slag viscosity and corrosion rates as functions of gas composition, temperature, and slag composition. Previous research at the NDEERC by Kalmanovitch and Frank and at Penn State by Jung and Schobert has led to the development of methods to predict slag viscosity with good accuracy based on slag composition and temperature as long as the slag is fully liquid. However, equations for predicting the actual temperature of freezing are in the development stage, so freezing temperatures are still best determined by a combination of calculation of slag composition on better developed ash formation and deposition models, then measurement of the freezing temperatures by laboratory methods. Using these techniques, the NDEERC has shown that the freezing temperature of slags formed from PRB coals can be increased by over 390°F by adding naturally occurring materials at rates of 2% on a coal weight basis. Doing this during HITAF operation would cause a slag layer to be frozen next to the radiant heat exchanger surfaces, dramatically reducing slag corrosion.

Critical Issues

As can be seen in the previous sections, the preliminary design work performed during Phase I has identified several critical technical issues:

- Slag properties in the radiant zone
- Refractory corrosion in the radiant zone
- Slag screen operation
- Convective air heater cleaning
- Convective air heater corrosion

Many of these issues are related to the effect of molten slag and dry ash deposition on the operation and lifetime of the HITAF components. For example, molten slag can cause corrosion and reduced heat transfer in the radiant zone.

238

Slag Properties in the Radiant Zone - As previously discussed, the slag characteristics in the radiant zone greatly affect the heat transfer and ash removal. Slag/ash viscosity, for example, controls both the sticking probability and the flow characteristics of the slag. The thermal conductivity controls heat transfer to the working fluid. In the HITAF system, these parameters are coupled to control the overall effectiveness of the slag screen. The viscosity of the slag controls the thickness of the flowing slag layer, and the ease at which slag flows to the slag tap and is removed. The thermal conductivity controls, in part, the thickness of the frozen slag layer next to the refractory tubes and the heat transfer through the entire slag layer. Therefore, the combination of the two characteristics defines the ease of operation of the HITAF for given coal characteristics and operating conditions.

During Phase II, it will be necessary to explore the effect of furnace operating conditions and coal characteristics on the slag viscosity and thermal conductivity with the goal of being able to better predict HITAF performance and minimize the associated technical risks. Measurement of slag properties under representative conditions and development of appropriate engineering models are needed.

One way of monitoring deposits is by using an existing commercial system such as Cleaning Advisor. It consists of one or more industrially hardened infrared video cameras (up to 4), connected to a central image processing computer. The computer colorizes and enhances the images while allowing the user to store and retrieve images and switch between cameras. A key feature of the system is the ability to compare and plot as a function of time the brightness of given area in the field of view as compared to some reference area. This technique allows the relative cleanliness and fouling rate of the selected area to be quantitatively evaluated. Several processing adjustments are available to enhance the sensitivity of this method. The system has been available for more than 4 years and has been proven in many utility applications.

Refractory Corrosion in Radiant Zone - Refractory slag corrosion in the high-temperature conditions of the HITAF is a critical issue. Previous studies have indicated that the corrosion of SiC refractory bricks by acidic and basic slags at 2730°F involved the formation of iron silicides, and basic slags corroded the SiC more rapidly than acidic slags. The investigations indicated that monolithic SiC-based refractories had reacted quite extensively with the high-calcium and high-iron slags at 2605°F. The evidence suggests that the phosphorus-based and calcium aluminate binders in these refractories may be the cause of some of these reactions. Some experimental refractories were developed under Phase I of this program; however, corrosion in the presence of PRB slags is still a critical issue. It is necessary to develop a more corrosion-resistant SiC monolithic refractory with less reactive binders.

Slag Screen Operation - Another critical issue identified is design of the slag screen. The slag screen serves a dual purpose in the current design, serving as both a particle collection device and a radiation shield for the radiant zone. It is critical to design a slag screen that efficiently removes ash particles with a minimum pressure drop. The main slag screen parameter that can be varied to affect

particle collection efficiency and pressure drop is tube arrangement. Optimization must be made over range of operating conditions in the combustor, i.e., gas velocity and ash size distribution.

This can be addressed by identifying tube placement to maximize particle capture, tube orientation in the flow to facilitate slag removal, location in the furnace for slag removal, and slag screen size. CFD modeling can guide optimum tube arrangements.

Convective Air Heater Cleaning - The slag screen cannot remove 100% of the particles that are likely to deposit in the convective air heater without incurring an unacceptable pressure drop. The design and operation of the convective air heater, therefore, must allow for controlled removal of deposits. Heavy, sintered deposits are undesirable because they may be difficult to removal and the removal process may damage the air heater. Therefore, to reduce the risk of failure in the convective air heater, a maximum gas inlet temperature has been specified. This temperature is such that deposits on the convective air heater surface will sinter slowly enough to allow removal by conventional sootblowers. Spacing between the tube sheets is wide enough to allow retractable sootblowers to clean between sheets.

The air heater in the convective pass of the HITAF will be most likely constructed of an aluminum containing high-temperature alloy. These alloys form a skin of aluminum oxide that is highly resistant to oxidation or chemical corrosion. For the situation where the HITAF is fired with 65% coal and 35% gas, the convective air heater is expected to operate with a skin temperature of up to 1660°F. At these temperatures, oxidation is expected to be minimal because of the low rate of oxygen transport through the alumina skin. Corrosion by other coal gases and ash should also be minimal.

Thermochemical equilibrium calculations can be used to indicate some of the most likely reactions. Data from the JANAF and Barin tables indicate that there will be several species within the products of coal combustion that will be reactive toward an alumina coating. The most common species will be glassy silicate ash particles, which will react to form aluminosilicate material. However, the reaction between the silica glass and the alumina coating will be slow unless fluxing elements like calcium or sodium are present, in which case sodium and calcium aluminosilicates will form. The alkali elements may be present in large quantity through the physical and chemical vapor deposition of sodium and calcium sulfate at these temperatures. Calcium sulfate may also directly react with the alumina coating, even if silica is not present, to form calcium aluminate and sulfur trioxide gas. However, it is not known how rapidly these reactions will occur, or if the reaction products themselves, which should be solid at these temperatures, will form a different protective coating to prevent further corrosion. Also, it is not known how much corrosion resistance will be provided by the other elements in the alloy. Finally, not all of the reaction products can be predicted by simple thermochemical equilibrium modeling because equilibrium data for all possible species is not yet available.

4.4 Duct Heater and Gas Turbine Integration

The combined cycle power plant described in Section 3 will utilize a nominal 160 MWe gas turbine powered generator. From thermodynamic analysis of the combined cycle it has been determined that the optimum input temperature to the turbine should be 2495°F at 225 psia. Since the high-temperature coal-fired air heater will operate with a discharge temperature of 1700°F, a boost heater is needed to provide the additional energy to operate the turbine at the required power output.

4.4.1 Preliminary Engineering Analysis

The key requirements in the design of the boost heater are:

- Pressure drop less than 1.5% of air flow total pressure
- Uniform exit temperature profile
- Ultra-low emissions of NO_x and CO

These requirements can be met with mixer/combustor designs which have been developed at UTRC as a result of research into gas turbine combustors for ground-based and aircraft turbines, and in micronized coal combustion research.

Heater Thermodynamics — The pressure drop through any combustor or mixer design is a direct function of the mass flow through the system. If the total mass flow of air to be heated is fixed, there is an optimum configuration which will provide the required heating rate, temperature profile, and pressure drop with piping that will match the physical dimensions of the gas turbine to be used. Based upon experience at UTRC on gas turbine combustor design, it is desirable to maintain duct velocities around 50 ft/s to reduce piping losses and to obtain a boundary layer of moderate size. Gas velocities in practical combustors are maintained below 200 ft/s for flame stability, and momentum ratios between air streams are typically 4 to 1 to aid in mixing. Using these criteria as general guidelines, the gas turbine air path was analyzed to determine the optimum method of providing the additional energy downstream of the air heat exchangers needed for the combined cycle.

Analysis shows that by splitting the flow into two streams, the size of ductwork, swirler dimensions, and mixing patterns can be optimized. However, each flow stream must experience a 795°F temperature rise, with a total heat input of 3.567×10^8 Btu/hr. To obtain this temperature rise, the flow could be further split so that 33% of the air would pass through a combustor, and 67% of the air would bypass the burner. This would reduce the overall pressure loss of the flow, since the burner is the high pressure loss side of the flow and only 1/3 of the airflow would experience this pressure drop. This flow split, however, is not practical because of the high temperatures required in the burner flow in order to provide the overall temperature rise of 795°F. Based upon the enthalpy of the total and split flow streams, the burner discharge temperature would approach 4000°F (2478°K). Not only would this present a materials problem, but more importantly, it would present a serious thermal NO_x problem.

Studies of the production of NO_x in flames (Semerjian, 1977, Tacina, 1990, Merryman, 1975) have indicated that the production of "thermal" NO_x increases dramatically when combustion

temperatures exceed 2420°F (1600°K). Therefore, to reduce NO_x emissions from the boost heater, it is imperative that temperatures above this level be avoided. For this reason, the burner concept incorporating a 33% flow split cannot be used due to the high NO_x levels which would result. The optimum configuration will involve staged mixing which maintains a fuel-lean mixture at all times and prevents temperatures from exceeding 2420°F. Premixing is not possible due to the high inlet temperature of the gas stream; the natural gas will oxidize very rapidly under the inlet conditions (reaction times <30 msec). Residence times should be kept to a minimum at elevated temperatures in order to curtail reactions in the high temperature, very fuel lean flow which is proposed by the cycle analysis.

Mixer Aerodynamics − To provide rapid mixing with low pressure loss, the concept of centrifugal mixing, which utilizes density gradients within swirling flow to promote instability and mixing, will be utilized. This concept has been investigated for over 15 years at UTRC and Pratt & Whitney Aircraft (Vranos, 1982, Freihaut, 1989, Markowski, 1976, Johnson, 1986). Experiments detailed in Freihaut have demonstrated complete mixing of gaseous fueled diffusion flames in as little as 1.5 duct diameters under high intensity flame conditions. This centrifugally-enhanced mixer concept has been demonstrated successfully in reacting (combusting) flow in a previous DOE-sponsored contract.

The concept of centrifugal mixing involves utilizing the instability created by density gradients within a swirling flow to enhance mixing between the flows. For an axisymmetric, swirling fluid with a small radial velocity, the condition for dynamic equilibrium is given by the equation:

$$\frac{\partial p}{\partial r} = -\varrho_u \frac{w^2}{r}$$

Here ρ_u is the density of unburned flammable mixture, w is the tangential velocity, p is the static pressure, and r the distance from the center of rotation. If an annular element of flammable mixture is suddenly ignited along its periphery (as in the case of an annular pilot flame), a local density change is introduced, and the dynamic equilibrium is upset. This leads to a radial acceleration, so that

$$\frac{\partial p}{\partial r} = -\varrho_b \frac{w^2}{r} + \varrho_b a_r$$

Finally, the radial acceleration of a fluid element is then given as:

$$a_r = \frac{w^2}{r} \left(1 - \frac{\varrho_u}{\varrho_b}\right)$$

The subscripts u and b refer to unburned and burned fluid, respectively. If the combustion kinetics are sufficiently fast, the acceleration is tantamount to inward flame propagation, and the propagation rate is controlled by the density ratio of burned and unburned gases, and the acceleration

term w^2/r. An excellent correlation has been found between turbulent flame speed and w^2/r. It is believed that inertial effects induced by fluid rotation can substantially increase the rate of heat and mass transfer between the two streams. Experimental data and theory indicate that the centrifugal acceleration effects become pronounced when the centripetal acceleration exceeds 1000.

In nearly every practical combustor design, gas temperature and local stoichiometry is controlled through the use of transverse jets which bring combustion or dilution air into the reaction zone. The design of a combustor incorporates air flow splits between dilution jets and the main flow to obtain the desired pressure loss, total mass flow, and staged stoichiometry to control emissions. Research conducted in the area of turbulent jet mixing in cross-flows has been conducted at UTRC for many years (Vranos, 1988). The results of these and other studies have indicated that the penetration of a jet of diameter D into a cross flow can be given by:

$$\frac{Y}{D} = 0.76 \left[\frac{\varrho_j V_j^2}{\varrho_0 V_0^2} \right]^{0.52} \left(\frac{\varrho_j}{\varrho_0} \right)^{0.11} \left(\frac{X}{D} \right)^{0.29}$$

where subscript j refers to the jet, X is the distance downstream from the jet discharge, and Y is height above the orifice discharge. The design of a natural gas fired boost heater requires complete oxidation of the natural gas and complete penetration of the air jets within the combustor length. The above correlation was used to evaluate the boost heater to ensure complete mixing in the length available.

Initially Proposed Heater Design — Based upon UTRC's experience in swirling flows, dilution jet mixing, NO_x formation chemistry, and advanced mixer concepts, a design concept, shown in Figure 4.4-1, was evaluated which was expected to provide a uniform hot gas stream to the turbine at minimum NO_x levels. The cycle analysis and heat exchanger design dictated that the air flow to the turbine would be divided into two gas streams. Therefore, two in-duct heaters would be required; the air mass flow through each heater would be 363.25 lbm/s, and fuel flow would be 3.63 lbm/s. The heater would operate with an inlet temperature of 1700°F at 225.1 psia, with a discharge temperature of 2495°F.

To minimize NO_x emissions, the fuel input must be tailored to maintain constant fuel-lean conditions. The kinetics of natural gas oxidation at the elevated temperature and pressure of the air stream were studied using a chemical-kinetics code (CHEMKIN©). The calculations determined that at an equivalence ratio (F) = 0.18, the fuel is completely oxidized in 29 msec. The important fact to note is that the inlet conditions to the heater promote rapid oxidation of the fuel. The heater is not a combustor in the conventional sense. No flame stabilization is required, no piloting zones, no recirculation for flame retention, and no dilution for temperature profiling is needed for this type of heater. What is most important is rapid mixing at minimum pressure loss, with stoichiometry carefully controlled to ensure complete oxidation with minimum NO_x production. This is the key concept of the design outlined below.

243
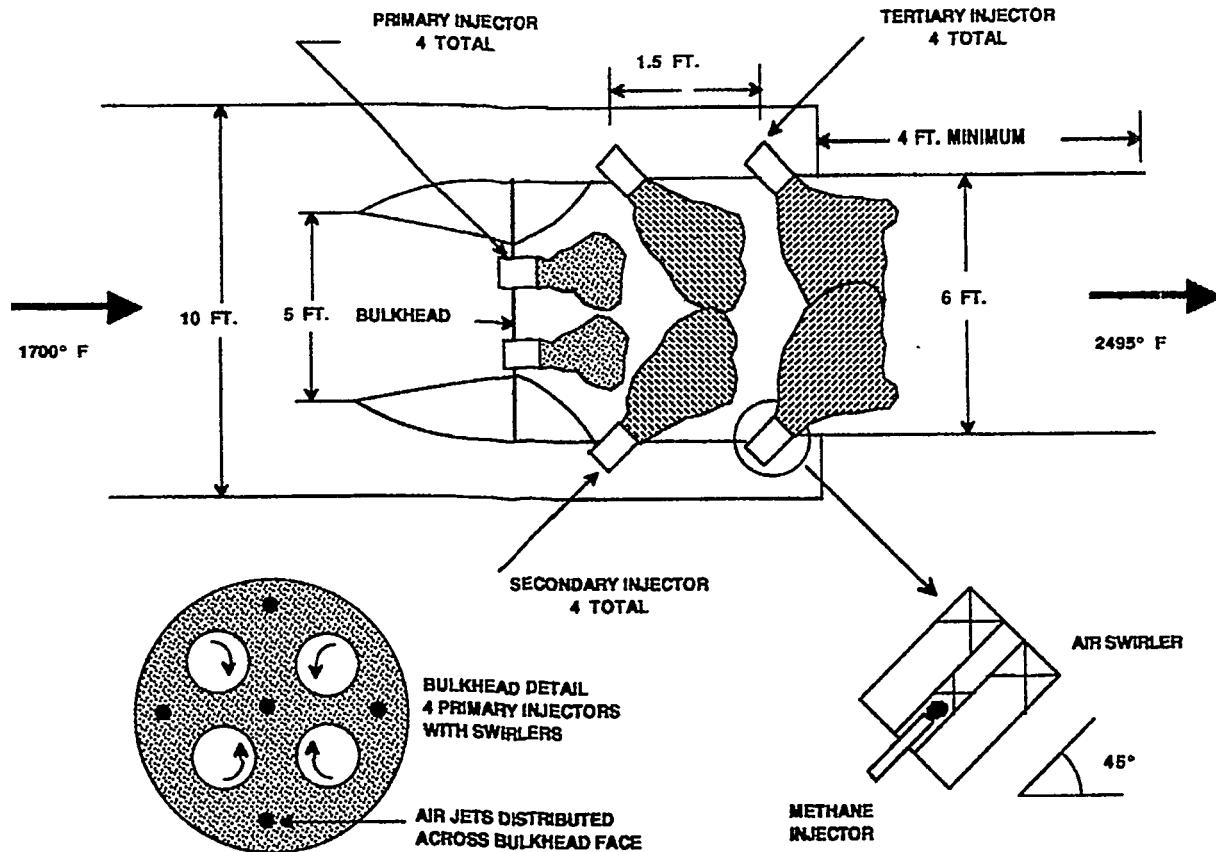
Figure 4.4-1   Initial Duct Heater Configuration.

The schematic representation of the initially proposed boost heater is shown in Figure 4.4-1. The fuel is injected in three stages through a total of 12 centrifugally-enhanced mixers. Each swirl module will pass 30.27 lbm/s of air, with fuel input through central injectors and swirlers to maintain F = 0.18. Each swirl module incorporates centrifugal mixing, due to the density ratio of 2.56 between the cold central fuel and the hot outer air. The swirl module is proposed to be of 9 in. outer diameter with a 1 in. inner swirl annulus for fuel flow. The mass-average velocity through the air swirler will be 195 ft/s, which will provide a centripetal acceleration (V^2/r) of 7000 g's if a 45° swirl angle is used. Based on the results of past studies, this acceleration would promote very rapid mixing and ensure that the local stoichiometry would remain very lean to avoid temperature peaks. This rapid mixing is essential for low NO_x emissions.

The spacing of injection stages was tailored to allow complete oxidation of each stage of fuel; the overall length of 7 ft would ensure a uniform profile at the discharge plane. The swirl module dimensions, duct size, and duct length were chosen theoretically to provide complete penetration of the "jets" by the discharge plane, and the velocity levels in the swirlers were comparable to those tested in Freihaut (1989), Markowski (1976), Johnson (1986).

244

The largest impact of this type of heater design is in pressure drop imposed upon the system. Based upon the results of Markowski (1976) and Johnson (1986), and theoretical calculations, the expected pressure loss through the swirl modules would be less than 1.5% of the air flow total pressure. This pressure loss will not have a significant impact upon the overall system efficiency.

The output from the two in-duct heaters, each of 6 ft. diameter, would feed into a common duct to the power turbine. Overall swirl would be minimized due to the interaction of the individual swirl modules in each heater. The first stage swirlers would reinforce the swirl in the annulus between swirl modules, but there would not be an overall net swirl to the flow. The individual swirl modules would interact in regions of high shear which would further enhance small scale mixing. The discharge of the two heaters into a common duct to the turbine could be tailored to provide minimum duct pressure losses and to provide a uniform total pressure profile to the turbine.

Concept Evaluation and Results — The objective of Phase I was to develop the concept for an in-duct gas fired heater which will raise the air temperature from 1700°F (the discharge of the air heat exchanger) to 2495°F, the temperature required at the turbine inlet for the proposed cycle efficiency. This heater was to have very low pressure loss and produce very low levels of NO_x. The key items to be examined were the effectiveness of mixing with the injector, and the overall penetration of the fuel-air mixture into the main air flow path.

To develop a low-pressure-loss, rapid mixer for the in-duct boost heater, it was most cost effective to screen preliminary concepts in a reduced scale cold flow apparatus. Efficiency of the mixer can be determined using planar digital imaging and probe sampling with the goal of minimizing pressure losses within the duct heater while maintaining a uniform mixture profile. The cycle analysis has indicated that the density ratio of the fuel to the main air flow in the in-duct heater will be 2.35, with a duct diameter of 6 feet. In the current program, it seemed most efficient to examine the centrifugally enhanced mixing concept in a 1/12 scale model of the duct heater, use air to simulate the fuel, and a mixture of air and helium to simulate the hot gas stream. These gases provide the appropriate density ratio between the injected "fuel" and the heated "air."

For ease of construction and to maintain manageable gas flows in a laboratory, the duct diameter was chosen to be 6 inches, with centrifugally-enhanced mixing injectors of 1 inch diameter. A mixture of helium and air (58% by volume of helium) was used in the outer swirl passage, with air in the central core. By seeding the central air flow (representing the high density fuel in the actual duct heater) with a methane trace gas, a total unburned hydro-carbon analyzer utilizing a flame ionization detector (FID) was used to probe the discharge of the swirler-injector at specific axial and radial locations in the duct to determine the concentration profile. Flow visualization was performed by seeding the central air flow with a mineral oil seed, and using Mie-scattered light intensity from an argon-ion laser to determine relative concentration of the seeded gas in the duct. Results from each of these investigations are discussed below.

Flow Visualization — The duct heater concept originally proposed utilizes an array of centrifugally enhanced mixers arranged in stages around the circumference of the duct as shown in Figure 4.4-1. The concept was based upon using the penetration of the individual jets into the main stream to provide a uniform exit temperature profile, while obtaining rapid mixing in each injector using the centrifugal mixing concept. To evaluate the mixing profile for an individual injector, tests were performed in a rectangular duct using planar digital imaging to determine concentration profiles of injected gas into the main flow. The jet flow was marked with mineral oil seed which was illuminated by sheets of light formed by an argon-ion laser and a rotating mirror system. The resultant image was captured and digitized by a CCD camera and associated data acquisition equipment. By normalizing the intensity of the image at any point in the duct with the intensity at the discharge of the jet into the duct, the relative concentration of jet fluid in the main flow can be determined. A conceptual representation of this apparatus is shown in Figure 4.4-2.
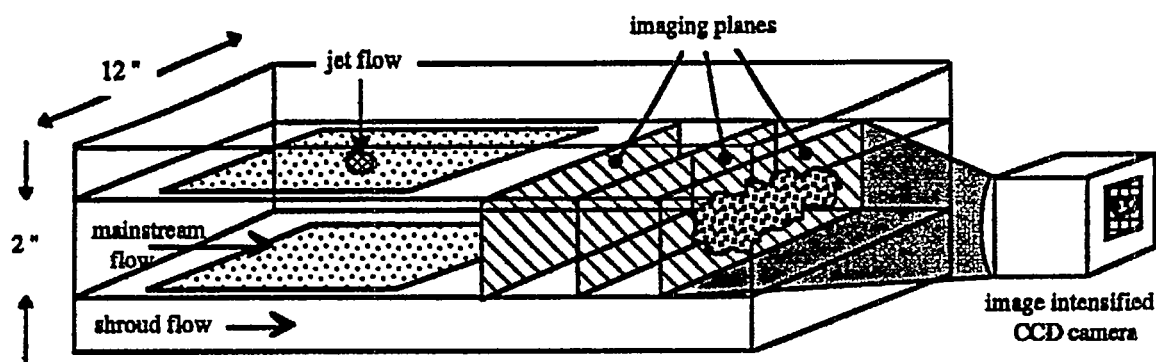
Figure 4.4-2   Flow Visualization Apparatus.

The main duct velocity as proposed was approximately 50 feet/sec, with each of the 12 injectors introducing 30.27 lbm/sec of air at a velocity of 195 feet/sec and 0.302 lbm/sec of fuel at a velocity of 87 feet/sec. Using the target velocity ratios, the sub scale experiment in injector mixing was operated at a main flow velocity of 4 feet/sec in order to provide a flow field that could be imaged properly and ensuring that the marker particles would faithfully follow the flow. Although this experiment was approximately 1/12 scale, the momentum ratios were maintained as close as possible to that which would be expected in the full scale apparatus. As has been previously demonstrated, the momentum ratio is a critical parameter in cross-stream jet mixing if the jet diameter is normalized by duct height in analyses. The mainstream flow was constant, and imaging was performed at several locations down-stream of the injector location for several velocity ratios in order to explore the effect of velocity on the jet penetration. The injector consisted of a double swirl module of 0.87 inch diameter with 45° swirl vanes in the center and annular flows, similar to the proposed full scale device. The swirlers were designed and manufactured using stereo lithography and CAD techniques which could be used to optimize the swirler design for pressure drop and flow characteristics.

246

The results of the flow visualization experiments demonstrated that the centrifugal mixer works too well to provide adequate penetration of the jet into the main flow. From the concentration contours measured, it was evident that the swirler flow spreads radially along the wall, indicating very rapid transverse mixing, but the majority of the gas does not penetrate into the main flow. This would result in very poor temperature profiles in the duct heater and probably areas of high NO production. The heater exit pattern factor, defined as the deviation of local temperature from the average temperature, normalized by the average, would be large and would therefore present problems for the turbine inlet guide vanes and first stage rotor due to large thermal variations and accompanying stresses.

Mixer Concentration Measurements – Based upon the flow visualization results, a new duct heater concept was developed. This concept, shown in Figure 4.4-3, consists of 12 centrifugally-enhanced mixers distributed in equal area sectors across the duct. Each injector will handle the same flows as listed above, and will be responsible for the fuel and air flow for each sector of 2.356 square feet area. It was apparent that the centrifugal mixer provides very rapid transverse mixing at the velocity and density ratios to be found in the duct heater, so this characteristic was used to an advantage in designing the duct heater concept shown in Figure 4.4-3.

To study the mixing in more detail, an experimental apparatus was built to perform probe sampling of the flow in both the near and far field of the mixer-injector. To accomplish this, the swirl module was designed with air flowing in the center passage (shown in Figure 4.4-4), and a mixture of air and helium flowing in the outer passage as described above. Based upon chemical kinetics studies using the CHEMKIN© computer code, the temperature rise needed in the duct heater is predicted to require an overall stoichiometry of 0.187, which calculates to a fuel mole fraction of 0.018. The more rapidly the mixer-injector can achieve this fuel mole fraction, the shorter the residence time at higher stoichiometries. Therefore the thermal NO_x can be minimized.

The sub scale test apparatus was designed with critical flow orifices or laminar flow elements used to meter the flows in each passage so that each gas flow could be measured accurately. The inner flow was seeded with methane tracer so that there was sufficient concentration at the discharge to measure with confidence while constantly monitoring the seed concentration to ensure it was stable. Typically, the inner air was seeded with 800 ppm of methane, with concentrations of 14 ppm measured when the flow was completely mixed. Once again, several flow velocity ratios were tested, with one being the anticipated ratio to be used in the full scale device. The density ratio was determined by the fuel-air density ratio in the actual duct heater.

The results of these gas composition experiments is shown for the expected density and velocity ratios in Figure 4.4-5. This figure shows radial composition profiles at 5 axial positions using a 0.0625 inch diameter sampling probe. The O.D. of the outer flow passage was 0.87 inches. From the figure, the data indicates that the inner and outer flows are completely mixed in 1.1 swirler diameters downstream of the swirler exit plane. Tests were also performed at various mass flows through the swirl

DUCT ID = 6 FEET

FUEL SWIRLER
OD = 1 INCH

AIR SWIRLER
OD = 9 INCHES

DUCT AREA = 28.27 SQ. FT.   SWIRL MODULE SECTOR AREA = 2.356 SQ. FT.
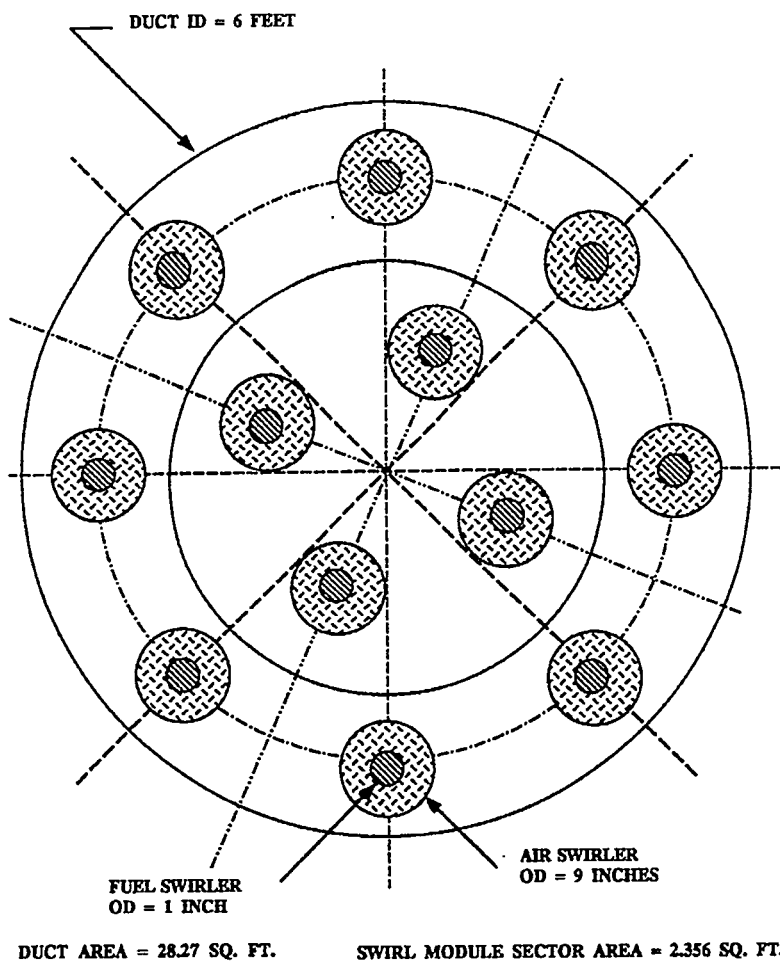
Figure 4.4-3   Revised Duct Heater Configuration

SWIRLER-INJECTOR

AIR WITH TRACE
METHANE SEED

AIR AND HELIUM
MIX (OUTER FLOW)

6 INCH DUCT

Y

X

SAMPLE PROBE
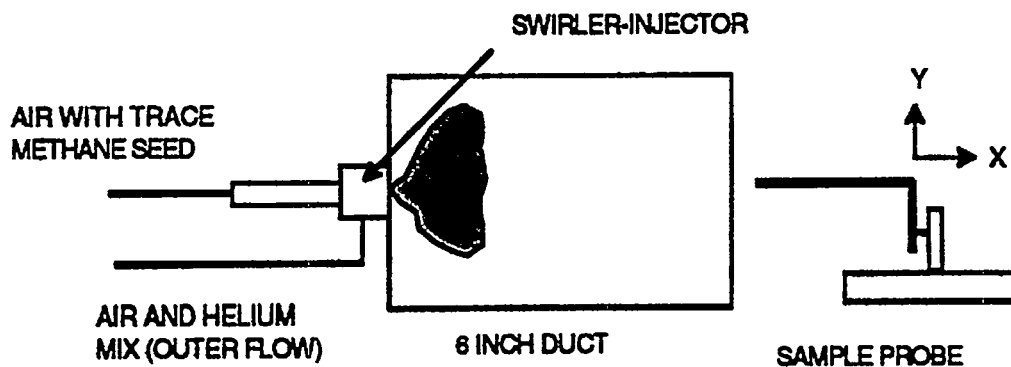
Figure 4.4-4   Schematic of Gas Composition Apparatus.

module to determine the effective C_DA for the swirl module design. A larger diameter swirler (1.875 inch O.D.) was also tested to examine scaling effects. From the air flow data, the pressure drop that can be expected in the full scale device under the operating conditions listed in the proposal will be 1.3%, which is within the target of 1.5% total pressure drop.
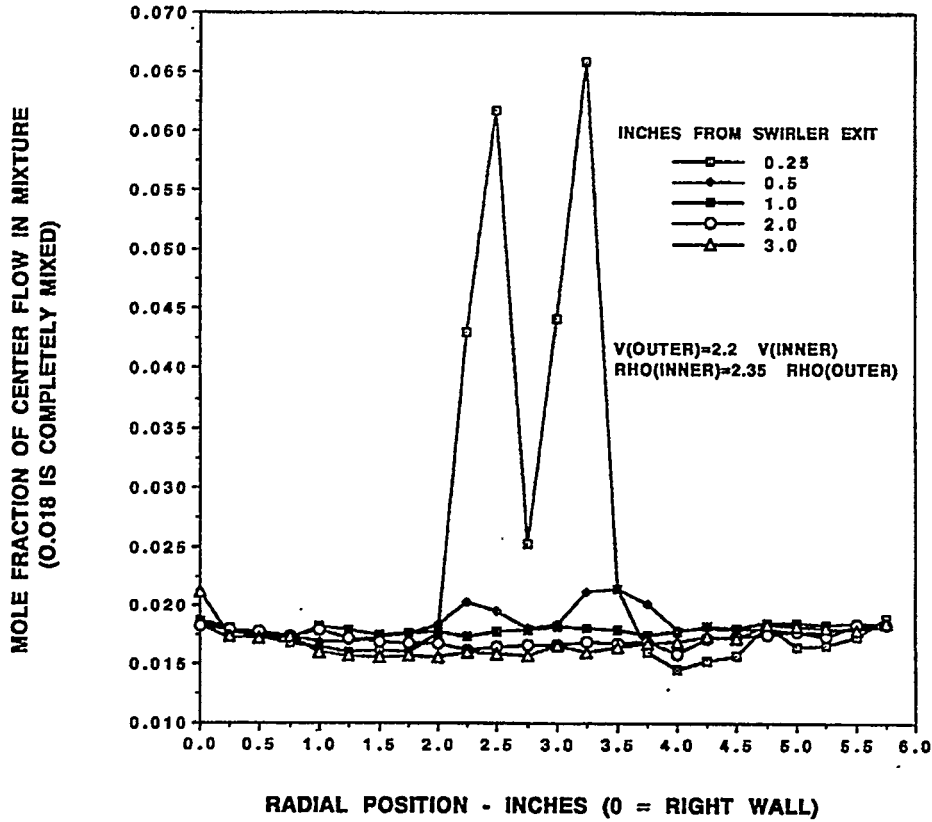
Figure 4.4-5   Duct Heater Mixture Profiles – Combustion 2000 Duct Heater.

Conclusions – The centrifugally-enhanced mixer concept will provide very rapid mixing of the fuel and air in the duct heater based upon projected mass flows and density ratios. The sub scale model has demonstrated the viability of the concept. From these experiments, it has been determined that transverse injection of the fuel and air into the duct will not provide adequate penetration of the fuel-air mixture into the main stream and will therefore not provide a uniform exit temperature and composition profile. With a distributed array of coaxial mixers, the centrifugally-enhanced mixer-injector concept will provide complete mixing within 1.5 mixer diameters. This rapid mixing should keep the production of thermal NO_x at a minimum. Preliminary sub scale pressure drop measurements indicate that the total pressure drop through the mixer will be 1.3%, which meets the program goal.

4.5 Air Pollution Control Systems and Combustor Control Systems

The level of NO_x control required for the HIPPS was originally 0.15 lb/MMBtu. However, it was decided that processes should be able to meet tougher future standards such as 0.06 lb/mmBtu, one-tenth the current New Source Performance Standards (NSPS) for coal-fired power plants. To achieve this target in a cost-effective manner, several different process for control of NO_x must be combined *in an integrated fashion*.

4.5.1 Integrated NO_x Control System

The technologies currently being considered for control NO_x in coal-fired power plants are as follows: combustion system modifications (low NO_x burners, over-fired air, staged combustion), reburning, selective non-catalytic reduction (SNCR), and selective catalytic reduction (SCR). These technologies have been demonstrated at full scale units, either as commercially available systems or as part of the Clean Coal Technology program.

Cost/Performance/Availability Trade-off – Selection of NO_x control options for HIPPS will involve consideration of the cost, performance, and technical readiness of the integrated system. Table 4.5-1 gives examples of the cost and performance of the NO_x control options as applied to conventional pc-fired boilers. The costs apply to systems which must meet the NSPS limit of 0.06 lb/MMBtu and thus may not be applied directly to HIPPS. Similarly, the performance values are for retrofit applications, not new systems. However, the table illustrates the relative cost and performance differences among various options.

The cost of low NO_x burners is not an issue for the HITAF in that the furnace is being designed with a low NO_x combustion system; the costs really apply for burners being installed in existing boilers. SCR is capable of reducing NO_x to the target level, however the cost may be prohibitive. Reburning and SNCR are less expensive to install and run than SCR, but have proven to have lower removal efficiencies. The main reasons for the lowest efficiencies with reburning and SNCR are poor temperature control and ineffective mixing of reactants with flue gas, both common problems in retrofit applications. However, the HITAF will be designed with adequate mixing and temperature monitoring and control such that both processes should achieve efficiencies at the high end of the range. A combination of SCR with a less expensive technique may provide the most cost-effective NO_x reduction.

250

Table 4.5-. NOx control options for coal-fired boilers

Control Method	Installed Cost, $/kW	Levelized Cost, mills/kWh	Removal Efficiency	Control Limit, lb/mmBtu[1]
Low NO$_x$ burner	15–25	<1	30–50[2]	0.25–0.3
SNCR	10–20	0.5–2.0	35–60[3]	0.2–0.25
SCR	35–75	5–7[5]	80–90[4]	0.05–0.06
Gas reburning	30–40	2–3	50–70	0.15–0.2

1 Assuming the uncontrolled NO$_x$ level is 0.5–0.6 lb/mmBtu
2 The higher efficiency is with overfire air (OFA).
3 Efficiency varies with boiler load; the higher efficiency is at 1700–1900°F.
4 Operated at the optimum temperature range of 700–800°F.
5 Based on four years catalyst life and 80% NO$_x$ removal.

4.5.2 Particulate Control

Although the focus of the effort is the high-temperature slagging furnace (including the radiant and convective air heaters), it will be important to characterize the flue gas stream and its constituents during each development step. Information on particulate emissions (mass loading, particle-size distribution, and chemical characteristics) obtained from these characterization activities will be helpful in defining emission control requirements and evaluating the application of commercial and developing technology options.

Present New Source Performance Standards (NSPS) for utility coal-fired boilers limit particulate emissions to 0.03 lb/MM Btu and require less than 20% opacity. The particulate control efficiency required to meet this standard varies from about 99% to 99.9%, depending on the heating value and ash content of the coal. This limit applies to facilities newly constructed or expanded after September 18, 1978.

More recent regulations concerning particulate matter have focused on ambient air concentrations of fine particulate material, 10 microns and smaller. The determination of regulatory need was based on the fact that fine particulate matter suspended in the air can be inhaled as a result of the normal breathing process and fine particulate suspended in the air contributes significantly to visibility impairment. Also, potentially toxic trace elements are known to be concentrated on fine particles. Therefore, the PM10 standard, effective as of July 1, 1987, was intended to address ambient air quality with respect to fine particulate matter relative to these health and visibility concerns.

As with the NO$_x$ emissions, the particulate emissions control target is 0.003 lb/MM Btu, an order-of-magnitude reduction in emissions compared to current regulations. A key goal of this emissions target is a significant reduction in fine particulate emissions in order to substantially reduce the release of potentially toxic trace elements (e.g., Sb, As, Ba, Cr, Mn, Mo, Ni, Zn) from coal-fired

251

ower plants. The particulate control efficiency required to meet this standard will vary from about 99.9% to 99.99%, depending on the heating value and ash content of the coal.

Particulate control technology currently being applied to coal-fired systems include electrostatic precipitators (ESPs) and fabric filters. The vast majority of coal-fired systems make use of ESPs for particulate control, with fabric filters playing a more significant role in the last 10 to 15 years. Current ESP designs and performance are adequate to meet current particulate NSPS for a wide variety of boiler designs and fuel types (bituminous coal, subbituminous coal, and lignite). However, ESP performance is highly dependent on flue gas and fly ash composition and sensitive to flue gas flow rates, temperature, and particulate loadings. Most importantly, although overall ESP particulate collection efficiency can be high, >99%, particulate collection performance is significantly reduced for particles between 0.1 and 1.0 microns in diameter. Reduced collection efficiency for fine particulate is caused by particles of different diameters having different effective migration velocities, as well as by particle reentrainment resulting from system-cleaning characteristics. Therefore, conventional ESP technology is least effective at controlling fine particle emissions and is anticipated to be the focus of future regulations.

Although fabric filtration predates ESPs as a method for removing particulate from a gas stream, it has only been in the last 10 to 15 years that fabric filtration has been used to a significant degree for controlling particulate emissions from utility coal-fired systems. This relatively recent market penetration by fabric filtration was motivated by the development of durable fabrics and a requirement for improved particulate collection technology in industrial and utility applications.

The single most significant area of development has been in the choice of fabrics for specific applications. Early fabrics were limited to natural fibers having a low temperature limit (<200°F) and no corrosion resistance. However, the advent of manmade fibers in the past 50 years has resulted in the development of a wide range of fabric types for filtration applications in the industrial and utility markets. Fabric types are available commercially for a wider range of temperature (<1200 to 600°F) applications with significantly improved abrasion resistance for extended bag life. Fabric types are also available for use in environments prone to chemical attack by acids as well as alkali materials. Current fabric development efforts include high-temperature glass and ceramic fibers for use at temperatures approaching 1000°F and 2000°F, respectively, as well as new or coated fabrics with a higher degree of chemical resistance.

A fabric filter is generally considered more efficient than an ESP for particulate control. Where ESPs have been observed to control total mass emissions at levels of 99% to 99.9%, fabric filters have been observed to control total mass emissions at levels of >99.9%. However, conventional fabric filtration experience (reverse-gas and pulse-jets) has shown that the collection efficiency of fabric filters for fine particles (0.1 to 1.0 microns) is reduced. Therefore, conventional fabric filtration as currently applied will not be universally capable of controlling fine particulate emissions to levels consistent with the more restrictive particulate emission limits anticipated.

Options for improving fabric filter fine particle performance include design modifications, chemical conditioning, electrostatic enhancement, and particle agglomeration applied individually or in combination. Of the commercially available particulate control technologies, fabric filtration has the highest probability of meeting stricter particulate emission standards in general and fine particulate standards specifically. In some cases, fabric filters currently operating in the industrial and utility sectors are capable of meeting an emission limit of 0.003 lb/MM Btu. However, in order for fabric filter technology to play a significant role in meeting future particulate emissions standards, it will be necessary to demonstrate improved fine particle capture at a cost competitive with other technologies. A more detailed discussion of fabric filter performance enhancement options is presented below.

Commercially available technologies such as ESPs and fabric filters are not expected to be capable of universally meeting the solicitation particulate emission objective of 0.003 lb/MM Btu. However, efforts are ongoing throughout the industry to develop low-cost technology enhancement options aimed at improving the performance of ESPs and fabric filters in order to effectively control fine-particle (<5 micron) emissions. In addition, new technology options are also being developed that address integrated approaches to controlling emissions of particulate, sulfur dioxide, nitrogen species, and air toxics.

Fabric Filters – Although one of the oldest methods for removing solid particles from a gas stream, fabric filtration began to play a prominent role in particulate emissions control in the utility sector only in the early 1970s. Initially, fabric filters were thought to be the answer to the performance problems experienced by ESPs. For many applications, specifically low-sulfur coals generating high-resistivity ashes, fabric filters were found to be a good alternative to ESPs. Full-scale performance results demonstrated particulate control levels ranging from 98% to nearly 99.99%. Operating differential pressure ranged from 4 to 8 inches W.C. and typical bag life has increased to three years since early installations in the 1970's. Baghouse reliability has been excellent, with problems corrected during scheduled outages or in service, resulting in essentially no impact on boiler availability. Fabric filters were also observed to more efficiently collect fine particles than conventional ESP's. Specifically, the fractional efficiency for a fabric filter is 99% versus 95% for an ESP for particles ranging in size from 0.1 to 1.0 microns.

Fabric filters have their own set of disadvantages. These include large space requirements, the application of expensive specialized fabrics for potentially chemically active environments, dust explosion and fire hazards, reduced performance for fine particles (<2.5 microns), and susceptibility to performance limitations (particulate collection efficiency and differential pressure) for problematic ashes. As a result, fabric filtration research has focused on several fundamental areas. These include dust cake formation, fabric development, pressure drop control, and improving fine particle collection.

Pilot-scale tests sponsored by the Electric Power Research Institute (EPRI) have shown that pulse-jet baghouses have broad application to utility systems. A slip stream baghouse operating on a

older cycling boiler firing a low-sulfur coal demonstrated particulate collection efficiencies of 99.99%, with an operating differential pressure of 4 inches W.C. Measured outlet emissions were generally <0.002 lb/MM Btu. Results on a high-sulfur application also showed good particulate collection performance with emissions generally <0.01 lb/MM Btu. However, in this case, bag failures began to occur after 3000 hours of operation. Based on the data from these pilot-scale tests it appears that pulse-jet fabric filters can successfully control particulate emissions from utility boilers to meet current NSPS standards and, in some cases, may be able to meet the solicitation objective of 0.003 lb/MM Btu.

Options for improving fabric filter fine-particle performance include design modifications, electrostatically enhanced filtration, chemical conditioning, and particle agglomeration, applied individually or in combination. In a fabric filter, a significant proportion of the emissions result from emission spikes from cleaning cycles. Therefore, any design or operational modification that would reduce cleaning cycle frequency or the resulting emission spike would improve the fine-particle collection efficiency of fabric filters. Another design approach that would improve the fine-particle collection in a fabric filter is to increase the fabric collection area, effectively operating at low face velocities. However, the cost of a fabric filter is directly related to its size. Therefore, simply increasing the size of the fabric filter to improve performance is cost prohibitive and more cost-effective design options are necessary.

Development of electrostatically enhanced fabric filters has been ongoing for more than 20 years. Results indicate that for some design variations, both particulate emissions and differential pressure can be significantly reduced, cost effectively. However, high ash resistivity can be problematic and power consumption in some cases can be significant. Commercial implementation of electrostatically enhanced fabric filters has not occurred because of the perceived complexity of a combined fabric filter and high-voltage components and the absence of a need for a technology capable of meeting performance goals beyond those possible with conventional fabric filtration. However, the recent interest in fine-particle emissions (<2.5 microns), air toxics, and the anticipation of more restrictive particulate emission regulations may motivate commercial development of electrostatically enhanced fabric filters.

Flue gas conditioning, as applied to fabric filters, has seen continued development success since the early 1980s. Early work on a full-scale utility baghouse demonstrated that ammonia conditioning improved particulate collection efficiency from <98% to >99.9% on a total mass basis but no fractional efficiency data were reported. Early pilot-scale data showed that using a combination of SO_3 and ammonia can be effective in reducing fine particulate emissions as well as total emissions by several orders of magnitude. In addition, operating pressure drop was reduced by 30% to 75%. The basis for improved performance is an increase in the cohesive strength of the dust cake, which reduces particle penetration but simultaneously increases the porosity of the dust cake, minimizing differential pressure.

A recent pilot-scale study on pulse-jet baghouse applications has shown that flue gas conditioning with SO_3 and ammonia can increase particulate collection efficiency to levels ranging from 99.95% to 99.99% (86). This work was completed using a range of coals and filter face velocities (4 to 16 ft/min). The operating differential pressure was also reduced in each case. These results indicate the potential for meeting the 0.003lb/MMBtu objective using a pulse-jet fabric filter in combination with dual flue gas conditioning.

Bench- and laboratory-scale tests evaluating alternative conditioning agents have been completed, indicating a significant reduction in the level of particulate emissions comparable to those observed with SO_3 and ammonia. Further development work will attempt to confirm these results at the pilot and full scale in an effort to identify a cost-effective alternative to SO_3 and ammonia.

The performance of fabric filters could also be improved by the successful application of particle agglomeration techniques. As stated previously in reference to ESP applications, particle agglomeration is an attempt to create one large ash particle from several small ash particles. Although fabric filters are generally better collectors of fine particulate than ESPs, a reduction in the quantity of fine particulate as a result of particle agglomeration would also benefit fabric filter performance and increase the potential to meet the solicitation objective of 0.003 lb/MM Btu.

4.5.3 SO_2 Control

Present New Source Performance Standards (NSPS) for utility coal-fired boilers limit sulfur dioxide (SO_2) emissions to a maximum of 1.2 lb/MM Btu and require a minimum of 70% to 90% SO_2 control, depending on potential SO_2 emissions. This limit applies to facilities newly constructed or expanded after September 18, 1978. The 1990 Clean Air Act Amendments require 111 uncontrolled utility plants to reduce SO_2 emissions to 2.5lb/MMBtu in 1995, and all plants must meet a 1.2 lb/MM Btu emission limit by the year 2000. More importantly, in the year 2000, all existing and new utility plants will be restricted to a combined emissions cap of 8.9 million tons of SO_2 annually. As a result, new plants will have to obtain SO_2 allowances from the control or closing of older units. Therefore, recent regulatory activities have provided a significant level of motivation for the development of highly efficient, cost-effective technology options for meeting these standards.

The selected objective for Combustion 2000 HIPPS for SO_2 emissions is 0.06 lb/MM Btu. For a low-sulfur subbituminous coal (0.5% sulfur and 9000 Btu/lb), 95% SO_2 control would be adequate to meet the objective. However, for a moderate-sulfur bituminous coal (4% sulfur and 12,000 Btu/lb), >99% SO_2 control would be required. Therefore, this objective is consistent with recent regulatory activities which placed an annual cap of 8.9 million tons on SO_2 emissions beginning in the year 2000.

Technology options for meeting the 0.06 lb/MM Btu objective are rather limited. Options may include enhanced conventional wet scrubbers, developing SO_2 control technologies, and developing integrated technologies for simultaneous SO_2 and NO_x control. Wet scrubbers in commercial use were originally designed to meet the 90% NSPS SO_2 control requirement. However, this level of

performance will not meet the 0.06-lb/MM-Btu objective or the performance level required to meet long-term control needs established by the SO_2 emissions cap in the 1990 Clean Air Act Amendments.

Recent pilot-scale studies sponsored by EPRI have evaluated the use of organic acid additives to improve wet scrubber performance. Results indicate that the use of an organic acid additive along with a reduction in the liquid:gas ratio was an effective method of increasing the performance of an existing scrubber from 85% to 95% SO_2 control. Field tests, sponsored by DOE/PETC, have shown that the use of organic acid additives is capable of improving scrubber performance from 85%-90% to 95%-98% SO_2 removal. Incremental costs for the additional SO_2 removal were estimated to be $30 to $50/ton depending on the baseline performance of the scrubber system.

The DOE Clean Coal Demonstration program has a few projects addressing high-efficiency SO_2 control technology development. A project being carried out by Pure Air is demonstrating the performance of a single-module limestone scrubber producing a wallboard-grade gypsum by-product. Scrubber performance has been excellent, demonstrating an SO_2 removal rate in excess of 95% and an availability rate of 99.9%.

A second Clean Coal Demonstration project is evaluating the performance of a technology referred to as SNOX. This project, being carried out by ABB Environmental Systems, is a combined SO_2 and NO_x control technology. Nitrogen species are controlled using selective catalytic reduction and the SO_2 is oxidized to SO_3 and recovered as sulfuric acid in a condensing heat exchanger. System performance has demonstrated SO_2 and NO_x control exceeding 95%.

A third demonstration project is evaluating the performance of the Chiyoda Thoroughbred scrubbing process. Results indicate SO_2 removal up to 95% is possible while producing a gypsum by-product. An added benefit of the three projects is the production of a saleable by-product rather than a waste requiring disposal.

Throughout the world, there is an ongoing effort to develop and demonstrate high-efficiency, cost-effective SO_2 control technologies. Although all of these development or demonstration efforts have or anticipate demonstrating >90% SO_2 control. Only a few have as an objective an SO_2 control level of >95%. In addition, there are a number of development efforts focused on the simultaneous control of NO_x and SO_2. Again, in these development efforts, only a few projects anticipate achieving SO_2 control levels of >95%. Therefore, the technology options available or under development with the potential to meet the SO_2 emission objective of 0.06 lb/MM Btu appear to be rather limited.

Near-commercial options appear to be additive-enhanced wet limestone scrubbers, an ammonia scrubbing concept producing ammonium sulfate, and wet condensation concepts recovering sulfur as sulfuric acid. In order for a particular SO_2 control technology to play a significant role in meeting future emissions standards, it will be necessary to demonstrate 95% to 99% SO_2 capture at a cost competitive with other technologies and to minimize the production of wastes requiring disposal.

The Combustion 2000 HIPPS unit must meet more stringent emission standards for NO_x, SO_2 and particulate matter than conventional coal-fired power plants at a lower overall cost. In order to satisfy both cost and emission targets, the HIPPS plant will take advantage of advanced processes for emission control that are now under development under the sponsorship of the DoE and other agencies. In particular, technologies under development in the Low Emission Boiler System (LEBS) program may be applied to the HIPPS program.

Integrated emission control processes (i.e., those that remove more than one pollutant) are desirable for the HIPPS plant because of the potential for lower capital cost than single-pollutant processes. Table 4.5-2 shows that most of the control options under development in the LEBS program are designed to remove multiple pollutants. The application of these technologies to the HIPPS plant is briefly discussed below.

TABLE 4.5-2 NOX/SOX/PARTICULATE CONTROL OPTIONS FROM THE LEBS PROGRAM

Process	NO_x	SO_x	PM	Description
Hot-SNOX™	X	X	X	— Catalytic removal of SO_2 — Catalytic baghouse for NO_x, particulate — H_2SO_4 product
Limestone Injection Dry Scrubbing (LIDS)		X	X	— Limestone injected 2200°F — Spray dryer for SO_2/SO_3 — FGD byproduct landfilled — Baghouse or ESP
SOXAL™		X		— Sodium-based regenerable process for SO_2/SO_3 removal — Elemental sulfur product
Moving Bed Copper Oxide-Copper Sulfate System	X	X	X	— Moving bed ($CuO-Al_2O_3$) for SO_2 removal — $CuSO_4$ catalyst for NO_x removal — H_2SO_4 or elemental sulfur product

The Hot-SNOX™ process uses the previously-developed SNOX™ process with an integrated particulate collection system and NO_x reduction catalyst. The process also uses a catalytic reactor to oxidize SO_2 to SO_3, thereby producing commercial-grade sulfuric acid as a byproduct. In the Hot-SNOX™ process, a small amount of ammonia is added to the flue gas for NO_x conversion prior to entering the integrated particulate collection system and NO_x SCR (PCS/SCR). The flue gas enters the PCS/SCR at approximately 700°F. Removal efficiencies are 99.5% and 80% for particulate matter and NO_x, respectively.

Currently, two different PCS/SCR systems are being considered: EERC's Catalytic Baghouse and Ceramem's Catalytic Ceramic Gas Filter. Following the PCS/SCR, the flue gas enters a catalytic reactor where 96-98% of the SO_2 is oxidized to SO_3. Excess NH_3, CO, and carbonaceous material are

also completely oxidized. After oxidation, the SO_3 gas is cooled in the air heater (of a conventional power plant) and then cooled further in a falling film condenser. In this last piece of equipment the SO_3 is completely converted to H_2SO_4 vapor and then separated from the gas as it condenses in the falling film. The sulfuric acid solution is a salable byproduct. Integration of this process with the HIPPS plant would require a low temperature heat exchanger since there is no air heater in the HIPPS system.

The Moving Bed Copper Oxide-Copper Sulfate process is being considered for LEBS as well (90). In this process, the flue gas (at approximately 750°F) enters the absorber, a moving bed reactor containing a sorbent (copper oxide supported on alumina) for desulfurization. The sorbent is regenerated in a separate reactor. The concentrated SO_2 stream resulting from regeneration may be oxidized to SO_3 and condensed to H_2SO_4 or converted to elemental sulfur in a Claus plant. The primary function of the moving bed absorber is to remove SO_2 from the gas. However, the absorber removes a substantial amount of particulate matter which should allow the final particulate control device to be more compact. More importantly, the copper oxide/copper sulfate bed acts as a selective catalyst for NO_x reduction with the addition of ammonia.

Limestone Injection Dry Scrubbing, or LIDS, is a process in which a limestone-based sorbent is injected into the flue gas at high temperatures (circa 2200°F). The limestone is calcined and decomposes into to lime and carbon dioxide gas. The calcined lime reacts with some of the SO_2 and all of the SO_3 in the flue gas. The reacted sorbent, the flyash, and the gas exit the boiler to a spray dryer vessel. The flue gas enters the top of the spray dryer where it contacts an atomized slurry of recycled solids collected from the spray dryer and the particulate collection device. The flue gas is humidified to a low approach-to-saturation temperature; the majority of the SO_2 captured by the LIDS process is captured by this means. Some of the solids are collected in the spray dryer and conveyed to the recycle system. The majority of the solids are conveyed to a baghouse for collection followed by disposal and/or recycle. The solids collected for disposal are transported to a landfill.

Finally, the SOXAL™ regenerative sodium-based wet scrubbing process is being considered for FGD in the LEBS program. The SO_2 in the flue gas is absorbed by a regenerated sodium sulfite solution. The process employs a single reaction vessel for SO_2 absorption to sodium bisulfate. The sodium bisulfite is regenerated to sodium sulfite and a concentrated SO_2 gas stream using bipolar membrane technology. The sodium sulfite is recirculated back to the absorber and the concentrated SO_2 gas is processed to a molten sulfur byproduct.

Other ongoing advanced emissions control development projects supported by DOE/PETC may have application to the high-temperature slagging furnace system. Although most of these projects focus on simultaneous NO_x and SO_x control, a few focus more specifically on fine particulate control. Flue gas conditioning projects have been previously discussed. However, there is one project focused on the development of a compact ceramic filter element that may be effective in both cold- and

258

hot-side particulate control applications. Further development and testing of the filter is necessary to verify performance with respect to filter cleanability and the control of differential pressure.

4.5.5 Air Toxics Control

Of the 189 substances identified as hazardous air pollutants by the Clean Air Act Amendments (CAAA, Title III), 37 are of particular concern for utility operators. These 37 species, including 11 metals, have been measured by EPRI in the flue gases of pulverized coal-fired utility boilers. Although utilities are currently exempt from CAAA mandated emissions limits, future regulations may require utilities to carefully monitor and control emissions of these hazardous air pollutants.

A significant level of effort is underway to validate existing and recently developed sampling and analytic techniques for speciation and quantifying organic and inorganic emissions. For existing systems, the emphasis has been on the completion of field studies to determine the type and quantity of hazardous air pollutants (HAPS) being emitted and the level of HAPS control that can be expected from the various emission control technologies currently in commercial use. Results from these field studies, being carried out in the U.S. by DOE and EPRI, are currently being reviewed and are expected to be the basis for the determination of need and possible promulgation of HAPS emissions standards by the U.S. Environmental Protection Agency. Clean Coal Technology demonstration projects have collected or will collect HAPS emissions data. However, very little data have been reported. Clean coal demonstration projects in the early stages of design and construction are expected to add HAPS emission measurements to their demonstration activities. For developing technologies it will be important to characterize HAPS emissions at each stage of technology development in order to adequately determine the potential for HAPS emissions and the technology options available or requiring development to effectively control emissions.

Most of the metals listed in Title III and found in effluent streams of coal-fired power plants occur as trace elements in coal. Results from the DOE\PETC field test efforts are still undergoing review and have not been published in their entirety. However, several papers have been published on selected topics as have results from the EPRI field tests. Typical metals concentrations in coal range from approximately 0.2-200 ppm. Many of these metals are relatively non-volatile and are captured with the bottom and fly ash. Other metals, including arsenic, selenium, mercury, lead, and cadmium, are either volatile or semi-volatile under conventional combustion conditions.

The highly volatile metals including Hg and, to a lesser extent, Se may escape all particulate control devices and pass through the stack as vapors. The less volatile toxic metals, including As, Cd, Pb, Sb, Zn, may nucleate or heterogeneously condense in the cooler regions of the unit and add to the submicron ash loading. Particles formed by this method are typically in the size range most likely to escape capture in particle control devices. Emissions data show that nonvolatile inorganic HAPS are effectively controlled by conventional technology (ESPs, fabric filters, spray dryers, and wet scrubbers) if overall fine particulate control is adequate. However, volatile species such as mercury are not consistently controlled at high levels using conventional technology.

Sampling and analysis for organic emissions show that organic species and concentrations can be highly variable from system to system but are generally observed at low concentrations. In most cases, investigators concluded that further development and validation of sampling and analytical procedures were necessary.

A recent study on the behavior of trace metals in coal combustion systems has identified an optimum control strategy for the capture of toxic metals from coal fired boilers based on currently available technology. This strategy employs an ESP followed by a spray dry scrubber and a baghouse. This system has been shown to achieve 99% capture of most metals. Mercury was the only major exception with capture efficiencies ranging from 35-85%. Other options for Hg control include lower flue gas temperatures in the scrubber and baghouse, and the injection of activated carbon based sorbents.

Bench- and pilot-scale results show that activated carbon can be used to remove elemental mercury from a flue gas stream. Sulfur and iodine-impregnated activated carbon are more efficient mercury sorbents than an untreated activated carbon. Mercury removal is temperature-dependent, with mercury removal increasing as flue gas temperature decreases. High mercury removal (>90%) has been demonstrated at 200°F using small amounts of activated carbon injected upstream of a fabric filter. At higher temperatures (300° to 400°F) an iodine-impregnated activated carbon effectively controlled elemental mercury emissions for both a subbituminous and bituminous coal in a pilot-scale system.

In general, it is safe to conclude that a lot remains to be learned concerning HAPS emissions from coal-fired systems and the technology options that may be needed for their control. For the high-temperature slagging furnace system, it is likely that trace element partitioning will be different from that observed for conventional pc- and cyclone-fired furnace systems. The furnace configuration and higher temperatures of the advanced slagging system may increase the concentration of volatile trace elements in the vapor phase. Also, initial concentrations of semi-volatile species in the vapor phase may increase, resulting in an increased enrichment for certain elements in the fine particulate. Since the size distribution of the entrained fly ash is expected to be somewhat smaller for the high-temperature advanced slagging system, effective control of HAPS will depend to a significant degree on the control of fine-particle emissions as well as vapor-phase constituents.

4.5.6 Fine Particle Formation in HITAF

Reduction of emissions of particulate matter to 0.003 lb/MBtu will require high efficiency particulate removal equipment. The most difficult particles to control, i.e., those with the lowest collection efficiencies, are in the range of 0.1 to 0.5 microns in diameter. These submicron particles are formed via a vaporization-condensation mechanism in the flame. Because of the high radiative heat transfer rates needed in the HITAF, the conditions in the flame should promote the vaporization of ash and the growth of the vaporized ash into the 0.1 to 0.5 mm range. Previous measurements, both from laboratory combustion systems and utility power plants, confirm that the temperatures in the

flame strongly influence the size and amount of ash in this submicron mode. Conditions associated with higher temperatures produce larger ash particles and higher rates of vaporization.

Since it is likely that particulate control for a full-scale, high-temperature advanced slagging furnace will make use of an enhanced ESP or fabric filter system, it will be important to thoroughly characterize the particulate component of the flue gas stream in order to evaluate emission control options and the potential to successfully meet the 0.003 lb/MM Btu emission objective. This information will be necessary for each of the fuel types evaluated in the system. No matter what the control device happens to be, it will be important to know the probable ranges of total mass loading, particle-size distribution (0.01 to 100 micron particles are likely), bulk chemical composition, and physical characteristics, including ash morphology and cohesive properties. For an ESP-based control system, flue gas composition and bulk ash resistivity data will also be necessary.

Detailed characterization of the entrained particulate is important in order to understand key penetration mechanisms that may influence the performance of an ESP or fabric filter. Both control devices are known to be susceptible to decreases in fractional collection efficiency for particles in the 0.1 to 1.0 micron range. For both ESPs and fabric filters, penetration mechanisms are fairly well understood. For a given ESP design, direct penetration will be a function of mass loading, particle-size distribution, and ash resistivity. For a given fabric filter design, direct penetration will be a function of the ash cohesive properties in combination with mass loading and particle-size distribution.

Therefore, in order to determine appropriate technology options for controlling particulate emissions from the high-temperature advanced slagging furnace system it will be necessary to characterize particulate emissions (mass loading, size distribution, chemical composition, cohesive properties, and resistivity) from the pilot-scale furnace. For both ESPs and fabric filters, penetration as a result of reentrainment will depend largely on ash cohesive properties. For ESPs, ash cohesive properties will affect reentrainment as a result of rapping cycles. For fabric filters, ash cohesive properties will affect dust cake characteristics with respect to bleed-through and differential pressure. Particle reentrainment in a fabric filter caused by bleed-through is usually not a significant contributing factor and is as much dependent on fabric characteristics as ash characteristics. Particle reentrainment resulting from fabric cleaning is a direct function of ash cohesive properties resulting from its effect on individual particle reentrainment and dust cake properties affecting pressure drop and cleaning frequency.

Hazardous air pollutants in the flue gas stream will also require thorough characterization. The emphasis in this case will be on inorganic trace elements, most of which are expected to be found in the fine particulate. However, vapor-phase species, such as mercury, and their concentrations will also be important. Although organic hazardous air pollutants are also of concern with respect to coal-fired systems, organic species and their concentrations are highly dependent on system design and operation.

261

4.6 HITAF SENSORS AND CONTROLS

4.6.1 Introduction

HIPPS is more complex than a conventional pulverized coal power plant or even a gas turbine-combined cycle due to the coupling of a "slow" (i.e., high thermal inertia) combustor with "fast" gas and steam turbines. The way in which we control HITAF must be determined in the very beginning of the design process because the control philosophy determines what equipment will be needed in the commercial plant and what the performance criteria will be for subsystems. Both affect the capital and operating costs for the commercial plant as well as the Phase III system. The combustor control philosophy is shaped by the need to accommodate following factors:

- Rapid load changes (startup, shutdown, equipment failure)
- Load following
- Heat flux distribution in radiant zone
- Integration of NO_x control subsystems

Procedures and equipment for starting up or shutting down (in either planned or unplanned mode) must be identified. The most critical needs fall in the area of emergency shutdown resulting from a failure in some component or subsystem. A failure of the gas turbine will result in rapid loss of vitiated combustion air to the furnace and of cooling air in the air heater. The air flow must be maintained at some level using a back up compressor or fan until the combustor can be cooled down. The combustor will have a maximum rate of temperature change, determined by the behavior of the refractory, the air heater, joints and seals, etc. On the other hand, in the event of a HITAF failure, provision must be made to continue running the gas turbine by increasing the output of the duct burner. As discussed above, a dynamic simulator will provide guidance in designing start-up and shut-down procedures, in predicting the ability of the system to change load, and in identifying system response to component or subsystem failure.

Load changes down to 50% must be accommodated in the HIPPS. There are several options for dropping load as far as operation of the HITAF is concerned. First, the turbine inlet temperature can be changed while keeping the air flow relatively constant. The natural gas supply to the duct burner is reduced, but the coal and air flow to the HITAF remains relatively constant. Although the overall efficiency decreases, the least expensive fuel, coal, is being used. Second, the turbine air flow can be reduced while keeping turbine exhaust temperature constant. As a consequence, the coal and air flow to the HITAF are changed as is the natural gas flow to the duct burner. At this point, there is not enough information to determine how far the load in the HITAF can be reduced. The minimum load may be determined by flame stability and/or by slag freezing on the radiant air heater.

In a multiple burner furnace, the radiant heat flux will not be constant over the entire high temperature heat transfer surface which may cause hot or cold spots. The former could result in loss of refractory and structural failure and the latter may cause build up of frozen slag with the related

262

problems for heat transfer and structural integrity. The new materials under development for the radiant air heater subsystem will have limitations on temperature. In turn, these considerations will affect the control required for individual burners in the firing system and may affect the choice of sensors for the high temperature furnace environment.

To meet the NO_x emissions level of 0.06 lb/MBtu, a multi-step approach must be taken, both to minimize the cost and to lower the technical risk. The total NO_x reduction strategy must include a low-NO_x firing system in combination with one or more of the following subsystems: air staging, reburning, SNCR and SCR. Performance and cost analysis will determine which subsystems are included. Each of these technologies has its own control requirements and limitations, each of them must be maintained at optimum conditions. For example, optimum stoichiometry on a burner-per-burner basis must be maintained for the firing system to achieve the lowest level of NO_x without increase in unburned carbon. Vertical temperature profile should be monitored for the air staging and reburning systems, optimum temperature windows must be maintained for the SNCR or SCR system.

The HIPPS project presents a formidable challenge for a process control engineer. It combines problems of system design for a very dynamically complex system containing many non-linear interconnections, limitations and restrictions, with selection of specialized instrumentation. Our review of the I&C issues includes the following sections:

1. Control system organization - major control subsystems (Functional Groups).

2. Dynamic simulation.

3. HITAF control.

    a. HITAF control philosophy.

    b. Sensor/instrument selection and development.

4. Additional information required in Phase II.

4.6.2 HIPPS Control System Organization – Major Control Subsystems (Functional Groups)

The HIPPS plant will be equipped with a state-of-the-art control and instrumentation system designed in accordance with the existing engineering practice with the scope sufficient to ensure the required level of plant availability and reliability, as per the plant design philosophy defined in the Quarterly Technical Report for July 1 through September 31, 1994.

The overall process control and monitoring functions will be performed in a central control room (CCR) utilizing a distributed control system (DCS) along with several dedicated control subsystems.

Conceptual design of the I&C system (system architecture) is illustrated in Figure 4.6-1. From the control point of view, the overall plant equipment will be divided into several functional groups (FG), some of them equipped with their own dedicated vendor-supplied controls, others will be controlled directly by DCS from the CCR. Control systems of individual FG's will provide control

263

interface and necessary inputs to DCS for centralized data acquisition, monitoring and reporting. The hardware and software basis of these individual systems should be uniform and compatible with the central DCS.

Table 4.6-1. lists major equipment components and systems (FG's) and indicate those which are normally supplied with their dedicated specialized control systems.

TABLE 4.6-1 MAJOR EQUIPMENT COMPONENTS

Acct No.	Functional Group	Qty	Dedicated Controls	Remarks
2.1	HITAF Combustor with radiant and convective air heaters	2	no	
5.1	In-duct gas-fired burner	1	yes	
2.3	HRSG #1 (clean)	1	"	
2.3	HRSG #2	2	"	
6.0	Gas Turbine Generator	1	"	
7.0	Steam Turbine Generator	1	"	
10.1	Coal receiving, storage & handling	1	"	
1.1	Coal prep and feed system, including 4 coal pulverizers	2	"	
12.2	Natural Gas supply system	1	"	
10.2	Limestone receiving, storage & handling	1	"	
1.2	Limestone prep and feed system	1	"	
10.3	Wet Ash handling and disposal	2	"	
8.3	SNCR (part of HITAF)	2	no	
2.3	SCR (part of HRSG # 2)	2	no	
2.1	Flue Gas Recirculation System (part of HITAF)	2	no	
8.1	Particulates Removal	2	yes	
2.5	ID Fans	2	no	
8.2	Flue Gas Desulph. System (FGD)	2	yes	
7.0	Feedwater System	2	no	
11.2	Raw Water Supply and Treatment	1	yes	
11.1	Circ. Water System	1	no	
12.1	Compressed Air System	1	yes	
12.1	Instrument Air System	1	yes	
8.0	CEM	1	yes	
2.1	Quench Air Blower	2	no	
12.7	Balance of Plant (Misc.) systems			
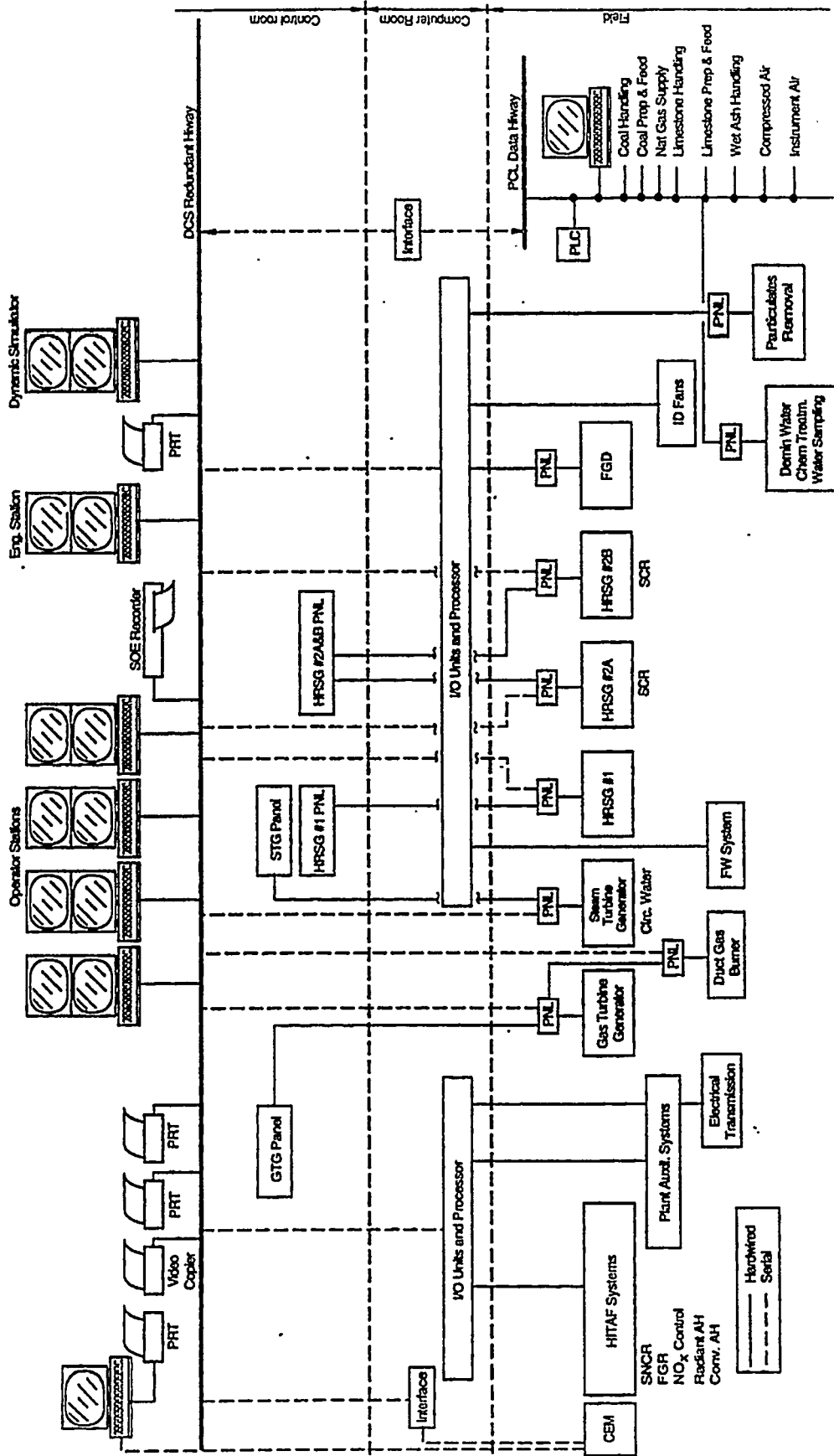
Figure 4.6-1 Control System Architecture.

The I&C design for the HiPPS plant will be conducted by the architect-engineer (A-E) in accordance with the existing engineering practice and industry standards. Along with the normal design procedures, which include the selection of DCS and instrumentation, one of the important tasks for the A-E will be the coordination of all dedicated I&C subsystems and their integration into the overall control system.

DCS Capabilities and Controls

The DCS will include dynamic controllers and color graphic displays. Operator selection and re-configuration of graphics will be performed via keyboards and CRT's.

The DCS will provide soft auto-manual stations for remote control of the various field devices and control loops. This control will be accomplished via the operator's CRT console. The soft CRT stations will be used for analog control loops. The open loop control functions, such as motor control and discrete monitoring, will be accomplished in the DCS using key selection and dynamic displays on the operator console. The configuration of function codes and control strategies will reside in the non-volatile memory and will be maintained in the event of a power failure.

The control schemes will be hardware and software configured with consideration for redundancy, as applicable. In the event of any single power supply failure, processor/controller or highway/communication link/data multiplexers, it will alert the operator while continuing to keep the process under uninterrupted automatic control from the CRT. If the primary control processor should fail, a secondary processor (operating in the "hot stand-by" mode) will assume control responsibility with bumpless transfer. In the event of a failure of both processors, the system will be configured such that each analog and digital output will go to a predetermined fail-safe position.

Communication to the individual dedicated PLC-based control systems will be accomplished via standard termination ports. A Performance Assessment program will be configured in the DCS. This software application will gather information for each system and will provide real-time displays to the operator.

Power supplies will be redundant, such that failure of a power supply will cause a back-up power supply to assume responsibility. The operator interface will provide a user-friendly environment for control and data acquisition functions. This interface will provide access to plant-wide operations allowing the operator to monitor and take corrective actions as required. The displays will provide dynamic information by updating information and status displayed to the operator.

An engineering workstation will allow personnel to configure the operator consoles and control hardware. The software package will enable the engineer to design, configure, monitor, trend, tune, modify and document process activities. Graphic symbols and function codes will be used to build the process logic control drawings on the CRT screen. The engineering workstation will be used during start-up and debugging stage of commissioning. It will also be used as a tool to maintain, troubleshoot, operate and reconfigure the system if required once the plant is operating.

By the time the A-E starts their design, all main control issues for individual FG's must be resolved. These control issues are primarily associated with the diagnostics and control of the HITAF process and include the following.

1. Plant operating procedures: description of all operational sequences for start-up, load shedding, load following within 50 to 100% MCR, normal shutdown, emergency run-down and shutdown;

2. Equipment failure modes, i.e., sequences of operation in case of a major component loss, such as HITAF, GTG, STG, HRSG, etc.;

3. Conceptual design of the main HITAF control systems:

   - Combustion and NO_x Control;
   - Radiant Heat Flux Management (Radiant Heat Transfer and Turbine
   - Air Temperature Control);
   - Ash Management

4. Dynamic Simulation System.

5. New sensors and instruments: development/selection/testing.

4.6.3 Dynamic Simulation

The Quarterly Technical Report for July 1 through September 31, 1994 indicates that "Dynamic modeling ... will be necessary to establish transient times and identify the key control parameters". At this point, we believe and emphasize that the dynamic simulation, started early, may be of particular importance and may play a key role to assure the success of the HIPPS project.

Use of dynamic modeling for this particular project offers a unique opportunity for solving difficult technical problems and for the overall project cost reduction.

In many publications and discussions related to dynamic simulation, an ideal case is often mentioned which allows realization of the maximum positive benefits from the use of dynamic simulation. This case occurs when dynamic modeling is started from the very beginning of the system design, before any serious design errors are made. In this ideal case, we start with an initial, relatively simple, dynamic model, limited by the available technical data. This initial model will gradually expand and grow in complexity, as the additional data become available. This model will be continuously utilized for replaying and testing of different design versions and options of various instruments, systems, design modifications, etc. In addition, this dynamic model will also be used as a static model to calculate and analyze technical characteristics of system components at steady-state conditions.

In the real-life situations, we almost never have a chance to utilize this ideal case because of various restrictions and limitations. Dynamic modeling is usually applied at later stages of the

equipment design, when the equipment is already purchased, built or commissioned. In the HiPPS case, we have that fortunate situation when we actually have a chance to fully utilize all advantages of dynamic simulation by maximizing design efficiency and minimizing technical risks and design time. In our opinion, **the HIPPS project offers us a unique opportunity to realize the great benefits of dynamic simulation, if we apply it early in the design stage.** One important reason why the simulation system should be selected and applied early in the process is that this system can actually be used as a design tool, starting with the development of process flow diagrams (PFD's).

The first important step will be the selection of the dynamic simulation system itself. This selection must be done at the earliest stage of the project. The main technical requirements to the selected dynamic simulation system (in addition to the commercial considerations) must be the following:

    a.   demonstrated ability to solve difficult non-linear control problems for the power plant systems;

    b.   ability to simulate both steady-state and transient conditions in real and compressed time scale;

    c.   flexibility (ease of modifications, additions, deletions);

    d.   portability (use of common computer software and hardware);

    e.   user-friendliness: the system should not require specific programming skills, both process design engineer and control engineer should be able to build and operate the modeling system.

In our opinion, the required simulation system should be developed as a design engineering tool emulating process equipment and controls. This system must be compatible with dynamic models of individual equipment, such as GTG, STG, HRSG, FGD, etc., which are to be developed and supplied by the equipment vendors. It also should interface with the CAD system used by the A-E.

PSI proposed to use ARUBA dynamic simulation system which meets all these criteria and offers the best technical and the most economical solution for the HIPPS process. However, in order to achieve an objective selection, we recommend, in the beginning of Phase II, to undertake a comparative study (with participation of the team members), which will invite presentations from several potential suppliers, conduct thorough analysis of their proposals and recommend the final selection.

The right decision at an early stage may hold the keys to the success of this project by avoiding dangerous and expensive design errors and problems with the demonstration HIPPS unit. The proposed dynamic model will be continuously updated, corrected and completed in the course of the design and commissioning process. In the future, it may be used for personnel training and for solving different operational problems.

4.6.4 HITAF Control

Combustion and NO_x Control

To meet the NO_x emissions level of 0.06 lb/MBtu (for 65% coal, this is 0.09 lb/MBtu for coal, assuming negligible NO_x emissions from natural gas), a multi-step approach must be taken, both to minimize the cost and to lower the technical risk. The total NO_x reduction strategy must include a low-NO_x firing system in combination with coal reburning, FGR, SNCR and SCR. Each of these technologies has its own control requirements and limitations and must be maintained at optimum conditions. For example, optimum stoichiometry on a burner-per-burner basis must be maintained for the firing system to achieve the lowest level of NO_x without increase in unburned carbon. Vertical temperature profile should be monitored for the air staging and reburning systems, optimum temperature conditions (temperature windows) must be maintained for the SNCR or SCR system.

The overall organization of the HIPPS control system will be quite different from that of a conventional fossil power unit. The HIPPS system includes several parallel and interconnected power trains: the GTG train, two HITAF trains and the STG train. The GTG train includes the duct burner, GTG and the clean HRSG #1. Each HITAF train starts with the pulverizer and includes the HITAF, HRSG #2, baghouse, ID Fan and FGD. The STG train includes all HRSG's and the steam turbine. The whole process in each train must be considered as one continuous technological process: operation of each train component affects other components. Therefore, any disturbances, limitations or restrictions in any individual train component must be translated into corrective actions feedforwarded to other components. For example, a trip of one of the circulating pumps in the FGD system leading to a reduced FGD capacity, should initiate a feedforward action to reduce the overall train load, followed by the increase of the GTG (or another train) load. Therefore, in addition to a usual Unit Load Controller, the system should include a Train Load Supervisory Controller which coordinates the operation and distributes the load between all trains.

The overall Unit Load Demand (ULD) system receives its set-point, the initial ULD signal, from the operator, and generates individual load demands for each major system component, i.e., for each HITAF, gas turbine, steam turbine and for each HRSG, via Load Distribution Controller and Train Load Supervisors. This system compares the ULD with the actual loads, limitations, restrictions, alarms, overriding commands, etc. for each component. Depending on the actual loading, availability and limitations of each piece of equipment, the load demands may be redistributed even during normal steady-state base-load operation.

The HITAF combustion control system includes several control subsystems: coal combustion, natural gas (warm-up and support fuel) combustion, NO_x control, control of individual burners, reburners control, flue gas recirculation control. All these systems are interdependent: any changes or disturbances in one of them affect operation of other systems and the overall HITAF performance. To achieve the target NO_x emissions, operation of all subsystems must be well coordinated. A conceptual presentation of the Unit Load Controllers and HITAF combustion controls is shown in Figure 4.6-2.

269
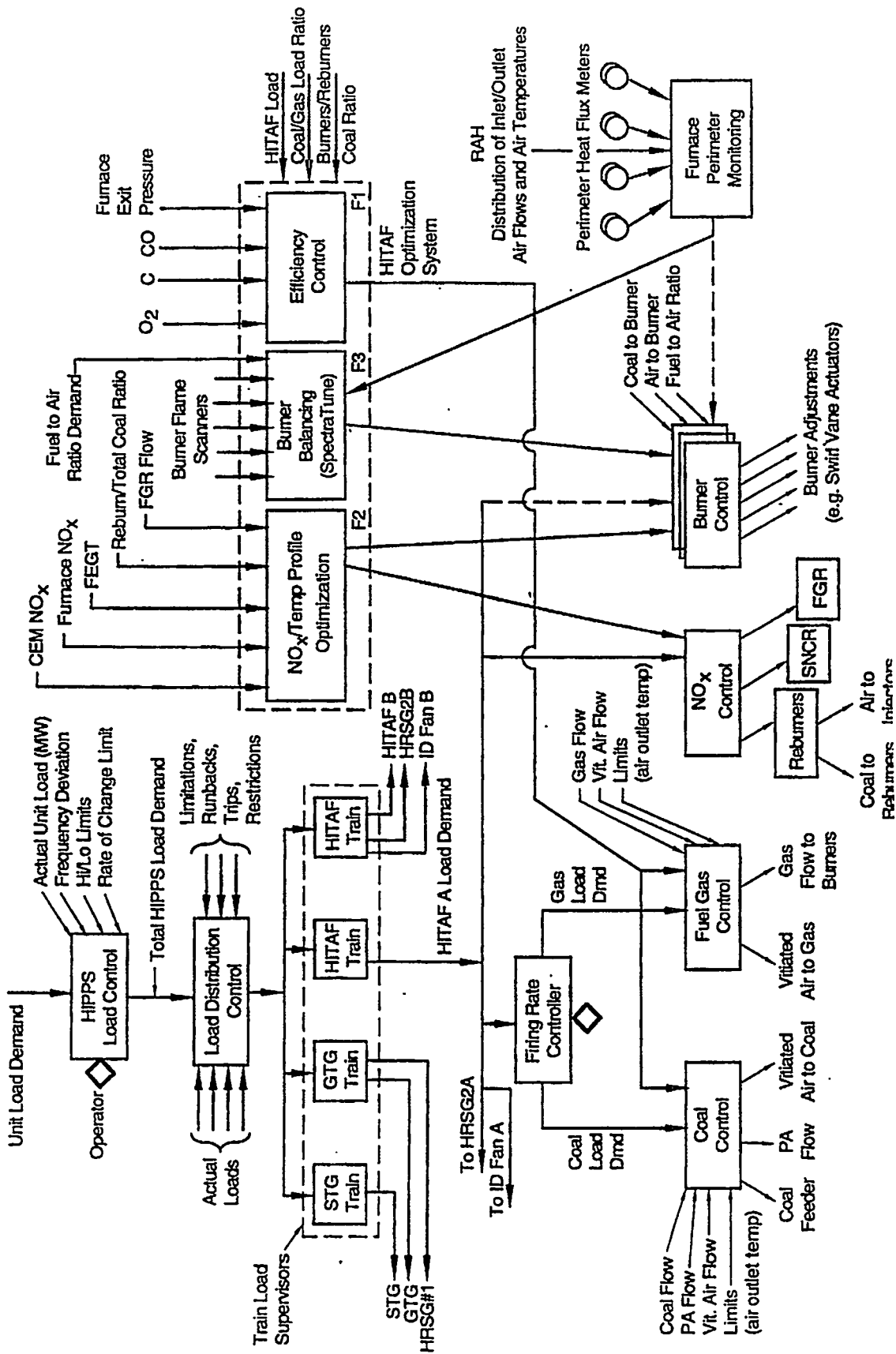
Figure 4.6-2 HITAF Control System Organization.

270

HITAF load demand signal governs two major combustion subsystems: coal and gas controls. The load demand for each subsystem is generated by the Firing Rate Controller (FRC) which forms the gas and coal load requirements depending on the load demand and the operator's input. Various factors will affect the desired coal/gas load distribution (furnace temperatures, slagging conditions, etc.). Many of them can be taken into account in the FRC program, but the main responsibility in distributing load between coal and gas will reside with the operator, particularly during the first stage of unit operation. Each subsystems will include two main portions: analog system and digital logic.

The natural gas controller will maintain the total gas and air flows to the burners in accordance with the gas load demand and current limitations and restrictions (mainly, radiant air heater air outlet temperature, gas pressure limits and burners availability). It will modulate both gas and air control dampers to maintain the required heat release from fuel gas, also taking into account a corrective signal from the efficiency control subsystem F1. The latter signal is formed as a cumulative corrective function reflecting deviations of average values of furnace outlet pressure, O_2, and combustibles from their set points.

The coal controller will maintain the total coal, primary and secondary air flows to the burners in accordance with the coal load demand and current limitations and restrictions, such as those associated with the radiant air heater air outlet temperature, with the pulverizer and coal feeder operation (e.g., mill outlet temperature) and burners availability. The coal controller will modulate pulverizer load and air control dampers to maintain the required heat release from coal burners, also taking into account a corrective signal from the efficiency control subsystem F1.

The ID Fan loading will maintain the air-flue gas balance by maintaining the constant (slightly negative) pressure at the combustor exit downstream of the slag screen. Since the ID Fans are located far downstream the combustor, after the HRSG and baghouse, they can be considered and controlled as a separate functional group coordinated with the HITAF operation via the Train Supervisor.

The **NO_x control subsystem** will combine a central logic F2 with several analog control loops. It will coordinate operation of coal reburners, SNCR and FGR systems, all designed with the main purpose of NO_x reduction. The SCR system will be coordinated via Train Supervisor.

We anticipate that NO_x Controller will set the initial capacities of each subsystem, as a preprogrammed function of the HITAF load. In addition, each subsystem will be modulated by the NO_x Optimization subsystem F2 to reflect the actual measured NO_x values, taking into account many limiting factors, such as furnace gas temperature, Reburn Coal to Total Coal ratio, FGR flow (or allowable ratio). Digital logic associated with NO_x control will initiate proper startup and shutdown sequences associated with the operation of reburners, SNCR and FGR. The system will incrementally and sequentially modulate controllable factors affecting NO_x formation in search of the best compromise between the lowest values of NO_x and unburned carbon at the combustor exit. These controllable factors may include air flow staging and distribution, reburn fuel flow, flue gas recirculation to the radiant zone. We envision this system implemented as an expert system operating

when the combustor is in the steady state mode. Depending on the research and design data and combustor operating conditions (FEGT and ash deposit values), the system will select the controllable parameters and determine the sequence, directions and rates of changes for their adjustments.

The initial NO_x reduction will be achieved by the application of Low-NO_x Burners. The next stage of NO_x reduction will be achieved in the furnace by reburning and then by FGR. Further NO_x reduction to the target level will be achieved in the post-combustion systems (SNCR and SCR). Each of these systems will be equipped with its own control. The optimum thermal conditions for their operation (temperature windows) will be maintained by modulating the quenching air and FGR flow to the dilution zone.

We anticipate that **control of individual burners** may play an important role in achieving the target performance parameters. Ideally, this system should balance the measured coal and air flows to each burner, and then to trim other available burner adjustments, such as swirl vanes, to achieve the optimum mixing rate for each burner. Based on recent tests of our new SpectraTune burner flame monitoring system conducted at full-scope power plants and at several single-burner combustion test facilities, we envision this system as autonomous and relatively slow, operating only when the base system is in operation and the unit is in the steady state mode. The base burner control system will set and maintain equal fuel and air flows to individual operating burners in accordance with the HITAF load demand. The burner balancing (SpectraTune) system F3 will receive and analyze signals from individual burner flame scanners, and will generate flame quality values Q_i for each burner. If, in the course of burner operation, the system detects significant imbalances among the Q-values of individual burners, it will adjust the appropriate burner(s), as illustrated in Figure4.6-3. We expect the burner manufacturer to indicate which burner adjustment(s) is the most suitable for burner balancing and to equip the burners with the appropriate actuators. Our experience with coal-fired LNB's has indicated that such adjustment could be the burner secondary air flow (controlled by a secondary air shroud) or the secondary air swirl (controlled by a swirl vane).

This system will also advice the operator in case of a serious burner problems (detection of out-of-tune burners). We anticipate that the SpectraTune system will be incorporated into the burner management system and will be further developed to continuously generate an optimum burner optimization algorithm, and also to include an expert subsystem generating advice to operator. We expect that a similar system may be used to control and balance the reburners. The operator will be able to intervene by changing the criteria of burner balancing and adjustment.

Radiant Heat Flux Management – Radiant Heat Transfer & Turbine Air Temperature Control

Sufficient heat transfer to the turbine air in the radiant and convective air heaters is one of the critical requirements to achieve high process efficiency in the HITAF. Maintaining even and balanced radiant heat flux distribution is critical in order to avoid overheating of the radiant panels. The axial and circumferential variations in radiant heat flux must be kept within a certain tolerance. A system of **perimeter monitoring** will be developed to ensure protection of the radiant panels. This system will be

272
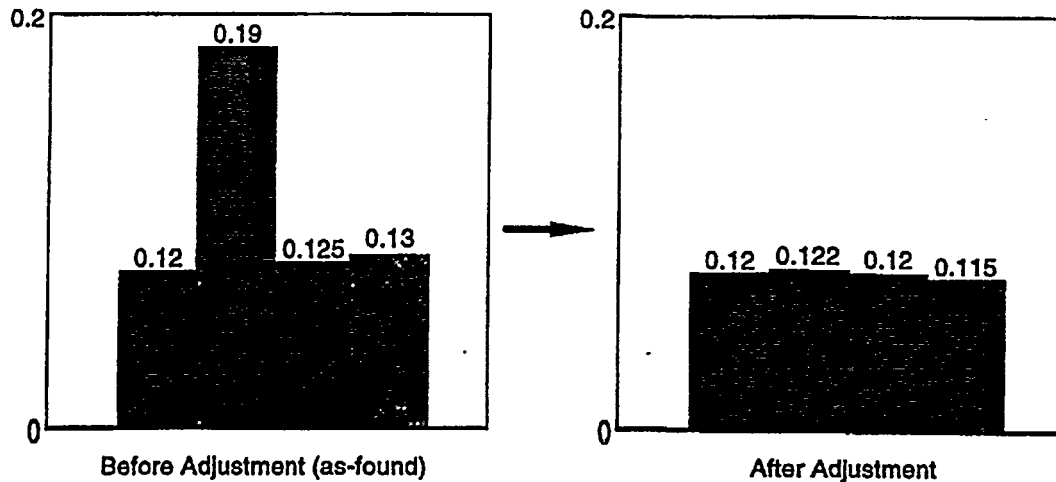
Figure 4.6-3   Illustration of Burner Adjustment (Burners C-row, Chalk Point
Plant, PEPCO).

based on monitoring of either radiant heat flux sensors in the HITAF walls, or on measuring circumferential distribution of air outlet temperatures in the radiant air heater and air flows to its individual sections. This system, in essence, will constitute an autonomous radiant heat transfer balancing system. When an imbalance in radiant heat transfer (or an overheated portion in the radiant air heater) is detected, the system will tilt or reposition individual burners and/or reburners to restore the balance of heat distribution in the combustor. It may also directly modulate individual dampers controlling air flows to individual sections of the air heater (provided such control dampers are available).

Turbine air from the gas turbine exhaust passes through convective and radiant air heaters and the duct burner. The temperature of air exiting the radiant air heater and duct burner and entering the gas turbine is one of the main cycle parameters. This temperature will be affected by many factors, such as the flame temperature and emissivity in the radiant zone, thickness of ash deposits in both air heaters, combustor outlet temperature and the quench air/FGR flows, and operation of sootblowers. The most direct and dynamically effective method of maintaining the GTG inlet temperature is by the fuel supply to the duct burner. Other methods may include burner flame adjustments, fuel biasing between burners and reburners, air flow distribution and convective air heater bypass. In Phase II, the optimum temperature control method (or combination of several methods) will be determined and the corresponding control system will be designed.

Ash Management Control

Ash deposits must be continuously monitored and controlled to maintain sufficient radiant heat transfer and optimum turbine air temperature. The sootblowing system must assure effective ash deposit removal from the slag screen, water walls and convective air heater (and possibly from the radiant air heater). The existing technology of soot monitoring and sootblowing will be suitable for this application. For example, such systems as Diamond's *FlameView* and *BurnerView* (based on TV

273

cameras application) and *Cleaning Advisor* (based on IR-viewing), in conjunction with the existing sootblower controls, will meet the requirements. In Phase II, we propose to develop/select, test and evaluate available sensors to measure physical properties of deposits, including deposit thickness. The optimum cleaning strategies shall be developed and analyzed. Cleaning procedures for convective air heater will be tested on small-scale combustors.

Sensor/Instrument Selection and Development

For successful implementation of the sophisticated HITAF control system, a number of advanced sensors, instruments and measuring techniques have to be developed/selected, tested and evaluated. Currently, based on the present status of our information, these sensors and techniques are the following (instruments/ sensors which are in the development stage or need to be developed are identified below by *bold and italics*):

> *Coal flow* and air flow measurements for individual burners. *New flow measuring systems are being developed and tested by Air Monitor Corporation, Sierra Instruments and by EPRI.*

- Flame diagnostics for individual burners:

  a. based on analysis of the temporal flame frequency spectra (VIR VI by Fossil Power Systems in Canada - commercially available, *SpectraTune* system by PSI Technologies, "Signature" flame scanner by Fireye Inc.);

  b. based on the *OH imaging* for individual burner flames (PSI);

  c. based on the *CH/OH ratio* analysis (Fireye Inc.);

  d. based on TV-monitoring (BurnerView by Diamond Power);

- On-line precision monitoring of the following flue gas parameters:

  a. gas temperature at furnace exit and at SNCR exit (GasTemp by PSI SDx);

  b. O_2;

  c. NO_x;

  d. CO;

  e. unburned carbon and/or LOI at furnace exit (combustion monitor series 4100 by Rupprecht&Patachnic, *new method of carbon* measurement proposed by PSIT);

  f. *NO, NH₃, N₂O* measurements at SNCR exit and at SCR exit;

- *Heat flux and perimeter monitors*;

- *Advanced expert systems and optimization methods based on neural net/fuzzy logic* (Lehigh Energy Research Center, Pavillion Engineering, EPRI);

- *Deposits and slagging monitoring* (physical properties and thickness).

4.6.5 Additional information required in Phase II

Quarterly Technical Report for July 1 through September 31, in Section "Operating and Maintenance characteristics" (p. 29-33), outlines the initial concepts of system startup, shutdown and

274

normal operation. This description can be used as a starting point for the conceptual control system design. This document stipulates that control system represents a key undefined "grey area" and offers a great challenge to the control engineer due to the dynamic complexity of the HiPPS and many unknown factors. When the actual design work starts, there will be many technical questions which will be resolved in close cooperation between the process and control design engineers. Currently, we will formulate some initial questions and additional information required in Phase II.

Startup Procedures

Figure 4.6-4 presents a simplified diagram of the HIPPS start-up sequence of operations, as described in the above report. First of all, we start the GTG train (GTG, duct burner and HRSG #1) and, within minutes, bring it to full power. At the same time, we are starting a preselected HITAF train (e.g., HITAF A and HRSG #2A) firing gas. The HITAF start-up program will initiate starting the HITAF gas burners and will slowly ramp up the gas flow, while monitoring all important parameters. The most significant factors will be the furnace gas temperatures (level and distribution), refractory temperatures, fuel and air flows. When FEGT and/or the refractory temperature reach the first critical point T_1, the program will open inlet dampers to the air heater (AH) to allow vitiated air flow to the air heater. From this moment, the control system will monitor the air flows to each section of the air heater and its temperatures. Continuous monitoring of air temperatures at the inlet and outlet of both convective and radiant air heaters, and their deviations at different sections of the air heater would provide us with additional information on the heat flux distribution in the furnace.

When FEGT and/or the refractory temperature reach the second critical point T_2, the program will initiate the coal firing system. When the coal flame is established, the system will gradually ramp up the total coal flow while simultaneously reducing gas flow to a minimum. When coal flame is fully stabilized, gas burners will be shut down and maintained in the hot reserve (some gas burners may be left in operation to support and stabilize the coal flame). When at least one of the HRSG's attains sufficient steam conditions, the STG train will be started.

After the HITAF train is started and stable base-loaded combustion conditions are attained, the HITAF control system will initiate auxiliary optimization systems, such as NO_x control, burner control and furnace perimeter monitoring.

This brief review immediately raises many questions which must be clarified in order to proceed with the I&C design. For example:

1. Define all conditions to be satisfied to allow natural gas firing (start permissives) for HITAF and other major equipment.

2. Determine critical FEGT points: T_1 - permissive to open vitiated air to the air heater, T_2 – permissive to start coal firing.

3. Determine recommended start-up curves with the indication of critical limiting factors for Fuel Gas Flow to HITAF, Coal Flow to HITAF, FEGT, Radiant Air Heater Outlet Temperature, Convective Air Heater Outlet Temperature.

Vitiated Air
Conditions OK
(Temp, O$_2$)

GTG and Duct Bnr
Start Permissives

HIPPS Start
Permissives

HRSG1 Perm

Start
HRSG #1

Start

Start GTG
and Duct Bnr

HITAF Perm

Start Gas
in HITAF

HITAF Startup Program

FEGT

T$_2$

T$_1$

Air Outlet Tmp.

Coal Flow

Gas Flow

Time

Open Vitiated Air to AH

Start Coal

Start HRSG#2

HRSG2 Perm

HRSG1 Stm Press OK
HRSG1 Stm Temp OK

HRSG2 Stm Press OK
HRSG2 Stm Temp OK

Start STG

STG Start
Permissives

Figure 4.6-4   Simplified Start-up Sequence.

4. NO$_x$ control strategy in HITAF: at what point and sequence we start individual NO$_x$ control subsystems (reburners, SNCR and FGR). Define starting conditions and limitations for each subsystem, initial capacities of each subsystem, as a preprogrammed function of the HITAF load. Prepare the following graphs: Coal Flow to Reburners, FGR Flow, SNCR capacity vs. HITAF load.

5. Determine all conditions which require immediate load shedding or emergency trip for HITAF and other major equipment.

Later, in the course of the I&C design, we should clarify many other questions, including the following:

* optimum set-point settings for individual subsystems versus load;

* burner turndown versus burner out of service (BOOS) strategy for load swings;

* distribution of various air flows (primary, secondary, staging, dilution) versus load;

* flue gas recirculation versus load;

* slagging limitations for individual subsystems.

276

5.0 RESEARCH, DEVELOPMENT AND TESTING PLAN FOR PHASE II

5.1 Commercial Plant Design

Commercial Plant Design

The commercial plant design work is a continuation of engineering performed in Phase I. In Phase II, the design and cost estimates will be updated and revised to reflect new information from other team members, industry and DOE programs such as LEBS. The objectives include preparation of engineering and cost estimating documents to establish the generating, environmental and economic performance of the HIPPS commercial plant.

Analytical Approach: Performance and operating conditions of the HIPPS and associated advanced processes or equipment will be established by team members and other qualified vendor organizations. This information will be used to specify the commercially available systems required to form a complete power plant. Technical and cost data from Bechtel's in-house experience, and from equipment suppliers will be used to complete the technical performance and cost estimating work.

Analysis of Results: The plant's generation performance, i.e., efficiency and emissions, and costs will be used to compare the commercial HIPPS power plant to alternate power generation technologies such as pulverized coal, coal gasification combined cycle, or others to be selected by the team.

Schedule: Much of the work will be conducted in Task 6, which is scheduled from months 30 to 42. However, data collection and coordination with other work related to the commercial design will be performed at other times.

HIPPS Prototype Plant Design

The overall objective of this effort is to design a prototype plant that will demonstrate the HIPPS technology. The design will be site specific, and for economics, utilize as many as possible existing facilities. Sufficient engineering will be performed in Phase II so that a cost estimate with a probable accuracy of 15 percent (class III) can be prepared. Detailed drawings for construction and any commitments for equipment or materials will be part of Phase III.

Analytical Approach: Designs for the HITAF and the power island section will be prepared to match the host site requirements for power/steam production. Additional balance of plant items and integration with the existing plant will be parts of the total design.

Analysis of Results: The Phase II design work will provide a detailed cost estimate for economic evaluation and decision making. Engineering drawings and other documents will prepare the team for completing detailed designs for construction during Phase III.

Schedule: Much of the work will be conducted in Task 7, which is scheduled from months 36 to 51. However, data collection and coordination with other work related to the prototype will be performed at other times during Phase II.

277

5.2 Cycle Optimization

The major driver for the HIPPS/HITAF program is the attainment of the highest efficiency (a minimum > 47% HHV) commensurate with cost and emission goals. Thus, a detailed cycle analysis activity will be maintained throughout the Phase II program. The objectives of this continuous cycle analysis are:

- identify the efficiency benefits resulting from increases in performance of the major components

- identify the technology goals to attain these performance increases

- evaluate the effect of attainment/nonattainment of the technology goals on other component characteristics

- evaluate alternatives and recommend different technology paths to attain the highest achievable efficiency.

Because of the complex inter-relationship of the various components in the HIPPS/HITAF system, the cycle analysis capability must be able to meet the above objectives at differing levels of complexity. These would range from the effect of introducing a single change in a component to sub-optimizing equipment groups through determining overall system perturbation resulting from a change in operating requirements. This capability will become even more important in Phase II as experimental results define more closely the abilities and limitations of components undergoing test and development.

Analytical Approach: The Combustion 2000 Team members each have models and codes that guide the design and development of their particular program responsibilities. For example, Reaction Engineering International uses JASPER for 2-D analysis of the combustor, Bechtel uses ME671M for plant design, and Fluor Daniel used GATE for conceptual cycle definition. Each of these models relates differently to SOAPP, the UTC-developed model that is used for cycle optimization. The results from JASPER are used as input to SOAPP while SOAPP output is used to determine final equipment configurations in the Bechtel ME671M models.

State-of-the-Art Performance Program (SOAPP): All of the cycle optimization studies for the proposed Phase II program will be carried out using a sophisticated power plant performance analysis computer code called "State-of-the-Art Performance Program (SOAPP)." This code utilizes modularized representations for each type of power plant component or subsystem permitting virtually complete freedom in selecting the desired configuration. It is capable of analyzing gas turbine engines, steam cycles, combined cycles, and Humid Air Turbine (HAT) cycles, plus a complete power station including coal combustor, heat recovery, and other types of advanced technology including the HITAF system. It is easy to use, versatile, and fast. It incorporates the most up-to-date calculation techniques available. The full system is currently in use on the IBM 3090 computer, and on special workstations in interactive modes of operation.

278

The development of SOAPP was done at Corporate expense. The basic system structure, communication techniques and mathematical routines were developed by Pratt & Whitney Aircraft (PWA) in 1970, as were the first component calculation modules and component map routines. Other maps and modules for aircraft gas turbines have been added continually by PWA. In the intervening years, PWA assisted the UTRC and the TurboPower Marine Division with the extension of the SOAPP library to include modules necessary for advanced industrial power plants. These additions included boilers, heat exchangers, coal and oil gasifiers, fuel gas cleanup systems, coal-fired conventional, fluid bed, and HITAF combustors. SOAPP has been used in a large number of Corporate-, Government-, and EPRI-funded projects.

SOAPP is a computer code comprised of a preprocessor coupled to a library of modules and maps. SOAPP modules all contain design, off-design, and dynamics representation capability. The SOAPP library also stores gas and physical property data for all potentially important working fluid constituents. The program automatically handles thermodynamic properties for mixtures in homogeneous streams.

A partial list of modules currently available in the SOAPP library includes:

Compressors	Steam Boilers	Pumps
Drive Turbines	Gasifiers	Flow Mixers
Oil and Coal Combustors	Regenerators	Flow Dividers
Ducts	Gas/Gas and	Two-Phase Flow
Valves	Gas/Liquid Heat	Turbines
Reformers	Exchangers	Saturators

The engineers can use the SOAPP system to complete an entire simulation problem from start to finish without any special computer programming, providing all necessary elements reside in the library. They can set up their system in the configuration mode, describe physical hardware and external conditions in the design mode, and run performance calculations in the run mode, with results automatically provided.

As appropriate, the models used by the Combustion 2000 Team in identifying performance will be further developed or adaptations made to increase model fidelity and robustness. For example, if empirical data were made available concerning the behavior of the saturator at the saturation line under a variety of pressures and temperature, both Fluor Daniel and UTC would evaluate changes in their saturator models.

Analysis of Results: The cycle optimization analyses deal with identifying the parameters that control design considerations. For example, the exit temperature from the duct heaters, referred to as combustor exit temperature (CET) is the controlling parameter for the performance of the gas turbine and, therefore, the overall power plant. However, the CET is made up of two components, the temperature rise from compressor discharge temperature to some level limited by material considerations in the HITAF (coal input) and the rise from HITAF discharge to CET in the duct

heater (gas input). The goal of a minimum 65% energy input from coal plus the real physical constraint of the available materials for construction of the radiant heater portion of the HITAF limit the CET to values below that projected for use in the advanced, aero-derivative engines that would be available at the time of program commercialization (>2700 F). Engines of this type would be used in both combined cycle and Humid Air Turbine configurations.

The results of the cycle analyses then must be reviewed to identify both performance and economic trade-offs as functions of such influence factors as material limitations, use of additional coal in HITAF to bring coal/gas ratio into balance, use of topping/bottoming heat recovery systems to utilize additional coal provided heat input, compromises to gas turbine operation to maximize performance while running at less than design point conditions, etc. These results are evaluated in the context of both the commercial plant and the demonstration plant designs.

5.3 HITAF Combustor

The eventual success of the HITAF depends on the performance of several interrelated subsystems: the firing system; the radiant air heater/combustion chamber; the slag screen; the flue gas recirculation dilution zone; the selective noncatalytic zone, and the convective air heater. This task has one overall objective: to predict the performance of the HITAF, consistent with materials capabilities, at various scales thereby demonstrating our ability to design systems for different scales, fuel combinations and applications.

There are two aspects to this problem: a) the inherent interdependence of the separate HITAF subsystems (the performance of the radiant heater depends on the design of the firing system; the slag screen, dilution zone, convective air heater and SNCR zone are coupled), and b) the need to account for transient phenomena (the effect of start-up, shut-down, turndown and a range of failure scenarios).

5.3.1 Analytical Approach

The computational tools that will be used in this task are based on software developed over the last fifteen years by Dr. Philip J. Smith, Vice President of REI. These tools simulate reacting and nonreacting flow of gases and particles, including gaseous diffusion flames, pulverized-coal flames, liquid sprays, coal slurries, isothermal and reacting two-phase flows, injected sorbents, and other oxidation/reduction systems. Particular emphasis has been placed on simulating coal combustion and pollutant formation. The tools have been applied to a wide variety of industrial systems including utility boilers, pyrolysis furnaces, gas turbine combustors, rotary kilns, waste incinerators, smelting cyclones and others. Applications have included basic design, problem solving, pollution control, etc. using many different fuels including natural gas, coal and waste.

The computational approach involves numerical discretization of the partial differential equation set which describes the physics of the system. Typically $10^5 - 10^6$ nodes are needed to resolve important features of a three-dimensional combustion process. Around 60 variables (representing,

e.g., gas velocity, temperature, concentration of various chemical species) are tracked at each node. Particle trajectories are followed by introducing them into the flow field induced by the mixing and reaction processes. Their position in turn influences the velocity, pressure, concentration and temperature fields of the combustion process. Computations include full mass, momentum and energy coupling between the gas and liquid or particles as well as full coupling between turbulent fluid flow, chemical reactions and radiative and convective heat transfer.

Accurate simulation of combustion processes requires accurate modeling of the dominant or controlling physical mechanisms in the process. Different industrial processes can have different controlling mechanisms, so it is important to include all potentially dominant mechanisms in the combustion model and to appropriately couple these mechanisms to account for their interactions (e.g., effects of turbulent fluctuations on local properties). The capabilities of the combustion simulation tools that will be used in this task include the following:

- Steady state, laminar or turbulent flows with relaminarization option
- Complex axisymmetric, three-dimensional cartesian or cylindrical geometries
- Periodic and symmetric boundary conditions with multiple arbitrary inlets and outlets
- Polydisperse phases of gases and particles, droplets or slurries with full mass, momentum and energy coupling between phases
- Full coupling between turbulent fluid mechanics, radiative and convective heat transfer, and chemical reactions
- Mixing and reaction of multiple fuels
- Multiple reaction rate processes for liquid vaporization, coal devolatilization and heterogeneous particle reactions
- Particle capture efficiency, dust carry-over, ash loading
- Particle deposition and slag formation
- Two-phase fluid mechanics, sorbent injection
- Radiative heat transfer for absorbing-emitting-anisotropically-scattering, turbulent, sooting media
- Thermal and fuel NO_x formation, taking account of coal properties, and NO destruction by reburning and selective noncatalytic reduction
- Variable thermal boundary conditions including adiabatic, thermal resistance and "heat exchanger"
- Sulfur capture by dry sorbents

5.3.2 Analysis of Results

In this task the term modeling means computer simulation of the HITAF including the coal fired radiant heater, the slag screen and dilution zone, the convective heater and the SNCR zone. All the modeling activities have been included in this task, even those that relate to experimental studies that

281

will be carried out in other tasks. The total effort has been divided into a series of subtasks for convenience.

Improve Existing Models — In addition to validation, two factors will improve the effectiveness of computer simulations: 1) the ability to more accurately portray real geometries, and 2) a reduction in the turnaround time for complex cases. Advances in computer hardware will reduce run times, but the need to include more detailed physical and chemical models and the necessity of evaluating real three dimensional geometries will tend to negate these advances without parallel improvement in computational techniques. Our computer tools will be modified to improve their computational efficiency and ability to simulate accurately various HITAF designs. The improvements can be classified into two categories:

1.   Computational improvements including:

    – the incorporation of solution adaptive procedures to enhance solution accuracy;

    – multi-grid convergence methods to reduce run times; and

    – domain decomposition to exploit parallel computing.

2.   Chemical and physical model improvements based upon advances in the basic science, these could include:

    – improved chemical submodels for char burnout;

    – coal devolatilization;

    – NO formation and destruction in flames and by SNCR;

    – the ability to handle an arbitrary set of chemical species in partial equilibrium;

    – enhanced particle transport models to improve the accuracy of particle deposition; and

    – spectral radiation submodels.

Simulate the Firing System/Radiant Heater — The objectives of this task are: 1) to continue the optimization of the HITAF design initiated in Phase I with the intent of reducing the overall costs without jeopardizing energy conversion efficiency and environmental performance; 2) to examine design alternatives that will result in a reduction of the amount of natural gas being fired in the duct burner in order to move towards an all coal fired HIPPS; and 3) to examine the performance of the HITAF when firing a wide range of US coals. As part of this task we will:

    – continue the evaluation of groups of circular burners in a down fired mode;

    – evaluate the use of advanced firing systems designed for wet bottom boilers; and

    – evaluate corner firing as an alternative approach for the HITAF.

These evaluations will be carried out for both a range of coal types (including dried lignite) and the fraction of the total heat input supplied to the HITAF as coal (from a minimum of 65%).

Model the Performance of the Small Scale Test System — As part of the program to evaluate the performance of the radiant heater and its refractory coating, a 2 MBtu test furnace will be constructed

by EERC. The best model available at the time will be used to aid the facility design. One important factor in the design of this subscale system is the radiant flux to the refractory panel, this should be the same as that expected in the full scale system. In addition, the model will be used in the planning and evaluation of the test program.

Modeling the Performance of the Pilot Scale Firing System – It is intended to build and test a pilot-scale firing system at ABB. The best model available at the time will be used to aid the facility design. In addition, the model will be used in the planning and evaluation of the test program. One of the key aspects of this evaluation will be extrapolation of the test results to multiple burner systems and different thermal conditions. The parameters that will be modeled will include, but not be limited to:

- heat flux distribution;
- carbon burnout;
- pollutant formation;
- particle deposition; and
- wall conditions.

Modeling the Performance of the Dilution Zone/Convective Heater/SNCR Zone – The performance of the Dilution Zone/Convective Heater/ SNCR Zone is a key factor in the overall success of the HITAF design. The effluent from the radiant furnace (gaseous combustion products and fly ash) must be cooled to protect the convective air heater and to prevent sticky ash deposition. Cooling will be accomplished by a combination of water walls and dilution by cooled recirculating flue gases. This process should produce a uniform flow of well mixed gases at a uniform temperature not only to maximize the overall performance of the convective air heater but also to provide optimum conditions for SNCR which might be required to reduce the NO_x emission below 0.6 lbs/MBtu.

Simulation of the Commercial Plant HITAF – The purpose of this task is to support the HIPPS commercial plant design, specifically the expected performance of the total system. Because of the coupling between the various subsystems involved in the HITAF, this task requires a simulation of the total system from the introduction of the fuel to the entry of the combustion products to the heat recovery steam generator system. The improved model will be used to evaluate the performance of the commercial plant HITAF for different fuel mixes. The following performance factors will be taken into account in the evaluation:

- heat release profile;
- air heater exit temperature;
- particle deposition on walls, slag screen and convective heater;
- carbon burnout;
- NO/NH_3 and CO emissions; and
- tolerance to variations in coal type.

Modeling the Performance of the Prototype HITAF — The improved model will be used to evaluate the performance of the Prototype HITAF similar to the simulation of the commercial plant.

Development and Application of a Transient Simulation — One of the factors that differentiate the HITAF from conventional water-wall coal-fired steam generators is the impact of transients on the integrity of the radiant heater. In this task REI's model will be adapted to evaluate the impact of varying firing rates on the radiant heater wall temperature as a function of time following the change in firing rate. This model will be used to assess the impact of the following on critical HITAF components including but not limited:

- start up;
- shut down;
- turndown for load following; and
- failure conditions that will affect the integrity of the HITAF.

5.3.3 Sensors and Controls

The HITAF is a new furnace design, one that has never been built. The fact that the HITAF is being designed "from scratch" provides an unprecedented opportunity to instrument the furnace and to create a control system which takes maximum advantage of advances in sensors and diagnostics. The overall objective is to meet the program goals for system efficiency, NO_x emissions, and system availability. Our approach to developing the control system for HITAF is based on the following principles. First, development of a control philosophy early in the design process will make the design process more efficient and will lower the technical risk involved in Phase II and Phase III. Second, analysis of the transient behavior of the HITAF-HIPPS is critical to the design process. Third, development of new sensors will be required to provide necessary inputs to the control system, allowing the control system to meet the program objectives in an efficient and cost-effective way.

Analytical Approach: The HIPPS process presents a very dynamically complex system with many unknown factors and non-linearities. Even if each individual system component is well designed, operates normally and meets the target objectives at steady-state conditions, the overall system behavior during transient situations may cause serious difficulties . The dynamic aspect of the overall system must be taken into account and one of the best solutions is to start developing the dynamic model of the process at an early stage of the design. Dynamic modelling will aid the design process by identifying sensors, control elements and their optimum locations required for the transient behavior of the system in terms of its stability, accuracy and flexibility. The model can identify potential problems with start-up, shutdown or load changes. Once identified, the system can be reconfigured and tested *in the design stage,* thus avoiding dangerous and/or expensive problems with the demonstration unit. The use of a dynamic simulator will reduce the technical risk as well as the design time of the HIPPS project.

PSI will use a commercial dynamic simulation package (ARUBA) to predict the transient behavior of the HITAF in the commercial plant design, particularly for the analysis of start-up,

shut-down, and "off-normal" conditions such as component failure, and for the analysis of the effect of changes in operational parameters on the behavior, reliability, and efficiency of the plant. PSI will support the design of the commercial plant by predicting transient behavior in HIPPS. The results of this analysis will provide guidance in designing start-up and shut-down procedures, in predicting the ability of the system to change load, in identifying system response to component or subsystem failure, and in identifying equipment needed to minimize the risk of component or system failure.

Experimental Approach: The control system (and sensors employed in the control system) must guarantee the performance of certain critical subsystems in the HITAF. The priorities, in terms of control system development, are as follows: I) the firing system (stability, NO_x emissions, unburned carbon and turndown ratio); 2) heat transfer to air heaters; 3) the integrated NO_x control system.

Control of the firing system will involve sensing qualities of the flame and using this information to insure a stable flame over the entire burner load range, to minimize the formation of NOx and unburned carbon, and to maintain the correct temperature distribution, both axially and circumferentially. Ideally, by simply measuring fuel and air flows to each burner we should meet most of these needs. Although air flow sensors are now available, there are currently no commercial coal flow sensors available capable of measuring coal flow to individual burners with sufficient accuracy. It is possible, however, to extract fuel-to-air ratio information (and much more) by analysis of the radiation signature of the flame. PSI has demonstrated in conventional power plants that the signal from existing flame sensors, *when properly processed,* can provide information on the fuel-to-air ratio and the flame aerodynamics. The latter information may be used as a measure of NOx production and unburned carbon. PSI Environmental Instruments Corporation (EIC) is now developing a commercial prototype of this instrument, SpectraTune™, for conventional power plants.

GasTemp™ by itself can provide temperature information at multiple points in the HITAF. Information on the state of ash deposits in the HITAF can be provided using a combination of GasTemp™ and another commercial product, Cleaning Advisor™. This system is available through B&W Diagnostic Systems. It consists of several industrially hardened infrared video cameras, connected to a central image processing computer. The computer colorizes and enhances the images while allowing the user to store and retrieve images and switch between cameras. A key feature of the system is the computer's ability to compare and plot as a function of time the brightness of a given area in the field of view as compared to some reference area. This technique allows the relative cleanliness and fouling rate of the selected area to be quantitatively evaluated. Several processing adjustments are available to enhance the sensitivity of this method. A strip chart of cleanliness versus time can be output on the screen. The system has been available for more than 4 years and has been proven in many utility applications.

Analysis of Results: Results from the HITAF dynamic simulation will be used to: a) improve accuracy of commercial plant design by providing a more complete equipment list, especially

equipment required for start-up and shut-down and b) reduce risk of Phase III prototype operation failure by contributing to Phase III design.

Data collected on pilot scale testing of sensors will be used to design beta-versions of the HITAF sensors for testing in the subscale system. Results of the subscale sensor tests will be used to 1) provide guidance for the control system design as to the type of sensor outputs available and 2) make recommendations for instrumentation to be delivered to the Phase III system.

Schedule: Definition of the control philosophy and sensor requirements (Task 2) will begin in the third month of the program and require approximately one year to complete. Time has been allocated for review and comment by team members on the control system. Dynamic simulation of the HITAF will be used to support both the Commercial Plant Design (Task 6) and the Phase Ill Prototype Design (Task 7). This work will take place throughout Tasks 6 and 7 in order to allow time for interaction with other team members.

Preparation for sensor testing in the pilot scale facility (Task 2) will begin in the sixth month. Testing will be completed by the twenty-first month. Design and fabrication of beta-instruments for subscale testing will require six months. Beta-instrument testing (Task 5) will take place in the third and fourth years of the program and continue until the end of Task 2. Evaluation of pilot scale test data will occur in the second and third years of the program.

5.4 HITAF Air Heaters

5.4.1 Introduction

Insofar as the successful commercialization of the HIPPS concept for electric power generation is dependent on the development of the HITAF which uses pulverized coal combustion to heat air for driving a gas turbine, various critical technical issues relate to the survivability of the radiant and convective air heaters which are major parts of the HITAF. Although material selections will be the principal technology requirement for successful development of the air heaters, heat transfer design of these air heaters will play a key role in this development process to ensure that materials are not subjected to excessively high temperature levels or thermal stresses while achieving performance goals. Thus, the primary objective of this RD&T effort will be to provide engineering analyses, modeling, and experimental R&D related to the heat transfer performance of the radiant and convective air heaters in support of the design and testing of small scale test units, subsystem test units, a prototype HITAF demonstration plant, and a full-scale commercial generating plant. In a supporting role to related activities, in particular development of materials and mechanical designs for air heaters, engineering analysis will be performed to ensure that performance goals are met and material requirements are accurately known.

5.4.2 Air Heaters Analytical Models

A major activity of this effort will be devoted to the development of analytical models which will describe in detail the heat transfer performance of the radiant and convective air heaters. Although

models have been developed for the stated reasons under Phase I of this program, these models will be improved to provide a more exact representation of the heat transfer performance and related processes. Improvements to be developed and incorporated in the convective air heater model will include: (1) more exact correlations for the convection coefficient and gas pressure drop on the hot gas side using CFD analyses and available literature data which better represent the geometry of the finned-tube-sheet configuration; (2) a prediction of the temperature profiles in three dimensions throughout the cross-counter flow arrangement of the convective air heater; and (3) an improved representation of the thermal performance degradation expected from ash deposition on the hot gas side. Improvements to be developed and incorporated in the radiant air heater analysis will include: (1) integration of the radiant air heater and the furnace combustion models to provide a more rigorous representation of radiative heat exchange between the hot combustion products and the air heater surface, accounting for spatial variations in radiative properties, temperature, and optical path or transfer function; (2) a more exact representation of the optical radiative properties (emissivity) of the slag layer in combination with the heater surface as a function of temperature, slag composition, and slag layer thickness; (3) more exact values for thermal resistance of interfaces and contacts between dissimilar materials (i.e. metal alloy, ceramic refractory, and slag) using experimental data from small scale test units and literature sources; and (4) a more exact correlation for slag viscosity as a function of composition and temperature for an improved prediction of the slag layer thickness and flow over the radiant heater surface.

The principal use of the engineering models for heat transfer performance of the radiant and convective heaters throughout Phase II will be to provide information on expected operating temperatures and temperature profiles for use in related material development and structural design activities. In addition, these models will be used for design of test units at the various scale levels and eventually for design of air heaters for a HITAF prototype demonstration unit and a full-scale commercial generating plant. Clearly, these engineering models for describing the heat transfer and thermal performance of the air heaters must be as rigorous as possible so as to provide accurate information for material development, mechanical and structural design, and cost analyses.

5.4.3 Slag Screen and Ash Management

(a) Slag Screen

The objective of this effort is to provide the information needed to design particle removal systems for the convective air heater and slag screen. Realizing that the slag screen and convective air heaters cannot be tested at the scale of the Phase III system, our approach is to carry out experiments designed to validate models which will be used for the design. Although the slag screen and convective air heater both remove ash particles, the operating conditions and constraints are different between the two devices. Thus, the priorities for the slag screen operation are to maintain a low pressure drop, to prevent slag from freezing, and to capture particles with the highest possible collection efficiency. On the other hand, the priorities for the convective air heater operation are to maximize heat transfer and to ·maximize the lifetime of the air heater.

Experiments at pilot scale will provide data on ash deposition, but these data will be difficult to scale up to the full size. We will, therefore, rely on complex heat transfer and CFD codes to conduct the design of the commercial plant and the Phase III system. We will validate these codes using results from well controlled flow visualization experiments and from the pilot scale combustor.

As discussed above, sensors will be developed, specific to the HITAF environment, for determining the state of the slag layer. One technique for determining the state of the slag layer is to monitor the emissivity of the slag: the temperature and the morphology of the deposit will both affect the emissivity. The use of an imaging camera provides spatial resolution in the radiant zone.

Analytical Approach: PSI will refine models developed in Phase I of slag flow in the radiant zone and slag screen using experimental data obtained by EERC on slag properties. PSI will coordinate this activity with REI's combustor modeling efforts. The results of these calculations will be used to predict heat transfer and ash removal rates in the radiant air heater and slag screen as a function of coal type and load.

PSI will design the slag screen by specifying tube location and placement. In addition, the Phase II work will address the need for sootblowers in the slag screen for operation under dry ash conditions, and minimization of technical risks for the Phase III design. PSI will design an ash removal system for the convective air heater.

Experimental Approach: PSI, working closely with UTRC, will conduct flow visualization experiments which will provide model validation of complex CFD codes used to design the slag screen and convective air heater. Work under Phase II will address several design issues including: optimum slag screen tube placement to maximize particle capture, slag screen tube orientation in the flow to facilitate slag removal, slag screen location in the furnace for slag removal, slag screen size, and deposition patterns in the convective air heater. Preliminary CFD modeling will provide guidance for optimum tube arrangements of the slag screen. The results of these experiments will be used to carry out design of the slag screen for the Phase III prototype plant.

Analysis of Results: PSI will use the data generated from the flow visualization experiments in the design of the pilot scale materials testing facility at EERC by specifying layout of the slag screen and equipment for testing of sootblower concepts in the convective air heater simulator. PSI will evaluate the pilot scale data on ash deposition and removal in the slag screen and convective air heater. The results of these experiments will be used to confirm ·model predictions of deposition and heater transfer and to use models to scale up experimental data to design the prototype systems and commercial plant.

Schedule: This work will begin in the third month of the program with slag flow calculations and initiation of the project with the Flow Analysis Laboratory. Engineering design of the slag screen and cleaning systems will begin early in the second and third years of the program.

(b) Ash Management

The HIPPS plant must be able to burn a wide range of American coals in order to meet the energy production needs of utilities. The choice of coal has a profound impact on the ash behavior during operation of the HITAF. The important coal characteristics, ash content and ash composition, control the operation of many of the *in situ* particle removal devices and directly affect the heat transfer efficiency in the unit. The coal choice also plays a major role in the production of fine ash particles in the HITAF system. Due to the high temperatures required in the radiant zone for efficient radiative heat transfer, vaporization of many ash species may occur at higher rates than in conventional units. These vaporized ash species can then nucleate and condense, creating an increased loading of fine particles as compared to conventional units. Particulate control devices may have a more difficult time in removing particles from HITAF as compared to those generated by a conventional coal-fired power plant.

PSI's expertise in the area of coal mineral transformations in combustion systems will be used to predict the size, composition and mass loading of ash at various points in the HITAF. This will provide a common basis for other modeling activities and will thus support the design of experiments in Phase II, the commercial plant design, and the Phase III prototype design.

Analytical Approach: PSI will evaluate coal mineralogy for two coals, one bituminous coal and one western, low rank coal and use this information to predict the impacts on the HITAF system. Existing models will be used as follows: Predict ash particle size, composition, and mass loading at HITAF exit; Predict vaporization of major, minor, and trace inorganic species in burner zone; Predict size and composition of submicron aerosol from burner zone to convective air heater exit; Predict partitioning of trace metals (including Hg, Se, As, Pb, Cr) from burner zone to convective air heater exit.

Results from the EMAF model, coupled with rates of vaporization calculated by SOLGASMIX, are used as input to a third code developed at PSIT to predict the size and composition of the submicron ash aerosol. These particles will ultimately determine the effectiveness of the particulate collection device and will contain a significant portion of the hazardous air pollutants (HAPs) produced in HITAF.

Analysis of Results: The results of these calculations will serve as input to other modeling efforts and be used to: 1) predict operating characteristics of the slagging combustor, slag screen, and convective air heater, 2) interpret results of pilot and subscale testing and 3) scale up experimental data to design the prototype systems and commercial plant.

(c) Slag Properties — Waste Utilization

The HITAF combustor will have liquid coal slag flowing continuously over its walls which are composed of radiant air heater panels coated with refractory material. In order for the HITAF to operate properly, the slag must flow under all possible wall temperatures and atmospheres. Also, slag

viscosity can affect corrosion/erosion of the refractory since viscosity and slag layer thickness control the rate of ion diffusion through the slag to the refractory surface, which controls the rate of refractory dissolution. Slag viscosity will also be affected by the refractory dissolution products. For proper operation, the slag properties must be predicted accurately and, if necessary, modified by varying operating conditions, coal blends, or additives. Finally, disposal options and commercial markets for the HITAF ash must be identified in order to keep operating costs as low as possible. This must be done by testing since all past coal by-product utilization attempts were empirically rather than scientifically designed.

Experimental Approach: The viscosity of two candidate coal slags will be measured over the predicted operating temperature range of the HITAF radiant zone. Variables to be tested will be atmosphere, dissolution of refractory, and coal additives. Additives will be chosen for their probable ability to form a protective, frozen layer of slag on the radiant air heater or to increase slag viscosity to decrease the corrosiveness of the slags. Four additives will be tested. In order to determine the mechanisms for measured viscosity changes, characterization of the slags will include mineral and bulk composition by scanning electron microscopy and x–ray diffraction.

To determine potential utilization or disposal problems of HITAF ash, ash produced at at the (EERC) during pilot–scale testing of the HITAF components will be characterized to determine chemical composition, mineralogical composition, and leaching characteristics.

Analysis of Results: Measurements of slag viscosity under HITAF conditions will be made in order to provide input data for existing models of slag behavior and to determine methods for modifying slag flow behavior by varying system operating conditions, fuel feed, or the use of additives. The ability to incorporate additives into the refractory slag to make the refractory self-healing will also be determined. Ash utilization and disposal testing will be done to determine the basic chemical and mineralogical composition of each material, any potentially problematic elements present in the materials, including radionuclides and radon, the concentration of these elements in the ash, and the leachability of the potentially problematic elements.

Schedule: Viscosity measurements of the raw coal slags and modified slags will occur over the first two years of the project. Tests of the leachability and commercial value of simulated HITAF slags and ashes will take place after samples are made in the pilot–scale activities, assumed to occur the last two years of the project.

5.4.4 Laboratory– and Bench–Scale Testing of Materials and Refractory Coating for HITAF Air Heaters

Because of the high working temperatures produced in the radiant heater that forms the walls of the HITAF, the materials used in its construction will be prone to failure from thermal shock, erosion, and corrosion. We propose to use a refractory coating on the radiant heater which will serve as a replaceable corrosion barrier. However, in order to provide confidence in the design to commercial

investors, the refractory coating should have a considerable lifetime. We propose to perform short-duration temperature cycling tests of refractory covered alloys, as well as long–duration bench-scale tests to determine the behavior of the refractories in a simulated HITAF environment. In addition, the EERC will provide support to the UTRC materials testing program under this task.

Experimental Approach: Thermal cycling of the refractory/alloy interface may cause spalling of the refractory. The spalling potential of 12 monolithic refractory/air heater material combinations will be investigated in laboratory thermal cycling experiments. Both commercially available and experimental refractories will be investigated. The binder in experimental refractories will be varied to determine the effect on spalling potential.

Flowing slag may corrode the refractory. To determine the lifetime of a refractory coating in flowing slag, the experiments need to be carried out for long periods under conditions as similar as possible to those in an operating HITAF, in terms of oxygen transport to the materials and slag erosion and corrosion. To get realistic slag erosion conditions, it will be necessary to have the slag flow over the materials under the influence of gravity. This will allow for a thin layer of slag to flow over the materials, which will best simulate realistic rates of oxygen transport to the material.

The EERC proposes to modify an existing 1650°C electrically heated bench–scale furnace to allow slag to flow over rectangular modulus-of-rupture bars of refractory. Test durations of a thousand hours or more may be necessary so that accurate determinations of the refractory lifetime can be determined. Therefore, in order to provide a large test matrix with a limited amount of equipment, many samples will have to be tested at the same time. To reduce downtime, the system will have few moving parts, and they will be at room temperature. To minimize operating costs, the reactor will be operable without continuous supervision or by a single technician when necessary. The slag will need to be recycled and also replenished at a rate that assures that its composition does not change significantly because of dissolution of the samples or reactor materials. Changes in slag composition will be monitored through x–ray fluorescence analyses of grab samples. Two types of coal slag will be tested: one from a bituminous coal, most likely an Illinois No. 6, and the other from a Powder River Basin subbituminous coal. These two types of coal slags will be tested because they represent economically important fuels and because they represent acidic and basic slags, respectively. In addition, mixtures of slag with additives to reduce slag corrosion as determined in laboratory tests will be tested.

Analysis of Results: EERC testing of HITAF refractories will provide low-cost design data on the useful lifetime of refractories that will be used in slagging environments and, second, will provide scientific data on rates and mechanisms of the combined effects of thermal shock, erosion, and corrosion on the materials so that better materials can be designed.

The corrosion mechanisms will be determined by x–ray diffraction and scanning electron and scanning auger electron microscope analyses of cross sections of the interfaces between the corroded

refractories and the slag. This information will be used to indicate possible coal additives to make the slag less corrosive and to indicate more corrosion—resistant materials.

Schedule: Laboratory refractory spalling tests will take place periodically throughout the Phase II effort as new materials arise. For the long-term refractory testing, an existing cyclone furnace at the EERC will be modified, including installing an automated slag feeder system, a slag tap, and a sloped internal chamber. Four 100-hour shakedown tests will be performed to finalize the design and operating parameters before materials testing commences. In the second year of Phase II, long—term materials testing will commence and continue to the end of Phase II. For Year 2 of Phase II, two of the four shakedown tests averaging 100 hours and two long-duration tests averaging 1000 hours each have been budgeted. In each test, four refractories will be tested for corrosion so that standard deviations in lifetime and corrosion rate can be determined for a total of eight refractory/slag temperature combinations. For Years 3 and 4 of Phase II, four 1000 hour tests have been budgeted. In each test, four refractories will be corroded so that standard deviations in lifetime and corrosion rate can be determined for a total of 32 refractory/slag/temperature combinations in Years 3 and 4.

5.4.5 Convective and Radiant Air Heater Structural Modeling

Detailed finite element analysis and experimental testing will be performed to support the design of the convective and radiative air heaters. The components of these systems to he designed include the cooling air passage geometries, the support structures, and the connections between air heater segments and other segments or headers.

The objective of the modeling effort is to optimize the design of the air heater components by meeting performance requirements while maximizing component life. Interaction with the materials effort of this program will ensure the selection of the best materials for the design. An all-ceramic design and an all-alloy design will be considered. Heat transfer analyses will be used to determine the temperature distributions and gradients, and stress analyses will predict deflections and stresses due to the thermal and mechanical loadings. Component life estimates will be obtained considering yielding and creep rupture for metals, and statistical failure for ceramics.

The experimental testing effort has two objectives: (a) mechanical property and creep testing to provide the analysis with accurate constitutive relationships at high temperature, and (b) concept testing of joints, seals and header connections, including leakage rate measurements. The combination of analysis and testing will provide verified designs of the convective and radiant air heater components that will meet life requirements.

Analytical Approach: Finite element analysis will be used to model both two—dimensional and three-dimensional models of the air heaters. Two-dimensional models will consider a cross-section of the component with assumptions in the out-of-plane dimension. Examples of two-dimensional formulations include plane strain, plane stress and axisymmetric assumptions. Temperatures throughout the structure will be determined based on the hot gas and cooling air temperatures and

292

flow conditions, including heat transfer coefficients at the surfaces. Stresses and deformations due to thermal gradients and cooling air passage pressures will be determined. Changes in geometry, material property and applied boundary condition or loading will be applied to the model to determine the effect on the structural response.

Prediction of the service life of the components will be accomplished using probabilistic failure analysis for brittle materials such as ceramics. In probabilistic failure analysis, a large number of ceramic specimens are loaded to failure, and the failure stresses are used to define a Weibull failure curve. Based on the stress results from a finite element analysis, the probability of survival of the design will be determined from the failure data. For metals, ductile failure will be predicted based on a deterministic method in which stress levels are compared to the yield stress to determine if plastic deformation will occur. In addition, time to rupture from creep effects will be calculated. Creep is the progressive deformation of a material at constant stress, encountered in temperature ranges that are typically 0.35 to 0.70 times the melting point. Even if creep does not lead to rupture, stresses will relax due to creep which can cause residual stresses to be present after cycling to room temperature. These effects will be addressed.

The MARC nonlinear finite element computer program will be used as the main analysis tool in this effort. MARC can be used to execute both heat transfer and stress analyses using the same mesh. MARC allows the input of advanced constitutive relationships that will include temperature effects, yielding, plasticity, creep and rupture. Any material data that cannot be obtained from other sources will be obtained from experiments to ensure accurate representation of the material behavior in the analysis.

The CARES/LIFE code, developed at NASA, will be used to predict probabilistic failure of ceramics. Failure data, obtain in experiments, will be used to determine the probability of failure of components in the ceramic design.

The convective air heater main component consists of tube sheets that provide for the heat transfer between the hot gases on the outside and the cooling air inside the tubes. This component will be analyzed and designed for the all-alloy case and the all-ceramic case. The main component in the radiative air heater is the cooling air passages in the walls of the air heater with a refractory coating on the gas side. This component will also be designed for both alloy and ceramic cases.

The main considerations in the analysis of the air heater main components is the ability of a selected geometry constructed from a selected material to withstand stresses from thermal gradients through wall thicknesses, thermal fight between different materials, and internal gas pressures. These stresses will occur in high temperature regimes which will result in degraded strength properties and creep situations for metals. Another consideration is the deflections due to thermal expansion, which may not hinder the main component design but will have a great effect on joining considerations. Design of the structural support systems for both air heater main components will be included.

Joining, sealing and headering of air heater segments will be designed based on a combined analytical and experimental approach. Candidate joining methods will be developed, and analysis will be used to rate the methods of joining, assuming both ceramic and metal components. The most promising joining geometries will be tested for verification.

Experimental Approach: Material property evaluation may be required to support the analytical effort. In particular, high temperature effects such as creep and rupture for alloys will be determined for selected materials. These tests will be performed in the Materials Testing laboratory at UTRC. The laboratory is well−equipped to handle a large array of high temperature testing of stress, strain and creep at high temperatures.

Testing will also be used to assist and verify the analytical models for joining air heater components. Experiments will be designed to include joining techniques that are subjected to large amounts of movement that will be present in the actual design due to thermal expansion. Elevated temperature environments will be included in the experiments, along with the appropriate pressure loading in the air passages. A measure of the structural integrity of the joints will be obtained from these experiments and will be compared with analytical results for verification. Additional information, such as leakage rates, will be measured. The Materials Testing laboratory at UTRC is experienced in designing, constructing and testing special purpose experiments.

Analysis of Results: Results from the air heater structural analysis and experimental testing will be used to guide the design of high temperature applications of ceramics and alloys, including the effect of pressure. Joining and headering the air heater components at the high temperature ranges is a challenging engineering problem which will provide state-of-the-art design methods for high temperature joining.

Schedule: The convective air heater analysis will start in month 1 and be completed in month 6. The radiative air heater analysis will start in month 6 and be complete in month 12. Any experimental work and collaborative efforts with the materials effort of this program will be performed at this time. The development and design of the joints, seals and headers will begin in month 13 and continue through the remainder of the program. Analytical and experimental work will be performed.

5.4.6 Air Heater Materials Selection and Screening

The HITAF air heaters must operate at high temperatures and resist the aggressive corrosive actions of combustion products such as coal ash and alkali sulfates. In addition the HITAF must posses the necessary thermal conductivity at the anticipated temperatures. These criterion make materials selection and prediction of behavior under extended service conditions (life) critical to the success of the HIPPS program.

For the convective air heater, wrought superalloys with inherent oxidation resistance, further supplemented by thin protective coatings, will be modified and evaluated for corrosion resistance and mechanical integrity. For the radiant air heater: 1) the integrity of the metallic/ceramic system will be

evaluated for heat transfer passageways, 2) thick refractory ceramic materials will be evaluated for protection of the alloys from molten coal slags, and 3) thin coatings (applied to metallic substrates) will be evaluated for providing corrosion resistance to gaseous and condensed corrodents and resistance to molten coal slags in the event of localized chemical or mechanical failure of the thick refractory lining.

Several materials combinations will be analyzed with respect to environmental durability and mechanical integrity in order to determine expected service life. This activity will culminate in limited life demonstration tests in a follow-on task, Air Heater Materials Engineering. The data acquired within this task will be utilized for: 1) materials selection, 2) design, 3) structural analysis, and 4) lifetime prediction of the convective and radiant air heater components.

Analytical Approach and Analysis of Results: The existing knowledge base for performance of materials in coal combustion and other similar hostile high temperature environments will be utilized to pre-select materials for detailed evaluation. Manufacturers data along with limited in house testing will be utilized to determine mechanical properties at room and elevated temperatures for pre-selected materials.

Corrosion performance will be evaluated through exposure of test coupons in: 1) an ash fed burner rig, 2) a running coal slag rig, and 3) condensed and corrosive gas exposure tests. The combination of these laboratory scale tests best simulate the HITAF air heater environment, while minimizing development costs as compared to running all the material combinations in a sub scale coal combustor. Reaction mechanisms and corrosion rates will be evaluated to provide a database for design and construction of the HIPPS pilot facility. Corrosion rates of weldments and other joints will also be evaluated. Lining and air tube materials will also be tested to ensure compatibility (non—reactivity) at interface temperatures typical of air heater operation. All physical properties (mechanical and corrosion related) will be correlated and utilized within the structural analysis and air heater design tasks.

Data to be acquired will include surface recession rates, and exposure related degradation in mechanical properties. These data will be analyzed to select materials optimal for air heater construction based on minimum cost for an expected service lifetime, commensurate with acceptable heat transfer performance. Where possible, statistically designed experiments will be utilized to decrease the number of individual tests needed to identify trends in materials performance.

Experimental Facilities: The necessary materials testing equipment is available at UTRC and described elsewhere in this proposal. Where possible, manufacturers data will be utilized for database construction, however, missing or highly critical data needed for design of air heater components will be obtained using UTRC facilities, or where necessary, at ORNL.

Rapid screening of material resistance to coal combustion environments will utilize various types of equipment. The UTRC corrosion/erosion rig will be modified so that heated ash particles will

impinge upon test surfaces, and run off into a collection chamber. Samples will be exposed for sufficient durations to determine recession rates and evaluate mechanisms. Recession rates and corrosion mechanisms will be examined and correlated for various types of refractory ceramics, and protective coatings. Metal alloys will be exposed to lower temperature "dry" coal ash as is expected within the convective air heater. In addition, the rig will be operated with injected gases typical of coal combustion environments to determine gaseous corrosion effects on materials.

The most promising materials will be subjected to longer term running coal slag exposures in a bench scale dynamic slag corrosion reactor at UNDEERC. The existing electrically heated cyclone furnace at the EERC will be modified for long term slag exposure testing. Modifications include installing an automated slag feeder system, slag tap, and a sloped internal chamber. This facility will be utilized for 1000 hour exposure tests of the more promising refractory ceramic lining materials. This will provide highly accurate surface recession rate data.

Air Heater Materials Development

The objective of this Task is to determine the best methods for protection and assembly of the materials identified and evaluated in the Materials Selection and Screening Task for fabrication of radiant and convective air heater. Methods for bonding, sealing, and attaching the various materials used to fabricate the air heater walls will be defined. The necessary modifications to chemistry and microstructure will be explored in order to maintain or improve oxidation and corrosion resistance or to enhance mechanical properties. Secondary objectives include: 1) exploration of structural ceramics (e.g. silicon carbide based) for use in air channeling or piping as required for growth to the all coal case,. and 2) a preliminary examination of how baseline materials (alloy air heater walls, protective refractory ceramic coatings) can be refurbished or repaired during HITAF operation or during shut down periods.

Analytical Approach and Analysis of Results: The joining processes used to construct the radiant and convective air heaters must produce components that possess the necessary physical and chemical properties for successful operation. The transient liquid phase bonding process will be modified for the on site joining of the cast nickel base superalloys. The traditional welding procedures will be used to join the wrought alloys.

The ambient and elevated temperature mechanical properties of the joined sections will be determined by the accepted tests employed by the welding community. Weld quality will be measured through evaluation of weld microstructure using optical and electron microscopy. Alloy compositions may be altered to improve weldability, oxidation resistance and elevated temperature strength. Improvements to oxidation resistance and/or high temperature strength will be evaluated using thermogravimetry and fast fracture testing, respectively.

A variety of methods will be considered for attachment of refractory ceramics. The types of attachment techniques to be considered will be dependent on the type(s) of refractory ceramics to be

attached. Refractory brick may be attached via interference fit, hanging mechanisms, transient liquid phase bonding, and various other techniques. Gunnable and castable refractories will utilize various types and configurations of ceramic anchors. Alloy/refractory lining assemblies will be fabricated, and joint quality will be analyzed through interrupted thermal cycling in combination with mechanical adherence tests. The goal will be to achieve a system which allows high lining adherence despite exposure to thermal cycling and consequent thermal expansion mismatch stresses.

A secondary effort will focus on evaluating structural ceramics for use in future "all coal" HITAF air heaters. Throughout Phase II, progress in the field of structural ceramics will be monitored. If significant progress is made in fabrication of reliable, large, complex shapes such as tubing, these materials may receive renewed consideration for the prototype HIPPS power plant.

A further effort will focus on methods for on-line and off-line repair of both the metallic and refractory materials. Methods for hot repair of refractory linings developed for the glass furnace industry will be evaluated for repair of cracked refractories in the presence of coal slags. On-line welding of cracks and repair of coatings for the metals and their protection systems will also be evaluated.

Experimental Facilities: No new or unique capital equipment items are needed to support this effort. A wide variety of mechanical testing equipment is available at UTRC and is described in the section on Experience, Capabilities, and Resources.

Air Heater Materials Engineering (Lifetime Demonstration)

The first objective of this Task is to evaluate the performance of sub−scale air heater walls in a coal combustor environment. The task described below serves mainly as a validation test for both materials of construction and design. The second objective of this task is to perform a cost/benefit analysis comparing materials lifetime and cost.

Analytical Approach and Analysis of Results: Sub−scale radiant air heater walls will be constructed similar to the designs planned for the HIPPS pilot facility. They will be installed in the 2 million Btu/hr coal combustor at UNDEERC and the 50 million Btu/hr combustor at ABB, and exposed to both bituminous and sub−bituminous coal combustion products. Clean, intermediate temperature air will be provided to the metallic air channels, to simulate actual HITAF use conditions. The subscale walls will be assembled in a manner which will allow change out of the refractory ceramic lining material to allow different lining materials to be evaluated. Following each exposure test, a postmortem analysis will be performed by UTRC and UNDEERC.

Data obtained in the test above, and from the Materials Selection and Screening Task will be used to perform a cost benefit analysis. UTRC, EERC and Bechtel personnel will compare expected service lifetimes and material costs. The most cost-effective materials capable of withstanding HITAF conditions for adequate lifetimes will be determined.

Experimental Facilities and Approach: The construction and operation of the 2 million Btu/hr coal combustor test facility is at UNDEERC described below. Construction of sub scale radiant air heater wall sections will be performed at UTRC and shipped to UNDEERC for insertion into the test facility. Results will be evaluated using UTRC and UNDEERC analytical equipment described within Section IV Experience, Capabilities and Resources.

5.4.7 Pilot–Scale Testing of the HITAF Combustor and Air Heaters

In addition to the laboratory- and bench-scale work to provide ash and materials data, the EERC will provide engineering analyses, support modeling activities, and complete material and component testing in support of the design and operation of a prototype HIPPS plant by performing pilot–scale work with a 2-million-Btu/hr high-temperature slagging combustor built for this purpose. The main design areas for which these data are required are: 1) overall HITAF design and operation, 2) radiant panel performance and survivability, 3) convective panel performance and survivability, and 4) slag screen performance and survivability. This task will involve the design, construction, and operation of the pilot-scale high-temperature slagging furnace and support systems.

Experimental Approach: All of the activities proposed by the EERC will be performed using facilities on–site at the EERC. A new pilot plant high bay area was recently constructed on the EERC site. In addition, all utility requirements (water, electricity, natural gas, compressed air, compressed nitrogen, and steam) are present in the new pilot plant. The availability of these resources substantially reduces the cost of building the pilot-scale high-temperature slagging furnace system.

This task will consist of four subtasks. Subtasks A, B, and C will involve the design, construction, and shakedown of the pilot-scale high-temperature slagging furnace system. Subtask D will involve operation of the pilot-scale high-temperature slagging furnace system. The EERC will be responsible for the design, construction, and operation of the pilot-scale system along with the analytical support required to evaluate performance thoroughly. Each subtask is described herein.

Design and construction activities will be performed in accordance with appropriate OSHA standards and codes concerning pressure vessels, pressure piping, structural steel, and electrical standards. During and after completion of the construction activities, the EERC will dispose of all wastes in accordance with all applicable federal, state, and local laws and regulations. The EERC does not expect that hazardous wastes will result from the construction effort; therefore, scrap metal will be recycled, if appropriate, and all nonrecyclable wastes will be properly landfilled. If hazardous wastes are produced as a result of the construction effort, EERC's hazardous waste disposal policy will be implemented.

A two-step approach will be used to complete the design of the pilot-scale high-temperature slagging furnace system. A preliminary system design will be developed by EERC personnel with input from other project team members. The preliminary system design will include a process flow diagram, equipment lists, size determination of system components, and a test unit layout. The preliminary

298

system design will be submitted to the prime contractor and DOE COR for review. Once the preliminary system design is approved by the prime contractor and DOE COR, the final system design will be prepared.

The final system design will include detailed component designs for the pilot-scale high-temperature slagging furnace, pulse—jet baghouse, and support systems, specifications for purchased components, instruments, piping and electrical specifications, basic engineering design data, utility and raw material requirements, and piping and instrument diagrams. Procurement of equipment and fabrication of parts will begin once written approval has been obtained from the prime contractor and DOE COR.

The design and construction of material test coupons in support of the convective and radiant air heater designs and the convective air heater (CAH) and the radiant air heater (RAH) panels that will ultimately be tested in the pilot-scale furnace will be provided by UTRC. The furnace design will include locations to accommodate installation of material test coupons and the CAH and RAH test panels as well as heated air for panel operation.

The preliminary design of the pilot-scale high-temperature slagging furnace system actually began with the preparation of this proposal. Figure 5.4-1 presents a conceptual illustration of the system. Primary components include: 1) combustion air system, 2) fuel feed system, 3) slagging furnace, 4) cooling air system, 5) cooling water system, 6) pulse-jet baghouse, 7) system instrumentation, and 8) data acquisition system. The pilot-scale high-temperature slagging furnace will be a downfired, vertically oriented unit. At this time, the firing rate is estimated to be 2 million Btu/hr using pulverized coal. Critical design features will include firing rate, temperature control, furnace access for material coupon testing, furnace access for the RAH panel, the slag tap and quench, furnace access for slag screen installation, the flue gas dilution and quench zone, furnace access for the CAH panel, sootblowing capabilities, ash removal, and optical access. The furnace will be primarily constructed of carbon steel with extensive refractory lining.

Furnace firing rate and temperature control are interdependent parameters. Proper furnace design will be critical to achieve the desired temperature regimes in the slagging furnace for a range of fuel types. Furnace temperatures approaching 2900°F are desirable. Therefore, the EERC anticipates designing the furnace to operate at a 2600°F to 2900°F exit temperature while firing a subbituminous coal. Comparable conditions should be easily attained when a bituminous coal is fired. When a lignite is fired, cofiring with natural gas is expected to be necessary to achieve the exit temperature target. Proper temperature control to the furnace exit will be important in maintaining proper slag conditions in the furnace.

Furnace access will be a key design issue. Removable panels in the furnace walls will be necessary to accommodate testing of material coupons possibly as large as 1 ft^2. A minimum of four small removable panels are anticipated at this time. In addition, one wall of the furnace will contain a single removable panel for the purpose of installing and testing the RAH panel, possibly as large as 8 to 18 ft2.
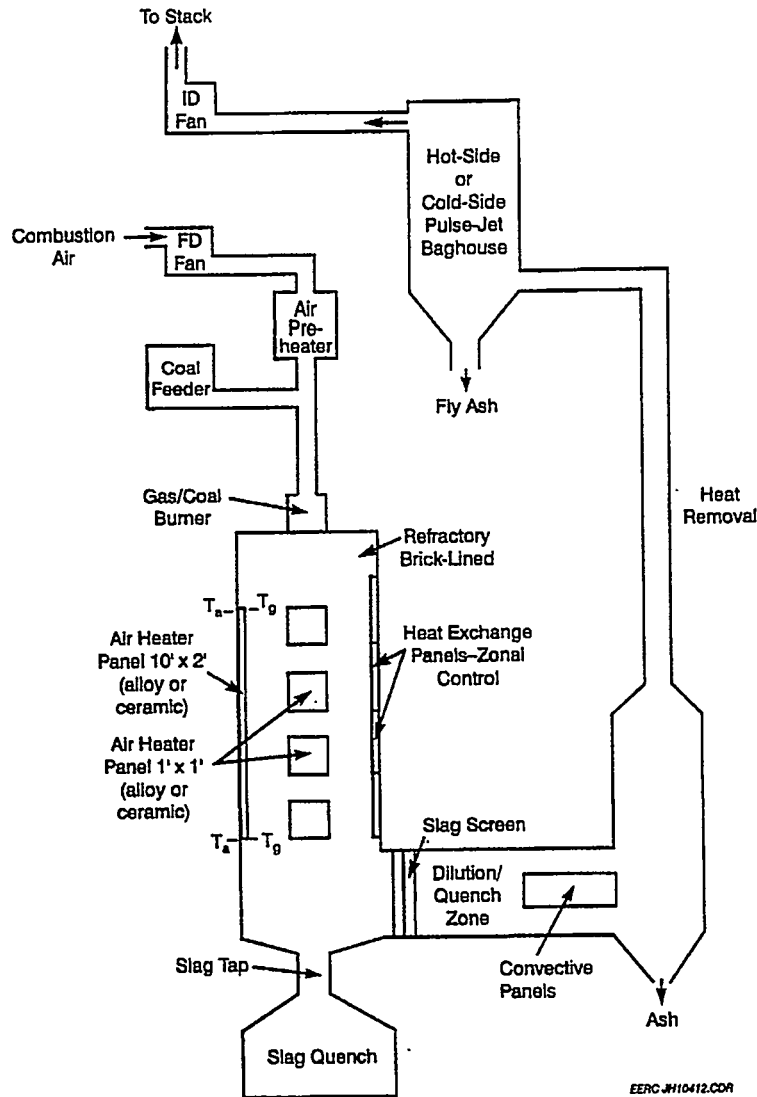
Figure 5.4–1 Proposed Pilot-scale High-temperature Slagging Furnace System.

Other heat removal panels for the purpose of furnace temperature control will also be factored into the design. The design of the access locations will depend largely on the design of the coupons and RAH panel to be evaluated. Therefore, it will be important to obtain information from the HITAF design team. The EERC is anticipating that other project participants will have responsibility for design and construction of the RAH and CAH panels and the slag screen that will be tested in the pilot-scale furnace.

A dilution/quench zone upstream of the CAH panel will be used to reduce flue gas temperature to a 1800°F to 2000°F temperature range. The size and geometry of the quench/dilution zone along with the number and size of the quench fluid nozzles will be a critical design activity relative to properly quenching the flue gas and possibly evaluating the use of selective noncatalytic reduction (SNCR) for partial NO_x control.

300

A pulse-jet baghouse will be used to control particulate emissions from the pilot-scale high-temperature slagging furnace system. Baghouse design will permit operation as a cold-side or hot-side unit at air-to-cloth ratios of 3 ft/min or greater while the entire flue gas flow from the slagging furnace is filtered. Actual baghouse size will depend on the size (thermal input and flue gas flow rate) of the slagging furnace. Based on a 2-million-Btu/hr furnace design and a face velocity of 3 ft/min, the pulse–jet baghouse will house 24 bags for hot-side operation, 6 in. in diameter by 10 ft long, providing a total cloth area of about 377 ft^2.

System instrumentation will include a large number of thermocouples in order to adequately monitor flue gas temperatures, cooling air temperatures, and material temperatures critical to the operation of the slagging furnace as well as the performance of the material coupons, CAH panel, RAH panel, and numerous support systems. The measurement of static and differential pressures will be required throughout the pilot-scale system to monitor performance and measure the flow rates of various process streams. Flue gas analyzers will be required to monitor system performance properly. Specific instruments will be purchased for on-line monitoring of flue gas oxygen (O_2), sulfur dioxide (SO_2), nitrogen species (NO_x and NO_2), carbon dioxide (CO_2), and carbon monoxide (CO) concentrations.

Analysis of Results: Subtask D is divided into three subtasks. Subtask D1 will deal with HITAF design evaluation. As much as one-third of the planned operating time (6 weeks) may be spent in this subtask. Key activities will include evaluation of burner and furnace performance with respect to slag flow characteristics, ash impingement, and deposition and evaluation of monitoring methods for developing information concerning heat transfer and loss of refractory. Materials issues to be addressed will include heat-transfer characteristics of alloys and ceramic samples, the performance of welds, seals, and joints, and the bonding of refractory and alloy materials. This series of tests will offer an opportunity to characterize the flue gas particulate mass loading, particle-size distribution, and · HAPS. Subtask D2 will deal with convective air heater panel evaluation including materials issues, ash deposition, ash corrosion/erosion, sootblowing, and CAH panel performance with respect to heat transfer. Two or more CAH panels will be tested. Subtask D3, dealing with radiant air heater panel evaluation, will focus on materials issues, slag corrosion/erosion, and RAH panel performance with respect to heat transfer. Two or more RAH panels will be tested.

In addition to specific component testing, the entire series of pilot-scale tests will offer an opportunity to characterize the flue gas particulate mass loading, particle-size distribution, and HAPS emissions so as to provide input data to the HITAF system design team. In addition, there may be an opportunity to evaluate methods in combination with the furnace system and pulse-jet baghouse for the purpose of meeting the 0.003 lb/MMBtu particulate and 0.06 lb/MMBtu NO_x emissions objectives, as well as the control of HAPS emissions. Options include, but are not limited to, flue gas conditioning, carbon-based sorbents, SNCR, and SCR.

Schedule: Preliminary design activities will be completed by EERC personnel with input from other project participants within a 3-month period of time for completion of preliminary design

301

activities. Final component design and procurement activities will begin following approval of the preliminary design by the prime contractor and DOE COR. The final design of system components will be performed by EERC personnel with input from other project participants. This proposal assumes a 6-month period of time for completion of final design and procurement activities. Construction activities will begin as soon as individual system component designs have been completed and approved by the prime contractor and DOE COR and required materials and components are procured. All of the construction activities will be completed by EERC personnel. This proposal assumes a 10-month period of performance of construction activities. EERC expects that the initial construction activities will overlap with the final detailed design activities.

Following completion of the construction activities, all process equipment, process controls, flow measurement systems, instrumentation, and data acquisition systems will be put through a rigorous shakedown for a 3-month period.

After shakedown, normal testing will commence. A total of 18 weeks of actual furnace operation has been budgeted, assuming 100 hours of operation per week. The duration of individual operating periods may range from a single day to as many as 14 days, depending on operational objectives and system performance. Testing will continue until the end of Phase 2, but may continue into Phase 3 as the need arises.

5.5 Duct Heater and Humid Air Turbine

Development of Low NO$_x$ Emissions Natural Gas Fired Boost Heater

The focus of this task will be the development and demonstration of a sub scale mixer and fuel injection device that will operate with an inlet temperature as low as 730°F and have a discharge temperature of 2495°F. This device should have a pressure drop $\leq 1.5\%$ of combustor total pressure, and have NO$_x$ emissions < 0.01 lbm/M Btu of fuel input and very low CO emissions. This natural gas fired boost heater will be capable of operating either with an inlet temperature of 730°F and supply the 2495°F discharge temperature whenever the gas turbine is being operated with 100% natural gas firing, or boost the output of the HITAF radiant heater from 1700°F to 2495°F for the gas turbine flow path. The ultimate priority is to develop a low pressure drop, low NO$_x$ and CO emissions boost heater to provide the energy required by the gas turbine.

Analytical Approach: In the initial phase of this task, the results of previous experiments on centrifugally enhanced mixing performed in Phase I will be evaluated using existing flamelet models and 2-D fluid dynamic codes. From this preliminary modeling effort, a basic understanding of the fluid dynamics governing the rapid mixing induced by inverse density gradients in rotating flows will be achieved Additionally, the kinetics of NO$_x$ formation in an ideal combustion environment, using a perfectly stirred reactor (PSR) model, will be studied. The residence time for complete fuel oxidation will be determined at various inlet air temperatures for the pressures to be expected in the gas turbine. NO$_x$ and other species production will be predicted; these predictions will dictate the rapidity at which

the fuel and air must be mixed for complete combustion in the physical space available for the boost heater. Preliminary designs for the mixer/injector will be modeled using the JASPER® Code in conjunction with FLUENT® and other 2-D CFD codes. The integration of PSR modeling with fluid dynamic models is a complicated process; this process will be aided by 3-D measurements of the velocity flow field in and near the centrifugal mixer evaluated in Phase 1 of this program. These boundary conditions will aid the modeling effort and aid in closure of the iterative nature of this type of model. The modeling, both of chemical processes and fluid dynamics will also investigate the effect of high water vapor content in the combustion process for humid air turbine cycle applications.

Experimental Approach: The development of the boost heater will involve the construction of a high temperature, moderate flow, high pressure facility that can deliver uncontaminated air at fixed humidity level for evaluation of the centrifugally enhanced mixer. Additionally, the program will involve extensive sub scale cold flow testing and development. The cold flow testing will be performed in two facilities: A 12 x 12 inch wind tunnel and a 4 x 4 inch facility for low flows. The models to be tested in these cold flow facilities will be designed and constructed using computer aided design and stereo lithography of UV cured polymers. Evaluation of the mixing efficiency of these models will be performed using flow visualization techniques that include smoke tracing of large scale structures, planar digital imaging using Mie-scattering, planar laser induced fluorescence (PLIF), and tracer gas mixing measurements. Three dimensional velocity measurements will be made using either a rotating hot film sensor or laser doppler anemometry. An optimum configuration will be developed in the reduced scale cold flow experiments before hardware is fabricated for the hot flow testing.

Testing at the pressures and temperatures expected in the FT4000 gas turbine will take place in the facility described elsewhere in this proposal. A multi-stage air heater will enable testing at inlet temperatures up to 1 700°F at mass flow rates up to 5 lbm/s. The optimum centrifugal mixers from the cold flow studies will be tested in the hot flow facility for flame stability and emissions. The primary diagnostics will be translatable thermocouple and gas sampling probes which will be used to map out the 3-dimensional profiles of temperature and species. Of particular interest for this program will be the NO_x, CO, and unburned hydrocarbon concentrations at the discharge of the boost heater, as well as the temperature distribution across the discharge plane. This distribution is critical for the operation and durability of the gas turbine. Three modes of operation will be investigated: (1) A boost heater to increase the temperature from the HITAF air heater from 1700°F to 2495°F, (2) operation with 100% natural gas firing with an inlet temperature of 730°F, and (3) operation with high inlet water mass fraction (HAT cycle). All of these tests will be performed on mixers that are as large as 1/6 scale, but at the operating temperature and pressure that will be used in the actual cycle.

Analysis of Results: The evaluation of the centrifugal mixer/fuel injector for the boost heater will be based upon pressure drop, uniformity of temperature profile at the entrance to the high pressure turbine, and emissions of NOx, CO, and UHC. An acceptable device will have a pressure drop $\leq 1.5\%$ of the combustor total pressure, and NO_x emissions ≤ 0.01 lbm per million Btu of fuel input. The modeling effort associated with this development program will be used to predict the performance of

the mixer in the hot flow tests. The velocity field in the vicinity of the mixer will be used as boundary conditions for 2-D fluid dynamic computations. The measured mixing rate between the two streams, as done in cold flow, will be compared with model predictions. If an acceptable agreement is seen between the model predictions and the measured mixing profiles, the model will be used to design the characteristics of a larger scale device. This will be tested in cold flow also, thereby providing confidence in scaling parameters in the model. The final test of the modeling process will be in the performance of the sub scale mixer in the hot test flow facility.

With any experiment that is coupled with an analytic model, an iterative process is required in order to determine the sensitivity of the variables being measured in actual physical hardware to the independent variables developed in the model. A blending of non reacting and reacting computational codes is required in this program. Additionally, the flow field in this type of mixer is sufficiently complex that an exact analytical model is computationally intractable. Assumptions will have to be made, but the experience base that is present at UTRC, along with the experimental facilities, will provide the best possibility for success in the development of this low emissions boost heater. For the case where 100% methane firing is desired, and in the humid air turbine (HAT) cycle, the ability to obtain stable combustion with acceptable emissions and pressure drop is the measure of success. The centrifugally enhanced mixer shows distinct promise for achieving these goals due to the fact that the combustor will be operating in a nearly fully premixed mode, which has been demonstrated to provide uniform temperature at the discharge and low emissions. The ultimate goal will be to provide an understanding of the centrifugal mixing process and apply this knowledge to design and test a sub scale mixer. From this knowledge base, a full scale mixer design can be suggested and the emissions predicted, so that the boost heater design can be further developed in the next phase of this program.

5.6 Gas Turbine Integration

Gas Turbine Integration

The gas turbine is the heart of the HIPPS/HITAF power system. Careful integration with the HITAF and other heat exchangers, the control system, and fuel supply is necessary to ensure efficient and reliable power generation. The gas turbine has flow interfaces with the HITAF at compressor discharge, duct heater inlet, and the gas turbine exhaust. The major integration requirement is the removal of the compressor discharge air at the end of the high pressure compressor and the return of the heated air from the HITAF to the duct heater. The heavy frame machine used as the basis of the Phase I commercial plant design has off−base combustors and requires little change to accommodate the HITAF. The advanced aero-derivative engine, however, will need design effort to identify the air handling requirements.

Approach: Generally, heavy frame gas turbines are arranged on a single shaft with the compressor followed by the combustor followed by the turbine (Figure 5.6-1). Aero engines often have multiple shafts with the low pressure spool (compressor and turbine) drive shaft concentric within the high pressure spool; often a separate power turbine to drive the electric generator is required (Figure

5..6-1b). The addition of intercoolers, recuperators, etc. call for large diffusers and collectors, extending the length of shafts, often requiring extensive changes in bearings and shaft load carrying capacity. To minimize this type problem, the FT4000 I/C has been designed as two separate spools, aligned end to end (Figure 5.6-1c). This results in a number of advantages:

- Direct drive from the LP spool at either 3000 or 3600 rpm (30 or 60 Hertz)
- Lower cost, industrial construction of the larger LP components
- Sufficient room for diffusers and collectors
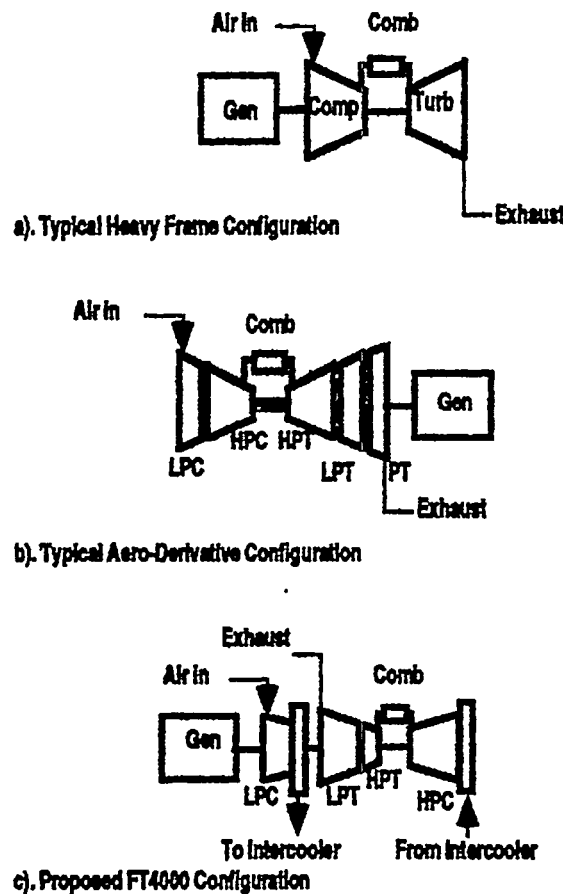- Flexibility in the combustor area.

a). Typical Heavy Frame Configuration

b). Typical Aero-Derivative Configuration

c). Proposed FT4000 Configuration

Figure 5.6−1   Gas Turbine Configurations.

This design concept reduces somewhat the constraints on the air handling at the end of the HPC. Nevertheless, the preliminary design of the diffusers and collectors for the HPC discharge/duct heater inlet will be an import part of the Phase II program plan. This design effort will be carried out by Pratt & Whitney in conjunction with UTRC; P&W will have cognizance over the diffuser/collector while P&W and UTRC will combine efforts on the duct heater arrangement.

305

Results: A typical diffuser for use at the end of the high pressure compressor is shown in Figure 5.6-2. It is anticipated that the design effort of P&W will result in a similar design, optimized for the operating conditions of the HITAF.
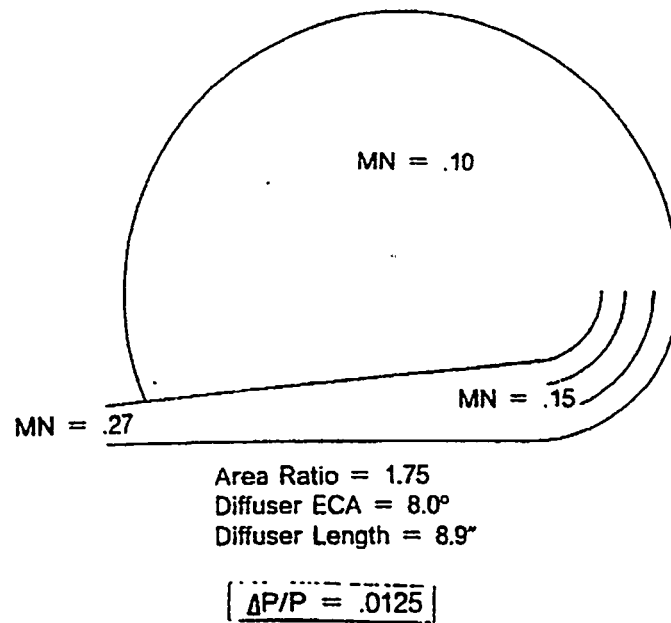

Area Ratio = 1.75
Diffuser ECA = 8.0°
Diffuser Length = 8.9"

$\Delta P/P = .0125$

Figure 5.6–2   HPC Diffuser/Collector Cross Section.

5.7   Subsystem Testing

To ensure successful operation of the HIPPS prototype plant, a 50 million Btu/hr test facility will be used to evaluate the performance of those critical subsystems for which a database for scale–up doesn't exist. The following subsystems will be tested 1) firing system, 2) radiant air heater, 3) convective air heater.

The objective of the firing system is to provide the appropriate heat flux distribution to the radiant surfaces to ensure heating of the process air from 1300°F to 1800°F, while minimizing NO_x emissions and carbon loss.

Performance and survivability of the radiant air heater will also be tested at this scale. The testing will establish the boundary conditions in terms of the gas (composition and temperature) and the particulate phase (concentration and physical state) at the air heater walls. Slag characteristics and their impacts on heater thermal performance will be evaluated. The effect of operating exposure on material/ component integrity (spalling, warping, etc.) will be assessed.

The testing will also provide the initial stage of the interaction between the ash/slag deposit and the air heater surfaces. However, long-term data on deposit-metal interactions will not be obtained in the testing. Smaller–scale testing will be used to examine the long-term performance of the radiant air heater materials using the boundary conditions determined from sub-scale testing.

306

A convective air heater section will be installed in the sub-scale test unit to evaluate the design for heat transfer effectiveness, extent of fouling and rate of degradation of heat transfer, as well as sootblowing effectiveness.

Analytical Approach: The simulation of pulverized coal combustion involves the modeling of a large number of complex, coupled physical and chemical processes. Use of computational modeling of furnaces at ABB Combustion Engineering Inc. is an important activity in the optimization of advanced firing systems. ABB C-E has evaluated and validated available computational fluid dynamic (CFD) codes from Reaction Engineering International (GLACIER), Brigham Young University (PCGC−3), and FLUENT, Inc. (FLUENT) for combustion and flow calculations at various laboratory scales as well as for field applications. Data from sub-scale testing on the Boiler Simulation Facility (BSF) has been used to validate the accuracy of both the flow fields and temperature/gas species levels for several cases. A simulation of a low-NO_x (staged) tangentially−fired coal combustion system is provided below.

The physical features of the BSF are outlined in Figures 5.7-3 and 5.7-4. An important aspect of these BSF simulations was to match the predicted and measured gas temperatures under coal firing. Predicted planar averaged temperatures at several vertical elevations, shown in Figure 5.7-1 as a function of boiler height, match reasonably the average measured temperatures. The oxygen concentration distribution at the horizontal furnace outlet plane (HFOP) for the measured and calculated cases also show good correspondence (Figure 5.7-2). For this particular test condition, the separated overfire air, located at the base of the arch, penetrates to the center of the furnace, but since the combustion is nearly complete, the oxygen is not fully consumed, yielding concentrations of up to 5% near the center of the test plane. A summary of the different types of CFD combustion simulations performed at ABB C−E is shown in Table 5.7-1.

ABB C-E in collaboration with REI will use computational fluid dynamic codes to support the combustor and firing system design. Various design alternatives will be studied to assess the following: (a) temperature distributions and heat flux to the walls, (b) thermal boundary conditions for radiant panels and ash deposition, (b) coal devolatilization rates and stoichiometry−temperature maps in the burner and overfire air zone to minimize NO_x emissions and (d) carbon burnout. The assessment will lead to selection of specific configurations which are likely to provide the desired thermal environment and the lowest carbon and NO_x emissions.
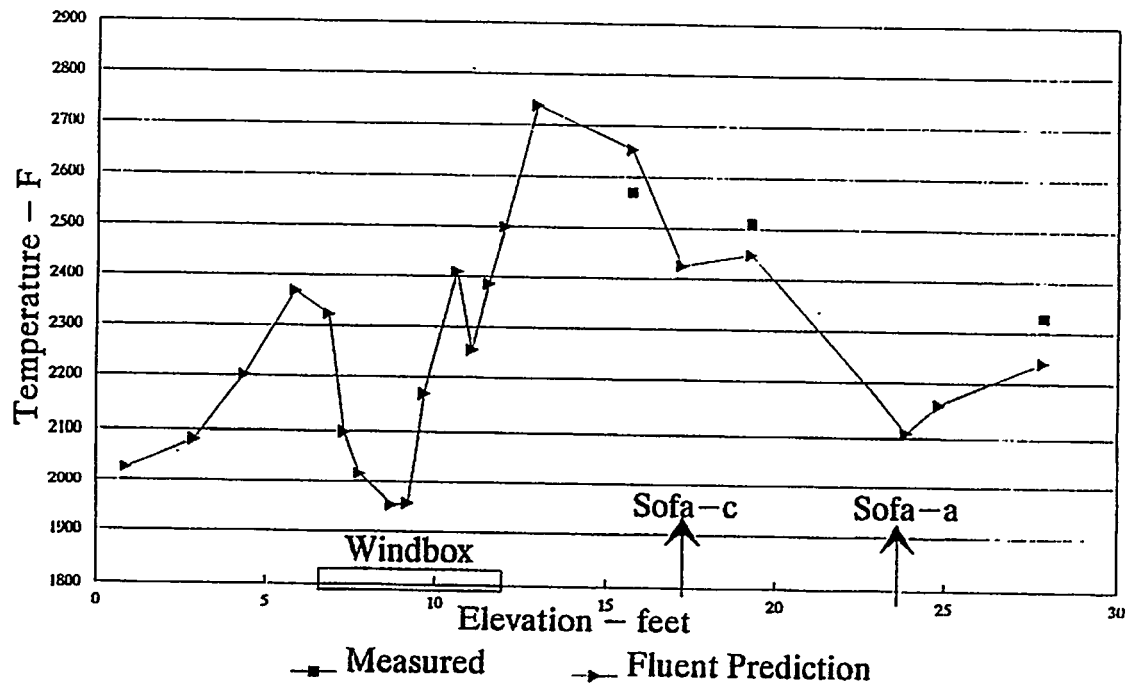
Figure 5.7−1   Comparison of Planar-averaged Predicted and Measured Gas Temperature in the BSF as a Function Of Elevation.

TABLE 5.7−1 CFD SIMULATIONS OF VARIOUS FURNACE TYPES

Furnace Types	Simulation Objectives	Details
Tangential, Pilot Scale	Coal and Oil combustion analysis	CFD reacting flow, Cartesian coordinates, 150,000 to 250,000 nodes, with coal combustion.
Recovery Boiler (CRU)	Air System Optimization, black liquor firing optimizations	Customized black liquor droplet combustion model, 200,000 to 250,000 nodes. Several units modeled to evaluate uprating potential.
Wood/Bark Furnaces	Furnace shape · optimization, minimization of CO and particulate carryover	Reacting and isothermal simulations of new and retrofit units for wood, biomass, and refuse derived fuels.
Incinerators	Overfire Air Optimization	Quasi−3D slice models with gaseous combustion. 60−80,000 nodes.

(a) Experimental

ARCH

LEFT — RIGHT

1.00, 4.10, 5.00, 1.75
1.25, 4.53, 5.00, 2.90
2.55, 4.85, 5.40, 1.75
3.00, 4.10, 3.50, 3.00

FRONT
0.00 0.34 0.67 1.01 1.34 1.68 2.01 2.35 2.68 3.02 3.35
2.21 1.99 1.77 1.55 1.33 1.11 0.88 0.66 0.44 0.22 0.00

(b) Calculated

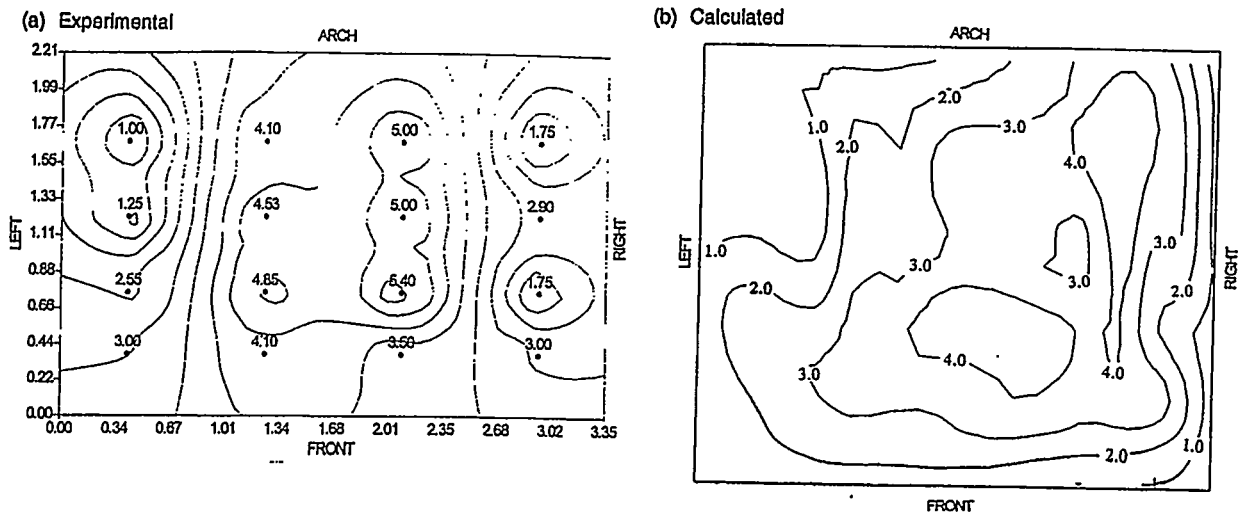ARCH

LEFT — RIGHT

1.0 2.0 3.0 4.0 2.0 1.0

FRONT

Figure 5.7−2 Comparison of Predicted and Measured Oxygen Mole Fraction Contours at the BSF Arch (HFOP) Elevation, (a) Experimental and (b) Calculated
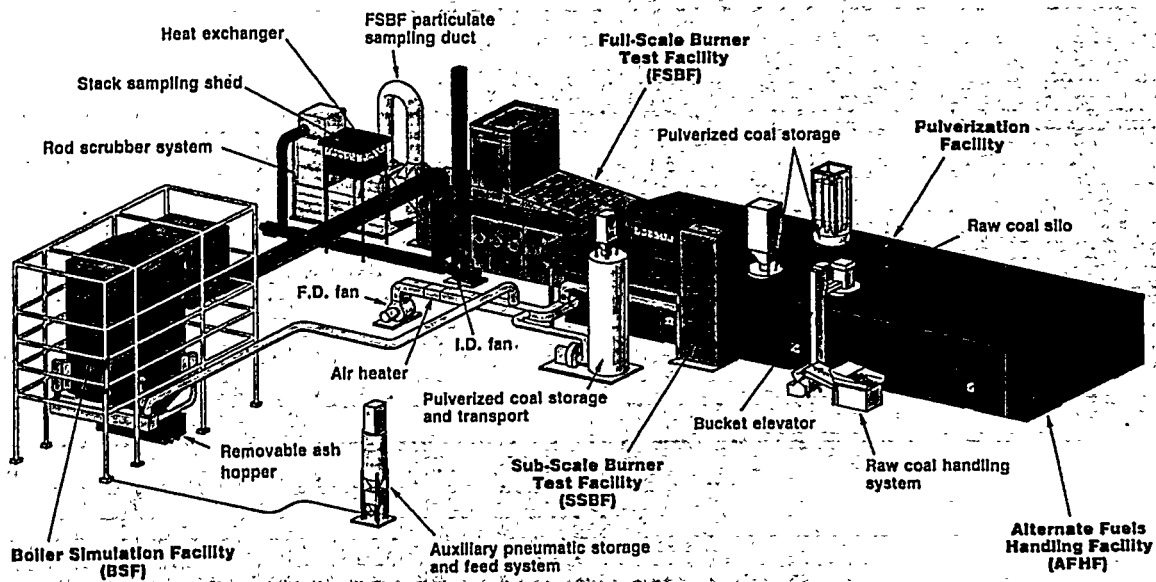

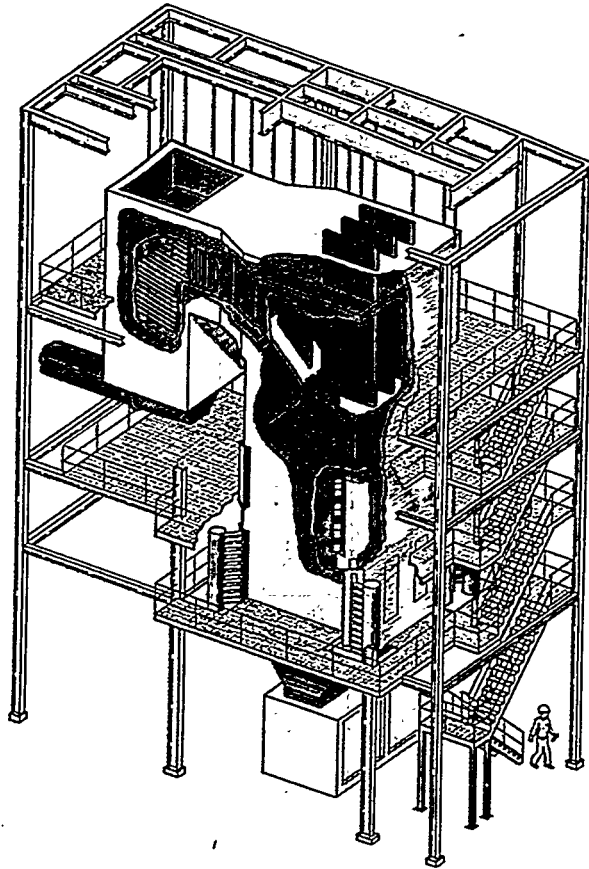Figure 5.7−3 ABB CE's Firing System Development Complex (FSDC).

309

Figure 5.7−4. ABB CE's 50x10^6 Btu/hr Boiler Simulation Facility (BSF).

Experimental Approach: *Description of Existing Facilities* − The sub-scale testing will be performed in ABB−CE's Firing System Development Complex (FSDC) shown in Figure 5.7-3. The current complex houses a 50x10^6 Btu/hr upward flowing tangentially-fired furnace, the Boiler Simulation Facility (BSF), which is shown in Figure 5.7-4. This combustion facility is designed to accurately model the aerodynamic and thermal conditions including the residence time-gas temperature profile, heat release and heat absorption characteristics of a large utility boiler. The furnace walls and heat transfer surfaces are cooled by a surrounding water jacket. Furnace gas temperature profiles as well as the horizontal furnace outlet plane (HFOP) gas temperature are replicated to full-scale by selective refractory lining of the furnace waterwalls.

The BSF includes simulated waterwall panels and deposition probes to obtain ash deposition data in the lower furnace. Ports located in proximity to these panels/probes are typically used to determine the deposition boundary conditions with respect to the gas and particulate characteristics. The upper furnace has simulated superheater and reheater panels, and downstream of these panels, the furnace gases enter a convective pass formed by a series of tube bundles similar to that in an actual boiler. The BSF also includes sootblowers for cleaning the heat transfer surfaces both in the furnace

310

and in the convective pass. Data on heat flux recovery at the various locations can be obtained as a function of the operating condition for different fuels.

The BSF is fully instrumented to monitor combustion phenomena. Access ports (Fig. 5.7-5) are located throughout the furnace, convective sections and stack for temperature (suction/acoustic pyrometer), gas composition, velocity (laser Doppler velocimetry) and particulate measurements. Continuous sampling for gas composition (analyzers, gas chromatograph, FTIR) is performed by transferring the furnace gases via a heated sample line to a gas conditioning system and then to the respective analyzers. Optical ports are also distributed around the furnace for visual observations and video. Critical furnace operating and test measurements are taken, recorded and displayed by the facility's computerized MOD300 Distributed Control System (DCS) and Data Acquisition System.
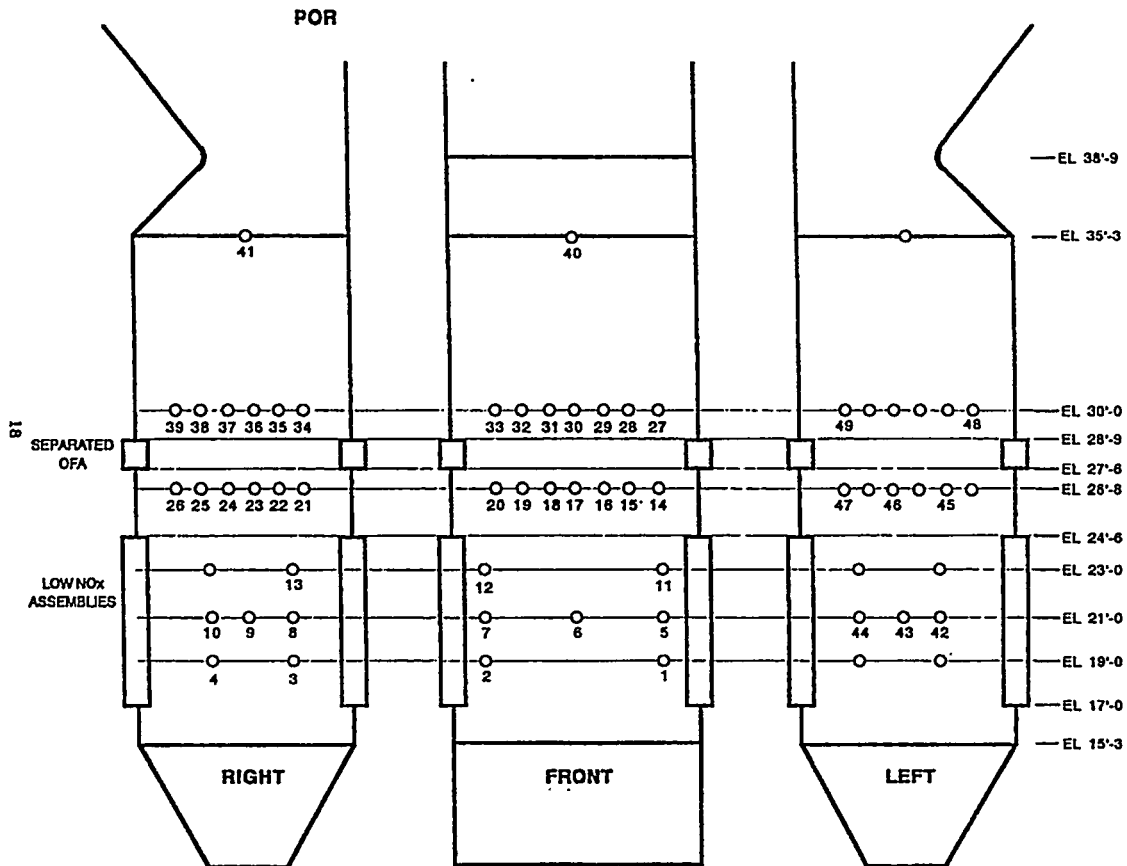
Figure 5.7–5   Sampling Port Locations at the Boiler Simulation Facility.

The FSDC includes complete coal handling and pulverizing equipment as well as oil and gas storage and supply systems. In addition to the BSF, the FSDC supports two large single burner combustion facilities capable of multi–fuel firing at rates up to 150×10^6 Btu/hr (45 MW$_t$). The FSDC houses the FD and ID fans, combustion air preheater, and the flue gas scrubbing systems.

311

The current state-of-the-art tangential firing system is incorporated into the BSF and includes the following:

1. ABB C−E's advanced HP series pulverizer with an integral dynamic classifier (Figure 5.7−6). The dynamic classifier is designed to produce coal fineness levels of approximately 98.5% smaller than 100-mesh and 85% smaller than 200-mesh. Rotating classifier vanes impart centrifugal forces on coal particles as they are transported, separating the smaller (than the design size) particles into the exit stream and retaining the larger particles for further pulverization. The improved classification approach reduces the population of coarse particles while not over-grinding the fine particles (Figure 5.7−3). A fine degree of control in pulverization offered by the above system minimizes combustible losses (unburned carbon) and helps control ignition at the coal nozzle tip, enhancing fuel−bound nitrogen conversion and its subsequent reduction to N_2 under staged conditions.

2. Flame attachment nozzle tips. The rapid fuel ignition associated with this tip produces a stable volatile matter flame and minimizes NO_x production in the fuel−rich stream.

3. Concentric Firing System (CFS). Horizontally offsetting some of the windbox secondary air flow makes less air available to the coal stream during the early stages of coal combustion. It also creates an oxidizing environment near the waterwalls in and above the firing zone, reduces ash deposition and increases lower furnace heat absorption. Increased O_2 levels along the waterwalls also reduces waterwall corrosion potential.
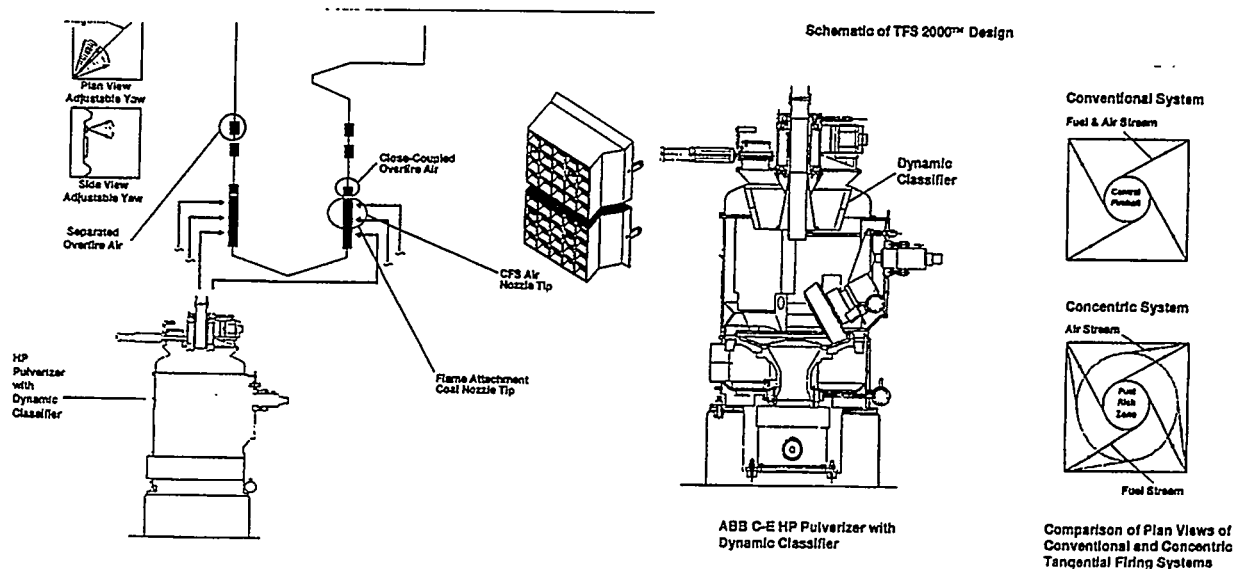

Figure 5.7−6   Schematic of ABB C−E's TFS−2000 Low−NO_x firing system, HP Pulverizer with Dynamic Classifier, and Plan View of Conventional and Concentric Tangential Firing System.

312

4. Close-coupled over fire air (CCOFA). A portion of the secondary air is introduced through registers at the top of the main windbox to improve carbon burnout without increasing NO_x production.

5. Firing zone stoichiometry control through multiple separated overfire air ports (SOFA). Two or more discrete levels of overfire air with adjustable tilt and yaw positioning are incorporated in the furnace corners between the main windbox and the furnace outlet to create the optimum stoichiometry-temperature history for NO_x minimization and carbon burnout.

Facility Modifications (Design, Preparation and Construction) – The existing Firing System Development Complex will be used in the proposed program along with a modification to the associated 50×10^6 Btu/hr Boiler Simulation Facility (BSF). Use of the existing facility is an extremely cost–effective approach to meet the objectives of the proposed project.

The main technical requirements that have an impact on the hardware include the following:

- Slagging furnace
- Secondary air preheating to $850°F$ and oxygen concentration 17–18%
- Flame temperatures around $3000°F$
- Bottom slag removal.

Since the HIPPS prototype furnace will be a slag–tap furnace, there are advantages to operating it in a down–fired mode particularly in terms of reducing slag buildup on the burners. Up-firing, on the other hand, will be less expensive to the program because of lower facility modification costs. Both up–firing (conventional design) and down–firing the BSF were therefore considered for subsystem testing and respective cost and performance benefits determined.

The down–fired configuration for the BSF included the following additional modifications compared to up–firing:

- – removal of the existing arch
- – extension of the waterwall to block existing backpass
- – rerouting of the fuel and air lines to the top of the furnace
- – installation of the windbox at the top
- – increased structural support
- – removal of existing convective surface and relocation at the furnace exit (bottom).

Costs associated with these additional modifications were judged to be disproportionate to the benefits for downfiring in this test.

Up–firing is the present choice for the project since the BSF testing is only required to evaluate the performance of the individual subsystems (firing system, radiant panels, convective section) and

313

not the integrated system. The correct boundary conditions (temperatures, heat fluxes and flow) for this evaluation can be provided equally well in the up−fired configuration. Two issues need to be considered when comparing up−firing vs. down−firing: buoyancy (natural convection) and particle settling. The bulk velocities in the furnace are sufficiently high compared to the natural convective velocity (low Grashof number) that forced convection remains the dominant flow characteristic. Also, the bulk flow velocities (15 ft/s) in the furnace are much higher than the terminal velocities for the largest coal particles (0.5 ft/s) so that particle settling is minimal.

The following modifications will be made to the BSF for the HIPPS subsystem testing:

- Modify firing system to obtain design heat fluxes for the HIPPS furnace (increased firing rate, add refractory to roof and waterwalls)
- Upgrade air heater and ductwork to 850°F
- Install new windbox components (integrate with pulverizer, control individual nozzle flows)
- Quench of combustion gases prior to SOFA introduction (add flue gas recirculation ducts, nozzles)
- Reconfigure hopper for slag collection
- Modify backpass, if necessary (ductwork, add convective surface to cool gases to acceptable exit level)
- Upgrade flue gas cleanup system (add baghouse)
- Install radiant air heater panels, convective air heater test section, other subsystem test units
- Modify MOD 300™ furnace control system
- Integrate flow, temperature and other test measurements to data acquisition system

The design of the subsystem test units will be based on the engineering R&D conducted in Task 2 and on the requirements of the HIPPS commercial plant design. Each subsystem will include all the instrumentation; materials of construction; and facilities for the delivery, storage, handling and disposal of all the materials and reagents required for operating the test unit. The subsystem test units will be designed to:

- Provide adequate instrumentation to achieve test objective
- Provide reliable testing conditions and operation periods necessary to obtain the data for scale-up to the commercial plant
- Provide for cost-effective evaluation of materials of construction suitable for use in the HIPPS commercial plant at the relevant conditions
- Comply with applicable codes and standards for personnel and operation safety
- Provide cost-effective operations by using to extent possible existing contractor facilities and components and performing cost-effective modification and construction of new facilities

314

Benchmarking Experiments — The Boiler Simulation Facility has demonstrated the ability to generate temperature profiles, carbon burnout and NO_x emission values consistent with utility boiler measurements on similar, retrofittable, combustion system arrangements. For example, the performance of an earlier low-NOx firing system design tested on the BSF and in a 160 MW$_e$ utility boiler in Italy is shown in Figure 5.7-7. Good correlation between the BSF and field data is evident.
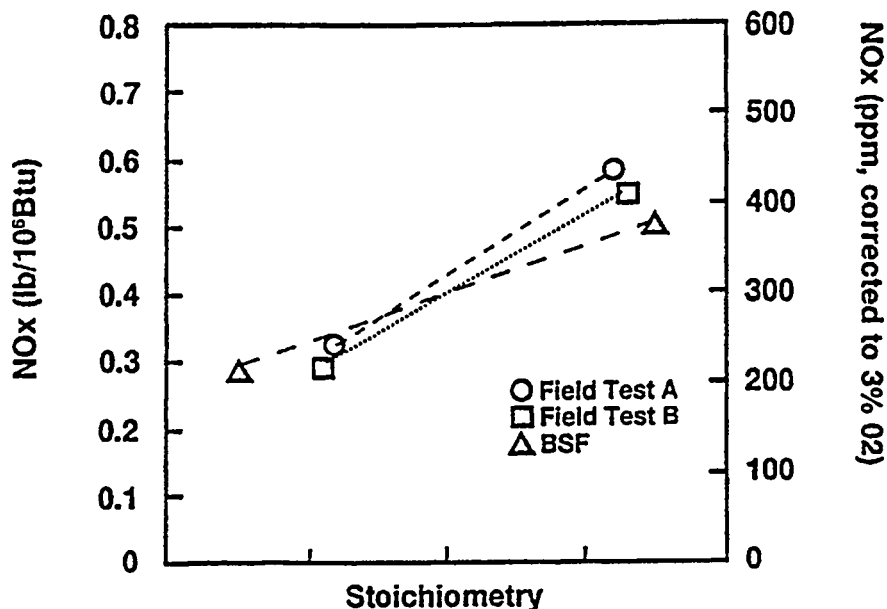

Figure 5.7-7   Comparison of Field and BSF NO_x Emissions.

With pulverized coal firing, NO_x emissions are strongly influenced by oxygen availability in the early stages of combustion. The availability of oxygen in the early stages is characterized by the parameter "main burner zone stoichiometry", the ratio of oxygen available to that required for complete fuel oxidation in the zone of fuel introduction. Figure 5.7-8 shows that as the main burner zone stoichiometry is reduced to optimum levels, NO_x levels are dramatically reduced to 0.14 lb./10^6 Btu (106 ppm). Figure 5.7-8 also shows that carbon emissions increase with reduced stoichiometry but are still less than 5% carbon-in-flyash at the optimum condition. Low levels of carbon and NO_x emissions have been demonstrated for a range of coals in the BSF and in the field.

Figure 5.7-9 shows the effect of improving coal fineness (using a dynamic classifier on the pulverizer) beyond current industry standards on unburned carbon and NO_x emissions for several candidate low-NO_x firing system configurations. Not only does the unburned carbon levels decrease substantially, NO_x emissions are reduced as well due to the release of a higher fraction of the coal nitrogen into the volatile phase and its subsequent conversion to N_2.

The advanced firing system with integration of the developments in coal pulverization technology, advanced fuel admission assemblies and in-furnace staging techniques has been able to control NO_x emission below 0.15 lb./10^6 Btu, while holding carbon-in-flyash levels to less than 5%, and CO emissions to less than 50 ppm. Good correlation of the BSF test results with data from field units
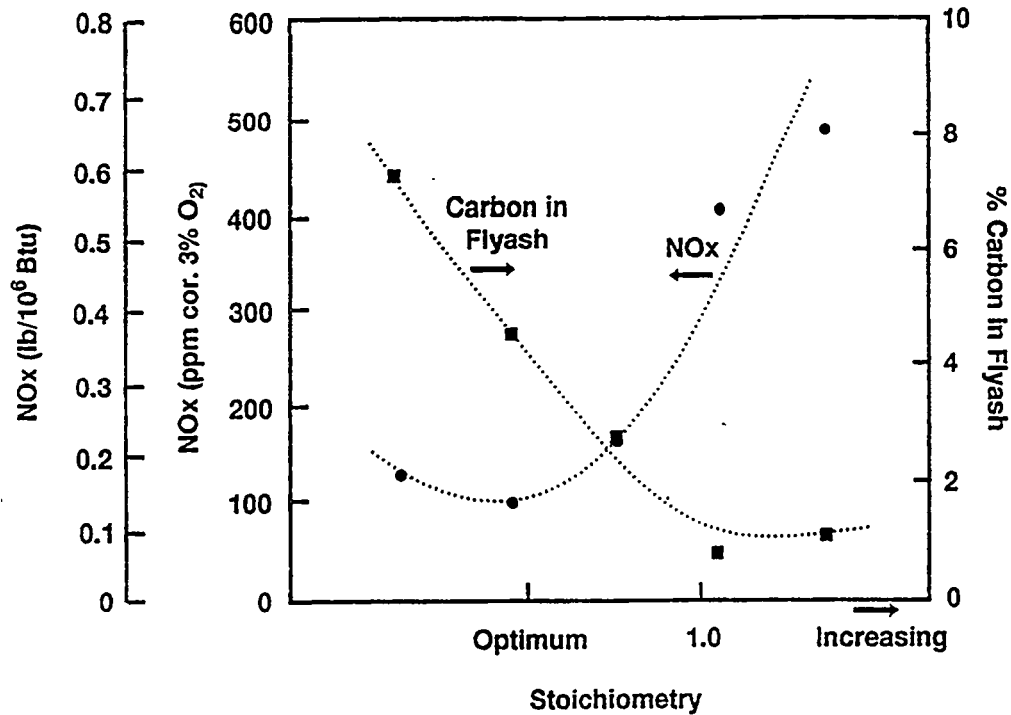
315

Figure 5.7-8   NO$_x$ and % Carbon in Fly Ash versus Main Burner Zone Stoichiometry (TFS 2000™ Firing System Firing Coal).
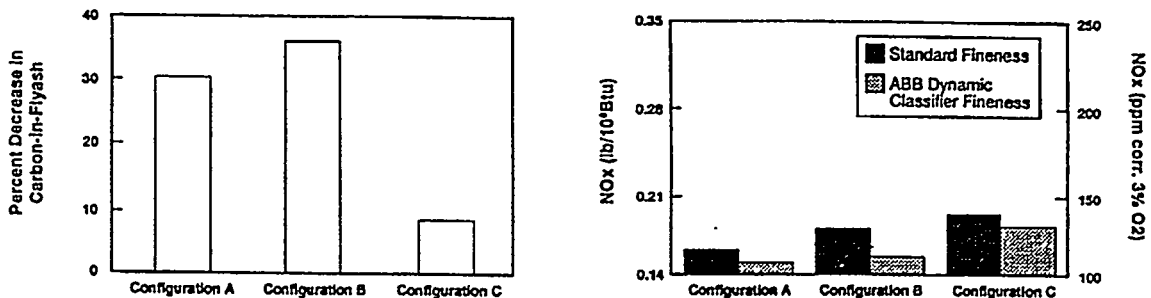
Figure 5.7-9   Effect of Coal Fineness on NO$_x$ and Unburned Carbon Emissions.

retrofitted with the advanced firing system provides confidence in being able to achieve the NO$_x$ levels in the HIPPS combustor as well as being able to subsequently scale-up to a larger demonstration unit.

Test Program (Test Matrix, Measurements, Use of Data) — Test Matrix — Tests will be performed in the BSF at a firing rate of 50x10^6 Btu/hr or higher, as determined by furnace design calculations, with the new firing system. The new firing system will have the capability to control individual air and coal nozzle flows to allow determination of the optimum firing configurations.

The following test matrix will be executed to examine the effect of the various operating variables on system performance including, heat transfer to the radiant panels and convection test section, NO$_x$ emission, carbon burnout, turndown and fuel flexibility.

316

A total of 3 weeks (360 hours) of testing with data collection will be performed on the project. A portion of the first week of testing will involve shakedown of the firing system, test panels and various measurement systems. Parametric testing will be performed in the remainder of the first two weeks as per the test matrix provided in Table 5.7-2. The objective of the parametric testing is to provide comprehensive data on the heat transfer to radiant and convective test sections, NO_x emissions and carbon burnout, while operating the firing system over a wide range of conditions. These tests will also help identify the set of optimum values for the operating variables, which will be used for detailed testing in the third week. Detailed testing will involve in-furnace maps of temperature, gas composition, velocities to establish conditions for model validation and scale-up. Continuous performance of the radiant and convective section test panels over a 120 hour period will also be obtained, as well as fly ash size and air toxics measurements to provide critical input for emission control system design.

Test Measurements – The measurements to be taken during testing and the use of the data are shown in Table 5.7-3. Gas temperature distribution at different locations will be obtained using suction pyrometer. An acoustic pyrometer will be used to continuously monitor the furnace outlet temperature (FOT) to note changes with operating conditions. The FOT is a critical parameter for proper operation of the convective air heater. It is expected that for a given fuel, fouling will accelerate and become unacceptable above a critical FOT value. All operating parameters such as air flows and fuel flows are recorded continuously by the data acquisition system. Burner set points and operating pressures are also recorded.

TABLE 5.7–2 TEST MATRIX

Test Series	Operating Variables	Comments/Objectives
1	Firing rate	Incident and transmitted heat flux to radiant panels, slag layer thickness, turndown capability
2	Air/coal flow split between main burner zone and SOFA, air split in SOFA ports	Heat transfer, NO_x, carbon burnout
3	Air/coal flow split to individual nozzles Nozzle design	Spatial heat flux distribution, slag flow distribution
4	Quench zone (between main burner zone	Effect of attached vs. lifted flame
5	and SOFA) characteristics – temperature, residence time, cooling media	Minimize thermal NO formation, impact on convective air heater – heat transfer and deposition
6	Pulverizer operation (transport air/coal, transport air temperature & composition, coal fineness	Integration of pulverizer with firing system to minimize carbon loss, NO_x
	Coal type	System performance vs. fuel composition
7		

TABLE 5.7-3 TEST MEASUREMENTS AND USE OF DATA

Measurements	Locations	Comments
Gas temperature	In–furnace, HFOP	Critical for heat flux
Gas composition	In–furnace, HFOP, stack	System performance (NO_x, CO emissions)
Gas velocity	In–furnace	Flow distribution
Particulates (size, concentration)	In–furnace	Carbon content, ash composition affects deposit properties and heat transfer
Deposit/slag	Test panels, furnace bottom	Affects heat transfer
Incident heat flux	Test panels	Heat transfer vs. operation
Transmitted heat flux	Test panels	Heat transfer vs. operation, time, cleanability
Flyash loading, size and composition	Duct before baghouse	Affects performance of particulate removal device, particulate emissions
Air toxics organics inorganics Advanced diagnostics	Before and after baghouse	Emission rates of VOCs, PAHs, metals

In-furnace gas composition measurements will be made using multiple techniques. Measurements of O_2, CO, CO_2, SO_2 and NO_x are made with dedicated analyzers. A Fourier Transform Infrared instrument will be used to measure additional species such as NH_3, HCN, H_2S, COS and hydrocarbons. A gas chromatograph will be used to measure H_2. Gas samples are extracted using a stainless steel water-cooled probe connected to a vacuum pump. Large capacity submicron filters are placed before the analyzer to separate unburned carbon and ash particles from the measured gas stream. Examples of test results are shown in Figure 1.4.7-10, where the furnace NO_x concentration distribution is shown. In-furnace gas velocities will be measured either with a five-hole pitot probe or with a laser-Doppler velocimeter. Both techniques have been used successfully in the BSF with coal firing.

Particulate samples will be collected using a water-quenched probe within the furnace, in particular at locations close to the radiant panel and convective test sections to determine the particle flux and composition (carbon content, ash composition and state) arriving at the heat transfer surfaces. Deposit and slag samples will also be collected from the test panels for subsequent analyses by microscopic techniques (computer controlled scanning electron microscopy) to determine the composition distribution from the heat transfer surface to the fireside.

Incident and transmitted heat fluxes will be obtained for the radiant test panels in a time–resolved manner through start-up, upon achieving steady state and during turndown. Incident heat flux will be determined using a radiometer, while transmitted fluxes will be determined by monitoring the air temperatures entering and leaving the test panels. Similar data will be obtained for the convection pass with the emphasis on measuring combustion gas temperatures and velocities in
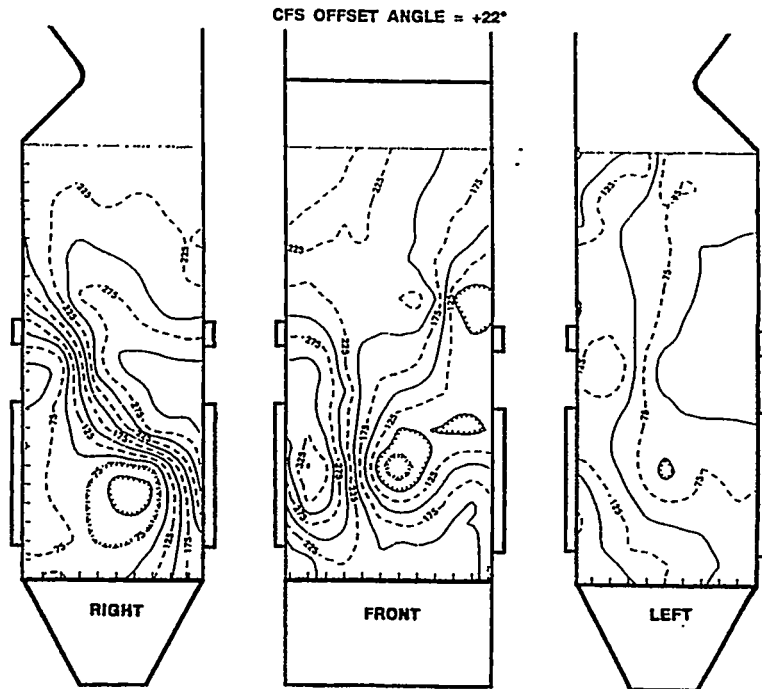
318

Figure 5.7–10 Gas Concentration on BSF Furnace Waterwalls (NO$_x$ in ppm by volume).

the vicinity of the test section. Cleanability measurements will also be obtained in regions where sootblowers will be operated by examining the heat flux recovery upon sootblowing.

The firing conditions in the HIPPS combustor is significantly different from standard PC firing in that higher combustion temperatures will be experienced. This is likely to increase the vaporization of the ash and hence skew the fly ash size distribution to smaller sizes. Since the size distribution entering the particulate removal device, in particular the concentration in the submicron size fraction, is critical in determining particulate emissions, detailed size-fractionated fly ash samples will be obtained at the stack. An Anderson cascade impactor will be used for this purpose. These samples can also be analyzed for trace metals to determine the potential inorganic air toxic emissions likely when this firing system is coupled to a specific particulate removal device. Organic air toxics (VOCs, PAHs) will also be measured using standard EPA methods.

Use of Data:

Analysis of Results: After the conclusion of the subsystem tests, ABB C-E will critically evaluate the results of all the tests performed with respect to firing system performance.

The evaluation of the firing system performance will include the following:

— Summary of all primary experimental data, data reduction, engineering analysis, and computations.

— Summary and analysis of all results

— Comparison of results with the objectives of the RD&T plan to determine the extent to which research needs were successfully addressed, and residual needs analysis

319

- Critical re-evaluation of the firing system to assess whether it is ready for further scale-up and inclusion into the final design of the POC Test Facility
- Development and analysis of a work plan, schedule, and resources required for continued firing system development.

The parametric testing of the firing system will yield the desirable optimal firing configurations and operations that will provide the correct thermal environment for heat transfer to the radiant air heater as well as minimize the carbon and NO_x emissions.

A procedure which sequentially optimizes the firing system operation for the critical variables will be used. First the optimum split of air flows between the main burner zone and the separated over fire air ports will be determined in the testing. Competing requirements of high flame temperature (achieved at burner zone stochiometry near 1.0) and low NO_x is likely to alter the air splits in comparison to current p.c. firing systems. The quench requirements between the main burner zone and the separated over-fire air ports will also be established from the testing. Again, high levels of NO_x formation will occur if the temperature in the region where the final burnout air is added is high. The residence time required at the reduced stoichiometry will also be determined by running tests with different splits among the overfire air ports.

The parametric tests will also provide information on how to minimize costs of the firing system. Reduction in the requirement of separated over-fire air, smaller windbox pressure drop, simplicity in windbox and nozzle design, smaller number of penetrations into the furnace, etc. will all contribute to reducing firing system costs. Test data for the different configurations will enable selection of the best firing system design with respect to both cost and performance.

The detailed mapping of in-furnace heat flux, gas composition, temperature, velocities and particulates will allow determination of the gas and coal transformation history that is responsible for the desirable firing system characteristics. Computational 3-D codes such as FLUENT, other in-house proprietary firing system performance models, and associated scaling criteria will be used to achieve the above desired distribution of values of heat flux, temperatures, etc., for the full-scale unit.

5.8 RD&T Summary, Schedule and WBS

The RD&T plan for Phase II of this program is outlined in sections 5.1 through 5.7. This plan includes a wide variety of analytical and experimental efforts. The analytical work includes modeling of complete power plants and cycle optimization as well as models of slag properties, heat transfer, structural mechanics, combustion, NO_x chemistry and 2-D and 3-D fluid flow. The experimental work proposed includes lab scale, pilot scale and subsystem testing. The program contains a logical progression of less expensive small scale testing of materials and components, to intermediate pilot scale testing of components in place, followed by the more expensive testing of those components whose performance can not be scaled up from small scale tests.

Our program has been laid out to maximize the testing benefit per unit cost. For the small lab scale testing we are utilizing existing facilities at UTRC and UNDEERC, including the UTRC Jet Burner Test Stand erosion/corrosion rig which can simulate the temperature and ash impingement conditions anticipated in the HITAF. We are also planning our subsystem testing at 50 M Btu/hr for the ABB CE boiler simulation facility (BSF). This is a well-documented facility with the full range of instrumentation in place and capability for FGR and flue gas treatment. The only new construction will be the 2M Btu/hr pilot–sized furnace at UNDEERC. This size was selected as optimum for testing both radiant and convective air heaters, slag screen designs and the refractory coating materials. While major savings can be realized by testing at the pilot size some systems are thought not to scale well from this size. This is true for the firing system which will be tested at 50 M Btu/hr subsystem size. Since the operation of the injectors, the flame itself, and radiative heat transfer are independent of buoyancy we have initially chosen to test the HITAF components in an upfired configuration. The cost savings from avoiding modification to the BSF is significant and should allow for a more thorough testing program.

6.0 REFERENCES

ACAA. "State Solid Waste Regulations Governing the Use of Coal Combustion Byproducts (CCBs)," American Coal Ash Association 1995.

ACAA. "Combustion Byproduct (CCB) Production & Use: 1966-1993," report for coal-burning electric utilities in the United States, American Coal Ash Association, 1994.

Anderson, D. W., R. Viskanta, and F. P. Incropera, *J. Eng. Gas Turb. and Pow.*, 109, 215, 1987.

Baker, W. B., S. M. Ray, and A. M. Landry, "Investigation of Coal Combustion By–Product Utilization for Oyster Reef Development in Texas Bay Waters," in Proceedings of the 9th International Ash Use Symposium – Volume 2: Stabilization and Aquatic Uses; Orlando, FL, Jan. 22-25, 1991; EPRI GS-7162, Project 3176, pp 48-1–48-14, 1991.

Barsotti A. F., and R. Kalyonco, "Implications of Flue Gas Desulfurization on the Mineral Industries," Proceedings of the 4th International Conference on FGD and Other Synthetic Gypsum, Toronto Canada, U.S. Bureau of Mines, May 17-18, 1995.

Bearce, B. C., D. L. Lentz, M. A. Woodard, and E. C. Townsend, "Coal Bottom Ash as a Root Substrate for Marigolds in a Closed Loop Nutriculture System," in Proceedings of the 10th International Ash Use Symposium – Vol. 1: High–Volume Uses/Concrete Applications; Orlando, FL, Jan. 18-21, 1993; EPRI TR-101774, Project 3176, pp. 13-1–13-16, 1993

Beeghly, J. H., J. Bigham, and W. A. Dick, "The Ohio-Based Study on Land Application Uses of Dry FGD By-Products," in Proceedings of the Tenth International Ash Use Symposium – Vol. 2: Ash Use R&D and Clean Coal By–Products, Orlando, FL, Jan. 18-21, 1993; EPRI TR-101774, Project 3176, pp. 59-1–59-14, 1993.

Bennett, O. L., J. L. Hern, and W. L. Stout, "Fluidized-Bed Combustion Waste, a Potential Agricultural Soil Amendment," in Proceedings of the Governor's Conference on Expanding the Use of Coal in New York State: Problems and Issues; Tress, M.H.; Dawson, J.C., Eds.; Albany, NY, May 21-22, pp.43-48, 1981.

Benson, S. A., and P. L. Holm, "Comparison of the Inorganic Constituents in Three Low-Rank Coals," *Ind. Eng. Chem. Prod. Res. Dev.* 24, 145-149, 1985.

Bergeson, K. L., and D. R. Overmohle, "Reclaimed High-Calcium Fly Ash Use as a Highway Base Material," In Proceedings of the 9th International Ash Use Symposium – Vol. 2: Stabilization and Aquatic Uses, Orlando, FL, Jan. 22-25, 1991; EPRI GS-7162, Project 3176, pp. 44-1–44-13, 1991.

Bird, R. B., W. E. Stewart, and E. N. Lightfoot, Transport Phenomena, John Wiley & Sons, New York, p.37, 1960.

Boni, A. A. et al., "Transformations of Inorganic Coal Constituents in Combustion Systems," Phase I Final Report, Contract DE–AC22–86PC 90751, 1990.

Burnham, J. C. "Use of Coal Ash Products as Alkaline Admixtures in the Sludge Stabilization Process," In Proceedings of the 10th International Ash Use Symposium – Vol. 1: High-Volume Uses/Concrete Applications, Orlando, FL, Jan. 18-21, 1993; EPRI TR-101774, Project 3176, pp. 1-1–1-1, 1993.

Butt, D. P., J. J. Mecholsky, and V. Goldfarb, Effects of Sodium Silicate Exposure at High Temperature on Sintered-Silicon Carbide and Siliconized Silicon Carbide, *J. Amer. Ceram. Soc.,* Vol. 72, pp. 1628-1635, 1989.

Calvert, S. et al., "Entrainment Separators for Scrubbers – Final Report", prepared for EPA, August 1975.

Clark, R. B., K. D. Ritchey, and V. C. Baligar, "Dry Matter Yields of Maize Grown with Coal Combustion By–Products," in Proceedings of the 10th International Ash Use Symposium-Vol. 1: High-Volume Uses/Concrete Applications, Orlando, FL, EPRI TR-101774, Project 3176; pp. 15-1–15-11, Jan. 18-21, 1993

Clarke, L. B., "Utilization Options for Coal–Use Residues: An International Overview," in Proceedings of the 10th International Ash Use Symposium-Vol. 2: Ash Use R&D and Clean Coal By–Products, Orlando, FL,Jan. 18-21, 1993; EPRI TR-101774, Project 3176, pp. 66-1–66-14, 1993.

Culley, R. W. and O. H. Smail, "Performance of Waste Coal Ash as a Highway Subbase Course," reprinted with permission for inclusion in Think Fly Ash, Proceedings of the Utilization of Ash and Concrete Pavement Repair Conference; University of North Dakota, Grand Forks, ND, May 14-16, 1986.

Courts, G. D. "The Aggregate of the Future is Here Today," in Proceedings of the 9th International Ash Use Symposium – Volume 1: Concrete and Related Products, Orlando, FL, Jan. 22-25, 1991; EPRI GS-7162, Project 3176, pp. 21-1 to 21-10, 1991.

Donnelly, J. R., E. S. Jons, and W. C. Webster, "Synthetic Gravel from Dry Flue Gas Desulfurization End–Products," reprinted with permission for inclusion in Think Fly Ash, Proceedings of the Utilization of Ash and Concrete Pavement Repair Conference; University of North Dakota, Grand Forks, ND, May 14-16, 1986.

Dunstan, E. R., Jr., "Freeze-Thaw and Dicer Scaling Resistance of Concretes Containing Fly Ash," in Proceedings of the 9th International Ash Use Symposium – Volume 1: Concrete and Related Products, Orlando, FL,Jan. 22-25, 1991; EPRI GS-7162, Project 3176, pp. 11-1–11-11, 1991.

Easler. T. E., C. Tan, and L. M. Putz, Influence of Oxidizing and Reducing Environments on Coal-Slag-Induced Corrosion of Silicon Carbide Ceramics, Report ANL /FE-85-11, 1985.

Federer, J. I., "High-Temperature Corrosion of Heat Exchanger Materials" in *Ceramic Transactions,* Vol. 10, R. E.Tressler and M. McNallan, eds., pp. 425-443, The American Ceramic Society, Westerville, Ohio, 1990.

Ferber, M. K. and V. J. Tennery, Evaluation of Tubular Ceramic Heat Exchanger Materials in Acidic Coal Ash from Coal-Oil Mixture Combustion, Report ORNL/TN-7958, 1981.

Ferber, M. K. and V. J. Tennery, "Evaluation of Tubular Ceramic Heat Exchanger Materials in Basic Coal Ash from Coal-Oil Mixture Combustion" ORNL/TN-8385, 1982.

Ferguson, G., and J. J. Zey, "Stabilization of Pavement Subgrade with Class C Fly Ash," in Proceedings of the 9th International Ash Use Symposium - Volume 2: Stabilization and Aquatic Uses, Orlando, FL,Jan. 22-25, 1991; EPRI GS-7162, Project 3176, pp. 42-1 – 42-14, 1991.

Flagan, R. C., and J. H. Seinfeld, Fundamentals of Air Pollution Engineering, Prentice–Hall, Englewood Cliffs, NJ, 1988.

Fox, D. S., N. S. Jacobson, and J. L. Smialek, "Hot Corrosion of Silicon Carbide and Silicon Nitride at 1000 C." in Ceramic Transactions, Vol. 10, R. E. Tressler and M. McNallan, eds., pp. 227–249, 1990.

Freihaut, J. D., W. Proscia, and B. A. Knight, "Combustion Properties of Micronized Coal for High Intensity Combustion Applications," Final Report DOE Contract DE-AC22-80263, April 1989.

Gallagher, N. B., L. E. Bool, J. O. L. Wendt, T. W. and Peterson, Combust. Sci. Tech., 74, 211, 1990.

Goldstein, S., Modern Developments in Fluid Dynamics, Dover Publications, Inc., New York, NY, 1965.

Gorsline, "The Use of Fly Ash and Pozzolans in the Production of Lightweight Aggregates for Industry," presented at the 3rd International Conference on the Use of Fly Ash, Silica Fume, Slag and Natural Pozzolans in Concrete, Madrid, Spain, April 21-25, 1986.

Gray, D. H., E. Tons, W. H. Berry, and U. W. Stoll, "Post Construction Monitoring and Performance Evaluation of a Cement Stabilized Fly Ash Base," in Proceedings of the 9th International Ash Use Symposium – Volume 2: Stabilization and Aquatic Uses, Orlando, FL, Jan. 22-25, 1991; EPRI GS-7162, Project 3176, pp. 45-1–45-16, 1991b.

Grimson, Trans. Am. Soc. Mech. Eng., 59, 583, 1937.

Hansen, M. and Anderko, K., Constitution of Binary Alloys, second edition, McGraw-Hill Book Company, p.713, 1985.

Hastie, J. W. and D. W. Bonnell, "A Predictive Phase Equilibrium Model for Multicomponent Oxide Mixtures – Part II. Oxides of Na-K-Ca-Mg-Al-Si," High Temp. Sci. 19, 275-306, 1985.

Hay, P. D., and E. R. Dunstan, Jr., "Lightweight Aggregate Production and Use in Florida," in Proceedings of the 9th International Ash Use Symposium – Volume 1: Concrete and Related Products, Orlando, FL, EPRI GS-7162, Project 3176, 1991, pp. 22-1 – 22-10, Jan. 22-25, 1991.

Henkel P. J., J. C. Gaynor, and N. F. Garceau, "The Conversion of United States Gypsum Company's East Chicago, Indiana Plant to NIPSCO FGD Gypsum" proceedings of Third International Conference on FGD and Chemical Gypsum, pp. 16.1–16.10, 1993.

Johnson, B. V., S. J. Markowski, and H. M. Craig, "Cold Flow and Combustion Experiments with a New Burner Air Distribution Concept,: *ASME Jrnl. of Engineering for Power*, pp. 370-375, April 1986.

Jones, D. "By-Product Lime and Fly Ash for Use as a Road Base on Secondary Roads," Ash at Work 1, American Coal Ash Association, 1986.

Korcak, R.F. "Utilization of Fluidized Bed Combustion By–Products in Horticulture," in Proceedings of the Tenth International Ash Use Symposium – Volume 1: High-Volume Uses/ Concrete Applications; Orlando, FL, Jan. 18-21, 1993; EPRI TR-101774, Project 3176, 1993, pp. 12-1 to 12-9, 1993.

Kuo, S. T., R. Huang, J. J. Chang, and C. M. Liu, "A Study of Engineering Application of Fly Ash Blocks," In Proceedings of the Ninth International Ash Use Symposium – Volume 2: Stabilization and Aquatic Uses; Orlando, FL, Jan. 22-25, 1991; EPRI GS-7162, Project 3176, pp. 49-1 – 49-16, 1991.

Hopkins, T. C., M. M. Wu, R. A. Winschel, and T. L. Robl, "The Ohio Coal Development Office Coolside Waste Management Demonstration Project," In Proceedings of the 10th International Ash Use Symposium - Volume 2: Ash Use R&D and Clean Coal By–Products; Orlando, FL, Jan. 18-21, 1993; EPRI TR-101774, Project 3176, pp. 60-1 – 60-16, 1993.

Hoy, H. R., A. G. Roberts, and D. M. Wilkins, "Behavior of Mineral Matter in Slagging Gasification Processes," *J. Inst. Gas Engrs.* 5:444, 1965.

Jacober, D. E., and M. J. Matteson, *Aer. Sci. and Tech.*, 4, 433, 1985.

Jones, M. L., B. P. Kalmanovitch, E. N. Steadman, C. J. Zygarlicke, and S. A. Benson, "Application of SEM Techniques to the Characterization of Coal and Coal Ash Products," in Advances in Coal Spectroscopy; Meuzelaar, M.L.C., Ed.; Plenum Publishing Co.: New York, 1992.

Keshawarz, M. S., U. Dutta, and N. E. Najib, "Laboratory Stabilization of Caliche with Fly Ash," in Proceedings of the 9th International Ash Use Symposium - Volume 2: Stabilization and Aquatic Uses, Orlando, FL, Jan. 22-25, 1991; EPRI GS-7162, Project 3176, pp. 46-1–46-10, 1991.

Kzukauskas, A., Advances in Heat Transfer, J. P. Hartnett and T. F. Irvine Jr., Eds, 8, Academic Press, New York, N, 1972.

Lisk, D. J., "Benefits and Hazards of Using Coal Fly Ash in Agriculture and Aquaculture; in Proceedings of the Governor's Conference on Expanding the Use of Coal in New York State: Problems and Issues; Tress, M. H.; Dawson, J. C., Eds.; Albany, NY, pp. 13-17, May 21-22, 1981.

Livingston, R. J., G. F. Brendel, and D. A. Bruzek, "Coal Ash Artificial Reef Demonstration," in Proceedings of the Ninth International Ash Use Symposium – Volume 2: Stabilization and Aquatic Uses; Orlando, FL, Jan. 22-25, 1991; EPRI GS-7162, Project 3176, pp. 50-1–50-9, 1991.

Mackenzie, J. K. and R. Shuttleworth, Proc. Phys. Soc.(London), B62, 833, 1949.

Marshack, J., Senior Environmental Specialist, Environmental/Technical Support, California Regional Water Quality Control Board, Sacramento, California. Memo to Pete Fuller, Division of Clean Water Programs, State Water Resources Control Programs, Oct. 26, 1992.

Manz, O. E., and M. J. Mitchell, "Selection of Ash for Utilization and Economics of Ash Use in Various Products," in Proceedings of the 13th Biennial Lignite Symposium: Technology and Utilization of Low-Rank Coal; Grand Forks ND; Jones, M. L., Ed.; NTIS: Springfield, VA, 1986; Vol. II, pp. 638-651, May 20–23, 1985.

Markowski, S. J., R. P. Lohmann, and R. S. Reilly, "The Vorbix Burner — A New Approach to Gas Turbine Combustors," ASME Jrnl. of Engineering for Power, pp. 123-129, Jan. 1976.

Merryman, E. L., and A. Levy, Fifteenth Symposium (International) on Combustion, p. 1073, The Combustion Institute, 1975.

Meyer, R. D., G. M. Nakamura, H. A. George, B. L. Willoughby, G. Markegard, and R. A. Shippey, "Recycling Wood Fueled Co-Generation Fly Ash on Agricultural Lands," presented at the Cogeneration Ash as a Low-Cost Fertilizer Meeting and Workshop and Work Group Meeting on Land Application of Power Plant Ash, Burney, CA, Jan. 22, 1992.

Mulder, E., and A. S. M. Houtepen, "Artificial Gravel as a Gravel Substitute in Asphaltic Concrete," in Proceedings of the 9th International Ash Use Symposium — Volume 1: Concrete and Related Products, Orlando, FL, Jan. 22-25, 1991; EPRI GS-7162, Project 3176, pp. 23-1–23-11, 1991.

Naik, T. R., L. H. Wei, and S. S. Singh, Low-Cost Ash-Derived Construction Materials: State-of-the-Art Assessment; interim report, EPRI TR-100563, Project 3176-1; 144 p, April 1992b.

Parker, J. H., Woodhead, P. M. J., I. W. Duedall, "Ocean Disposal and Construction with Stabilized Coal Waste Blocks," in Proceedings of the International Conference on Coal-Fired Power Plants and the Aquatic Environment; CONF-8208123, Copenhagen, Denmark, pp. 287-299, Aug. 16, 1982.

Pauken, D. G., and G. W. Wieskamp, "Producing Marketable Gypsum — Hindsight is 20/20," in Proceedings of the Tenth International Ash Use Symposium - Volume 2: Ash Use R&D and Clean Coal By–Products; Orlando, FL, Jan. 18-21, 1993; EPRI TR-101774, Project 3176, pp 77-1–77-12, 1993.

Payne, J. C., and R. A. Carroll, "Advances in the Use of Fly Ash as a Raw Material in the Manufacture of Autoclaved Aerated Concrete," in Proceedings of the 9th International Ash Use Symposium - Volume 1: Concrete and Related Products, Orlando, FL, Jan. 22-25, 1991; EPRI GS-7162, Project 3176, pp. 26-1–26-15, 1991.

Phillips, B. and A. Maun, A., Amer .J. Sci., Vol. 42, p. 414, 1959.

Price, K. S., C. E. Schlekat, and K. M. Hansen, "Project Ash Clutch: A Report on Optimal Oyster Clutch Based on a Prepared Fly Ash Substratum," in Proceedings of the Ninth International Ash Use Symposium – Volume 2: Stabilization and Aquatic Uses; Orlando, FL, Jan. 22-25, 1991; EPRI GS-7162, Project 3176, pp. 47-1–47-15, 1991.

Perry, R. H., and C. H. Chilton, Chemical Engineer's Handbook, 5th Ed., McGraw Hill, 1973.

Phillips, B. and A. Maun, *Amer. J. Sci.*, Vol. 42, p. 414, 1959.

Price, J. R. and M. van Roode, "Corrosion Resistant Coatings for Silicon Carbide" in *Ceramic Transactions*, Vol. 10, R. E. Tressler and M. McNallan eds., pp. 469-493, The American Ceramic Society, Westerville, Ohio, 1990.

Puccio, M, and L. Nuzzo, "Utilization of Thermoelectric Power Plant By-Products after Granulating and Thermal Sintering Treatments," in Proceedings of the 10th International Ash Use Symposium - Volume 1: High-Volume Uses/Concrete Applications, Orlando, FL, Jan. 18-21, EPRI TR-101774, Project 3176, pp. 11-1–11-7, 1993.

Pytlik, E. C., and J. Saxena, "Fly Ash-Based Autoclaved Cellular Concrete: The Building Material of the 21st Century," in Proceedings of the 9th International Ash Use Symposium – Volume 1: Concrete and Related Products, Orlando, FL, Jan. 22-25, 1991; EPRI GS-7162, Project 3176, pp. 25-1–25-12, 1991.

Raask, E., Mineral Impurities in Coal Combustion, Washington, D.C.: Hemisphere Publishing, 1985.

Reid, W. T. and P. Cohen, "The Flow Characteristics of Coal Ash Slags in the Solidification Range," Furnace Performance Factors, suppl. to Trans. ASME, 66:83, 1944.

Rodgers, M. W., Slag Layers in Coal-Fired MHD Generators. PhD Thesis, Stanford University, 1979.

Santhanam, C. J., R. R. Lunt, C. B. Cooper, D. E. Klimschmidt, I. Bodek, W. A. Tucker, and C. R. Ullrich, Flue Gas Cleaning Wastes, Disposal and Utilization; Noyes Data Corporation: Park Ridge, NJ, 646 p, 1981.

Sauber, B. "Status of Development Project Using Fly Ash in Cellular Concrete," in Proceedings of the 9th International Ash Use Symposium – Volume 1: Concrete and Related Products, Orlando, FL, Jan. 22-25, 1991; EPRI GS-7162, Project 3176, pp. 27-1–27-7, 1991.

Semerjian, H., and A. Vranos, "NO_x Formation in Premixed Turbulent Flames, Sixteenth Symposium (International) on Combustion, p. 169, The Combustion Institute, 1977.

Soroushian, P., and J. Hsu, "Fly Ash Effect on the Scaling Resistance of Concrete: A Literature Survey," In Proceedings of the 9th International Ash Use Symposium – Volume 1: Concrete and Related Products, Orlando, FL, Jan. 22-25, 1991; EPRI GS-7162, Project 3176, pp. 13-1–13-15, 1991.

Smith, C. L., "Commercial Aggregate Production from Fly Ash and FGD Waste," In Proceedings of the 10th International Ash Use Symposium - Volume 1: High–Volume Uses/Concrete Applications, Orlando, FL, Jan. 18-21, 1993; EPRI TR-101774, Project 3176, pp. 10-1–10-13, 1993.

Stultz, S. C. and J. B. Kitto, Steam/its generation and use, 40th Ed., The Babcock & Wilcox Company, Barberton, OH, 1992.

Swain, L. M., *Proc. Roy. Soc. London*, 125, 647, 1929.

Tacina, R. R., "Low NO_x Potential of Gas Turbine Engines, AIAA-90-0550, 1990.

Tyson, S. S., "Freeze-Thaw Durability of Coal Fly Ash Concrete," in Proceedings of the 9th International Ash Use Symposium - Volume 1: Concrete and Related Products, Orlando, FL, Jan. 22-25, 1991; EPRI GS-7162, Project 3176, pp. 10-1–10-14, 1991.

van der Sloot, H. A., P. M. J. Woodhead, D. Hockley, and F. J. Roethel, "The Long–Term Behavior of Stabilized Coal Ash in the Sea," in Proceedings of the Ninth International Ash Use Symposium - Volume 2: Stabilization and Aquatic Uses; Orlando, FL, Jan. 22-25, 1991, EPRI GS-7162, Project 3176, pp. 53-1–53-17, 1991.

Varallo, G. "Reclamation of Fly Ash from Electricity Generating Plants Through Cocomposting with Source–Collected Vegetable Waste," in Proceedings of the Tenth International Ash Use Symposium - Volume 1: High–Volume Uses/Concrete Applications; Orlando, FL, Jan. 18-21, 1993, EPRI TR-101774, Project 3176, pp. 14-1–14-10, 1993.

von Fay, K. F., W. F. Kepler, and R. Drahushak-Crow, "Freeze-Thaw Durability of Concretes with Various Fly Ashes," in Proceedings of the 10th International Ash Use Symposium - Volume 2: Ash Use R&D and Clean Coal By–Products, Orlando, FL, Jan. 18-21, 1993; EPRI TR-101774, Project 3176, pp. 40-1–40-14, 1993.

Vranos, A., and D. S. Liscinsky, "Planar Imaging of Jet Mixing in Crossflow," *AIAA Journal*, Vol. 26, No. 11, p. 1297, November 1988.

Vranos, A., B. A. Knight, and M. F. Zabielski, "Centrifugal Mixing: A comparison of Temperature Profiles in Non-Recirculating Swirling and Non-Swirling Flames," *Combustion and Flame* 48, pp. 109-119, 1982.

Wain, S. E., W. R. Livingston, A. Sanyal, and J. Williamson, Proceedings of Engineering Foundation Conference on Inorganic Transformations and Ash Deposition During Combustion, p. 459, ASME, New York, NY, 1991.

Ward, M. E., N. G. Solomon, M. E. Guldeb, and C. E. Smeltzer,Development of a Ceramic Tube Heat Exchanger with Relaxing Joint, US Department of Energy, Report FE–2556–30, 1980.

Wei, L., T. R. Naik, and D. M. Golden, "A Study on the Properties of Coal Ash Masonry Blocks," in Proceedings of the 10th International Ash Use Symposium –Volume 2: Ash Use R&D and Clean Coal By–Products, Orlando, FL, Jan. 18-21, 1993; EPRI TR-101774, Project 3176, pp. 78-1 to 78-10, 1993.

Wheelabrator Shasta Energy Co. "Project Summary WFPPA.801," Sept. 12, 1991.

Wibberly, L. J. and T. F. Wall, Alkali−ash reactions and deposit formation in pulverized coal-fired boilers: the thermodynamic aspects involving silica, sodium, sulfur, and chlorine, *Fuel*, Vol. 61, pp.87−92, 1982.

Zimmels, Y., G. Shelef, and A. Boas, "Utilization of Coal Fly Ash for Land Reclamation from the Sea and Offshore Islands," in Proceedings of the Ninth International Ash Use Symposium - Volume 2: Stabilization and Aquatic Uses; Orlando, FL, Jan. 22-25, 1991, EPRI GS-7162, Project 3176, pp. 56-1−56-15, 1991.

Zygarkicke, C .J., S, A, Benson, D. L. Toman, E. N. Steadman, D. Brekke, T. A. Erikson, and J. P. Hurley, "Combustion Inorganic Transformations," Final Report for the period July 1989 to June 30, 1990, work performed under Contract DE-FC21-86NC10637, 1990.